E.O. Paton Electric Welding Institute
of the National Academy of Sciences of Ukraine

Laser Technology Research Institute
of the National Technical University of Ukraine
«Kiev Polytechnic Institute»

International Association «Welding»
Local Charity Foundation «Welding Community»

Laser Technologies in Welding and Materials Processing

Proceedings of the Second International Conference

May 23–27, 2005, Katsiveli, Crimea, Ukraine

Edited by
Prof. B.E. Paton and Prof. V.S. Kovalenko

E.O. Paton Electric Welding Institute, NASU
Kiev 2005

(2005) **Laser Technologies in Welding and Materials Processing.** Kiev: E.O. Paton Electric Welding Institute, NASU, 208 pp.

The book contains papers presented at the Second International Conference «Laser Technologies in Welding and Materials Processing», covering the latest achievements in the field of laser welding, cutting, surfacing and other advanced processes of laser machining of materials. Prospects of application of laser technologies are considered. Authors of the papers are the known specialists from many countries all over the world.

The papers are published as they are submited by the authors without editing.

Compiled by *V.S. Kovalenko, I.V. Krivtsun*

Publishing Project *A.T. Zelnichenko*

Translation *T.K. Vasilenko*

State Registration Certificate DK 166 of 06.09.2000

ISBN 966-8872-01-0

© E.O. Paton Electric Welding Institute, NASU, 2005

Sent to press on 06.12.2005. 60×84/8 form. Offset paper. Offset print. Ukr. Pet. Font. 44,0 cond. print. sheets. 30,2 publ. print. sheets.
Camera-ready copy: ITB Advertising Agency.
Published by «Esse». 34/1, Vernadsky Ave., Kiev, 03142.

Contents

Preface 7

Kovalenko V. S. Laser Technology: From Macro to Nano 9

PLENARY PAPERS

Albert F., Jahrsdorfer B., Mys I., Schmidt M. Innovative Laser Based Micro Joining Techniques in Electronic Production 19

Bachmann F. Impact of High Power Diode Lasers on Solid-State Lasers and Materials Processing Applications 24

Dilthey U., Gumenyuk A., Turichin G. Towards Kinetical Description of Phase Transformation Phenomena in Metals under Laser Welding Conditions Using Reaction-Diffusion Formalism 29

Golubev V. S. Melt Removal Mechanisms of the Gasjet-Assisted Laser Fusion Cutting 34

Klimpel A., Lisiecki A., Janicki D., Stano S. High Power Diode Laser Welding of Aluminum Alloy EN AW-1050 A 39

Man H. C., Zhang S., Guo X. Synthesis of a Porous Coating on NiTi Shape Memory Alloy by Laser Surface Alloying for Enhanced Osteointegration 43

Thomy C., Kohn H., Vollertsen F. Application of High-Power Fibre Lasers in Laser and Laser-MIG Hybrid Welding 46

Turichin G., Lopota V., Zemliakov E., Pozdeeva E., Grigoriev A., Gumenyuk A., Dilthey U. Kinetics of Optical Discharge in Plasma Plume During Laser Welding in Shielding Gas 49

EQUIPMENT

Borisov Yu., Bushma A., Fomakin A., Khaskin V., Kislitsa A., Krivtsun I., Shelyagin V., Voynarovich S. Integrated Laser-Arc Plasmatron for Laser-Plasma Spraying and CVD Processes 57

Garashchuk V. P., Sidotrets V. N. Optical Properties of Excited Active Medium of Slab CO_2-Laser 60

Kovalenko V., Mamalis A., Kolpakov V. Web-Technologies Application to Increase the Efficiency of Laser Industrial Systems 64

Oleschuk L. M., Kovalenko V. S., Anyakin M. I., Zhuk R. O. Configuration of Industrial Laser System (ILS) for Layer by Layer 3-D Forming of Solid Objects 67

HEAT TREATMENT

Borisova G. V., Lysenko A. B., Korovina N. A., Kravets O. L., Lysenko A. A. Amorphing of Alloys by Laser Glass Glazing of Surface 73

Golovko L. F., Kaglyak A. D., Krasavin A. P., Soroshenko V. G. Increase of Rigidity of Thin Laminas by Creation and Optimum Arrangement of Metallurgical Stress Raisers 76

Golovko L. F., Serditov A. T., Klyuchnikov Y. V., Daszherdi A. Application of Laser Treatment for Increase of Wear Resistance of Details of the Heavy Loaded Units of Friction 80

Lysenko A. B., Korovina N. A., Pavluchenkov I. A. Metal Crystallization Kinetics in Conditions of Laser Rapid Hardening 85

MODELLING

Kovalenko V. S., Zhuk R. O. Prerequisites to Numerical Modelling of Aerodynamic Phenomena at Gas-Laser Metal Cutting 91

Lopota V., Turichin G., Valdaitseva E., Malkin P. E., Goumeniuk A. CAE System for Laser and Electron Beam Welding 96

Pretorius T., Woitschig J., Vollertsen F. Simulation of Thermal Bending — Acceleration of Temperature Field Calculations 100

Seyffarth P., Makhnenko O. Calculational Prediction of Total Distortion of Tailored Beams in Laser Welding 103

OTHER ADVANCED PROCESSES OF LASER MACHINING OF MATERIALS

Chivel Yu. A., Beliavin K. E., Pavlenko V. K., Petrushina M. V. Research of Direct Laser Sintering of Metal Powders 113

Kovalchenko A., Ajayi O., Etsion I. Tribological Behavior of Laser Textured Surfaces under Oil Lubrication Conditions 116

Kovalenko V. S., Golovko L. F., Exsan O., Goncharuk A. A., Novikov N. V., Shepelev A. A., Sorochenko V. G. Features of Application of Laser Technology for Sintering Diamond Composite Materials 121

Teplova L. A. Laser Surface Alloying of Titanium and Titanium Alloys 126

Vertiy A. A., Gavrilov S. P. Inspection of Reinforced Concrete Units Using Tomography Techniques 130

RAPID PROTOTYPING

Anyakin M., Kondrashov P., Mukhoid A., Stepura A., Kovalenko V. Optimal Conditions for Process of Rapid Prototyping 135

Anyakin M., Rudakov K., Lutay A., Kozakova T., Kovalenko V. Study of the Process of Rapid Prototyping Using Numerical Experiments 141

SURFACING

Chivel Yu. New Method of Laser Power Delivery to Powder Stream in Laser Cladding and Nanopowders Production 151

Devojno O. G., Kardapolova M. A. Influence of Laser Treatment on Structure and Properties of Plasma Ceramic Coatings 154

Klimpel A., Janicki D., Lisiecki A. Thermal Stress Analysis of Nozzle for Powder Feeding in High Power Diode Laser (HPDL) Powder Surfacing 158

Radziejewska J., Kalita W., Bartoszewicz A. Modification of Surface Layer Properties by Laser Alloying Combined with Burnishing 162

WELDING

Cheng C. H., Chan L. C., Chow C. L., Lee T. C. Laser Welding and Formability Study of Tailor-Welded Blanks of Different Thickness Combinations and Welding Orientations 167

Cheng C. H., Chan L. C., Chow C. L., Lee T. C. True Stress-Strain Analysis on Weldment of Heterogeneous Tailor-Welded Blanks — an Experimental Approach 171

Gedopt J., Verwimp J., Geerinckx E. Laser-MIG Hybrid Welding of Aluminium Alloys 175

Kalita W., Kolodziejczak P., Kwiatkowski L., Grobelny M., Hoffman J. Properties of CO_2-Laser Welded Joints of Dissimilar Magnesium Alloys 182

Karfoul M. K. Effect of Presence of the Active Metal in ODS Laser Weld Metal 186

Shelyagin V. D., Krivtsun I. V., Khaskin V. Y., Nabok T. N. Some Results of Research in Hybrid Laser-Arc Technologies at the E.O. Paton Electric Welding Institute of NASU 190

Sokolova T. N., Surmenko E. L. Study of Chemical Element Distribution in a Laser Weld Joint 195

Stano S., Banasik M., Dworak J., Pilarczyk J. Laser Welding of Steel Sheets Differentiated in Thickness for Tailored Blanks. Investigations Conducted at the Instytut Spawalnictwa 198

Thomy C., Seefeld T. Basics and Applications of Laser GMA Hybrid Welding 203

Name Index 207



Participants of the Second International Conference «Laser Technologies in Welding and Materials Processing»,
May 23-27, 2005, vil. Katsively, Crimea, Ukraine

PREFACE

This Proceedings cover the materials of the 2nd International Conference on Laser Technologies in Welding and Material Processing (LTWMP-05) which took place in Katsively town, Crimea, Ukraine on May 23–27, 2005.

The International Conference had been organized by the experts in laser technology from the Paton Welding Institute of the National Academy of Science of Ukraine and from the Laser Technology Research Institute of the National Technical University of Ukraine (Kiev Polytechnic Institute) where pioneering research in this field in Ukraine and in the former Soviet Union was conducted since 1963. The Conference had been supported as well by the International Association «Welding».

At the 1st similar conference held in May 2003 the decision to arrange such conferences once per every 2 years was accepted. And thus again in 2005 the experts from 19 countries (Ukraine, Russia, Belorus, USA, Germany, Poland, PRC, Switzerland, Israel, Italy, Belgium, Iran and others) in the field of laser technology have presented the results of their last researches.

The lasers have dynamically come practically to all spheres of human activity in the last years. More 350 various applications of lasers are known now. The global market of lasers and laser technologies makes more than 90 billions American dollars per year (not considering military applications). Use of lasers for processing materials in various industries is especially efficient. And the customer's interest to these technologies has increased especially for last decades because of development of new generations of lasers with increased efficiency: solid-state, powerful CO_2, excimer, metal vapor, compact diode, fiber optics etc.

To this and to other last achievements in the field of laser technology the program report and few plenary papers had been devoted. In total three plenary sessions were carried out.

The further work of a conference was held on following topics: welding, modeling, synthesis of three-dimensional objects, heat treatment, coating, equipment, other advanced processes (8 sessions). The special session was allocated to poster papers (24 in total).

A number of the reports was devoted to urgent problems of laser sintering of powder materials at realization of processes of synthesis 3D products The study of opportunities to use laser radiation for sintering the diamond containing composites at manufacturing the diamond cutting tool was considered.

The significant accent at the Conference was made on process simulation. The models of different processes were presented which had been visualized in dynamics giving quite adequate mechanism of different effects at laser beam interaction with materials. Such simulation not only helps to understand better these effects but also provides eventually the improvements in laser material processing.

The final report of a conference was devoted to the problem how to increase the efficiency of operation of the laser industrial equipment. In the report the basic principles of work of the virtual enterprise using as industrial base the laser industrial equipment of various organizations for performance of the orders on laser processing with application of modern information systems and the Internet were shown.

Members of Organizing Committee and the stuff of the House of Scientists actively helped to make the participant's stay in Katsively not only useful but pleasant as well.

The conference has shown, that laser technology still remains the most dynamically developing area of science and engineering stably raising efficiency of existing processes of laser processing and constantly opening new applications of lasers in industrial sphere.

Friendly, hospitable and creative atmosphire of the conference promoted development of useful discussions, establishment of business contacts. The participants of the conference from different countries marking unconditional success of a conference, expressed wishes to take part in next 3d International conference LTWMP-07 in 2007. Thus it becomes the traditional conference on laser technology in the post-soviet countries.

Prof. Volodymyr S. KOVALENKO
Co-Chairman of the Conference
Director of the Laser Technology Research Institute of NTUU «KPI»

LASER TECHNOLOGY: FROM MACRO TO NANO

V. S. KOVALENKO
Laser Technology Research Institute of NTUU «KPI», Kiev, Ukraine

Along with classic piercing of small holes, cutting and welding different materials of significant thickness (up to 30–40 mm) in automotive and airspace industry, hardening of large camshafts and cylinder linens for diesel engine of locomotives, attempts were made to use lasers to drill rocks for oil rigs, to clean rails from leaves at railroads, to remove old paints from the air dynamic surfaces of planes, cars and buses bodies etc., to change the shape via controlled thermal deformations of large sheet components for machine building and shipbuilding industries, to record and to read the enormous (macro) volumes of information with unprecedented speed. Recently achieved possibilities to obtain laser pulses of very short duration in nano and femtosecond range with different wavelengths brought to life the new multyphoton processes of radiation interaction with matter. Very short wavelength in combination with super high power density allow to perform very precise laser processing with dimensions of affected region in the range of micrometers and nanometers. Thus from macro processing laser technology has come to micro and nanoprocessing.

Introduction. Global economy development discloses new challenges in human activity. Advent of information technologies, airspace developments, new success in health care, new results in biotechnology and other science and technology achievements are possible among others due to fundamental changes in manufacturing science and possibilities to use new approaches in product developments.

Laser technology born in the middle of the last century continues to bring new challenges and to open new horizons for scientists and manufacturers up to now.

From the beginning of the laser era it started from the use of focused laser beam to pierce small holes and to cut precise slots in super hard materials. First industrial systems had been too inefficient to find broad and more sophisticated application.

With the development of new types of powerful lasers the fields of industrial applications are becoming broader and laser processing itself becomes not so much exotic and expensive. Thus from one side laser industrial application may be found now at treatment of large components, at use on wide production scale, in functioning multy million business etc. From another side the unique abilities of laser technology allow to treat micro components, to perform unique machining operations, to achieve product manufacturing at nano scale.

Laser as energy converter. It is known that laser efficiency «from wall plug to radiation» is extremely low. For the first industrial lasers it had been even less than 1%. The main consumed electrical energy is transformed into heat and the main problem is how to remove this heat. Thus the most significant drawbacks of the majority of lasers are as follows:

- heavy energy losses on intensive cooling;
- large dimensions;
- too much complicated design;
- expensive maintenance.

© V. S. KOVALENKO, 2005

I recollect my experience of doing research at McMaster University, Hamilton (Canada) at the end of 80-ies when the well known electric power company «Ontario Hydro» used to sponsor laser technology research considering powerful lasers as the most prospective and efficient consumer of electric power.

From the beginning of laser era it started from the use of focused laser beam to perform unique machining operations: piercing small holes and cutting precise slots in super hard materials. First industrial systems had been too inefficient to find broad and more sophisticated application. Because of low efficiency lasers has suffered some decline of interest to them from industrialists during the past decades in spite of general increase of laser industry (Figure1).

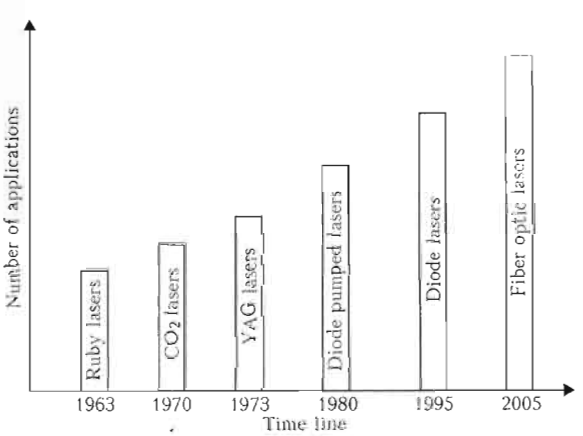
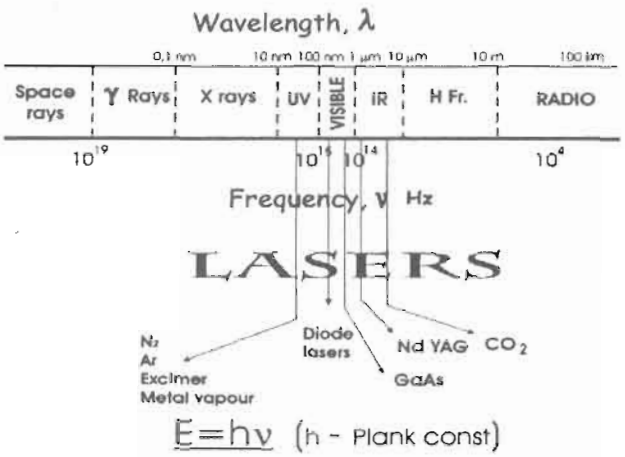


Figure 1. Fluxes of interests to laser types and their application

Laser developments. Looking back into the history of laser technology we can see that the first industrial application were based mainly on the use of ruby and He–Ne lasers generation in the visible part of electro-magnetic spectrum. With further laser developments great amount of different types of lasers appeared both in infra red (IR) and ultra violet (UV) parts of the spectrum (Figure 2). It is important to note that the shorter wavelength of laser radiation



Part of the Spectrum	ν, Hz	E, eV	Note
IR	$3x10^{13}$	0.124	
UV	$3X10^{15}$	13.6	2 orders higher
X-rays	$3x10^{17}$	$1.2x10^{3}$	4 orders higher than at IR
γ- rays	10^{20}	$4.0x10^{5}$	

Figure 2. Types of lasers

the higher photon energy and more powerful is the laser beam. At the same time shorter wavelength enables to decrease the diameter of the focused spot and thus the power density may be increased significantly for the focused laser radiation.

Next generation of lasers – Nd-glass and Nd:YAG lasers – became widespread very fast and up to now the Nd:YAG laser with some improvements is still a «working horse» in industrial laser applications. The same role has the CO_2 laser which became very popular especially at large production scale applications. CO laser has a lot of advantages in comparison with CO_2 laser, especially at materials cutting but because of some problems with maintenance its use up to now is still limited.

Table 1. Efficiency for different laser types

TYPE OF LASER	*EFFICIENCY*
Ruby laser	< 0.1%
Nd-glass laser	< 1.0%
Nd:YAG laser	< 1.0%
CO_2 laser	< 10%
CO laser	< 12%
Excimer laser	< 25%
Diode laser	> 40%
Fiber optics laser	> 40%

Excimer laser with its UV radiation became quite widespread in different precise micro machining and has its own very good niche in microelectronics.

The real boom in industrial application was caused by the development of very efficient high power diode lasers. The main advantage of this type of laser in comparison with others is their unique efficiency (Table 1) and thus the possibility to get very compact with low mass laser system and even to fit it to the hand of anthropomorphic robot (Figure 3). Thanks to diode laser the efficiency of Nd:YAG lasers had been increased as well when to pump the active rod instead of flash lamps the pumping diodes became possible to use.

The new exciting achievement is the development of very compact fiber optics laser with very high efficiency (Table 2).

Many other types of laser are under development now and their use will bring new features in industrial laser applications. Quite unusual applications, for example, may be found with the development of the powerful X-ray laser [1].

Mechanisms of laser radiation interaction with matter. The process of laser radiation interaction with material has very complicated nature. The mechanism

Table 2. Characteristics of fiber optics lasers

Typical Specification

Optical Parameters	**Unit**	**YLR-1000**	**YLR-2000**	**YLR-4000**	**YLR-10000**
Mode of operation		CW	CW	CW	CW
Central emission wavelength [1]	nm	1070	1070	1070	1070
Nominal output power [2]	W	1000	2000	4000	10,000
Typical beam quality [3]	mm·mrad	6	18	20	25
Output power stability (long term)	%	+/-3	+/-3	+/-3	+/-3
Output fiber delivery diameter	μm	100-200	200-300	300-400	400
Electrical Parameters					
Typical electrical requirements	VAC	208-480	380-480V,3P+PE, 50 - 60Hz		
Maximum power consumption	kW	7	15	30	80
Max. cooling water consumption	m^3/h	0.6	1.2	3	5
Cooling water temperature	°C	5-30	5-30	5-30	5-30
General Parameters					
Dimensions (WxDxH)	cm	60x79x110	60x79x110	60x79x160	120x79x160
Weight	kg	150	300	450	1000
Ambient temperature	°C	0-45	0-45	0-45	0-45

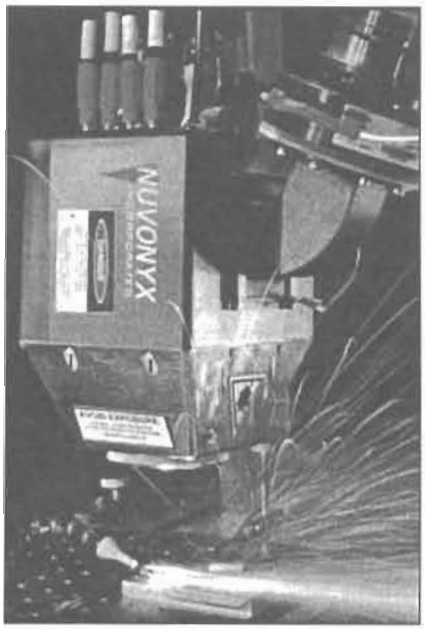


Figure 3. High power diode lasers

of this interaction depends on many factors: characteristics of the radiation, properties of the material, working media, etc. Basically all types of processing have the same nature – thermal effect on media, causing its heating, melting, evaporation, explosion, ablation, etc. At the same type each type of laser treatment has its own features: for hole piercing and cutting – melting, evaporation air dynamic and hydrodynamic phenomenon; for heat treatment – phase transformations and element migration; for welding – melting, key hole formation etc.; rapid prototyping – the whole bunch of features starting from polymerization of liquid media and ending with sintering of powder materials under laser radiation influence.

Looking into fundamentals of light interaction with matter it is the energy of photon which plays the decisive role in causing different effects, because it destroys the chemical bonds in affected material (Figure 4). Three mechanisms may take place in material depending on wavelength (photon energy) and laser pulse duration [2].

The photon energy is required
to destroy chemical bonds
in material
$E=h\nu \sim 3\text{-}10$ eV

Three mechanisms:

1. Thermal or pyrolitic
   (Long waves)
2. Photolitic
   (Short waves UV – E=3-7 eV)
3. Multiphotonic impact on electrons
   (ultra short pulses)
   - Nanoseconds 10^{-9} s
   - Picoseconds 10^{-12} s
   - Femtoseconds 10^{-15} s
   - Attoseconds 10^{-16} s

To shorten the wavelength — To shorten pulse duration

Figure 4. Various mechanisms of laser beam interaction with materials

Macro machining. At the beginning of industrial laser applications laser systems used had very small pulse energy (few joules) with frequency of up to few pulse/min or 10–30W of CW radiation. That is why the applications were limited only by micro machining. With the development of high power lasers (pulse energy up 100–500 J and power of CW radiation up to 5–20 kW) the scale of laser use became much larger.

One of such macro application is laser hardening of different components. Automotive industry has implemented hardening technology to increase the wear resistance of dies, moulds, cutting tools, engine camshafts, cylinder linens, gear blocks, valves etc [3]. Good example of large components treated with laser was the hardening of working surfaces of long slides for thin polymer film manufacturing (Figure 5).

Research has been done on use laser hardening on more broad scale. The positive result has been obtained at hardening working surfaces of rails for rail roads. The international project (Canada, FSU, PRC) had been initiated to put two 50 kW CO_2 laser on the platform the power supply source being at another platform with locomotive moving with the speed few km/h to perform rails heat treatment.

Laser welding became now widespread for joining components of aluminum car bodies. Among such macro application the laser cleaning operations may be named too as efficient method of old paint removal from large surfaces of airplanes, cars, buses etc. The cleaning speed may reach few thousands square millimeters per min. Just recently there were disclosed the results of tests of laser system developed for cleaning railways at train movement. Quite high efficiency was demonstrated at removal grease, old leaves and other dirt making safer railway transportation.

Due to conversion of the developed military laser systems one more macro application is coming under investigation. Thanks to very high power radiation in the range of few hundreds kilowatts it became possible to study laser drilling of the rocks and concrete to produce holes of large diameters instead of mechanical drilling. Because of melting and glazing of the sand and rocks containing soil it is expected to realize the

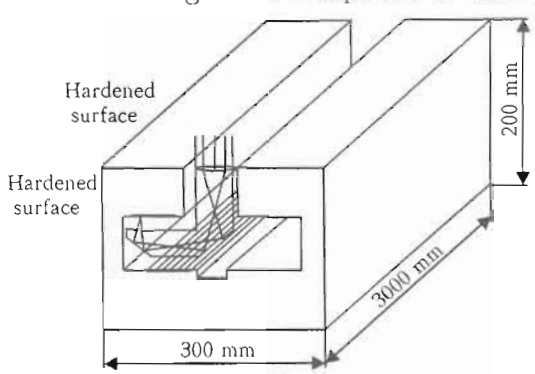


Figure 5. Laser hardening of the internal working surfaces of the long slides, used in special equipment for thin polymer film manufacturing

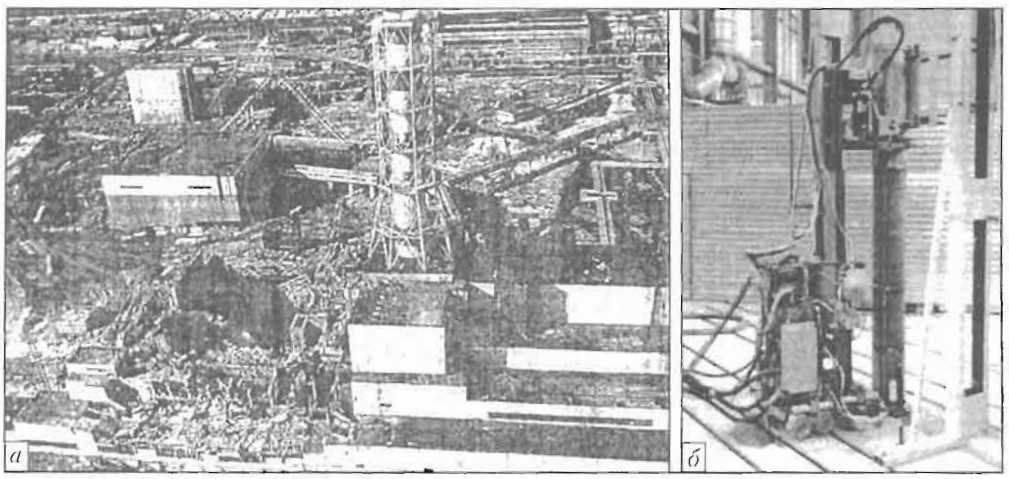


Figure 6. Aerial view of the destroyed reactor #4 at the Chernobyl Nuclear Power Plant (*a*) and the developed robotized laser system for disintegration of object «Shelter» (*b*)

possibility to eliminate the use of special tubes in forming oil (gas) rigs [7].

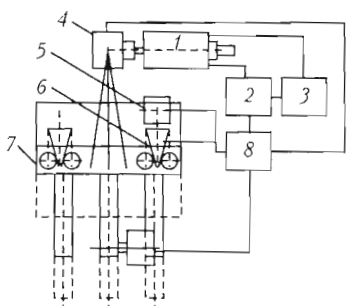
Among macro applications the important role belongs to laser cutting or shearing of steel sheets in airspace, automotive and ship building industry. The material thickness may vary from fraction of millimeter up to 40–50 mm. Thanks to careful study of air dynamic and hydrodynamic phenomenon at gas-laser cutting it is possible significantly to improve the quality and productivity of the process. One more specific macro application of laser cutting technology had been proposed and developed at Laser Technology Research Institute (LTRI) of the NTUU «KPI» — the use of laser radiation to dismantle the radioactive remnants of the Object «Shelter» of the Chernobyl Atomic Station. It had been demonstrated that with help of remote controlled laser robotized system it is possible to perform some demolishing operations in a highly complicated and dangerous conditions (Figure 6) [4].

By macro laser application we may call as well the huge use of different laser systems for printing information and its reading. The scale of this application is indeed global and through it almost everybody may personally be acquainted with laser and laser technology.

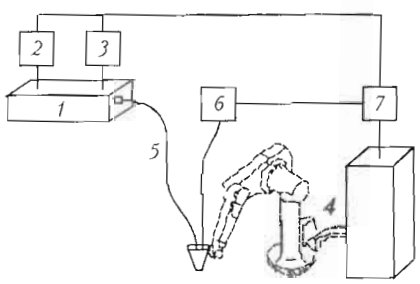
Micro machining. As it was mentioned earlier micro machining was the first industrial application but up to now it is still wide spread because there is no alternative technology to perform precise micro holes piercing with very high productivity in different super hard and usual materials or to cut narrow precise slots and cuts in brittle materials, etc.

In many cases laser hardening is done by pulsed lasers when there is need to treat small working areas of components ant tools with high precision. Good examples of such applications are dyes and punches, different cutting tools, etc. Laser micro welding is usually done with pulse radiation, not only dot welding but seam welding as well. These operations are performed mainly with systems based on Nd:YAG lasers.

The real revolution in manufacturing technology may be considered the development of Laser Rapid Prototyping (RP) technique. Using laser beam scanning according to program it is possible to «grow» the component layer-by-layer from different powder materials. Such technology is based on micro volume material laser treatment and thus it lies between macro and micro technology (and even nano technology). It is possible to manufacture with this technology both small size and large size components. New universal rapid prototyping equipment was developed at LTRI which is based on the use of two schemes of process realization (Figure 7) — with help of anthropomor-



Oscillator *1* to the technological laser with a supply unit *2* and cooler *3*; *4* — scanning system; *5* — dosing device; *6* — device of powder preparation; *7* — work table; *8* — control system;



Oscillator *1* to the technological laser with a supply unit *2* and cooler *3*; *4* — technological robot with programming system; *5* — optical fiber with systems of radiation input-output; *6* — dosing device; *7* — control system;

Figure 7. Combined laser system for rapid prototyping (LTRI)

phic robot and by powder layer distribution with roller. The new step in development of this promising process is the scheme when powder irradiation according to program is formed with help of diode matrix (Figure 8).

The schemes described above actually represent the layer by layer material deposition. So in some cases such technology is called direct metal deposition. It may be used for forming the body of composite diamond tools, large dyes or matrix with hollow internal channels for cooling or even from layers of different materials with higher heat conductivity.

Starting from micro laser treatment the new technology was developed to change the shape of sheet materials. Due to thermal deformation it became possible to control the deformation by programmed irradiation of the sheet. First application was the bending of different contact elements for electro technical and electronic industry. Later it became possible to provide the regular waviness for sheet metal components with this technology. And now we witness quite wide research in the field of development laser deformation technique for ship building and airspace industry.

Laser marking and engraving is actually micro volume phase transformation in local zones of the material according to the program. It may be done both on the surface of component and inside of the transparent for laser radiation materials. The scale of engraved signs may be different thus changing in size from micro to macro. The main advantages of such technique is very high productivity, precision and ability to treat any materials

Very high precision may be achieved at using for micro machining the material destruction mechanism like ablation (at very high power density). In combination with such modern type of manufacturing system like parallel kinematics (tripod, hexapod, hexaslide) it is possible to perform 3D machining like mechanical milling without applying to component any mechanical forces or heat treatment.

To increase the precision of laser micro cutting it is proposed to add the water jet coaxial to laser beam at material processing. The process is called laser-water jet cutting and has three main features. First, water stream serves like a light guide, second – due to cooling effect helps to decrease the size of the heat affected zone, third – evacuates the laser erosion products from the working zone. It is recommended for machining very hard and brittle materials mainly in micro electronics.

Nano machining. The possibility to concentrate very high power in a very small spot makes laser technology very prospective for its use in nanomachining, nanomaterials and in nanoworld in general.

Considering the prediction that in 21st century the mankind will have the nanotechnological revolution it is possible to trace already the first steps in moving laser technology in this direction.

For the moment there is a success already in manufacturing nano size powder. The technique is almost

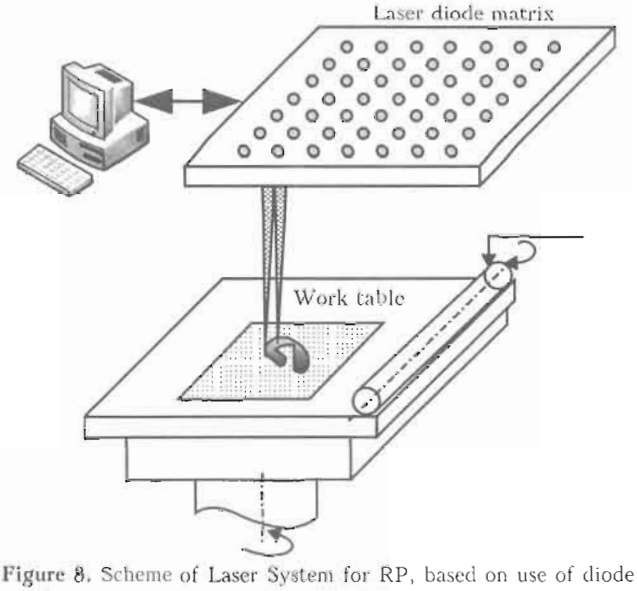


Figure 8. Scheme of Laser System for RP, based on use of diode matrix

the same used in electro discharge method. Laser beam is directed onto target and then the erosion products are condensed on the cool walls of the screen surface, streaked by generated plasma. Particles with size down to few nanometers may be obtained.

The further step in nano-material manufacturing is the development of carbon nanotubes, which may be one wall hollow tube, two-walls tubes etc. Such materials have one order higher mechanical properties and are very light. So, to machine components from such materials will be possible only with help of laser technology.

Nanomachining are widely used now for manufacturing microelectronics elements. Widely implemented into electronic industry is laser lithography which provides the microchips manufacturing with ability of storage of huge volume of memory. Thus, the 256M DRAM contains 340 millions of transistors and capacitors which form the memory volume equivalent to the information contained at 2100 standard newspaper pages. For manufacturing structural elements the excimer laser radiation with wavelength 248 nm is used. It is likely that 64 Gb DRAMS will be in production in 2009 using for processing shorter wavelength of 193 nm or even 157 nm. This will be achieved by decreasing the size of structural elements (Figure 9).

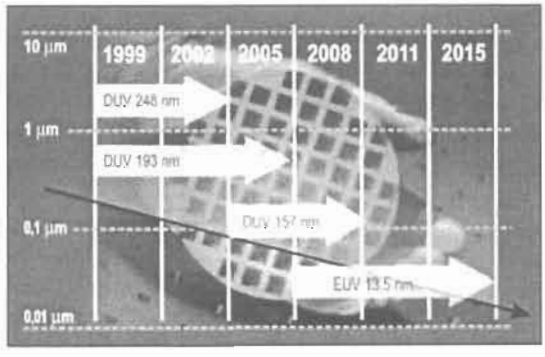


Figure 9. Trends of decreasing the structural elements dimensions with decrease of applied radiation wavelength

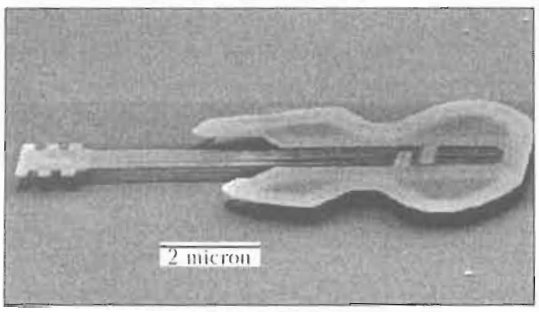


Figure10. Nano guitar made with laser stereo lithography technique

At this level of technical achievement and laser technology implementation the microelectronics and communication industry has very interesting and impressive results:

1. Optical lithography generates global revenues – 1 billion Euro.
2. Microchips produced using these systems generates global revenues – 155 billion Euro.
3. Sales of computers, digital cameras, mobile telephones, dependent on microchips generates total revenues – 1160 billion Euro.

So, every Euro earned with laser lithography generates approximately 1000 Euro of industrial production. No other scientific or technical innovation could bring such brilliant economic result – 100% efficiency. Thus the Optical (Laser) lithography is of crucial importance for the microchips' production. Further miniaturization of the manufactured microprocessors will demonstrate even more.

In microelectronics the removal of nano-layers of impurities and dirt from the components surface is becoming quite efficient. Using scanning technique with high power short pulses it is possible and economically justified as well to remove the dirt from the priceless artifacts at the rate of less than one micron per pulse.

The technology of laser rapid prototyping based on laser stereo lithography has good prospects in nano scale field. Figure 10 demonstrates micro guitar from polymer only few microns long many elements of which are less then one nanometer in size.

Using such technology it is possible to manufacture 3D microprocessor with unique properties which are nevertheless the solid background for the technology of nano-scale photonic devices such as wave guide, miniaturized light sources and plastic based electronics.

Laser technology + information technology = high efficiency. It is impossible to develop modern laser technology without mutual integration with information technology. Such integration is moving along the following directions:

- Process simulation;
- CAD&CAM in product realization;
- E-enterprise.

Laser radiation interaction with substance is very complicated process itself influenced by more than 100 parameters and causing many physical and chemical phenomenons in material. To study them experimentally and to find optimal working conditions is a very serious problem. This problem is much more complicated when the process is augmented by the action of additional energy source – electric arc, magnetic field, plasma, electrical discharge, gas or liquid stream, mechanical force, etc. So the process simulation is the only one right way to find the optimal solution at minimum cost. The developed up to moment software is reliable enough to find the adequate model for the process.

Usage of CAD & CAM in laser technology are just the right means to fully realize he unique advantages of laser treatment – very high processing speed, precise and localized laser beam action, impossibility to control the super high-speed processes with conventional techniques, non contact laser beam interaction with material, etc.

The mutual integration advantages are mostly obvious at performing such processes like programmed laser sheet material cutting, marking and engraving, different techniques of Rapid Prototyping, surface cleaning, thermo-deformation treatment of sheet material, etc. One of the last promising developments in laser technology implementation into industry is the use of the main principles of e-commerce to improve the work efficiency of the available industrial laser systems. It is well known that except of some particular cases (highly specialized industrial laser systems) the majority of equipment is in operation only 25–30% of its possible working term. The main reason of such situation is the absence of enough orders to keep in maximum operation this equipment. This is true mainly for small and medium enterprises of different types of ownership. To find the way out from situation and thus to increase the competitiveness of different enterprises interested in implementation

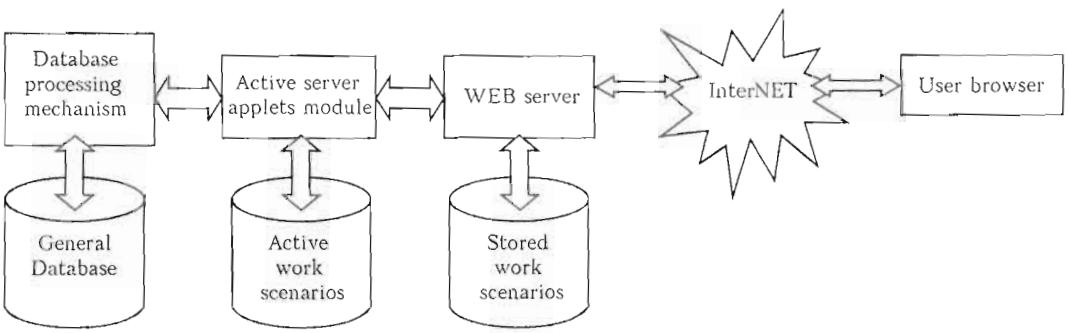


Figure 11. Principal scheme of LTRI e-enterprise

high techs in their product manufacturing the laser e-enterprise had been created at LTRI of the NTUU «KPI» [5]. Based on the developed data bank on different available industrial systems and gained experience in developing the large variety of processes the LTRI may help to solve the problem in fulfilling the order using both its own facilities and Internet resources. LTRI uses its own WEB-server (Figure 11) and can serve the customers from any region and even from abroad.

Mutual integration of laser technology and information technology for sure will increase the global laser market. If now it is assessed at more that 90 billion American dollars (not considering military application) very soon we will witness even wider laser technology implementation into different fields of global economy.

CONCLUSIONS

Laser beam became the highly efficient universal tool. Laser technology has found the wide application in global economy. The mutual integration of laser technology and information technology is the main way to enhance the processing efficiency. Laser technology growth is far from saturation. The manufacturers' interest to laser processing is increasing. The prospects are bright!

1. Kovalenko V.S. *Recent developments in laser material processing*, «Proceedings of International Conf. ILLA/LTL-2003», September 27 – October 1, 2003, Plovdiv-Smolyan, Bulgaria, p. 174.
2. Meijer J., Gillner A., Hoffman D. et al, *Laser machining by short and ultra short pulses: state of the art*, Proceedings of CIRP General Assembly, San Sebastian, Aug. 18–25, 2002, 22 p.
3. Kovalenko V.S. *Opportunities to use laser technology in automotive and aerospace industry*, «Electron material machining», #36, 2002, p. 9–18.
4. Kovalenko V., Anyakin M., Karpachov Y., *Robotized laser technology – solution for the problem of destroyed reactor dismantling at Chernobyl Atomic Station*, Proceedings of the 12th International Symposium for electromachining, (ISEM), Aachen, 1998, p. 613–623.
5. V. Kovalenko, L. Golovko, N. Novikov, B, Shepelev, V. Sorochenko, *On the possibility of using laser technology for diamond tool manufacturing*, «Journal of Engineering manufacture», IME, London, UK, August 2004, vol.218, #B8, p. 1029–1036.
6. V. Kovalenko, M.Anyakin, W. Duley, J. Meijer, D. Roessler, *Laser 3D components forming from powder metal and ceramic materials*, Proc. of ICALEO-2003, Jacksonville, FL, October, 2003.
7. Philip L Crouse and Lin Li, Cutting 500 mm *Thick Concrete Using High-Power Lasers Below 2 kW*, Proc. of ICALEO-2003, Jacksonville, FL, October, 2003.
8. Frank Wagner, Ochelio Sibailly, Nandor Vago, Rafal Romanowicz, Bernold Richerzhagen, *The Laser Microjet® Technology. – 10 Years of Development (M401)*, Proc. of ICALEO-2003, Jacksonville, FL, October, 2003.
9. *Proceedings of the International Congress on Nanotechnology*, Indian Academy of Engineering and Technology, India, 2003.

Conference Sponsors

PWI Laser Systems and Technology Center

Ministry of Education and Science of Ukraine

Information Support

«The Paton Welding Journal»

www.nas.gov.ua/pwj

Conference Sponsors

PWI Laser Systems and Technology Center

Ministry of Education and Science of Ukraine

Information Support

«The Paton Welding Journal»

www.nas.gov.ua/pwj

Conference Sponsors

PWI Laser Systems and Technology Center

Ministry of Education and Science of Ukraine

Information Support

«The Paton Welding Journal»

www.nas.gov.ua/pwj

INNOVATIVE LASER BASED MICRO JOINING TECHNIQUES IN ELECTRONIC PRODUCTION

F. ALBERT, B. JAHRSDORFER, I. MYS, M. SCHMIDT
Bavarian Lasercenter GmbH, Erlangen, Germany

Laser application in electronics production constantly gains industrial significance. After laser single point soldering or laser spot welding has already been established in many production lines, today new requirements on these joining processes are increasing. This paper is dealing with three different solutions which are currently of special importance in electronics production: The simultaneous laser based soldering and rework of SMD electronic devices, the laser beam welding of materials for high-power electronics and the special procedure laser droplet welding.

Selective laser-based soldering and rework. *Hardware for laser soldering.* Today single point soldering with cost-efficient diode laser systems is an industrially established procedure. It is used for example for the production of electronic devices with only few soldering joints, for contacting of individual electronic components on already reflow soldered devices or also for subsequent contacting of temperature-sensitive components. Wellknown low controllability of laser soldering processes is today significantly improved by the application of pyrometer-based control systems.

The modern soldering industry focuses on the enlargement of the components variety having regard to flexibility of laser systems and possibilities of full process automation and process control.

The major purpose here is the achievement of high process stability of soldering and rework processes. To realize it, flexible laser beam shapes (e.g. single point, point line, continuous light line) are required. Such light sources allows the component handling and soldering independent of component geometry, connection forms, number of leads and substrate materials. On the other hand for realization of flexible solder processes a flexible mounting hardware for different electronic components must be implemented. One possible realization of such flexible system with integrated pick & place-unit and laser soldering head with galvanometer mirrors for fast beam deflection is presented here.

For a high degree of automation of complex soldering and rework procedures information about the soldering or the defective joint, the electronic component, the defect and the position of the defect related to reference marks must be applied. By means of data from the reference IPC-A-610 [4] about component specific defects and tolerances the optimal repairing strategy (component mounting and reworking), position coordinates and laser parameters can be generated (Figure 1).

Quality of laser-based reworked solder joints. The quality of solder joints, particularly for rework procedures on complex electronic devices, is of substantial importance. In general, quality of solder joints produced with laser beam is comparable to the quality of the conventional solder joints that are made in a mass soldering process like reflow soldering [5, 6].

Important criteria for a high quality rework are the growing of intermetallic phases at the diffusion zone between solder, pads and leads, the formation of acceptable wetting angles and the providing of high mechanical stability as well as good electrical properties throughout product life.

In rework processes, especially by exchanging electronic components, some solder rests remain on the pads also after removal of old solder. Investigations in [4, 5] show that a removal of the old solder from the pads is not essential for the quality of reworked solder joints, however the degree of the first wetting is of substantial importance for a high-quality reworked joint. The joints created with Sn95Ag5 and Sn95.5Ag4Cu0.5 solder with predefined volume proportion of new and old solder are produced on 35 µm copper with chem. tin finish. Old solder means in this context solder that has wetted the pads during a first soldering and remains on the pad after removal of an electronic component. New solder is the quantity of supplied fresh solder, necessary for a 100% solder quantity, after removing the defect component.

Shearing tests immediately after rework as well as after different artificial aging tests show that the strength of reworked solder joints insignificantly depends on the volume rate of old solder in the joining area. Micrographs and EDX analyses show that because of the short solder process times even with in-

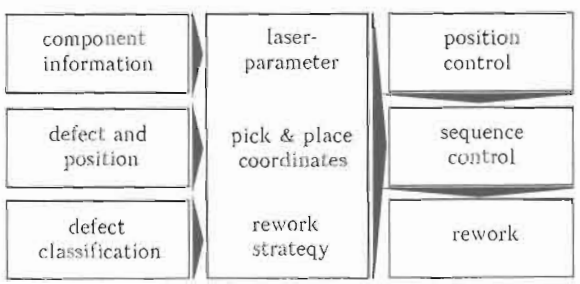


Figure 1. Automation of rework processes

© F. ALBERT, B. JAHRSDORFER, I. MYS, M. SCHMIDT, 2005

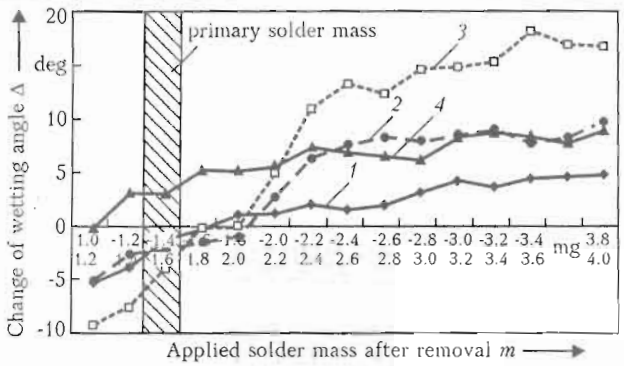


Figure 2. Change of wetting angle in dependence on secondary applied solder mass and different aging processes: *1* — reference: wetting, removal of solder, secondary wetting; *2* — wetting, aging 12 h/ 150 °C, removal of solder, secondary wetting; *3* — wetting, aging 24 h/150 °C, removal of solder, secondary wetting; *4* — wetting, removal of solder, aging 12 h / 150 °C, secondary wetting

creased reworking repetitions only very slow growing of intermetallics at the diffusion zone between solder and pads can be observed. A substantial quality influence is not recognizable.

Another important quality factor of solder joints is the wetting angle between pad and solder and/or component lead and solder. As shown in [7] the remaining solder depots after removal of the defect components don't wet a further pad surface if it is soldered one more time. This fact determines that the quality of reworked joints is particularly predefined by the wetting degree of the primary solder joint as well as the position of the lead of the new component on the pad. On closer consideration the wetting degree of reworked joints depends on oxidation degrees of pads and «non-wetted» pad surface that wasn't wetted during the first primary soldering.

In order to determine the main influence of the wetted and non-wetted pads predefinied solder quantities between 1.4 and 1.6 mg are applied and laser melted. The solidified solder depots were remelted with laser beam and removed from the pad by means of a desoldering pump. After the artificial aging of the pads the fresh solder with predefined quantities between 1.0 and 4.0 mg was applied and again laser melted.

After each solder solidification the wetting angle (Figure 2) and the wetted pad size of the solder depots was measured. Linear change of wetting angle (wetting angle secondary wetting process — wetting angle primary wetting process) can be observed up to a critical solder mass of approx. 1.4 to 1.8 mg for the reference soldering without intermediate steps of artificial aging. According to it a nearly constant angle increase is observed between 3 and 5° independent of the volume of new solder. This range corresponds to the primary wetted areas with non-removable (during desoldering) phases.

For larger solder masses the small increase of the wetting angle clarifies the influence of the second / multiple laser application concerning the oxidation of the pads. The similar tendencies are also recognizable for the samples, which were thermally aged after the primary wetting process. New solder wets the primary wetted areas; a change of wetted surface between with primary and secondary solder wetted pads does not exist. Only afterwards and with rising wetting angle ranges of the not wetted pads will be wetted with solder.

The oxidized landing surfaces after removal of primary solder show a similar trend to the reference samples. After 12 hours aging at 150 °C with already removed primary solder a laser based secondary wetting process leads at first to a linear change of the wetting angle change. Started above the critical solder mass of 1.6–1.8 mg an approximately constant value of the attainable wetting angle of 7°–8° is appeared. Due to an interruption in the rework process between the removal of defect element and the removal of remaining old solder a new soldering process causes a low increasing of the wetting angle. Changes depend on the volume of fresh-applied solder.

Increase in reliability of laser welding of materials for electronic applications. *Problem statement.* Copper and copper alloys are definitely the main materials for mechanical and electrical contacting in the electronic industry. However the excellent thermal and electrical properties of these materials lead to limitations in manufacturing with lasers and especially in laser spot welding. Good thermal conductivity ($\lambda_{Cu} \approx 397$ $Wm^{-1}K^{-1}$) and high optical reflection in NIR-spectral range (where most industrial lasers for welding operate) ($R_{Cu} \approx 95$–98%) require high laser energies to initiate the material melting. After generation of the keyhole, the total absorption increases up to 80–100% due to the Fresnel absorption in a keyhole and the thermal dependence of the absorption and the thermal conductivity [8]. This makes the welding process unstable and causes welding defects, such as welding splitters, substrate damages, etc.

Would the moment when the surface is fused superficially be known and be always the same, it should be possible to reduce the laser power at this moment so that the keyhole formation is avoided or controlled. Unfortunately there is another important source of instabilities during laser welding: The dependence of absorption on the surface condition of the material that lead to fluctuations of initial time of keyhole formation and energy needed for material fusion. This dependence is caused by variable oxidation, roughness and contamination as well as by other imperfections on the material surface. These factors are determined by manufacturing, storing and handling of materials and their influence on the initial absorption and hence on the process stability is very difficult to predict.

To eliminate the influence of above-mentioned instabilities in copper welding (in spot welding particularly), a realtime process control is essential. However the high complexity of a welding process, short interaction time of laser beam and material and lack of a fast controlled laser system are the main obstacles for successful implementation of such a process control. The enumerated problems become less critical if

a preliminary control is applied before the welding process takes place.

Process control with prepulse. The main idea for preliminary process control is the measurement of the local absorptivity and reflectivity on the surface and the corresponding adjustment of process parameters (laser energy) before the main welding process. One possibility to get information about the local surface conditions online is the use of a laser measuring pre-pulse. In this case before the main laser pulse a relatively short and weak laser pulse is applied — in our experiments we use a laser pulse with pulse duration of 0.6 ms. The reflected prepulse light is detected by the combination of one on-axis and two off-axis Si-diode detectors, which detect the radiation of two opposite spatial directions (Figure 3, *a*). Both off-axis detector signals are used for calculation of an average signal value in order to eliminate possible errors caused by inaccurate positioning of the welding partners or a different grain structure of copper.

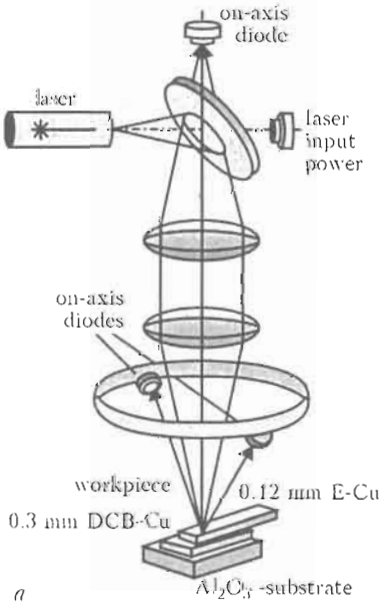
In order to achieve certain and constant absorption conditions on the surface in the experiments the thin copper sheets are systematically pretreated by means of oxidizing, etching and sandblasting. For every type of the pretreated specimens the reflection signals during the pre-pulse are detected and the optimal process parameters (laser power and pulse duration) are determined.

After amplification and signal filtration the diode signals are digitalized with the DAQ-board and normalized by the laser input power signal. As our data analysis shows a proper differen-tiation of the local absorption conditions can be achieved by using a quotient of the on-axis signal and average off-axis diode signal.

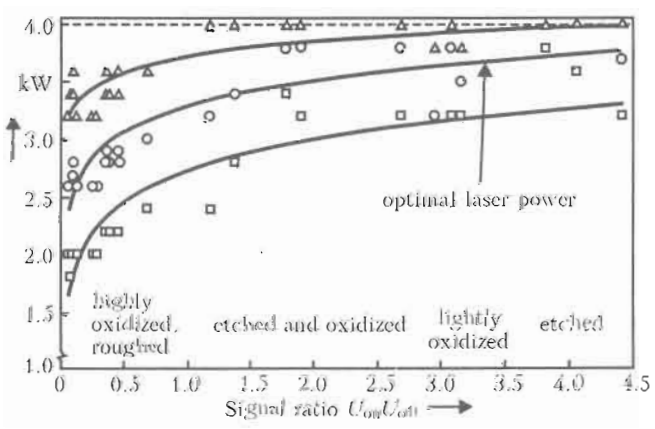
Figure 3, *b* shows dependencies between the particular process windows for welding of different pretreated specimens and their corresponding absorption condition with signal ratio U_{on}/U_{off}. A logarithmic dependence between the signal ratio (i.e. absorption on the surface) and laser power can clearly be shown: the highly oxidized or roughed surfaces with small signal ratio and high absorptivity (left) require significant smaller laser energies for good welding than etched surfaces with large signal ratios (right). The alignment of the fitting curve on the single process window suites very well. The scattering in the higher range of signal ratio at the etched surfaces can be explained as an inaccuracy of process windows definition restricted by the laser power range. According to these results, the application of a pre-pulse signal ratio in welding of copper and low-doped copper alloys provides very good adjustment of process (laser) parameters concerning the actual surface conditions [9].

The implementation of the process control using pre-pulse is shown in Figure 4, *a*. Generally it can be split into two separate blocks: authentical on-line process control running in real time and a database that collects information off-line before the material processing. The database provides the detailed optimal process parameters that will be transmitted to the laser. It in-cludes «card indices» with the dependencies of optimal parameters and signal ratios. For every joining geometry (differences in material, thickness and arrangement) such a card has to be created. The optimal process parameters are preliminary defined off-line from the particu-lar process windows for different surface conditions and corresponding signal ratios.

The pre-pulse used in our experiments can be implemented as a part of the main laser pulse. Figure 4, *b* shows a slightly modified «ramped-down» laser pulse shape traditionally used for the reduction of the weld splitter in spot welding. It consist of three main regions: The short pre-pulse area to get the information about the surface conditions t_{pre}, the adjustable initial pulse area t_{init} and the non-adjustable «ramped-down» area for splitter reduction t_{ramp}. In process control the



a



b

Figure 3. Experimental setup (*a*), and dependence between signal ratio and laser power (*b*): *1* — power limit of laser; *2* — upper process window limit; *3* — optimal laser power; *4* — lower process window limit

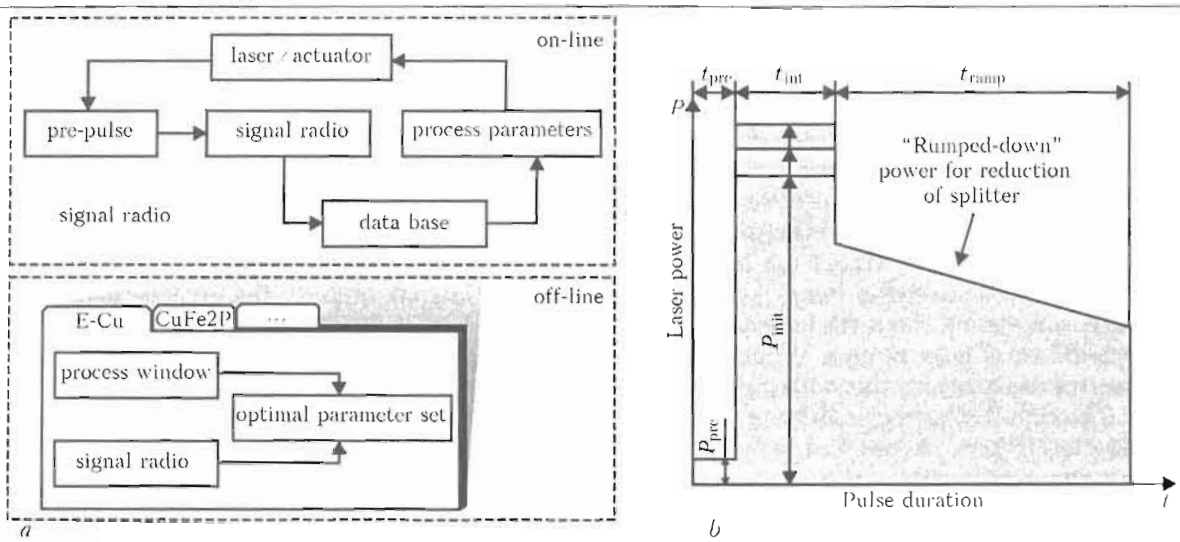


Figure 4. Process control with pre-pulse (*a*), and special pulse shape for pre-pulse control (*b*)

information about local absorptivity, collected during pre-pulse stage, is used to on-line adjust the laser power P_{init} in the initial stage according to the actual absorption conditions.

Laser Droplet Welding. *Procedure characterisation.* A further possibility for the realization of selective joining tasks for electrical and/or mechanical contacting offers the Laser Droplet Welding process. The main parts of the Laser Droplet Welding-setup are a pulsed Nd:YAG-laser, a wire feed system with positioning nozzle and a shielding gas supply. The wire is fed in an angle of 45° into the focus of the vertical laser beam. Within the Droplet Welding process a liquid metal droplet is created at the end of the wire. The molten material is subsequently placed onto the joining partners to achieve material conclusive connections. The heating of the wire material generally can be realized with different sources. The investigations presented here refer to laser radiation as a heating source. The droplet is created during a single laser pulse; thus the wire has to move in a controlled way during the pulse [10]. The wire movement adjusts the self wetting of the wire and guarantees the presence of wire material between laser beam and joining

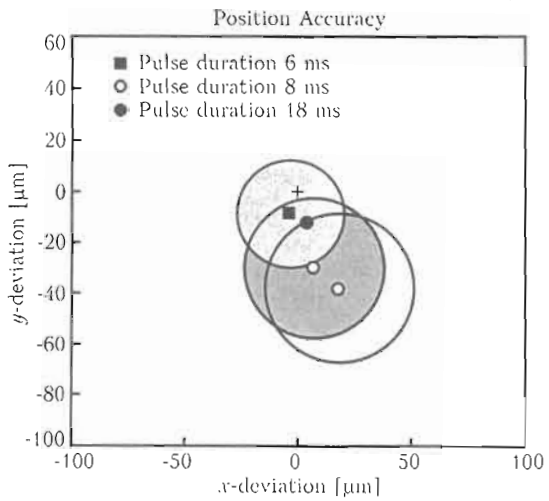


Figure 5. Position accuracy (nickel wire of 0.25 mm)

partners [11, 12]. In such a way uncontrolled irradiation of the joining partners with the laser can be avoided.

For a more exact view of the process it is meaningful to split it up into different process stages. It can be differentiated between drop production and drop separation, drop flight, drop landing and drop weld. During the drop production the wire is moved in a controlled way and the laser is active. The drop production with the separation of the drop occurs within a single laser pulse. Subsequently, the drop is separated from the wire, but still not in contact with the joining partners (drop flight). Calculations and measurements show that the drop cools down in the flight only insignificantly for typical working distances (~30 K) [13]. During the drop flight a clear deviation from the ideal drop form is recognizable and can be explained by two effects: On the one hand it occurs during the recording of one individual picture to a drop movement, which can amount up to 25% of the drop diameter. On the other hand there are dynamic, thermally induced flow processes in the drop, affecting again the form of the drop. During the following drop landing it comes to the contacting of the joining partners by the molten drop. The drop keeps first its spherical shape and warms up the joining partners over a relatively small contact area. After a certain warm-up time it comes to the wetting of the joining partners and thus to the material-conclusive connection.

The described process flow of the Laser Droplet Welding process can be supplemented by modified variants. With these variants the process is changed in such a way that e. g. there is no drop flight. It is possible to produce a molten drop at the end of the wire, to move the wire with this drop contacting the joining partners and to pull the wire out of the solidifying melt after a defined waiting period («Touch and Retract»). Within a further variant the wire is positioned closely above the joining partners. During the drop production the drop contacts the joining partners by the wire feed motion and the constant enlar-

gement of the molten drop. This arrangement permits further variations such as preheating the adding partners and postheating of the placed drop by the laser beam, which in particular can be interesting if tensioninduced cracking represents a problem.

Additional Materials (Drops). For the industrial use of the Lasers Droplet Welding process connecting filigree components the positioning accuracy of the drops becomes crucially important. Joining tasks within the range of micro technology only can be fulfilled with high position accuracy. Figure 5 shows the achievable positioning accuracy of nickel drops. The diagram shows the average deviation of the drop center from the goal ($x = 0$, $y = 0$) for different process parameters. Around the average value a circle is drawn for each parameter setting. Within these circles all drops are positioned. Regarding the positional variations – the maximum deviation from the goal is smaller than 80 µm – in the comparison to the diameter of the welded drop, which amounts to typically at least 500 µm, it can be noted that the procedure offers a very high and reproducible positioning accuracy. The positional deviation increases with rising process duration and rising energy input.

The Lasers Droplet Welding process offers advantages that make it in many cases to an interesting alternative or addition of conventional joining processes. Thus the process offers the possibility of bridging gaps between the joining partners by auxiliary material. A further advantage is the well adjustable droplet size, whereby the energy for welding can be adapted on the respective adding situation optimally. This makes a controllable thermal load of the adding partners possible as well as the welding of filigree geometries, thin metallic coatings, heat sensitive components and strongly different partial geometries without negative effects on their mechanical and electrical characteristics.

Potential for contacting in electronics production. The possibility of the Laser Droplet Welding process to place liquid and defined metal droplets of different materials exactly onto the joining partners to achieve material conclusive connections offers an interesting possibility for many joining tasks in electronics. The Laser Droplet Welding process can be used in an ideal way for the contact between wire and leads of planar circuit carriers. By using intelligent clamping devices and process adapting on very sensitive substrate materials – for example on semiconductors such as GaAs or silicon – welding is even possible. Figure 6 shows a joining example where a filigree wire is connected by a nickel droplet with a metallic contact area of a leader plate. The various

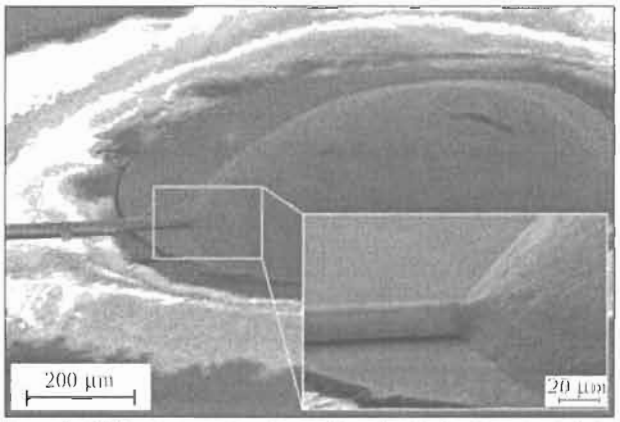


Figure 6. SEM-picture of a «Laser-Droplet Welded» Joint (nickel droplet)

possibilities of the Laser Droplet Welding for electronics production can be anticipated by this Figure [16].

1. Bielefeld, M.; Clair, D.; Gering, H.: *Modulare, skalierbare Karosserie-Steuergerate.* In: Automotive, Marz 2003, S. 24–26.
2. Veen, N.J.A van: *Laser-Lottechnologie.* In Tagungsbericht Leiterplatte ?92, Band 2, Dusseldorf: VDI-Verlag GmbH, 1992, S. 39–52
3. Fleckenstein, M.; Bickert, M.; Frohlich, T.; Abert, A.; Schneider, M.: *Strategien fur die Elektronikfertigung.* In: Laser, Marz 2001, S. 70–73
4. IPC-A-610, *Acceptability for Electronic Assemblies,* Northbrook, Illinois, 2000
5. Hierl, S.; Fleckenstein, M.; Frohlich, T.: *Innovative Strategien zum Laserstrahl-Mikroloten in der Elektronikproduktion.* In Geiger, M.; Otto, A. (Hrsg.): Tagungsband LEF 1999, Bamberg, Meisenbach, 2004, S. 23–35
6. Fleckenstein, M.: *Qualitat laserstrahlgefugter Mikroverbindungen elektronischer Kontakte.* Dissertation Erlangen-Nurnberg, In: Geiger, M.; Feldmann, K. (Hrsg.): Reihe Fertigungstechnik, Bd. 125, Bamberg, Meisenbach, 2002
7. Albert, F.; Esser, G.: *Laserstrahlbasiertes Reparaturloten in der Elektronikproduktion.* In: VDI – Tagungsband Fachtagung «Optische Technologien fur die Mikroproduktion», Band 1810, Dusseldorf, VDI, 2003, S. 187–194
8. Blom, A.; et al.: *Process spread reduction of laser microspot welding of thin copper parts using real-time control.* In: Photon Processing in Microelectronics and Photonics II, Proceedings of SPIE, Vol. 4977, 2003, pp. 493–507
9. Mys, I.; Geiger, M.: *Use of pre-pulse in laser spot welding of materials with high optical reflection.* In: Laser Precision Microfabrication LPM 2003, Proceedings of SPIE, Vol. 5063, 2003, Belligham, WA: SPIE, pp. 314–318
10. Geiger, M.; Jahrsdorfer, B.; Schmidt, M.: *Laser Droplet Weld – an innovative joining technology.* In: Production Engineering – Annals of the WGP, 2003, Vol. X/2, pp. 141–144
11. Huimin, L.: *Science and Engineering of Droplets,* New York: Noyes Publications; 2000
12. Clift, R.; Grace, J. R.; Weber, M. E.: *Bubbles Drops and Particles,* London: Academic Press, INC. LTD., 1978
13. Brandes, E.A., Brook, G.B.: *Smithells Metals Reference Book,* Butterworth-Heinemann, 1997
14. Jahrsdorfer, B.; Schmidt, M.; Geiger, M.: *Laser Droplet Welding and its potential for joining dissimilar materials.* In: Geiger, M.; Otto, A.: Proceedings of the LANE 2004, Volume 2, Bamberg, Meisenbach Verlag, S. 651–659
15. Schmidt M.; Jahrsdorfer, B.; Mys, I.; Esser, G.: *Laser Micro Welding of Dissimilar Metals.* In: Proceedings of the 23rd International Congress on Applications of Lasers & Electro-Optics ICALEO 2004, 2004, M502

THE IMPACT OF HIGH POWER DIODE LASERS ON SOLID-STATE LASERS AND MATERIALS PROCESSING APPLICATIONS

F. BACHMANN
ROFIN-SINAR Laser GmbH, Hamburg, Germany

Introduction. The appearance of reliable laser diodes has revolutionized the technology of high power solid state lasers in several ways. The original idea, which is almost as old as diode lasers and optically pumped solid state lasers, and which among others has driven the development of high power laser diodes, namely to use them as pump source for solid state lasers [1] has become reality at the end of the century: diode pumped rod lasers in the kW range are available on the market place as industrial products. However, beyond that in the mean time new diode pumped solid state lasers have appeared, which do not have a conventional, i.e. lamp pumped counterpart. Such laser types, which are exclusively possible by use of laser diodes as a pump source are e.g. the disk laser and the fiber laser, which are now entering the materials processing market. Furthermore, diode laser technology itself has developed to such a high power and quality, that even direct diode lasers can be used for materials processing.

Semiconductor laser technology. Laser action on GaAs or GaAsP laser diodes at cryogenic temperatures has been demonstrated as early as 1962 [2]. What has started as a physical curiosity as a basis for extremely expensive lasers with very short life time, is nowadays the basis for very long-lived and cheap laser sources covering the biggest market of laser sources, with a volume of 3.20 billion US$ in 2004 [3]: The lion's share of today's diode laser market is related to rather low power applications in telecommunication and optical storage, but the technology has also very strong impact to materials processing with high power lasers. Careful investigation of the crystalline structures, detailed understanding of failure mechanisms and considerable improvement of the manufacturing processes has lead to this success. Nevertheless, even if sophisticated cooling concepts allow a power increase far beyond the telecom requirements the emission of a single emitter is still limited to a few watts. Therefore, several emitters are combined in one monolithic element called a laser bar, which is then mounted onto a micro- channel heat sink for efficient cooling [4]; 50 W are a typical power of a commercial bar, but more than 300 W are reported from laboratory experiments recently [5]. Aspheric cylindrical lenses are used for the collimation of the highly divergent beam. The brilliance, however is limited because of the limitations of beam quality of the individual emitters and especially because of their incoherent coupling [6].

Diode pumped solid state lasers: technology and applications. Even if the replacement of flash or arc lamps has originally boosted the development of the diode lasers as a pump source, laser diode pumping offers much more than that. New laser concepts, which could not be realized by lamp pumped configurations, e.g. because of limited focusability, and new laser materials, which have been almost impossible to be pumped by lamps for reasons of the required power density are now accessible.

Diode pumped (side pumped) rod laser. The original and still mostly used shape of the active medium in a high power solid state laser (Nd:YAG) is the cylindrical rod; typically this rod has a diameter of 4 to 8 mm and a length of 150 to 200 mm and excitation is performed by krypton arc lamps. Even if this type of solid state laser has been the most prominent solid state laser over the past years, it has two system inherent disadvantages: First, the life time of the krypton arc lamps is rather short — several hundred hours only — and thus, need frequent replacement. Second and even more severe, only a very little fraction of the light provided from the krypton arc lamps is actually used for the pumping of the laser process; the rest is generating heat and thus, wasting energy and causing problems, especially creating the thermal lens effect. By diode pumping we get rid of these problems: laser diodes provide a long life of more than 10000 hours and their emission wavelength can be exactly matched to the absorption peak of the active material, 808 nm in case of the Nd:YAG crystal. The reduced heat load to the crystal allows higher power output of one rod as well as it provides better beam quality: typically, diode pumped rod lasers in the (multi-)kilowatt range are specified with a beam parameter product[1]) of ≤12 mm mrad, whereas lamp pumped rod lasers show about 25 mm mrad. Therefore, smaller fiber diameters (typically 300 μm) can be used. Furthermore a wall plug efficiency of 10% is characteristic

[1] According to European standard (IEN 11146) beam parameter product (BPP) is defined as (beam waist radius) × (half divergence angle)

© F. BACHMANN, 2005

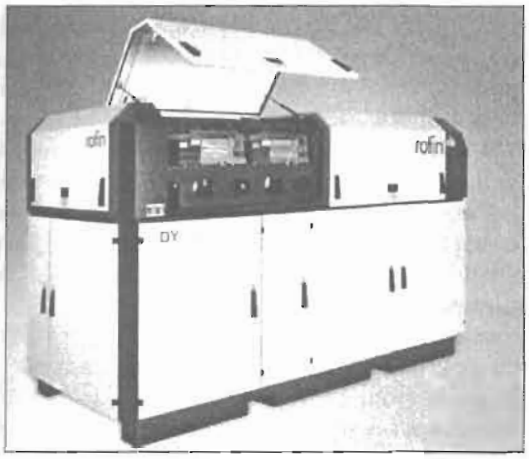


Figure 1. ROFIN DY 044 – diode pumped rod laser with 4.4 kW output

for these lasers, compared to about 3% for lamp pumped devices. A typical high power diode pumped rod laser is shown in Figure 1. This laser is the top model in a series from 550 W to 4.4 kW and is equipped with eight laser chambers.

Besides the fact, that the already existing applications as cutting and welding of mild steel and stainless steel could be extended to larger material thickness or higher speed, the increase in power density, which can be reached with diode pumped rod type Nd:YAG laser did also lead to the ability to cut and weld materials, which have been hardly accessible before as especially aluminum based alloys. This is shown in Figure 2, where welding curves for AlMg3 (5457) with a ROFIN DY 044 (see Figure 1) laser are presented.

Diode pumped rod laser at 8 kW. As a laboratory prototype based on the ROFIN DY-Series described above a rod-type diode pumped Nd:YAG laser with an output power of max. 8 kW has been realized in cooperation with the Fraunhofer Institute for Laser Technology in Aachen, Germany. The goal of the project is to gain better understanding for high power materials processing in the 1 µm wavelength range. The radiation of the 8 kW laser has been delivered to the workstations by fibers with a core diameter of 600 µm and a length of up to 50 m.

Stainless steel cutting has been performed for materials thicknesses between 4 and 10 mm. The maximum speed, which could be reached for oxide free cuts has been 2.5 m/min; to reach this speed with a CO_2 laser about 20% higher power is required despite the superior beam quality [7]. Welding experiments have been performed at stainless steel and mild steel material in the range between 6 and 10 mm thickness. An unexpectedly strong vapor plume during the weld has been recognized in these experiments. Sufficient suppression of the plume could not be reached by conventional standard nozzles without disturbing the weld pool. Thus, the important challenge has been to develop a special nozzle, which could effectively suppress the plume on one hand but leave the weld pool undisturbed on the other. A successful new nozzle

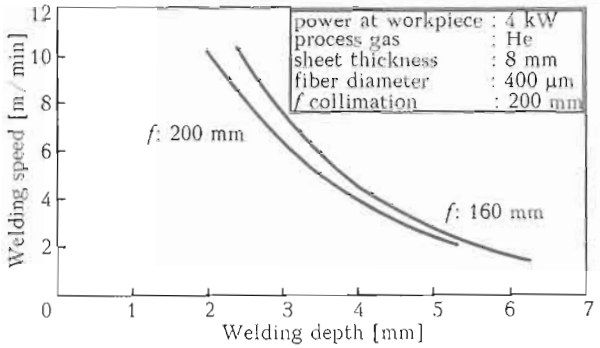


Figure 2. Welding curves for welding of 8 mm thick AlMg3 with a 4.4 kW diode pumped Nd: YAG laser

design was proven to fix the problem: Figure 3 shows the actual welding results for mild steel and stainless steel. Further investigations of the vapor plume, especially the interaction between the plume, the laser radiation and the process gas flow shall be investigated further and open the potential of high power solid state lasers further.

The Q-switched high power Nd:YAG laser. Triggered by a special application, namely the removal of leaf contamination from railway tracks [8], a high power Q-switched Nd:YAG laser (ROFIN DYx85QS) has been developed. Leaf contamination creates mainly two problems, which influence the safety of the train system: low adhesion of the wheels causing breaking and acceleration problems and interference with safety relevant electrical track circuits. Laser ablation has been detected to be the process of choice for the efficient removal of this layer. As well known, laser ablation needs short pulses in the range of several ten nanoseconds. Thus, excimer lasers have been mainly used so far; however, as the laser systems for this application have to be run on trains, excimer lasers have been ruled out among others for safety considerations. An average power of about 1 kW has been requested since average power determines the removal rate of the contaminant and a minimum average train speed of about 70 km/h must be reached for economic

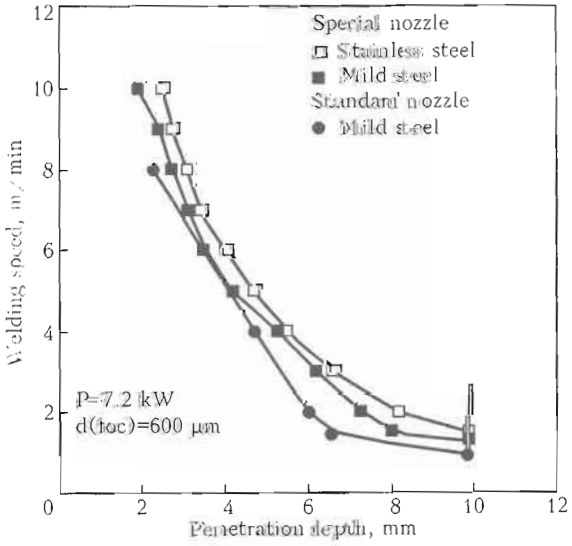


Figure 3. Welding with 8 kW solid state laser and radial jet nozzle [7]

use of the method. Based on the diode pumped rod laser design described above a Q-switched Nd:YAG unit has been realized which provides an average power of 850 W in Q-switch mode in pulses of about 200 ns and at a repetition rate from 20 to up to 60 kHz (950 W cw). The energy is delivered through a 600 µm fiber into a special working head, which forms a line focus with the width of the trail and a length, which ensures overlapping pulses even at highest train speed to perform full cleaning of the tracks; the working heads are mounted underneath the car of the «cleaning train». The system has been tested successfully and fulfils technical and economic requirements. The laser described here is to our best knowledge the strongest Q-switched commercial laser available. Applications may emerge in the field of paint stripping, surface cleaning, high speed structuring and others.

End-pumped rod laser. In longitudinally (or end-) pumped solid state lasers the pump radiation is provided along the optical resonator through the end mirror of the laser. Of course, pumping in this geometry is only possible, if the beam quality of the pump source is good enough so that the pump light can be efficiently coupled into the laser rod. Thus, the concept is only feasible with (diode-) laser pumping; the rectangular highly astigmatic emission of the diode bars must be rearranged to fit into the circular shape of the rod. Contrary to the side pumped concept in such a configuration the pumped region can be matched to the mode volume of the resonator and thus, a very efficient laser source with high beam quality can be realized. Diode pumping qualifies also other laser active materials than the well known Nd:YAG crystal for lasers: end pumped lasers often use Nd:YVO_4 (Yttrium-Vanadate), which among others has a wider absorption band for the 808 nm radiation of the diodes and thus, is less sensitive to the temperature shift or the aging of the diodes. The high beam quality (fundamental mode) and short resonator configuration of the end pumping concept as well as the short fluorescence lifetime of Nd:YVO_4 make this setup a preferred combination for the generation of short Q-switch pulses and also for frequency conversion.

Typical applications for such lasers are in the area of high precision marking and high precision machining. A typical and very representative example for a marking application of this laser is the generation of smart cards, shown in Figure 4: The high pulse peak power and high repetition rate of the laser reduces the printing times for many applications. ROFIN-lasers for this application utilize an innovative grey scale software allowing different intensities for individual laser pulses. Grey scale imaging makes it possible to reduce the number of bits in a given image, noticeably shortening the marking time compared to conventional black-and-white images affording high quality photography printing.



Figure 4. Marking application with end pumped, Q-switched solid state laser (ROFIN RSM103D)

An example for thin film removal is the structuring of solar cell material: The transparent electrode, typically made from Indium-Tin-Oxide must be structured in stripes with as narrow separating lines as possible as the area of these lines is lost for energy conversion and thus, influence the efficiency of the solar cell. Lines with a width as small as 10 µm and can be written with a speed of up to 1000 mm/s. For another application the complete removal of the thin film on the solar cells is required. The laser can perform this task with a rate of 5 cm^2/s.

End pumped slab laser. As mentioned above, for the end pumped rod concept the rectangular beam of the diode laser stacks for pumping must be matched to the circular symmetry of the rod by special beam forming optics. This step can be avoided, if a slab geometry is used as the active medium as it has been proposed from the Fraunhofer Institute for Laser Technology [9]. Thermal lensing is almost ruled out by the cooling geometry in the direction perpendicular to the active plane and by the small thickness of the active plane. Thus, of course the concept provides a high beam quality as well as a high differential optical-to-optical efficiency (about 50%), but beam clean-up as well as a hybrid resonator are required. Short and powerful pulses can be generated in a q-switch configuration; the high beam quality and high peak power also favor the concept for frequency conversion. 130 W with $M^2 > 2$ have been reached in the fundamental mode, delivery through a 100 µm diameter, 0.22 NA fiber is possible. The lasers are preferably used for machining of glass and surface cleaning.

Contrary to the end pumped rod concept described above, the technology is scalable into the kW range [10]: More than 1 kW have been reached with two laser heads with $M^2 > 5$ [11].

Disc laser. One of the limiting factors for rod type lasers in terms of beam quality even if diode pumping is used is the «thermal lens effect». One idea to circumvent that has been published in 1994 by A.Giesen [12], who proposed to use a thin disc (about 150 to 300 µm in thickness and about 7 mm diameter) as a laser medium. This thin disc is mounted to a heat sink with its rear side and thus, can be cooled axially. As active material Yb:YAG is used in this case as among others this material allows much higher doping levels (up to 30%) than Nd-doping; high doping levels are important for this technology as the volume, where the laser light is extracted is much smaller than in case of the rod type. Pumping is of course performed

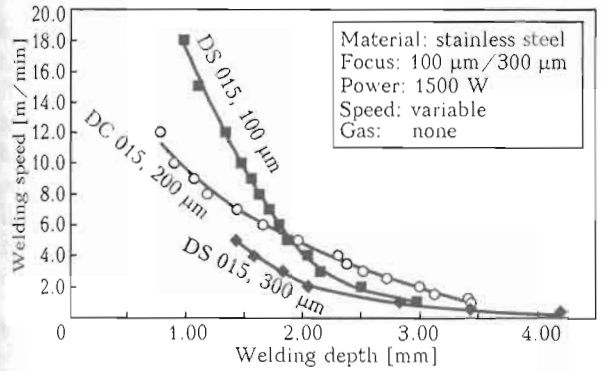


Figure 5. Welding curves for stainless steel welding with a 1.5 kW disk laser (DS015) in comparison with a slab-type CO_2 laser (ROFIN DC015): clearly visible is the advantage of the disc laser for thin material. By plasma effects, the CO_2 laser is advantageous for thicker material

with diodes, the wavelength of which is tuned to the main absorption of the Yb:YAG crystal (940 nm); as not all of the pump light can be absorbed in one path a multiple pass configuration is realized. Furthermore, the quantum defect is much smaller than in case of the Nd:YAG rod laser, which leads to a further reduction of heat load. For these reasons, a further improvement compared to diode pumped rod lasers is expected and in fact, 7 mm mrad can be achieved in a typical disc laser set-up. At the same time higher efficiency is reached, which is as high as 50% optical-to-optical, which results in a wall plug efficiency of about 20%!

Nowadays high power disk lasers are delivered from 750 W (ROFIN DSx75HQ) from one disk with a 100 µm fiber up to a power of 4 kW (ROFIN DS040) from two disks and a 300 µm fiber (used NA = 0.12). Welding curves for a 1.5 kW laser and for two different focus diameters (100 µm and 300 µm) are depicted in Figure 5 for stainless steel welding in comparison with a CO_2-slab laser. The advantage of the disc laser for thin material is clearly visible.

An example for industrial application is the welding of a battery case made from stainless steel 1.4301 (Figure6); with 700 W and a spot diameter of 100 µm the part can be perfectly welded with a speed of 5 m/min under a He atmosphere. The disc laser is of course also well suited for cutting: 0.5 mm (4 mm) thick stainless steel foils have been cut with a power of 1.5 kW at a speed of 40 m/min (2 m/min); oxygen assisted cutting of mild steel was performed at 1 mm (10 mm) thick material with 10 m/min (1 m/min).

High power fiber laser. The other possibility to avoid the thermal lens effect is to «make the rod thinner and thinner and longer and longer», so that finally the active medium has degenerated to an optical fiber and even radial cooling does not cause a temperature profile over the cross section of the fiber. In fact, the diameter of the active core can be so thin, that only one single mode is amplified and thus, high beam quality single mode radiation can be generated. Pumping is typically performed by the use of a so called double-clad fiber: the pump light is coupled into the inner cladding surrounding the active fiber core and successively absorbed from the active fiber core over the entire length of the fiber. There are two general possibilities for the coupling of the pump light into the pump core: (*a*) the end-pumped concept, which requires a diode stack with a rather high beam quality to fit into the pump cladding of the fiber, and (*b*) the «Y»-coupling configuration, which needs a high number of fiber coupled diodes, which must be fed into the pump core by rather complex methods, e.g. fiber splicing or Bragg gratings.

By the maximum power density in the active core in the fiber, the power which can be extracted from a single fiber (not necessarily single mode!) is limited. In commercial systems this limit is at about 200 W for the time being with about 1 to 2 times diffraction limited beam quality, whereas in the laboratory 1.3 kW have been demonstrated [13], with a beam which is «almost diffraction limited». Power scaling is performed by «side-by-side» combination of several fibers and thus, goes along with a loss of beam quality.

Fiber lasers in the high power range are in an evaluation phase for industrial applications at the moment and have not yet passed the threshold to industrial manufacturing. They are, however, a technology with a high potential, if they can be manufactured for reasonable costs and can provide the same performance and beam quality as the disc laser, especially in the high power range.

High power diode lasers. Instead of using the diode laser for pumping high power solid state lasers they can also be used for direct processing. Such units impress by extremely small size even at high power: the 3 kW laser head shown in Figure 7 is as small as 555 (including the optics tubus) × 260 × 200 [mm] and the weight is just 25 kg. A control unit and a chiller with a size of about 600 × 800 × 1000 [mm] each are to be added to complete the entire laser sys-

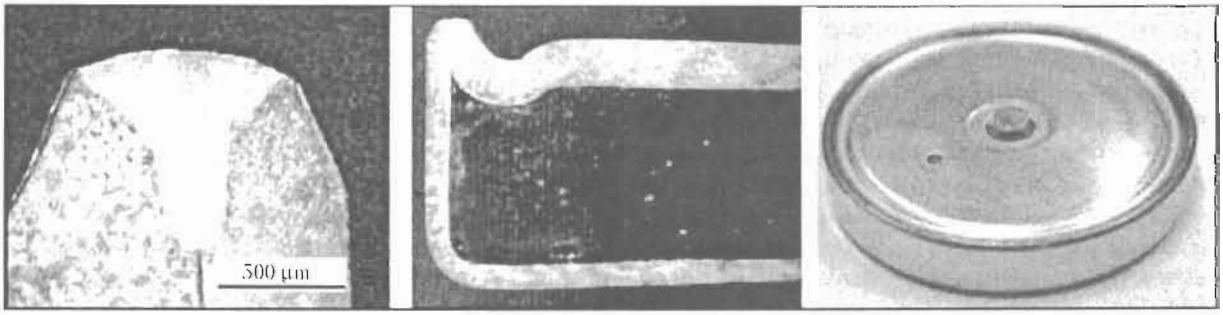


Figure 6. Battery case (1.4301) welded with a 750 W thin disc laser (ROFIN DSx75) spot size 100 µm, welding speed 5 m/min



Figure 7. Head of a high power diode laser, 3.1 kW (ROFIN DL031Q)

tem. High power diode lasers, however, cannot provide such high beam quality as the diode pumped lasers described above. This is a consequence of the incoherent coupling of the individual emitters of the diode laser bars [6]. With increasing power P the beam quality decreases by a factor $\sqrt{P}$ as long as the brilliance[2] of the individual emitters remains unchanged. Polarization coupling and wavelength coupling are used to improve the situation: High power diode lasers are typically unpolarized and emit at two or three wavelengths. The spot is rectangular (1.3×0.8 [mm] at a focal length of 66 mm for the 3 kW system shown in figure 7) with a top hat profile in one direction and a Gaussian in the other. Therefore these lasers cover rather new application fields, which can be performed with moderate beam quality as surface processing, brazing and heat conduction welding as described in the literature [4, 14].

CONCLUSIONS

All solid state lasers have become possible by the arrival of reliable high power diodes; this did not only lead to a considerable improvement of the existing solid state laser technologies, but even enabled new concepts, which provide higher efficiency, better beam quality, shorter pulses and higher performance. High power diode lasers for direct applications opened new fields for laser materials processing, which could not be economically covered with lasers so far; this is a consequence mainly of their high efficiency, small size and high reliability. Whichever laser is the best for a distinct application and material must be found out individually, and even if CO_2 lasers are still the workhorses in the industrial materials processes; all solid state laser technology is looking into a bright future.

1. R.J.Keyes, T.M.Quist, *Injection luminescent pumping of $CaF_2:U^{3+}$ with GaAs diode lasers*; Appl. Phys. Lett. 4, (3), 50 (1964).
2. R.N.Hall, G.E.Fenner, J.D.Kingsley, T.J.Soltys, R.O.Carlson; *Coherent light emission from GaAs junctions*; Phys. Rev. Lett. 9, 366 (1962).
3. R.V.Steele, *Review and forecast of the laser markets – part II: Diode lasers*; Optoelectr. Report Vol. 12, No. 3, p. 1 (2005).
4. F.Bachmann, *Present technology, industrial applications and future prospects of high power diode lasers*; Proc. SPIE Vol. 4762, p. 1 (2001).
5. N.Lichtenstein, Y.Manz, P.Mauron, A.Fily, B.Schmidt, J.Mullerm S.Arlt, S.Weiss, A.Thies, J.Troger, C.Harder; *325 Watt from 1 cm wide 9xx laser bars for DPSSL- and FL-applications*; presented at Photonics West 2005, San Jose, USA; Proc. SPIE Vol. 5711 (2005) to be published.
6. F.Bachmann, *Chances and limitations of high power diode lasers*; Proc. SPIE Vol. 5336, p. 95 (2004).
7. D.Petring, *Innovative Entwicklungen im Bereich des Laserschweissens und – schneidens*; Aachener Kolloquium für Lasertechnik; Aachen, April 26–29, 2004.
8. M. Higgins, *The lasers railhead cleaner*, see www.laserthor.com.
9. K.Du, Y.Liao, P.Loosen; *Nd:YAG slab laser end-pumped by laser diode stack and its beam shaping*. Opt. Comm. 140, p. 53 (1997).
10. C.Schnitzler; *A 500 W high brightness diode end pumped NdYAG slab laser*; OSA Trends in Optics and Photonics, Vol. 68, Ed. By M.E.Farman, published by Opt. Soc. of America, 2002.
11. P.Loosen, Fraunhofer Institut fur Lasertechnik, Aachen, Germany; *personnel communication*.
12. U.Brauch, A.Giesen, A.Voss, K.Wittig; *Laserverstarkersystem*, Patent DE 4344227 A1 (1993).
13. A.Liem, J.Limpert, H.Zellmer, A.Tuennermann, V.Reichel, K.Moerl, S.Jetschke, S.Unger, H.-R.Muller, J.Kirchhof, T.Sandrock, A.Harschak, *1.3 kW Yb-doped fiber laser with excellent beam quality*; Conference of Lasers and Electro-Optics, May 16–21, 2004, San Francisco, C A, USA; post-deadline paper CPDD2 (2004).
14. F.Bachmann; High Power Diode Lasers: *A New Tool for Laser Materials Processing*; Proc. of LTWMP 2003, Katsiveli, Crimea, Ukraine, May 19–23, 2003, p. 17.

[2]Brilliance $B = P / BPP^2$ (P = power, BPP = beam-parameter-product – see footnote 1)

TOWARDS KINETICAL DESCRIPTION OF PHASE TRANSFORMATION PHENOMENA IN METALS UNDER LASER WELDING CONDITIONS USING REACTION-DIFFUSION FORMALISM

U. DILTHEY[1], A. GUMENYUK[1], G. TURICHIN[2]
[1]ISF-Welding and Joining Institute, Aachen University, Germany
[2]State Technical University, St. Petersburg, Russia

A mathematical model, which is based on the self-consistent solution of problems of solute diffusion and kinetics of chemical reactions with consideration of the mutual influence in ensemble of growing nuclei, is developed. This approach allows description of a number of metallurgical processes driven by kinetics of phase transformation in metals under welding conditions. Of the particular interest are the welding methods with high heating and cooling rates, like laser beam welding. In such systems conditions are usually far from the equilibrium state and conventionally used approach of thermodynamics and quasi-equilibrium kinetics does not work. A number of examples, like columnar and dendritic solidification, precipitation growth, kinetics of phase transformation in HAZ under different heating and cooling conditions and their description using CCT-diagram technique are given in order to illustrate the application of the described method.

Introduction. A prediction of the mechanical properties in the welded material and the heat affected zone (HAZ) is the key factor for a constructive design as well as for a choice of welding parameters and materials. For the high cooling rates, which are typical for electron beam, laser and plasma welding, the phase transformations in HAZ have a number of peculiarities. All these methods are characterised by very high heating and cooling rates in the zones, where new structures are formed. Equilibrium conditions of the microstructures formation are practically never reached, so that the microstructures and the properties of the material in HAZ and melting zone are determined by the far from equilibrium kinetics of the phase transformation. Beside this, the transformations take place in a very short time at strong variation of temperature and correspondingly diffusion coefficient.

The scope of controlled by diffusion metallurgical phenomena includes grain growth, phase transformation in solid, precipitation, solidification etc.

Practically all of them are determined by the mentioned specifics of thermal cycles during laser welding. So it seems to be reasonable to develop a universal approach based on the description of kinetics of the phase and microstructures transformation suitable for significant deviation from equilibrium conditions.

There are a number of models for the description of precipitation and phase transformation in solid for classical heat treatment [1] and conventional welding conditions [2]. The common way of description of transformation kinetics in solid state is based on the theory of new phase nucleation [3] and applies the Avrami equation for transformed volume fraction and exponential dependence of nucleation rate from phases thermo-dynamic potentials. Also, non-steady state character of diffusion in the initial stage of nuclei growth does not find an appropriate consideration. The classical theory of diffusion-controlled precipitation by Lifshitz-Slyozov-Wagner [4, 5] is commonly used for the calculation of the inclusion size.

From the point of view of the non-equilibrium stationary kinetics the ferrite grain grow was considered in [6]. For a reliable and applicable procedure of material structure calculation in the HAZ for high cooling rate welding it is necessary to clarify the mutual influence of chemical kinetics and non-stationary diffusion during nucleation and growth of a new phase. The theory of constitutional supercooling is applied to prediction of solidification structures and morphologies under consideration of dependencies between cooling rates, solidification velocity, temperature gradients at the solidification front, concentration of the constituent elements and distribution coefficient. The temperature of solute correspondent to the temperature of liquidus $T_l(x)$ is usually obtained from the phase equilibrium diagram. If the real temperature $T(x)$ is lower than hypothetical temperature $T_l(x)$ of the concentration layer, the region of constitutional supercooling appears ahead of the solidification front, which becomes unstable. The ratio between solidification velocity of dendrite tip its curvature and grade of supercooling can be obtained in frame of KGT (Kurz-Giovanola-Triverdi) model. The dendrite tip radius R corresponding to stable growth condition can be taken from analytical solution for diffusion field around an ellipsoid of revolution first obtained by Ivantsov.

All the presented models are based on assumption of near-equilibrium limit, in which the solidification

© U. DILTHEY, A. GUMENYUK, G. TURICHIN, 2005

speed is largely controlled by the rate of transport of latent heat away from the interface. However during rapid solidification, like that, taking place during laser beam welding with high welding velocity, the substantial departure from equilibrium at the interface may exist. It was found that although the total free energy of the liquid dropped during solidification, the chemical potential of the minor component of dilute binary alloys often increased. Solute concentration far in excess of the equilibrium solid solubility limit have been attained in this manner. This phenomenon referred as «solute trapping». The theory of a solute trapping was proposed by Aziz and includes the following formulation of solidification velocity dependence

Statement of the problem. The main assumptions made in the present theory are following:

- reaction take place only on the interface between the old and the new phases
- the symmetry of the problem depends on the shape of the growing inclusions and correspondent size of particles and diffusion length
- initial conditions for the problem is a radius of inclusion and is an external parameter in the present model
- the convective term connected with an inclusion boundary motion can be neglected because of the smallness of diffusion Peclet number
- new phase is considered to be diffusionless
- diffusion in the old phase is non steady state problem depending on the thermal history
- no assumption about local thermal equilibrium is made.

The speed of growth of the second phase volume can be expressed by difference of the velocities of formation and destruction: [18]:

$$\frac{da}{dt} = K_1(T)\cdot C - K_2(T) \qquad (1)$$

where $K_{1,2}(T) = K_{1,2}^{(0)} \exp\left(\frac{U_{f,s}}{kT}\right)$ are constants of velocities of the direct and inverse reaction, U_f, U_s are activation energy of the direct and reverse reaction, $K_1^{(0)}$, $K_2^{(0)}$ are frequency factors One of the velocities C is free carbon concentration on the inclusion surface, T and t are local temperature and time.

The superficial concentration in (1) is determined by a solution of the diffusion equation.:

$$\frac{dC}{dt} = D\Delta C = D\frac{1}{r^2}\frac{\partial}{\partial r}\left(r^2\frac{\partial C}{\partial r}\right) \qquad (2)$$

The equation (1) represents a boundary condition for solute flux on the surface of the growing inclusion. The is a problem of the reaction-diffusion type.

Precipitation growth. The solution of the problem of inclusion growth stated in the equations (1) and (2) has been obtained by standard methods of mathematical physics [21]. The solute concentration on the surface of the growing inclusion (at $x = 0$) is given by the expression:

$$C = C_0 - \frac{1}{\sqrt{\pi}}\int_0^t \frac{\alpha(\tau)}{a(t)}\cdot\frac{K_1C_0 - K_2}{\sqrt{D(t-\tau)}}\left[1 - \left(\frac{K_1}{D} - \frac{1}{a}\right)\times\right.$$
$$\left.\times\sqrt{\pi D(t-\tau)}\exp\left(\left(\frac{K_1}{D}\frac{1}{a}\right)^2 D(t-\tau)\right)\left(1 - erf\left[\left(\frac{K_1}{D} - \frac{1}{a}\right)\sqrt{D(t-\tau)}\right]\right)\right]d\tau \qquad (5)$$

where K_1, K_2, D are functions of $T(\tau)$, a is a function of τ.

The expressions (1) and (5) forms a system of equations for temporary values of the inclusion size and solute concentration on the growing inclusion interface. The expression can be simplified by using typical scales of the values under integral sign for the stage, when it is possible to assume diffusion as a steady-state process. According to [18] it is possible to obtain for the stage of inclusion growth:

$$C = C_0 - \frac{1.56}{D\sqrt{\pi}}\frac{(K_1C_0 - K_2)}{\left(\frac{K_1}{D} - \frac{1}{a}\right)}.$$

Since the carbon concentration and relative volume of the cementite are small, the probability of collisions of the growing inclusions is small too. Nevertheless, the dynamics of the inclusion ensemble growth is properly determined by their mutual influence, especially in the final growth stage. The physical reason is a decrease of the average solute concentration owing to the solute absorption by the ensemble of growing inclusions. Having denoted the solute concentration in the growing phase as C' and inclusion number density as n, one can get for the ensemble of spherical inclusions

$$C_0 = C_0 - nC'\frac{4}{3}\pi a^3, \quad \text{were} \quad n = \frac{C_0 - C_{lim}(293)}{\frac{4}{3}\pi a_{lim}^3 C'}$$

The value of the parameter n, was determined from solubility limit at room temperature taken from the phase diagram. Here a_{lim} is a limit size of the growing inclusion. C_{lim} solubility limit. An example of calculation of the growth of carbide particle is obtained from the solution of the growth equation by using the *Euler's* method. Because the result of calculation (a_{lim}) has to be included in the equation, the hooting method of solution was used, i.e. such preliminary value of a_{lim} should be introduced, which provides the same final value of the inclusion radius a. The temporal behavior of temperature was calculated by the laser welding process model for the point on the axis of the weld seam. [22] (Figure 2). The calculated values of the inclusion radius generally correspond with the experimental ones. It can be seen also, that inclusion size is not changed in the different parts of the HAZ correspondent to different heating temperature. The reason for this is about the same cooling rates everywhere in HAZ. Opposite to this, the inclusion size strongly depends on the welding velocity and decreases

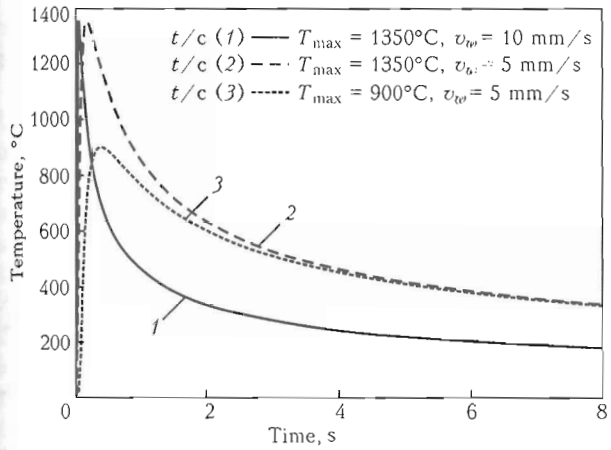


Figure 1. Different thermal cycles in HAZ

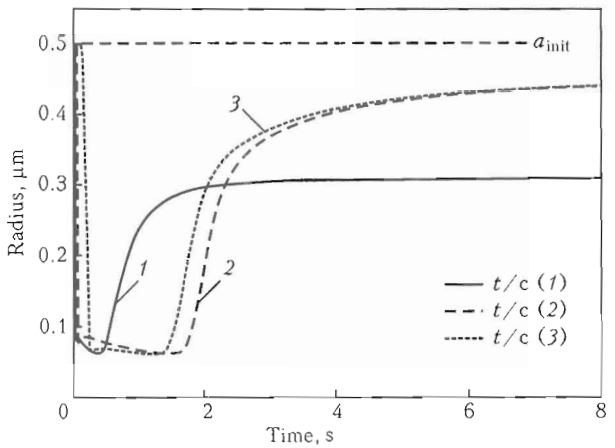


Figure 2. Example of the calculation of inclusion radius with different thermal cycles

with the welding velocity increasing.These figures are a visible illustration of the influence of kinetic effects on the process of microstructure formation. The calculated average carbon concentration in the solid solution exceeds significantly the limit of solubility (≈0.1%).

Simultaneously, the final carbon concentration on the cementite — α-phase interface is less than the carbon concentration in the solid solution.

Phase transformation. In order to obtain an expression for TTT and CTT diagram it is necessary to use a non-steady state solution of diffusion problem, for initial moment of transformation. The beginning of transformation corresponds to the condition $\frac{da}{dt} = 0$. This condition defines a connection between the temperature and the time of the transformation beginning, i.e. it describes mathematically a C-type curve of the phase transformation.

$$1 + \frac{2}{\sqrt{\pi}}\frac{K_1}{D}\left[\sqrt{Dt}\left(1 - \frac{a_1}{p}\sqrt{\pi}\right) - \frac{a_1}{p^2}\sqrt{\pi}\,\frac{A}{\frac{1}{a} - \frac{K_1}{D}}\right]$$

$$\frac{dT}{dt}\,\frac{2K_1}{\sqrt{\pi}}\,\frac{\frac{d}{dT}(K_1C_0 - K_2)}{K_1C_0 - K_2}\,0.1t\left[\sqrt{Dt}\left(\frac{1}{a} - \frac{K_1}{D}\right)\right] = 0$$

Here $a_1 = 0.348$; $p = 0.47$, $A = \ln\left(1 + p\sqrt{Dt}\left(\frac{1}{a} - \frac{K_1}{D}\right)\right)$.

Supposing $\frac{dT}{dt} = 0$, we obtain the equation of the isothermal curve (TTT-diagram). If $\frac{dT}{dt}$ is not equal to «0», we have the equation of the continuous cooling curve (CCT-diagram).

To determine five unknown values governing the equation above, five independent conditions have to be used. There are: condition on stationary transformation temperature, which is given by binary phase diagram; condition on difference of activation energy for forward and inverse reactions, which should be equal to formation enthalpy; condition, which connects value of initial nuclei radius with maximum transformation temperature (eutectoid) ; and two conditions, which are given by experimental TTT — curves: minimum value of transformation delay and diagram shift with maximum heating temperature changes. The values of parameters, used for calculation in this article for steel S690QL, are given in table 1.

Diffusion constants for carbon diffusion in α-Fe were taken following [7]. For the analysis of microstructure transformation of the HAZ material in welding the CCT diagrams, taking into account the cooling rates which are typical for welding conditions, are generally used. The diagram technique, developed above, allows to obtain the region of CCT diagram, which corresponds to bainite transformation, by substitution of the typical dependence for the welding cooling cycle.

The displacement and shape changes of transformation diagrams due to influence of peculiarities of temperature cycle and initial microstructure of steel,

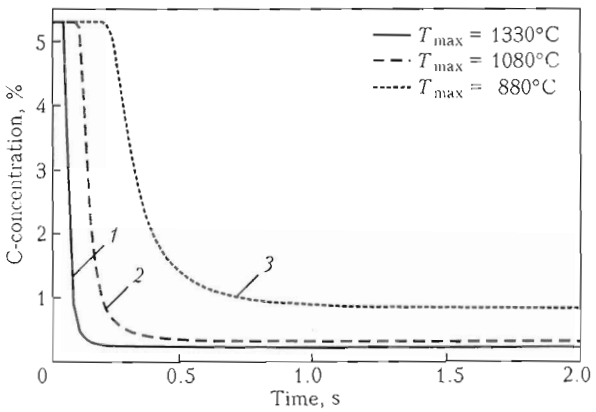


Figure 3. Calculated values of initial carbon concentration in different parts of HAZ

Table 1. Values of the used constants

Parameter	$K_1^{(0)}$, m/s	$K_2^{(0)}$, m/s	U_f, J/atom	U_s, J/atom	D_0, m²/s	U_d, J/atom	a_{cr}, m	A
Value	45	2.2	$1.26\cdot10^{-19}$	$1.60\cdot10^{-19}$	$2\cdot10^{-6}$	$1.38\cdot10^{-19}$	$1.1\cdot10^{-8}$	3.35

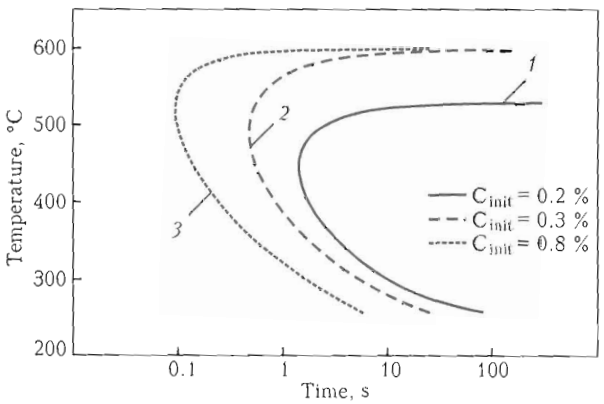


Figure 4. Calculated CCT-curves for different values of initial local carbon concentration in γ-matrix

observed experimentally, are also described by the developed theory. Initial values of grain size, vacation and dislocation density, making strong effect on diffusivity, effect, therefore, also the diffusion- controlled phase transformation. The initial size of cementite inclusion, together with temperature cycle parameters such as maximum heating temperature and heating and cooling rate, dramatically influence transformation diagrams. A reason for this fact is dependence of transformation beginning and cementite nucleus growing rate from the initial value of local carbon concentration in the transformation moment. Assuming that transformation, i.e. cementite origination, begins in regions with maximum initial carbon concentration, i.e. on the place of former cementite grains, it is possible to estimate the initial carbon concentration by the solution of the problem about carbide particle dissolution. Examples of temporal behaviour of rest carbon concentration corresponding tothree different regions of HAZ are shown in Figure 6 for calculated welding temperature cycles. correspondent transformation curves are shown in Figure 7.

The electron beam welding experiments with low-alloyed steels were carried out as an illustration of the developed theory. Two plates of S690QL high-strength low-alloyed steel with 15 mm thickness were welded in butt-joint with 20 mA and 150 kV electron beam focussed at 800 mm distance on the surface of the workpiece. The welding velocity was 5mm/s, that resulted in a cooling time $t_{8/5}$ of 4 s in the middle part of the HAZ. This time was estimated to be insignificantly varying with a growing distance from

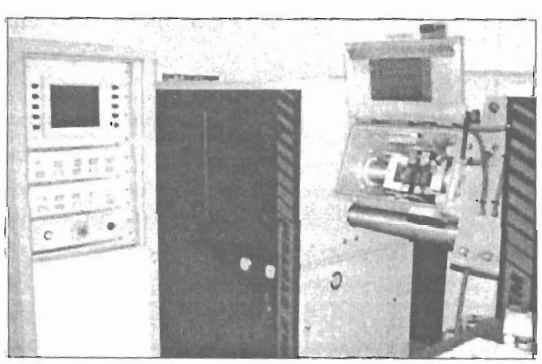


Figure 5. Thermo-mechanical simulation equipment GLEEBLE 3500 at SLV-Rostock

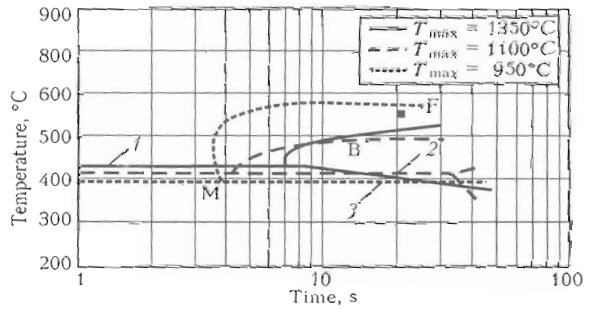


Figure 6. Experimentally obtained CCT-diagrams for steel S690QL for different maximum temperatures

the solidification line (SL). The microhardness profile, measured across the weld joint on the halfplate thickness distance from the specimen surface, is an evidence of transition from martensite to bianite microstructure with growing distance from SL (Figure 8).

The experimental CCT curves corresponding to conditions, having place during beam welding, were obtained for the same steel by the thermo-mechanical simulation on GLEEBLE 3500 equipment at SLV-Rostock (Figure 5) using a combined method of dilatometery and microstructure evaluation. The Figure 6 shows such transformation curves corresponding to three different maximal heating temperatures 1350 °C, 1100 °C and 950 °C. The predicted behaviour of curve shift is reproduced by the experiment in general. The deviation in the theoretically predicted and experimentally observed magnitudes of the transformation curve shift values can be explained by more complicated chemical composition of the real steel and the influence of such alloying elements like Mn etc., which have been not taken into account in the present theory.

Analysis of rapid solidification phenomena. The methods of the solution of kinetics equation together with diffusion equation can be applied for analysis of solidification phenomena having place during laser welding. The growth of dendrite cell will be considered here to illustrate the applicability of the method. The process will be considered as a steady state in the frame of reference moving with a solidification front. The latter moves with a constant velocity v_S cosa

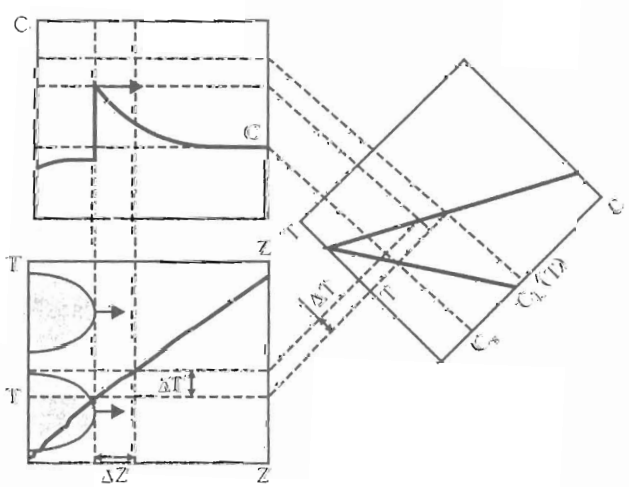


Figure 7. Illustration of solidification kinetics during welding

where α is the angle between directions of the temperature gradient and the welding velocity v_S.

Assuming, that there is a temperature gradient in the direction of dendrite axis, which can be considered as a constant in the near of the melting front, the concentration profile like depictured on the Figure 7 appears in the near solid-liquid interface. The maximal superficial concentration of the solute is lower than the concentration corresponding the equilibrium conditions at the local temperature. It is a reason for dendrite cell growth. I.e. the interface moves towards a region with higher temperature. From the other side the existence of a concentration gradient in the near of phase interface is a reason for diffusion of the solute from the latter to the volume of the liquid phase. For described process the following diffusion equation for the case of plane geometry is valid:

$$\frac{\partial C}{\partial \tau} = D\frac{\partial^2 C}{\partial x^2}. \qquad (6)$$

In case of steady moving boundary it is possible to transfer from the temporal coordinate to the second spatial coordinate like follows: $\tau = z/V\cos\alpha$. On the interface between solid and liquid phase the following boundary condition must be satisfied. The net mass flux of the admixture through the moving boundary should be equal to the diffusion flux. Latter is proportional to the concentration gradient at the interface:

$$\frac{\partial V}{\partial \tau} = -D\frac{\partial C}{\partial x}\Big|_{x=x_0} S = K(T)\left(C_L(T) - C\Big|_{x=x_0}\right) S. \qquad (7)$$

The left part of this equation describes diffusion and the right one kinetics of the growth of dendrite cell. $C_L(T)$ is an equilibrium liquidus concentration at the temperature T. The coefficient $K(T)$, in the right part is an exponential function of the temperature $K(T) = A\exp\left(-\frac{\Delta F}{kT}\right)$, where ΔF is an change of free energy between solid and liquid phase. The solution of such a problem is known [41]:

$$C(x(\zeta,\eta),z(\eta)) = C_0 + \frac{1}{\sqrt{\pi}}\int_0^z \frac{d\eta^*[C_0 - C_L(T(\eta^*))]}{\sqrt{\eta - \eta^*}} \times$$

$$\left[\exp\left(-\frac{\zeta^2}{4(\eta-\eta^*)}\right) - \sqrt{\pi(\eta-\eta^*)}\,\exp(\zeta + (\eta-\eta^*)) \times \left\{1 - \Phi\left(\frac{\zeta}{2\sqrt{(\eta-\eta^*)}} + \eta - \eta^*\right)\right\}\right] \qquad (8)$$

where the expression $[C_0 - C_L(T(\eta))]$ is a known function of the argument η.

In Figure 8. the concentration profiles on different distances from dendrite tip are represented. It can be recognized, that concentration in inter-dendritical space rise with progressing solidification. This prevents further growth of dendrite in transverse direction. In the same time the diffusion in the liquid terminates because the solute concentration becomes distributed steadily. Dependence of the dendrite radius from the distances from dendrite tip is depicted in lower Figure.

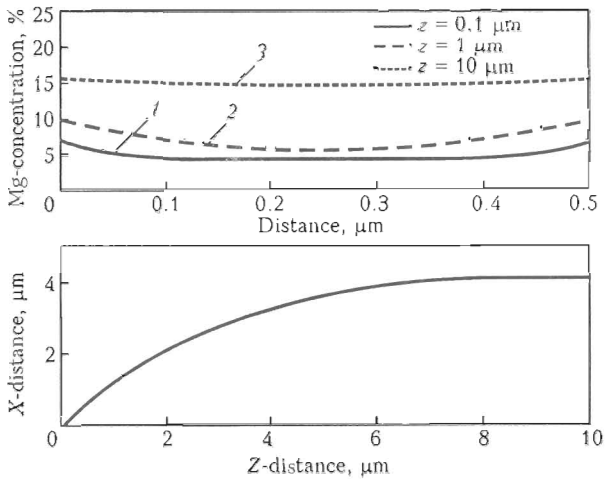


Figure 8. Concentration profile (above) in inter-dendritic space and dendrite half width (below) depending on distance from dendrite tip

CONCLUSIONS

The developed mathematical model, based on solution of connected problems of diffusion and kinetics of chemical reaction with consideration of mutual influence in inclusions ensemble, allows to describe processes of cementite growth and carbon redistribution in the ferrite phase. The evaluated size of cementite inclusions corresponds to that, known from experiments.

The developed method, based on the simultaneous solution of complex diffusion-kinetic problems, allows to obtain a parametric description of isothermal and continuous cooling transformation diagrams. Operating with a small number of easy interpretable physical constants, the proposed model allows to describe the influence of the initial structure of the material and the parameters of the welding thermal cycle on the course of the transformation curve. In combination with experimentally obtained TTT and CCT-diagrams, the method enables to broaden possibilities of diagram technique for the analysis of the microstructures and properties of weld joints.

1. Matsuda H. and Bhadeshia H.K.D H. *Avrami theory for transformation from non uniform austenite grain structures*, Materials Science and Technology, Vol. 19, 2003, p. 1330–1334.
2. Grong O. *Metallurgical modelling of welding*, Cambridge, The Institute of Materials. 1994.
3. Cahn J.W. *The kinetic of the grain boundary nucleation reactions*, Acta Metallurgica V 4, 1956. p. 449–459.
4. Lifshitz I.M. Slyozov V.V. *The kinetics of precipitation from supersaturated solid solutions*. Journal of Physics and Chemistry of Solids V. 19, 1961. p. 35–50.
5. Wagner, C., *Theorie der Alterung von Niederschlagen durch Umlosen*, Z. Elektrochemie, V 65, 1961. p. 581–591.
6. Lubov B.Ya. *The kinetic theory of phase transformations*, Moscow: Metallurgy, 1969.
7. Umanskii Ya.S., Skakov Yu.A. *Physics of metals*, Moscow: Atomizdat, 1978.

MELT REMOVAL MECHANISMS OF THE GASJET-ASSISTED LASER FUSION CUTTING

V. S. GOLUBEV
Institute on Laser and Information Technologies of RAS, Shatura, Russia

A physical analysis is presented on melt removal and melt layer instability mechanisms of gasjet-assisted CW laser fusion cutting. The published models are considered and specified: melt squeezing-out due to gas pressure gradient; melt dragging by the friction force between melt surface and gas flow; formation of moving shelves at the cutting front. Additionally, some new hydrodynamical mechanisms are proposed and discussed.

Introduction. The problem of melt removal in laser cutting (LC) processes continues to be actual [1–3]. The aim of this study is to review the published models on the gas-assisted cw-laser fusion cutting mechanisms and to discuss some new hypotheses on nonstationary mechanisms of melt removal. The main attention is given to qualitative physical ideas on possible nonstationary hydrodynamic phenomena accompanying melt removal.

The published models of LC process consider mainly the stationary melt removal from the cutting front by assist gas flow pressure gradient [2, 4, 7] and gas flow-melt friction force [2, 5–7]. A detailed model of stationary melt removal mode has been developed in [2]: as well, this model considers hydrodynamical instability of the flowing melt layer, similar to the classic instability of the boundary layer [8].

During last decades, models of several mechanism of hydrodynamically unstable, periodical melt removal LC-process have been published:

- periodically arising shelves, moving along the cutting front [10];
- melt droplets at the top of the cut front due to pulling effect of the gas flow [11];
- melting front instability [11];
- forced oscillations of the melt layer due to assist gas pressure fluctuations [5];
- melt droplets tearing-off due to development Kelvin-Helmholz instability [3, 9].

Additional hydrodynamic mechanisms are proposed in the present study. One of these mechanisms is the melt surface flow instability, caused by flow velocity gradients. The second mechanism is the periodical (along the cutting front) melt squeezing-off («snow-plough» effect) the melt layer, caused by dynamic pressure of the gas flow.

All these instabilities cause the strata formation on the cut edges and influence the energy efficiency of LC process. Analysis of the discussed mechanisms allowed to propose a qualitative explanation of experimentally observed dependencies of energy efficiency and cut edge roughness amplitudes upon the cutting velocity and gas pressure. This helps to propose some practical recommendation to optimise laser power, cutting velocity, gas flow parameters and laser beam intensity profile.

© V.S. GOLUBEV, 2005

LC melt removal mechanisms. process instabilities. *Geometry and gasdynamics of the LC process.* We suppose the «classical» geometry of the nozzle, laser beam and gas flow [1]. In this case the nozzle cross-section exceeds the cut kerf width. As a rule, the gas flow inside the cut slot is supersonic, and the behaviour of its gasdynamical parameters is far from being optimal for the LC process [12]. Though, an optimal gas flow geometry was proposed by Prof. La Rocca [12]: the nozzle diameter should be equal to the kerf width. Still, this proposal, seemingly, is not applied to running technology of LC [1].

Supersonic gas flow entering into the cut slot expands and deccelerates in a system of oblique shocks. Mean values of the static pressure p and Mach number M change in accordance with computation [11, 13]. In the upper zone of the cutting front, $M > 1$; in the lower zone, the flow is subsonic; $p < p_{atm}$; local values of p and M oscillate along the direction of the front [13]. Such a situation hampers the process of melt removal, resulting in formation of wide and deep strata on the cut edge and in dross adhesion.

The stationary process of melt removal. Estimating the models of stationary melt removal process, we point out the existence of three flowing sublayers inside the frontal melt layer [3]. The flow mode is changing, when melt travels along the cutfront: there exist a critical distance h^*: if $z < h^*$, melt flow has no boundary layers. At $z > h^*$, the melt layer consists of three sublayers: near-bottom, intermediate and near-surface. Our model considers the driving forces of pressure gradient and of shear stress between the gas jet and melt surface versus the forces of inertia and viscosity. The value of h^* depends upon cutting velocity v_c, shear force τ_f and kinematic viscosity ν of the melt: $h^* = \nu\tau_f/\rho v_n^3$; $\tau_f = 2{\cdot}10^{-3}\,\rho_g v_g^2$ in the case of turbulent gas flow [8]; ρ_g, v_g — gas density and gas flow velocity; ρ is the melt density. If $h > z > h^*$, then $v_c > v_{th} = Pe_{th}{\cdot}\chi/b$, with Pe_{th} determined by

(1), χ being the thermal diffusivity of the substrate and b-width of the cut kerf. The near-surface sublayer is subjected to the «surface-flow» instability. We have found, (see 2.3.), that the pressure driven intermediate melt layer can be subjected to forced oscillatons, initially considered in [5]. Though, the melt flow at $z \le h^*$ can be unstable as well [2, 3, 6, 7]. The analysis [2, 7] has revealed a possibility of LC melt flow hydrodynamical instability, similar to the instability of the classical boundary layer [8], with its subsequent turbulization.

Forced oscillations of the melt layer. Free oscillations of the melt layer are enhancing when in resonance with fluctuations of the gas flow pressure or of the laser power (Prof. D. Schuoecker, [5]). Our simplified model [14] gives a condition for onset of the instability:

$$v_c > (\nu\tau_f/\rho h)^{1/3} \cong 2 \div 3\ cm/s;$$
$$Pe \equiv (v_n b/2\chi) > 10^{-1}(b/\chi)(\partial v/\rho h)^{1/3} \equiv Pe_{th} \qquad (1)$$

and the wavelength of striations at the cut edge: $\Lambda \cong 2\pi h v_c(\rho/p)^{1/2} \cong 10^{-2} \div 10^{-1}$ cm Within (1), Pe is the Peclet number, h is the thickness and χ is thermal diffusivity of the sample).

Kelvin-Helmholz («wind») instability and droplets tearing-off [9], (Figure 1). Increment (γ) of the instability is maximal for the wavenumber $k = k_m$:

$$\begin{cases} k_m = (\rho_g v_g^2/3\sigma) \cong (10^2 \div 10^3)\ cm^{-1} \\ \gamma = v_g k^{1/2}(\delta\cdot\rho_g/\rho)^{1/2} \cong (3\cdot 10^4 - 10^6)s^{-1}\ (\text{if } \delta \cong 10^{-2}\ cm) \end{cases} \qquad (2)$$

Droplets velocity: $v_d \cong (3\cdot 10^2 \div 10^3)$ cm/s ; droplets dimensions: $d \cong (8/\pi)^{1/2} k_m^{-1} \cong 10^{-2} \div 10^{-3}$ cm; edge striations wavelength: $\Lambda \cong 10^{-1} k_m^{-1} \cong 10^{-4} \div 10^{-3}$ cm.

«Moving shelves» [10]. At low cutting speeds ($Pe < 1$) the scanning laser beam permanently overlaps and heats the upper surface of the specimen, and the area of this surface, adjacent to the cutting front, melts earlier, than the front surface (Prof. V.S. Kovalenko et al., [10]). For a case of Gaussian laser intensity profile, the criterium of low v_c, found in [14], is: $Pe < Pe_{cr} \cong 3$.The melt on the heated area is removing by pressure gradients in the gas flow [11]; diameter of the teared-off droplet: $d \cong (\sigma b/p_{din})^{1/2}$ (σ is surface tension of the melt, p_{din} — dynamic pressure of the gas flow). Rough estimation [14] gives, that at the depths $z \ge (0.1 - 0.3)h$, the melt vapor pressure over the shelf surface exceeds the dynamic pressure of the gas flow; travel velocity v_z of the shelf downwards the cutting front: $v_z \cong 10^2$ cm/s, and the droplet's size $\cong 3\cdot 10^{-4}$ cm. Experiments [15] seemingly are consistent with this model, having found the value $\sim 10^{-2}$ cm/s of velocity of the bright spot, moving alongside the cutting front.

Cutting front instability at Pe >> 1. Physical reason of instability (Figure 2) is the increasing of local heat flux to the depressions of a spontaneously perturbed cutting front. It occurs, if the laser beam intensity profile's slope is negative in the direction of cutting [11]. The melt, moving alongside the front, is ejected by the centrifugical force from the humps of developed perturbations of the surface [14]. The jets of the melt are transforming into droplets due to the effect of capillary collapse. The conditions and parameters of instability [11]:

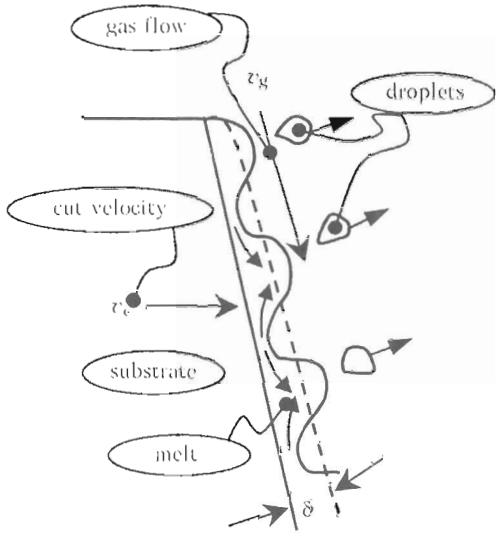


Figure 1. Kelvin-Helmholz («Wind») instability and droplets tearing-off*

$$Pe >> 1;\ k_m << \frac{v_n}{\chi};\ \gamma = -\frac{\partial}{\partial z}\left(\frac{q}{E_m}\right) \cong = \frac{v_n}{r_0};\ v_{ph} \approx \frac{q}{E_m} \qquad (3)$$

Within (3), q is laser beam intensity, E_m — full specific heat of the melt per cm^3; v_{ph} — phase velocity of perturbations travel along the front. The wavelength of striations is: $\Lambda \cong b/2 \cong 10^{-2}$ cm.

Melt surface flow instability. The fast film flow over the liquid substrate (at $z > h^*$) is unstable due to the centrifugical force in the humps and grooves of spontaneously emerging perturbations on the flowing melt surface (Figure 3). The instability is accompanied by subsequent tearing-off of the melt droplets . Thus, the instability participates as an additional mechanism in the melt removal process, and in the generation of cut-edge striations, due to the adhesion of the ejected

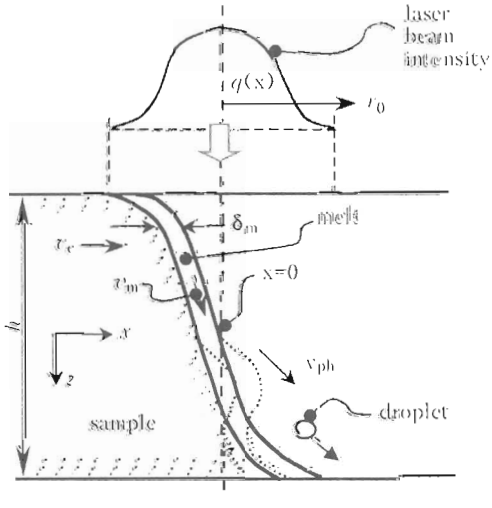


Figure 2. Cutfront instability * at $Pe >> 1$

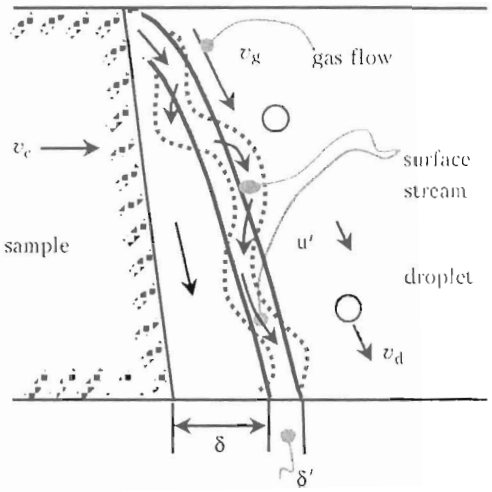


Figure 3. Melt surface flow instability

droplets. The threshold of instability is determined by conditions, found in [14]:

$$z \geq \left[\left(\frac{\sigma}{\rho}\right)^2 \rho v / v_n^3 \tau_f\right]^{1/3}; \; Pe > (p/\rho)^{1/3}(\nu^{1/2}/\chi) b h^{-1/2} \qquad (4)$$

Within [14], z is the distance downside the cutting front, and p is the gas pressure. Droplets velocity:

$$u_\tau \cong \left(\frac{\sigma}{\rho}\frac{(\tau_f/\rho)}{\nu}\right)^{1/3} \cong 10^2 \text{ cm/s}$$

Droplets size d and edge striations wavelength Λ:

$$d \cong \Lambda \cong 10^2 \cdot \nu^{2/3}(\sigma/\rho)^{1/3}(p/\rho)^{-2/3} \cong 10^{-3} \div 10^{-2} \text{ cm}$$

«Moving humps», or «Snow-plough» mechanism. At $Pe > Pe_{cr}$, the «moving shelf» intstability of the cutfront does not exist. Instead, we have considered [3, 14] a hypothesis of moving melt «humps», without deformations of the melting front. Any spontaneous perturbation of the melt surface can be increased by dynamic pressure of the gas flow. This perturbation transforms, due to the «snow-plough» effect, in a moving hump, succeeded by periodical tearing-off of droplets. This process generates both transversal and longitudinal striation on the cut edge.The condition of the instability:

$$Pe >> 16(\sigma/\rho h)^2(b/\chi)(\rho/p)^{1/2} \qquad (5)$$

The wavelength of transversal striations:

$$\Lambda \cong 4(\sigma/\rho)v_n^{1/2}(p/\rho)^{-3/4} \cong 3\cdot10^{-4} \div 3\cdot10^{-3} \text{ cm}$$

2D-map for different mechanisms of melt removal. The map on Figure 4 presents 2D-area of $\{h, v_c\}$ parameters for possible mechanisms of melt removal and melt layer instabilities. To generalize the map for others, than steel, materials, the nondimensional parameters $\bar{h} = h/b$ and $Pe = v_c b/2\chi$ are used as well. Moving alongside the border-line 4 of sample's throughcut, one can determine qualitatively the possible modes of melt removal and of expected types of striations. An expression for the line 4 is presented in part 3, formula (6). The expressions for lines 1, 2, 3 are presented respectively by formulaes (5), (4) and (1).

Figure 4 demonstrates, that LC process of the specimens with high thermoconductivity, increased thickness and at low cutting speeds (i.e., when $Pe << Pe_{cr} = Pe$ (5)) is running in the «moving shelves» mode. In this case it is principally difficult to avoid the formation of edge strata (grooves). The edge roughness (R_a) at mostly favourable (i. e., «top-hat») focal spot intensity distribution was calculated in [10]: in this case, the Ra values are pretty small.

If the speciment is of low thermoconductivity, of small thickness and if the LC process runs at elevated speeds, (i. e., $Pe > Pe_{cr}$), this process can proceed in the classical mode of melt removal by gas flow pressure gradient and shear force. The edge roughness is minimized by using high values of gas pressure and velocity, according to analysis of parts 2.7, 2.8 and 3. As well, application of «top-hat» intensity distribution is favourable, because it prevents the cutting front instability (part 2.6). The striations formed by forced oscillations of melt layer can be minimized by strong stabilization of laser power (at frequencies 10^2–10^3 s^{-1}) and laminarization assist gas flow.

Striations on the cut edge. LC process (as well as nonlaser cutting processes) succeeds by formation of striations on the cut edge.The measured surface roughness height Ra exhibits a minimum at some intermediate cutting speed [16–18, 22]. It is noteworthly to mention, that a similar minimum manifests the experimentally measured [18] dependence of the samples' temperature growth versus cutting velocity (Figure 5).

The explanation of mechanisms of strata formation can be given on the basis of LC front melt layers instabilities. The stratification occurs either due to the striped melting of the edge by oscillating heat flux from the cutting front, or by periodical adhesion of droplets [17], emitting from the front melt waves [14].

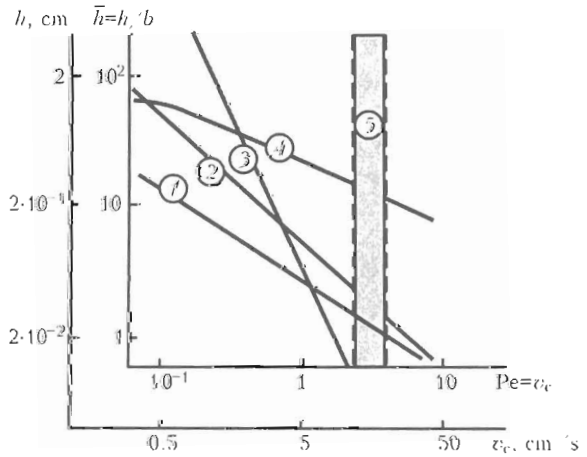


Figure 4. 2 D-MAP $\{v_c, h\}$ of LC melt removal models (rough estimations): Borders of: *1* — «Snow-plough» mechanism at $Pe >> 1$; *2* — surface flow instability at $Pe > Pe$ (2); *3* — bottom and surface sublayers at $Pe > Pe$ (3), forced ocscillations; *4* — limit of throughcut at $Pe > Pe$ (4) (steel, b = 0.2 mm; P = 4kW); *5* — critical Pe for «moving shelf» at $Pe < Pe$ (5)

As the dynamic pressure of the cutting gas flow or melt vapor pressure (this is important for «moving shelf» and «snow-plough» mechanism) are always decreasing in the lower parts of the cutting front, the wavelength and heights of the strata increase in the direction to the lower zone of the front [e. g., see (3), (4)]. The adhesed and solidified droplets form the periodical crests, i. e. striations, on the cut edges. An estimation [14] of heat transfer and hydrodynamic processes in adhesing droplet has shown that the roughess height increases with increasing cutting velocity and decreases with increasing assist gas dynamic pressure.

We tried [14] to interprete the dependence $R_a(v_c)$, presented at Figure 5. If $Pe < Pe_m$, the heating of edges decreases with growth of Pe. Simultaneously decreases the depth of melted strips on the edge, produced by moving «shelf». If $Pe > Pe_m$, the heating of edges increases with growth of Pe due to adhesion of melt droplets to quickly cooling edges. Simultaneously, these adhesed and frozen droplets make periodical «crests», or striations, on the edge surface. The measured cut edge roughness as well depends upon gas pressure, p. It was stated in [7]: with the growth of gas pressure, p, the value of R_a increases, if $Pe < 1$; but, R_a decreases, if $Pe > 1$. A qualitative explanation [14] of this behaviour of R_a: if $Pe < 1$, LC process is running in «shelf» mode, succeeded by striped melting of cut edges by heat flux from the moving shelf. The less is the value of p, the slower is squeezing of the melt out melted strips and consequently the less it the value of R_a. If $Pe > 1$, the adhesion of droplets on cut edge occurs, producing the regular stratification by «crests», formed by solidified droplets. The more is the value of p, the less it the height of crests due to «flattening» of the adhesed melt by the gas flow.

LC process energy efficiency. The analysis of LC melt removal mechanisms is inevitable as well for estimation of energy efficiency of the process as for interpretation of cut edge striations. The treatment [14] of experimental LC parameters [1] shows the consistency of «moving shelf» model for LC energy efficiency η_T estimation (Figure 6). The η_T value is determined as $\eta_T = (E_m b v_c h)/AP$, with A defined as the total absorption coefficient of laser beam energy plus the energy of exothermic reaction of the assist gas with the melt. For the case of inert assist gas we suppose $A \cong 1$, according to [19, 20]: the absorption of laser radiation by metallic melt sharply increases due to effects of surface capillary and electromagnetic waves. For the case of oxygen gas, we suppose $A \cong 2$, i.e. the share of the exothermic reaction energy roughly equals [1] to the share of the absorbed laser energy.

Model «moving shelves» considers heat expenses for front melting and side heating of the substrate and evaporation of the melt on upper surface of the shelves,

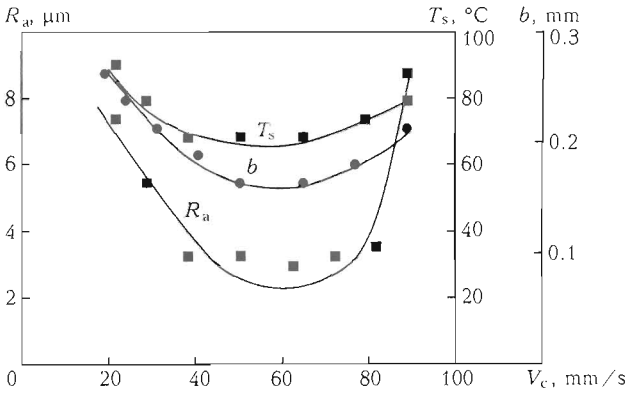


Figure 5. LC kerf parameters versus cutting speed [18]

similarly to the analysis [21] of laser hole punching. An interpolation formula for η_T in Pe range $0.3 < Pe < 5$ and $q = 10^6 - 10^7$ W/cm^2 was found [14].

$$\eta_T \equiv \frac{E_m b v_c h}{AP} = \left[\left(1 + 1.2Pe^{-0.75}\right)\left[1 + 0.3(q/q_1)^{0.6}\right]\right]^{-1} \quad \text{with} \left(q_1 = \frac{E_{ev}}{kT_B} p_A a_s\right) \tag{6}$$

Within (6), E_{ev} is the evaporation energy per one atom of the substrate; k is Bolzmann constant, T_B — boiling temperature of the melt (usually, $(E_{ev}/kT_B) \cong 14$), p_B — vapor pressure at 1 ata, a_s — sound velocity in the vapor (e.g., for iron vapor: $q_1 \cong 1.2 \cdot 10^5$ W/cm^2). According to (6), the expression used for $\bar{h}$ in the curve 4, Figure 4, is: $\bar{h} = AP\eta_T/2\chi b E_m Pe$. The widespread model of the stationary melt removal gives:

$$\eta_T \approx \left[1 + \left(\chi h/u_m b^2\right)Pe^2 + \left(\frac{1}{2Pe} + \frac{1}{PE^2}\right)^{1/2}\right]^{-1} \tag{7}$$

where u_m is melt removal velocity along the cutfront. As it is seen on Figure 6, the model of stationary melt removal is less consistent with the experiment, than the model of «moving shelves».

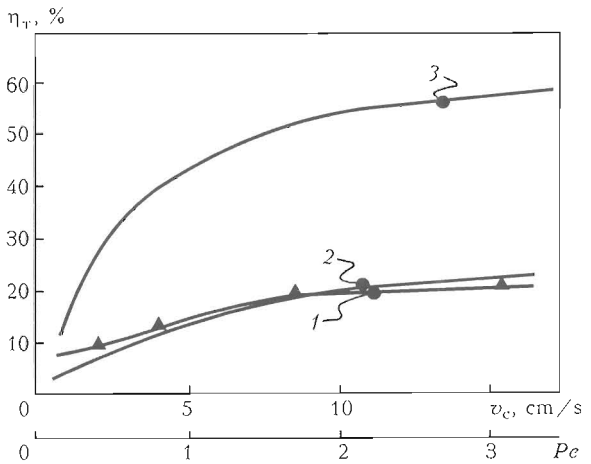


Figure 6. Thermic efficiency of steel LC: *1* — points (▲): the results for $h = f(v_c, P)$ of experiments [1] P_{LAS} = 1.5kW; b = 0.2 mm, $P(O_2) = P_{LAS}$ (supposition), used in: $\eta = E_m b h v_c/AP$; *2* — model of moving «shelves»; *3* — classical model of stationary melt removal by gas pressure gradient

CONCLUSION

1. Instabilities of the melt flow and subsequent tearing-off of droplets affect the mechanisms of the LC process and cause the formation of cut-edge strata.

2. Hydrodynamical phenomena, important in LC-melt removal mechanisms:

- Unstable film flow on the melt surface.
- Generation of moving «shelves» at low ($Pe < Pe_{cr}$) velocities, melt droplets tearing-off.
- Melting front and melt surface instabilities at increased velocities ($Pe > Pe_{cr}$) cause the growth of melt removal rate and the roughness of striations due to adhesion of droplets on the cut edge.

3. New hypotheses on mechanisms and properties of LC have been [3, 14] proposed:

- Three sublayers in the stationary flowing melt layer along the cutting front.
- Melt droplets ejection due to hydrotynamic instabilities.
- Appearance of moving melt humps along the cut front by «show-plough» effect (at $Pe > Pe_{cr}$), with subsequent droplets tearing-off.

4. It is difficult to give an explicit juxtaposition of presented qualitative models and experimentally measured strata parameters. The thoroughful systematic experimental investigations of strata roughness (R_a) and wavelength (Λ) in the representative range of LC parameters and sample's materials need to be done. Summarizing, one can only cautiously say, that the estimations of strata wavelengths reveal the same range of Λ, as the range of experimentally observed values Λ (10^{-3} – 10^{-1}cm). Besides, the character of observed dependencies of the R_a upon cutting speed,gas pressure and location on the cut edge are qualitatively the same as it follows from estimations (parts 2.3–2.8). The simultaneous presence of the strata with different wavelengths (e.g., 10^{-3}, 10^{-2} and 10^{-1} cm) is not in contradiction with the map of Figure 4.

5. Practical recommendations. The presented qualitative analysis of melt removal in LC-process allows to propose some additional practical recommendations:

- Adjusting the values of laser power, focal diameter and processing velocity to the thickness of the sample and its thermophysical properties. The criterium for optimal adjusting should be the value of Peclet number of the order of few units.
- Forming the special laser intensity profile in the focal spot.
- Laminarisation of the assist gas flow.

1. *LIA Handbook of Laser Materials Processing* 20, J.F. Ready, D.F. Farson, Ed., Laser Institute of America, 2001.
2. Ming-Jye Tsai, Cheng-I.Weng, J. Phys. D: Appl. Phys. 26, pp. 719–727, 1993.
3. Golubev V. S. *Proc. of Intern. Conf. «LTWMP»*, pp. 24–31, May 19–23, 2003, Katsively, Crimea, Ukraine. Ed. By B.E.Paton and V.S.Kovalenko. Publ. E.O.Paton Electric Welding Institute, NASU, Kiev 2003.
4. Flemming O. Olsen, *Proc. SPIE 2207*, pp. 402–413, 1994.
5. Schuocker D. *«Ind. Las. Handbook»*, Ed. D. Belforte & M.Levitt, Penwell, Tulsa, OK, pp. 65–79, 1987.
6. Sforza P., Santecesaria V. *Proc. SPIE 2207*, pp. 836–847, 1994.
7. Vicanek M., Simon G., Urbassek H. M., Decker I., Phys J. D: Appl. Phys. 20, pp. 140–145, 1987.
8. Schlichting H. *Grenzschicht-Theorie*, Verlag G. Braun, Karlsruhe, 1967.
9. Johnson R. L., O'Keefe J. D. AIAA Journal 12, N8, pp.1108–1109, 1974.
10. Kovalenko V. S., Romanenko V. V., Oleshuk L. M. *Waste-Free Processes of Laser Cutting*, Kiev, Tekhnika, 1987.
11. Makashev N. K. et al., *Kvantovaya Elektronika 19*, N 9, pp. 910–915, 1992.
12. Aldo V.La Rocca, *Proc. SPIE 2097*, pp. 100–111, 1993.
13. Leidinger D., Penz A., Schuoecker D. et al., *Proc. SPIE 2207*, pp. 469–479, 1994.
14. Golubev V. S. *Melt removal mechanisms in the gas-assisted laser cutting of materials* Eprint №3, ILIT RAS, Shatura, 2004.
15. Takashi Fushimi, Hideyuki Horisawa, Shigeru Yamaguchi et al., *Proc. SPIE*, 2888, pp. 90–95, 2000.
16. Decker I., Ruge J., Atzert U. *Proc. SPIE 455*, pp. 81–87, 1984.
17. Shariff S. M., Sundararajan G., Joshi S. V. Journal of Laser Applications 11, N 2, pp. 54–63, Apr. 1999.
18. Bazyleva I. O., Galushkin M. G., Golubev V. S., Dubrovina E. A., Karasev V. A. *Proc. SPIE 4644*, pp. 77–86, 2001.
19. Samokhin A. A. *Proc. IOFAN*, vol 13, pp. 3–98, Moscow, «Nauka», 1988.
20. Akhmanov S. A., Emelyanov V. P., Koroteev N. I., Seminogov V. N. «Uspekhi Fys. Nauk», 1985, vol.147, pp. 675–745.
21. Von M. Allmen, *Laser Beam Interactions with Materials*, Berlin, Springer-Verlag, 1987.
22. Grigoriants A. G., Sokolov A. A. *«Laser cutting of metals»*, Moscow, «Vysshaya shkola», 127 p., 1988.

HIGH POWER DIODE LASER WELDING OF ALUMINUM ALLOY EN AW-1050 A

A. KLIMPEL, A. LISIECKI, D. JANICKI, S. STANO
Welding Department of Silesian University of Technology and Welding Institute, Gliwice, Poland

In this work, results of study on the process of HPDL laser welding of aluminum alloy 1050A are presented. Butt joints of thin aluminum sheets were produced using high power diode laser ROFIN SINAR DL 020. The influence of diode laser welding procedure on mechanical properties and joints structure were determined. It was proved that it is possible to produce high quality joints in a wide range of diode laser welding parameters.

Introduction. Thanks to high mechanical properties and low density, high corrosion resistance and good plasticity, aluminum alloys are widely used as construction material in industries such as automotive, aircraft, chemical, power construction industry [1, 2]. In the last five years, the consumption of aluminum alloys in automotive industry has increased over 80%. It is predicted that the mass of aluminum alloys used for manufacture a single car can be increased from approximately 110 [kg] in 1996 to 250–340 [kg] in 2015 if used for auto-body panels, Figure 1.

High quality joints of aluminum alloys sheets can be produced by GTA, GMA, PTA but welding of thin sheets under 3.0–5.0 [mm] is very difficult, and impossible by GMA method. Fast development of high power molecular and solid state lasers make that automated and robotized laser welding of aluminum alloys joints are competitive to GTA, GMA and PTA technologies in wide range of thickness because of quality and economical reasons [1, 4, 6].

Laser welding consist in rapid melting of the contact area of sheets to be welded by the heat of focused, concentrated and high intensity laser beam [1, 3, 4]. Laser as a flexible heat source of high power density (intensity), over 109 [W/cm^2], enables key-hole welding of single side joints of aluminum alloys in the thickness range from a few hundredths millimeters up o 20 [mm]. Mechanical properties of laser welded joints are not lower then properties of base material, the joints are distortions free, the weld is very narrow and the HAZ is almost undetectable [1, 3, 6, 8].

Main difficulties during laser welding of aluminum alloys are the results of high chemical activity, intensive oxidation, high thermal conductivity and high thermal expansion, susceptibility to porosity, loss of alloying elements such as magnesium and zinc during welding, and very low absorption of laser beam energy. For low intensity laser beam, only 1% of the laser beam energy is absorbed by polished surface of aluminum [3, 4].

Nd:YAG and molecular CO_2 lasers, emitting at 1.06 [mm] and 10.6 [mm] respectively, have found the most extensive application for welding of aluminum alloys [3, 4, 6]. Laser welding of aluminum alloys without any absorbents, that are used for increasing the absorption of joint surface, is possible only during key-hole welding technique.

Slight deviations of laser beam spot size of CO_2 and Nd:YAG lasers lead to significant changes of penetration depth and other weld shape defects and also increase of porosity even when potential sources of hydrogen, as a maim reason of porosity of aluminum alloy welds, are eliminated [3, 6].

High-power diode lasers, emitting in a range 800–960 [nm], are of interest for material processing in many branches of industry. HPDL's have many beneficial features compared with molecular CO_2 and solid state Nd:YAG lasers, especially significantly lower investment and running costs [4, 5, 8].

Conventional HPDlL's, with power density (intensity) of laser beam spot in a range 104–105 [W/cm^2] and size of beam spot about several square millimeters, can be used only for conduction mode welding. Application of a special optics for focusing and forming the laser beam enable to produce circular beam spot of 1.0 [mm] in diameter. Circular beam spot of HPDL was successfully used for key-hole welding of butt joint of AlMg3 alloy 1.5 [mm] thick, at laser power 1400 [W] and welding speed 0.32 [m/min], and also AlMg1 alloy 2.0 [mm] thick, at laser power 2300 [W] and welding aped 0.35 [m/min] [8]. Other solution is application of special absorbents for increasing the absorption of laser beam energy on the surface of welded sheets [9]. In this work, the process of HPDL laser welding of butt joints 0.8, 1.0 i 1.5 [mm] thick of aluminum alloy

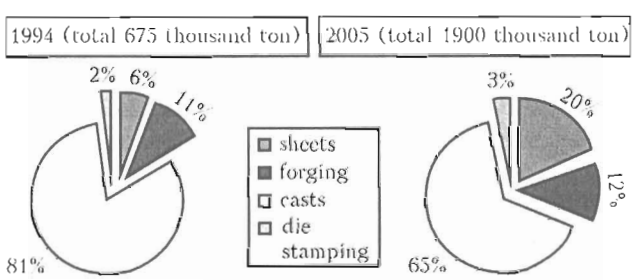


Figure 1. Increase of aluminum alloys consumption in automotive industry [2]

© A. KLIMPEL, A. LISIECKI, D. JANICKI, S. STANO, 2005

Table 1. Technical data of the high power diode laser acc. to Figure 1

Wavelength of the laser radiation	808 nm ±5 nm
Maximum output power of the laser beam (continuous-wave)	2300 W
Laser power range	100÷2300 W
Focal length	82 mm/32 mm
Laser spot size	1.8×6.8 mm/1.8×3.8 mm
Range of the laser intensity	0.8÷36.5 kW/cm^2

EN AW-1050A, used mainly in chemical and food industry for containers and cans, was investigated.

Results. The investigations were carried out to determine the influence of laser welding procedure during high power diode laser welding of aluminum alloy EN AW-1050A butt joints 0.8, 1.0 and 1.5 [mm] thick, Table 2, and also to determine the influence of basic laser welding parameters on the quality and properties of the joints.

High power diode laser HPDL ROFIN DL 020 with maximum output power 2300 [W] was used in the investigations, Table 1. The laser beam spot was focused on the top surface of the joints to be welded at focal length 82 [mm] and beam spot size 3.8×6.8 [mm]. CNC ISEL Automation positioning system was used for positioning and moving the joints and laser head. The positioning system consist of three linear stages x, y, z, and one rotary positioner powered by 4-axis servo-controller connected with PC computer via PC-card. The laser head was fixed to a vertical stage on the axis «z» to ensure precision control of the beam spot position. Directly under the laser head a cross-table with two linear stages was placed. The linear stages were moving in two direction along axis «x» and «y». An aluminum positioning plate was fixed to the cross-table with special clamping system and with a graphite backing bar forming and protecting the weld root, Figure 2.

Initial laser welding tests have shown that even at maximum laser power full penetration of 0.8 [mm] thick but joint of surface cleaned aluminum alloy sheet can not be achieved. To increase the absorption of the laser beam energy, top surfaces of the joints were covered by alcoholic solutions of black dye manufactured by Pentel. The tests of laser welding of aluminum alloy joints with the absorbent have proven that the absorption of laser beam energy on the joint surface is significantly increased, and it is possible to produce high quality joints in wide range of laser welding parameters. Prior to laser welding edges of the samples to be welded were mechanically cleaned to remove oxides and also degreased, and then the black absorbent was supplied on the surface in joint area. The test joints oh aluminum alloy sheets 200 [mm] long were laser welded at different heat input by means of different welding speed and different laser power, Table 3. The weld pool and whole welding area were

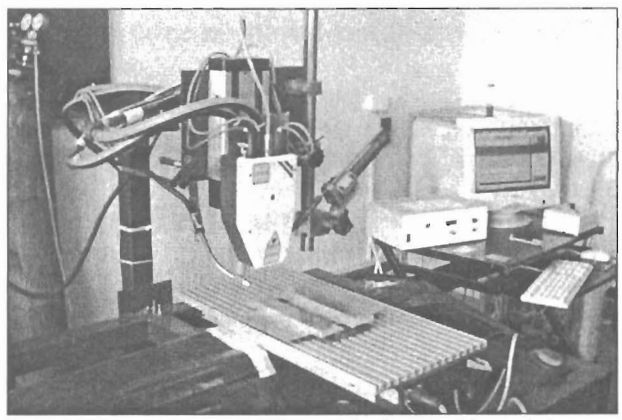


Figure 2. View of experimental setup for laser welding of aluminum alloy butt joints with high power diode laser ROFIN DL 020

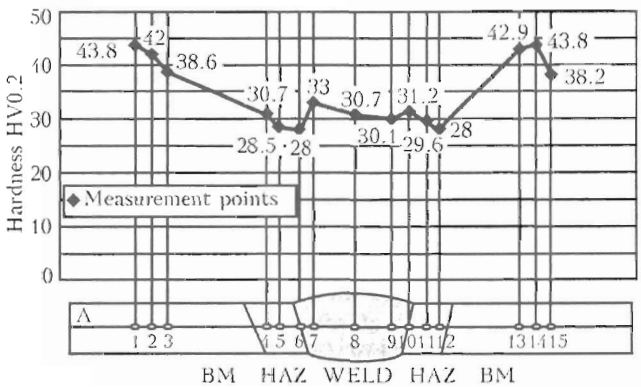


Figure 3. Microhardness HV 0.2 distribution on cross-section of butt joints of aluminum alloy sheets EN AW-1050A 1.0 mm thick, acc. to Table 3 laser beam power of 2.5 kW, welding speed of 1.9 m/min

Table 2. Chemical composition of aluminum alloy sheet EN AW-1050A

Chemical composition [%]									
Al min.	Accepted contamination content								
	Fe	Si	Cu	Mn	Mg	Zn	Ti	other	
								separately	all
99.50	0.40	0.25	0.05	0.05	0.05	0.07	0.05	0.03	–
Mechanical properties									
Thickness [mm]	State of strengthening			*Rm* [MPa]		R_{p02} [MPa]		*A* [%]	
0.8	H24 – semi hard partially recrystallized			105		75		4	
1.0				105		75		4	
1.5	H14 – semi hard			105		85		4	

Table 3. Influence of laser welding parameters with HPDL ROFIN DL 020 laser on mechanical properties of butt joints of aluminum alloy sheets EN AW-1050A 0.8, 1.0 and 1.5 mm thick

Butt joint 0.8 mm thick					
Laser power [kW]	Welding speed [m/min]	Rm^* [MPa]	Area of sample breaking	Angle of bending from weld face	Angle of bending from weld root
1.5	1.1	73	HAZ	180°	180°
1.7	1.65	78	HAZ	180°	180°
2.5	1.85	74	HAZ	180°	180°
2.5	2.63	73	HAZ	180°	180°
Butt joint 1.0 mm thick					
Laser power [kW]	Welding speed [m/min]	Rm^* [MPa]	Area of sample breaking	Angle of bending from weld face	Angle of bending from weld root
1.5	0.8	80	HAZ	180°	180°
1.8	1.35	83	HAZ	180°	180°
2.5	1.3	72	HAZ	180°	180°
2.5	1.9	75	HAZ	180°	180°
Butt joint 1.5 mm thick					
Laser power [kW]	Welding speed [m/min]	Rm^* [MPa]	Area of sample breaking	Angle of bending from weld face	Angle of bending from weld root
2.0	0.7	85	HAZ	180°	180°
2.3	1.0	82	HAZ	180°	180°
2.5	0.85	84	HAZ	180°	180°
2.5	1.25	85	HAZ	180°	180°

Remarks: * – results for mean value of three samples, focal length 82 mm, top surface of joint was covered by black absorbent.

protected by argon flow via cylindrical nozzle 12 [mm] in diameter at constant flow 10 [l/min]. The results of mechanical tests, metallographical analysis and microhardness tests are given in Tables 3 and 4 and Figures 3–6.

Summary. Study of the HPDL laser welding process of butt joints of aluminum alloy sheets EN AW-1050A of 0.8, 1.0 and 1.5 [mm] thick, showed that the black absorbent applied on the top surface of joint increases significantly the absorption of laser beam energy. Thanks to higher absorption of laser beam energy high quality joints can be produced in a wide range of laser parameters, Table 3, Figure 6. As a result of grains recrystallization of the strengthen base material, microhardness in the area of HAZ is significantly lower compared with base material and also plasticity of HAZ and weld metal was increased, Figure 3, 4 and 5, Table 4. During tensile tests the samples

Table 4. Results of microhardness HV 0.2 tests determined for butt joints of aluminum alloy sheets EN AW-1050A 0.8, 1.0 and 1.5 mm thick acc. to Table 3

Joint thickness [mm]	Welding parameters P [kW], V [m/min]	Base material			HAZ			Weld			HAZ			Base material		
		Points, Figure 3														
		1	2	3	4	5	6	7	8	9	10	11	12	13	14	15
0.8	1.5, 1.1	33.6	36.4	37.1	27.1	25.8	26.6	25.3	28.5	28.5	25.8	26.6	26.2	22.6	24.5	35.6
	1.7, 1.65	35.6	34.5	20.2	22.3	18.4	20.4	21.9	21.3	23.0	23.4	23.4	25.3	26.2	35.6	38.6
	2.5, 1.85	37.1	36.4	33.6	23.0	24.9	24.5	28.5	28.0	25.8	26.2	22.3	22.6	28.5	37.1	37.1
	2.5, 2.63	39.4	37.1	35.6	21.9	21.0	20.4	29.6	27.1	26.6	24.5	29.6	22.3	33.6	37.1	37.1
1.0	1.5, 0.8	38.6	37.1	40.2	29.6	28	30.7	29.0	31.2	29.0	28.5	29	26.6	24.9	35.6	37.1
	1.8, 1.35	42.0	39.4	38.6	27.1	26.6	24.9	26.6	23.7	24.1	27.1	25.3	24.5	22.3	38.6	42.0
	2.5, 1.3	42.9	42.0	37.1	26.6	28.5	27.1	29.6	29.0	29.0	27.1	27.1	27.1	24.9	40.2	37.1
	2.5, 1.9	43.8	42.0	38.6	30.7	28.5	28.0	33.0	30.7	30.1	31.2	29.6	28.0	42.9	43.8	38.2
1.5	2.0, 0.7	39.4	36.4	23	24.9	22.6	25.3	25.3	26.6	26.6	27.1	25.8	25.3	39.4	42	42.9
	2.3, 1.0	37.1	38.6	36.4	27.1	25.8	27.1	27.6	26.6	26.6	29.6	26.2	25.8	23.4	42.0	40.2
	2.5, 0.85	40.2	40.2	27.1	29.6	29.0	28.0	28.0	24.9	27.6	27.6	27.6	27.6	26.2	37.1	42.0
	2.5, 1.25	45.8	41.1	37.8	28.5	28.5	28.0	28.0	27.1	26.2	29.6	26.6	28.0	24.9	39.4	42.0

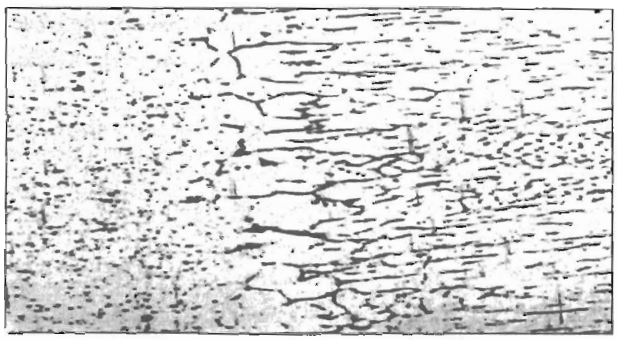


Figure 4. Microstructure (×200) of HAZ in butt joint of aluminum alloy sheets EN AW-1050A 0.8 mm thick, acc. to Table 3 laser beam power of 2.5 kW, welding speed of 0.4 m/min. Base material from left. Etching by Keller reagent

were breaking in area of HAZ and the tensile strength was at level approximately 70% of the strength of base material, Table 3. High plasticity of the joints was proven by bending tests carried out for bending from weld face side and also from weld root side, Table 3. To ensure mechanical properties of the joints at level

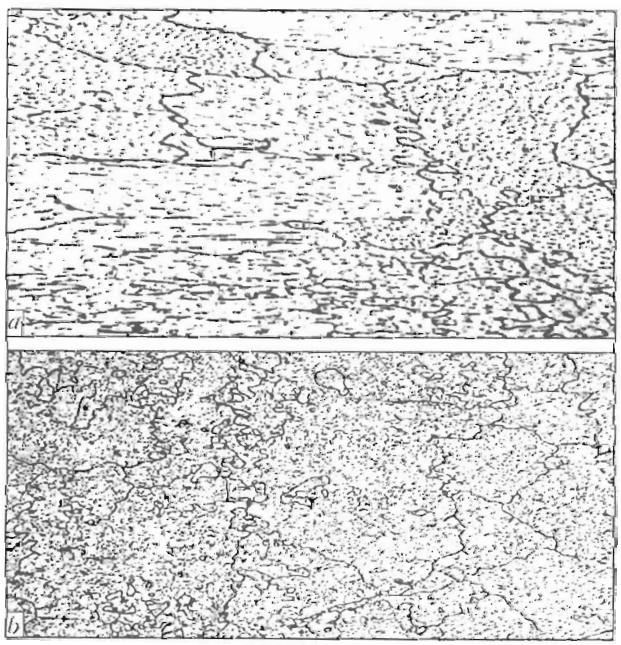


Figure 5. Microstructure (×200) of butt joint of aluminum alloy sheets EN AW-1050A 1.5 mm thick, acc. to Table 3 laser beam power of 2.5 kW, welding speed of 0.85 m/min: *a* – microstructure of HAZ, *b* – microstructure of weld metal. Etching by Keller reagent

not lower than properties of base material, a heat treatment of the joints after laser welding is required [1]. To produce high quality butt joints of aluminum alloy sheets, prior to HPDL laser welding of the edges of joints must be precisely prepared and the top surface

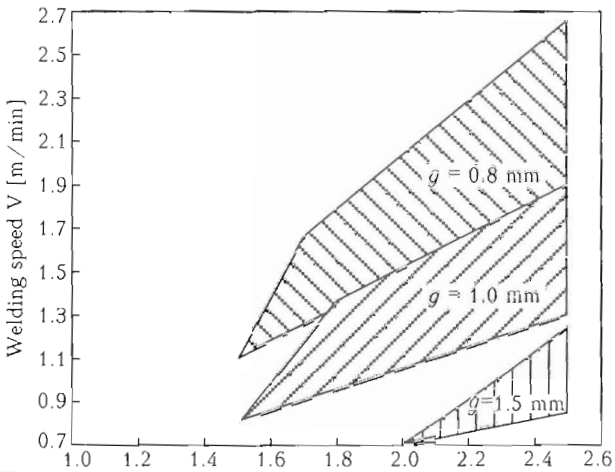


Figure 6. Fields of optimal parameters for laser welding of butt joints of aluminum alloy sheets EN AW-1050A 0.8, 1.0 and 1.5 mm thick using high power diode laser HPDL ROFIN DL020. Focal length 82.0 mm, shielding gas flow 10.0 l/min

must be covered by black absorbent to increase the absorption of laser beam energy. Initial tests of HPDL laser welding of aluminum alloy sheets using activating flux ActivaTec 500, originally designed for GTA welding, showed that the welding speed can be additionally increase up to 30 [%] but the quality of joints was unacceptable because of oxides inclusions inside the weld metal. Further investigations of HPDL laser welding process will be concentrated on applications of activating flux AT 1000, originally designed for GTA welding of aluminum alloys.

1. *Welding Handbook*. Materials and Applications. – Part 1, AWS, 1996, Ed. 8, vol. 3, Aluminum and aluminum alloys, 257–306.
2. Miller W.S. et al. *Recent development in aluminum alloys for the automotive industry*. Materials Science & Engineering A280, 2000, 37–49.
3. Venkat S., E. Albight C., Rammasamy S., Hurley J. P. *CO_2 Laser Beam Welding of Aluminum 574-O and 6111-T4 Alloys*. Welding Journal. 1997, vol. 76, no.7, 275–282.
4. Klimpel A. *Spawanie, zgrzewanie i ciecie metali*. WNT. Warszawa, 1999.
5. Klimpel A. *Lasery diodowe duzej mocy w spawalnictwie*. Przeglad Spawalnictwa. 1999, no 8, 1–8.
6. Pastor M., Zhao H., Martukanitz R. P., Debroy T. *Porosity, Underfill and Magnesium Loss During Continous Wave Nd: Yag Laser Welding of Thin Plates of Aluminum Alloys 5182 and 5754*. Welding Journal. 1999, vol. 78, no. 6, 207–216.
7. Klimpel A., Lisiecki A. *Spawanie polwyrobow karoseryjnych laserem diodowym duzej mocy*. Przeglad Spawalnictwa 1999, no 12, 1–6.
8. Bleidtner. J., et al. *Experiments relating to deep welding using a fibre-contact high- power diode laser*. Welding & Cutting. Schweissen und Schneiden. 2000, vol. 52, no. 4, E.78–E.83.
9. Kuo M., Sun Z., Pan D. *Laser welding with activating flux*. Science and Technology of Welding and Joining. 2001, Vol.6, no.1, 17–22.

SYNTHESIS OF A POROUS COATING ON NiTi SHAPE MEMORY ALLOY BY LASER SURFACE ALLOYING FOR ENHANCED OSTEOINTEGRATION

H. C. MAN[1], S. ZHANG[1], X. GUO[2]
[1]Department of Industrial and Systems Engineering, Laser Processing Centre, Hong Kong
[2]Department of Rehabilitation Science, Hong Kong Polytechnic University, China

To facilitate the in-growth of cells to the implant of Nickel Titanium for enhanced fixation, porous NiTi implants have been investigated by many scientists recently. Porous NiTi component can be fabricated by conventional powder sintering method. However, the mechanical properties such as the strength, superelastic and shape memory characteristics of the porous structure are worse than conventional NiTi alloy. The feasibility of using such porous component for implant is therefore questionable. This paper reports the results of our investigation on the fabrication of a porous surface on NiTi substrate. By using laser surface alloying method, a 0.8 mm thick porous coating with open and connected pores were successfully fabricated on NiTi substrate. Metallurgical bonding between the porous coating and the substrate was found. The corrosion properties of the coated specimen was investigated.

Introduction. Among the important biocompatible metallic alloys, NiTi shape memory alloy, a relatively new biomaterial, has attracted immense research interest because of its unique properties such as pseudoelasticity, damping capacity and shape memory effect. However, as similar to other metallic alloys, the strength of this alloy is higher than that of the human bone. The mismatch between the alloys and the bone would induce stress shielding effect and result in bone degradation. In addition, the compact surface of the alloy is very different from the porous nature of human bone. This unavoidably limits the fixation of the implants with the body tissue and also affects the transport of body fluid. To overcome these problems, porous biocompatible metals have been produced by powder sintering method (1–8). The open porous structure makes the in-growth of the bone tissue into the body of the implant possible and enhances fixation of the implant-bone system. However, it is unclear whether the mechanical properties and shape memory effect of the completely porous NiTi SMAs are adequate if the implant is for load bearing, i.e. the skeletal system. Another approach is to fabricate a porous coating with a gradient of porosity on a solid substrate. The corresponding Young's modulus would change from the value of the compact material down to the level of cortical bone. This paper reports the result of our feasibility study of fabricating such a graded porous NiTi SMAs coatings on a compact NiTi substrate using laser surface alloying technique.

Experimental details. NiTi plates of nominal composition of Ni49.2 at % and Ti–50.8% was used as the substrate material. The plate was cut into specimen of size of 40 × 25 × 5 mm and then sandblasted and cleaned thoroughly. NiTi alloy powder (Ni 49.6 at %, Ti 50.4 at %) of particle size of 43 μm and commercial pure Titanium Hydride powder of average particle size of 38 μm were mixed at different ratio to form a paste using polyvinyl alcohol as the binding agent. The powder mixture was then pasted on the specimen and the paste thickness was controlled at 0.7 mm. Laser surface alloying of the specimen was carried out inside a gas chamber. Nitrogen of 99.95% purity was flowed through the chamber to maintain a nitrogen atmosphere for the surface alloying and gas nitriding process. In some experiment, a mixture of Argon and Nitrogen were used to study the nitriding effect during the alloying process.

A high power Nd-YAG laser was used for the surface alloying process. The power, speed, Nitrogen and Argon ratio in the gas chamber were varied After some preliminary experiments, a set of parameters (25 mm/s, 600 W power, 3 mm diameter) was chosen for surfacing by overlapping individual tracks at 50% track width interval.

Results and discussions. Based on the cross section micrographs of a series of specimens using various laser processing parameters and powder mixtures, it was found that the aspect ratio (height to width) of the individual track was influenced by the laser energy

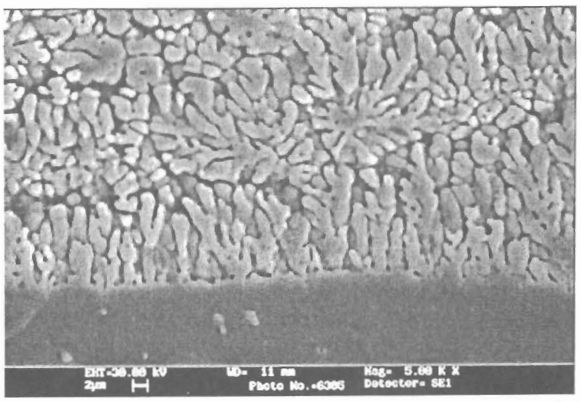


Figure 1. Cross-section micrograph of a specimen using 100%TiH_2 powder, 1 kW, 25 mm/s, 30 l/min N_2, acid etched

© HC MAN, S ZHANG, X GUO, 2005

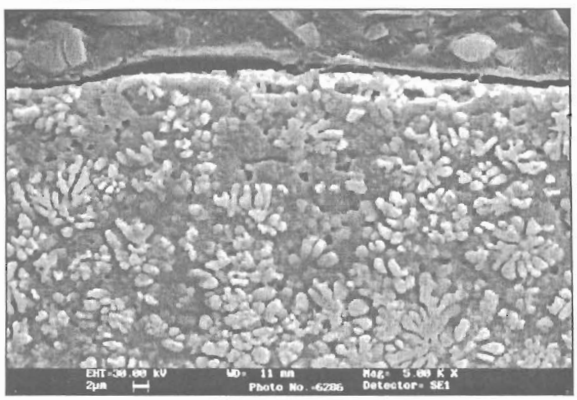


Figure 2. Specimen with 60%TiH_2–40%NiTi powder mixture on NiTi substrate, 1 kW, 25 mm/s, 30 l/min N_2

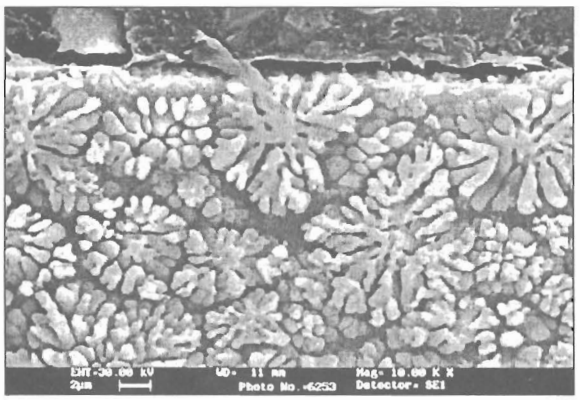


Figure 3. Specimen with 40%TiH_2–60%NiTi powder mixture on NiTi substrate, 1 kW, 25 mm/s, 30 l/min N_2

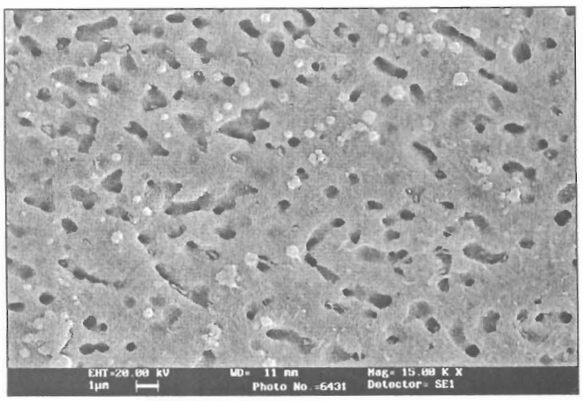


Figure 4. Top surface of speciment with 40%TiH_2–60%NiTi, 0.6 kW, 25 mm/s, 30 l/min N_2. Note the interconnected pores

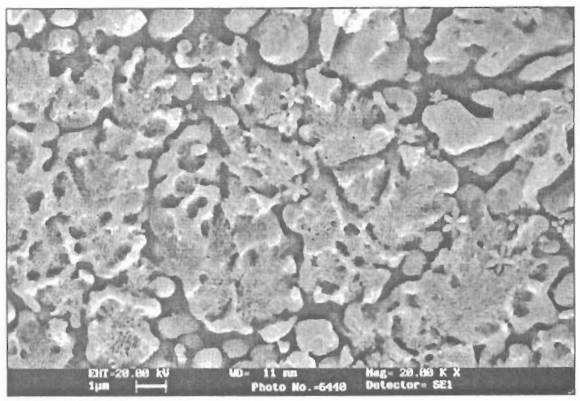


Figure 5. Same as in Figure 4 except 0.8 kW, polished and acid etched. Note the coral structure within the Ti_2Ni dendrites

input and the composition of the powder mixtures. The effect of laser energy input is well expected that the higher the energy input, the more substrate of solid NiTi was melted and therefore a wider track was formed. It was found that the higher the percentage of TiH_2 in the powder mixture, the lower the aspect ratio the individual track was found. This was due to the energy gained from the exothermic reaction when TiH_2 is dissociated under the irradiation of the laser beam. The heat of formation of TiH_2 is $-$ 80.3 kJ/mol. The extra energy resulted from the exothermic reaction effects the formation of wider track.

The integrity of the coated layer is also affected by the processing conditions and the composition of the powders. Generally it was found that at the same processing conditions and low dilution with the substrate, the higher the percentage of TiH_2, the higher the tendency of cracking of the coated layer. Since the cladding process was carried out in a nitrogen rich atmosphere, the dissociated and nascent Ti has a tendency to react with Nitrogen to form TiN phase which has the appearance of flower like structure, as shown in Figure 1 (100% TiH_2 powder on NiTi substrate). According to X-ray spectrum, the main phases are Ti_2Ni and TiN. The interface between the substrate and the coated layer is of metallurgical type and epitaxial growth of the dendrites at the interface is clearly shown in Figure 1.

Figure 2 and 3 show the microstructures of the laser surface alloyed specimens using 60%TiH_2–40%NiTi and 40%TiH_2–60%NiTi powder mixture respectively. It can be seen that the amount of the matrix phase of NiTi increases correspondingly.

Figure 4 shows the micrograph of the top surface of a laser surface alloyed specimen using 40%TiH_2–60%NiTi as the powder mixture, 0.6 kW laser power, 25 mm/s processing speed and 30 l/min Nitrogen gas flow rate. The top surface was ground flat and no chemical etching has been carried out. It can be seen that the porosities are interconnected in a three dimensional manner. The size of the porosity is in the order of 1–5 micron. It was reported by other researchers that for the bone cell to anchor successfully to a porous structure, the ideal porosity size should be in the order of 200–400 micron. The sizes of the pores formed in the present study are a long way short of that. Nevertheless, it is believed that the small size porosities formed in this work could help the deposition of hydroxapatite and other cell deposition function. Some more work will be carried out to address these points. Figure 5 shows another top surface micrograph at a higher magnification. The specimen details are 40%TiH_2–60%NiTi 0.8 kW, 25 mm/s, 30 l/min N_2, acid etched after polishing. It is clearly shown in the figure the coral structure within the $NiTi_2$ phase.

Another advantage of fabricating the porous layer on NiTi solid substrate using the method developed from this work is the reduction of Ni content at the surface. Because of the extra supply of Ti from TiH_2,

the stable compound formed at the surface are mostly $NiTi_2$. SEM EDAX results indicated that the Ni content has been reduced from 49.2 at% to 12.5 at% at the outmost surface. The reduction will greatly alleviated the potential release of Ni into the body fluid system.

The corrosion properties of the alloyed porous layers (40%TiH_2–60%NiTi powder mixture) in Hanks' solution, 310 K, are similar to the NiTi, substrate, as shown in Figure 6. The porous structure therefore does not affect the corrosion characteristics of NiTi.

CONCLUSIONS

By laser surface alloying a 40%TiH_2–60%NiTi powder mixture on the surface of NiTi using optimised laser process parameters, a porous NiTi layer can be fabricated on the NiTi substrate. The metallurgical interface between the porous layer and the substrate assures excellent bonding strength between them. The pores, in the range of 1–4 micron in dimension, are interconnected three dimensionally. The Ni content of the porous layer was found much less than that of the original NiTi surface. Possible biomedical application for this porous surface with good mechanical strength provided by the substrate are being sought.

Acknowledgements. *The work described in this paper was fully supported by a grant from the Research Grants Council of the Hong Kong Special Administrative Region, China (Project No. PolyU 5190/02E). Support from the infrastructure of the Hong Kong Polytechnic University is also acknowledged.*

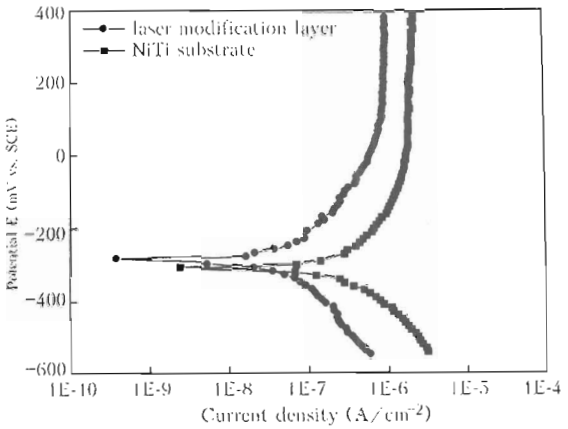


Figure 6. Polarisation curves of NiTi and specimen of Figure 4. Hanks solution, 310K

1. Li B.Y., Rong L.J., Li Y.Y., Gjunter V.E. Acta Mater. 48 (2000) 3895–3904.
2. Kujala S., Ryhanen J., Danilov A., Tuukkanen J. Biomaterials 24 (2003) 4691–4697.
3. Entchev P.B., Lagoudas D.C., Mech. Mater. 34 (2002) 1–24.
4. Chu C.L., Chung C.Y., Lin P.H., Wang S.D. Mater. Sci. Eng. A, 366 (2004) 114–119.
5. Castillo M., Moore J.J., Schowengerdt F.D., Ayers R.A., Zhang X., Umakoshi M., Yi H.C., Guigne J.Y. Advances in Space Research, 32 (2003) 265–270.
6. Kang S.B., Yoon K.S., Kim J.S., Nam T.H., Gjunter V.E. Mater. Trans. 43 (2002) 1045–1048.
7. Hey J.C., Jardine A.P. Mater. Sci. Eng. A, 188 (1994) 291–300.
8. Li B.Y., Rong L.J., Li Y.Y. Mater. Res. 13 (1998) 2847–2851.

APPLICATION OF HIGH-POWER FIBRE LASERS IN LASER AND LASER-MIG HYBRID WELDING

C. THOMY, H. KOHN, F. VOLLERTSEN
BIAS-Bremen Institute of Applied Beam Technologies GmbH, Germany

Latest developments in laser physics have enabled the production of high-power fibre lasers with beam powers up to 10 kW at excellent beam quality. Adding to these properties their high energetic efficiency, their considerable estimated lifetime and their compact size, they might well be considered to be a viable alternative to both conventional lamp- or diode- pumped Nd:YAG- as well as to CO_2-lasers. However, due to the novelty of the system, very few experiences on their usability for materials processing and in special for welding of steel and aluminium sheet material are existing. To help this situation, both a 7 kW and a 10 kW high-power fibre laser system have been tested by BIAS, and their potentials for welding steel and aluminium sheets have been assessed. By the help of these results for pure laser and laser GMA hybrid welding, of which a selection is presented here, it could indeed be demonstrated that it is possible to remarkably enhance process limitations considering welding speed and sheet thickness previously regarded to be inevitable when welding with solid-state lasers.

Introduction. New developments in laser physics have recently enabled the construction of novel type laser sources such as the disc laser or the high-power fibre laser. The high-power fibre laser in special has undergone a rapid development in the past three years and could (not least due to its modular structure) be scaled from a few hundred Watts up to 10 kW and more [1]. Currently, it is commercially available with beam powers up to 10 kW, thus possessing a sufficient beam power for the vast majority of applications in laser materials processing. However, these systems still have to be qualified e.g. for laser and laser GMA hybrid welding processes [2].

The fibre laser just like the Nd:YAG-laser belongs to the large group of solid-state lasers. The laser-active medium normally consists of a glass fibre doped with Ytterbium and optically pumped by diodes at the ends and through the cladded shell surface by bragg grating. The wavelength is 1070+/−5 nm.

This novel type laser has various advantages. Its efficiency (up to 25%) exceeds the efficiency nowadays achievable with lamp- or diode-pumped Nd:YAG-Lasers. Due to the improved beam quality (2003: BPP 17.5 mm·mrad for a 10 kW system, 8.5 mm·mrad for a 5 kW system; 2004: 12.5 mm·mrad for a 10 kW system, 5 mmpmrad for a 5 kW system; source: IPG) compared to lamp-pumped systems (BPP typically around 25 mmpmrad at 4 kW) smaller fibre diameters can be used, thus enabling increased power densities in the focal spot. Moreover, the beam source is extraordinarily compact taking into account its beam power and (due to robust construction, low power supply as well as the long fibre lengths up to 200 m) is fit for flexible and potentially mobile use especially for those fields of application currently not accessible to laser technology. In view of operating costs, the lifetime of the pumping diodes is of crucial importance. It is expected to be significantly longer than for other diode-pumped beam sources.

Properties of the Beam Source. In table 1, a comparison of some basic beam parameters of the high-power fibre lasers YLR 7000 and YLR 10000 with those of the diode-pumped Nd:YAG-Laser Trumpf HL 4006D, the diode-pumped Nd:YAG-Laser Rofin DY044 and the CO_2-lasers Trumpf TLF 6000 and TLF 15000 at their respective maximum beam powers is given. All measurements have been carried out by BIAS.

The YLR 10000 fibre laser (Figure 1), less than one year after the YLR 7000 system, comes with a significantly improved performance in terms of both output power and beam quality. It delivers 10 kW to the work piece through a 200 µm fibre and is typically focused by a set of 125 and 200 mm optics for collimation and focusing, respectively to a beam diameter of 360 µm. The beam parameter product is as low as

Table 1. Comparison of basic beam parameters for various laser systems (BIAS)

		YLR 7000	YLR 10000	HL 4006D	DY 044	TLF 6000	TLF 15000
Max. beam power at work piece	[kW]	6.9	10	4.0	4.2	5.5	13.6
Fibre core diameter	[µm]	300	200	600	400	–	–
Focal length (typical)	[mm]	200	200	150	200	350	300
Beam diameter (focus)	[µm]	510	360	430	434	262	512
BPP	[mm·mrad]	18.5	11.6	23.9	15.7	6.7	15.3

© C. THOMY, H. KOHN, F. VOLLERTSEN, 2005

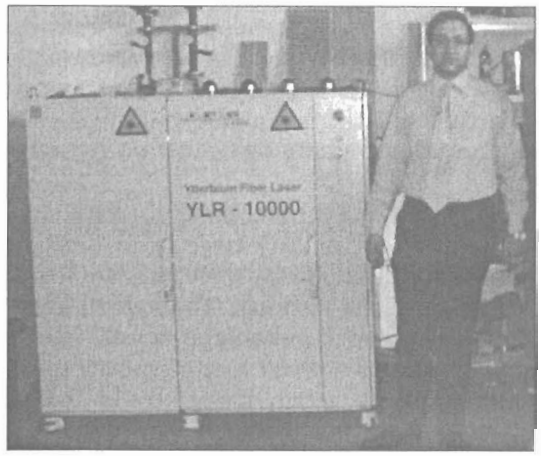


Figure 1. High-power fibre laser IPG YLR 10000

11.6 mm·mrad. Moreover, due to a compact design this laser has a very small footprint. The wall plug efficiency is 25% (source: IPG).

It may be concluded from tab. 1 that the high-power fibre lasers have beam properties comparable or superior to those of the diode-pumped Nd:YAG-Laser. The BPP of both fibre lasers is still higher than the BPP of the CO_2-laser with 6 kW maximum beam power. However, both fibre lasers have surpassed the YAG laser systems in terms of both power and beam quality, and that they are now approaching the performance of CO_2-lasers in this respect.

Welding Performance in Steel and Aluminium. To assess the potentials of both fibre laser systems, bead-on-plate welds have been performed for various steel (mild steel S235 JR, pipeline steel X70, austenitic stainless steel 1.4404) and aluminium materials (AA 5083, AA6056 and AA 6082). Shielding gas for all welds was Argon.

It is evident from Figure 2 that both mild steel grades yield a similar penetration depth at a given welding speed. Roughly, a penetration of 8, 6 and 4 mm was achieved at 3, 6, and 11 m/min. For the stainless steel grade, the attainable welding speed was significantly (up to 50%) higher compared to the mild steel grades. The most noticeable observation, however, is the penetration depth in the two aluminium materials which is by far superior in particular with

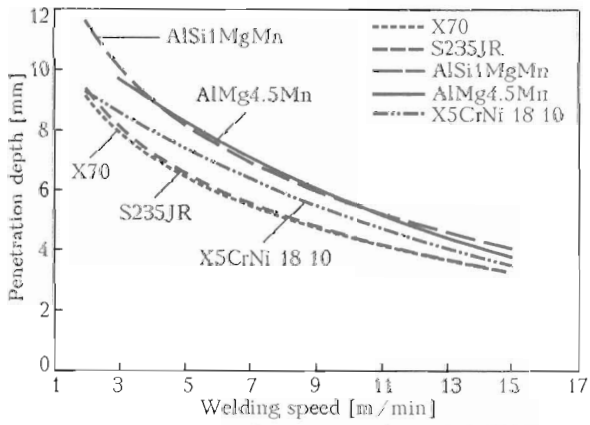


Figure 2. Penetration curves for a variety of materials (YLR 10000, focal position $z = 0$, P_L = 10 kW, Precitec YW50, f = 200 mm, coaxial shielding gas supply, Ar 20 l/min)

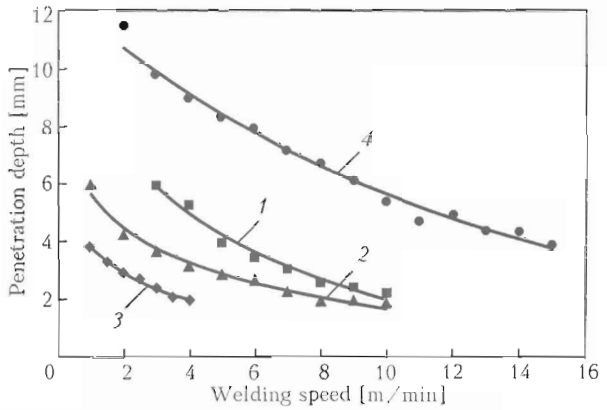


Figure 3. Penetration for various laser systems in aluminium (6XXX) (P_L = max, $z = 0$, f = 200 mm): *1* — 6.9 kW high power fibre laser YLR 7000; *2* — 4 kW diode pumped Nd:YAG laser DY044; *3* — 4 kW lamp pumped Nd:YAG laser HL4006D; *4* — 10 kW high power fibre laser YLR 1000

respect to the mild steel grades. For aluminium, a depth of 8, 6 and 4 mm was exceeded at velocities of 5, 9 and 14 m/min, respectively.

From Figure 3 it can be concluded in comparison with other solid state lasers (table 1) that with respect to penetration the 10 kW fibre laser offers a tremendous performance, in particular for aluminium, which can be attributed to the unique combination of laser power and beam quality at a near infrared wavelength, and which to the best of our knowledge outclasses the performance of any other common laser systems.

A typical bead-on-plate weld on aluminium AA 6082 (Figure 4) obtained during the first tests of the IPG YLR 10000 shows a penetration of 10 mm at a welding speed of 3 m/min, which is ca. 2.5 times the penetration achievable with today's diode-pumped Nd:YAG-Lasers of the 4 kW class. The weld is extremely narrow with parallel fusion lines and features a nail-head shape at the top. Moreover, the microstructural integrity of the weld is noticeable. In particular, the level of porosity is comparatively low. This coincides with the observation of a remarkably calm and smooth welding process. Despite of using a monofocus beam with a comparatively small waist diameter of 360 µm, instabilities which are frequently observed

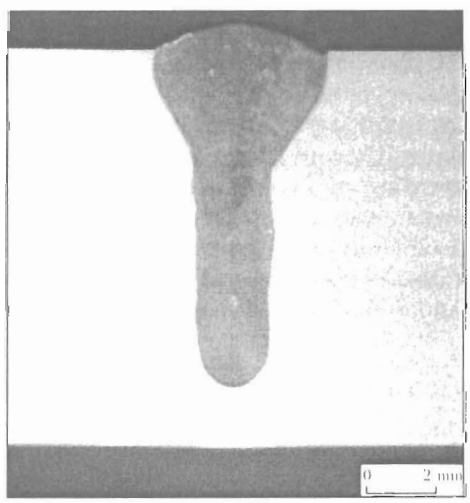


Figure 4. Bead-on-plate weld on AA 6082 (t = 12 mm, P_l = 10 kW, v = 3 m/min)

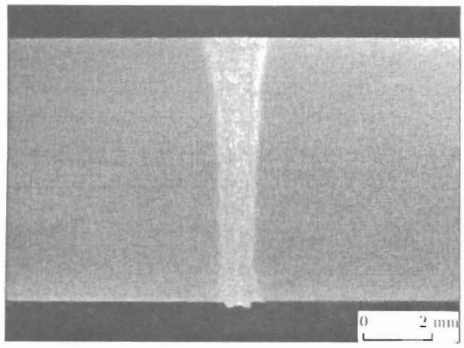


Figure 5. Butt weld of X70 steel (t = 11.2 mm, P_L = 10 kW, v = = 2.2 m/min)

in highly dynamic laser welding processes of aluminium were not detected here.

Another aspect is the sensitivity to variations in focal position e.g. due to positioning tolerances. It was concluded that especially for aluminium for a focal position from $z = -5$ mm to $z = +1$ mm the effect on the penetration depth is rather low. During these tests, which have been performed for both steel and aluminium with perpendicular beam incidence angle, the fibre laser unexpectedly proved to be insensitive considering backreflection problems.

Fibre Laser Applications for Welding of Steel and Aluminium. An example of butt welding of X70 steel is given in Figure 5. At a welding speed of 2.2 m/min, full penetration was comfortably achieved in 11.2 mm material. The weld seam is narrow, and there is only a small reinforcement on both the crown and the root side. No cracks occurred. Currently, BIAS is developing an all-position welding process for this type of material in various thicknesses for pipe laying applications in the field.

For welding of aluminium extruded profiles for the railway industries, the IPG fibre laser YLR 10000 was applied to hybrid welding, too. Figure 6 shows two first results obtained on EN AW 6008 (wall thickness 4 and 8 mm, respectively) with filler wire AlSi 5. Welding speed was 6 m/min in all cases with laser powers up to 10.5 kW for the 8 mm material. The process was very stable and weld quality was acceptable. Further optimisation might result in even higher welding speeds especially for a wall thickness around 4 mm.

These results have been rated so promising that further tests to pre-qualify fibre laser GMA hybrid welding for welding railway structures are scheduled.

Conclusions and outlook. The experimental studies on welding with both high-power fibre lasers performed by BIAS showed very promising results for all materials investigated. Especially in comparison with lamp-pumped or diode-pumped Nd:YAG lasers, a significant enlargement of the process window towards higher welding speeds and thicker materials could be realized due to the higher beam power at competitive beam quality of the fibre laser. With this highly promising laser, the BIAS Bremer Institut fur angewandte Strahltechnik GmbH – aside from other applications – intends in cooperation with their partners from industry to open those applications for laser welding which up to now have not or not successfully used laser sources only due to their properties disadvantageous for their applications.

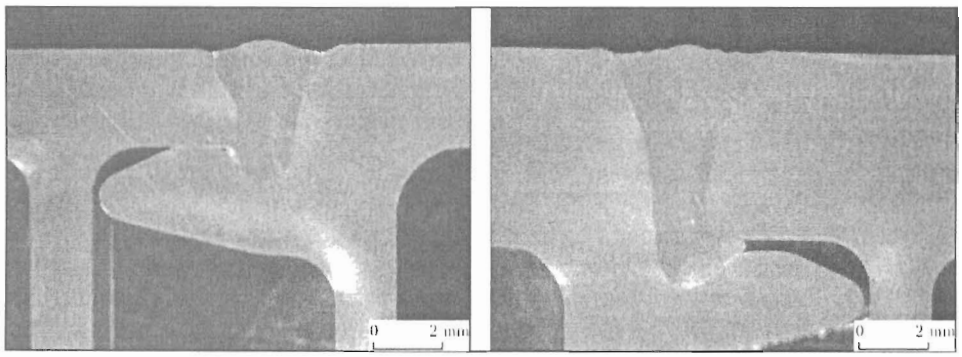


Figure 6. First fibre laser GMA-hybrid welds (EN-AW 6008, 4 mm and 8 mm)

Acknowledgements. *The authors are particularly grateful to the Deutsche Forschungsgemeinschaft for funding considerable parts of the study in the framework of the Gottfried-Wilhelm-Leibniz-Programm (VO530/7).*

1. Grupp M., Sepold G. *Laser System Technology.* In: Landolt-Bornstein Laser Applications, Gruppe 8: Advanced Materials and Technologies, Band1/Teilband C: Laser Physics and Laser Applications, Springer Verlag Berlin, Heidelberg, New York, 2004.
2. Thomy C., Grupp M., Seefeld T. Vollertsen, F.: *Schweiben mit dem Hochleistungs-Faserlaser.* In: «Strahltechnik». – Vortrage der 6. Konferenz «Strahltechnik» in Halle vom 26. bis 28. April 2004. Halle, Deutschland, 26–28. April 2004, 39–45.

KINETICS OF OPTICAL DISCHARGE IN PLASMA PLUME DURING LASER WELDING IN SHIELDING GAS*

G. TURICHIN[1], V. LOPOTA[1], E. ZEMLIAKOV[1], E. POZDEEVA[1], A. GRIGORIEV[1], A. GUMENYUK[2], U. DILTHEY[2]
[1]Institute of Laser and Welding Technology of St. Petersburg TU, Russia
[2]ISF-Welding and Joining Institute, RWTH, Aachen, Germany

Article devoted to the analytical description of ionization degree in plasma plume during laser welding. A model of non-equilibrium two-component plasma was used. For description of chemical composition of plasma plume the problem about axial symmetrical submerged jet of hot metal vapor, flowing to cold shielding gas, has been solved in boundary layer approximation. Developed approach allows to determine a refraction index distribution in the plasma plume. The interferometry experiments was made for verification of developed model.

The theoretical descriptions of laser induced and hybrid plasma are usually supposed as thermodynamic equilibrium. The temperature of equilibrium plasma is defined ionization degree and others plasma parameters [1]. However, supposition about thermodynamic equilibrium of plasma is not correct for optical and hybrid discharge. Arc discharge plasma is really near equilibrium condition, but for laser induced plasma the electron energy distribution is not Maxwellian, i.e. supposition of thermodynamic equilibrium is not correct [2]. So the description of laser induced plasma, and also of plasma combined laser-arc discharge is to be developed in the view of kinetic approach. For description of the macroscopic characteristic of such a plasma, it is necessary to solve a Raiser kinetic equation [3] for electrons energy spectrum, like it was done for laser induced plasma in the keyhole [2], taking into account the rate of electron energy increases due to arc electric field and chemistry of plasma plume.

To take into account real chemistry of plasma it is necessary to introduce probabilities of electrons collision with ions and atoms of different elements in plasma which are proportional to local concentrations of these elements. The element concentration field of plasma is determined from mixture task.

For the calculation of spatial components distribution in the plasma plume during laser-arc welding it is necessary to solve a gas-dynamic task about subsonic hot metal vapor jet in cold shielding gas with consideration of heat conductivity and vapor-gas diffusion. The numerical schemes [4] or well-known analytical solution for non-compressive submerged jet [5] are usually applied for calculation of the parameters of steam-jet plasma vapor. The approximate analytic description of plasma plume in vapor jet — shielding gas mixture with consideration of heat conductivity, diffusion and compressibility effects is a subject of present paper.

Formulation of jet dynamic problem. Introducing metal vapor concentration as «C», it is possible to write $\rho_g = (1 - C)\rho$; $\rho_V = C\rho$, where ρ — total mixture density, ρ_g — shielding gas density, ρ_V — vapor density.

Using boundary layer equation in cylindrical coordinates according to [6] for description of jet velocity field one can write:

$$\rho\left(V_z\frac{\partial V_z}{\partial z} + V_r\frac{\partial V_z}{\partial r}\right) = \frac{\partial}{\partial r}\left(\mu\frac{\partial V_z}{\partial r}\right) + \frac{\mu\partial V_z}{r\partial r} \qquad (1)$$

The diffusion equation can be presented as:

$$\rho V_r\frac{\partial C}{\partial r} + \rho V_z\frac{\partial C}{\partial z} = \frac{1\partial}{r\partial r}\left(r\rho D\frac{\partial C}{\partial r}\right), \qquad (2)$$

in approach of quasi-steady boundary layer. Considering local equality of mixture components temperatures, energy equation we can presented as follows:

$$\rho V_r\frac{\partial h}{\partial r} + \rho V_z\frac{\partial h}{\partial z} = V_z\frac{\partial p}{\partial x} + \frac{1\partial}{r\partial r}\left(\rho\lambda\frac{\partial T}{\partial r}\right) + q, \qquad (3)$$

where q — heat sources density, h — mixture enthalpy. Along with constitutive equation:

$$p = \sum\frac{\rho_i}{\mu_i}RT = \left(\frac{C}{\mu_V} + \frac{1-C}{\mu_g}\right)\rho RT,$$

equations (1)–(4) are complete formulation of metal vapor jet in the gas atmosphere problem. They can be appreciably simplified after introduction of Howarth-Dorodnitsin variables:

$$ydy = \frac{\rho}{\rho_\infty}rdr;\ x = x.$$

Believing that $\rho(r)$ is slowly changes with r, it is possible to assume that in the right part of equation $r^2 \approx \frac{\rho_\infty}{\rho}y^2$. Introducing

* This investigation was supported RFBR (grant 03-02-04030) and DFG (grant 436 RUS 113/774/0-1)

© G. TURICHIN, V. LOPOTA, E. ZEMLIAKOV, E. POZDEEVA, A. GRIGORIEV, A GUMENYUK, U DILTHEY, 2005

$$\tilde{v} = u\frac{\partial y}{\partial x} + v\frac{\partial y}{\partial r}, \qquad (4)$$

one can get equation set as for constant density gas case:

$$\begin{aligned} u\frac{\partial u}{\partial x} + \tilde{v}\frac{\partial u}{\partial y} &= \frac{1\partial}{y\partial y}\left(\frac{\mu}{\rho_\infty} y \frac{\partial u}{\partial y}\right), \\ u\frac{\partial C}{\partial x} + \tilde{v}\frac{\partial C}{\partial y} &= \frac{1\partial}{y\partial y}\left(D\frac{\rho}{\rho_\infty} y \frac{\partial C}{\partial y}\right), \\ u\frac{\partial h}{\partial x} + \tilde{v}\frac{\partial h}{\partial y} &= \frac{1\partial}{y\partial y}\left(\frac{\lambda}{\rho_\infty C_p} y \frac{\partial h}{\partial y}\right). \end{aligned} \qquad (5)$$

The mixture kinetic coefficients μ, D и λ are functions of the enthalpy and concentration values.

Solution of gas mixture task. For diffusion coefficient of mixture components according to [7] it is possible to write:

$$D = \frac{1}{3}\left(\frac{\rho_2}{\rho}\lambda_1\overline{V}_1 + \frac{\rho_1}{\rho}\lambda_2\overline{V}_2\right).$$

Because $\frac{3}{2}kT = \frac{m_1V_1^2}{2} = \frac{m_2V_2^2}{2}$, then for diffusivity one can get $D \approx \frac{1}{3}\lambda\sqrt{3kT}\left(\frac{C_2}{\sqrt{m_1}} + \frac{C_1}{\sqrt{m_2}}\right)$. Mixture viscosity is defined as $\mu = \frac{1}{3}\lambda\sum m_i n_i \overline{V}_i = \frac{1}{3}\lambda\rho\sqrt{3kT} \times \times \sum_i \frac{C_i}{\sqrt{m_i}}$. As long as the main mixture component in submerged jet is surrounded gas, one can assume that $C << 1$. Taking, that scattering cross sections of atom of different mixture components are the same, one can assume that $\sigma_{gg} = \sigma_{gV} = \sigma_{VV} = \sigma$. Then, taking into account that $\lambda = (n\sigma)^{-1}$, $\rho = n\left(\sum\frac{C_i}{m_i}\right)^{-1}$, $C_g = 1 - C$, it is possible to write, taking into account $\frac{m}{M} << 1$:

$$\mu = \mu_\infty\sqrt{\frac{h}{h_\infty}}\left(1 + C\left(\sqrt{\frac{m}{M}} - \frac{m}{M}\right)\right), \qquad (6)$$

where m — gas atom mass, M — vapor atom mass, $\mu_\infty = \frac{\sqrt{3kT_\infty}}{3\sigma}\sqrt{m}$ — surrounded gas viscosity at temperature «on infinity». With consideration of the vapor concentration is small, for diffusivity one can write $D = \frac{\sqrt{3}}{3}\frac{(kT)^{3/2}}{p\sigma m^{1/2}}$, and introducing D_∞, which is suitable to T_∞: $D_\infty = \frac{\sqrt{3}}{3}\frac{(kT_\infty)^{3/2}}{p\sigma m^{1/2}}$, one can obtain:

$$D = D_\infty\left(\frac{T}{T_\infty}\right)^{3/2} = D_\infty\left(\frac{h}{h_\infty}\right)^{3/2}. \qquad (7)$$

Having made the same assumptions and having introduced we get for the heat conductivity:

$$\lambda = \lambda_\infty\left(\frac{h}{h_\infty}\right)^{1/2}\left[1 - C\left(\frac{m}{M} - \left(\frac{m}{M}\right)^{3/2}\right)\right], \qquad (8)$$

where λ_∞ is heat conductivity at temperature «on infinity». In fulfilling conditions $\frac{m}{M} << 1$, $C < 1$ the kinetic coefficients of the mix are entirely determined by the lightweight component. In this case the system (5) assumes an essential simplification. Really, as $D = \mu/\rho$, comparing the first and second of the equations (5), it is easy to be made sure of their full similarity in changing «C» on «u». Hence, a Krocco's integral takes place for the vapor concentration $C = \gamma u + \delta$, and the problem is reduced to solution of the momentum and energy equations from system (6). We shall search flow function and enthalpy as:

$$\psi = xa\left(\frac{y}{x}\right) + a_0\left(\frac{y}{x}\right) + \frac{a_1\left(\frac{y}{x}\right)}{x} + \ldots, \; h = \frac{1}{x}b_1\left(\frac{y}{x}\right) + \frac{1}{x^2}b_2\left(\frac{y}{x}\right) + \ldots \qquad (9)$$

having designated $\frac{y}{x} = \eta$. Substitution of these expressions in system (6) will not allow, as it is done for an incompressible liquid [6], to obtain system of the ordinary hooked equations for functions $a(\eta)$ and $b(\eta)$, having equated factors at exponents of «x». The reason of it is «not exponential» dependence of viscosity and heat conductivity factors on enthalpy. In this case replacement of a square root with linear function (Chapman-Rubezin approximation) will be too rough because of significant change of the mix enthalpy in area of calculation.

Let's designate h_0 — the maximal value of enthalpy. On the interval $[h_\infty; h_0]$ one can approximate $\sqrt{\frac{h}{h_\infty}}$ by square-law function, instead of linear one. It is possible to do, having expanded $\sqrt{\frac{h}{h_\infty}}$ in Taylor series around of a point h^*, laying inside (or on border) this interval.

The numerical analysis shows, that at changing temperature from 300 up to 8000 K and h^*, corresponding 0.7–0.9 h_0, the mistake of approximation does not exceed several percents.

Let's introduce a relative enthalpy

$$\overline{h} = h - h^*. \qquad (10)$$

Substituting (9), (10) in the first and third equations of system (5), having designated to simplify records $\eta = \sqrt{\nu\zeta}$, $a(\zeta) = \nu c(\zeta)$, $b(\zeta) = \nu d(\zeta)$, and equating factors at identical exponents of «x», one can obtain:

$$\left(\frac{c'}{\zeta}\right)'' + \frac{1+c}{\zeta}\left(\frac{c'}{\zeta}\right)' + \left(\frac{c'}{\zeta}\right)^2 = 0, \; -(cd_1)' = \frac{\chi}{\nu}\left(\zeta d_1'\right)', \qquad (11)$$

the stroke designates differentiation on «ζ». First equation of (11) completely coincides with the well-

known solution for equation for the submerged jet of incompressible gas [6]. Integrating (11) in view of the initial conditions, one can obtain:

$$c(\zeta) = \frac{\alpha^2\zeta^2}{1+\frac{1}{4}\alpha^2\zeta^2},\ d_1 = \frac{\beta}{\left(1+\frac{1}{4}\alpha^2\zeta^2\right)^{2\frac{\nu}{\chi}}}, \qquad (12)$$

where the constants α and β are determined by initial conditions. To determine α it is possible to use a condition of momentum flux conservation: $\int_0^\infty 2\pi\rho u^2 r dr = J_0$. Taking into account, that by virtue of Howarth-Dorodnitzin transformation, $\rho r dr = \rho_\infty y dy$, having integrated one can obtain: $\alpha = \left(\frac{3J_0}{16\pi\eta}\right)^{\frac{1}{2}}$. The constant β determines from condition of enthalpy flux conservation: $\int_0^\infty 2\pi\rho h u r dr = \text{const} = W_0$. Taking into account, that $h = \frac{\nu}{x}\frac{\beta}{\left(1+\frac{1}{4}\alpha^2\zeta^2\right)^{2\frac{\nu}{\chi}}}$, after integration one can obtain: $\beta = \frac{\left(1+2\frac{\nu}{\chi}\right)W_0}{8\pi\nu^2\rho_\infty}$. Constants γ and δ in the distribution of vapor concentration $C = \frac{2\alpha^2\gamma}{x}\frac{1}{\left(1+\frac{1}{4}\alpha^2\zeta^2\right)^2} + \delta$ can be determined by the same way. It is obvious, that $\delta = 0$, and one can determine γ from condition of substance flux conservation along the axis «x»: so $\int_0^\infty 2\pi\rho c u r dr = \text{const} = I_0$ as $\gamma = \frac{I_0}{J_0}$.

For calculations of full fluxes of vapor I_0, jet momentum J_0 and enthalpy W_0 on the cavity outlet have been used. The solution of the problem should be transformed to «usual» cylindrical coordinates. Taking into account a connection of density ρ with the gas mix enthalpy «h» and using Howarth-Dorodnitzin formulas, it is possible to write after elementary transformations:

$$h = \left[\left(\frac{\nu\beta}{x}\frac{\chi/2\nu}{1-\chi/2\nu} - \frac{\alpha^2 Pm C_p}{2\eta k x^2}\frac{r^2}{2}\right)\frac{1-\chi/2\nu}{\chi/2\nu\left(\frac{\nu\beta}{x}\right)^{\chi/2\nu}}\right]^{\frac{1}{1-\chi/2\nu}}.$$

Substituting the obtained expression for «h» into expressions for «u» and «C», one can get distributions of velocity and concentration fields of the mix in «physical» coordinates.

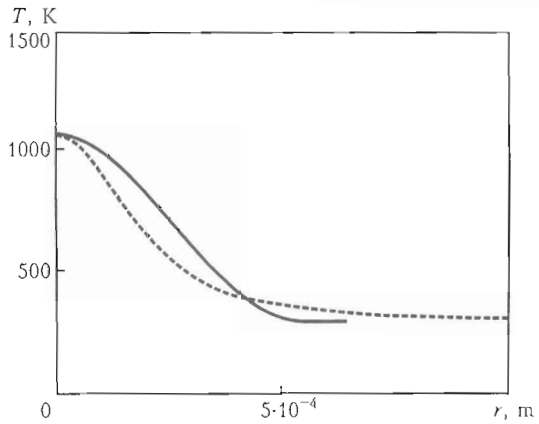


Figure 1. Jet radial temperature distribution 1 cm above surface: solid line — compressible gas; dot line — non-compressible

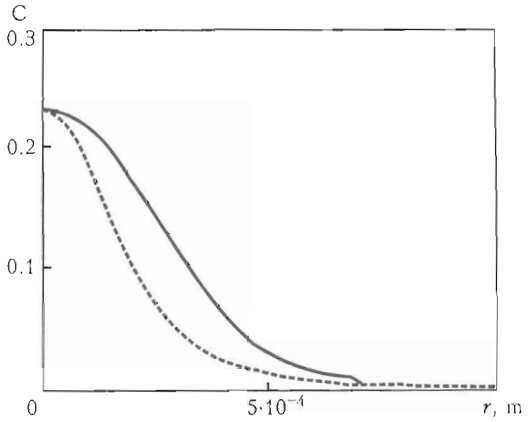


Figure 2. Iron concentration field in jet 1 cm above surface: solid line — compressible gas; dot line — non-compressible

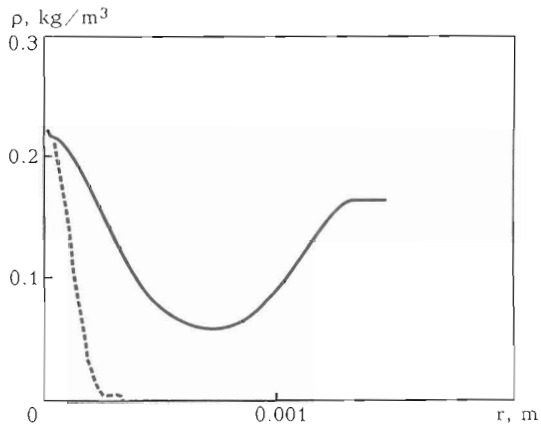


Figure 3. Density distribution on keyhole outlet: solid line — total density; dot line — iron vapor density

The figures 1, 2, 3 shows an examples of calculation of distributions of temperature, mix density and concentration in the iron vapor jet with initial temperature 3000 K, flowing with initial speed 200 m/s into the helium atmosphere of room temperature.

Against the «classical» submerged jet, in considering compressibility, diffusion and heat conductivity of the gas mix the jet becomes physically limited. There is a distance from the axis on which the temperature of the mix becomes in accuracy equal to temperature of the surrounded gas. The radius of the jet rises thus proportionally to a square root of longitudinal coordinate, i.e. the jet has a parabolic rotation shape, instead of a cone, as in a classical case.

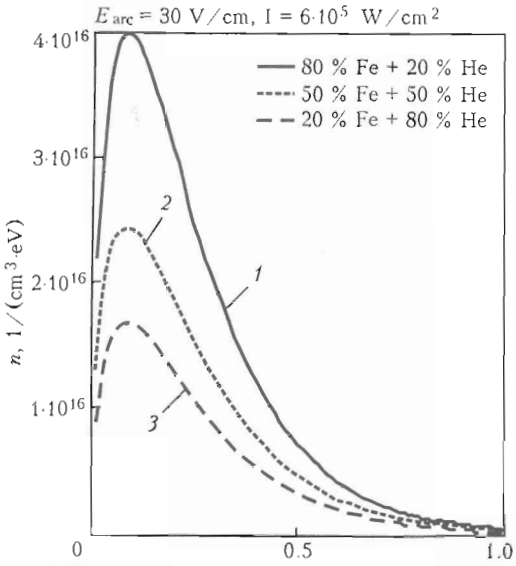


Figure 4. Energy spectrum of plasma electrons for different chemistry

Discharge kinetics in plasma plume. Follow [2], kinetic equation for energy spectrum of plasma electrons can be written as:

$$\frac{\partial n(\varepsilon)}{\partial t} = \frac{\partial}{\partial \varepsilon}\left[A\varepsilon^{3/2}\frac{\partial}{\partial \varepsilon}\frac{n(\varepsilon)}{\varepsilon^{1/2}} + 2m\,\varepsilon\, n(\varepsilon)\sum_{j=1}^{4}\frac{\nu_{tj}}{M_j}\right] \quad (13)$$

where:

$$A = \frac{e^2}{3m}\left\{\frac{2E_d^2}{4} + \frac{E_l^2\sum_{j=1}^{4}\nu_{tj}}{2\left[\sum_{j=1}^{4}\nu_{tj}\right]\left[\left(\sum_{j=1}^{4}\nu_{tj}\right)^2 + \varpi^2\right]}\right\},$$

E_d — strength of arc field; $E_l = \left(\frac{8\pi}{c}I\right)^{1/2}$ — strength of laser field; I — laser radiation intensity; $\nu_{tj} = \nu_e\sigma_{trj}N_j$ — collision rate of electrons with heavy particles of j kind; v_e — electron velocity; σ_{trj} — transport cross-section of electron scattering on particle of j kind; M_j — mass of heavy particle (atoms, ions) of j kind; N_j — j kind particles concentration.

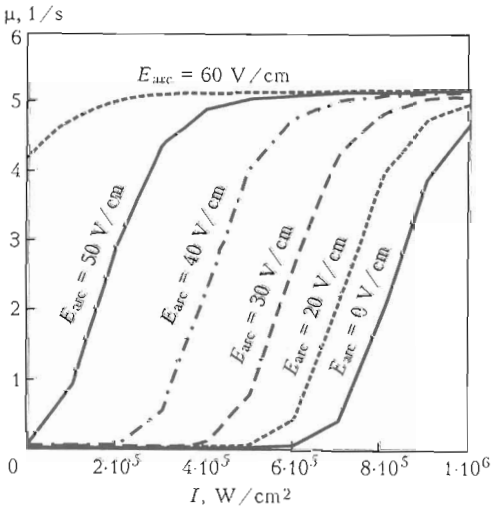


Figure 5. Absorption factor μ versus laser beam intensity for different arc field strength (100% Fe)

Boundary conditions:

$$1.\ -\frac{A}{2}n\Big|_{\varepsilon=0} = 2\left(A\varepsilon\frac{\partial n}{\partial \varepsilon} - \frac{A}{2}n + \frac{2m}{M}\sum_{j=1}^{4}\nu_{tj}\varepsilon n\right)\Big|_{\varepsilon=J}$$

$$2.\ n(\varepsilon)|_{\varepsilon=J+0} \to 0$$

The first boundary condition is responsible for conservation of particles number, the second — for his scantiness.

Solving kinetic equation for energy spectrum of electrons with such boundary conditions by the method that was proposed in [2], one can obtain normalized electrons energy spectrum as:

$$n(\varepsilon) = \frac{2}{\sqrt{\pi}}\left(\frac{2m}{A}\sum_{j=1}^{4}\frac{\nu_e\sigma_{trj}N_j}{M_j}\right)^{3/2}\varepsilon^{1/2}\exp\left(-\frac{2m}{A}\varepsilon\sum_{j=1}^{4}\frac{\nu_e\sigma_{trj}N_j}{M_j}\right) \quad (14)$$

For the vapor mixture of iron and helium, concentration of particles is represented in the following way: $N = N_{Fe} + N_{He}$, where $N_{Fe} = N_{Fe^+} + N_{Fe^0}$ — concentrations of iron atoms and ions, $N_{He} = N_{He^+} + N_{He^0}$ — general concentration of helium atoms and ions. General concentrations of particles are given by mixture task solution. Ions (atoms) concentrations of each plasma component can be determined from ionic balance condition:

$$\frac{dN_{Fe^+}}{dt} = \sigma_{trFe}v(\varepsilon = J_{Fe})N_{Fe^0}n(\varepsilon \geq J_{Fe}) - \alpha_{Fe^+}N_{Fe^+}N_e \quad (15)$$

where σ_{trFe} — transport cross-section of electron scattering on neutral iron atom; $v(\varepsilon = J_{Fe})$ — velocity of electron with energy e equal to iron ionization potential J_{Fe}; $n(\varepsilon \geq J_{Fe}) = \int_{J_{Fe}}^{\infty}(N_{Fe^+} + N_{He^+})n(\varepsilon)d\varepsilon$ — concentration of electrons which are able to ionize iron atom (with energy $\varepsilon \geq J_{Fe}$); α_{Fe^+} — recombination coefficient.

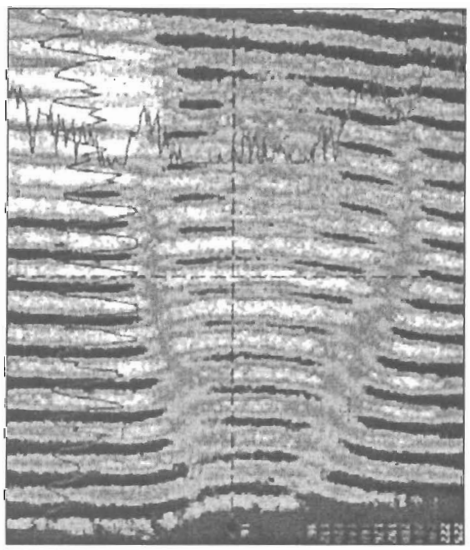


Figure 6. Plasma plume interferogram with calculated boundary of the jet (solid line)

ent of iron ions [8]. Obviously, that the first term of right part of equation (15) is respond to ionization of neutral atoms, and the second — for recombination of ions. From equation of ionic balance (15) we obtained expression for concentration of iron ions N_{Fe^+}:

$$N_{Fe^+} = \frac{\sigma_{tr Fe}\nu(\varepsilon = J_{Fe})n(\varepsilon \geq J_{Fe})N_{Fe}}{\alpha_{Fe^+}N_e + \sigma_{tr Fe}\nu(\varepsilon = J_{Fe})n(\varepsilon \geq J_{Fe})} \qquad (16)$$

Similarly for helium:

$$n(\varepsilon \geq J_{He}) = \int_{J_{He}}^{\infty}(N_{Fe^+} + N_{He^+})n(\varepsilon)d\varepsilon \qquad (17)$$

$$N_{He^+} = \frac{\sigma_{tr He}\nu(\varepsilon = J_{He})n(\varepsilon \geq J_{He})N_{He}}{\alpha_{He}N_e + \sigma_{tr He}\nu(\varepsilon = J_{He})n(\varepsilon \geq J_{He})} \qquad (18)$$

The solution of the equations set (15)–(18) is permit to determine concentration of atoms and ions for iron and helium. Taking into account plasma electro neutrality, one can defined general number of free electrons $N_e = N_{Fe^+} + N_{He^+}$, as well as plasma ionization degree. Value of the free electrons number allow to find plasma electro conductivity σ and absorption factor μ as [9]: $\sigma = \frac{e^2}{m\nu_t}N_e$, $\mu = \frac{4\pi N_e e^2}{mc}\frac{\upsilon_t}{\omega^2 + \nu_t^2}$. Dependences of these magnitudes from laser radiation intensity, strength of arc field and chemistry of mixture are shown on figures 4, 5, 7. The plasma plume interferometry experiments (Figure 6), made with the Michelson scheme, confirm the developed theory.

CONCLUSION

The boundary layer gas dynamic solution has been obtained for the hot jet, flowing to cold surrounded gas with consideration of gases compressibility and mutual diffusion.

The mathematical model of plasma plume in metal vapor — shielding gas mixture has been developed.

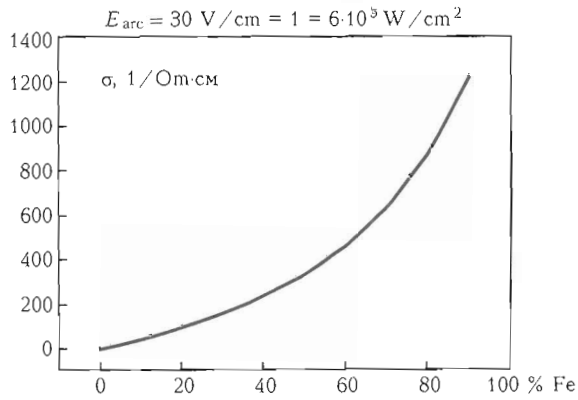


Figure 7. Dependence of plasma conductivity on chemistry

Developed model is permit to calculate plasma conductivity and laser radiation absorptivity and also to determine their dependence on laser radiation intensity.

Calculation with developed model allows to conclude, that mutual influence of gas dynamics and plasma kinetics during co-axial laser-arc action produce a thin conductive channel in plasma plume. The electric arc, compressed to this channel, form the heat source on the workpiece surface with higher power density, then in the free arc case. It explain a synergy effect, which is one of main advantages of hybrid welding.

1. V. Golant, A. Gilinskiy, I. Saharov, *Basis of plasma physics*, Moscow, Atomizdat, 1977, 348 p.
2. U. Diltey et all, *Kinetic description of keyhole plasma in laser welding*, J.Phys.D, 2000. — 33, №21, 2747–2753.
3. Yu. Raizer, *Laser spark and discharge propagation*, Moscow, Science, 1974, 308 p.
4. K. Ramachandran et al. *Structural analysis of converging jets in a triple torch plasma system*, J. Phys. D: Appl. Phys. 2003 36 p.1198–1203.
5. A. Revuelta et al., *Confined axisymmetric laminar jets with large expansion ratios*, J. Fluid Mech., 456, 319 2002.
6. Loitzynski L.G. *Mechanics of liquid and gas.* Moscow, Drofa, 2003.
7. A.K.Kikoin, I.K.Kikoin. *Molecular physics.* Moscow, Nauka, 1976.
8. V. Berestetskiy, E. Lifcis, L. Pitaevskiy, *Quantum electrodynamics*, Moscow, Science, 1989, 723 p.
9. Yu. Raizer, *Physics of gas discharge*, Moscow, Science, 1987, 592 p.

Conference Sponsors

PWI Laser Systems and Technology Center

Ministry of Education and Science of Ukraine

Information Support

«The Paton Welding Journal»

www.nas.gov.ua/pwj

Conference Sponsors

PWI Laser Systems and Technology Center

Ministry of Education and Science of Ukraine

Information Support

«The Paton Welding Journal»

www.nas.gov.ua/pwj

Conference Sponsors

PWI Laser Systems and Technology Center

Ministry of Education and Science of Ukraine

Information Support

«The Paton Welding Journal»

www.nas.gov.ua/pwj

INTEGRATED LASER-ARC PLASMATRON FOR LASER-PLASMA SPRAYING AND CVD PROCESSES

Yu. BORISOV, A. BUSHMA, A. FOMAKIN, V. KHASKIN, A. KISLITSA,
I. KRIVTSUN, V. SHELYAGIN, S. VOYNAROVICH
E. O. Paton Electric Welding Institute of NASU, Kiev, Ukraine

An integrated laser+non-transferred arc plasmatron for laser-plasma spraying and CVD processes was designed, and its prototype was manufactured. This plasmatron is based on the combined laser-arc discharge arising from coaxial joining of a focused CO_2-laser beam and a non-transferred arc in the plasma forming channel blown with an inert gas flow. The testing of the plasmatron carried out proved high stability of its work in the arc current range of 20...60 A and the beam power being up to 3.5 kW. The preliminary investigations of technological possibilities of the plasmatron designed bear evidence of wide prospects of using similar devices for spraying different ceramic materials, as well as for synthesis of diamond and diamond-like coatings.

Along with the well-known processes of surface modification and coating production using arc discharge plasma or laser radiation [1], the greater attention is paid to hybrid laser-plasma processes involving both of the heat sources [2]. The preliminary analysis shows, that while spraying ceramic powder materials such a combination permits to ensure uniform heating and melting of the particles being sprayed, to reduce the required laser power, as well as to provide dosed heat input into the spray material and the coating [3] (the process given is not to be mixed with the known methods of the two-step laser deposition [4], in particular at predeposition with plasma spraying).

Another current area in the field of coating production is Chemical Vapor Deposition (CVD) process activated by plasma or laser radiation. This method provides deposition of such coatings as diamond and diamond-like carbon, amorphous silicon, Si_3N_4, SiO_2, AlN, TiC etc. Unfortunately, the well-known plasma activated CVD processes are realized using RF or microwave gas discharge at low pressure ($< 10^3$ Pa) and provide insufficient rates of deposition [1]. Laser activated CVD processes [5] can ensure higher deposition rates, but require high power lasers with high beam quality, allowing to form and maintain continuous optical discharge at atmospheric and higher pressures. A way of solving these problems can also be simultaneous using of arc discharge plasma and laser beam to realize CVD processes.

Theoretical and experimental studies of the physical phenomena occurring in interaction of focused beam of cw CO_2-laser and dc arc plasma at atmospheric pressure, carried out at the E. O. Paton Electric Welding Institute, showed that a special type of the gas discharge may be formed in the system under consideration. This discharge is a combined laser-arc discharge [6], which differs both from the conventional dc arc and from the continuous optical discharge maintained by laser radiation. It was justified that the combined discharge can be used as a basis for making a new class of plasma devices, i.e. integrated laser-arc plasmatrons for hybrid welding and surface modification [2]. Principles of design and methods for calculation of coaxial laser + transferred or non-transferred

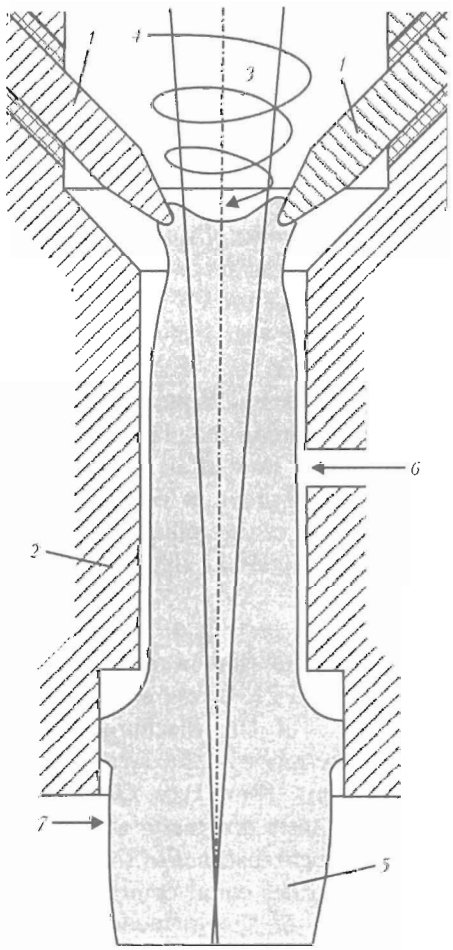


Figure 1. Schematic diagram of integrated laser + non-transferred arc plasmatron for hybrid laser-plasma spraying and CVD process: *1* — thermionic cathodes; *2* — plasma forming nozzle-anode; *3* — focused laser beam; *4* — inert plasma gas; *5* — combined laser-arc discharge plasma; *6* — reactive gas; *7* — powder feed

©Yu. BORISOV, A. BUSHMA, A. FOMAKIN, V. KHASKIN, A. KISLITSA, I. KRIVTSUN, V. SHELYAGIN, S. VOYNAROVICH, 2005

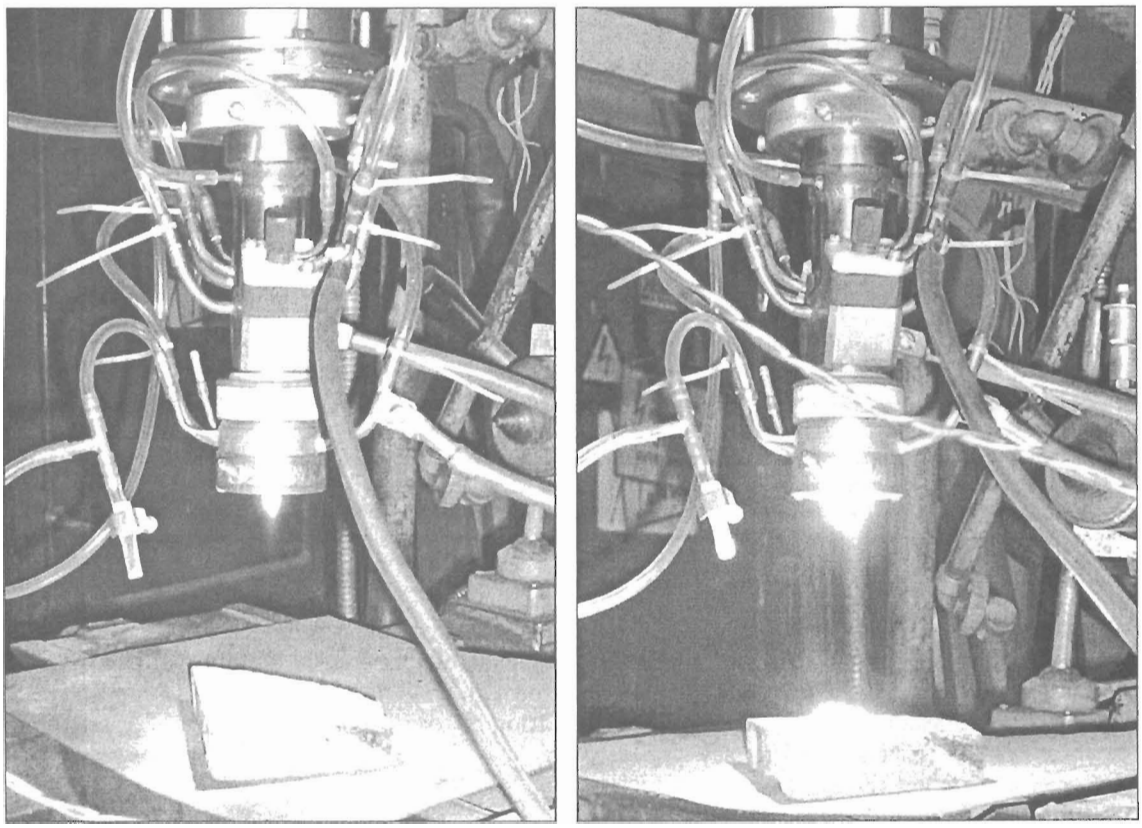


Figure 2. Operation of the integrated plasmatron in arc (left) and hybrid laser-arc (right) modes

arc plasmatrons operating in laminar or turbulent modes of the plasma gas flow at atmospheric pressure were developed.

Within the frameworks of these studies, an integrated laser + non-transferred arc plasmatron for realization of laser-plasma spraying and CVD processes was designed, and its prototype was manufactured. This device is based on the combined laser-arc discharge arising from coaxial joining of a focused beam of cw CO_2-laser and a non-transferred dc arc in the plasma forming channel blown with turbulent flow of an inert gas (Figure 1). The plasmatron design provides feeding the reactive gas into the combined discharge plasma region or feed of the powder being sprayed into the plasma jet generated by this plasmatron.

The experimental testing of the developed plasmatron was carried out first in arc mode and than in laser-arc one (Figure 2). These experiments showed a certain decrease of the discharge voltage from $U = 50$ V in the arc mode at the current $I = 45$ A and plasma gas (argon) flow rate $Q = 15$ l/min to $U = 47$ V in the laser-arc mode at the laser beam power $P = 3$ kW (focal distance of the lens used being $F = 500$ mm) and other equal conditions.

At investigation of the influence of plasma gas flow rate, laser beam power and focusing on the absorption of laser radiation in the combined discharge plasma, it was determined, that at $I = 45...47$ A, $P = 3.5$ kW, $F = 500$ mm the variation of total plasma gas flow rate from 6 to 12 l/min does not practically influence on the absorption of laser beam. The level of laser beam absorption is 40...44 %. Substitution of the lens with focal distance of 300 mm for the lens with $F = 500$ mm, which corresponds to the increase of maximum power density in the laser beam from 1.5×10^6 W/cm^2 to 6.1×10^6 W/cm^2, resulted in a substantial increase in absorption from 42 % to 71 %. Finally, the reduction of the laser power from 3.5 kW to 3.0 kW ($F = 300$ mm), on the contrary, led to the decrease in absorption from 71 % to 31 %.

Generally, the integrated plasmatron testing carried out proved high stability of its work in the arc current range of 20...60 A, the total plasma gas (argon) flow rate of 6...18 l/min and the laser beam power being up to 3.5 kW. The results of the preliminary investigations of technological possibilities of the designed laser-arc plasmatron show wide prospects of using similar devices for laser-plasma spraying of different coatings, as well as for hybrid laser-plasma CVD processes performance, such as deposition of diamond and diamond-like coatings (Figure 3).

The advantages of the integrated laser-arc plasma generators over the optical (laser) plasmatrons [7] and the arc ones can be summarized as follows:

- Increased stability of the combined discharge plasma;
- Higher efficiency of utilization of the laser beam energy (decreased power of laser);
- Wider range of steady-state conditions in flow rate and composition of the plasma forming gas;
- Additional possibility of controlling the process through varying the arc burning conditions and laser beam parameters.

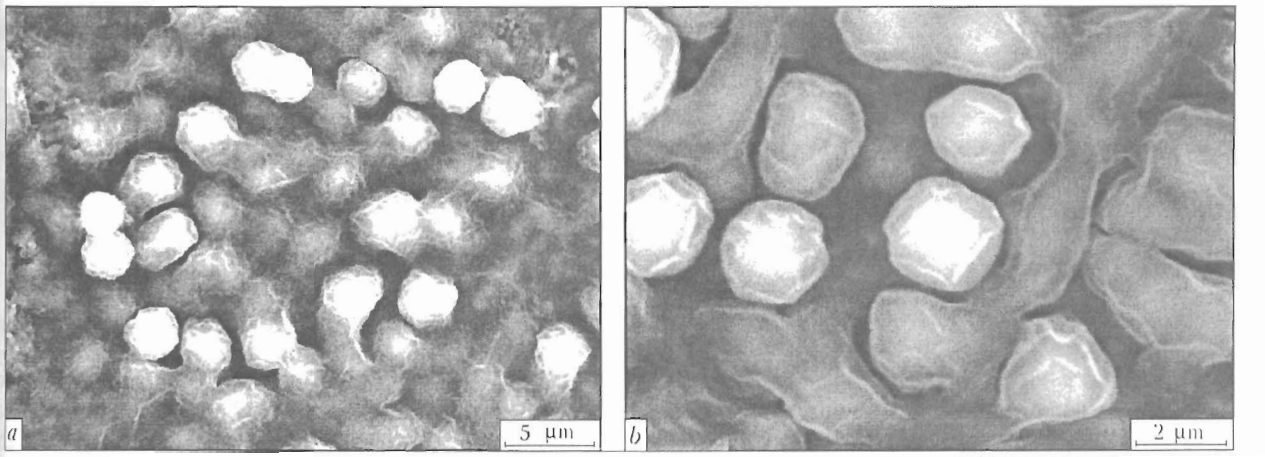


Figure 3. Diamond-like coatings obtained with hybrid laser-plasma CVD process: *a* — ×3000, *b* — ×8000

In this connection, usage of the integrated laser-arc plasmatrons for practical realization of the spraying and CVD processes provides broader technological capabilities and lower costs associated with carrying out of these processes, compared with other laser or plasma methods.

1. Hocking M.G., Vasantasree V. and Sidky P.S. (1989) *Metallic and ceramic coatings: Production, high temperature properties and applications.* London: Longman Scientific and Technical.
2. Seyffarth P. and Krivtsun I.V. (2002) *Laser-arc processes and their applications in welding and material treatment.* London: Taylor and Francis Books.
3. Borisov Yu.S., Bushma A.I. and Krivtsun I.V. (2005) *Simulation of powder particles motion and heating in laser, plasma and hybrid spraying.* Dopovidi of NASU, 1, 86–94.
4. Pawlowski L. (1999) *Thick laser coatings:* A review. Journal of Thermal Spray Technology, 8 (2), 279–295.
5. Konov V.I., Prokhorov A.M., Uglov S.A. et al. (1998) *CO_2 laser-induced plasma CVD synthesis of diamond.* Appl. Phys. A, 66 (5), 575–578.
6. Gvozdetsky V.S., Krivtsun I.V., Chizhenko M.I., et al. (1995) *Laser-arc discharge: Theory and applications.* In: Welding and Surfacing Rev., 3, Harwood Academic Publishers.
7. Metev S., Brecht H., Schwarz J. et al. (2002) *New technology for high rate synthesis of PC-diamond coatings in air with photon plasmatron.* Diamond and Realated Materials, 11, 472–477.

OPTICAL PROPERTIES OF EXCITED ACTIVE MEDIUM OF SLAB CO_2-LASER

V. P. GARASHCHUK, V. N. SIDOTRETS
E.O. Paton Electric Welding Institute of NASU, Kiev, Ukraine

For achievement of high generation efficiency the CO_2-laser active medium need intense cooling because of at $T > 500$ °K the efficiency falls sharply [1]. In lasers with radiation power greater then 1–1.5 kW a convective cooling is applied. Such pumping active medium through a volume of discharge and resonator complicates laser design. If ever diffusion (thermal convection) cooling is applied then in pipe laser from one meter of pipe a laser beam with power no more than 100 W can be obtained that not enough for more thermal technologies.

Specific power CO_2 laser with diffusion cooling increases significantly in the so called slab laser. In this laser as a pumping source the α-type glow discharge is used which burns between two plate electrodes with width is equal to several centimeters, length is equal to several tens of centimeters and a gap between them is equal to several millimeters (see Figure 1). As long as gas discharge is supplied by high frequency current the electrode surface does not take place in creation of current carriers [2] because of metal water cooling electrodes with large operative surface can be used that cools efficiently an active medium in discharge gap. Small distance between electrodes increases significantly stability of a burning of glow discharge that prevents its transformation to the arc discharge. This allows reaching values of volume energy contribution up to several tens of watts per cubic centimeter [2].

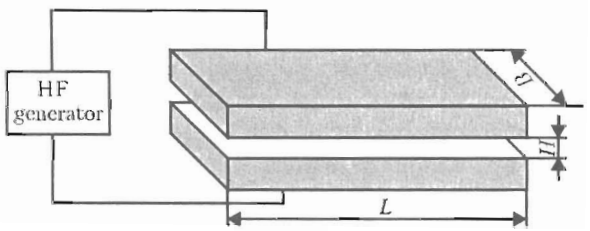


Figure 1. Connection circuit for electrode system of slab laser

Constructive peculiarity of this laser is a resonator which has to form a laser beam in small height volume. Practices show that the best for this aims is a resonator stable on height of discharge and unstable on width, so called stable-unstable resonator. Such resonator can be realized by mirrors which have different curvatures in named above mutual orthogonal planes. It is obviously that cylindrical mirrors with one curvature are produced more technologically then complicated mirrors with two curvatures. In this case both resonators (stable and unstable) will be formed by flat and cylindrical mirrors. Moreover, it is desirable the laser to generate one beam. It can be achieved by using unstable resonator which be formed by flat and convex mirrors. At this case the laser beam on each path will be move away from axis to one side.

It does not difficult to create unstable resonator. But at calculation of stable resonator it need to take to account the optical power of active medium which appears because of its density heterogeneousness. The cause of this is clear. At excitation of the medium is heated by current and is cooled by electrodes. Maximum of temperature locates on symmetry plane, minimum of temperature — on electrode surfaces. Since gas density is inversely proportional to temperature, minimum of density locates on symmetry plane, maximum of density — on electrode surfaces. Because of medium located between electrodes represents the cylindrical lens with negative optical power which is determined by distribution of refraction index that is proportional to molecule density according to Lorenz-Lorentz law. Optical power of thermal lens may be significant and it must be take to account at the calculation of curvature radius of the stable resonator mirror. Moreover the presence of divergent lens leads to increase of harmful losses in resonator because of more frequent beam reflection from electrode surfaces.

To solve the problems enumerated above need to define the distribution of gas density and refraction index across discharge height. In present paper this is implemented by solution of thermal problem employing numerical technique.

GAS DENSITY DISTRIBUTION IN DISCHARGE GAP. Calculation of optical power of thermal lens. Pumping power with density $\sigma_{\text{ВАК}}$ is bring in discharge gap into whole volume and its liberal share is required for heating of active medium which is cooled by electrode surfaces. Their dimensions are greatly more then distance between electrodes. Therefore the problem of finding of temperature distribution and gas density can be reduced to one-dimension one as far as the deflection of heat through the side boundaries and butt-ends of discharge gap substantial smaller then by electrodes surfaces. The origin is located in any point on symmetry plane. Axis of x is directed normally to electrode surfaces, axis of y — parallel to electrode width, axis of z —

© V. P. GARASHCHUK, V. N. SIDOTRETS, 2005

parallel to electrode length and it coincides with resonator axis. In chosen co-ordinates with taking to account conditions fixed above the temperature distribution across discharge height will be described following thermal conductivity equation:

$$\frac{\partial T}{\partial t} = \frac{\lambda}{\gamma\rho}\frac{\partial^2 T}{\partial x^2} + \frac{\sigma_T}{\gamma\rho}. \qquad (1)$$

Stationary operation of a laser will be considered. In this condition temporary changing is absent and equation (1) is simplified

$$\frac{dT^2}{dx^2} + \frac{\sigma_T}{\lambda} = 0, \qquad (2)$$

here σ_T – thermal power density which is determined by relation $\sigma_T = (1 - \eta_{c.o.})\sigma_{pump.}$, $\eta_{c.o.} = P_{gen}/P_{pump.}$ – electro-optical efficiency; λ – heat conductivity factor of the gas medium, γ and ρ – thermal capacity and density accordingly. Boundary conditions for the problem are:

$$T(x = \pm a) = 300\ ^\circ K, \qquad \frac{dT}{dx}(x = 0) = 0$$

Density of pumping power $\sigma_{нак}$ [W/m^3] is determined from relation $\sigma_{pump.} = jE$, where j – current density, E – electric field strength in plasma discharge. Glow discharges as DC as AC are characterized by values of electric field strength per one molecule $\frac{E}{N}$[$V{\cdot}m^2$] which does not depend on gas temperature. For mix of carbonic acid gas, nitrogen and helium which are active medium of CO_2-laser the value of $\frac{E}{N} \approx 3.4{\cdot}10^{-20}$ $V{\cdot}m^2$ [3]. Power pumping density with taking into account specified electric field strength is written so:

$$\sigma_{pump.} = j\frac{E}{N}N, \qquad (3)$$

that is evidence of its dependence on molecule concentration N in active medium.

In CO_2-lasers with diffuse and convective cooling a discharge volume occupies little part of total gas volume in laser. Therefore a gas heating in discharge does not practically change its pressure in device that is cause a decrease of molecule concentration in discharge at that accordingly to temperature on given distance from electrode. In accordance with eq. (3) the power density is proportional to gas density in given discharge site.

Using formula (3) and equation for gas pressure $p = NkT$ the relation (2) is written as:

$$\frac{d^2T}{dx^2} + (1 - \eta_{e.o.})\frac{j\frac{E}{N}}{\lambda}\frac{p}{k}\frac{1}{T} = 0, \qquad (4)$$

that allows us to calculate temperature distribution across discharge height and using the equation for gas pressure to obtain its density distribution and energetic contribution yet. Accounts are carry out at the following values of physical quantities incoming in eq. (4) $p = 6.6$ kPa; $\eta_{c.o.} = 0.15$; $\lambda = 0.18$ $W/(m{\cdot}^\circ K)$ (It is considered that heat conductivity factor depends completely on helium as long as in lasers with diffuse cooling more often an active medium consisting of component in volume part ratio CO_2:N_2:He = 1:1:8 is used). Here it is necessary to note that keeping in eq. (4) ratio $\frac{j}{\lambda} = const$ constant we shall obtain the same solution at other values of conductivity factor but the current density have changed accordingly.

In slab CO_2 laser the distance between electrodes is small that creates favorable conditions of stable glow discharge burning and because of this allows to enter in active medium large power density. Therefore it is possible the case when because of overheating gas mix the effectiveness of laser generation decrease sharply. This is observed when gas temperature exceeds 450... 500 °K. Therefore the calculation was carried out up to such current density when on symmetry plane the temperature 450 °K is achieved.

Temperature distribution across discharge height is shown on Figure 1 for four values of discharge height, and gas density distribution across discharge height according to curves presented on Figure 1 is shown on Figure 2. The last ones are approximated by relations $N(x) = A + Bx^2 + Cx^4$ and $N(x) = a + bx^2$. The factors of approximating functions are given in table 1.

Analyzing the obtained approximating functions it is clear that calculated relations with high accuracy are described by fourth degree polynomials and less accuracy – by second degree polynomials, i.e. by parabolas. Both approximating functions can be presented by relations:

Table 1. Approximating functions for gas density across discharge height

Discharge height $2a$, mm	A	B	C	Root-mean-square error, %	a	b	Root-mean-square error, %
6	10.645	0.324	0.028	0.55	10.449	0.542	3.8
4	10.643	0.73	0.143		10.447	1.22	
2	10.644	2.92	2.283		10.448	4.88	
1	10.645	11.68	36.51		10.449	19.516	
General	10.644	2.92	2.283		10.448	4.88	

$$N(x) = \left[10.644 + (2.92a^2)\frac{x^2}{a^2} + (2.283a^4)\frac{x^4}{a^4}\right]10^{23}\ [\mathrm{m}^{-3}]$$

and (5)

$$N(x) = \left[10.644 + (4.8a^2)\frac{x^2}{a^2}\right]10^{23}\ [\mathrm{m}^{-3}],$$

which in Table 1 are called «Generalized».

The obtained results earnestly is evidence that active medium in electrode gap possesses distortion properties and is negative cylindrical lens with a shape although differ but close to parabolic one. For determination its focal power we have considered that gas density distribution across discharge height in all cases is described by parabola that allows us to employ the mathematical technique of matrix optics [4].

As well known [5] the increase of refractive exponent of medium consisting of m kind of atoms to comparison with refractive exponent of vacuum is described by Lorenz-Lorents formula:

$$n - 1 = 2\pi e^2\left(\sum_i^m N_i \frac{1}{\mu_i}\frac{1}{\omega_{0i}^2 - \omega^2}\right),$$

here N_i — atom concentration of i — kind in optical medium; μ_i — their mass; e — electron charge; ω_{0i} — frequency of absorption line; ω — frequency for which refractive exponent is determined.

At calculation of the refractive exponent will be taken to account only two components: nitrogen and helium. Third component will not be taken to account because of following reasons. In non-excited medium the carbonic acid gas includes its portion in value of refractive exponent by absorption line between levels 000→001. In excited gas the level 001 is populated inverse and therefore it creates negative dispersion on laser transition 001→100. Overpopulation on transition 001→100 not yet says about overpopulation on absorbent transition 000→001. For estimation combined action these two transitions in CO_2 molecule on refractive exponent with different signs it is necessary to know occupation degree of level 001 that is difficult,

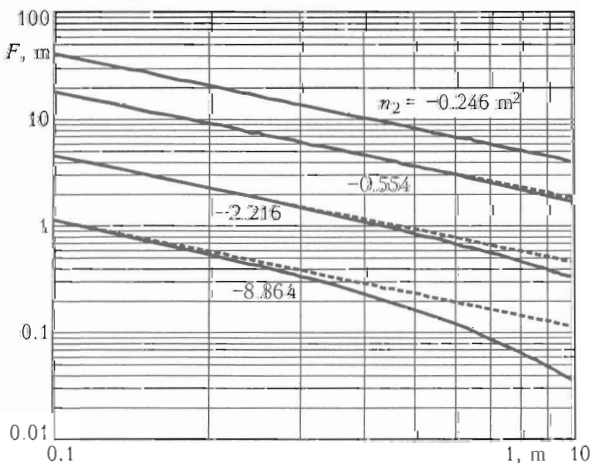


Figure 2. Focal distance of medium vs. discharge length

in general case. Therefore it will consider that positive dispersion of non-excited molecules is compensated by negative dispersion of excited molecules, i.e. contribution of the carbonic acid gas on refractive exponent can be neglect. The accuracy of relation (5) is the higher, the more difference between frequency of absorption line and frequency w. Resonance absorption lines nitrogen and helium locate in far ultraviolet region but CO_2 laser generates in middle infrared region. So the accuracy of relation (5) is satisfied surely.

In relation (5) component partial concentrations will take to account with their relative molar contents γ_i in medium: $N_i = \gamma_i N$, here N — total atom and molecule concentration in medium. Mix refractive exponent n_Σ was calculated to according with relation:

$$n_\Sigma(x) - 1 = \frac{N(x)}{N_0}\left[\gamma_{He}(n_{He} - 1) + \gamma_{N_2}(n_{N_2} - 1)\right], \quad (6)$$

here $N(x)$ and N_0 — particle concentrations on coordinate x and at standard conditions accordingly. Then in calculations the values $\gamma_{He} = 0.8$, $\gamma_N = 0.1$, and refractive exponents for helium and nitrogen at wave length $\lambda = 10.6$ μm and normal conditions $n_{He} = 1.000035$, $n_{N_2} = 1.000291$ recalculated by Cauchy formula [6].

Using the approximating parabolic equation (5) and relation (6) write the relation of refractive exponent vs. coordinate x in form: $n(x) = n_0 + 0.5n_2x^2$. For studied values of discharge heights the values n_0 and n_2, and also according to them focal distances in account on 0.1 and 1 m its length are put in Table 2. The focal distances were determined from element C of beam matrix for lens-like medium with length l [4]:

$$F = -\frac{1}{\sqrt{-n_0 n_2}\ sh\left(l\sqrt{\frac{-n_2}{n_0}}\right)}$$

From Table 2 it follows that focal distance of negative thermal lens is the less, the less the discharge height and the more its length. Absolute values of F for small discharge height so much small that one cannot but take to account them in calculations focal distance of resonator curve radius.

With the purpose of detail analysis a family of relations of medium focal distance vs. discharge length

Table 2. Factors in equation for refractive exponent across discharge height and focal distances per 0.1 and 1 m its length

Discharge height 2a, mm	Refractive exponent on symmetry plane n_0	Factor at quadratic term n_2, m^{-2}	Focal distances of medium per 0.1 и 1 m its length, m	
1	1.000002215	−8.864	−1.112	−0.034
2	1.000002215	−2.216	−4.496	−0.319
4	1.000002215	−0.554	−18.034	−1.649
6	1.000002215	−0.2462	−40.601	−3.9

for various values of parameter n_2 was plotted (see Figure 2).

Evidently from figure the relations very closed to hyperbolas (dashed lines, scales is logarithmic). Just at large values of parameter n_2 and l a deviation from this relation is observed. So one can make conclusion that the more cases with sufficient accuracy the focal distance can be calculated by reductive formula:

$$F = -\frac{1}{n_2} l$$

Calculated distributions of particle density across discharge height allow to us also calculate the permissible power which can be entered in active medium per area unit of electrodes at the condition that gas temperature on symmetry plane is equal 450 °K:

$$\frac{P}{S} = 2j\frac{E}{N}\int_0^a N(x)dx.$$

The values of permissible current density and power per electrode area unit and averaged per volume unit are given in Table 3.

Obtained values of power density per volume unit coincide with experimental data in Ref [2].

Table 3.

Discharge height $2a$, mm	Current density, A/cm^2	Power density per area unit of electrodes, W/cm2	Averaged across discharge height power density per volume unit, W/cm^3
1	0.660	27.3	273
2	0.165	13.5	67.5
4	0.041	6.9	17.3
6	0.018	4.5	7.5

CONCLUSION

1. Gas density in electrode gap of slab laser increase in direction to cooling electrodes accordingly to law closed to parabolic and has minimum on symmetry plane.

2. The active medium of slab CO_2-laser with optical means is the negative lens. Optical power of this lens which can be calculated on the base of solution of thermal problem increase with deceasing the distance between electrodes. It is necessary take to account at calculation of resonator mirrors.

3. At the optimal conditions of heating of active medium namely the temperature on symmetry plane 450 °K and on electrodes электродов 300 °K the permissible current density, power per electrode area unit and averaged per volume unit decrease at increasing the distance between electrodes.

1. V. Vitteman, *CO_2-laser.* — Moscow: Mir. 1990.
2. Yu. P. Raizer, M. N. Shaider, N. A. Yatsenko, *High Frequency Capacitance Discharge.* Physics. Technique of Experiment. Applications. — Moscow: MPhTI, Nauka, 1995. (In Russian)
3. N. V. Karlov, Yu. B. Konev, *Pulsing CO_2 Lasers High Pressure.* In book: Handbook on Lasers. In 2 Vol. By ed. A. M. Prochorov. — Moscow: Sov. Radio, 1978, V.1, Chapter 5. — P. 133–146.
4. H. Cogelnick, T. Li, *Resonators and Light Beams of Lasers.* Proceeding of IEEE, 1966, V.54, No.10. — P. 96–113.
5. D. V. Sivuhin, *General Curse of Physics.* Optics. — Moscow: Nauka. 1980.
6. C. W. Allen, *Astrophysical values.* — Moscow: Foreign Literature. 1960.

WEB-TECHNOLOGIES APPLICATION TO INCREASE THE EFFICIENCY OF LASER INDUSTRIAL SYSTEMS

V. KOVALENKO[1], A. MAMALIS[2], V. KOLPAKOV[1]
[1]Laser Technology Research Institute of NTUU «KPI», Kiev, Ukraine
[2]National Technical University of Athens, Greece

Technical solution intended to increase the competitiveness of engineering plants through reduction of the production time, centralization of manufacturing and distribution of orders using Web-technologies have been identified. Main principles of development of a web-site as an acceptor of orders have been considered, and version of software implementation of a central server and acceptable versions of transfer, reception and performance of a product manufacturing order have been analyzed by considering the example of the server of the Laser Technology Institute of the National Technical University of Ukraine «Kiev Polytechnic Institute». The need to promptly set up a centralized web-structure to control orders of small and medium-sized engineering plants of Ukraine for raising their foreign competitiveness is proved.

Introduction. Under globalisation of the economy one of the decisive factors for plant competitiveness is their ability to be integrated into a new system of obtaining orders, maximum shortening of the turnaround time and lowering the cost of a unit of product. Companies are pressed now with great amount of factors from various directions and of different intensities. The environment is determined by the global competition, the individualisation of customer needs, shorter product lifecycle and by the rapid development of information and communication technology [1]. The increasing probability of a company being subjected to specific turbulence due to intensely changing market leads to the conclusion that adaptability is becoming the crucial competitive factor for enterprises. Three basic elements influence substantially the success of the enterprise activity:

- resource time;
- resource capital;
- the complexity of product manufacturing.

It should be taken into consideration that each enterprise has its own, subjective perception of the environment and its changes should be adapted to the needs and possibilities of the enterprise.

Thus the aim of a company specific adaptability is therefore the permanent and efficient fulfilment of market requirements.

Problem solution. To get fastest breakthrough in the engineering industry of Ukraine and to reach the external market using the existing potential is the development of a market-oriented, fast system of support in securing orders for small- and medium-sized plants, based on web-technology of processing, analysis and transfer of the data. Such a technology is currently being developed by a number of global corporations [2–5], and may be considered as the main administrative tendency to improve the manufacturing efficiency. Practically the considered approach means partial reanimation of the idea of a centralized industry, but in an electronic format, global market oriented and independent of governmental bodies. Implementation of the system is based on interfacing databases of product characteristics, network analysis of the load on process equipment in a specific plant, its production capacity and additional aspects of order fulfillment. In the proposed version of export potential reanimation the Ukrainian engineering industry will have the role of a major industrial corporation of Western type with spatially dispersed and indepen-dent affiliated branches. Unlike the regular projects of support and development of small- and medium-sized plants, it is intended to increase the competitiveness of such plants by fast processing of all possible orders and widening the product range, using an «external order acceptor», providing their increased competitiveness and not losing their independence in selecting development strategy. As a result, not a single plant with limited capacity, but an entire industry with the complete capacity range and possible product range joins the international market. In technical terms the central web-site can have the role of external accumulator of orders for manufacturing the products of local plants. This site should use as the basis the data base with XML – marking, which will permit interfacing the software of the main customers and manufacturers from the engineering industry in the Internet without creating intermediate archivated files of technical documentation [6]. Site activation for «acceptance» and transfer of product prototypes for direct manufacturing to a Ukrainian plant via the Internet enables increasing the competitiveness of the local manufacturing, fitted with laser systems, against Western plants fitted with the same equipment, but having, through obvious reasons, a higher product cost.

Technical solution for the software development to ensure order acceptance. Main elements of the software for the order acceptor web-site. Principles and methods of programming the electronic business

© V. KOVALENKO, A. MAMALIS, V. KOLPAKOV, 2005

plants are filled with new capabilities avalanche like. The main technical solutions for creation of an external Internet-acceptor of orders have been defined in the general case. A typical web-site for electronic processing of orders includes the following program modules (Figure 1) [7]:

- presentation of general information in the form of HTML-files with possible inclusion of active advertising pages («saved scenarios»);
- formation and processing of the data base of orders with active acceptance modules;
- information about customer («common data base»);
- formation and processing of a data file from / for the data base of orders, using active modules of acceptance of information on the characteristics of the product suggested for manufacturing («mechanism of data base processing»);
- processing the file of order payment and issuing a command for manufacturing and realize of goods («mechanism of active server applications»);
- support and recording of receiving of the order by the user («mechanism of data processing»);

During construction of a virtual manufacturing the last listed items should be complemented by:

- evaluation of accessibility of equipment, which enables fulfilling the order and calculation of the possible manufacturing time;
- preparation of technical documentation for manufacturing and transfer for performance.

Principles of coordination of data base and grafic documentation in the internet. The most widely accepted are JPEG, GIF, PNG and BMP formats. Unfortunately, the basic formats of CAD systems for mechanical engineering products cannot be used for presentation in the web-site, because of different data communications protocols, principles of structure formation and data archiving. It should be taken into account that the above Internet-formats are raster ones and lose the image quality at scaling, do not accommodate command performance of graphic constructions and, therefore, are unacceptable for providing step-by-step execution of geometrical elements by a PNC machine tool. The main current CAD formats are DWG, DXF and DWF. A figure compatible with www and simultaneously preserving the specifics of transferring the drawing to a plotter or PNC board can be created in DWF-format specially developed for inclusion into a web-page or another text document. Use of a DWF-file to place and fulfill an order requires each user to have not only an additional program module of file exchange, I-drop, disseminated by AutoDesk free of charge, but also a copy of the main AutoCAD program module of this company [8]. Automated functions of file layout on a web-page were a new feature of AutoCAD product and in addition to MeetNow functions, providing joint viewing and editing of documentation in the local network they became a significant element in the tendencies of joint developed of the CAD and Internet systems.

The most promising software base for setting up a web-acceptor of orders for the mechanical engineering industry can be the intensively developing areas of design software for CAD systems, principles of web-support of access to common resources and capabilities of forming generalized data bases in the format of extensible markup language XML [5]. World producers of the software have mastered commercial release of XML-interfacing of data base and presentation of web-browsers in 2000–2002. AutoDesk Company has also commercially introduced DesignXML-module as a standard extension for generating an XML-file of the designed item in AutoCAD. XML-file of the part designed and transferred for manufacturing can be generated in this most powerful CAD software product, isolating the structure object saved in the file and forcedly replacing standard extension .dwg by .xml. This will result in a file structured for XML-marking and acceptable for presentation in the Internet.

In view of the above-said, selection of XML-programming as a basis for special software in implementation of a web-acceptor and distributor of orders is practically obvious.

Selection of software and operationg system for web-site implementation. A large number of publications on electronic commerce of Western market are helping the advertising campaign of the actual field of electronic sales and specialized self-advertisement of the authors. In addition, these publications are designed for financially secure businesses, purchasing Microsoft license programs, thus advertising the products of this company. As a rule in Western publications Microsoft Windows NT-server is selected as the server operating environment, IIS as the mechanism of server function support, ASP as the basic environment for programming server applica-tions, and Microsoft SQL-server of various modifications as the environment for forming the data base. Java (producer is SUN company) and JavaScript (Microsoft) are the most often mentioned language environments for activation of the applications.

Considering the need for programmers working on specialized programs and server operation support, the cost of the work will add up to a considerable sum for a government organization, small business or unit of an educational establishment. Use of unlicensed software by the authors to create commercial extensions is regarded as unacceptable and is not considered.

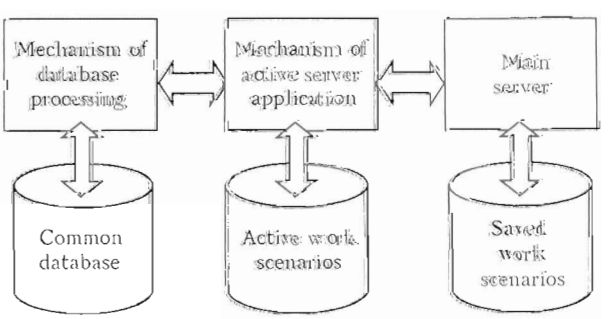


Figure 1. Schematic of implementation of web-site of order acceptor

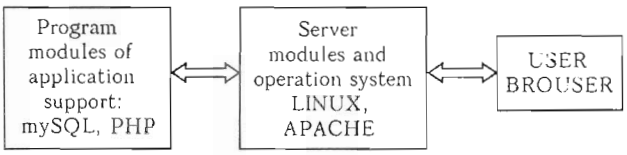


Figure 2. General schematic of data communication between the server and user in the case of using program products with an open code

Open-code programs, namely LINUX and FreeBSD (among operating systems), APACHE (among server programs), PHP (in the field of language structures of dynamic programming of web-pages) and MySQL (in the field of data base construction) have become an acceptable alternative to software products of Microsoft class. Openness of the initial program code, ability to use them without licensing and low cost of these software products determined their wide acceptance and popularity with the Internet providers and qualified programmers, developing specialized web-applications. The general schematic of data communication between the server and user in the case of using software products within open code is given in Figure 2.

Most of the providers offer disc space for placing active user servers, applying exactly this software. Disadvantages of selecting open-code programs to implement server applications of electronic commerce are high requirements to the qualifications of the programmer managing the web-project.

CONCLUSIONS

1. The proposed web-approach is aimed to increase the efficiency of the small and medium size (SMS) plants activity.

2. The use of Internet technology for centralized obtaining of export orders, as well as their analysis, processing and optimum distribution in the SMS businesses of the engineering complex of Ukraine is a real way for a significant increase of the competitiveness of the industry and reducing the small-batch shadow manufacturing.

3. The main order acceptor may be a web-site which uses the capabilities of conversion and XML-presentation of technical documentation for product manufacturing, data base of plants interested in getting the order, characteristics of their engineering facilities and load schedule.

4. Order forming and its transfer for manufacturing can be performed both directly trough XML-file of the central web-site, and using the file of an electronic drawing of the part, acceptable for output to the machine plotter.

5. The plan of plant workload should be made by a program module of network planning, with criteria selection of the next load site by price, speed and quality estimates.

1. Kovalenko V. S., Kolpakov V. V., *Use of web-technologies to improve the competitiveness of Ukrainian engeneering plants*, «The Paton welding journal», # 7, 2004.
2. S. Mc. Mains, C. Sequin, C. Smith, P. Wright, *Internet-based Design and Manufacturing Computer Science Department and Mechanical Engineering Departments University of California*, Berkeley, California 94720.Final Report 1999–2000 for MICRO project 99–10.
3. C. Smith *«The Manufacturing Advisory Service: Web Based Process and Material Selection»*, U. C. Berkeley Mechanical Engineering Depart., Ph. D. Thesis, August 1999.
4. J. H. Kim, F. C. Wang, C. Sequin, P. K. Wright, *«Design for Machining Over Internet»*, the Design Engineering Technical Conference (DETC) on Computer Integrated Engineering Paper Number DETC'99/CIE-9082. Las Vegas, Sept. 1999.
5. S. Mc. Mains, C. Sequin, J. Smith, *«SIF: A Solids Interchange Format for Rapid Prototyping»*, Technical Paper PE99-117, Society of Manufacturing Engineers, Dearborn, MI, 1999.
6. P. Spencer, *XML Design and realization*, «Lori», Moscow, 2001.
7. CHEN Ying QU Junsheng GE Hualan YANG Canjun, *«How does the WEB based design of hydraulic system work»*, State Key Lab of Fluid Power Transmission and Control, Zhejiang University, 310027, Hangzhou, China.
8. S. Frizell, *«A Pattern-Based Design Methodology for Web-based Instruction»*, Department of Computer Science and Software Engineering 107, Dunstan Hall, Auburn University, AL 36849 USA, Research Summary 09/2001.

CONFIGURATION OF INDUSTRIAL LASER SYSTEM (ILS) FOR LAYER BY LAYER 3-D FORMING OF SOLID OBJECTS

L. M. OLESCHUK, V. S. KOVALENKO, M. I. ANYAKIN, R. O. ZHUK
Laser Technology Research Institute of NTUU «KPI», Kiev, Ukraine

Nowadays, the usage of CAD and CAE systems along with modern technologies of parameterization, associative assembling is on increase. This helps to create an integrated system for automated development of technological equipment, simulation of its performance and the outcome of technological processes.
In this work a structural analysis of the variety of laser technological equipment for layer-by-layer 3D solid objects forming was performed. There were selected configurations which meet premeditated requirements to the equipment arising from peculiarities of the technique mentioned above. There was developed and manufactured technological equipment for 3D solid objects layer-by-layer forming using local selective sintering and melting of powder particles jet.

Introduction. Nowadays, industrial communities are revising exiting approaches towards industrial engineering due to rapid and steady increase in the efficiency of computer-aided systems of 3D modeling which employ novel technologies of designing, parameterization, associative compositions of units and Figure processing. Application of 3D modeling allows creating an integrated system of automated item or process design. This system offers a complete designkit for Figure, engineering analysis, development and imitation of tool control systems and executive routines for item processing. Its further integration with global informational databases for automated item design, production control and flexible manufacturing systems may result in creation of unified engineering system.

Modern technologies of Rapid Prototyping, Rapid Tooling and Rapid Manufacturing meet this approach in full. Latest achievements of information technologies in 3D modeling and the development of laser processing techniques gave way to the implementation of layer-by-layer material growth for 3D solid object's forming. Forming process starts with computer-aided designing of any desired object, so called spatial mathematical model of solid object. Consequently, this model is transformed into a set of discrete 2D cross-sections in layers. Control routines which govern the laser beam movement are developed respectively for 2D model of each layer of 3D solid object. Having created all necessary control routines it is now possible to simulate the whole process of object forming. In case of successful simulation, these routines are transferred to control units of industrial laser systems, thus materializing layer-by-layer the existing 3D mathematical model. The completion phase of forming process consists of final polishing, in order to change the properties of the obtained object (if needed), and quality control procedure.

Layer-by-layer material growing in object forming process is usually performed when material is in its intermediate state between liquid (powder) and solid phase. This range of materials comprises of photopolymers, thermoplastics, ceramics and metals. In some cases paper or foil can be used.

Among the basic methods of layer-by-layer material growing with help of laser beam is:

- local selective powder sintering
- melting of powder jet
- solidification of liquid photopolymer
- cutting through stacks (rolls) of paper or foil sheets

Layout of Industrial Laser Systems. General configuration of industrial laser systems for layer-by-layer 3D forming of solid objects by selective local sintering or powder jet melting has some peculiarities. This type of equipment must include technological laser, system for formation and propagation of laser beam, system of manipulators, auxiliary technological units, control system and at least 3-coordinate positioning worktable (Figure 1).

The proper choice of layout and configuration of industrial laser system is a core routine a developer has to undertake. It reflects kinematical structure of the equipment, position of its stationary and mobile elements along with guiding ways. This layout should be developed and taken into account on the technological phase of industrial system's design prior to designing of its main elements. It is the stage when the developer considers all technical and economical characteristics of the equipment and investigates its impact on the overall quality characteristics of the object being formed.

The design of in general requires following steps to be taken: the development of technological, coordinate and structural layouts. The first and the most crucial step is to develop a technological scheme and structure of future laser system. According to the tasks and purposes of the equipment all necessary types of movement and rotation are selected and analyzed. Coordinate layout reveals the composition and pattern

© L. M. OLESCHUK, V. S. KOVALENKO, M. I. ANYAKIN, R. O. ZHUK, 2005

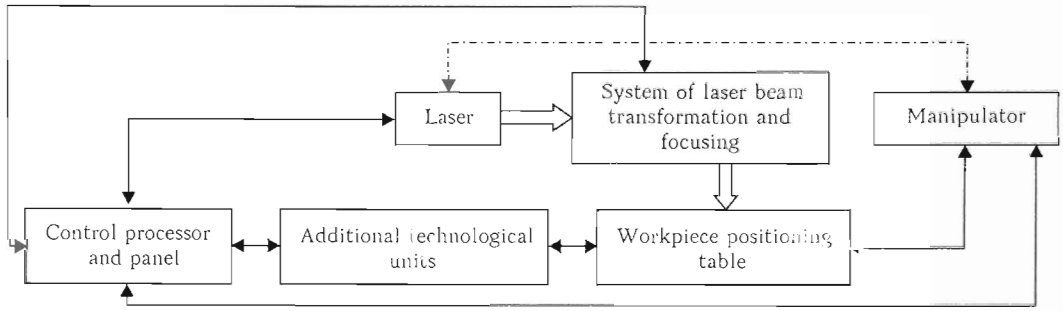


Figure 1. Layout of industrial laser system for 3D forming of objects

of all movements done by all part of technological equipment. The proper choice of kinematical structure greatly influences on laser beam propagation and transformation, as well as on form, position and size of active area during laser processing.

The theory of composition of industrial laser systems' layout might be of a great use for designers and developers at the very beginning of designing process. For its development an analytical apparatus of research was created and quality factors were assessed and classified. The first part of the task was intended to find a mathematical formulation of industrial laser system's layout that would facilitate the research process. The other task was to determine the quality characteristics of the layout of industrial laser system in order to be able to compare and contrast different layout's configurations that would eventually lead to the improvements in quality. Formalized factors and characteristics of the layout's configurations is one step toward automated design of industrial equipment.

Theory of Arrangements of Industrial Laser Systems (ILS). For the purpose of the research it was estimated that the systems for laser forming of 3D solid objects could be designed to operate in polar, cylindrical, spherical and 3D Cartesian coordinate systems.

The layout of industrial laser systems has blocked structure. It consists of one stationary and a number of mobile blocks. The translational movements of the laser beam and worktable along axis of coordinates mean the same as an applicable axis (X, Y and Z). The rotations around of X, Y and Z axes mean accordingly by characters A, B or C. It would be reasonable to treat all other blocks which are not responsible for the formation of the movement patterns as one stationary block and to label it with letter O. Another special function of stationary block is to separate blocks of industrial laser system which govern laser beam movement and propagation from those which control the movements of worktable. The laser head and focusing unit are represented as indexes of the blocks which are responsible for the movements of each unit.

The block of focusing device of laser system means by the character F at the sign of the block: X_F, Y_F and Z_F. The focusing device can be connected both with stationary and with movable blocks. This joint mean by the character L at the sign of the block: O_L, X_L, Y_L and Z_L. If focusing device and emitter are connected together with stationary or movable blocks, in a structural formula of the character F and L stand at the sign of the block, on which one they are established: O_{LF}, X_{LF}, Y_{LF}.

These symbols could be written in order of the arrangement of blocks, and mathematical apparatus of set theory and algebra of logic could be implemented for the development of structural formulas of the arrangement and layout of industrial laser system. Blocks which represent movements of laser focusing unit and those responsible for the movements of worktable are written in the left- and rightmost parts of structural formula and they are separated by the stationary block. If one imagine that laser system consists of immobile laser head, worktable that moves along axis Z and laser focusing unit that moves along axes X and Y, then the structural formula of this arrangement will be $ZO_L XY_F$.

Main logical relations among elements in a set could be represented with conjunction and disjunction operators from logic of algebra. Commutative and Distributive laws could be implemented as well.

The whole set of structural formulas of industrial laser systems designed to operate in 3D Cartesian co-

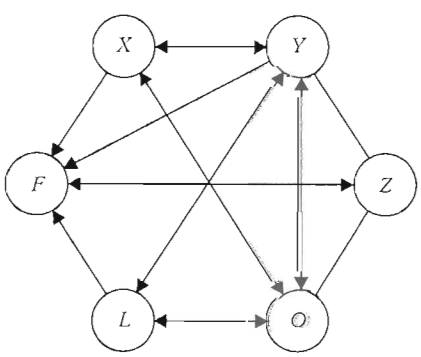


Figure 2. Oriented graph of the layout and arrangement of industrial laser system in 3D Cartesian coordinate system

	X	Y	Z	O	L	F
X	0	1	1	1	1	1
Y	1	0	1	1	1	1
Z	1	1	0	0	1	1
O	1	1	1	0	1	0
L	1	1	1	0	0	1
F	0	0	0	0	0	0

Figure 3. Matrix of interconnections of graph nodes which is intended to trace all possible structural formulas along ribs of graph

ordinate system could be represented as oriented graph, matrix of interconnections of graph nodes which is intended to trace all possible structural formulas along ribs of graph and matrix of the set of structural formulas (Figures 2, 3, 4).

The whole set of structural formulas of the arrangement of industrial laser system with regards to the mobility of focusing unit could be derived from the following expression:

$XYZO_{LF}$	$XYOZ_{LF}$	$XOYZ_{LF}$	XYO_LZ_F	XO_LYZ_F	$OXYZ_{LF}$	O_LXYZ_F
$YXZO_{LF}$	$YXOZ_{LF}$	$YOXZ_{LF}$	YXO_LZ_F	YO_LXZ_F	$OYXZ_{LF}$	O_LYXZ_F
$ZXYO_{LF}$	$ZXOY_{LF}$	$ZOXY_{LF}$	ZXO_LY_F	ZO_LXY_F	$OZXY_{LF}$	O_LZXY_F
$ZYXO_{LF}$	$ZYOX_{LF}$	$ZOYX_{LF}$	ZYO_LX_F	ZO_LYX_F	$OZYX_{LF}$	O_LZYX_F
$XZYO_{LF}$	$XZOY_{LF}$	$XOZY_{LF}$	XZO_LY_F	XO_LZY_F	$OXZY_{LF}$	O_LXZY_F
$YZXO_{LF}$	$YZOX_{LF}$	$YOZX_{LF}$	YZO_LX_F	YO_LZX_F	$OYZX_{LF}$	O_LYZX_F

Figure 4. Matrix of the set of structural formulae of industrial laser system in 3D Cartesian coordinate system

$$Pn = n! + [n! - (n - 1)!],$$

where Pn denotes the whole set of possible structural arrangements of industrial laser systems and n is a number of blocks of laser system.

The set of blocks which are included in the arrangements of laser systems for 3D Cartesian coordinate system is given by $\mathbf{M}\{O,X,Y,Z\}$. Thus, the number of possible arrangements of industrial laser systems with vertical orientation of coordinate axes will be: $Pn = 4! + [4! - (4 - 1)!] = 42$.

Using the same apparatus, graphs and matrixes of possible arrangements of laser systems could be obtained as well for polar, cylindrical and spherical coordinate systems. The set of blocks which are included in the arrangements of laser systems for cylindrical coordinate system is given by $\mathbf{M}\{O,X,ZC\}$ and $\mathbf{M}\{O,Y,Z,C\}$. It comprises stationary block O, block C that is responsible for the rotation around Z-axis, and blocks with linear movement along axes X, Y and Z respectively. Arrangements of industrial laser systems which were designed for spherical coordinate system there are two sets of blocks: $\mathbf{M}\{O,Z,A,C\}$ and $\mathbf{M}\{O,Z,B,C\}$. One block is responsible for linear movement, latter two — for rotational.

Of all variety of generated arrangements it is now necessary to pick a limited amount that would meet necessary technological tasks and requirements. Formalized criteria are required and mathematical principles of selection could be used to solve this problem.

Coordinate and Constructional arrangements of ILS. Basic requirements to industrial laser systems for laser forming of 3D solid objects with layer-by-layer material growing could be written as generalized structural formula, which in turn reflect diversity in the structure of arrangements.

For instance, if it is needed to avoid the impact of weights of both laser resonator and worktable on dynamic characteristics of laser beam manipulator, than resonator should be connected to stationary block and all technological movements are bound to be performed by the laser beam only. A generalised structural formula that describes the set of arrangements could be written as:

$$M_1 = O_L\overline{Z}\overline{Z}Z_F + O_LZ\overline{Z}\overline{Z}_F + O_L\overline{Z}Z\overline{Z}_F.$$

An upper dash above block's signs represents the inversion or logical negation:

$$\overline{Z} = X + Y.$$

Taking into account the fact that worktable moves along Z-axis in-between the process of powder layer formation it would be reasonable to add to our selection those arrangements where worktable moves only vertically. This extra regulation could be written as

$$M_2 = ZO_L\overline{Z}\overline{Z}_F$$

A general set of arrangements that responds to conditions stated above would be:

$$M_{1+2} = ZO_LXY_F + ZO_LYX_F + O_LXYZ_F + O_LYXZ_F + O_LZXY_F + O_LZYX_F + O_LXZY_F + O_LYZX_F$$

Further analysis of structural formulas show that this set of eight structural formulas could be reduced down to two main arrangements:

$$M = ZO_LXY_F + O_LXYZ_F.$$

Coordinate layouts, which would reveal the content of each block of equipment and the order of coordinate movements, should be done for each element from matrix of arrangements of ILS in various coordinate systems. These coordinate layouts are intended to give a spatial pattern of industrial laser system using structural formulas from matrixes of arrangements of ILS. Simplified images of laser head, resonator, focusing unit and other blocks were used (Figure 5).

When industrial robots are used in O_LXYZ_F arrangement, it is necessary to use optical fiber for laser beam delivery.

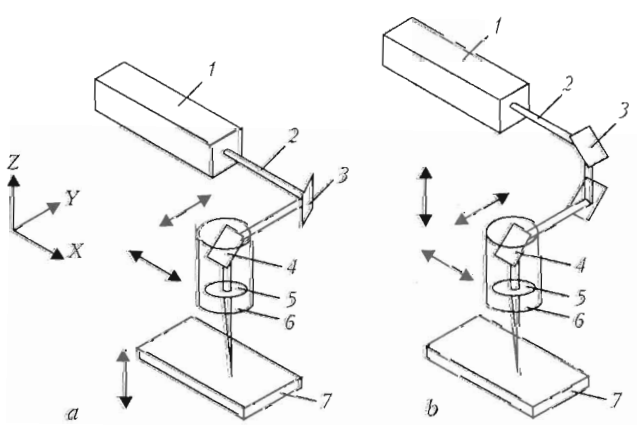


Figure 5. Coordinate layouts of ZO_LXY_F and O_LXYZ_F arrangements: *1* — resonator, *2* — laser beam, *3, 4, 8* — rotational mirrors, *5* — lens, *6* — focusing unit, *7* — worktable

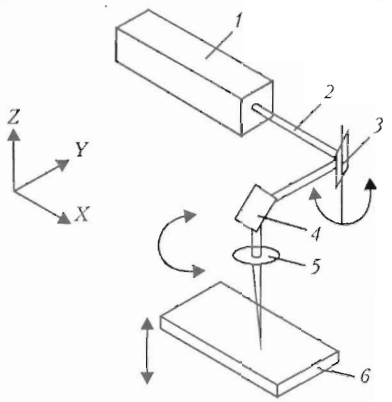


Figure 6. Coordinate layout of ZO_LCA_F arrangement

In the same way, coordinate layouts for cylindrical and spherical coordinate systems could be developed as well. The coordinate layout for ZO_LCA_F arrangement in spherical coordinate system is shown in Figure 6. Parts of its optical elements are now widely used in laser beam scanning applications.

Constructional layout of arrangement is a logical extension of the coordinate layout. The ZO_LCA_F arrangement was chosen to be the basis for constructional layout industrial laser system for layer-by-layer 3D forming of solid objects by selective local sintering. Stationary and movable blocks are connected with help of guiding rails (Figure 7). Taking into account the peculiarities of laser 3D forming of solid objects the following technological modules were added:

- module for creation of powder layer
- powder dispensing mechanism
- supporting He–Ne laser

The powder material is supplied form dispenser's nozzle *4* onto the module *3*, which usually rest in left-most or right-most positions and is involved in forming of a uniform layer of powder material. On a carrier of module *3* there is a bin with powder material, which acts as a bleed feeder. While module *3* moves along the slides the powder is dispended on a worktable *2* ore on a previously sintered layer of powder. The scraper attached to a bleed feeder evens the powder layer. At the same time, the newly formed layer of powder is tamped with a roll which moves along

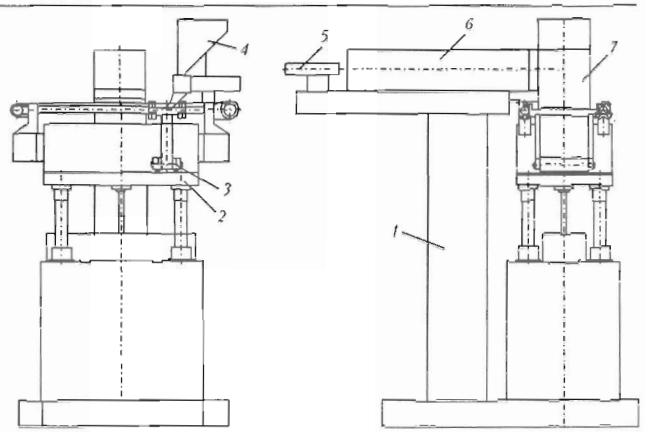


Figure 7. Constructional layout industrial laser system for layer-by-layer 3D forming of solid objects by selective local sintering; *1* — stationary block; *2* — work table; *3* — module of powder layer preparation; *4* — powder dispenser; *5* — supporting laser; *6* — laser; *7* — optical head

with the scraper. Attaching two rolls on both sides of module *3* will intensify the process. A layer of sintered powder with needed configuration is formed when laser beam scans powder bed following previously created control routine. The worktable then descends one step down, and feeder moves in backward direction, thus creating a new layer of powder. All this helps to create a 3D solid object out of powder material.

The worktable has a transparent tank for working zone's protection and for the ability to supervise the formation process.

CONCLUSIONS

Upon the result of the structural analysis of possible arrangements there were developed and designed two industrial laser systems for-by-layer 3D forming of solid objects by selective local sintering. The arrangement ZO_LCA_F of ILS was used for the laser forming with local sintering of powder, and the arrangement was used in the case of 3D forming with the stream of molten powder. In the latter case an industrial robotic system was used to manipulate the focusing unit and molten powder dispenser. The laser beam was propagated along the waveguide.

Conference Sponsors

PWI Laser Systems and Technology Center

Ministry of Education and Science of Ukraine

Information Support

«The Paton Welding Journal»

www.nas.gov.ua/pwj

Conference Sponsors

PWI Laser Systems and Technology Center

Ministry of Education and Science of Ukraine

Information Support

«The Paton Welding Journal»

www.nas.gov.ua/pwj

AMORPHING OF ALLOYS BY LASER GLASS GLAZING OF SURFACE

G. V. BORISOVA[1], A. B. LYSENKO[1], N. A. KOROVINA[1], O. L. KRAVETS[1], A. A. LYSENKO[2]
[1]Dneprodzerzhinsk State Technical University, Ukraine
[2]Dnepropetrovsk National University, Ukraine

The heat-transfer and glass forming particularizes at laser treatment of metal materials with surface fusion, has been investigated. It has been shown, that laser rapid quenching technology provides higher cooling melt rates, but it is less effective alloy amorphization method in comparison with quenching of liquid metal thin layers on heat-conducting substrate. By kinetic diagrams, built for bottom and top laser bath levels with account their transfer to undercooling state and probably crystallization mechanisms, the research results has been explained.

Materials and research methods. In the given paper a comparative structural analysis of a number of glassforming alloys, prepared in the form of rapid quenching foils 40–90 μm thick (l ~ 40–90 μm) fused by impulse laser radiation approximately to the same depth has been carried out. The objects of research were Fe-based alloys with elements-amorphiers (B, P, C), Al–Y–Ni-alloys, and also Ni–Nb alloys know for their high tendency to non-crystal hardening under the conditions of quick quenching of their liquid phases.

The liquid phase quenching was carried out by the injection of a small portion (~100 mg) of a melt onto the surface of a rotating cooper cylinder. Laser fusion of cast specimen was conducted on the plant GOS-1001 in the mode of free generation. X-ray structural studies were carried out using the diffractometer DRON-3 in monochromatic radiation Co_{K_α}. The microstructure was investigated with the help of the metallographic microscope Neophot 32, the microhardness — with the device PMT-3.

The results of the investigations and their discussion. The compositions and the structural analysis results of the alloys under investigation which were prepared by 2 methods of rapid quenching are presented in Table 1. It is evident that by solidifying on the surface of a rotating quenching unit alloy 1 acquires amorpho-crystal structure, and alloys 2–5 become complete amorphous in the cross-sections 43–88 μm. It confirms high glass-forming ability of all the alloys studies, and it increases in the order they are presented in Table 1.

Table 1. Structure of the investigated alloys obtained by rapid quenching on a heat-conducting base (QHCB) and laser treatment with surface fusing (LTSF)

Alloy number	Alloy composition	l, μm	h, μm	Structure of specimen studied	
				QHCB	LTSF
1	$Fe_{79}B_{21}$	40	33	$A + C$	C
2	$Fe_{78}P_{13}C_9$	43	37	A	C
3	$Fe_{84}B_{10}C_6$	46	42	A	$C + A$
4	$Al_{87}Y_8Ni_5$	65	58	A	$A + C$
5	$Ni_{85}Nb_{15}$	88	75	A	A

Note: A — amorphous phase; C — crystal phase

By fusion with millisecond laser impulses the indications of surface amorphing are revealed in alloys 3–5. The amorphic structure without any traces of crystal phases is observed only in alloys $Ni_{85}Nb_{15}$, which according to Table 1 is characterized by the highest tendency to non-crystal hardening. In the normal cross-sections of the specimens made of alloy 5

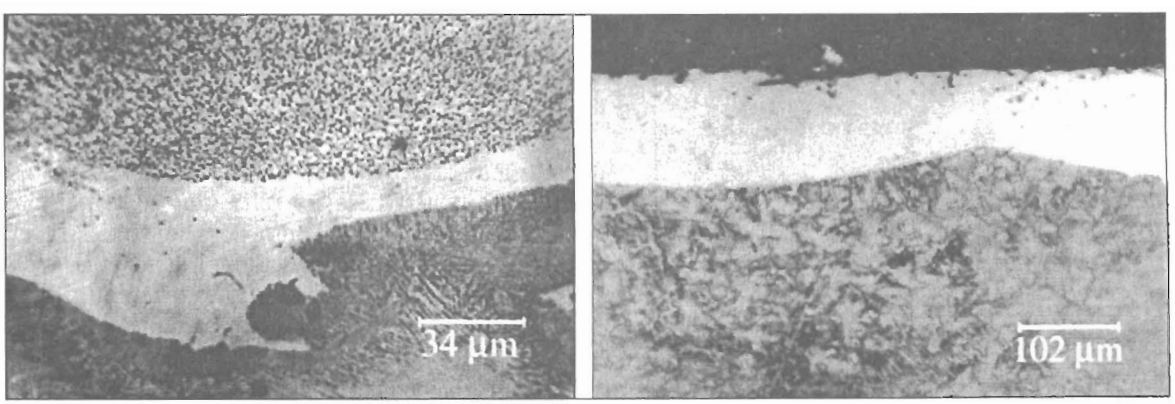


Figure 1. Microstructures of laser fusion zones: a — alloy $Ni_{85}Nb_{15}$, normal cross-section; b — alloys $Fe_{84}B_{10}C_6$, treated surface

© G. V. BORISOVA, A. B. LYSENKO, N. A. KOROVINA, O. L. KRAVETS, A. A. LYSENKO, 2005

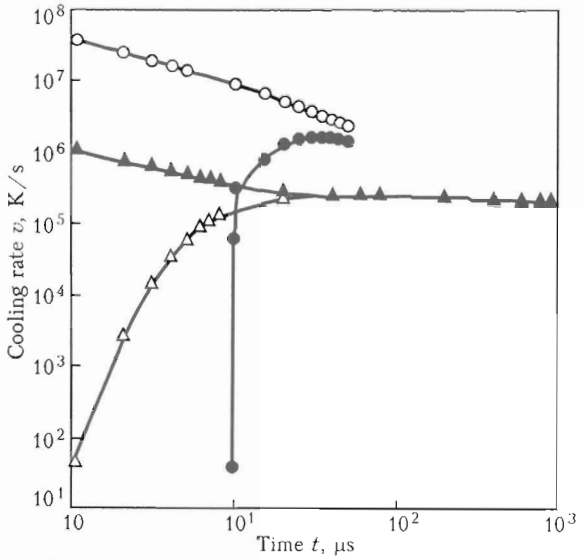


Figure 2. Dependencies of cooling rate on the time for melt areas, adjoining to free surfaces (light points) and adjoining the base or boundary of a laser fused zone (dark points)

and fused by a laser the surface layer looks like a continuous white stripe and its lower edge coincides with the fusion boundary (Figure 1, *a*). In this stripe limits no metallographic indications of the alloy crystal structure can be found.

The zone of laser glass glassing in alloys 3 and 4 possesses an amorphous-crystal structure and when in alloy $Fe_{84}B_{10}C_6$ the amorphous phase is relatively small, in alloys $Al_{87}Y_8Ni_5$ it is the prevailing structural constituent. The presence of the amorphous phase in the zone of laser treatment is revealed by the rise of intensity in the interval of reflection angles, which is characteristic of the first galo place on the scattering curves of the rapid quenched amorphous foils of the corresponding chemical compositions. With the help of metallography in the alloys with partly amorphized structure extent areas of unrestricted forms without any indications of etching can be revealed (Figure 1, *b*). These areas possess higher microhardness as compared to the ajoining areas having quasieutectic structures. For example, in alloy $Fe_{84}B_{10}C_6$ the average meanings of H_{50} for non-etched zones are 15.9 GPa, that perfectly agrees with the amorphous foils properties made of the same alloy, and also with the known literature data for amourphized by laser radiation Fe-based alloys [1].

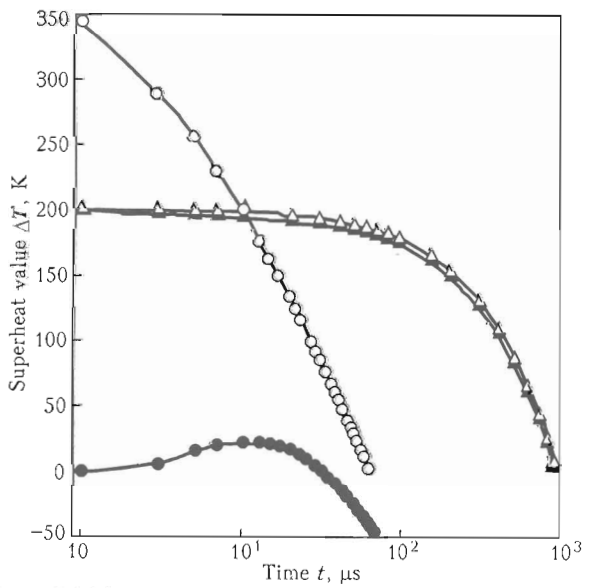


Figure 3. Melt superheat vs. time of cooling for surface levels (light points) and levels, which contact with substrate or crystal regions of laser target (dark points)

The experimental data testify that laser glass-glazing method is less effective means of alloy amorphing than rapid melt quenching on a cooler surface. To explain this conclusion we compare the modes of cooling in the investigated techniques of rapid quenching which were separately studied in the works [2, 3].

Using mathematical models offered in the sources mentioned, we obtain numerical solutions of the heat task, formulated to be applied to the QHCB and LTSF methods. All the calculations are be executed supposing that up to the moment of the surface zone mounting to the fusion temperature the liquid metal layer thickness is the same ($l = h = 50$ μm). To avoid possible influence on the results of simulating of the treated metal and base properties we shall study the processes of rapid quenching of copper on a copper base and also the cooling of a laser fusion zone on the surface of a semi-infinite copper plate.

The graphs of the speed variation of a melt cooling and its preheating data depending on the time are shown on Figure 2 and 3. The corresponding calculations were executed for two zones, one of them occurs near the liquid layer free surface, and the other along the boundaries with a heat-receiver or non-fused areas of a laser target.

The analysis of the simulation results shows that in both methods of rapid quenching at the early stages of the process the opposite sides of the liquid metal layers are cooling in a rather different way and by the application of the QHCB method the highest cooling rates are reached in the zone of the melt contact with the base. By the application of LTSF method these rates are the highest in the upper levels of the melt bath (Figure 2). In the course of time these differences in the quenching modes decrease, resulting in establishing a regular operation in the layers cooled on a heat-conducting base, and in the layers fused by a laser the operation is approaching a regular mode.

As we can see in Figure 2, when the melt reaches the fusion temperature, the speed of the laser bath cooling is by an order higher than the speed of the melt foil cooling on the quenching unit. As follows from it, laser treatment with surface fusion possesses higher potentialities for obtaining metastable, structural states in alloys. But according to the experimental data given above, this advantage of laser technique is not adequately realized in the structure of the alloys under investigation. To our minds the main reasons of this disparity of the potentialities and actual results of laser rapid quenching are non-synchronesm in reaching the fusion temperature by different zones of a laser bath and the existence (on the boundaries be-

tween phases) of crystals from the laser target material which are capable of growing, according to the simulation results the first to come to a supercooled state are the layers lying near the fusion boundary (Figure 3). As these layers come in contact with non-fused crystals of the target, the latter began to penetrate into the melt.

The possibility of realization of the matrix crystal growth mechanism, decreases the melt stability in the low undercooling zone, that is equivalent to appearing on the diagram «temperature-time-transformation» of an additional projection on the kinetic curve (Figure 4, *a*). It can be seen that as a result of such TTT-diagram transformation the cooling rates causing the suppression of homogenous crystallization processes are not able to avert crystal growth from the fuse boundaries. So, amorphing of the bottom part of the laser bath is hampered by crystal growth on the fusion boundary.

The upper levels of the laser bath are superheated to the maximum and are cooled at the highest speeds (Figure 2, 3). During the melt cooling to the fusion temperature a structural rearrangement in its bulk doesn't have time occur, that promotes the processes of crystallization of equilibrium phases. As a result in these areas preconditions for non-crystal hardening are created. As a result in these areas preconditions for non-crystal hardening are created. But by the upper layers transition to the critical area of the temperatures $T < T_m$ the melt cooling is rather slowed down because of releasing of latent conversion heat on the front of matrix crystal growth that is shown on Figure 4, *b* hampering in the form of a sharp change of the temperature curve slope $T(t)$.

Following the decrease of speed of the surface layers cooling, the processes of homogenuous crystallization are taking place and the rate of completion of these processes depends on the factual ratio of cooling rates to the rates of nucleation and growth of the crystal phases. So, the main cause, hampering amorphing of the upper layers of the zone fuse by a laser, is a sharp slowing down of cooling due to exothermal effect in the zone of columnal crystals growing from the fusion boundary.

CONCLUSIONS

1. The investigations of the structures of glass forming Fe-, Al- and Ni-based alloys were carried out (QHCB and *LTSF methods had been applied). It was shown*

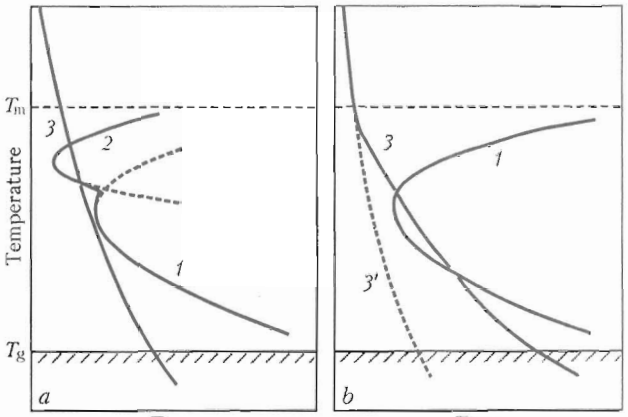


Figure 4. Scheme of kinetic diagrams and cooling curves for bottom (*a*) and top (*b*) levels of a pool; *1* — TTT-diagram corresponding to homogenuaous crystallization; *2* — TTT-diagram, corresponding to matrix crystal growth process (mechanism); *3* — curves $T(t)$; *3'* — curve path $T(t)$ without exotermal effect in the bottom part of a pool; T_m, T_g — temperature of fusion and glass temperature, respectively

that by comparable thickness of liquid metal layer its non-crystal hardening is most likely to occur in the case of its cooling on the quenching unit.

2. By the mathematical simulation of heat-transfer processes it was stated that the laser technique of rapid quenching provides higher speeds of melt cooling at the moment of its transition to a undercooled state than traditional methods of liquid metal foil quenching on a heat-conducting base.

3. A lower tendency of alloys to amorphing under the condition of laser rapid quenching is due to asynchronic transition to a undercooled state of different zones of a fused layer and also to the existence of equilibrium phases which, on the one hand, initiate crystallization of the bottom part of a laser bath and, on the other hand, influence the cooling modes and the transformation mechanism of the bath upper levels.

1. Yu.A. Skakov, N.V. Edneral, Kh.A. Mazorra, V.S. Kraposhin. *Producing amorphous layers on the surface of massive substrates using laser radiation.* In coll.: Amorphous metal alloys. — M: Metallurgy, 1983. — 814 p.
2. A.B. Lysenko, G.V. Borisova, O.L. Kravets. *Calculation of cooling rate in quenching alloys from the liquid state.* — Phyzika in tekhnika vysokikh davlenij, 2004. — V. 14. — #1. — 4453 p.
3. A.B. Lysenko, N.A. Korovina, G.P. Brekharya. *Influence of technological factors on thermal process dynamics in the zone of metal surface melting by laser radiation.* Mathematical simulation. — 2001. — # 2(7). — 99105 p.

INCREASE OF RIGIDITY OF THIN LAMINAS BY CREATION AND OPTIMUM ARRANGEMENT OF METALLURGICAL STRESS RAISERS

L. F. GOLOVKO[1], A. D. KAGLYAK[1], A. P. KRASAVIN[1], V. G. SOROCHENKO[2]
[1]National Technical University of Ukraine «KPI», Kiev, Ukraine
[2]V. N. Bakul Institute for Superhard Materials of NASU, Kiev, Ukraine

The analysis of the problems connected to rigidity of thin plates is resulted, results of mathematical modelling of them is intense – deformed statuses depending on conditions of the application of loading. It is informed on results of studying of features of structural – phase transformations in thin steel plates at local laser heating and laws of formation of residual pressure. The original way of increase of rigidity of thin steel plates is offered and investigated at the expense of creation on their surface with the help of a laser irradiation in the special image of the located local sites with the changed structure. It is shown, that, operating size and character of distribution of residual pressure on these sites, and also their arrangement on a surface of a plate, it is possible, depending on conditions of the application of loading, essentially to lower size of the elastic deformations arising from action of working loadings, and. Thus, to raise rigidity of products. The opportunity of application of the offered way for improvement of quality of the diamond tool and his productivity is illustrated.

Introduction. One of major factors which essentially influence quality and serviceability of a product such as «a thin plate» is its rigidity.

Rigidity is a property of a design and its elements to resist to external loadings concerning deformations (change of the form and the sizes). At the set loadings of deformation should not exceed the certain sizes which are established according to requirements to a design. The successful choice of this characteristic allows to use more effectively thin products, to increase its service life.

Now to increase of rigidity thin metal products apply a line of ways. This application composite materials reinforced with particles or fibres with the high module of elasticity. To the same purposes apply constructive receptions which are based on connection of geometrical parameters of a product and its rigidity. To increase rigidity of a design it is possible creating in her the closed cavities, manufacturing of edges of rigidity, fringing, thickenings, etc. In many cases the basic requirement is that thus its sizes did not change, for example thickness, and weight. The problem of low rigidity is characteristic for space technical equipment (the aerial, solar batteries), radio engineering, motor industry, aircraft construction, shipbuilding, tool manufacture, etc.

One of such products of tool manufacture is the thin diamond detachable circle. Its low rigidity results during work

To deformation of a circle. As a result of it accuracy and productivity processings, a resource of work of the tool and area of its application are essentially limited to sizes of loadings.

The basic problems of existing manufacturing techniques of thin diamond circles sintering in mould is the big heterogeneity of structure of the layer containing diamonds, and the residual deformations of the case of a circle connected to it, low rigidity of a circle in an axial direction, its insufficient wear resistance which is reduced in process of reduction of thickness diamond of a containing layer, low productivity. As base the design of a diamond detachable circle with the following parameters was considered. External diameter of – 125 mm; thickness of a diamond layer – 0.7 mm; the width of a diamond layer measured on radius of a circle – 7 mm; thickness of the case of a circle – 0.5 mm; depth of immersing of the case of a circle in a diamond layer – 2.5 mm. The case of a circle is made of steel 13Kh. After manufacturing he is exposed to special heat treatment which stabilizes structure of a material. To manufacturing tools apply synthetic diamonds such as ACC 35. The analysis of a design of the tool and requirements to it has shown what to solve the named problems it is possible application of laser technology. For this purpose it is necessary to execute correspon-ding researches. Researches are expedient for leading in three directions. To study an opportunity of application of laser radiation for increase of uniformity and dispersiveness of structure of materials, including layer with diamonds.

To investigate an opportunity of increase of axial rigidity of the tool due to increase in hardness of a material of the case of a circle on separate, special image the located, local sites. To study an opportunity of indemnification of pressure and the deformations arising in a product at action of working loadings, preliminary formation in the case of a circle by local change of structure of a special intense condition.

The results of researches corresponding to first two directions, are in part published by us earlier [1, 2]. The given work is their logic continuation and reflects some results concerning the third direction.

© L. F. GOLOVKO, A. D. KAGLYAK, A. P. KRASAVIN, V. G. SOROCHENKO, 2005

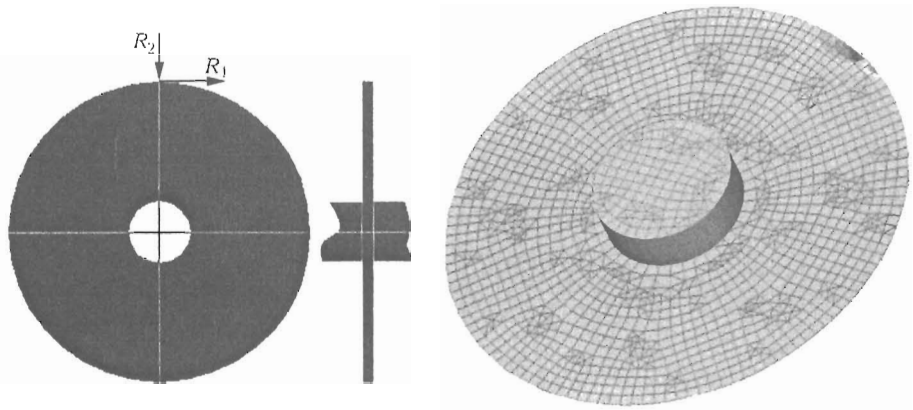


Figure 1. Circuit of settlement model of a disk and breakdown it on elements

The modeling is intense — deformed condition of a disk. Modelling is intense — deformed statuses of a steel disk under various conditions loading with used software MSC Nastran. For this purpose the three-dimensional geometrical model of a disk with a part of a shaft on which he is fixed (Figure 1) was formed all over again two-dimensional, then. At carrying out of calculations it was necessary, that the thin disk made of chromic steel (1.3%C, 1%Cr), thickness of 0.5 mm, 200 mm in diameter. Disk rigidly planted on a shaft (diameter — 30 mm) to which torque M. Modul's of elasticity E, the shear modulus G, Poisson's ratio μ, density of a material ρ was accepted for carbonaceous steel. As boundary the pressure corresponding to yield point $\sigma_т$ steel at a stretching, compression and shift were accepted

For realization of account the method of final elements chose the sizes of elements researched area, the boundary conditions and areas are given, to which they concern (internal diameter of a disk), condition loading. In process of contact of a rotating disk to a processable material, on it work radial and tangential of reaction R_1, R_2. Their correlationcan vary in a wide enough range. The accounts were carried out at various characteristic correlation R_1:R_2 (table 1). The direction of forces is shown in a Figure 1. The distributions normal, tangential, maximal tangential of pressure and deformations in various planes paid off.

The capacity of radiation was continuously supervised with the help specially developed through passage measuring instrument, working on branch of a part of radiation (1%) from the basic beam (accuracy of measurement 2%). For an estimation of distribution of capacity of radiation in a plane focusing and definition of an actual diameter of a stain in coaxial planes focusing the technique of scanning of cross section of a beam diaphragm, and also analyzer of laser bunches(beams) such as LBA of firm «ALL GmbH» was used. Were investigated carbonaceous steel (1%C), alloyed began 95Kh and V2F. Samples thickness of 1 mm were processed by laser radiation at the following modes: diameter of a stain of focussing, d_0 = 5 mm, capacity of radiation, P = 1 kw, speed of processing, V = 0.5; 1; 1.5; 2; 2.5 m/min. The irradiated samples of plates were cut on the electroerosive machine tool by a wire electrode in a direction perpendicular to a direction of moving of a laser beam (across «pathes») and along them on two equal parts. From one of half prepared by a standard technique metallurgical section.

Table 1.

№ calculation	Tangential R_1	Radial R_2	№ calculation	Tangential R_1	Radial R_1
1	20	10	8	260	220
2	80	50	9	270	320
3	100	110	10	280	420
4	110	130	11	100	420
5	170	140	12	80	200
6	170	170	13	100	250
7	180	210	14	300	100

Revealing of a microstructure of zones of laser heating was carried out with use of 3% spirit a solution of nitric acid.

Studying of a microstructure of the superficial layers strengthened by laser radiation, was carried out on metallurgical microscopes MMP-2P, Neopfot 23. Metallurgical microscopes have been advanced by their equipment by the digital television camera connected to a computer.

Measurement of microhardness of zones of laser heating was carried out on mikrohardometer PMT-3 at loading on indentor 100.

Influence of conditions loading on distribution of pressure in a disk. The analysis of results of cal-

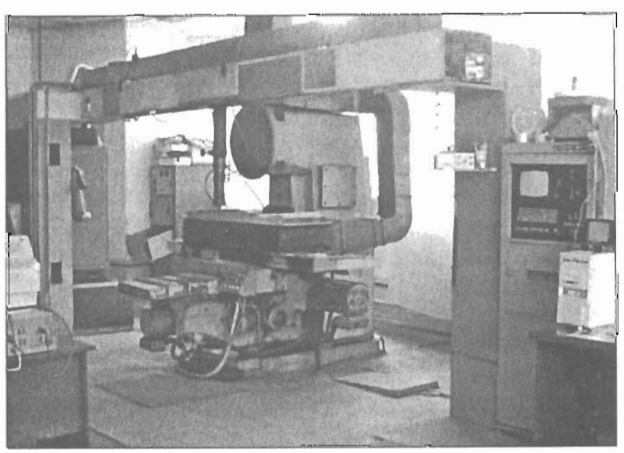


Figure 2. General view of experimental laser technological complex «Comet-2» on CO_2-laser base

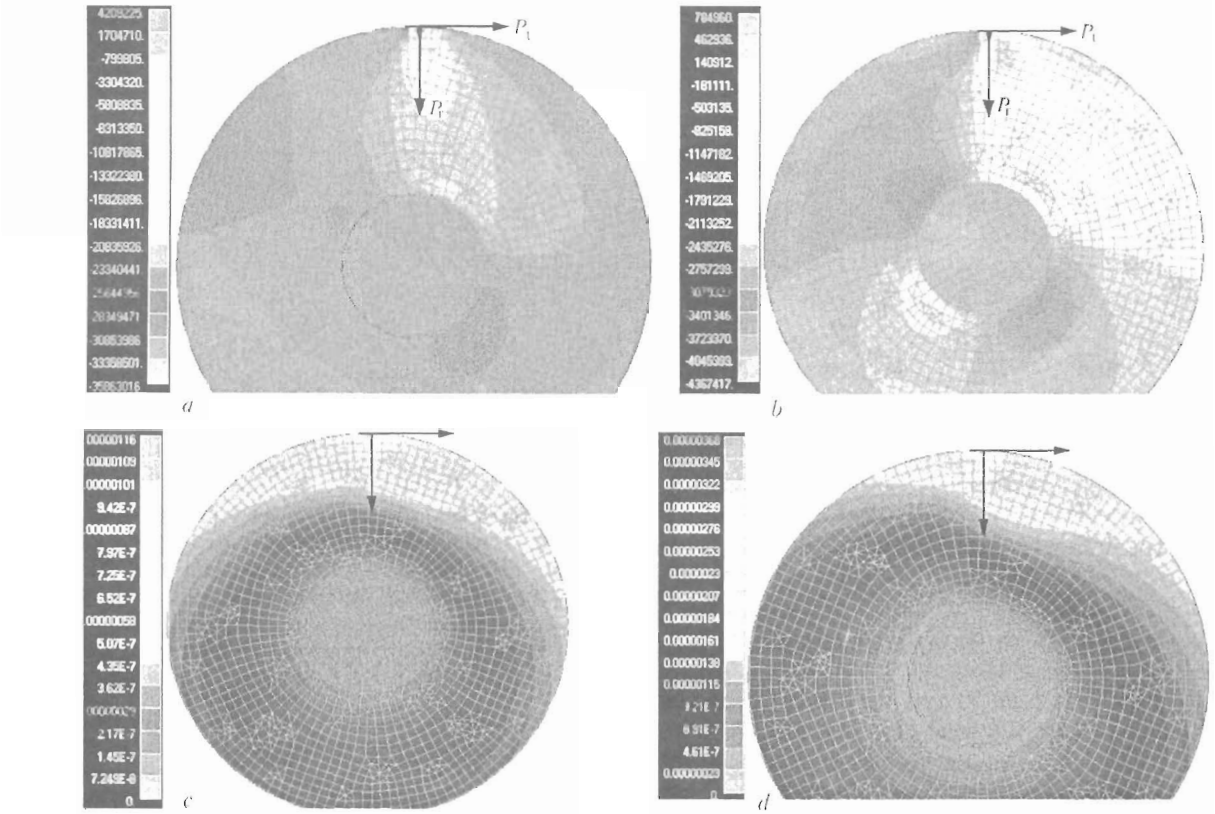


Figure 3. Distribution of normal pressure (*a*, *b*) and deformation (*c*, *d*) pressure in a disk at ratio of making loading P_r:P_t — 50:10 N (*a*, *c*); 80:20 N (*b*, *d*)

culations has shown, that in the case of a circle at the appendix external loadings (Figure 1) are formed various on size, a sign and a configuration of distribution of a pressure. In area, adjoining to a point of the appendix of loading, normal compressing pressure, in peripheral — stretching (Figure 3, *a*, *b*) take place. The configuration of their distribution essentially depends on a ratio of radial and tangential making loading. At the big radial component compressing pressure are concentrated along radius (Figure 3, *a*). With increase in a tangential component a trajectory of distribution of normal compressing pressure. It is curved aside opposite to a direction of rotation of a circle (Figure 3, *b*). This law has steady character. An intense status of a circle so also its deformation, at known components of loading it is possible to predict. Being set by limiting values of deformation it is possible to establish critical values of loading. These values of loading define rigidity of a circle and the maximal productivity of process of cutting. For increase of productivity of the tool it is necessary to increase value of critical loadings. It is possible to achieve preliminary formation in a material of a circle in the field of a concentration of working compressing pressure of residual pressure of an opposite sign. Such problem is offered to be solved application of local laser heating.At laser heating in steel depending on a chemical compound, an initial structural condition and conditions of an irradiation it is possible to generate both compressing, and stretching residual pressure[1]. Due to localness of process it is possible to receive their various distribution on a surface of a circle.

Feature of structural — phase transformations at laser heating of thin steel disks. The structure of steel V2F in the ambassador of thermal processing represents granular pearlite and the rests carbide grids.

On Figure 4 a the submitted zone of heating which is received as a result of a laser irradiation of a plate from steel V2F by thickness of 1 mm at capacity of radiation of 1 kW, diameter of a stain of focussing of 4.5 mm, speeds of moving of a sample of 0.5 m/min.

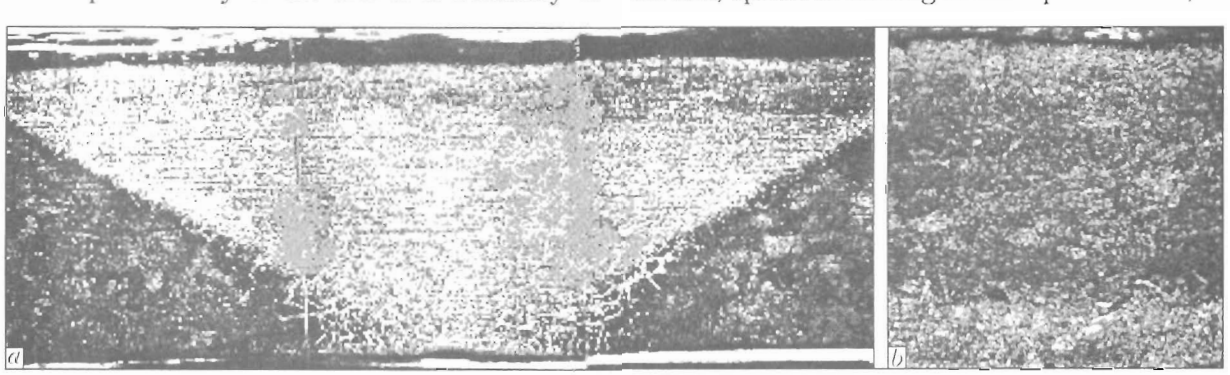


Figure 4. Zone of laser heating of a plate 1 mm thick of steel V2F at P = 1 kW, d_0 = 4.5 mm, V = 0.5 m/min (*a*) and 1.0 m/min (*b*)

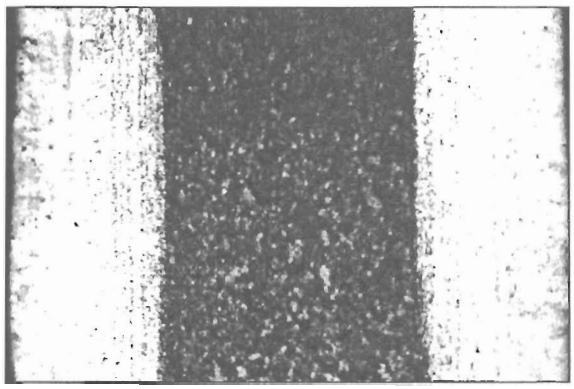


Figure 5. Steel thin plate (1 % C), strengthened from two parties by laser radiation (P = 1 kW, d_0 = 5 mm, V = 2 m/min)

This zone can be divided into some layers. In the first layer where the temperature exceeded critical point AC_m there was a full dissolution carbide. Structure of this layer: highalloyed residual austenite and a small amount martensite (Figure 4, *i*). Microhardness of structure 7500 MPa.

In the second layer of temperature of heating is closer to optimum temperatures of training for the given steel, and speed of cooling — sufficient for formation martensite carbide the grid is shattered, were formed superfine carbide. Hardness of this layer makes also 7500 MPa.

At the further removal {distance} from a surface the structure of incomplete training which includes martensite, a quantity residual austenite, small inclusions carbide is found out. Hardness of a layer — 7000 MPa.

The transitive layer as against processing massive details has dim borders. Structure of this layer: troostite with sites martensite.

At increase in speed of processing up to 1.0–1.5 m/min the sizes of a zone sharply decrease and become less thickness of a plate. Structure-martensite, residual austenite and part carbide. The maximal hardness reaches 10000 MPa.

Changing diameter of a stain of focussing and speed of processing it is possible to receive the strengthened layer which thickness is equal to thickness of a plate, and the form — it is close to rectangular. It is one of ways of reception of edges rigidity as the strengthened layers — metallurgical concentrators of pressure.

Other way of management of an intense condition of the case of a circle is possible also. At this way the sites of the case laying strictly against each other on opposite surfaces (Figure 5) are exposed to a laser irradiation.

At a laser irradiation carbide steel in a superficial layer the structure with hardness at a level of 1000–1100kg/mm^2 (Figure 6) is formed dispersion martensite-austenite Operating speed of an irradiation it is easy to change depth strengthened of a layer. For

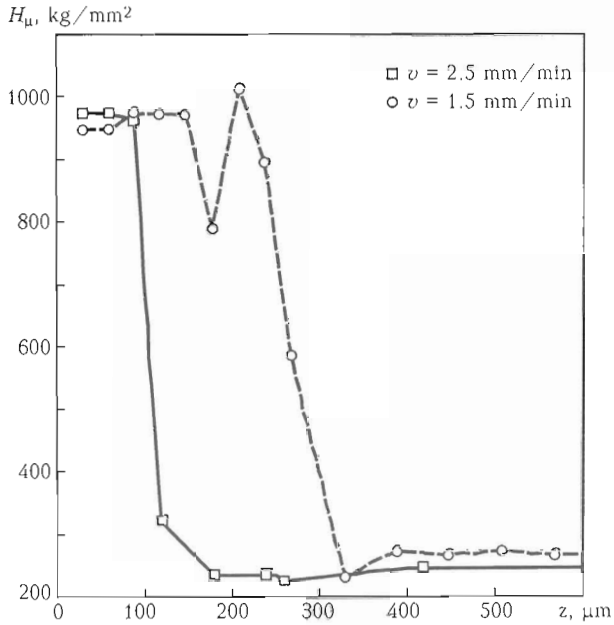


Figure 6. Distribution of hardness on depth in steel (1%C)

exception of occurrence of intermediate deformations of the case it is expedient for processing by laser radiation in detented a condition. At definition of modes of laser processing steel, stretching(dragging out) residual pressure, (voltage,) ensuring formation, it is expedient to take advantage of results of researches stated in [1, 2].

CONCLUSION

1. Existing methods of increase of rigidity of thin plates are analysed and the expediency of use for these purposes of local laser heating is shown.

2. Working pressure which arise in the case of a circle at external loading, their sign, size and character of distribution it is possible to define and predict applying software MSC Nastran.

3. Depending on a ratio of radial and tangential making loading in the case of a circle the compressing pressure concentrated along radius or along a curve curved aside opposite direction of its rotation are formed.

4. The new way of increase in rigidity of a plate is offered due to local change of structure of sites of a circle where working compressing pressure are concentrated.

5. Two circuits of increase of rigidity of thin plates at which one surface of a circle or both it is exposed to a laser irradiation are offered surfaces

1. *Handbook of Laser Materials Processing*. 7.5.3. L.F. Golovko et all. Laser Institute of America. Orlando, USA, 2001, p. 249–258 (715p.).
2. *Laser Surface Hardening and Electric-Spark Surface Hardening of Materials*, V. S.Kovalenko, A. D. Verkhoturov, L. F. Golovko, I. A. Podchernyaeva, New York, Plenum Publishing Corporation, 1986, 274 p.

APPLICATION OF LASER TREATMENT FOR INCREASE OF WEAR RESISTANCE OF DETAILS OF THE HEAVY LOADED UNITS OF FRICTION

L. F. GOLOVKO, A. T. SERDITOV, Y. V. KLYUCHNIKOV, A. DASZHERDI
National Technical University of Ukraine «KPI», Kiev, Ukraine

The analysis of problems of wear resistance of heavy loaded units of friction is represented. It is explored and analysed application for the solution of these problems of technologies of the laser thermal consolidating superficial microalloying and cladding, their technological possibilities are outlined. Offered and realized original method of increase of antifriction properties of surfaces of friction, working in extreme conditions: at high specific pressures, promoted temperatures influence of aggressive environments. Conformities to the law of forming are studied in the conditions of laser irradiation of wearproof superficial layers, their sizes parameters structure and tribotechnic descriptions. The results of application of the developed technology are represented for the increase of operating descriptions of boring instrument and bearings of the system of turbo-supercharging of diesel engine of heavy cars and tractors, information of industrial approbation.

Introduction. Resistance to the wear is the most important description of materials, to a great extent determining the resource of work of details of machines and mechanisms. Especially sharply this question stands for details working in the heavily loaded knots of friction, where high contact specific pressures take place, over high rates of relative movement, streams of working liquids, presence of aggressive environments, action of cyclic changing temperatures. Such terms are characteristic for supports of boring chisels, footstep-bearing of billows of turbines of the system of turbo-supercharging of engines, shoulder-blades of gas turbines and other. The laboured or in general impossibility of delivery and withholding in the area of contact of details of knots of friction of greasing is the distinctive feature of their work.

Technological measures, developed to the present tense, including creation on the contacting surfaces of oil-retaining regular microrelief, application of hard lubricating materials including with the rotaprint method of delivery of greasing, causing of antifriction coverages by galvanic methods, plasma, detonation and other in combination with different methods of the superficial consolidating (by plastic deformation, the HFC (high-frequency current) hardening, chemical-termical treatment (by nitriding, chrome-plating, nitriding and other), allowed to decide a lot of the intricate technical problems related to providing of capacity of different mechanisms. However much comparison of terms of work of the heavyly loaded knots of dry friction with the terms of work of machines with the traditional types of greasing shows that they on the resource of work in ten and hundred one time yield to the last. By the principal reasons of low resource of work of knots of dry friction there are the small volumes of lubricating material and absence of his circulation in a mechanism [1].

Laser radiation, due to high its energy, possibilities strictly dosed to bring energy into the processed material, allows due to the local high speed heating to create on a surface areas with specific structures, possessing high dispersion, containing metapermanent phases, supersaturated hard solutions. Such structures possess high hardness, in 1.5–2 times exceeding hardness arrived at at the use of traditional methods of heat treatment.

In structures along with hard consolidating phases (by martensite, carbides, borides and other) plastic γ-phases can be fixed, besides sometimes in great numbers, to 30% and anymore. The repeatedly observed redistribution in the hard phase of row of alloying elements is instrumental in it: one, for example carbon, — to the surface, other, for example heavy — vice versa [2]. It is necessary to mark that the mentioned redistribution carries anomalous character and is not inscribed in classic presentations of theory of diffusive processes. All adopted features of the structures got at the laser irradiation, stipulate their high resistance to the wear. The process of wear differs by a smoothness, absence of fragile destruction (extractions, splitting off), forming on the surfaces of friction of the characteristic texture oriented in the direction of sliding [3].

By additional backlogs of laser treatment, from point of increase of wearproof of knots of friction, are the directed change of chemical composition of local areas of superficial layers of details by the laser microalloying or cladding, and also management by sizes and location of these areas on contacting surfaces [4].

This work is devoted to the further study of possibility of application of technology of laser superficial treatment for the increase of wearproof of details of heavyloaded knots of friction, that the same is the actual question of industrial machine-building production.

© L. F. GOLOVKO, A. T. SERDITOV, Y. V. KLYUCHNIKOV, A. DASZHERDI, 2005

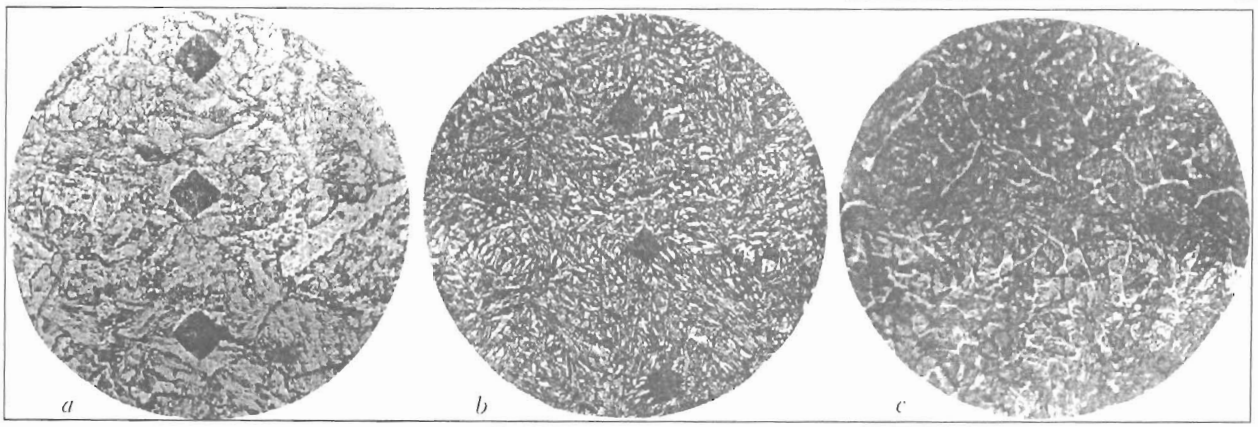


Figure 1. Microstructure of steel 14Xkh3MA in the initial state (*a* — ×500), aftereutectoid areas of the laser hardening (*b*) and transitional from aftereutectoid to ZTI (*c*) in preliminary cemented and hard-tempered HFC

Experimental equipment and method of conducting of researches. Experimental researches were conducted with the purpose of study of features of structure-phase transformations, flowing in carbon and alloyed steels at the laser irradiation, and also establishment of conformities to the law of process of laser cladding. Standards from steel 45 and 14KhN3MA with a different initial structure with sizes 40×40×5 mm was processed by the radiation of the CO_2-laser on the technological complex, equipped by the devices of control of parameters of bunch, system of dosage and serve of cladded powder, four by a coordinate table. Power of radiation made 1.2 kW, speed of treatment was varied within the limits of 0.5–2 m/mine, the diameter of spot of focusing changed within the limits of 2–5 mm. For the increase of taking in ability, standards preliminary were exposed to the chemical oxidizing.

On part of standards the method of laser injectional gas-powder cladding inflicted coverages from an alloy on the nickel basis PS12NVK, alloy on the basis of stainless steel of 12Kh18N10T and the Br bronze. OSTc10-1. The powder cladded under the corner of 45 degrees by transporting gas was given in track of ray. The expense of powder changed within the limits of 0.1–0.5 g/s.

After laser treatment standards, as well as model details, undergoed by metallography and dyurometrycheskym researches, during which was studied structure, microhardness and size descriptions of areas of the laser heating and cladded layers. After the analysis of results, on the chosen modes model details (pins of boring chisels and footstep-bearing of turbines) which were exposed to the tests in the real terms were processed.

Influence of the laser heating on the structurally-phase changes in steels. For making of details of the heavily loaded knots of friction, working in aggressive environments, apply lowcarbon cemented alloyed steels type 14KhN3MA. In the initial state after normalization the structure of this steel consists of corns of ferryta, having the wrong form of a different orientation, and unevenly distributed carbides. Between corns the small areas of perlyt are disposed (Figure 1, *a*). Laser irradiation became in a state of delivery after normalization, cemented and t cemented with the HFC hardening results in forming in the superficial layer of the consolidated layers substantially differentiating on structurally-phase composition and distributing of microhadness (Figure 2). Laser treatment became after normalization results in formation of two characteristic areas of phase transformations. Directly at a surface the area of hardening from hard solution is disposed. Tracks of its crystalline structure are revealed only at the frequent polishing and poisoning. A microstructure is a austenite-carbide. Carbides have the form of shallow-cell net prolate in the direction of taking warm. A layer is disposed in lower part of this area, the structure of which consists of needle-shaped martensite and remaining austenite. Austenite has the appearance of the triangles located between the plates of martensyta. The second area has also the structure of martensite with austenite. However much the needles of martensite become less. On a border with an initial metal the needle-shaped of martensite is almost unnoticeable, troostite formations on the Figure of initial austenite corns take place. Microhardness on a depth distributed unevenly and hesitates within the limits of 4.6–6 GPa.

Laser treatment became after carburizing on the modes (P = 1200 W, d_0 = 5 mm, V = 0.2–0.6 m/min)

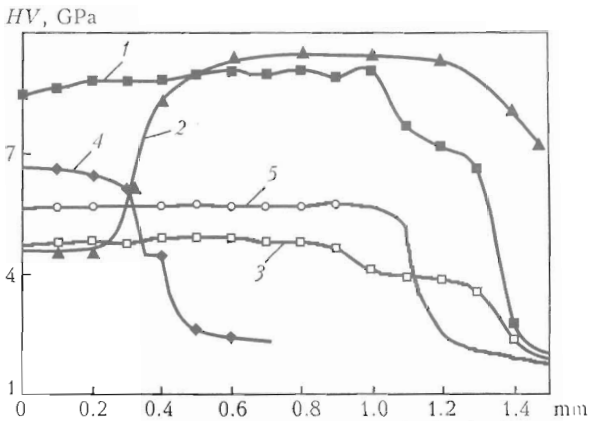


Figure 2. Distributing of microhardness on the depth of area of the laser heating in steel 14KhN3MA: carburizing+hardening; HFC+laser hardening (*1* — d_0 = 5 mm; V = 0.8 m/min; *2* — d_0 = 5 mm; V = 0.4 m/min); carburizing+laser hardening (*3* — d_0 = 5 mm; V = 0.8 m/min; *4* — d_0 = 5 mm; V = 1.6 m/min); normalization+laser hardening (*5* — d_0 = 5 mm; V = 0.6 m/min)

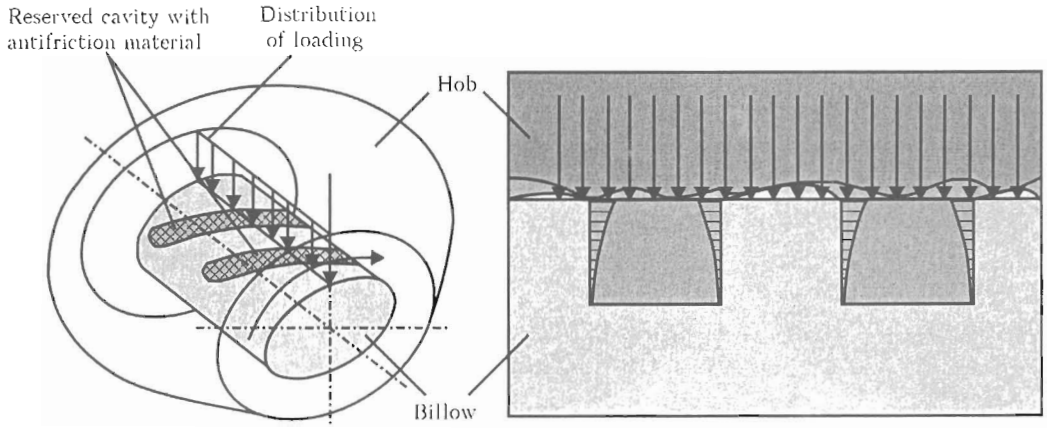


Figure 3. The chart of organization of the forced hard greasing

causing flaching off of surface, causes education at the surface of structure of amorphous martensite with a few of spherical carbide particles. The layer of large-needle martensite with the shallow-cell net of carbides of cement type is below disposed, oriented in the direction of taking warm. Microhardness of structure hesitates within the limits of 4.2–4.5 GPa. At speeds of treatment of 0.8–1.6 m/mine structurally-phase transformations flow in a hard phase. Dispersion of structure rises, is multiplied its microhardness to 5.1–6.5 GPa.

In cemented and hard-tempered steel after laser treatment a martensite-austenite structure with free carbides in the form of globuley is formed (Figure 3). A up-eutectic hard-tempered area is below than «white layer» disposed. Its microstructure consists of martensite and carbides of cement type in the form of net (Figure 1, *c*). Character of structure and its microhardness, its distributing on a depth is special, so much depend on time of the laser heating. There is the narrow enough range of speeds of treatment (0.8–1.2 m/min) at which the structure of the consolidated layer has even on a depth and high enough microhardness (7.5–9 GPa). In the other cases both at low speeds (0.2–0.6 m/mine) and at high – (1.4–1.8 m/mine), characte-ristic there is comparatively small hardness at a surface 4.5–5.5 GPa to the depth 0.2–0.3 mm, and large – 9–10.5 GPa at back.

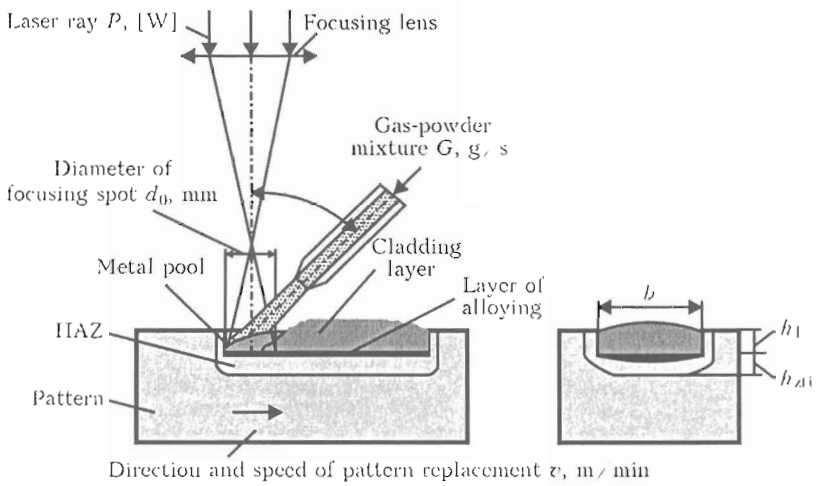


Figure 4. The chart of laser gas-powder cladding

The analysis of the got results showed that laser treatment on the optimum modes became 14KhN3MA, subjected preliminary to carburizing and the HFC hardening, to 1.3 mm allows to form at a surface the consolidated layer in depth, capable on the structure and hardness to provide necessary bearing strength to the details of the heavily loaded knots of friction.

Method of organization of the hard greasing of the heavily loaded knots of friction. For providing of high resistance to the wear besides good bearing strength of surface of friction must possess high antifriction properties. For the examined knots of friction such properties it is possible will substantially promote due to application of the hard greasing. For its organization it is suggested on one of surfaces of friction to create the evenly placed deepenings having a different form in a plan, but the necessarily reserved contour. Hard antifriction material takes place in these deepenings (Figure 3). In the process of work of such knot under action of loading effort of wall of deepenings resiliently become deformed and cause diminishment of their volume. Antifriction material filling these reserved deepenings is squeezed out in the area of contact, fills micro gaps and provides, thus, the forced greasing.

As antifriction materials it is suggested to apply depending on the terms of work of knot of friction the bronze OTcS10-1(high speeds of sliding at the small loadings) or composit being combination the bronze matrix OTcS10-1 (80%) with disseminations of particles became 95 Kh (20%) [5] (large loading efforts, comparative low speeds of sliding).

For placing in deepenings of information of antifriction materials it is expedient to apply laser gas-powder cladding. At this method in the cladded superficial layer of deepening of detail moving on a certain law, in track of ray the stream of transporting gas gives powder-like cladding material. The subsequent polishing of allowance provides necessary sizes and quality of surface.

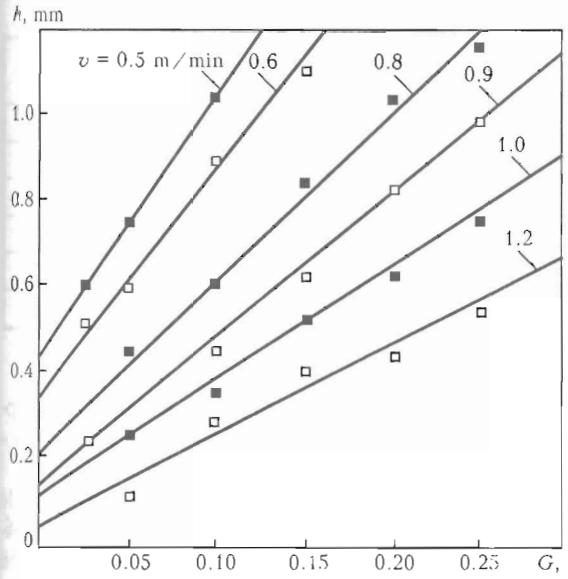


Figure 5. Dependence of thicknesses of the layer (h) got by the laser cladding on speed (V) and expense of powder (G)

Dignities of the offered method of causing of antifriction materials are: high electoral and productivity of process, possibility of organization of different compositions due to application of complex of different powder-like materials, high durability of coupling of cladded layer with material of basis because of presence between them metallurgical communication.

Application of laser radiation for cladding allows simultaneously to decide another very important task — to consolidate the superficial layers of walls and bottom of slot due to autohardening of steel basis. As a result, during the process of work plastic antifriction material will be situated between details, the contacting surfaces of which have high hardness.

The study of process of laser gas-powder cladding was conducted with the purpose of establishment of conformities to the law of change of sizes and properties of building up layers depending on the parameters of treatment. Figure 5 shows the depen-dences reflecting influencing of speed of treatment V, expense of powder of G and diameter of focusing spot d_0 on the thickness of cladded layer. This information was got at cladding of bronze of OTcS10-1. Bronze as powder by dispersion 60–80 μm was given under the corner of 45° in track of focused radiation of CO_2-laser. The diameter of focusing spot made 3.5 mm, power

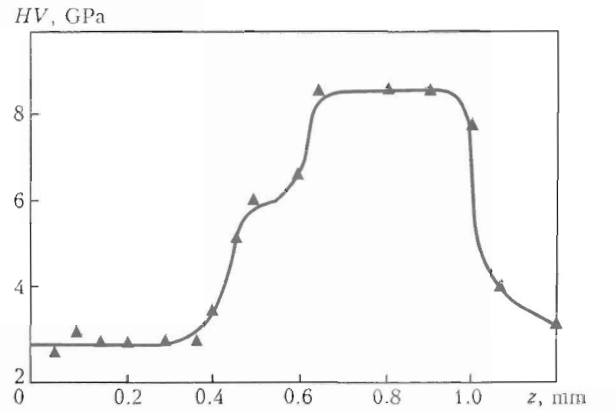


Figure 6. Distribution of microhardness HV on the depth of building up layer of bronze of OTcS10-1 on steel (0.45%C)

radiations — 1.2 kBt. The depth of area of alloying of bronze with steel of underlay was 30–80 μm. As an underlay carbon steel was used (0.45%C). Figure 5 represents the distribution of micro hardness on the depth of cladded layer. As follows from this dependence, directly on a surface the layer of bronze is disposed in thick 0.4 mm, below is layer of alloy bronzes with steel of basis, what fluently rising hardness testifies to. Yet below is small transitional layer, area of hardening became in the hard state with micro hard 8–8.5 GPa and initial structure of steel. Figure 7 representes microphotographs illustrating the microstructures of the mentioned layers.

In the process of laser gas-powder cladding on the surface of steel the layer of bronze, filling deepening special with the reserved contour, is formed. On the microphotograph taken off directly from the surface of pattern, (Figure 7, *a*) the unmelted particles of powder of brony, inculcated in got cristalline fusion which in layers, situated below has a homogeneous enough structure, are visible (Figure 7, *b*). The layer of bronze is connected firmly with underlayers, due to the presence of layer of its alloying with steel. The structure of transitional layer is represented on Figure 7. Under the area of fusion of basis the thermal affected zone is disposed, in part of which the temperature of heating was higher than the point of AC3. It stipulated flowing of process of austenization and subsequent education as a result of autohardening of high-dispersional martensite structure with high micro-hardeness (Figure 7, *c*).

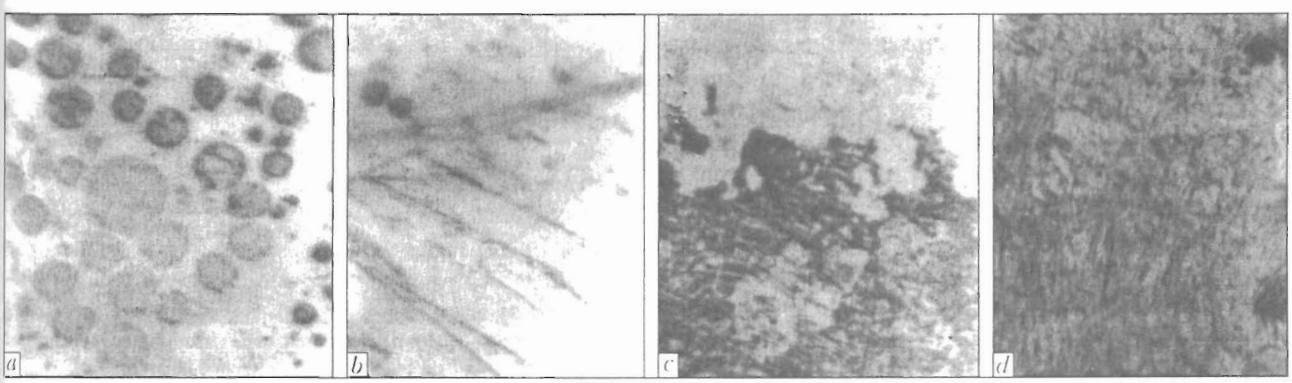


Figure 7. Microstructures of different areas of building up layer of bronze on steel: *a* — on the surfaces, *b* — under a surface, *c* — transitional layer, *d* — area of steel hardening

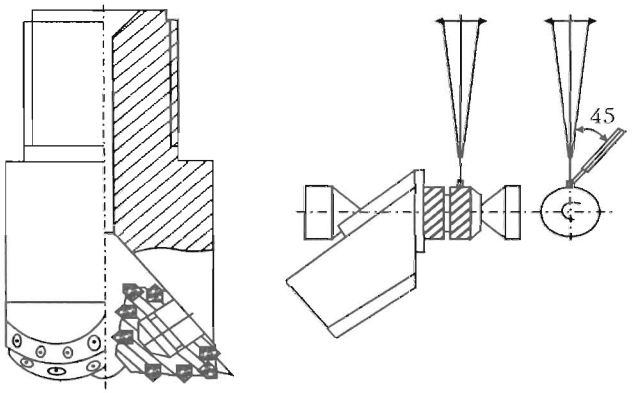


Figure 8. Boring chisel and chart of laser gas-powder cladding of bronze

Application of the got results of research in industry. At the boring drilling of mining holes the special chisels, being an instrument destroying a mountain breed and forming its trunk, are widely used in a geological survey (Figure 8). He is a corps a threesome, connected with each other by welding, brackets. On the pins of brackets, forming bearing of sliding, three breed-destroying disks are placed. Brackets and disks are made from the steel 14KhN3MA. With the purpose of increase its wearproof it is cemented and subjected to hardening with heating by the currents of high-frequency. Disks are supplied by the special insertions from a hard alloy. A chisel is the basic element of technological equipment, limiting productivity and prime price of the boring drilling. It is related to low his longevity, stipulated by extreme terms of work of knot of friction of sliding (high specific pressures, action of the aggressive abrasive-carrying liquid given under large pressure, absence of greasing).

The pins of brackets, preliminary cemented and hard-tempered HFC, were exposed to the laser consolidating on the optimum modes. On the pins of separate part of brackets the special deepenings which by the method of laser gas-powder cladding was filled by a bronze were made (Figure 8). After cladding the pins of brackets were polished for giving of the required sizes and roughness of surface. On the pins of the consolidated and deposited brackets disks with the insertions were set. Brackets with disks were going on three units, welded forming a chisel thus. Standard chisels and made on new technologies with the use of process of the electrospark alloying and laser consolidating passed the tests in the field terms. The results of tests are resulted in table 1. As is obvious from the resulted results, application of the laser consolidating is most effective. It allows to promote wearproof of boring chisels, advance driving by one chisel on 30–60%. It is possible to expect that expansion of base of tests, number of alternative technologies, including with the use of laser cladding, will allow to improve the got result, reduce labour intensive and cost of the boring drilling.

Table 1.

Characteristics of breed	Type of chisel	Tested	Bored, m	Driving, m	% to base of comparison
Granite	Serial	11	132.5	12.0	100
	Electrospark	10	133.4	13.3	110.8
	Laser	10	146.5	14.7	122.5
Albinite	Serial	10	84.9	8.5	100
	Electrospark	10	110.3	11.0	129.4
	Laser	10	134.9	13.5	158.7

Causing of bronze antifriction coverages was approbated on cladded of turbine of the system of turbosupercharging of diesel engine of heavy car.

On the butt end surfaces of footstep-bearing made from carbon steel (0.45%C), concentric circular ditches which by laser gas-powder cladding were filled by the bronze OTcS10-1 were made.

After cladding the butt end surfaces of center bowls were gnawed through in a size, the special oilretaining slots were inflicted.

The stand tests of footstep-bearing, made on a new technology with the use of laser cladding, found out two multiple increase of wearproof at the simultaneous decline of prime price of good.

CONCLUSION

1. The laser consolidating of lowcarbon alloyed steel type of 14KhN3MA is expedient to conduct after carburizing and the HFC hardening. Thus the depth of the consolidated layer makes 1–1.3 mm, microhardness – 7.5–9 GPa.

2. The laser consolidating of details of the heavily loaded knots of friction of type of pins of boring chisels provides the increase of resource of work of instrument on 30–60%.

3. Laser cladding of antifriction materials of bronze type on steel details is instrumental in forming under plastic coverage of layer of hard-tempered steel with high microhardness 8–8.5 GPa.

4. The offered method of the forced hard greasing, including making on the contacting surface of the special deepenings with the reserved contour and their filling by antifriction material of type bronze by laser cladding, is the effective mean of increase of resource of work of the heavily loaded friction units.

1. Drozdov Y. N., Pavlov V. G., Puchkov V. N., *Friction and wear in extreme terms.* – M.: Engineering, 1986, 224 p.
2. *Laser and electroerosional consolidating of materials* / V. S. Kovalenko, A. D. Verkhoturov, L. F. Golovko, I. A. Podchernyaeva. – M.: Science
3. Kovalenko V. S., Golovko L. F., *Laser hardening of chrome steels. The industrial laser handbook.* Springer-Verlag New York Inc., 1992, p. 121–122.
4. Kovalenko V. S, Golovko L. F Mikulyak O. V. and other, *Wearproof of the eutectic coverages treated by a laser.* Electronic treatment of materials, 1984, p. 33–36.
5. *Research of thermal processes and structure of superficial layer at laser cladding of powder-like materials* / B. A. Break, A. D. Podol'tsev, V. P. Lihoshva and other, Kiev, NAS of Ukraine, Institute of electrodynamics, 1998, 47 p.

METAL CRYSTALLIZATION KINETICS IN CONDITIONS OF LASER RAPID HARDENING

A. B. LYSENKO, N. A. KOROVINA, I. A. PAVLUCHENKOV
Dneprodzerzhinsk State Technical University, Ukraine

Theoretical analysis of crystallization kinetics of partial melting zone of metals by laser emission has been made. Kinetic equation taking into consideration the possibility of realization mechanisms in laser bath has been produced. The algorithm of developed model use for analysis of structure formation processes in conditions of laser treatment with partial melting of surface has been suggested.

Introduction. According to the results of experimental research [1–3] two structural zones reveal in cross sections of surface layers partial melted by laser: the zone preferably oriented dendrites (columnar crystals), which germinate from substrate and the zone of equiaxial crystals above it. It permits to suppose that laser bath by forging ahead of matrix crystals front (MCF) into melt and by means of spontaneous formation and consequent isotopic growth of crystals.

It has been noticed that under partial melting of metals to relatively little (up to 50 μm) dept the columnar crystals which grow from interface occupy the whole cross section of repeatedly hardening layer achieving its free surface. As a rule, in deeper layers the zone of columnar crystals takes only lower part of section while upper areas have the structure of equiaxial crystals.

Partial melting of some alloys with high glass formation capacity is known to accomplish by amorphization of surface layer [4, 5]. Hence under certain conditions of treatment both competitive mechanisms of laser bath crystallization can be suppressed.

In the given work the conclusion of kinetic equation which allows to take into consideration relative contribution of two alternative mechanisms of crystallizations to total quantity of crystallizing volume has been given. The consideration about the principles of its use with the purpose of investigation of formation processes of primary alloys structure in conditions of laser rapid hardening have also been expressed.

Physical Preconditions and Kinetic Aspects of a Model. Suggested kinetic model is based on the assumption that laser bath solidification happens by means of simultaneous action of two mechanisms of crystallizations above-considerated. One of them is realized in interface areas of partial melted zone, and the section — in upper increment which subjected to transformation. Let's designate these contributions in the following way: x_g — volume quota, occupies by columnar crystals, which grow from the interface of partial melting; x_h — volume quota which crystallizes spontaneously. It is apparent that magnitudes x_g and x_h are connected with relative quantity of liquid phase preserved x_l by ration

$$x_g + x_h + x_l = 1 \qquad (1)$$

We'll consider the crystallizations of partial melted zone begins when the metal bath gains the melting temperature T_m and continues right up to some temperature T_k at which the increment of crystallized volume stops either because of complete exhausting of liquid phase or in consequence of melt transition into hard amorphous state. In the latter point T_k has the meaning of glass-transition tempe-rature T_g. The process of crystallizations occupies time interval $t_m - t_k$.

Suppose, that crystals growing from the interface of partial malting by some moment of time $t_m < t' < t_k$ moves ahead into the dept of melt at the distance $h(t')$ and occupied the volume $V_g(t')$. It the growth of these crystals was free, their front would move with velocity $u(t')$ which is determined by process mechanism and concrete heat physical conditions on the interface. However, owing to the action of the second crystallizing mechanism columnar crystals meet on their way with homogenously forming crystal and as a result the increase of quota volume x_g is reduced. This effect is equivalent to the decrease of grown velocity of crystal and it reveals when the more degree the less quota volume in area occurring above matrix crystals front the liquid phase occupies. According to afore-said, the velocity of columnar crystals growth we shall characterize by effective parameter u_{ef} which is calculation by means of expression:

$$u_{ef}(t') = \frac{1 - x_g(t') - x_h(t')}{1 - x_g(t')} u(t') \qquad (2)$$

As it's seen from (2), if crystallization happens only owing to the growth of matrix crystals ($x_h(t') \to \to 0$), the latter are not blocked by homogenously forming crystals and in this case $u_{ef}(t') \to u(t')$. If because of any reasons the processes of germination into the melt of columnar crystals ($x_g(t') \to 0$) appear to be impossible, the layer partial melted by laser solidifies with the help of a single spontaneous mechanism and the formula for u_{ef} is transformed into:

© A. B. LYSENKO, N. A. KOROVINA, I. A. PAVLUCHENKOV, 2005

$$u_{ef}(t') = (1 - x_h(t'))u(t') \quad (3)$$

In this maximum permissible case parametr u_{ef} allows taking into account the effect of crystallizations retarding by interaction of neighbors homogenously forming crystals. This effect increases as relative volume of melt reduced [6].

Therefore, according to the model suggested, during laser bath solidification the crystals grow with real (physical) velocity $u(t')$ only in the earliest stages of conversion when magnitude $x_h(t')$ is too little. But on the stage of mass crystallization of upper horizons the crystals which are formed homogenously block both each other and crystal front growing from the interface. As a result, less values $h(t')$ and averaged linear dimensions of equiaxial crystals are achieved. For quantitive estimation of these changes in kinetic equations parameter $u_{ef}(t')$ depending upon liqud phase quota is used instead paramrtr $u(t')$.

Proceeding from assumption about effective velosity of crystal growth we can determine the values of volume increment of crystallization. First of all, we can determine the increment of volume quota, occupying by columnar crystals for short period of time between t' and $t' + dt'$:

$$dx_g(t') = (1/V_0)S(t')dh(t') = (1/V_0)S(t')u_{ef}(t')dt', \quad (4)$$

where V_0 — laser bath volume; $S(t')$ — MCF area.

Integration (4) in assumption of constant value $S(t')$ and taking into consideration (2) we obtain kinetic equation, describing contribution to the value of crystallized volume of growth mechanism of matrix crystals:

$$x_g(t) = (1/h_0)\int_{t_m}^{t'} \frac{1 - x_g(t') - x_h(t')}{1 - x_g(t')} u(t')dt', \quad (5)$$

where h_0 — primary depth of laser bath.

Then we'll determine the number of crystallization centers forming spontaneously during the period of time $t' \div t' + dt'$ in liquid part of the volume investigated:

$$dN(t') = V_0 x_l(t')I(t')dt', \quad (6)$$

where $I(t')$ — velocity of homogenous forming of crystal nucleus.

For simplicity let's set to spheric form of crystal nuclei and consider that it is inherited by crystals during their further isotropic growth linear velocity $u_{ef}(t')$. It means that in the developed model the forming of hypothetical spherical-type crystals is considered, but retardation of grown processes in consequence of mutual blocking of crystals are taken into consideration by means of expression (2).

Being based on the latter comment we can determine dimensions of imaginable crystals formed at time moment t' and further isotropically growing with velocity u_{ef} up to some final moment $t' \le t \le t_k$:

$$R(t',t) = R_k(t') + \int_{t'}^{t} u_{ef}(t'')dt'', \quad (7)$$

where $R_k(t')$ — radius of crystal nucleus of critical size.

The increment of crystallized volume quota owing to formation and further evolution of this crystals will have the following kind:

$$dx_h(t',t) = \frac{1}{V_0}\frac{4}{3}\pi R^3(t',t)dN(t') = \\ = \frac{4}{3}\pi x_l(t')I(t')\left[R_k(t') + \int_{t'}^{t} u_{ef}(t'')dt''\right]^3 dt' \quad (8)$$

Integration expression (8) with relation (1) and (2), we'll obtain summary kinetic equation for calculating of volume quota, crystallizing in the limits of laser partial melting zone by homogenous mecha-nism during the time observation $t_m \div t$:

$$x_h(t) = \frac{1}{V_0}\frac{4}{3}\pi\int_{t_m}^{t} (1 - x_g(t') - x_h(t'))I(t') \times \\ \times \left[R_k(t') + \int_{t'}^{t} \frac{1 - x_g(t'') - x_h(t'')}{1 - x_g(t'')} u(t'')dt''\right]^3 dt' \quad (9)$$

It is apparent that total volume quota of laser bath transformed into crystals state at any moment of time t, is determined by the sum:

$$x(t) = x_g(t) + x_h(t) \quad (10)$$

Principles of Kinetic Equation Use. Equations (5) and (9) allow to calculate volume quota of laser bath, which solidify owing to the action of two mechanism of crystallizations by values of the most important kinetic parameters — linear velocity of crystal growth, velocity of spontaneous forming of crystals nuclei and radius of steady crystal nucleus. According to formulas of crystallizations theory [7–9] these parameters depend upon the temperature. At the primary stages of laser bath (at $T > T_m$) the motion of temperature curves $T(t)$ is set to laser treatment and heat physical properties of metal [10]. However, during bath transition into critical area of temperatures $T < T_m$ quenching regime has supplementary influence of hidden heat release effect of crystallizations, the value of which depends upon value quota $x(t)$ underwent transformation by specified moment of time t. Therefore, dependences $T(t)$ at temperatures $T < T_m$ can be calculated only by means of coordinated solution of heat and kinetic task formulated according to the conditions of laser rapid hardening.

The development of similar solution algorithm introduce independent scientific interest and it is wider than the given report. Preliminary results obtained in the given direction is considered to be useful for studying of metal structure formation peculiarities in specified conditions of laser treatment with partial melting of surface.

1. Lysenko A.B., Kozina N.N., Miroshnichenko I.S., Borisova G.V. (1995) *Peculiarities of structure formation in steels subjected to laser surface alloying.* MiTOM, 12, 10–12.
2. Lysenko A.B. (2001) *Influence of technological factors on composition, structure and properties of laser chemical-thermal treatment zone.* FiTOM, 2, 25–30.
3. Lysenko A.B., Brekharya G.P., Nemoshkalenko V.V., Shpak A.P. (2002) *Role of treatment modes and «substrate effect» in laser surface alloying technology.* Metallofizika i Novejshie Tekhnologii, 24(7), 935–948.
4. Grigoriants A.G., Safonov A.N., Baskov A.F., Kauts E.V., Kraposhin V.S. (1985) *Producing fine crystalline and amorphous structures on the surface of massive samples using the continuous CO_2-laser.* MiTOM, 11, 17–20.
5. Lysenko A.B., Kozina N.N., Borisova G.V., Tolok A.A. (1994) *Conditions of amorphisation of metal alloys in laser surface melting.* Dep. in UkrNIINTI, 538-Uk94, Publ. 16.03.94.
6. Lysenko A.B., Shuleshova O.V. (2002) *Modeling of structure formation processes under the conditions of rapid cooling of metal melts.* In: Abstr. of Papers of the Nation. Conf. onCrystal Growth – NCCG. Moscow, IK RAN.
7. Skripov V.P., Koverda V.P. (1984) *Spontaneous crystallization of supercooled liquids.* Moscow: Nauka.
8. Gutzow I. (1979) *Kinetics of crystallization process in glass forming melts.* Journal of Crystal Growth, 48, 589–599.
9. Ovsienko D.E. (1994) *Nucleation and growth of crystals from the melt.* Kiev: Naukova Dumka.
10. Lysenko O.B., Korovina N.O., Girzhon V.V. (2005) *Peculiarities of heat transfer and crystallization processes under the conditions of ultrarapid tempering of metals.* Visnyk Lvivskogo Universytetu. Seriya Fizychna, 38, 147–156.

Conference Sponsors

PWI Laser Systems and Technology Center

Ministry of Education and Science of Ukraine

Information Support

«The Paton Welding Journal»

www.nas.gov.ua/pwj

Conference Sponsors

PWI Laser Systems and Technology Center

Ministry of Education and Science of Ukraine

Information Support

«The Paton Welding Journal»

www.nas.gov.ua/pwj

Conference Sponsors

PWI Laser Systems and Technology Center

Ministry of Education and Science of Ukraine

Information Support

«The Paton Welding Journal»

www.nas.gov.ua/pwj

PREREQUISITES TO NUMERICAL MODELLING OF AERODYNAMIC PHENOMENA AT GAS-LASER METAL CUTTING

V. S. KOVALENKO, R. O. ZHUK
National Technical University of Ukraine «KPI», Kiev, Ukraine

Despite numerous investigations in dross and striations formation which nevertheless are significant quality factors during laser cutting, the understanding of these mechanisms leaves much to be desired. This paper presents an attempt to numerically simulate the propagation of assisting gas exiting laser cutting nozzle. A comparison of different cases of further interaction of exit jet with melt pool and its behaviour inside cut kerf were investigated. Various configurations of laser cutting nozzles together with the ways of assisting gas delivery and their influence on general cut quality were analyzed. A design of high-speed laser cutting nozzle was introduced.

Introduction. With the development of new progressive technologies and a current trend towards micro units and nano processing the question of quality and accuracy of material processing becomes as important as never. Laser cutting was one of the first technological implementations of laser beam and over the years a great deal of industrial laser systems was developed for this purpose, and among them are laser cutting equipment that uses assist gas, either reactive or inert, along with laser beam. Despite the fact that the laser cut quality has improved drastically, we are still far from deep understanding of all those processes that are involved in laser cutting process. The main goal nowadays is to improve overall quality of side walls and width of the cut. Among the variety of factors that influence on the outcome of cutting process, the cutting speed, assist gas pressure and flow rate, configuration of cutting nozzle and stand-off distance are of particular interest.

Assist has a vital role in laser cutting process. It creates a mechanical force that exerts the molten material from the cutting zone and at the same time enhances the efficiency of heat conduction process. Having known that molten material is removed both by pressure driven and viscous drag mechanisms, it is possible to state that inefficient melt removal directly influences the kerf geometry. Moreover, assist gas has a protective function that results in the protection of laser cutting zone and optical system. In the latter case it prevents lenses and mirrors from contamination by metal vapours or pieces of solidified material. In case of reactive gases, extra thermal energy is added to energy flux into the cutting zone, which in some cases increases the rate of creation of molten layer.

Absence of solid theoretical background does not allow predicting accurately the influence of means of assist gas delivery and gas content on cutting results. The development of computer technologies and new computational algorithms for the simulation of laser cutting together with experimental verification of mathematical models may provide engineers with a versatile tool for prediction of final laser cut dimensions and quality control.

Main components of laser cutting process and their influence on overall quality. *Influence of proper laser cutting nozzle on the cutting results.* Cutting nozzle is an indispensable part of industrial systems for laser cutting that directs a compressed air jet into the cutting zone and drags or exerts the molten layers off the kerf. In general, the most desired features of laser cutting nozzle are maximal outlet pressure and ability to control the shape of a compressed jet. Although these features are somewhat limited due to the restrictions which are caused by laser beam properties, i.e. the laser beam should be in the centre of the nozzle and it should not have any restriction towards it propagation to the workpiece. Usually, ordinary laser cutting nozzles, so called sonic nozzles have inner surface of a conical shape with an exit diameter of 0.5... 2 mm. Assist gas, exiting this type of nozzle is highly underexpanded, has sonic or subsonic speeds and quickly propagates in space just after the nozzle exit or creates stagnation bubbles, sonic lines and shock waves, thus resulting in an uneven melt removal. It means that for this type of nozzles the distance between nozzle exit and work piece is crucial for successful cutting and has to be as minimal as possible but big enough in order to avoid contact between nozzle and material to be cut. A literature survey shows that there are some special means and techniques that allow to control and manipulate with this distance.

A complicated shape of assist gas jet and instabilities of its hydro-dynamical parameters also significantly influence a cut formation process. Gas jet interaction with boundary layers of molten material leads to wave-like character of melt flow along the cut walls and appearance of oscillating striations, which in turn increases the roughness of kerf walls. Moreover, the jet of assist gas loses its momentum

© V. S. KOVALENKO, R. O. ZHUK, 2005

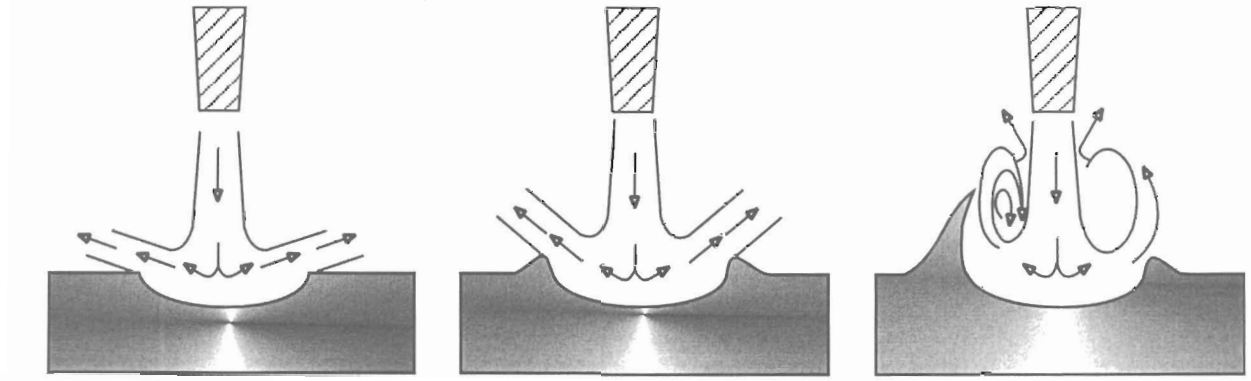


Figure 1. Possible ways of gas jet — melt interaction

significantly while interacting with work piece, which means that a great deal of gas streams would change its direction from axial to radial, with further formation of wakes, standing waves and whirls and would consequently shape the cut edges making them more of a round or of uneven form.

Three basic types of compressed gas jet interaction with bead of molten material are shown on Figure 1.

Apart from using ordinary nozzles, new applications for already existing nozzles or new types of nozzles with complicated shapes are developing nowadays. The main goal of such activities is to obtain such hydro-dynamical properties of assist gas jet that would allow to lower radial expenses of gas and to increase the amount of gas entering cutting zone. Another aspect of using modernized sonic and supersonic nozzles is to increase the gas jet pressure and mass flow rate to achieve higher melt removal rates. This can be achieved by using a converging — diverging nozzles or De Laval nozzles, changing the form of cross-section of exiting orifice. The most commonly used nozzles are presented in Figure 2.

More over different means of assist gas supply are used:

- Co-axial with laser beam
- At certain angle
- Gas delivery at transonic speed
- Tangential supply of gas jet into nozzle
- Combination of two or more nozzles
- Gas delivery at supersonic speeds

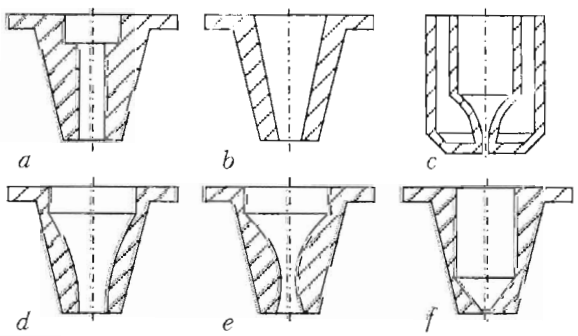


Figure 2. The most commonly used nozzles for gas-assisted laser cutting: *a* — nozzle with parallel walls; *b* — conical nozzle; *c* — ring nozzle; *d* — convergent nozzle; *e* — convergent-divirgent nozzle; f — conical + cylindric nozzle

Engineers have not come to an agreement whether it is necessary to use high speed gas delivery in laser cutting processes. Among major drawbacks are high gas consumption and complexity of gas propagation.

High speeds and pressure are the main causes of huge expenses of assist gas and the cutting process might be very costly comparing to convenient cutting methods. Supersonic nozzles are designed to operate with specified values of pressure, whereas subsonic nozzles can create a wide range of pressure values using only one nozzle.

The proper choice of the nozzle for gas-assisted laser cutting process should be based on requirements of technological task and above mentioned peculiarities should be considered prior to final decision.

Periodical instabilities of laser cutting process. The process of laser cutting itself is thought to be a relatively constant process. The only transient processes are the initial stage of penetration, cutting along the edges (heat accumulation effect is observed), oxidation, dross formation and melt front instabilities [2]. The conditions of energy and mass balance are satisfied periodically and in series, thus forcing the thickness of molten layer to vary with time, and it consequently leads to variable kerf width.

Moreover, the melt formation process starts at the initial stage of penetration. Melt, which is blown away by gas jet, is replaced with newly formed molten layer and this process repeats as long as cutting process lasts. These cyclical actions may also lead to formation of wave-like structure of kerf walls or striations. In case of reactive assist gases, the molten layer thickness and its removal rate are dependant on the formation of ferric oxides or other metallic oxides and their physical properties, viscosity in particular.

It is also necessary to take into account periodical appearance of metal vapors which interfere with the laser beam propagation and may cause plasma formation effects or may change the absorption coefficient. The jet of compressed gas, if it is delivered co-axial with laser beam would drag metal vapors in backward direction. As a result of vapors and molten layer interaction one may observe changes in viscosity of molten layer and ratio of metal oxides, in case if reactive gases are used. These uncontrollable changes are also of periodical nature.

To sum up, while attempting to simulate gas-assisted laser cutting process it is vital take into consideration the instability of its main parameters, and to correlate the frequency of their appearing with total roughness of obtained surfaces (the frequency of striations formation).

Optimal choice of assist gas speed and pressure, configuration of assist gas jet, cutting speed, cutting regime and cutting nozzle configuration, which would result in desired quality and configuration of the kerf with minimal time consumption and at low costs, is one of the main engineering tasks. This could be achieved by preliminary computation and simulation of laser cutting using principles of hydrodynamics. These measures would allow investigating the influence of each factor by changing the key parameters of the model.

Main factors, that complicate numerical computation of assist gas laser cutting. Assist-gas laser cutting could be represented through the series of complicated hydro- and thermodynamic properties, where the heat conduction, fluid movement and exothermic reactions interact with each other. The result of this interaction is significant influence on productivity and results of laser cutting which is impossible to describe it in full with existing analytical methods.

The goal of the researcher is to simulate these processes with help of numerical computation. One possibility is the development of dynamic mathematical model of movement of molten boundary layer that would describe and compute instabilities of formation and propagation of molten layer inside the kerf.

The Table 1 portrays a comparison analysis of different computational and experimental techniques.

Turbulence. Turbulence is a very complex phenomenon, since its appearance leads to radical changes of the gas flow which can have either positive (efficient mixing) or negative (energy losses) effects depending on one's point of view and the results needed. Periodical fluctuations associated with turbulence significantly increase Reynolds stresses in the flow.

It is very difficult to compute turbulence due to uneven fluid flow and different length and time scales of motion, eddies and shock waves. Some large-scale eddies could be compared to the geometrical dimensions of compressed gas or molten layer flow. Turbulence also causes significant energy dissipation, that is transferred from large-scale eddies to smaller ones. Moreover, turbulence is always a three-dimensional that is why its detailed computation and visualization requires powerful computational resources [1].

Although, there are some computational algorithms which facilitate general form of Navier-Stokes equations and in a way are set aside to compute turbulence: standard κ-ε model (Launder and Spalding, 1974) and Prandtl mixing length model, that deal with kinetic energy and velocity scales respectively.

Uncertainty of molten layer behavior inside the cutting kerf. A majority of fluid flows, which are of a great importance for engineers, are very hard to compute numerically. They include turbulent, multi-component and reactive flows. The development of a detailed mathematical model for these flows is impractical from the point of time needed to perform computation. That is why it is important to use semi-empirical models with second-order differential equations [3].

Depending on the character of the flow, these equations can be of three types: parabolic, hyperbolic and elliptic.

In case of supersonic nozzles and high pressure assist gas delivery the flow ought to be described as hyperbolic since we have to deal with discontinuities caused by shock waves. This characteristic becomes more complicated when model of viscid compressed gas is used since it is almost impossible to simulate it with existing numerical methods. If one tries to compute compressed gas flow with help of boundary layer theory the character of equations changes to parabolic since it is possible to get a smooth but not accurate solution.

Taking into account that during laser cutting the assist gas flow, molten layer flow and vapours of molten metal interact may speed or slow each other, one may consider equations for this system to be of elliptic character. The areas of recirculation of the flows usually occur with sonic or subsonic gas delivery speeds.

Dealing with shock waves in laser cutting nozzles. In order to obtain accurate results the following definition of a shock wave should be considered while creating a computational algorithm.

A surface or sheet of discontinuity set up in a supersonic field or flow, through which the fluid undergoes a finite decrease in velocity accompanied by a marked increase in pressure, density, temperature, and entropy. In other words, shock is a thin section of a control volume where there are abrupt changes in fluid properties. Formed due to the compressibility effects of fluids, normal shock occurs in a plane perpendicular to the flow. Fluid velocity increases in converging part of the nozzle lowering pressure until

Table 1. Pros and cons of different computational methods

Method	Advantages	Disadvantages
Experimental	Real results Direct control of parameters	Complicity and high costs Complicated data analysis Time and material consuming
Theoretical	Ready to use empirical equations	Narrow field of use Lack of precision
Numerical	Ability to describe and trace complicated dynamic processes Calculations could be easily repeated if parameters are changed All calculations are directly applied to physical model	Detailed computations are time-consuming Approximation of boundary conditions and initial state leads to inaccuracy in results There is a problem of precise description of boundary conditions

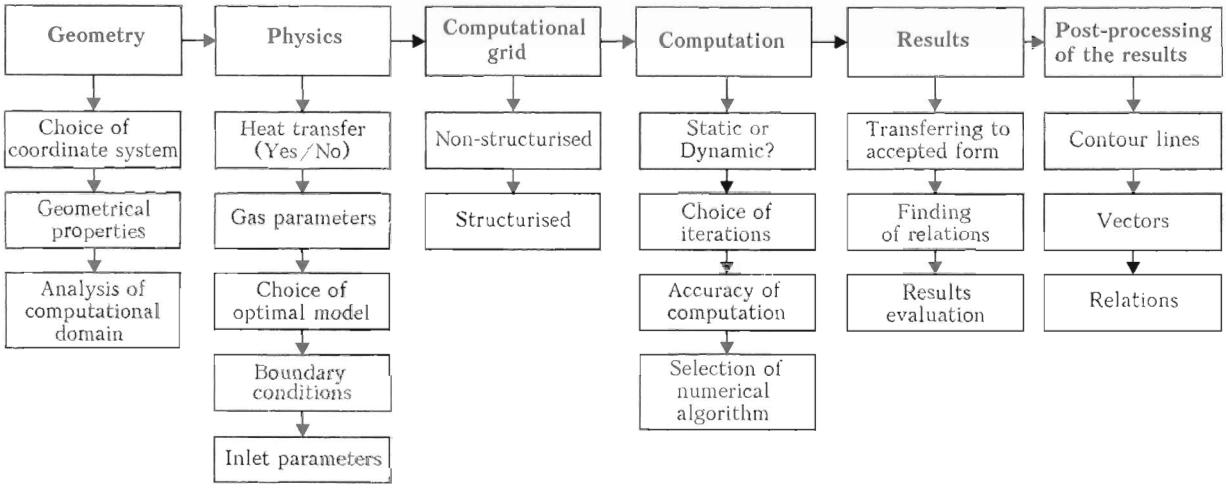


Figure 3. General stages of CFD process

max velocity reaches at throat (Mach number is equal to 1).

Diverging section continues to accelerate fluid to supersonic speed with continued drop in pressure until we hit region of normal shock in nozzle. At normal shock region pressure and temperature increase across the wave and velocity drops.

Possibility of prediction of overall quality of cutting process using computational methods. *Main components of computational model.* An indispensable part of any computational algorithm is a mathematical model which represents a set of differential equations and boundary conditions. In the case of assist-gas laser cutting process, differential equations are intended to describe the motion of a compressed assist gas, thermal influence of laser beam, temperature distribution and motion of melt. General stages of computational process are described in Figure 3.

It is advisable to use already existing general models, such as those that describe propagation of compressed or uncompressed gas, of a turbulent or laminar character of motion in one-, two-, or three- dimensional coordinate system. Mathematical model needs to be developed only for a specific task, since any generalisation is either impractical as it was mentioned earlier or impossible [5].

When the proper model is chosen it is now necessary to draw attention to method of approximation of differential equations to a system of algebraic equations with set of variables of a discrete position in time and space. Among the variety of solutions three methods are of the most extensive use: finite difference method, finite elements and finite volume methods. The popularity of these methods rests with minimal amount of computational time comparing to more sophisticated ones.

A proper coordinate system has to be chosen afterwards depending on the character of gas or melt motion, and differential equations had to be adjusted to it. The rational choice of coordinate system influences on the discretization method of differential equations and computational grid.

Discrete positions where the values of variables had to be determined are located on a computational grid, which is a discrete image of geometrical domain of computational model. The grid separates it into the finite number of elements. Depending on the size of these elements the grid could be adaptive, structurized or unstructurized. The example of computational domain and grid for computation of gas-assisted laser cutting process are shown in Figures 5 and 6.

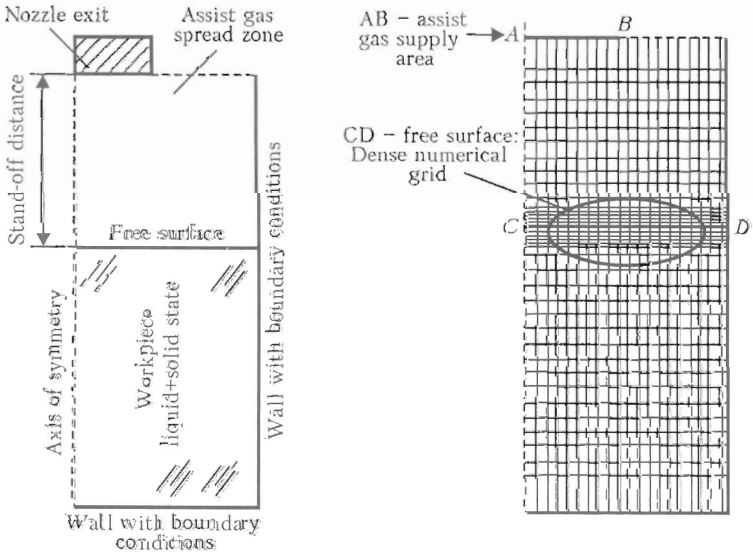


Figure 4. General form of computational domain and grid

Requirements to the computational models of gas-assisted laser cutting. The perfect computational model that can describe and investigate the laser cutting process had to include:

1. Mechanism of laser beam – work piece interaction
2. Mechanism of compressed gas jets, metal vapors and melt interaction
3. Thermal influence of laser beam and compressed gas jet
4. Energy losses and distribution inside the kerf that would help to develop a method

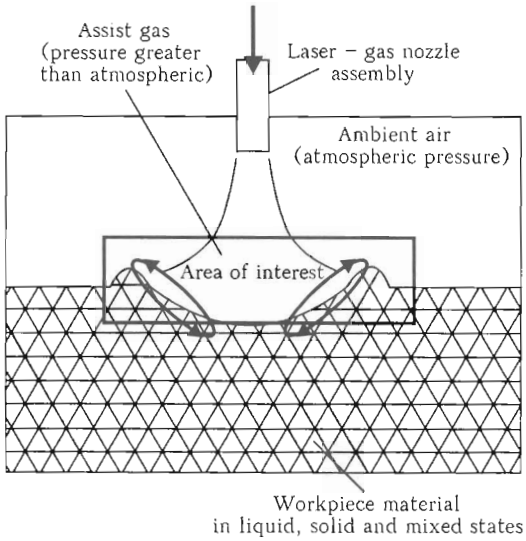


Figure 5. General form of geometrical domain

of energy losses optimisation and to evaluate those energy losses which are unavoidable.

5. Possibility to determine and control the dynamic characteristics of the process

CONCLUSIONS

A development of a special algorithm and conducting computational routines would be a versatile tool for intensification of the choice of means of assist gas supply and cutting nozzle configuration and visualization of fluid flow inside the cutting zone on the stage of the development of technological process and designing of necessary equipment. Principles of hydrodynamics may be of a good use for this purpose, although it is necessary to consider peculiarities of interaction of workpiece, laser beam and compressed gas jet.

1. H. K. Versteeg, *«An Introduction to computational fluid dynamics. A Finite volume method».*
2. Alexander F. H. Kaplan, *«Theoretical Analysis of Laser Beam Cutting»*, Shaker Verlag, Aachen, 2002.
3. Yilbas, B.; Shuja, S.; Budair, M. *Jet Impingement Onto a Hole with Constant Wall Temperature.* Numerical Heat Transfer, Part A 2003, 43, 843–865.
4. El Golli, S.; Aissia, H. B.; Zaouali, Y. *Numerical Study of the Influence of Dynamic and Thermal Exit Conditions on Axisymmetric Laminar Buoyant Jet.* Numerical Heat Transfer, Part A 2002, 42, 427–444.
5. Chai, J. C. *One-Dimensional Transient Radiation Heat Transfer Modeling Using a Finite-Volume Method.* Numerical Heat Transfer, Part B 2003, 44, 187–208.

CAE SYSTEM FOR LASER AND ELECTRON BEAM WELDING

V. LOPOTA[1], G. TURICHIN[1], E. VALDAITSEVA[1], P.E.MALKIN[1], A. GOUMENIUK[2]
[1]State Technical University, St. Petersburg, Russia
[2]ISF-Welding and Joining Institute, RWTH-Aachen University, Germany

The level of development of modern industry assumes active introduction and use of new methods of designing of technological processes. Systems of the automated designing considerably accelerate process of development of new technologies, and also allow creating more and more complex objects from the technical point of view.

Now there are many various kinds of CAD-CAE-CAM-systems intended for use in different branches of industry and research activity. However in the field of beam technologies there is patent deficit of them.

The modern program of engineering designing should have all necessary properties for ensuring competent designing on all or separate design stages of technological process, such as usage of adequate physical and mathematical models of processes, wide information base, the speed, the convenient dialogue interface.

LaserCAD is intended for the decision of a different kind of engineering problems, namely: calculation of geometrical characteristics of supposed connection, selection of optimum parameters of a processing mode, choice of the necessary process equipment according to the obtained parameters, selection of materials in view of supposed properties of connections.

The system includes model of laser welding and model of electron beam welding with deep penetration, model of hybrid welding with deep penetration and with surface melting, a multilevel database of materials, including data of physical properties and a chemical composition of alloys, a database of technological equipment, means of dialogue optimization of modes of the laser, electron beam and hybrid welding processes, the convenient intuitive — clear dialogue interface (Figure 1).

All listed models of beam processing represent a set of physically adequate models of the processes proceeding at various kinds of processing. The model of laser welding with deep penetration includes the solution of problems of heat transfer in metal in liquid and solid phases, hydrodynamics of the melt flowing, about metal vapor flowing and formation of laser-induced plasma and about beam-plasma interaction.

The model of hybrid welding except for characteristic processes for laser welding takes into account also heating from an additional heat source (arc, plasma or light) in case of deep penetration and expects temperature fields in case of surface melting on the basis of the numerical solution of a three-dimensional

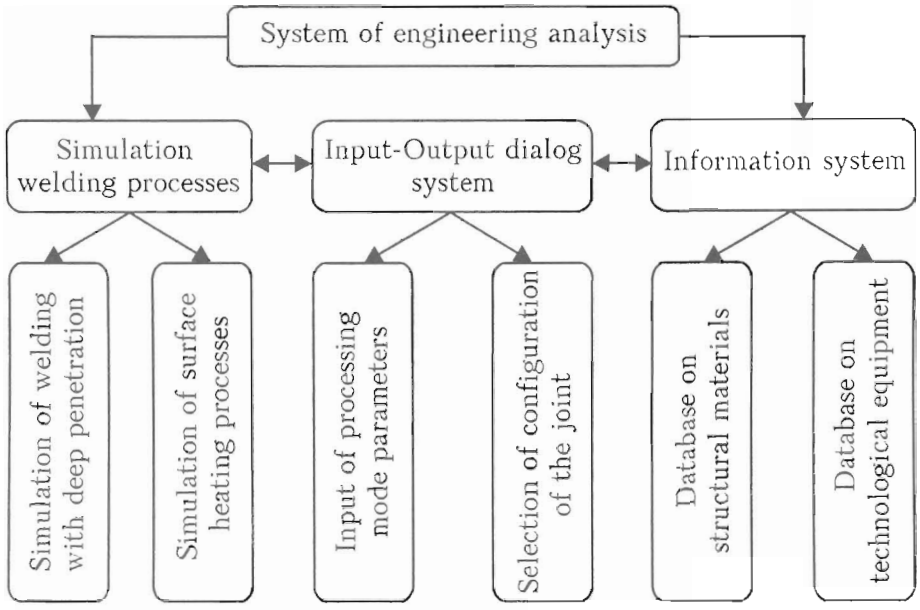


Figure 1. Block-diagram of the LaserCAD system of beam welding of metals

© V. LOPOTA, G. TURICHIN, E. VALDAITSEVA, P. E. MALKIN, A. GOUMENIUK, 2005

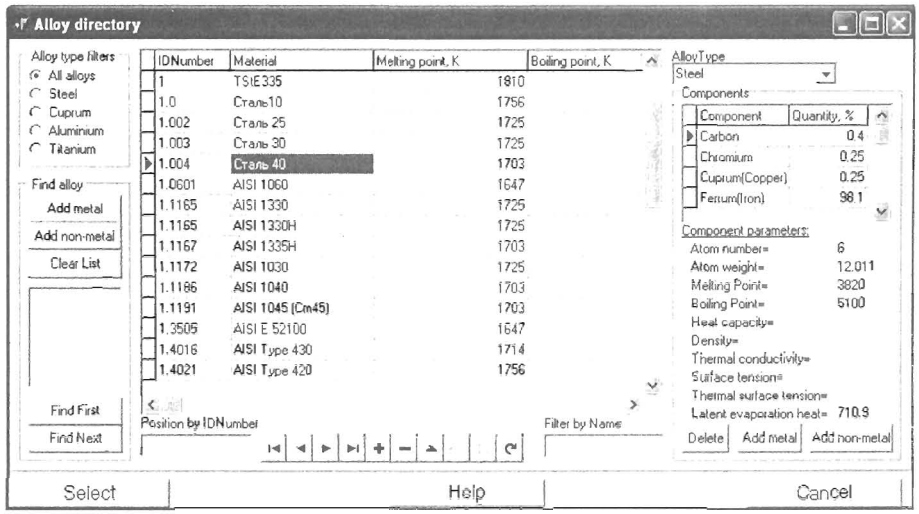


Figure 2. Database on welded material properties

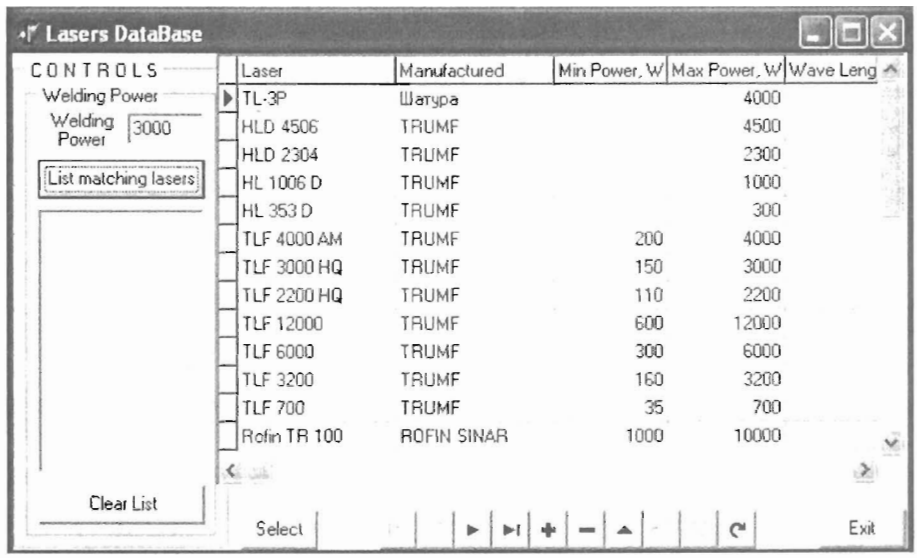


Figure 3. Database on the laser equipment

problem of non-stationary heat conduc-tivity. The electron beam model includes solution of problems about heat mass transfer, gas dynamics and kinetics of dispersion of metal vapors into vacuum, of a beam scattering on the metal vapor at welding with deep penetration.

Program LaserCAD includes multilevel multipurpose directory system. The system includes materials databases (Figure 2) which contain data on physical properties of metals, nonmetals and alloys, about their chemical composition, and also data of steels structure obtained on the base of CCT-diagrams of decay of austenite. On the basis of these data in aggregate with calculations on models it is possible to predict properties of received welded connections from the point of view of structure of metal of a seam and heat affected zone. The directory system contains also data on various sorts the process equipment, which can be chosen according to the requirements, showed to a mode of processing and operating conditions (Figure 3).

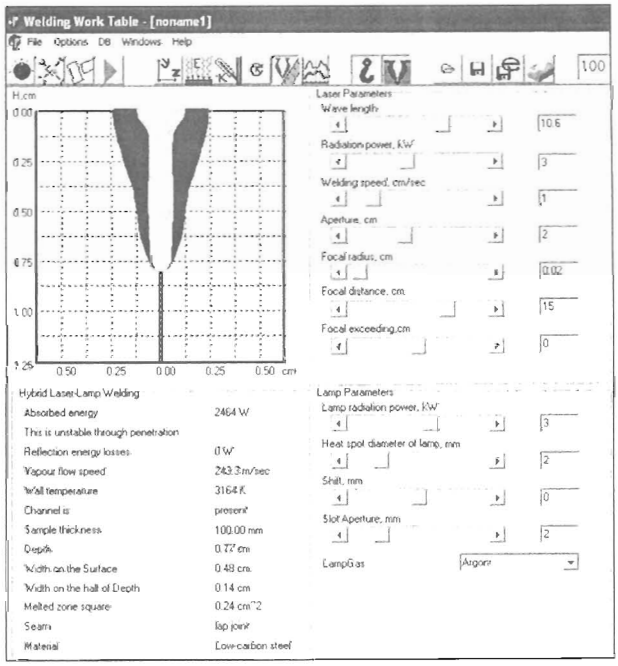


Figure 4. Dialogue optimizer for searching

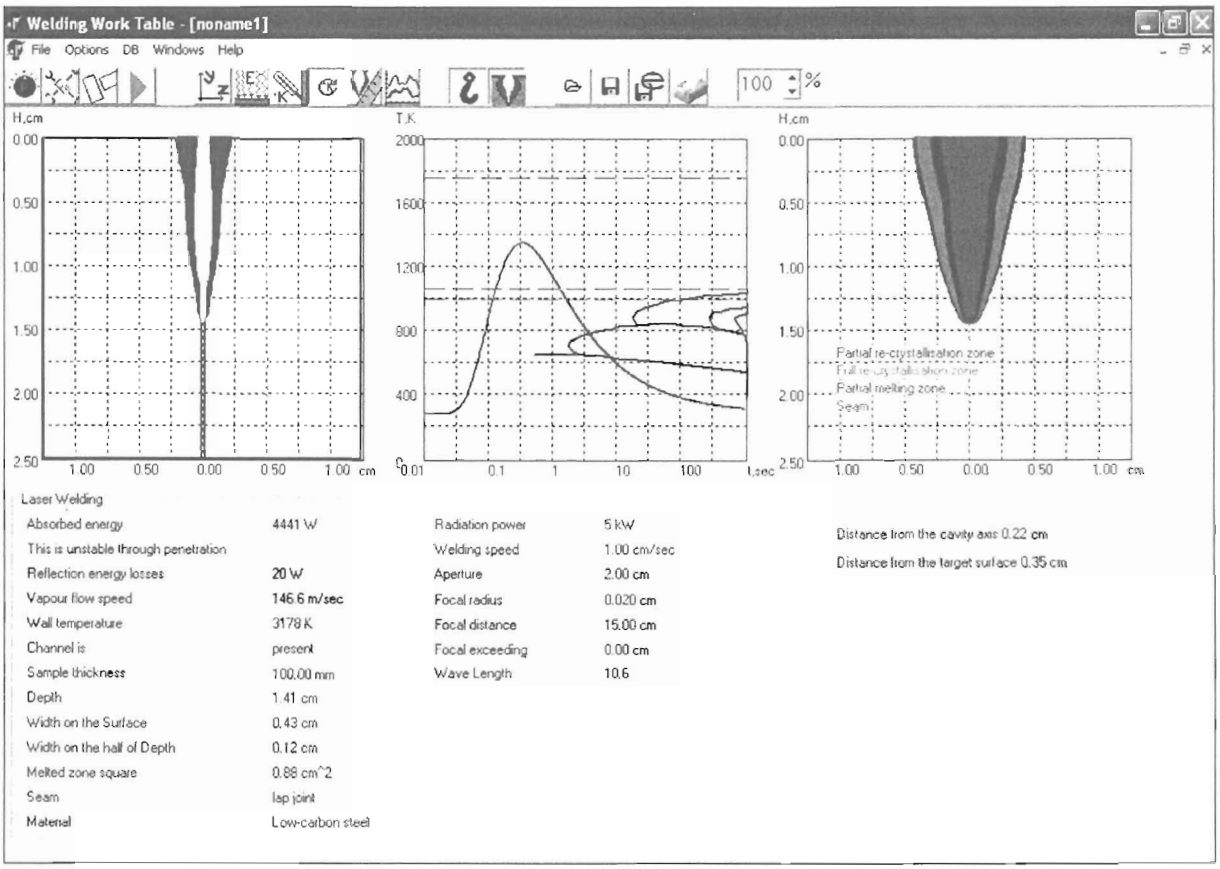


Figure 5. Analysis of structure of steel 30XM welded connection in laser welding required mode of hybrid welding example

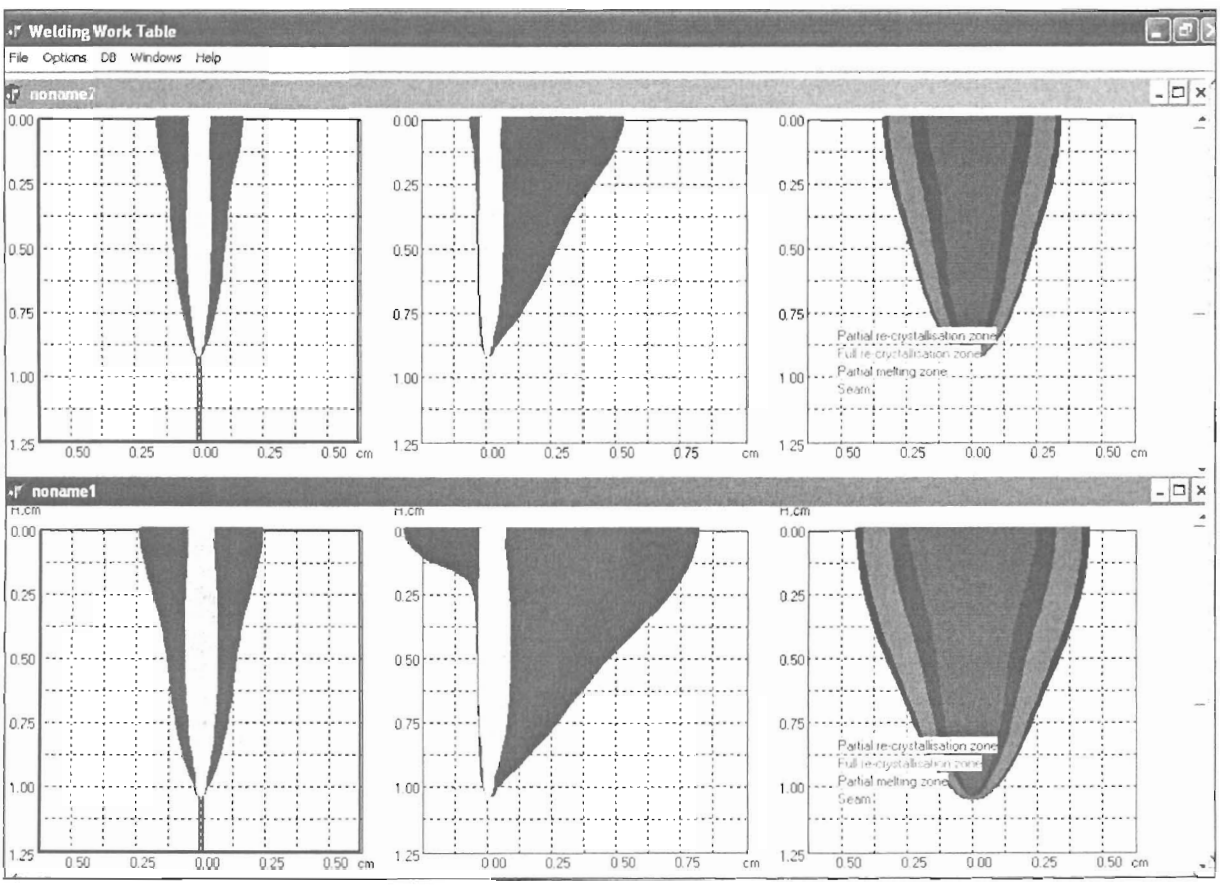


Figure 6. Example of simultaneous work of system with laser and laser-light welding

Databases are open for editing and updating by the new information, and also have function of a direct connection with global network Internet.

Program LaserCAD has the convenient interface, allowing to work in a dialogue mode. Special function «Manual optimizer» facilitates and accelerates selection of a necessary mode of processing for achieving required result (Figure 4).

The LaserCAD system is means of engineering computer analysis (CAE) of welding processes of metals the high-density energy fluxes. It allows to predict the sizes and the form of a welded seam and also to analyze change of a chemical composition of metal of a welded seam during welding, to predict structure and properties of metal of the seam and heat affected zones.

The system is organized as MDI program and can work in a multi-window mode, which expands opportunities of the simultaneous decision of several problems of comparisons, and the analysis of obtained results.

The program is written in Object Pascal in Delphi6 development system. In developing the system there were taking into account main principles of the organization of the modern CAD-CAM-CAE-systems. The program can operate under Windows'95/98, Windows'2000/XP, the minimal system requirements — Pentium-III/700, 128 Mb RAM. Use of the optimized algorithms permit to provide the speed of system operating necessary for it to be used in industrial practice (calculation of one variant of welding mode occupies no more than one minute).

Now LASERCAD and its analogues are successfully applied in our country and abroad (Figures 5, 6): in CSRI RTK and CSRI of Shipbuilding in Saint Petersburg, in Bauman STU and SRIH in Moscow, in a number of German institutes and the companies, such as IWS, Weldaix, NMB, SLV Rostock. Moreover, the system can be used not only in designing technological processes but in training the personnel and as a computer simulator of beam technologies.

SIMULATION OF THERMAL BENDING — ACCELERATION OF TEMPERATURE FIELD CALCULATIONS

T. PRETORIUS, J. WOITSCHIG, F. VOLLERTSEN
BIAS-Bremen Institute of Applied Beam Technologies GmbH, Germany

The simulation of thermal forming processes using complete finite element modelling of the specimen requires rather long calculation times. In order to accelerate the simulation of the time dependent temperature field of the process, calculations were carried out in which only the process zone was modelled using finite elements. The parts of the specimen outside this zone were accounted for by a boundary condition function which provides the heat transfer between the process zone and the other parts of the specimen (generalized heat flux function). Using this reduced modelling the calculation of the temperature field could be accelerated by a factor of 3.4 while the accuracy of the result is nearly as high as using complete finite element modelling. The method was developed for plasma jet bending, but is also applicable for other heat sources (e.g. laser beam).

Introduction. Thermal bending processes are a flexible method for the forming of simple components as well as complex geometries. The processes are characterised by a local elastic-plastic deformation zone that is driven through an elastic structure. An advantage of thermal forming processes over mechanical forming processes is the fact, that there is nearly no spring back effect [1]. A detailed description of the thermal forming mechanisms can be found in [2] for the case of laser bending. Thermal bending processes were investigated by various authors [3–8]. To keep the experimental effort small, a proper process planning is necessary for the forming of complex geometries. This could be done by simulating the process with different processing parameters and beam sequences. Unfortunately the simulation of these complex processes requires long calculation times. The goal of the work presented in this paper is the development of a system for the fast simulation of thermal forming processes. As a first step the calculation of the temperature field should be accelerated. For laser beam bending processes approaches to accelerate the thermal calculations by reusing the temperature field in incremental processes were done in [9]. This paper discusses an approach which reduces the finite element modeling to the deformation zone.

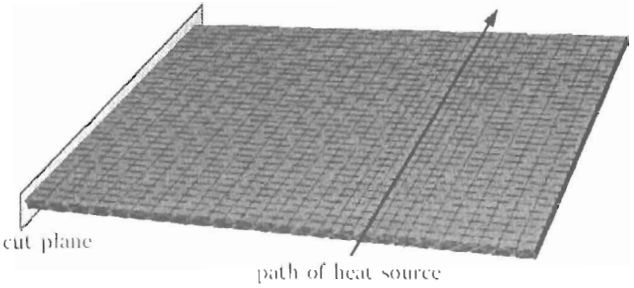


Figure 1. Mesh of the reference model

© T. PRETORIUS, J. WOITSCHIG, F. VOLLERTSEN, 2005

Geometry. As a model system the bending of steel sheets using a plasma jet as heat source was chosen. Assuming a non transferred plasma arc with electrical parameters 400 V and 15 A and an efficiency of 20 % resulted in 1.2 kW transferred energy into the sample. A description of experiments to measure the heat input parameters and a comparison between experimentally measured bending angles and simulation results can be found in [10]. The geometry of the samples was 200 mm × 70 mm × 2 mm. Each sample was used for two bending experiments. The paths of the plasma jet on the samples were positioned in such a way, that the two experiments are independent from each other. The material parameters used for the simulations were those of steel (St37). The simulation method can be easily transferred to other materials or heat sources if the parameters necessary for the simulation are known.

Simulation of the thermal bending process. Simulations of the thermal bending process were carried out using the FEM packet Abaqus standard 6.4–4 on a PC with two 2.8 GHz Xeon processors and 2.0 GByte RAM (operating system: Linux, SUSE 9.2). As a reference model for the simulation half of the sample geometry was modeled with finite elements (Figure 1).

4480 linear 8-node 3D elements were used. In the deformation zone the mesh was locally refined. The calculation of the temperature field using the reference model took about 22 min per cycle of the heat source. In figure 2 the results of a simulation using the reference model are shown. At the first cycle of the heat source (*a*) a significant rise of the temperature can be observed only in the deformation zone. During the following cycles the heat flows also into the regions of the sheet beside this zone (*b*). The reference model simulation allow for detailed investigations of the time dependent temperature field and the heat fluxes at every time everywhere in the modeled samples. Special respect was given to the transition region between the deformation zone and the remainder of the sheets. The

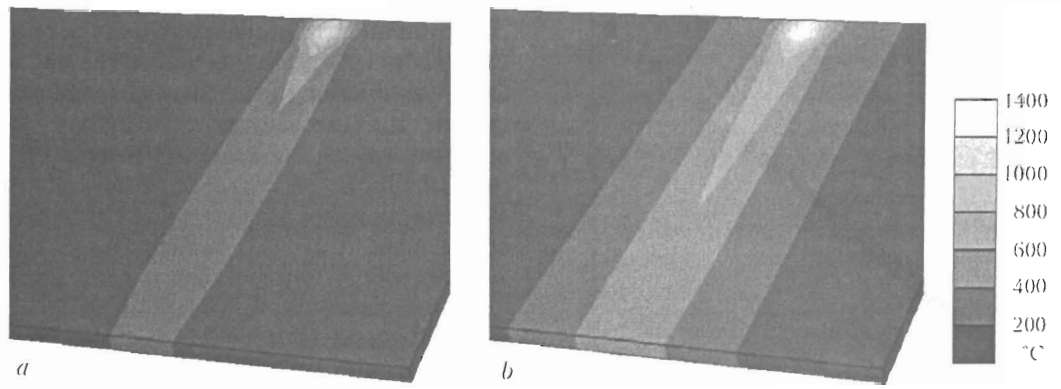


Figure 2. Results of a reference model simulation near the end of cycle 1 (*a*) and 4 (*b*) of the heat source; material St37, sheet thickness of 2 mm, velocity of heat source of 2500 mm/min

heat flux through this transitional region was investigated. It can be described by a generalized function, which moves parallel to the position of the heat source. In figure 3 such a heat flow function through a cutting plane 4 mm beside the path of the heat source is plotted for the first 4 cycles. The heat flux is described in dependence of the relative boundary position dy, which is calculated as the difference of the y-coordinate y_b at the border and the y-coordinate of the heat source y_{pl} by $dy = y_{pl} - y_b$. For thin sheets (up to 2 mm thickness) this function is independent of the z-coordinate of the boundary position and changes only slightly from cycle to cycle. During the cycles the shape of the function does not change.

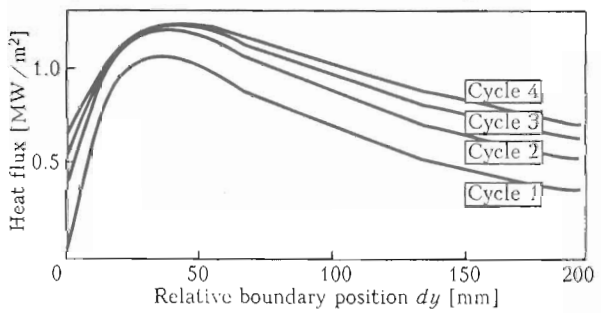


Figure 3. Generalized heat flux function: material St37, sheet thickness of 2 mm, velocity of the heat source of 2500 mm/min

After about four cycles of the heat source the maximum of the heat flux function does not increase any more, only the decrease section of the heat flux function shifts higher. This section can be interpolated linearly, if the time difference between to cycles is not to large (3 s for the case shown in Figure 3).

Acceleration of the temperature field simulation. To accelerate the simulation of the temperature field, calculations were carried out, were only the deformation zone was modeled using finite elements. The reduced model includes only 1/4 of the elements of the reference model (1120 elements). The parts of the sheet which were not modeled are accounted for by a boundary condition function (arrows in Figure 4) which provides the heat transfer between the deformation zone and the remaining parts of the sheet (Figure 3).

The accuracy of the simulation using the reduced model can be observed by comparing the calculated temperature fields with those resulting of the reference

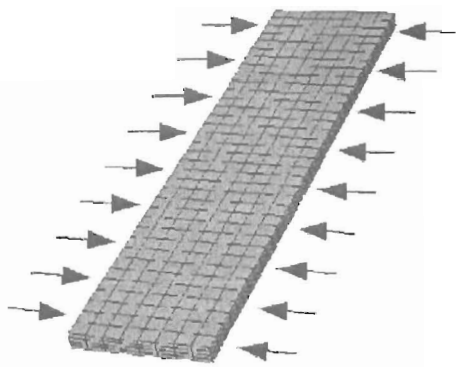


Figure 4. Reduced mesh with heat flux boundary condition function (arrows)

model simulations. In Figure 5 the temperature fields near the end of the second cycle of the heat source are shown. The temperature fields calculated with the two different models are in very good agreement. The isothermal line of 200 °C lies in both cases just inside the cutting edge of the reduced model. The maximum temperatures at the center of the heat source area differ only by 9 °C (reference model: 1240 °C, reduced model: 1249 °C). The good agreement between the calculated temperatures holds for the complete modeled region, as can be observed by comparing the temperatures of corresponding points of the two models.

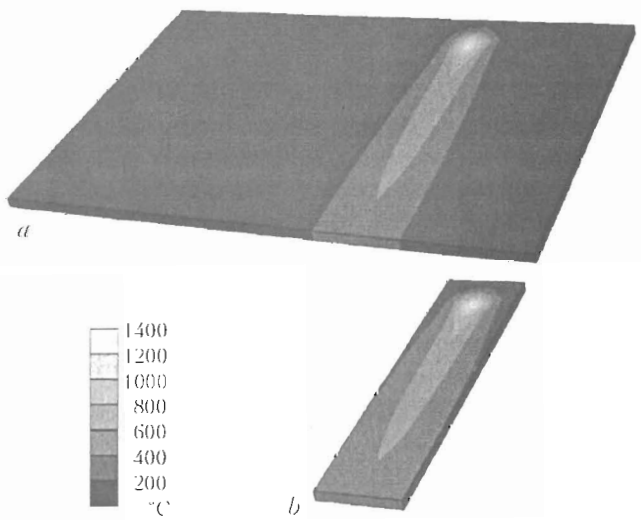


Figure 5. Simulated temperature field near the end of the cycle 2 of the heat source using the reference (*a*) and reduced (*b*) model

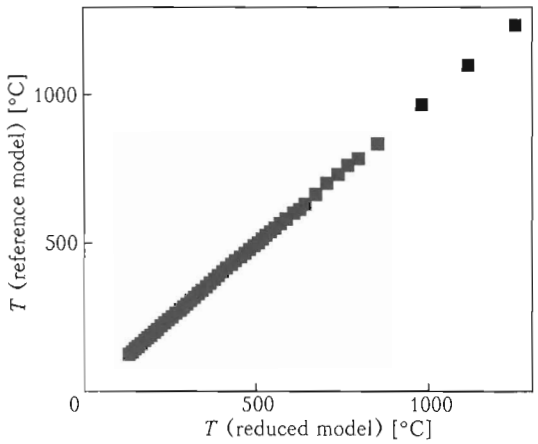


Figure 6. Comparison of the temperature fields shown in Figure 4

In Figure 6 the temperatures of the reference model calculation are plotted against those of corresponding points of the reduced model calculation. For an exact agreement all points should lie on a straight line with slope 1. As can be seen, the deviations are very small. The highest temperature differences are about 10 °C.

The calculation time for the simulation using the reduced model was about 6.5 min per cycle of the heat source, which is faster (by a factor of 3.4) than the calculation using the reference model.

CONCLUSION

With standard FEM packages, as Abaqus, the simulation of the thermal forming process is possible. Comparing the results with experiments reveal a good agreement. A full modeling of the geometry with finite elements results in inadequately high calculation times. A significant acceleration of the simulation of the temperature field can be achieved by reducing the modeling with finite elements to the deformation zone. For the investigated samples the calculation was accelerated by a factor of 3.4. Necessary for the reduced modeling is the knowledge of the heat flux from the deformation zone into the remainder of the samples. The heat flux can be observed in detail using simulations with complete finite element modeling (reference model). As a result a generalized heat flux function was defined, which was used as a boundary condition for the simulations using the reduced model. Further investigations to reduce the calculation time for the simulation of the thermal forming process will include the mechanical calculations. If a similar approach can be implemented successfully, the FEM calculation can be reduced on the deformation zone for the complete calculation. Especially for large components, this will reduce the calculation time significantly, which will allow for the use of simulations for parameter optimization and path planning for the forming of large and complex components.

Acknowledgement. *This work has been funded by the DFG (German Research Foundation) through SPP 1146 «Modellierung inkrementeller Umformverfahren» Project «Entwicklung eines Systems zur Simulation des Plasmastrahlbiegens» (VO 530/8-1). The authors wish to acknowledge the DFG for their support.*

1. Geiger, M.; Kraus, J.; Vollertsen, F.: *Laserstrahlumformen raumlicher Bauteile. Bestrahlungsreihenfolge wichtig.* Bander Bleche Rohre, vol 35, no 11 (1994) 26–37.
2. Vollertsen, F.: *Laserstrahlumformen – Lasergestutzte Formgebung: Verfahren, Mechanismen, Modellierung.* Meisenbach, Bamberg (1996).
3. Geiger, M.; Kraus, J; Vollertsen, F.: *Laserstrahlumformen raumlicher Bauteile. Bestrahlungsreihenfolge wichtig.* Bander Bleche Rohre, vol 35, no 11 (1994) 26–37.
4. Vollertsen, F.; Geiger, M.: *Laserstrahljustieren mechatronischer Komponenten.* In Strahltechnik 10: Laser – Von der Wissenschaft zur Anwendung, W. Juptner (edt.) BIAS-Verlag, Bremen, 1997, 309–320.
5. Holzer, S.; Vollertsen, F.: *Laserstrahlbiegen – Ein beruhrungsloses Blechumformverfahren.* Production Engineering, vol 84, no 1/2, 1994.
6. Geiger, M.; Vollertsen, F.; Amon, S.: *Flexieble Blechumformung mit Laserstrahlung – Laserstrahlbiegen.* Bleche, Rohre, Profile, vol 38, no 11, 1991, 856–861.
7. Klocke, F.; Demmer, A.; Dietz, C.: *Process analysis and practice-oriented modelling of laser bending operations using the temperature gradient mechanism.* Production Engineering, vol 6, no. 1, 1999, 39–42.
8. Male, A.T.; Li, P.J.; Chen, Y.Q.; Zhang, Y.M.: *Flexible forming of sheet metal using plasma arc.* SheMet, Internat. Conf. on Sheet Metal, 7 (1999) 555–560.
9. Komlodi, A.; Otto, A.; Geiger, M.: *On the way to real-time simulation of incremental laser beam bending.* Laser Assisted Net Shape Engineering 4, LANE 2004, Erlangen, 1059–1070.
10. Pretorius, T.; Woitschig, J.; Vollertsen, F.: *Fast Simulation of the Temperature Field for Plasma Jet Forming.* In Strahltechnik 26: Thermal Forming, F. Vollertsen; T. Seefeld (edt.) BIAS-Verlag, Bremen, 2005, 203–210.

CALCULATIONAL PREDICTION OF TOTAL DISTORTION OF TAILORED BEAMS IN LASER WELDING

P. SEYFFARTH[1], O. MAKHNENKO[2]
[1]SLV M-V GmbH, Rostock, Germany,
[2]E.O. Paton Electric Welding Institute, Kiev, Ukraine

Introduction. The rapid development of laser technology in welding causes the need of solving of new problems. One of the most important problems of laser welding is high requirements for accuracy of laser beam positioning. During welding a long tailored beam (Figure 1) is deforming and a displacement of laser beam, which move on a straight trajectory, from adjusted edges may exceed a tolerance (Figure 2). For example, this tolerance for tailored beams with wall thickness 4... 19 mm is about ±0.3 mm.

To reduce transient distortion of beams the restraint devices are used. At welding of the long tailored beams (4... 6 m) setting of a great amount of restraints decrease the productivity of technological process. Defining of a optimal distance between restraints by experimental way is unprofitable for modern small series welding production of tailored beams. Therefore, the calculation program for prediction of transient and residual welding distortions of tailored beams was developed. This program allows optimizing the distance between restraints to satisfy the given tolerance for displacement of laser beam. Also, the program evaluates the magnitude of forces in restraints during welding. This information is important for design of restraint devices. Also the program predicts residual general distortion of tailored beams after taking down restraints. The program takes possibility to evaluate the influence of both pre-bending and post-bending, made by restraints, on residual general distortion of tailored beams. Post-bending simulates the process of mechanical straightening after welding. The optimal value of pre-bending and post-bending are defined automatically for given tolerance for residual longitudinal deflection.

Computation Model. Using of the three dimensional FEM model of a long tailored beam in the stress-strain analysis requires long time of calculation and significant computational resources. Therefore, the following assumptions were taken in our calculation model.

Taking into account the high speed of laser welding, the assumption of high speed welding heat source is used in temperature problem. Since, three dimensional welding heat conduction FEM can be replaced by set of two dimensional FEM in the computation

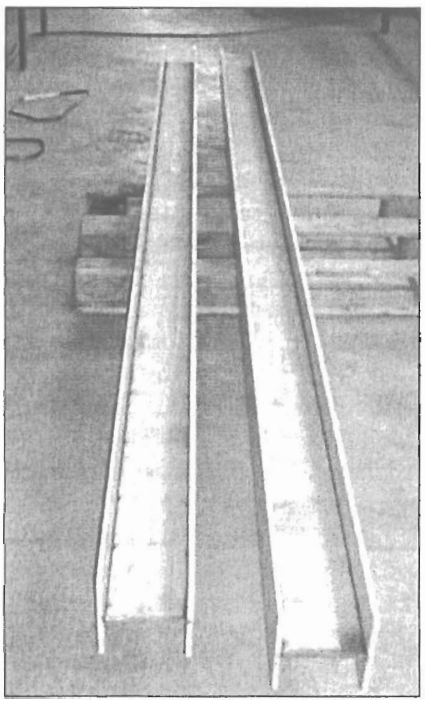


Figure 1. Laser welded long (4 m) tailored beams

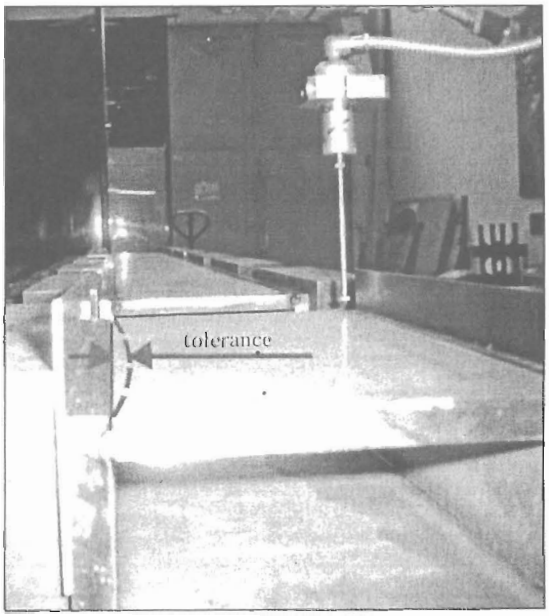


Figure 2. Layout of tolerance to displacement of laser beam from adjusted edges.

© P. SEYFFARTH, O. MAKHNENKO, 2005

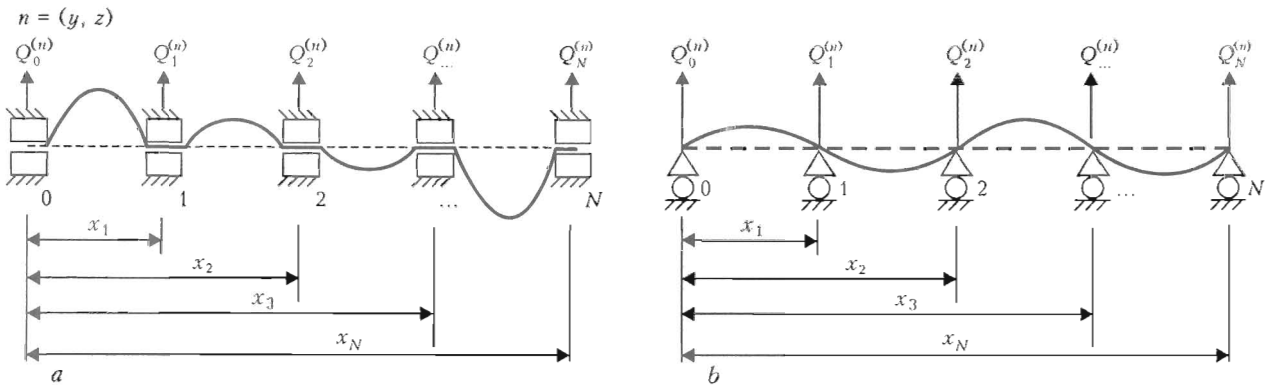


Figure 3. Built-in supported restraint conditions of a beam: *a* — built-in supported restraint; *b* — simply supported restraint

of the temperature distribution in selected cross-sections of a beam.

In mechanical problem the hypothesis of plane deformation or generalized plane strain is used. Stresses and strains can be computed by thermal elastic plastic FEM [1] in all selected cross-sections. It is known, that generalized plane strain FEM shows a good accuracy in the analysis of stresses and strains in comparison with three dimensional FEM [2].

Two variants of restraint conditions of a tailored beam were considered: built-in supported (Figure 3, *a*) and simply supported (Figure 3, *b*) restraints. Built-in supported restraint simulates restraint of a tailored beam by restrained devices with length along beam non equals zero. In this case the distortions of a beam between different restraints doesn't influence on each other. Other way, in the case of simply supported restraint, when restraint device acts at one point along beam, the deformation kinetic of a tailored beam is more complex.

The distinction of the used computational model is considering of statically indeterminate beam (Figure 3, *a*) with simply supported restraints along the length, where displacement equals zero $\Delta U_n(x_i) = 0$, $(n = y, z)$, $(i = 0, 1, 2, \ldots, N)$. Therefore, a solution for linearized problems of thermal elastic plastic FEM in all selected cross-sections are seek as sum of two solutions. First is a solution for the free beam with given temperature changes. Second solution corresponds to distortion of a beam by forces, defined from condition that sum displacements at all restraints equals zero.

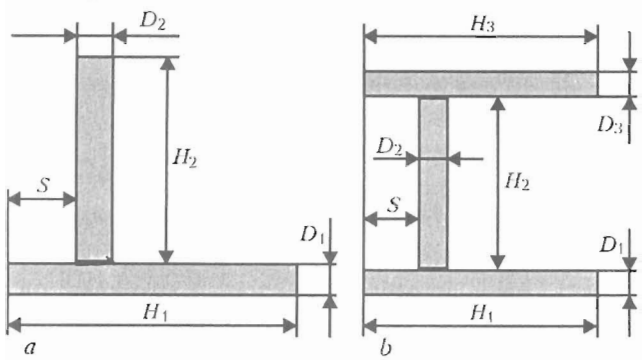


Figure 4. Profiles of tailored beams: *a* — T-profile; *b* — H-profile

Content of Computation Investigation. The developed calculation algorithm was used to predict displacements U_z and U_y of points of axes line of beam, passing throw the weight center of cross-section, at laser welding of longitudinal welds. Computations were conducted for long tailored beams with length 4 meters with different shapes of cross-sections (T- and H-profile) (Figure 4) and different distances between restraints. The material of tailored beams was assumed to be stainless steel. The physical properties of steel and their temperature dependency used in welding heat conduction FEM analysis are shown on Figure 5. Effective power of laser heat source is 8.5 kW, welding velocity — 1.3 m/min. Both restraint conditions were used in computations, but for the most part results are presented for simply supported restraints of tailored beams, because of economy of paper place and similarity effect on different factors.

The investigation evaluated the effect of a distance between restraints on the magnitude of transient displacements of points of axes line of beam, when welding heat source is passing these points. This information is important for optimization the distance between restraints for given tolerance for displacement of laser beam.

The effect of welding speed on the magnitude of transient displacements of points of axes line of beam, when welding heat source is passing these points, was studied.

Also the effect of a distance between restraints on the magnitude of general residual distortion of beams after taking down restraints was studied.

The investigation evaluated the magnitude of transient and residual forces in restraints during welding and after cooling. This information is important for design of restraint devices.

The calculation algorithm was added by possibility to define optimal pre-bending and post-bending, made by restraints, to minimize residual general distortion of tailored beams. Post-bending simulates the process of mechanical straightening after welding. The optimal value of pre-bending and post-bending are defined automatically for given tolerance for residual longitudinal deflection.

Computational results of general distortion of tailored beam. On Figure 6 the example of computational results of displacement U_y of points of axes line of beam, passing throw the weight center of cross-section, at laser welding of longitudinal weld is presented. The computation was performed for the tailored beam of T-shape cross-section ($H1$ = 80 mm, $H2$ = 80 mm, $D1$ = 8 mm, $D2$ = 8 mm, S = 36 mm) with length 4000 mm. Effective power of laser heat source is 8.5 kW, welding velocity – 1.3 m/min, restraint condition – simply supported restraints. The shape of cross-section and distribution of welding heating were choose symmetrical relative to axe Y, therefore displacement U_z equals zero. The quantity of restraints was five, that corresponding the distance between restraints equals 1000 mm. The results show the maximum value of transient displacement of points of axes line of beam, when welding heat source is

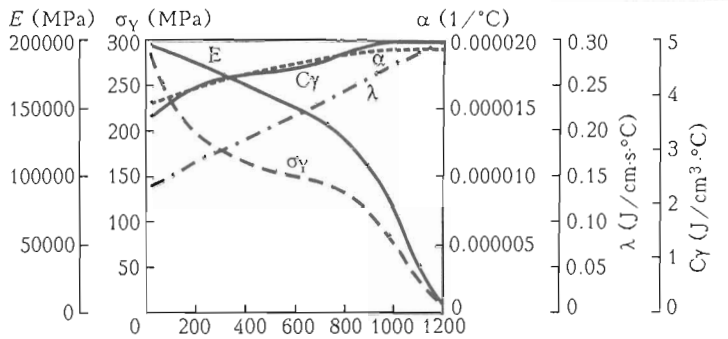


Figure 5. Temperature-dependent physical properties of a stainless steel used in FEM analysis

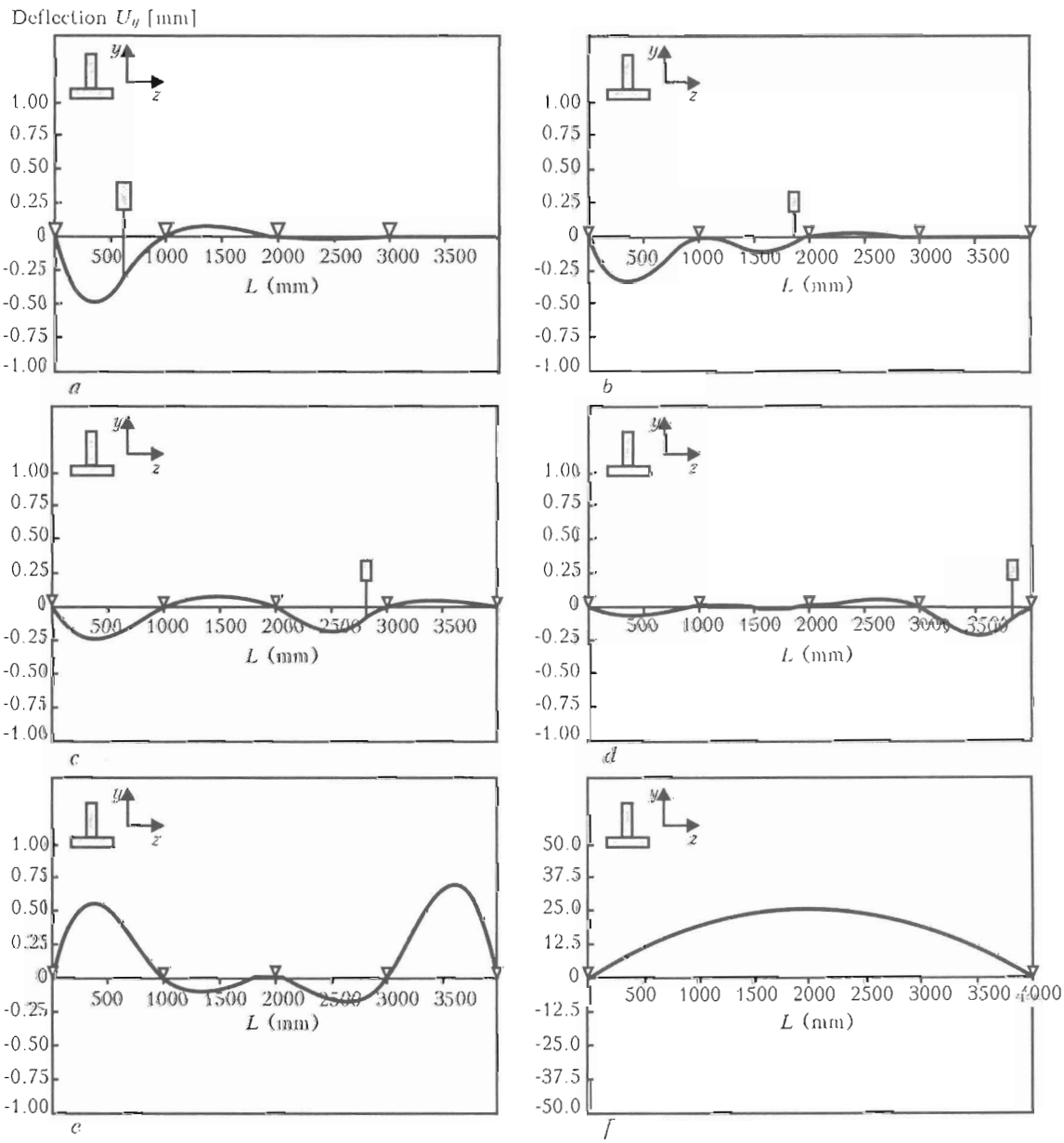


Figure 6. Computational results of displacement U_y of points of axes line of T-profile tailored beam ($H1$ = 80 mm, $H2$ = 80 mm, $D1$ = 8 mm, $D2$ = 8 mm, S = 36 mm) with length 4000 mm in laser welding of longitudinal weld in simply supported restraints $U_{y\,max\,u}$ = = –0.34 mm: *a* – 28 s from start of welding ($U_{y\,max}$ = –0.50 mm); *b* – 85 s ($U_{y\,max}$ = –0.33 mm); *c* – 130 s ($U_{y\,max}$ = –0.24 mm); *d* – 176 s ($U_{y\,max}$ = –0.22 mm); *e* – after cooling ($U_{y\,max}$ = 0.70 mm); *f* – after unloading restraints ($U_{y\,max}$ = 26.20 mm)

passing this points, reaches 0.34 mm at the moment 20 sec from start of welding (Figure 6, *a*) and exceeds the given tolerance for displacement of laser beam (±0.30 mm). It requires increasing the quantity of restraints. The value of residual deflection U_y of the beam after taking down restraints equals about 26 mm on the length 4000 mm (Figure 6, *f*). It is obvious, that this welded beam requires a mechanical straightening.

Figure 7. Shows the computational results of displacement U_y of points of axes line of beam at laser welding of longitudinal weld for similar T-shape tailored beam and welding conditions but another restraint conditions. Built-in restraint of a beam realized by restraint devices with length 30 mm. The quantity of restraints was five and the distance between restraints equals 970 mm. Simply to see that maximum value of transient displacement of points of axes line of beam, when welding heat source is passing these points, is significantly lower (0.04 mm) then for simply supported restraints (Figure 6). Next computations defined that for this tailored beam with length 4000 mm three restraint devices along beam length will be enough to satisfy the given tolerance for displacement of laser beam (±0.30 mm). But the value of residual deflection U_y of the tailored beam after taking down restraints also equals about 26 mm on the length 4000 mm (Figure 7, *f*). Therefore, the built-

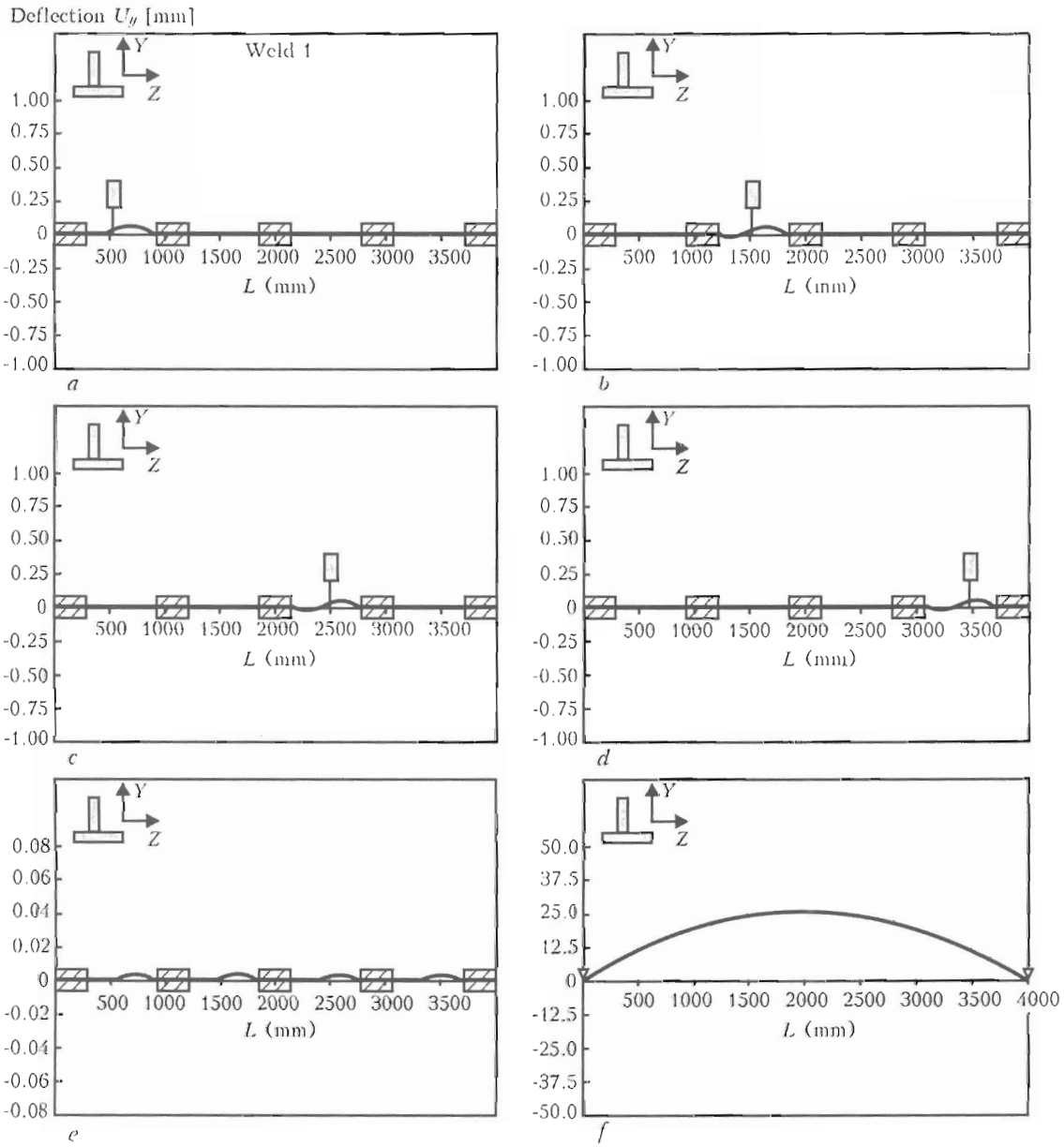


Figure 7. Computational results of displacement U_y of points of axes line of T-profile tailored beam ($H1$ = 80 mm, $H2$ = 80 mm, $D1$ = 8 mm, $D2$ = 8 mm, S = 36 mm) with length 4000 mm in laser welding of longitudinal weld in built-in supported restraints: *a* — 24 s from start of welding (t = 23.9 s, T_{max} = 1777 °C, $U_{y\,max}$ = 0.06 mm, $U_{y\,max\,w}$ = 0.03 mm); *b* — 67 s (t = 66.8 s, T_{max} = 1777 °C, $U_{y\,max}$ = 0.06 mm, $U_{y\,max\,w}$ = 0.04 mm); *c* — 111 s (t = 110.6 s, T_{max} = 1777 °C, $U_{y\,max}$ = 0.06 mm, $U_{y\,max\,w}$ = 0.04 mm); *d* — 154 s (t = 153.7 s, T_{max} = 1777 °C, $U_{y\,max}$ = 0.05 mm, $U_{y\,max\,w}$ = 0.04 mm); *e* — after cooling (t = 178.8 s, T_{max} = 20 °C, $U_{y\,max}$ = 0.00 mm, $U_{y\,max\,w}$ = 0.04 mm); *f* — after unloading restraints (t = 181.8 s, T_{max} = 20 °C, $U_{y\,max}$ = 26.10 mm, $U_{y\,max\,w}$ = 0.04 mm)

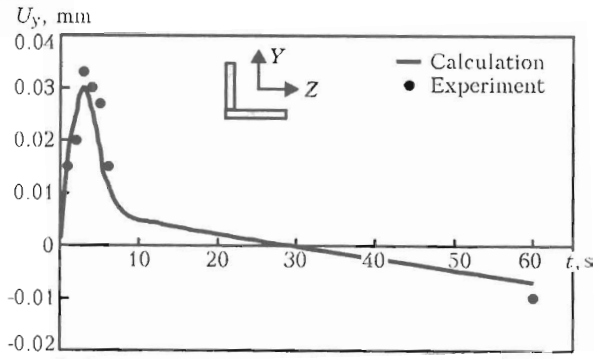


Figure 8. Comparison of calculation and experimental kinetics of transverse displacement of T-profile beam (material – steel 1.4301, $H1$ = 80 mm, $H2$ = 77 mm, $D1$ = 8 mm, $D2$ = 8 mm, S = 0 mm) in the middle point between two built-in supported restraints, positioned with distance 220 mm, in laser welding of longitudinal weld (P = 10.5 kW, V_w = 3 m/min)

in restraint conditions of tailored beam allows significantly decreasing the temporary welding deflections.

Experimental validation. During welding longitudinal weld (P = 10.5 kW, V_s = 3 m/min) of T-profile tailored beam ($H1$ = 80 mm, $H2$ = 77 mm, $D1$ = 8 mm, $D2$ = 8 mm, S = 0 mm) made by stainless steel 1.4301, the measurement of kinetic of transverse displacement U_y in the middle point between two built-in supported restraints, positioned with distance 220 mm, was conducted. Comparison of these calculation and experimental data on Figure 8 shows rather good agreement, when efficient coefficient of laser welding source assumed to be η = 0.5. After welding, cooling and unloading down restraints the measured residual deflection U_y of the beam equals 11.0 ÷ 11.5 mm. Calculation predicts residual deflection U_y = 11.7 mm

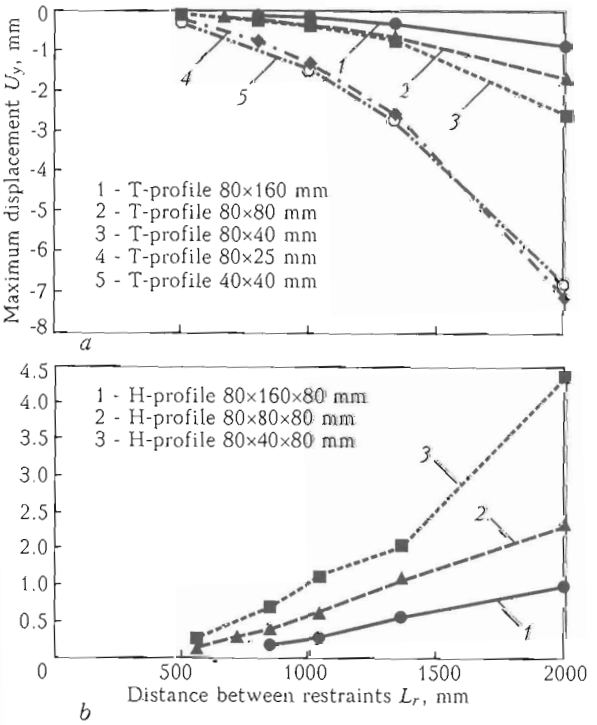


Figure 9. Effect of distance between restraints and rigidity of tailored beams with length 4000 mm on the magnitude of transient displacements of points of axes line of beam, when welding heat source is passing these points: *a* – T-profile beams; *b* – H-profile beams

Effect of distance between restraints on the magnitude of transient displacements of beam, when welding heat source is passing. Figure 9 shows the computational results of maximum transient displacements U_y of beams in the moment, when welding heat source is passing, for different value of distance between restraints. For comparison this results were calculated for five variants of T-shape tailored beams with one longitudinal weld and different ratio of web width $H1$ and flange width H2: 80×160 mm, 80 × 80 mm, 80 × 40 mm, 80 × 25 mm, 40 × 40 mm, and for three variants of H-shape beams with two longitudinal welds: 80 × 160 × 80 mm, 80 × 80 × 80 mm, 80 × 40 × 80 mm. The thickness of all webs and flanges are similar $D1 = D2 = D3$ = 8 mm. Welding conditions and material for all tailored beams are similar too. The results show, that with decreasing distance between restraints, the maximum transient displacements of beams in the moment, when welding heat source is passing, becomes significantly smaller. At distance between restraints equals 500 mm this maximum transient displacements of all examined beams does not exceed the tolerance value 0.3 mm. For beams with cross-section profiles 80 × 80 mm, 80 × 40 mm requirement of the tolerance is satisfied at distance between restraints equals 800 mm, for beams with cross-section profile 80 × 160 mm, 80 × 160 × 80 mm – at distance between restraints equals 1000 mm. With increasing beams rigidity, the maximum transient dis-

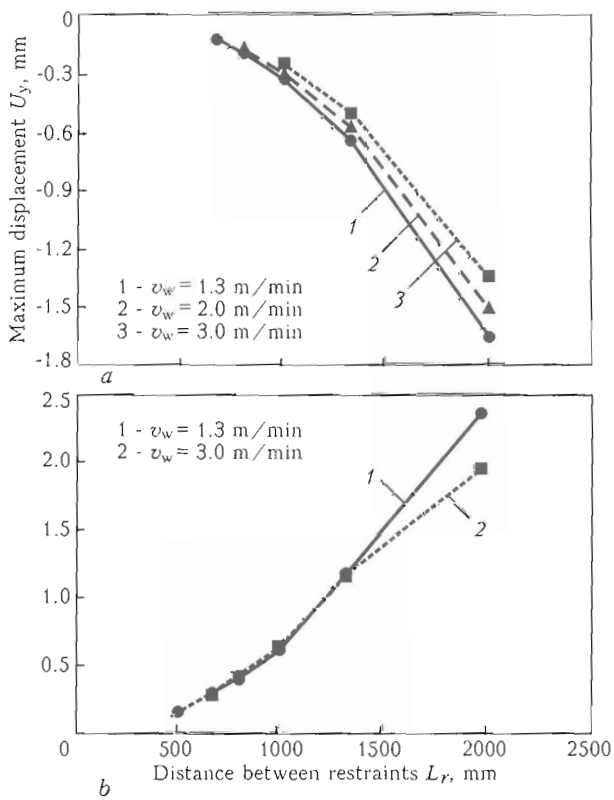


Figure 10. Effect of distance between restraints and welding speed on magnitude of transient displacements of points of axes line of beam, when welding heat source is passing these points: *a* – T-profile beams 80×80×4000 mm; *b* – H-profile beams 80×80×80×4000 mm

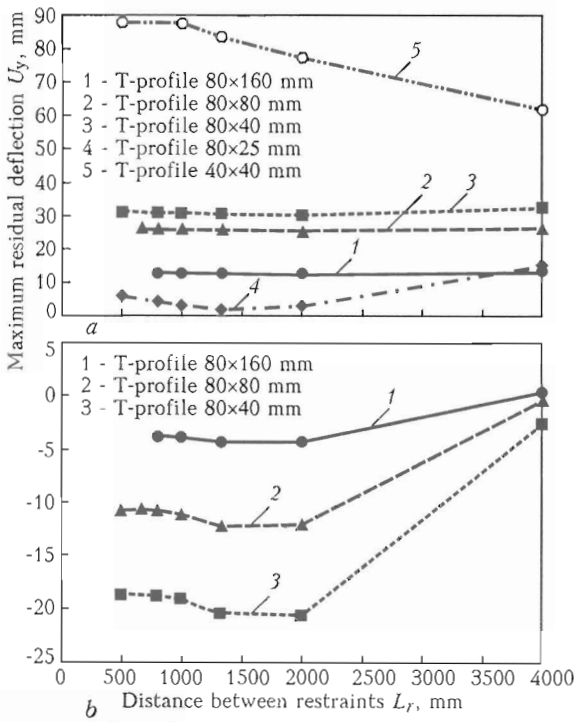


Figure 11. Effect of distance between restraints and rigidity of tailored beams with length 4000 mm on magnitude of residual deflection after removing restraints: *a* — T-profile beams; *b* — H-profile beams

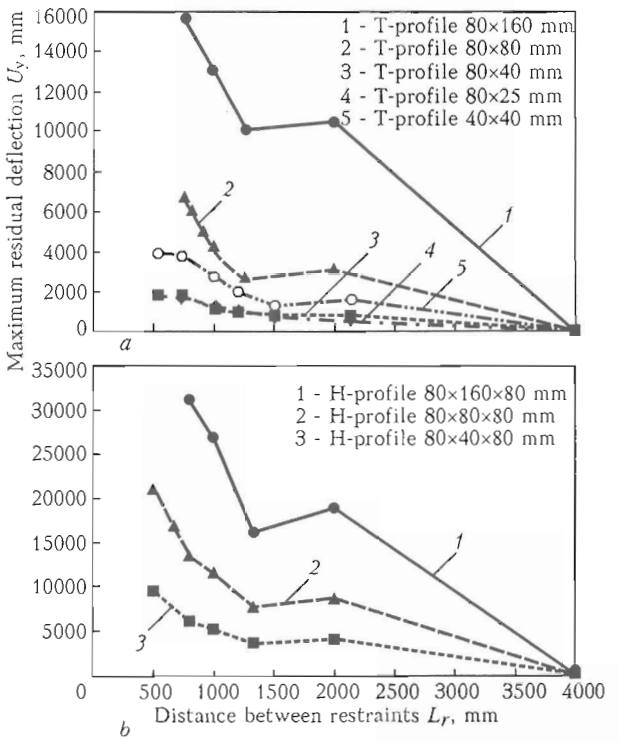


Figure 12. Effect of distance between restraints and rigidity of tailored beams on magnitude of maximum forces in restraints: *a* — T-profile beams; *b* — H-profile beams

placements of beams in the moment, when welding heat source is passing, decreases.

Effect of welding speed on the magnitude of transient displacements of points of axes line of beam, when welding heat source is passing. Figure 10 shows the computational results of maximum transient displacements U_y of T-profile and H-profile beams with length 4000 mm in the moment, when welding heat source is passing, for different welding speed with saving the constant value of heat input. Results on Figure 10, *a*, calculated for T-profile tailored beam with one longitudinal weld and web width H1=80 mm and flange width $H2$ = 80 mm, thickness of web and flange are $D1 = D2 = 8$ mm, demonstrate the little decreasing of magnitude of transient displacements on increasing of welding speed. For H-profile tailored beam ($H1$ = 80 mm, $H2$ = 80 mm, $H3$ = 80 mm, $B1 = B2 = B3 = 8$ mm) with two longitudinal welds (Figure 10, *b*) the influence of welding speed on the magnitude of transient displacements of beam nearly don't be observed, because the second weld is performed when a tailored beam is residually deformed after the first weld.

Effect of distance between restraints on the magnitude of residual deflection. Along with computation of transient distortions of tailored beams the residual deflection of beam after removing restraints were defined. Figure 11 shows the computational results of residual deflection U_y of examined beams for different value of distance between restraints during welding. For beams with T-profiles 80 × 160 mm, 80 × 80 mm, 80 × 40 mm the distance between restraints does not effects on the value of residual deflection U_y. For another beams this effect is more significant. For a beam with T-profile 80 × 25 mm and for all H-profile beams with decreasing distance between restraints, the residual deflection at first becomes smaller and then increases. For T-profile beam 40 × 40 mm the residual deflection becomes larger, when distance between restraints is decreasing. In general, it is confirmed the fact, that restraining of a beam during welding is not an effective technological measure to reduce general residual deflection. It can be seen that for H-profile beams with two longitudinal welds the restraining during welding causes increasing of residual deflection in comparison with welding in free condition. Free condition in this investigation corresponds the distance between restraints equals length of a beam 4000 mm. Also it can be seen that with increasing rigidity of tailored beams, the residual deflection becomes smaller. However, the distance between weight center of beam profile and longitudinal weld has the great influence on residual deflection of a beam. For example, for T-profile beam 80 × 25 mm the weight center is so close to weld that, in spite of small rigidity of this beam in *Y* direction, the residual deflection U_y is little.

Effect of distance between restraints on the magnitude of maximum forces in restraints. Forces acting in restraints during welding and cooling may reach significant value and it is necessary to consider this information for design of restraint devices. On Figure 12 the computational results of maximum forces in restraints of examined beams for different value of distance between restraints. This results show that

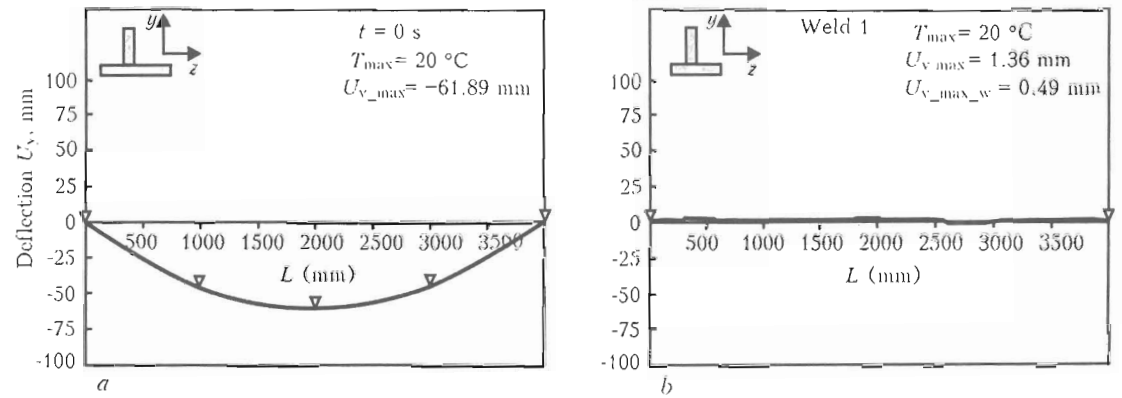


Figure 13. Example of computational results of defining optimal pre-weld bending, made by five restraints, to reduce residual distortion of the T-profile beam ($H1$ = 80 mm, $H2$ = 80 mm, $D1$ = 8 mm, $D2$ = 8 mm) with length 4000 mm: *a* — pre-bending before welding; *b* — after welding and unloading restraints

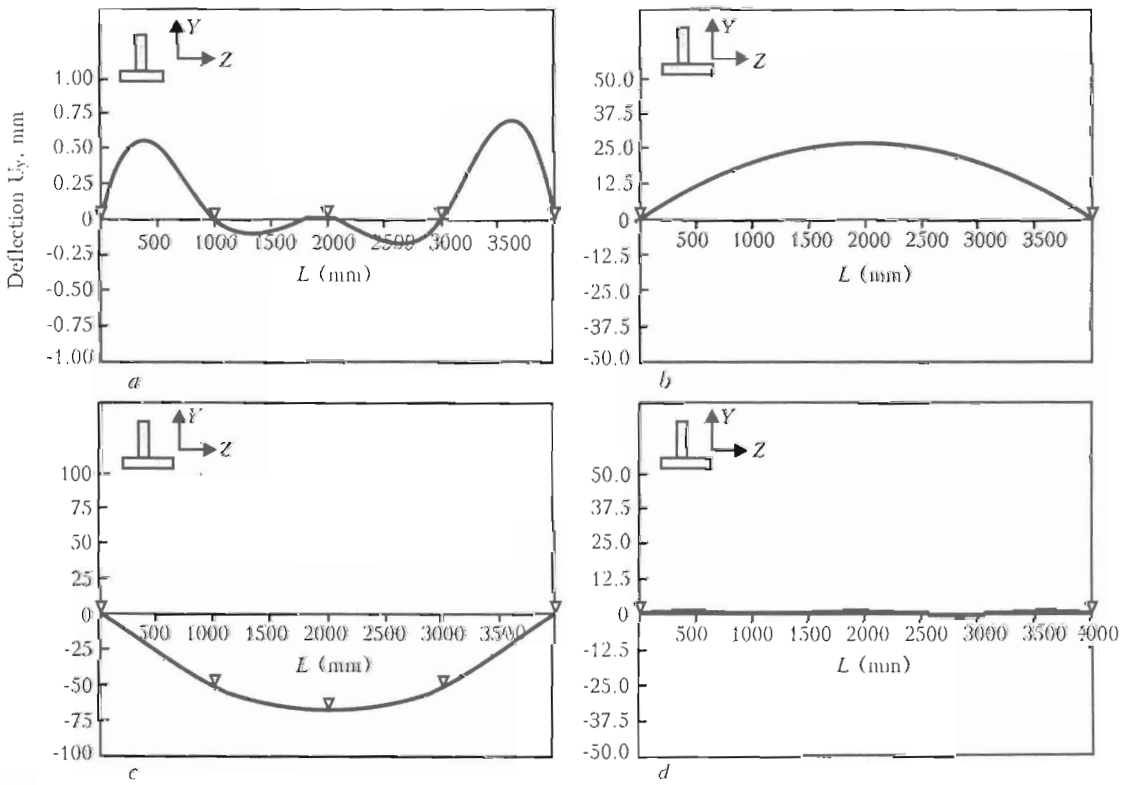


Figure 14. Example of computational results of defining optimal post-weld bending, made by restraints, to reduce residual distortion of the T-profile beam ($H1$ = 80 mm, $H2$ = 80 mm, $D1$ = 8 mm, $D2$ = 8 mm) with length 4000 mm (T_{max} = 20 °C): *a* — after welding ($U_{y\,max}$ = 0.70 mm; $U_{y\,max\,w}$ = −0.34 mm); *b* — after unloading restraints (t = 198 s; $U_{y\,max}$ = 27.00 mm; $U_{y\,max\,w}$ = −0.34 mm); *c* — post-weld bending ($U_{y\,max\,w}$ = −67.78 mm); *d* — after unloading restraints (t = 0 s; $U_{y\,max}$ = 1.14 mm; $U_{y\,max\,w}$ = −0.34 mm)

with decreasing distance between restraints and increasing rigidity of beams, the maximum forces in restraints becomes larger.

Computational defining of optimal pre-weld and post-weld bending. The calculation algorithm was added by possibility to define optimal pre-bending and post-bending, made by restraints, to minimize residual general distortion of tailored beams. Post-weld bending simulates the process of mechanical straightening after welding. The optimal value of pre-bending and post-bending are defined by iteration method for given tolerance for residual longitudinal deflection.

The example of computational defining of optimal parameters of pre-bending, made by five restraints, for T-profile tailored beam ($H1$ = 80 mm, $H2$ = 80 mm, $D1$ = 8 mm, $D2$ = 8 mm) with length 4000 mm is presented on Figure 13. Welding and cooling of this tailored beam in the pre-bended state (Figure 13, *a*), when pre-bending deflection equals — 62 mm, produce maximum residual deflection of the beam after unloading restraints nearly 1.4 mm (Figure 13, *b*). For comparison, in a case of welding this tailored beam without pre-bending (see Figure 12, *f*) maximum residual deflection is much greater and reaches 26 mm.

Figure 14 shows example of computational results of defining optimal post-weld bending, made by five

restraints, to reduce residual distortion of the similar T-profile beam. Bending to the value – 68 mm (Figure 14, *c*) reduces the maximum residual deflection of the tailored beam down to 1.1 mm (Figure 14, *d*).

It is necessary to note, that such bending with producing plastic strains in tailored beams requires action of significant efforts in restraints. That complicates structure of restraint devices. However, for a small series production of tailored beams the proposed technologies of welding with low residual distortions may be quite attractive.

Developed mathematical model allows:

1. To predict both temporary total distortions of laser welded tailored beams with big quantity of restraints and residual total distortions after unloading of restraints.

2. To optimize the distance between restraints to satisfy the given tolerance for displacement of laser beam.

3. To define optimal parameters of pre-bending or post-weld bending, made by restraints, to reduce residual deflection of tailored beams.

1. Makhnenko, V. I. (1976) *Numerical methods for investigation of kinetics of welding stresses and distortions.* Kiev: Naukova Dumka.
2. N.X.Ma, Y.Ueda, H.Murakawa and H.Maeda, *FEM Analysis of 3-D Welding Residual Stresses and Angular Distortion in T-type Fillet Welds* JWRI, Vol. 24 (1995) No.2, pp. 115–122.

Conference Sponsors

PWI Laser Systems and Technology Center

Ministry of Education and Science of Ukraine

Information Support

«The Paton Welding Journal»

www.nas.gov.ua/pwj

Conference Sponsors

PWI Laser Systems and Technology Center

Ministry of Education and Science of Ukraine

Information Support

«The Paton Welding Journal»

www.nas.gov.ua/pwj

RESEARCH OF DIRECT LASER SINTERING OF METAL POWDERS

Yu. A. CHIVEL, K. E. BELIAVIN, V. K. PAVLENKO, M. V. PETRUSHINA
Institute of Molecular and Atomic Physics NASB, Minsk, Belarus

Theoretical and experimental investigations of the direct sintering of powder coverings from metal spherical particles by pulsed laser radiation was made.

Introduction. When solving a number of problems of powder metallurgy including selective laser sintering of medical implants [1] the high degree of porosity of product must be conserved at minimal particles deformation. This can be arranged by contact welding of particles the layers each and particles of two sequential layers of powder coverings. The central problem is sintering a two layer without complete fusion penetration of upper layer.

We carried out theoretical and experimental researches of sintering of covering from two layers of spherical metal particles by pulse and pulsed-periodic laser radiation with length of a wave $\lambda = 1.06$ μm, duration 1–5 ms. Numerical calculations are conducted with use of program LS-DYNA on a supercomputer «SCIF» [2]. As a criterion of sintering achievement in points of a contact of spheres the temperature of fusion of a material of powder particles is chosen.

Modeling. Three-dimensional differential thermal conductivity equation may be written:

$$\rho c \frac{\partial T}{\partial t} = k\nabla^2 T + Q \qquad (1)$$

at boundary data: $k\frac{\partial T}{\partial n} = -(1-R)q + \acute{\varepsilon}\,\sigma T^4$ (2)

and initial conditions: $T = T_0$ при $t = t_0$.

where ρ, c, k — density, heat capacity, thermal conductivity of particles material, $\acute{\varepsilon}$ — emissitivity factor, σ — Stephen-Boltzmann constant, Q — intensity of internal heat source, q — laser radiation intensity, n — surface normal.

At the environment of Mechanical Desktop the solid — state model in the form of four balls was created (Figure 1). At the ANSYS programme the finite-element grid on a surfaces was built.

A boundary conditions was determined by given values of power flow through the finite-elements on the surface $(1-R)q$. In the model under consideration the laser radiation power density at focal spot on the particles surface is in the form of Gaussian distribution $q = q_m \exp(-r^2/R_s^2)$ with half-width R_s = = 0.02 – 0.2 mm, peak pulsed power density P = 10 – – 600 W, particles diameter — 200 μm, reflection

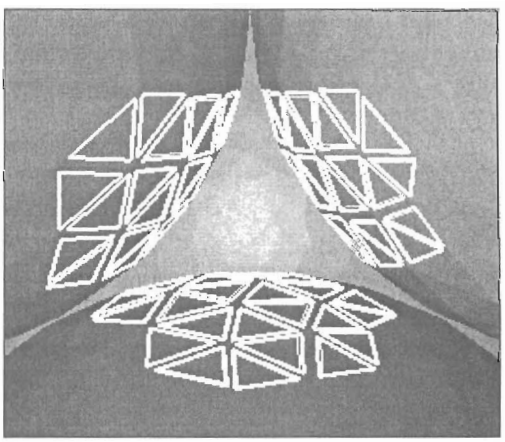


Figure 1. Finite-element grid on a surfaces of solid-state model

coefficient R = 0.6. The laser pulse shape is taken as rectangular.

Calculations are performed at a directional arrangement of an irradiation spot on a surface of powder covering at the one pulse influence (Figure 2).

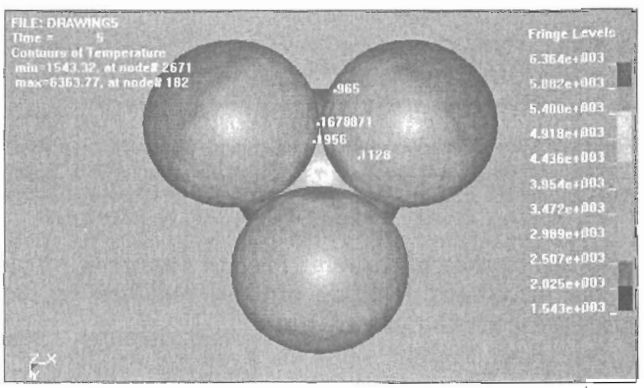


Figure 2. Temperature field on the surface of solid model at t = 5 ms

For maintenance of calculations of process of sintering and a choice of parameters of influencing laser radiation the measurements of factors of reflection and transmission of laser radiation by layers of a titanic spherical powder particles in diameter 200 μm and 400 μm are carried out. It is found that [3] only 15% of laser power fall on the underlayer particles at density packing and for two-layer sintering it is essential to melt the particles of upper layer.

© Yu. A. CHIVEL, K. E. BELIAVIN, V. K. PAVLENKO, M. V. PETRUSHINA, 2005

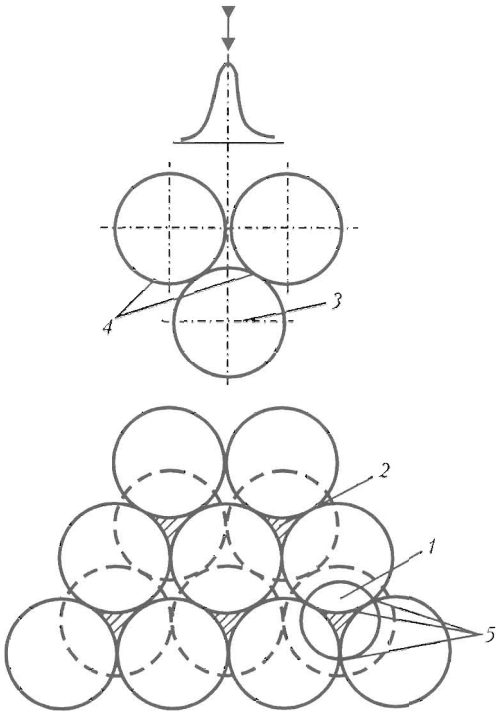


Figure 3. Schematic view of the directional focusing of laser radiation

As calculations implied, the optimal regime of sintering without particles melt down can obtain using

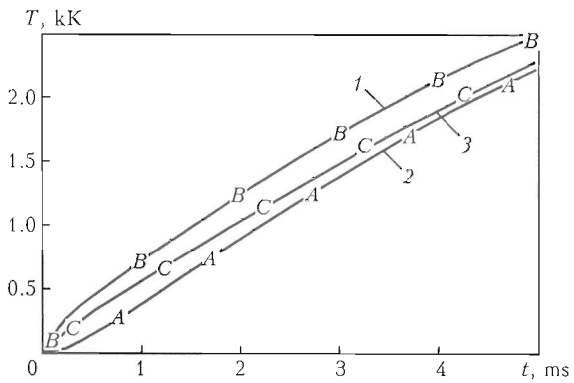


Figure 4. Time dependence of temperature at the contact points at optimal regime of operation: *1* — contact between balls of upper layer (point *B*); *2*, *3* — contact between balls of upper and lower layers (point *A*, *C*); D = 200 μm, P = 12.5 W, R_s = 0.02 mm

proposed method of sintering [4], the essence of which is the directional focusing of laser radiation to the space between the particles of upper layer. Redistribution of pulsed power between the layers provides optimal surface heating of the particles contact regions.

Serial focus spot reduction from R_s = 0.1 mm to R_s = 0.02 mm (Figure 4, 5) tends to temperature balance at upper and lower contact points. Particles heating down may be occur at the small region of lower layer particles (Figure 2). The focus

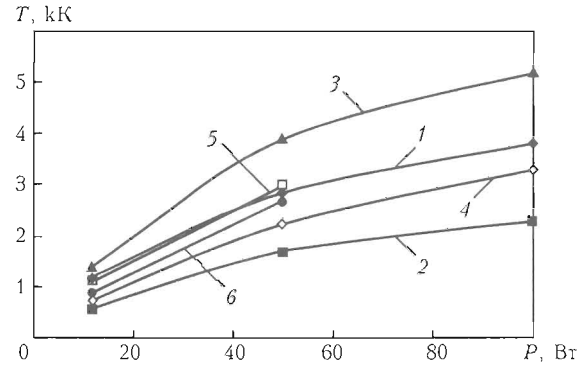


Figure 5. Power dependence and focus area size dependence of temperature at contact points (D = 200 μm). Focus area size: *1*, *2* — 0.1 mm; *3*, *4* — 0.05 mm; *5*, *6* — 0.02 mm; *1*, *3*, *5* — point *B*, *2*, *4*, *6* — points *A*, *C*

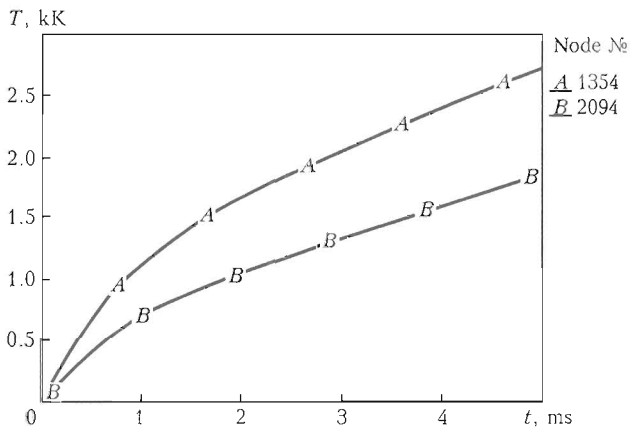


Figure 6. Time dependence of temperature at contact points at optimal regime of operation: D = 400 μm, P = 50 W, R_s = 0.05 mm

sport size and laser power will rise as the particles diameter increases (Figure 6) and temperature difference will gain.

Experimental. The preliminary experimental studies of sintering of fragment of powder covering from Ti — powder diameter 400–600 μm at the non — and directional influence by pulsed Nd-YaG laser (pulse duration 1–3 ms with energy in a pulse 0.1–1 J) have confirmed results of calculations. The sintering was made in Ar-atmosphere. The agreements are observed in laser power level and spot sizes (Figure 7).

Real time technology of sintering. For realization of idea of directional focusing of laser radiation in an interval between particles a apparatus and program

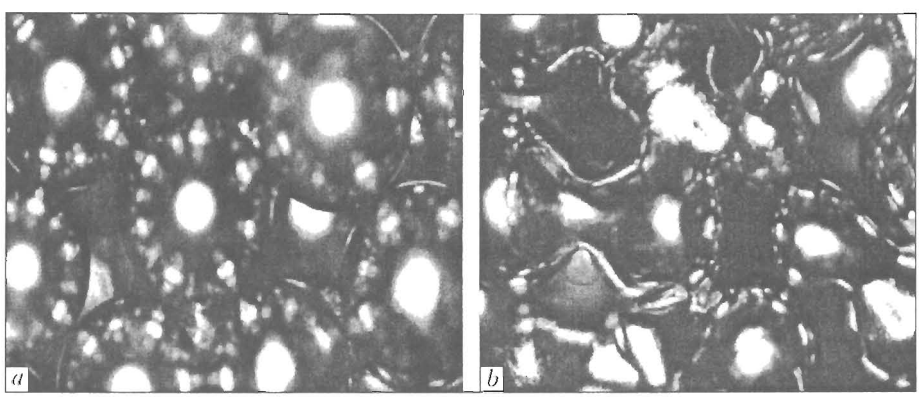


Figure 7. Image of sintering coverings: *a* — two layer, R_s = 0.05 mm (P = 53 W); *b* — two layer, R_s = 0.2 mm (P = 200 W) (non-directional mode)

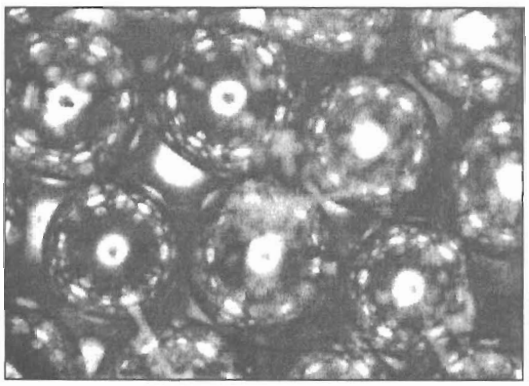


Figure 8. Image of powder covering

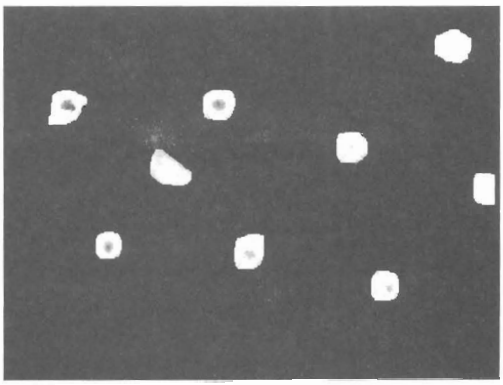


Figure 9. Result of image segmentation and filtration

components were designed [5]. The coaxial observation system with videocamera, the optical axis of which is concurrent to the laser beam path, makes it possible to observe the processing zone and surrounding area ~2 mm in diameter (Figure 7) during the process. The obtained images are identified in the real time regime (Figure 8) and coordinate of laser action points are determined. The laser focus spot is moved over the surface initially in a equidistant curves with a step smaller than particles diameter. According the determined coordinates the trajectory is varied in magnitude < particles radius in the real time under velocity of laser spot motion 20 mm/s and laser pulse frequency 50 Hz.

CONCLUSIONS

The modelling of sintering of covering from two layers of spherical metal particles in pulse mode of operation and the preliminary experimental studies validate the efficiency of proposed method of sintering, the essence of which is the directional focusing of laser radiation to the space between the particles of upper layer under appropriate focus spot dimension.

Optimal modes of spherical particles coverings sintering such that the porosity is preserved and particles deformations are minimal under synchronized reduction at about 5 times required laser power was determined.

Hardware and software tools for adaptive control mode of SLS-process has been devised.

1. Santos E., Osakada K., Abe F. et al. // Proc. X Intern. Conference *«Laser-Assisted Microtechnology»*, St-Petersburg. (2003). – P. 59.
2. *LS-DYNA.* Theoretical manual. Livermore software technology corp. 1998. – 498 p.
3. Chivel Yu. A., Petrushina M. V., Pogudo E. L. // High Temperature, 10 p., (2004) (to be published).
4. Chivel Yu., Beliavin K., Pavlenko V. et al. // Bulletin of invention, № 1. – P. 21, Minsk, (2004).
5. Chivel Yu., Inyutin A., Vatkin M., Zavedeev V. // Summary II Real Time Conference, Stockholm, Sweden, (2005), 2p. (to be published).

TRIBOLOGICAL BEHAVIOR OF LASER TEXTURED SURFACES UNDER OIL LUBRICATION CONDITIONS

A. KOVALCHENKO[1], O. AJAYI[1], I. ETSION[2]
[1]Energy Technology Division of Argonne National Laboratory, USA
[2]Technion Department of Mechanical Engineering, Haifa, Israel

Laser surface texturing (LST) is an emerging effective method for improving the tribological performance of friction units lubricated with oil. In LST technology, a pulsating laser beam is used to create thousands of arranged microdimples on a surface by a material ablation process. These dimples generate hydrodynamic pressure between oil-lubricated parallel sliding surfaces. The impact of LST on lubricating-regime transitions was investigated in this study. Tribological experiments were conducted with a pin-on-disk apparatus at sliding speeds in the range of 0.015–0.75 m/s and nominal contact pressures that ranged from 0.16 to 1.6 MPa. Two oils with different viscosities (54.8 and 124.7 cSt at 40 °C) were used as lubricants. The test results showed that laser texturing expanded the contact parameters in terms of load and speed for hydrodynamic lubrication, as indicated by friction transitions on the Stribeck curve. The beneficial effects of laser surface texturing are more pronounced at higher speeds and loads and with higher viscosity oil.

Introduction. The need to reduce friction and the amount of wear on machine element components involved in sliding contact is ever present. The efficiency, reliability, and durability of such components depend on the friction that occurs at the sliding-contact interface. In addition, there is always the desire to increase the load capacity or the power density of machine elements, which of course will lead to higher severity of surface interaction. Both the need to reduce friction and the desire to increase load capacity require effective lubrication strategy for sliding surfaces.

Surface lubrication involves many aspects of the physical and chemical properties of the surface material and the lubricant. The viscosity of the lubricant and some of its other rheological properties determine the thickness of the lubricant fluid film. A thicker lubricant fluid film leads to better lubrication. Similarly, the roughness of the contacting surfaces has a major impact on the friction and wear behavior of lubricated surfaces. In general, smoother surfaces are better for fluid film lubrication. Indeed, the effects of lubricant film thickness and surface roughness on lubrication are combined in the so-called λ ratio parameter, defined as the ratio of the lubricant fluid film thickness to the composite surface roughness of contacting surfaces. The higher the λ ratio, the more effective the fluid lubrication mechanism; and very low values of λ indicate higher severity of interaction between asperities on contacting surfaces. Of course, higher friction and wear are expected under the relatively severe contact conditions of low λ values.

In recent years it has been shown that the presence of artificially created micro-features can significantly affect friction and wear behavior of lubricated surfaces. For instance, «undulated» surfaces created by machining of 50–800-μm-deep and about 20–500-μm-wide periodic grooves on the surface of a titanium alloy disc were shown to reduce friction in lubricated reciprocating contact when compared to nonundulated surfaces [1]. The friction reduction was attributed to the trapping of wear debris in the groove, thereby eliminating the «plowing» contribution to friction. In the mechanical-seal community, it has been recognized that micro surface patterns, such as radial taper, hydropads, lobes, and grooves can exert beneficial effects on the lubrication of mechanical seals. With this recognition, Etsion et al. [2, 3] recently developed a method to texture seal surfaces with a laser. The process, known as laser surface texturing (LST), involves creation of an array of microdimples on the seal surface by a material ablation process with a pulsating laser beam.

Laser surface texturing (LST) was shown both analytically and experimentally to enhance hydrodynamic and hydrostatic lubrication of mechanical seals. The result is a significant improvement in the load capacity, wear resistance, and friction coefficient of mechanical seals [2, 3]. The LST mechanical seals have been successfully field tested, and showed a substantial reduction in wear and surface damage when compared with untextured seal surfaces.

With the excellent results in seal applications, LST technology is now being considered and evaluated for other tribological applications, especially those that involve conformal contacts. Analysis of lubrication mechanisms and optimization of LST for piston-ring and cylinder-liner contact interface has been conducted [4]. This analysis showed that the dimple area density and the dimple diameter-to-depth ratio are important parameters for this application. Experimental results from conformal reciprocating sliding contact tests showed that LST reduced the friction coefficient by 30–40% when compared with an untextured surface under flooded adequate-lubrication conditions [5]. The results were consistent with analytical predictions. Under starved lubrication, LST also provided beneficial results in terms of friction reduction

© A. KOVALCHENKO, O. AJAYI, I. ETSION, 2005

and increase in load capacity before seizure. It is assumed that the dimples act as an oil reservoir. It was, however, observed that, when the dimples are relatively deep or when the oil viscosity is relatively high, LST may be detrimental to tribological performance under starved-lubrication conditions.

In view of the promise, and perhaps some limitations of the new LST technology for applications on various lubricated tribological components, it will be very useful to assess the impact of LST on lubrication regime transition. Such an assessment could provide a guideline and better understanding of the application of LST to various tribological components. This paper presents our experimental investigation of the effect of LST on lubrication regime transitions.

Experimental details. Friction tests were conducted with a pin-on-disk friction machine in unidirectional sliding. The «pin» was a 9.55-mm-diameter hardened 52100 steel ball with a nominal hardness of 60 HRC. Inasmuch as the LST technology was developed and, so far, optimized for conformal contacts, a flat contact area was created on the ball sample by first sliding the ball against a flat sample that contained a series of SiC abrasive papers, ending with very fine, 4000-grit paper. The final flat area created on the ball is 4.7 mm in diameter; its surface roughness is 0.01 μm Ra. The disc samples, 50 mm in diameter and 10 mm thick, are made from hardened H-13 steel with 60 Rc hardness. Figures 1, *a–c*, respectively show a schematic diagram of the contact configuration, and pictures of the test machine and pin specimen used for friction testing.

Disc samples with various surface preparations were used for frictional tests. Table 1 lists the characteristics of the tested discs, which are identified with numbers 1 through 6. Discs 1 and 2 were not laser textured. Disc 1 was polished smooth to a surface roughness of 0.01 μm Ra, and Disc 2 was ground and has a surface roughness of about 0.12 μm Ra. These two discs represent typical manufacturing practices of superfinishing and grinding, with which the results of LST surfaces can be compared. Various parameters of the dimples on the laser-textured discs and their surface roughness are presented in Table 1. The roughness between dimples is determined by a post-texturing lapping process. The area density of dimples (total dimple area/total surface area) on Disc 3 is optimized with the dimples situated on parallel lines that are, on average, 200 μm apart. The dimple density of Disc 4 is higher with 80–100 μm between dimples that are situated on parallel lines. The dimple density of Disc 5 is standard, but without the post-laser treatment lapping to remove bulges or burrs around their rim. The dimple density of Disc 6 is lowest, as indicated in Table 1. Optical images of disc surfaces after various treatments are shown in Figure 2.

Friction tests were conducted at normal loads of 2, 5, 10, and 20 N, corresponding to nominal contact pressures (load/nominal contact area) of 0.16, 0.4, 0.8, and 1.6 MPa, respectively. The diameter of the contact track on disc sample was 29 mm. Tests were performed at rotation speeds of 10, 25, 50, 75, 100, 200, 300, 400 and 500 revolutions per minute, corresponding to linear sliding speeds of 0.015, 0.0375, 0.075, 0.125, 0.15, 0.3, 0.45, 0.6, and 0.75 m/s. Two fully formulated commer-

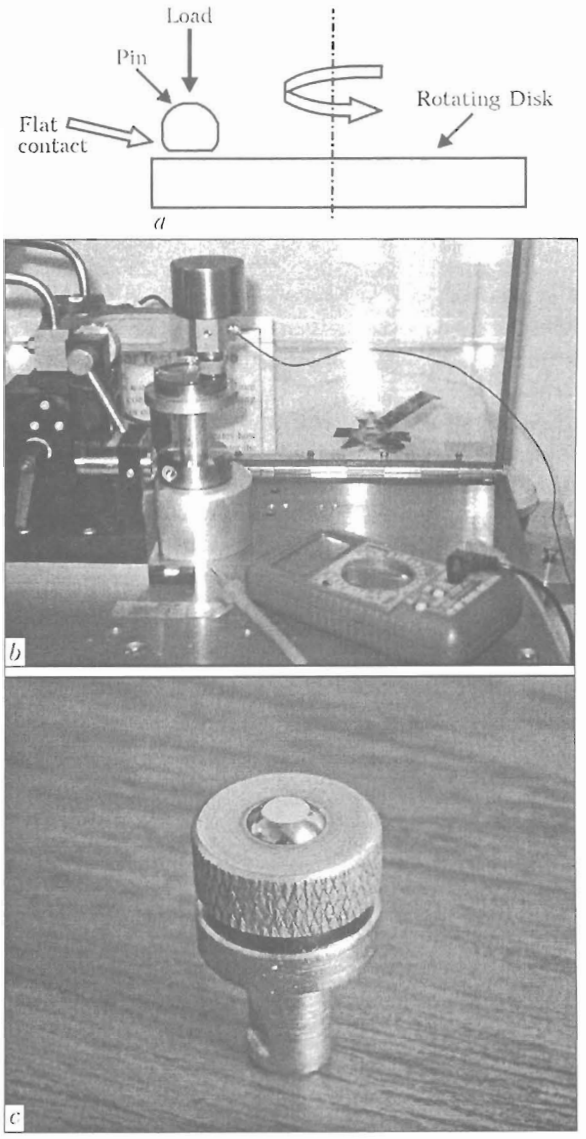


Figure 1. Schematic diagram of contact configuration (*a*), picture of pin-on-disc test rig (*b*) and picture of ball specimen with flat contact area (*c*)

Table 1. Surface parameters and characteristics of test discs

Parameter	1 Polished	2 Ground	3 Standard LST	4 Higher dimple density	5 Standard unlapped	6 Lower dimple density
Depth of dimples (μm)	–	–	5.5	5	6.5	4.0
Surface roughness between dimples R_a (μm)	0.01	0.12	0.03	0.06	0.07	0.09
Diameter of dimples (μm)	–	–	78	58	80	58
Distance between dimples (μm)	–	–	200	80–100	200	200
Dimples density (%)	–	–	12	15	12	7

Table 2. Physical properties of lubricant oils used for testing

Oil	Specific gravity	Pour point, °C	Flash point, °C	Kinematic viscosity (cSt) at	
				40 °C	100 °C
Lower viscosity	0.852	−54	232	54.8	10.1
Higher viscosity	0.863	−45	255	124.7	17.7

cially available PAO-based lubricant oils (Mobil-1) with differing kinetic viscosities were used for this study; the properties of the oils are presented in Table 2. Each friction test was conducted at a constant load, and, starting with the lowest speed of 0.015 m/s, the sliding speed was increased in a stepwise manner after 3 min at each speed, until the maximum speed of 0.75 m/s was reached. With this procedure, each test starts with very thin fluid film, and as the speed increases, the lubricant film thickness, and hence the ratio increases, allowing the contact to move from a boundary to a mixed, and, finally, to a hydrodynamic lubrication regime. Indications of the operating lubrication regime were assessed from the friction coefficient.

Results and discussion. Figure 3 shows the friction variation observed in tests with higher viscosity oil at a 20-N load. Significant differences are seen in the friction behavior in tests with ground, polished, and standard LST discs (Figure 3, *a*), especially at low speed. With a ground disc, the friction trend shows a clear transition from a high friction coefficient of about 0.11 at the lowest speed to lower values as the speed increases in a manner consistent with the Stribeck curve. A similar trend was observed with the polished disc, but with a lower magnitude of friction coefficient. The difference between the friction of the

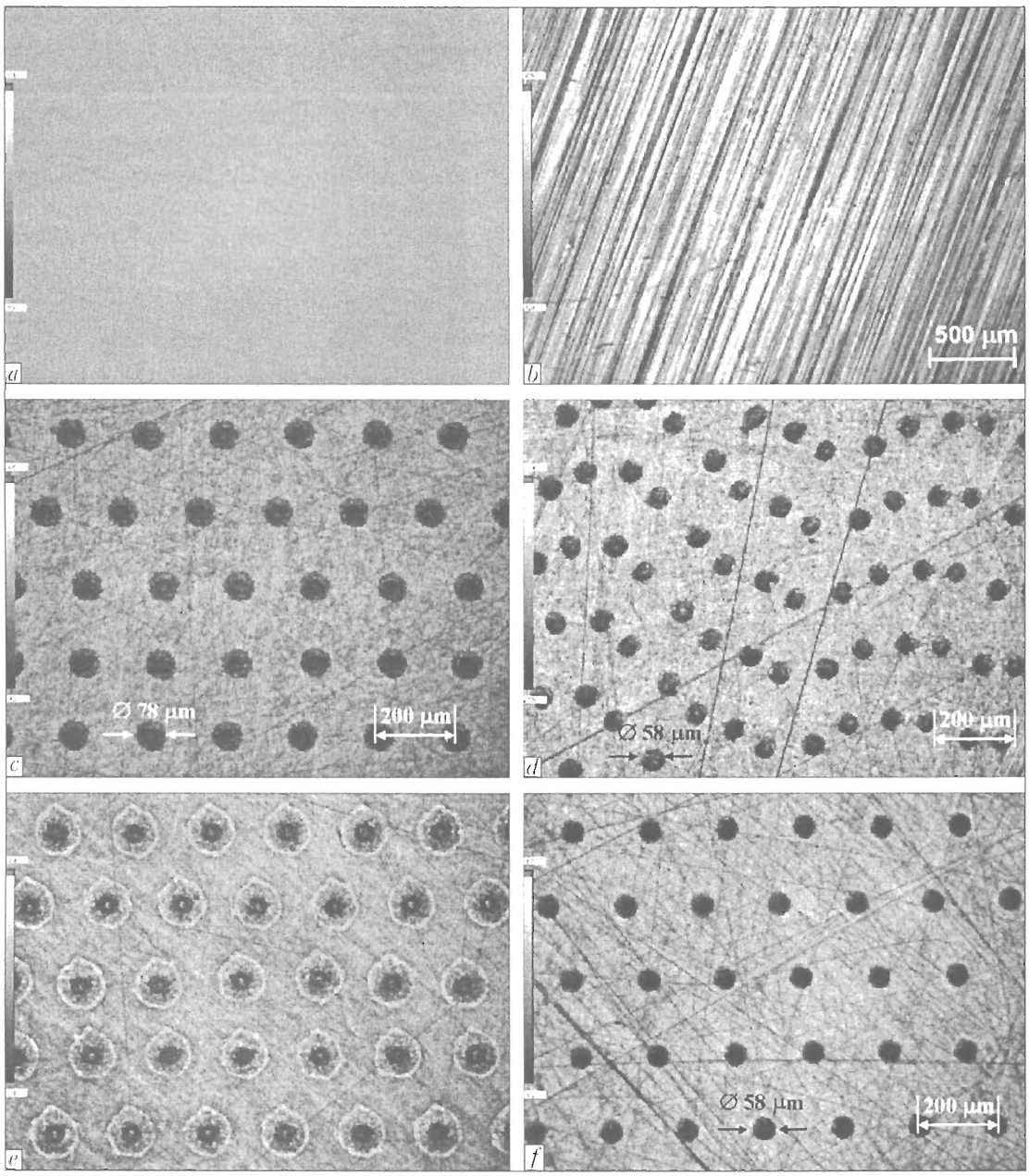


Figure 2. Optical micrographs of disc surfaces used for friction measurement; *a* — polished, *b* — ground, *c* — standard LST, *d* — higher dimple density, *e* — standard without lapping, *f* — lower dimple density

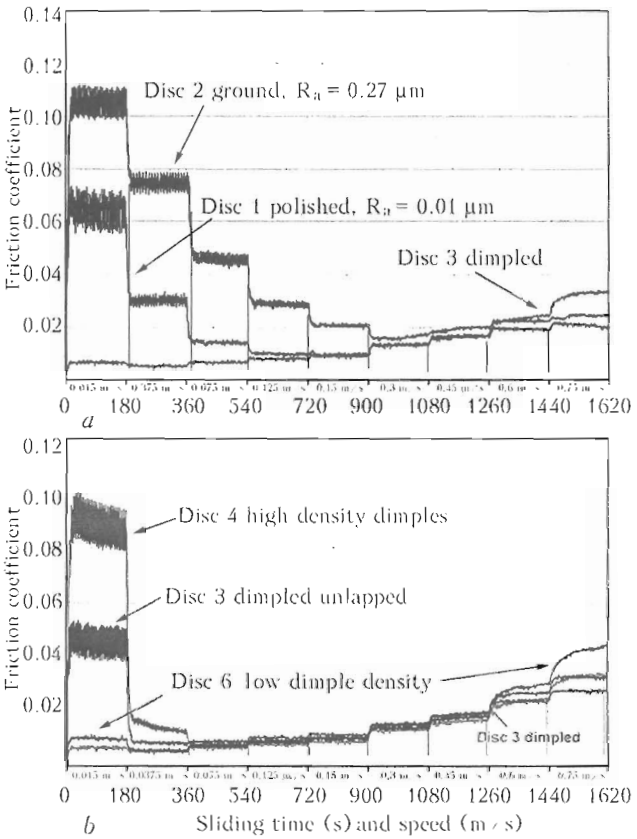


Figure 3. Variation of friction coefficient with sliding speed for various discs during tests with high-viscosity oil

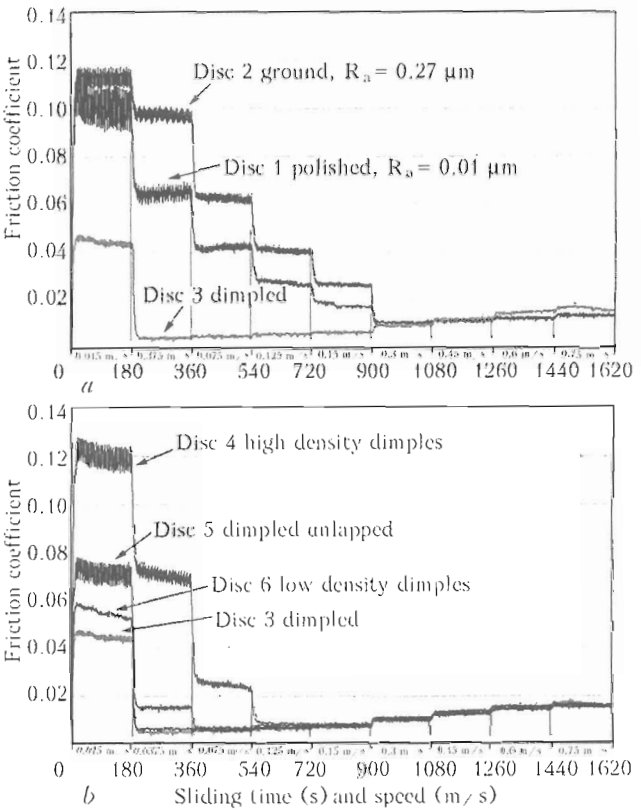


Figure 4. Variation of friction coefficient with sliding speed for various discs during tests with low-viscosity oil

ground and polished disc reflects the difference in the λ ratio (ratio of fluid film thickness to the composite surface roughness) in the two tests. With fluid film lubrication more effective in the test with the polished disc (higher λ ratio), lower friction is expected, and indeed, was observed. In the test with the standard LST disc, however, the friction coefficient remained low, even at the lowest sliding speed. Note that the surface roughness between dimples in the standard LST (Disc 3) is similar to that of the polished disc. Thus, differences between the friction trend of the polished disc and the standard LST disc are due to the dimples. At higher sliding speeds, differences between the friction in the tests with the three discs became insignificant because of the increase in lubricant film thickness with sliding speed. As the lubricant fluid film thickness increases, its behavior dominates the friction as the contact enters the full fluid film lubrication regime. Under such condition, the surface texture is expected to play a minimal role in friction behavior. It was also observed that the LST parameters have effect on the friction behavior at very low sliding speed (Figure 3, *b*). Under the present test conditions, the frictional behavior of the standard and low-dimple-density discs was more or less the same. Higher dimple density, however, resulted in high friction coefficients. Similarly, when the bulges around the rim of the dimples were not removed by posttexturing lapping, the friction coefficient was higher. This finding is, perhaps, due to the fact that bulges reduce the effective lubricant film thickness in the vicinity of the dimples. At higher sliding speeds, when full-film lubrication is effective, all of the LST surfaces showed similar friction behavior.

The friction behavior of tests conducted with lower viscosity oil is shown in Figure 4. The trends are very similar to those of tests with higher viscosity oil. A clear frictional transition was observed in the test with

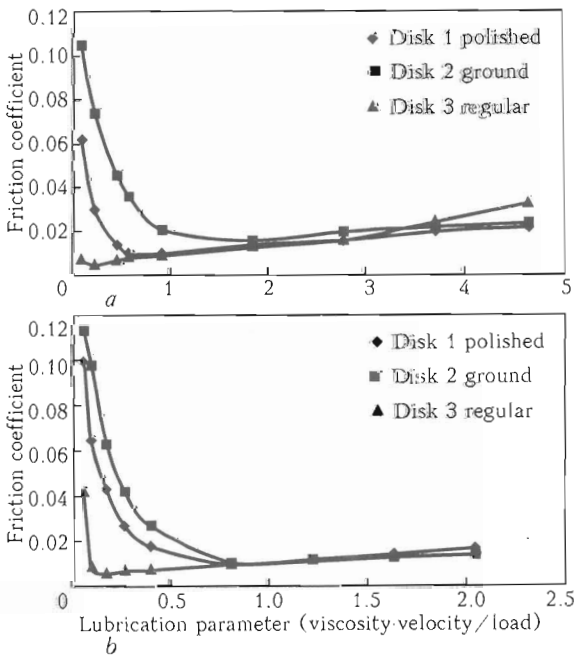


Figure 5. Summary of friction behavior in Stribeck curve format for high- (*a*) and low-viscosity (*b*) lubricant

the standard LST disc and is shown in Figure 4, *a*; although the magnitude of the friction coefficient is still substantially lower for the LST disc than for the polished disc. Transitions also occurred at higher sliding speeds, when compared with tests with higher viscosity oil. These differences are due to the thinner fluid film thickness in tests with lower viscosity oil. The effects of dimple parameters on friction are shown in Figure 4, *b*. At the lowest sliding speed of 0.015 m/s, differences are seen in the four discs with the high dimple density still showing the highest friction coefficient. Again, at higher sliding speeds, the friction behavior for all of the LST-treated discs was essentially the same.

The impact of LST on transitions in operating lubrication regimes is summarized in Figure 5, which shows Stribeck curves generated from the tests for ground, polished, and standard LST-treated discs. With high-viscosity oil, the transition from a boundary to a mixed, and finally to a hydrodynamic lubrication regime occurred at lower speeds and higher loads for polished discs than for ground discs (Figure 5, *a*). This result is expected, because the λ ratio will be higher for tests with polished discs under similar contact conditions. The presence of microdimples shifted the transitions to much lower speeds and much higher loads. Indeed, no transition was observed in the test with the LST disc in high-viscosity oil. All of the tests operated in the hydrodynamic regime. Because the surface roughness between the dimples is approximately the same as that of the polished surface, the dimples increased the λ ratio, perhaps, by increasing the fluid film thickness. In tests with lower viscosity oil, transitions in lubrication regimes were observed for all three discs represented in Figure 5, *b*. Again, LST shifted the transition to mixed and boundary lubrication regimes to much higher loads and lower speeds. Also, the friction coefficient under the highest load and lowest speed for the LST disc is much lower than the highest load and lowest speed for the polished disc, as shown in Figure 5, *b*.

The results of the present study have major technological implications. Oil-lubricated tribological components that operate under the low-efficiency, high-friction boundary lubrication regime can be made more efficient by simply applying LST to the lubricated surfaces. This will enable such components to operate in the low-friction hydrodynamic lubrication regime. Of course, this is only from the frictional standpoint. The impact of LST on the wear and durability of the components must be evaluated. The LST process is expected to modify the microstructure of the material in the vicinity of the dimples. The effect of such changes on surface damage and wear mechanisms is unknown at this time. Nevertheless, under a hydrodynamic lubrication regime, the extent of surface damage and wear is expected to be minimal when compared with surfaces operating under boundary lubrication.

CONCLUSIONS

The effect of laser surface texturing (LST) by microdimpling on lubrication regime transitions during unidirectional sliding was experimentally investigated by measuring friction coefficients with a pin-on-disc machine. LST was observed to expand the range of the hydrodynamic lubrication regime in terms of load and sliding speed for both high- and low-viscosity oil lubricants. Removal of the bulges at the edge of dimples by lapping after laser texturing is essential to optimize the positive effect of LST on lubrication regime transitions.

Furthermore, LST was observed to reduce the friction coefficient substantially under similar operating conditions, when compared with untextured surfaces of comparable surface roughness. In the present study, it appears that a lower area dimple density is more beneficial for lubrication regime transitions. LST can be used to reduce friction in oil-lubricated tribological components that are operating under a boundary lubrication regime.

Acknowledgments. *This work was support by the Heavy Vehicle Systems, Office of FreedomCar and Vehicle Technologies of the U.S. Department of Energy, under Contract W-31-109-Eng-38. The authors are grateful to Program Manager Dr. Sid Diamond for his support and encouragement.*

1. H. Tian, N. Saka and N. P. Suh, *«Boundary Lubrication Studies of Undulated Titanium Surfaces»*. Trib. Trans. 32 (1989) 289–296.
2. I. Etsion, Y. Kligerman and G. Halperin, *«Analytical and Experimental Investigation of Laser-Textured mechanical Seal Faces»*, Trib. Trans., 42 (1999) 511–516.
3. I. Etsion and G. Halperin, *«A Laser Surface Textured Hydrostatic Mechanical Seal»*, Trib. Trans., 45 (2002) 430–434.
4. A. Ronen, I. Etsion, and Y. Kligerman, *«Friction-Reducing Surface Texturing in Reciprocating Automotive Components»*, Trib. Trans., 44 (2001), 359–366.
5. G. Ryk, Y. Kligerman and I. Etsion, *«Experimental Investigation of Laser Surface Texturing for Reciprocating Automotive Components»*, Trib. Trans. 45 (2002), 444–449.

FEATURES OF APPLICATION OF LASER TECHNOLOGY FOR SINTERING DIAMOND COMPOSITE MATERIALS

V. S. KOVALENKO[1], L. F. GOLOVKO[1], O. EXSAN[1], A. A. GONCHARUK[1],
N. V. NOVIKOV[2], A. A. SHEPELEV[2], V. G. SOROCHENKO[2]
[1]Laser Technology & Material Science Department of the NTUU «KPI», Kiev, Ukraine
[2]V. N. Bakul Institute of Super Hard Materials of the NASU, Kiev, Ukraine

The analysis of techniques and problems in manufacturing tool composites containing super hard materials is given. The solution to solve these problems based on laser application is proposed. The results of systematic study of diamond composites sintering with laser radiation are discussed. Using mathematical modeling the heat transfer process at high speed laser beam scanning is studied and connections between working conditions and irradiated material characteristics are found. Results of experimental study of laser parameters influence on diamonds strength, their bond wetness and composite materials structure changes are demonstrated. The advantages to use the iron-based alloys as bonding material to manufacture diamond-containing composites are shown.

Introduction. One of the trends in development of modern mechanical machining is the creation of universal tools to produce the components of different shape and size. Such tools should have the very high durability and reliability. To meet this demand such tools should be made of special super hard composite materials.

To the present time the different manufacturing methods of tools of such type are known. Among them are thermal sintering of powdered materials by passing an electric current, manufacturing of tool composites by ways of a galvanic deposition, plasma, detonation and electron-beam spraying etc. [1–3].

The primary goal of tool manufacturing from super hard materials, including diamonds, is obtaining the indispensable shape and sizes, maintenance of strong fixing of diamonds on working surfaces, securing them the cutting ability which should be continuously kept during work. Listed above technologies differ by ways of cutting surfaces shaping, of diamond fixing, types of binders etc. Any of listed technologies has the advantages and lacks, area of expedient application.

The most perspective and efficient way of manufacturing of the discussed universal tools is the method of a level-by-level laser sintering of powder composites. At first, it allows to form the tool practically of any configuration, secondly, to use at sintering considerably more broad spectrum of binders, including those, which demand heating temperatures significantly higher than limiting one, for example, corresponding to diamonds oxidation. Besides, such heating temperatures allow to ensure metallurgical bond between diamond containing layer and steel body of the tool, that also causes increase of its strength properties.

As a heating source laser radiation has a number of considerable advantages. It allows at the expense of high speed of noncontact introduction of energy into material and its precise dosage to execute in a broad band of temperatures super fast heating of local areas of material. It enables to form layer by layer both single-row, and multirow working elements of tools, it is easy enough to control the concentration of components in composite, to thermal harden the binder and to obtain structures with high dispersivity [4].

The feasibility of laser radiation use for sintering of powder materials were studied by a number of researchers [5]. Laser sintering of powders from nickel, molybdenum, oxides, carbides, nitrides and borides on a steel substrate was studied experimentally. The laser heating of metal and ceramic powders freely scattered on the surface[5] has shown, that the most interest has the process of a liquid-phase sintering. Laser powder sintering in solid phase discloses no positive results. At the same time the theoretical possibility of solid phase laser sintering of ultra dispersed powders was pronounced [1].

The given research is dedicated to analysis of laser irradiation influence on properties of diamond-containing tool composites, and also to processes of their liquid-phase sintering in conditions of super fast local heating.

Simulation of laser sintering process. Structural and phase transformations in studied systems are uniquely determined by temperature conditions at laser heating and subsequent cooling. The characteristics of temperature field (level of temperatures, their distribution in a heated up volume, heating and cooling rates) are determined by a number of factors, bound with a heating source, treated material characteristics, conditions of their interaction [2].

To perform the experimental study of composite laser sintering the basic data reflecting connection of

© V. S. KOVALENKO, L. F. GOLOVKO, O. EXSAN, A. A. GONCHARUK, N. V. NOVIKOV, A. A. SHEPELEV, V. G. SOROCHENKO, 2005

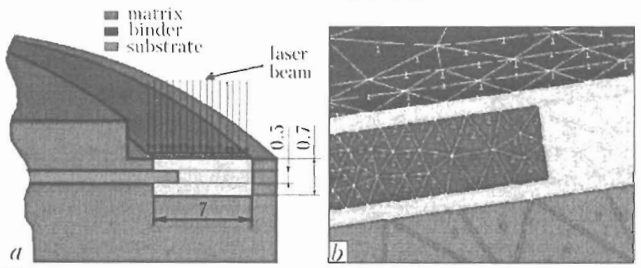


Figure 1. Scheme of a physical analog and considered boundary conditions (*a*) and the scheme of model segmentation on elementary tetrahedrons (*b*)

characteristics of laser heating of material with the main technological parameters of processing are as follows: power radiation (P, W) and its distribution in irradiated surface (P (x, y), W/cm^2), focusing spot size ($d_0 = 2r_0$, mm), laser beam movement speed (V, m/min), frequency (f, Hz) and scanning amplitude (B, mm).

The estimation of the characteristics of a thermal condition of material at laser irradiation was conducted on model, for which one the non-steady non-linear homogeneous equation of heat transfer in the Cartesian coordinate system X (x, y, z) was used. Simulation of thermal process was conducted with help of the software ANSYS 7. For this purpose the parametric program was developed, in which one all data on model were considered: model size (Figure 1, *a*), thermal properties of each material, heat affected zone, time of a laser beam action. At simulation there were selected conditions of irradiation, shown in Table 1.

Table 1. Parameters of composite laser irradiation

Parameter	Value
Power, W	1500
Heating spot size, mm	0.7
Scanning frequency, Hz	200
Amplitude of scanning, mm	7
Time of irradiation, s	0.2–1.0

The following materials were accepted for model: circle body — steel 13Kh), matrix — steel 45, binde — on the base of steel 12Kh18N10T (Table 2). At simulation the following simplifications were accepted:

• considering high speed of scanning, small amplitude and rather high inertness of material to thermal influence, it was accepted that in each point of a scanned surface (7×0.7 mm) the light source with a power density of 10^4 W /cm^2 was acting;

Table 2. Element contents of powdered materials, %

Material	Fe	Ni	C	Cr	Ti	B	Al	Si
13Kh	Base	–	1.2–1.4	0.4–0.7	–	–	–	0.1–0.3
Steel 45	Base	–	0.4–0.5	–	–	–	–	–
12Kh18N10T	Base	10	0.12	18	0.7–0.8	–	–	0.8
PG-10N-01	3–7	Base	0.6–1.0	14–20	–	2.8–4.2	0.8–1.2	4.0–4.5
KhTN-23	Base	6–8	–	20.0–20.5	2.4–2.5	2.5–2.6	–	–

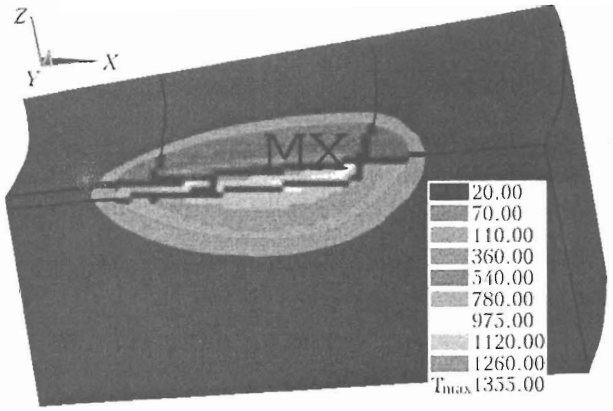


Figure 2. Temperature distribution in a zone of laser heating of tool composite

• at simulation, for flow bundle the thermal characteristics were taken for binder(12Kh18N10T) as for monolithic material;

• the absorptivity of material at irradiation was constant;

• the availability of synthetic diamonds in composite was not considered.

At calculation of temperature field in the program ANSYS the finite element method is used. At the stage of segmentation of integrated model into separate parts (demonstrated at Figure 1, *b*) which have definite thermal properties, the model was broken into elementary tetrahedrons.

Thus, each of them has number corresponding to material with definite properties. Approaching to the heat affected zone the step of segmentation was decreased to get more precise calculations results.

The outcomes of simulation are shown in a graphic presentation Figure 2.

Experimental procedure and technique. The experimental study of laser sintering of composites with diamonds was conducted on a special techno-logical complex based on. CO_2 laser and including device for transportation, focusing and control of radiation parameters, 5 axes NC work table. Laser radiation with a wavelength = 10.6 microns and power P = = 200...1500 W was focused with KCl lens by focal distance F = 300 mm. Thus the focused beam spot size could be changed in limits d_0 = 0.7...8 mm, speed of beam movement — V = 0.2...4.8 m/min.

One of primary goal of study was to find maximum temperatures of high speed laser heating of different synthetic and natural diamonds and conditions of irradiation, at which no deterioration of their strength is observed. Methodically given problem was solved by two ways — by straight irradiation of diamond grains arranged on a graphitic substrate, (Figure 3, *a*) and indirect heating of diamonds at laser melting of different powdered materials, which encircle and contact them, (Figure 3, *b*). After laser treatment diamonds were tested on a static strength using standard technique.

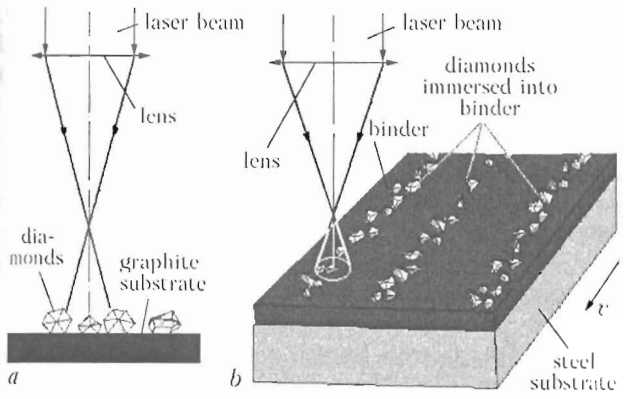


Figure 3. Schemes of irradiation of diamonds: direct (*a*), melting of binder with diamonds at different exposure times and melting of binder with diamonds migrating at laser beam movement (*b*)

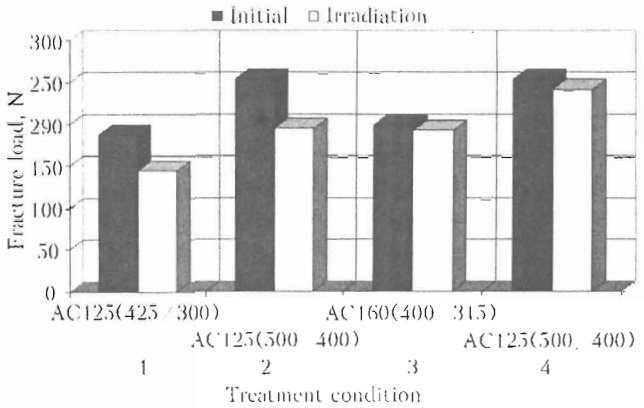


Figure 4. Influence of the characteristics of synthetic diamonds and conditions of laser irradiation on the level of destroying load: *1* — $W_p = 1.7 \cdot 10^3$ W/cm^2, $t = 0.09$ s; *2* — $0.6 \cdot 10^3$, 0.15; *3* — $0.4 \cdot 10^3$, 0.18; *4* — $0.2 \cdot 10^3$, 0.24

The analysis of laser irradiation influence on nature of material structure (hardness, dispersivity, uni-formity, distribution of alloying elements) was conducted on binders samples of following composites: PC-12NBK01-Co-diamond; XTN-Co-diamond. As experimental the powdered materials were studied, which have different bases. PC-12NBK01-Co-diamond is a material on nickel base, a mechanical mixture of powders: 65% PG-10N-01 and 35% WC. XTN — powder alloy on the basis of a stainless steel 12X18N10T with hardening phases TiB2 and CrB2. The elements content of powders PG-10N-01 and XTN-23 is listed in Table 2. Samples of materials as packed beds of a powder composites, were set on working table of laser system and were treated on air by a laser radiation at different power density in the limits $1.4 \cdot 10^3 - 1.4 \cdot 10^4$ W/cm^2 and processing speed (0.2–2.0 m/min). After irradiation samples were studied with application of methods of a raster sub microscopy and local X-ray spectral element analysis.

Study results. The synthetic diamonds of the types ACC125 (500/400), ACC125 (425/300) and ACC160 (400/315), taken on 60 pieces in a batch and selected by color (yellow and green-yellow), were subjected to a laser irradiation. The conditions of laser heating responded to calculated, which were planned to apply to structural improvement, and also for composites sintering with different types of binders. The results of tests of the irradiated diamonds on a static strength are given at Figure 4. The analysis of these data demonstrates that laser irradiation can in some extent reduce the strength of diamond grains. First of all it is caused by appearance of cracks, which arise on a surface of grains and are spread along their ribs. The cause of cracks occurrence are the internal stresses of diamonds, presence of defects, irradiation condition and first of all — its duration. Generally it is possible to state, that the grains of defectless and strong synthetic diamonds at selected conditions of a laser irradiation practically do not lose their strength.

At direct irradiation of synthetic diamonds (Figure 3, *a*), which are partially transparent for the given wavelength, to forecast the amount of absorbed energy is practically impossible. Therefore in parallel grains of diamonds were subjected to indirect high speed heating at the expense of laser melting of dusts Co, PC12NBK, XTN-23, in which one previously the synthetic and natural diamonds were placed (Figure 3, *b*). The analysis of diamond grains has shown, that they had a good thermal contact to molten metal during at laser irradiation. The prove to this is the data of a raster electron beam microscopy, the availability on a surface of diamond grains of a layer of a molten cobalt by depth from 180 A up to 400 A established with the help of a qualitative and quantitative microanalysis.

As the melting point of a cobalt makes 1450 °C it is possible to suggest that diamond grains were heated to the same temperatures. Thus no noticeable thermal destruction of diamonds was observed. The availa-bility of a film of metal testifies also a good wet ability of diamonds by a cobalt, that is very important for a strength improvement of mechanical fixing of diamond grains by binder, and also processes of heat transfer. It is known, that the liquid cobalt dissolves well carbon, that may have negatively effect on mechanical properties of diamonds. However at such small life times of a liquid phase (10^{-2}–10^{-3} c) the existence of noticeable diffusion processes is improbable. Nevertheless to exclude this effect it is expedient to use in binders cobalt together with carbide forming metals or carbides, for example tungsten carbide. Laser melting of powders XTN-23 and PC12NBK with diamonds, which have lower melting points (1220 °C and 1320 °C accordingly), neither has found thermal destruction of diamonds or loss of their strength. The single cases of a cracks initiation were marked, that may be considered as outcome of initial presence of defects in diamond grains.

Previous experiments on a sintering of a system PC12NBKC1 (10%)-diamond at power density $5.1 \cdot 10^3 \ldots 2.0 \cdot 10^4$ W/cm^2, beam diameter 3...5 mm, and scanning speed 0.8 m/min have revealed the coating cracking.

Therefore to increase plasticity of composition to powder PC12NBKC1(10%) cobalt (90%) was added. At lower cobalt content it was not possible practically

to get composite preform of satisfactory strength. The conditions of laser sintering were following: power density $5.1 \cdot 10^3 \ldots 1.4 \cdot 10^4$ W/cm^2, beam diameter 3...5 mm and scan rate 0.8...1.2 m/min. It is found that at $W_p = 1.4 \cdot 10^4$ W/cm^2, d_0 – 3 mm, $v = 0.8$ m/min the temperature in an irradiated zone was equal and even higher than cobalt melting point. Thus, the diamonds in composite were displaced to a surface of a melt and were located in chains or regular groups (Figure 5). At power density $5.1 \cdot 10^3$ W/cm^2 melting of binder is not detected.

It is interesting to comment the above effect of rearrangement of diamonds in the organized chains. Apparently it is caused by difference in density of diamonds and binder. This fact can be considered as basic effect in development production process of single-row multilayer diamond tools.

Thus, the discussed above results have shown, that for a sintering of composition PC12NBKC1(10%)-Co (90%)-diamond the radiation power density should be within the limits of $5 \cdot 10^3$ W/cm^2, beam diameter 5...6 mm and scan rate 0.8...1.2 m/min. The conditions of sintering with power density of $1.4 \cdot 10^4$ W/cm^2 is «critical», at which one the cobalt is melted intensively.

Sintering composite of a system XTN (10%)-cobalt (90%)-diamond) was performed at power density $5.1 \cdot 10^3 \ldots 1.4 \cdot 10^4$ W/cm^2, beam diameter 3...8 mm, and scanning speed 0.8...1.2 m/min. At processing on the upper modes ($Wp = 1.4 \cdot 10^4$ W/cm^2, $d_0 = 3$ mm, $v = 0.8$ m/min) the powder of composition was fluxed. It demonstrated considerable porosity, which appeared at border diamond – binder. The structure of molten material consists of cobalt grains surrounded with Co–Ni phase and impregnations of a Co–WC phase.

The aggregate size of cobalt varied from 5 up to 8 microns. At laser processing the tungsten carbide content is less by factor 2.0...2.5 than in initial powder. From our point of view for the mentioned above condition (quite rigid) the temperature in the irradiated zone considerably exceeded cobalt melting point. As the result at such temperatures cracks initiated on a diamonds surface. In an ostium of some cracks of width not less than 1.3 microns metal drops were watched. To establish the nature of these droplets (either initial molten binder powder or metal-solvent of diamond) the qualitative analysis of droplet material was made. The data analysis testifies that a ratio Fe:Co in composite makes 4.3%, and in an ostium of a crack – 1.4%. It testifies that in an ostium of a crack there are metals-solvents, which come out at external surface after crack initiation owing to laser radiation thermal influence on diamond.



Figure 5. Features of laser sintering of system PC12NBKC1 (10%)-Co (90 %)-diamond with formation of regular groups of diamonds

As a whole the demonstrated results testify that in this case, as well as at a sintering of composition PC12NBK (10%)-cobalt (90%)-diamond the radiation power density should be within the limits of $5 \cdot 10^3$ W/cm^2, diameter of a beam 5...6 mm and scan rate 0.8...1.2 m/min.

Generally, it is possible to state that laser irradiation allows to sinter the studied composites without negative thermal influence on single crystals diamonds.

The metallurgical surveys have shown, that after laser sintering the composite binder from alloy XTN has highly dispersive structure. The comminuting of excessive crystals of hardening phases (TiB_2, CrB_2) and eutectic are much higher, than for plasma coatings. In molten layers the segments of higher etching ability, similar to martensite needles are watched. They represent eutectic local sites with dispersed structure. The hardening phases and γ-phase are oriented in a direction of a heat removal. The value of a cooling rate in near-surface layers counted on depth crystals of hardening phase made approximately $5 \cdot 10^4 \ldots 10^5$ °C/s. With increase of distance from surface the dispersivity of structure decreases, crystal dimensions of hardening phases increase. The microhardness of structure with depth of melted layer changes smoothly, depends on working conditions and makes 7000–7500 MPa.

Hardness of melted layers increases with increase of degree of dispersion of their structural components, growth of a part of more hard eutectic and hardness of matrix.

The tribotechnical characteristics of composite binders obtained by laser melting (value and nature of wear, friction coefficient) were studied in conditions of dry friction. The binders from XTN and PC12NBKC1 were studied. The tests were conducted at different specific pressures 1–9 MPa. The slip velocity made 0.1 m/s. For comparison the friction tests were performed for XTN coating obtained by plasma spraying.

The greatest wear resistance was found for XTN coating, having smaller hardness from compared surfacing (Figure 6). It works better both at small unit loads, and at large (up to 9 MPa). In the latter case difference is very essential. The profile records of friction surfaces after tests for deterioration demonstrate, that melted layers are generally weared uniformly, without visible brittle failure. It is conditioned by a high disperse of structure, even distribution of hardening phases and plastic γ-phases. The laser melting as

contrasted to plasma spraying essentially increases wear resistance of alloys of a hypereutectic structure containing excessive diboride crystals. At laser melting by virtue of high speeds of a crystallization and formation of supersaturated solutions the quantity of excessive crystals and their sizes decreases. The coating in its structure displaces to the eutectic type, though the absolute values of hardness of plasma coatings are higher, than hardness of powder alloys melted with laser radiation. Laser melted layers as against plasma coatings have no brittle wear.

The results of tests demonstrate, that the powdered materials on the basis of steel after laser surfacing do not worse but surpass self fluxing nickel based alloys. It is possible to explain such effect by influence of oxidation on friction and by formation of secondary structures which are capable to self-organization.

CONCLUSIONS

1. The laser short-term heating of diamonds AC125 400/315, AC160 400/315 on air at times of influence 0.2–0.4 with up to temperatures 1200–1500 °C does not result in their thermal destruction and appreciable transformation into graphite.

2. The exception is made by (with) diamonds having initial defective structure.The mathematical modeling reveals character of distribution of temperatures in sintering a layer, case of a circle and adjoining part of a matrix, that allows by regulation of process of their rational compulsory cooling to operate quality of process of laser sintering.

3. The basic opportunity of use in quality binders wearproof and strong powder alloys on a basis nickel and iron with the additives of cobalt is proved, that can be applied at manufacturing the single-row multilayered diamond tool.

4. This is promoted by the established fact dense embrace of diamond grains a sheaf with formation on their surfaces metal films, and also effect of formation in conditions laser melting precise ordered single-layered groups or chains of diamond grains.

5. For elimination of residual thermal deformations, which arise at laser sintering, the receptions of

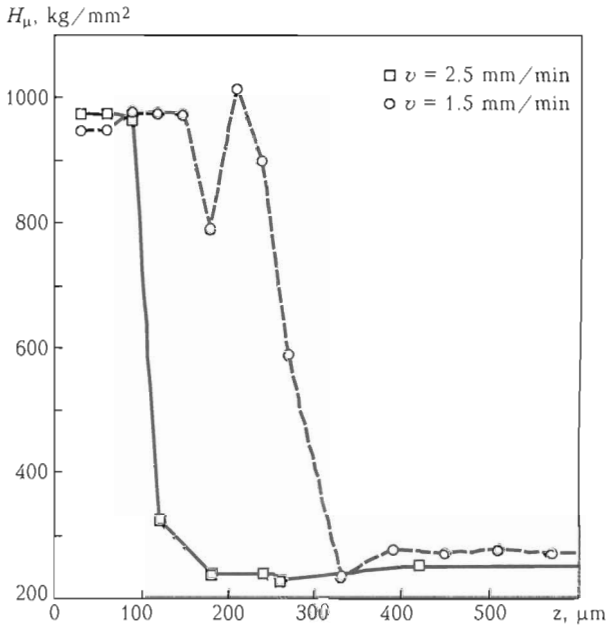


Figure 6. Histograms of weight loss (light field) and friction coefficient (dark field) for different melted layers: *1* — alloy XTN (plasma spraying); *2* — XTN; *3* — PC12NBKC1

necessary geometry and qualities of a surface of the diamond tool are expedient process of a laser irradiation for uniting with local deformation of a layer contaning diamond, in the heatet up status.

6. The ways and technological circuits thermo-deformation of sintering of composites containing diamonds are developed, bay the example of detachable circles with application of a scanning laser bunch (beam) and method of level-by-level escalating are developed.

1. Skorohod V. V. *Sintering of powder materials at electro thermal, plasma and laser heating* // Modern material science of XXI century / Edit. by I. K. Pohodnja. — Kiev: Naukova dumka, 1998. — P. 228–248.
2. Pat. 4938816 USA. *Selective Laser sintering with assisted powder handling* / J. J. Beaman, C. R. Dekard. — Publ. 1989.
3. Raichenko A. I. *Fundamentals of process of sintering of powders with an electrical current.* — M.: Metallurgy, 1984. — 128 p.
4. Webster J. *Innovations in Abrasive Products for Precision Grinding,* Annals of the CIRP, Vol. 53/2/2004
5. Tolochko N. K, Hlorkov U. V., Moscharov S. E. et al. *Absorptivity measurement of freely located one component metal powders and its change during laser processing* // Powder metallurgy. — 1997. — № 7/8. — P. 89–94.

LASER SURFACE ALLOYING OF TITANIUM AND TITANIUM ALLOYS

L. A. TEPLOVA
Moscow Automobile-Road Institute, Russia

Introduction. At present, new industry branch-laser industry is formed and developed in close connection with scientific and technical achievements in Russia. The elaboration of titanium alloys strengthening technologies is actual problem. Laser technological processes are classified as critical at the modern development stage of the national mechanical engineering.

Research results. The investigations were fulfilled on the samples and details from the technical pure titanium VTI-0, titanium α-alloys AT-3 (Al-2.5%, Cr-0.4%, Fe-0.3%), AT-6(Al-5%, Cr-0.4%, Fe-0.3%), (α+β)-alloy VT-22 (Al-5%, Cr-1%, Fe-1%, Mo-4.5%, V-4.8%).

Laser alloying process in the air atmosphere from powder coats was elaborated for titanium alloys on the base of the effectiveness, simplicity, technological ability requirements.

The non-metals, metals, ferro-alloys, metal melts, intermetalides, boronides, carbides, nitrides, molybdenum disulphite were used as the saturated mediums and complex laser alloying was also realized.

The technological laser complex «Quantum-16» (active element — core from glass with neodime) was applied, with the impact duration 4–6 mcs, radiant energy up to 15 joules, with different extent of the laser beam focusity (in the focus and out of the focuse). The gas CO_2-laser complex with continues working duty, with laser ray splitting systems and power up to 2 kilowatts were used too.

Laser alloying with the saturated coats from non-metals (amorphous boron, silicon, lamp soot), metals (iron, cobalt, niobium), ferro-alloys (ferrochromium, ferromolybdenum, ferromiobium, ferromanganese, double titanium, chromium boronide) promotes the significant hardness rise in the laser influents zones, but the hardness increase is insufficient for the wear resistance effective rise of the details hardening surface.

The top effect of the hardness increase is observed by laser alloying from boron, carbide and silicon carbide coats, more over, the hardness is regulated within the wide limites, attached to the process parameters changes.

Laser carboboroniding of technical pure titanium has optimal effect of the microhardness increase — 25000 MPa, that suffices to keep up the plasticity level.

© L. A. TEPLOVA, 2005

Laser carbosiliconiding of technical pure titanium has optimal effect of the microhardness increase — 16800 MPa, that is enough to preserve the sufficient plasticity level.

For α-alloy AT-6 the largest microhardness increase, by laser carboboroniding amounts to 19000 MPa, by laser carbosiliconiding — to 13500 MPa in alloying zones, that is to retain plasticity level.

For (α+β)-alloy VT-22 optimal microhardness rise achieves 16800 MPa in the alloying zones, as a result of laser carboboroniding, and reaches 11300 MPa as a laser carbosiliconiding result.

The investigations of the laser alloying regimes from the coats, with technical nitrogen jet supply into treating zone of α-alloy AT-3 and (α+β)-alloy VT-22, donTt show the essential microhardness increase, in comparison with laser alloying from the coats in the air atmosphere.

Laser alloying of (α+β)-alloy VT-22 from the silicon carbide coat and technical nitrogen jet supply, under 4–6 atmospheric pressure into treating zone, promotes the alloy fragility and the microcracks appearance in the alloying zones with the top microhardness 8940–10200 MPa.

In comparison with laser alloying from the coats in the air atmosphere, the more effective rise of the zone sizes by laser influence is observed with beam energy growth and technical nitrogen jet supply.

Laser alloying of alloys AT-3, AT-6 and VT-22 from tungsten, tantal, copper, niobium, cobalt (each separately) powder coats conduces to strengthened zones formation with the top microhardness 4200, 6500, 2500, 6800, 8000 MPa, in accordance with alloying component. α′-solid solution of alloying element in titanium is formed in alloying zones. Also, laser alloying of alloys AT-3, AT-6 and VT-22 in air atmosphere from composite foils (copper-tungsten, copper-tantal and other components) with 30–50 μm thickness, which are obtained by vapor phase crystallization in vacuum, contributes to the formation of α-solid solution of strengthened element in titanium alloying zones, but this laser influence zones have the lesser sizes in comparison with laser alloying from the powder coats.

The microstructures were investigated on the microscope — microanalysator «Jeol» «JXA-50A» under enlargement ×5000.

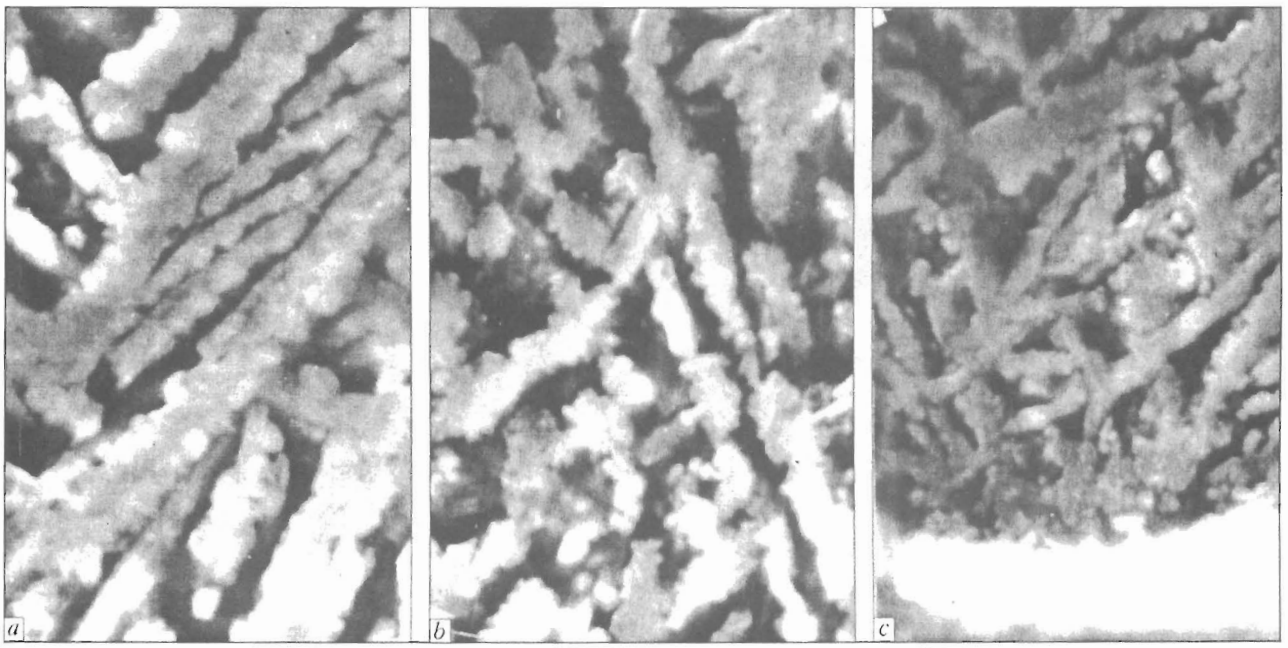


Figure 1. Morphology changes of the boronide phases along the thickness of alloy VT-22 alloying zone after laser carboboroniding: *a* — upper layer of the alloing zone; *b* — middle layer of the alloing zone; *c* — lower layer of the alloing zone

The main cause of the effective hardness rise of titanium and its alloys in the laser alloying conditions is the compound — alloying α′-solid solution formation, which makes stronger by boronides after laser carboboroniding (Figure 1) and by siliconides after laser carbosiliconiding (Figure 2).

Laser carboboroniding of titanium and its alloys AT-3, AT-6 and VT-22 peculiarity is the superior phase TiB_2 large quantity existence, compared to laser carboboroniding with the superior phase $TiSi_2$ lesser quantity availability and with the lowest phase TiSi large content. This peculiarity may be explained by the greater ability of the boron atoms (compared to silicon atoms) to instill in titanium metal lattice and by the more high energy stability of the superior boronides, compared to superior siliconides energy stability.

The phase analyze shows the titanium carbides absence in the alloying layer after laser carboboroniding and laser carbosiliconiding, this is contributed to the greater titanium activity to boron and silicon, then to carbon in the laser influence conditions.

The titanium reaction ability to boron and silicon is defined by lesser boron ionization potential — 8.28 ev and lesser silicon ionization potential — 8.26 ev, in comparison with carbon — 11.24 ev.

Besides, the value of dissolving change of the saturated element in liquid and solid states for boron is 34%, for silicon — 26%, for carbon — 20%.

The microhardness top increase along the thickness of carboboronided and carbosiliconided layers is observed on the areas, which are the most enriched by boron or silicon and contains carbon.

The microhardness rise effect reduces by titanium alloying with aluminium, during the transfer from titanium to alloys AT-3, AT-6, VT-22, jwing to the molten volume growth, *tj* the decrease of the saturation extent of α′-solid solution matrix by carbon, on account of the distribution density of intermetalide phases in alloying zones.

Technological parameters, which regulate strengthened layer structure and hardness, are saturated coat chemical composition, its quantity, laser influence power dencity and the ceiling degree of the laser influence zones.

During the cavitative and the hydroabrasive testing, the best results are come out with the ceiling coefficient $k = 0.5$, moreover the details are not subjected to the following mechanical process — to the polish, for the profile improvement and the roughness jf the laser alloying surface parameters amendment.

The coat quantity increase and the power density lowering tj the values, which are essential for the metal melting and alloying, lead to the rise of alloying elements, saturation degree in melting zone, to the microhardness growth and the metal fragility development.

The largest effect of the laser influence zone sizes rise, in accordance with the energy growth, is discovered in alloying of titanium alloys by aluminium, owing to the increase of melted metal volume. Laser influence zone sizes put up on account of aluminium content rise, with the transfer from the technical pure titanium to α-alloys AT-3, AT-6.

The distribution density of intermetalide compounds decreases in alloying zone with transfer from titanium VTI-0 to alloys AT-6, vt-22. The distortion degree of α′-solid solution matrix reduces, therefore the resirual strain level diminishes after laser alloying and the strengthened layer microplasticity grows.

Siliconaders, which make stronger α′-solid solution matrix, have the dendrite-structure after carbosiliconiding (Figure 2). Boronides. Which make strjnger α′-solid solution lattice, have needle structure after

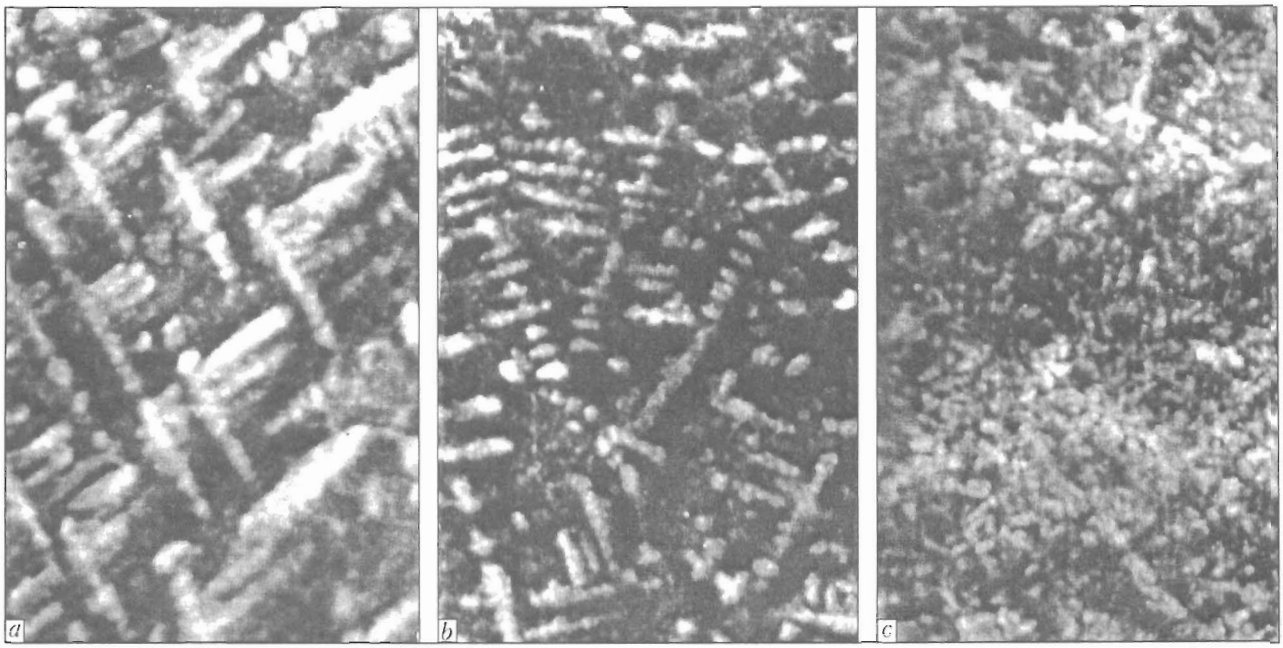


Figure 2. Morphology changes of the siliconide phases along the thickness of alloy VT-22 alloying zone after laser carbosiliconiding: *a* — upper layer of the alloing zone; *b* — middle layer of the alloing zone; *c* — lower layer of the alloing zone

carbosiliconiding (Figure 1). The formation of siliconide dendrites is accompanied by residual strains lesser level, than needle boronides discharde, therefore the relative microplastic deformation, in the alloying zone and in the thermal influence zone, has the more large value after the laser carbosiliconiding as to the laser carboboroniding. Also, the lesser quantity of high composition strengthened phases are formed by laser carbosiliconiding. This phases — titanium decompounds have.the most high toughness module of crystalline lattice.

The relative value of the microplastic deformation in the alloy AT-6 thermal influence zone decreases after laser carbosiliconiding, in comparison with laser carbosiliconiding. It is caused by the formation of titanium small dispersive globular borides, along the bouneds of α′-solid solution grains.

With the hardness rise of the strengthened layer of titanium and its alloys, wear resistance to the static friction-sliding increases and has been maximal after leaser carboboroniding.

«Shcoda-Savin» machine investigations shows that the alloying zones heterophase structure, which consists from α′-solid solution, titanium monoboronide TiB and titanium diboronide TiB_2 has ben ensuring the most high wear resistance to static friction-sliding. Optimal maximal microhardness is H_{100} 25000 MPa in the alloying zone. The highest wear resistanceis caused by the rise of boron and carbon saturation degree in alloying zone and by the microhardness growth of the strengthened phases.

As the result of titanium alloys alloying by aluminium, the wear resistance increase effect reduces, this is stipulated by the molten volume extention, by the increase of strengthened layer thickness, by the reduce of intermetalides saturation density in the alloying zone volume unit.

The investigations of the hydroabrasive resistance of titanium and its alloys were fulfilled on the machine «PV-12» with the rate of hydroabrasive wear medium (plumbing water with 0.5 mass per cent of quartz sand) — 27 m/sec, attack corner — 30°, time of one test cycle — 20 minutes.

The main parameters, which determine hydroabrasive wear resistance of strengthened, by laser alloying, surface layer of titanium and its alloys, are the hardness, the form and the size of intermetalide phase and the solid solution matrix plasticity.

The more propitious structure of the surface layer for the hydroabrasive wear resistance consists of the fine titanium of intermetalides, which are connected by the thin net of α′-solid solution plastic matrix.

Solid intermetalide phase role consists of perseption and dispersal of the impact force of the torrent abrasive particles, plastic copula defense from the destruction during the abrasive particles collisions.

The hydroabrasive wear resistance of the strengthened layer reduces in the VTI-0, AT-3, AT-6 row in consequence of the quantity decrease and the sizes rise of the high boronide phase TiB_2 after laser carboboroniding and quantity decrease and the sizes rise of the high siliconide phase $TiSi_2$ after laser carbosiliconiding, the distribution dencity reduction of the intermetalide phases in alloying zone volume, the increase of the intermetalide surface layer continuity.

Titanium alloying by molybdenium and vanadium promotes the reduction of the formation rates or the titanium boronides and titanium silsconides. The continuous boronide layer after laser carboboroniding, which consists of the needle tangles TiB_2, TiB, Ti_2B, don't provide demphiration ability in the conditions of the hydroabrasive wear resistance. The continuous siliconide layer on the alloy VT-22 surface, which consists of the thin dendritic tangles $TiSi_2$, TiSi,

Ti_2Si_3, has more plasticity, therefore the hydroabrasive resistance of alloy VT-22 reduces after laser laser carbosiliconiding.

The hydroabrasive wear resistance sharply increases by cobalt laser alloying, in accordance with the formation of the intermetalide phase TiCo and plastic phase α'-solid solution in the surface layer.

As the result of investigations in the hydroabrasive wear conditions, laser alloying is recommended for the surface treatment of details, which are making from titanium VTI-0, α-alloys AT-3, AT-6 and laser carbosiliconiding or laser alloying, by cobalt are advisable for the surface treatment of details, which are prepared from $(\alpha+\beta)$-alloy VT-22.

Titanium and it alloys cavitation wear resistance was determined on the magnetic-strictional vibrater of Central Scientific Researching Institute of Mashinery Technology with vibration frequency 8100 gerz and the vibration amplitude 70 mcm of samples.

In the working part of installation the efford didn't 30 v. The samples were investigated after laser alloing and laser heat treatment in the are atmosphere.

As to results of the cavitation wear resistance investigations the laser carbosiliconiding in the most effective strengthened treatement. In accordance with alloy VT-22 tests of staying power to cavitation, the titanium alloys cavitation were resistance is depend upon the hardness, the plasticity and the strengthened layer thickness after laser alloying. The cavitation were resistance rise, after laser heat treatment in air atmosphere, is determined by the formation of two-phase structure, which consists of α'-solid solution and titanium nitrides TiN, the contact strengthening in crystalic lattice, the hardness increase of strengthened phase, in comparison with the hardness of $(\alpha+\beta)$-solid solution of the alloy initial structure. The laser carbosiliconiding effectiveness in many hours wearing conditions, compared to laser heat treatment effect, is coursed by the more thickness of the strengthened layer, and also, by the more propitious form and the lesser sizes of titanium siliconides dentrites after laser carbosiliconiding, in comparison with fine needles of titanium nitrides after laser heat treatment.

The ceiling zones are the more treated to the cavitation were, owing to the rise of the intermetalide phases sizes and the more course structure formation.

The laser alloying of titanium and its alloys increases working resource of details in 1.5–1.6 times more. Besides, the details with optimal ceiling coefficient $k = 0.5$, are not subjected to the additional mechanical treatment to the polish.

Laser alloying technologies may be used in different industry branches, they are actual and have the demand on the laser technologies international market.

INSPECTION OF REINFORCED CONCRETE UNITS USING TOMOGRAPHY TECHNIQUES

A. A. VERTIY, S. P. GAVRILOV
TUBITAK-MRC, TUJRL, Gebze-Kocaeli, Turkey

Introduction. Reinforced concrete constructions are widely used at building of important civil and military objects. They are edifices, roads, bridges, aerodromes and others. Reinforced concrete structure is changed in length of time, under influence of environment and constructions made from it are estimated to be structurally deficient or functionally obsolete after some time [1]. Detection, localization, and image defects (hollows, poor welding connections) in reinforced concrete is complex problem. In present time different physics methods and signal processing algorithms are developed and created for solution of this problem. Use of eddy current and microwave subsurface tomography techniques gives possibility to obtain images of defects in concrete as well as images of the rebar mesh elements. In this case the entire 3D structure of the investigated object is fully inspected and the object state can be found out. These techniques are described in this work.

Employment of the eddy current and microwave subsurface tomography techniques for the reinforced concrete inspection is new idea. Tomographic algorithm is employed for the cross-section imaging of dielectric and metal objects within a reinforced concrete block. The cross-section restoration of studied objects is based on the tomography integral equation. The integral equation is obtained as a result of the inverse electromagnetic scattering problem consideration [2].

The scattered field of object is measured on a direct line parallel to the block wall. The solution of this integral equation gives the possibility to find the function representing the normalized polarization current distribution in the probing cross-section which is normal to the wall surface and in which the scan line lies (vertical cross-section). The normalized polarization current distribution depends on frequency and can be calculated for a set of frequencies. The image function is defined as modulus of the sum of the normalized polarization current distributions. If the wall material in vertical cross-section is not homogeneous because of presence of defects or quests within block, one can see these inhomogeneities. Set of images in different vertical cross-sections allows reconstruct 3-D image of the object.

Spectral approach, including in tomography algorithm the near-field information, which contains in the scattered field near to the scattering object, and opportunity of use of tomography algorithm in the

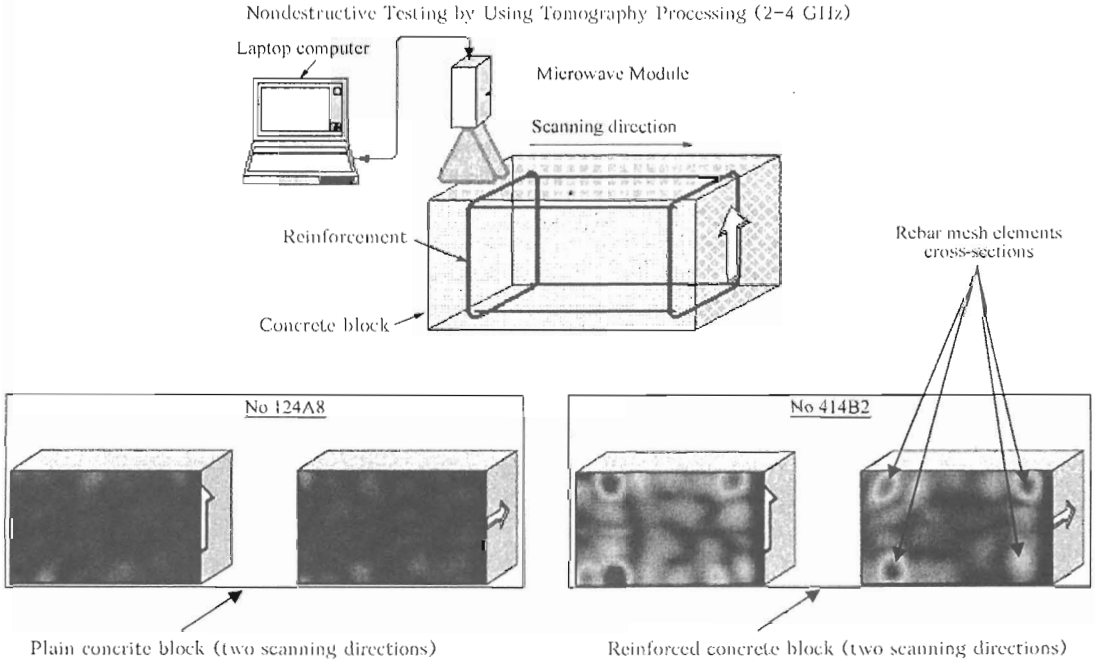


Figure 1. Concrite and reinforced concrite block cross-section images reconstructed by using the tomography processing (2–4 GHz)

© A. A. VERTIY, S. P. GAVRILOV, 2005

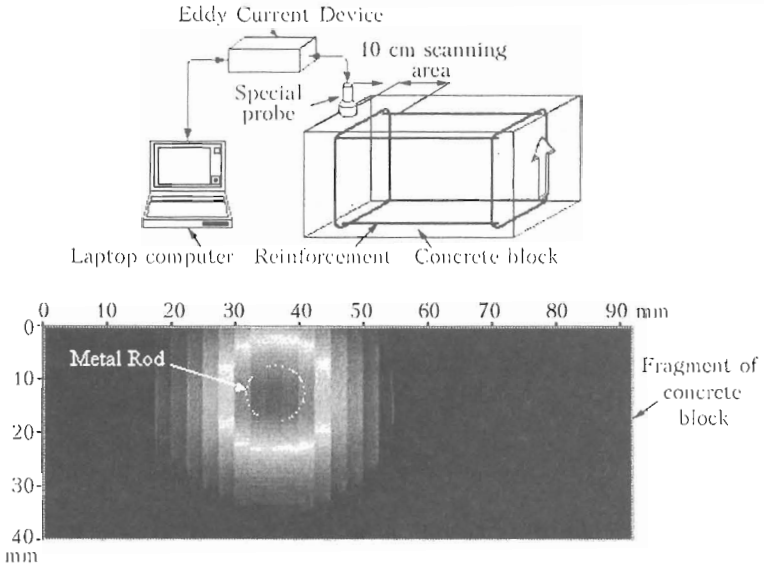


Figure 2. Reinforced concrite block cross-sections image reconstructed by using the eddy current tomography processing (0.8–5 KHz)

case of strongly absorbing environments allow to improve essentially the quality of the reconstructed images of the investigated objects.

The investigation results. The radar technology developed for the reinforced concrete inspection has been optimized for portability. This version of the system contains:

- Desktop or portable computer equipped with data acquisition board (DAQ-board);
- Small-sized and light weighted vector measuring unit (2-4GHz frequency range);
- Eddy current measuring block;
- Dielectric microwave antenna-probe;
- Eddy current probe;
- Scanning control block.

In the microwave subsurface tomography regime, positioned against an inspection wall the transmitting antenna sends out continues waves with a frequency step in the band from 2 GHz to 4 GHz. The waves pass through the wall material and scatter by objects and movement in the in probing space. The return signal from the receiving antenna is fed to a processor. The transmitting and receiving antennas form the antenna block, which can be moved by the operator hand in front of the target area along a direct line. Analysis software allows to reconstruct images of scattering regions in the probing cross-section which is normal to the wall surface and in which the scan line lies (vertical cross-section). Experiments were conducted with reinforced concrete and concrete blocks. Figures of the investigated objects and cross-section views are presented in Figure 1. One can see in Figure1 images of the rebar mesh elements within of the sample No 414B2. The images allow to trace the state of this rebar mesh.

The eddy current tomography experiment has been also conducted. In this case, the eddy current probe could be moved by the scanner in front of the target area along a direct line. Distance between the probe and reinforced concrite block surfaces was small and defined by irregularities of the concrite block surface. The return signal from the eddy current probe is fed to a processor. Analysis software allows to reconstruct images of scattering regions in the probing cross-section which is normal to the wall surface and in which the scan line lies (vertical cross-section). In the reconstruction used portion of the plane wave spectrum was limited by values of ν from -500 m^{-1} to 500 m^{-1}. The metal material parameters are conductivity $\sigma_2 = 3.54\times10^7$ S/m, permittivity $\varepsilon_{r2} = 0.8$. They were used the measured signals at 16 frequencies in the band 0.8–5 KHz with the constant frequency step $\Delta f = 0.28$ KHz. The magnitude β [2] assumes complex values but only real part $Re(\beta)$ of β in reconstruction was used, because $|\mathrm{Im}(\beta)|$ is large at the metals conductivity ~10^7 and imaginary part $\mathrm{Im}(\beta) < 0$. In this case the inverse is ill-posed problem and the reconstruction can be executed at complex values of β only for the sufficiently small values of $y > 0$.

The eddy current tomography image of a vertical cross-section of the probing reinforced concrite block is shown in Figure 2. It is clearly seen the rebar mesh element cross-section in the presented image. The real positions and shape of the rebar mesh element is shown in these pictures by white contour line.

CONCLUSION

The proposed techniques can be used to image structure of the reinforced concrete constructions and assess the condition of them. The images of the object cross-section are obtained by modern signal processing algorithms that are accurate and rapid. The conducted experiments validate the methods performance.

1. *«Our Nation's Highways: Selected Facts and figures»;* US Department of Transportation, Federal Highway Administration; Publ. № FHWA-PL-90-024.
2. A. A. Vertiy, S. P. Gavrilov, S. Aksoy, I. V. Voynovskyy, A. M. Kudelya, V. N. Stepanyuk, *«Reconstruction of Microwave Images of the subsurface Objects by Diffraction Tomography and Stepped-Frequency Radar Methods»*, Zarubejnaya Radioelektronika. Uspehi Sovremennoy Radioelektroniki (Russia), № 7, 2001, pp. 17–52.

Conference Sponsors

PWI Laser Systems and Technology Center

Ministry of Education and Science of Ukraine

Information Support

«The Paton Welding Journal»

www.nas.gov.ua/pwj

Conference Sponsors

PWI Laser Systems and Technology Center

Ministry of Education and Science of Ukraine

Information Support

«The Paton Welding Journal»

www.nas.gov.ua/pwj

Conference Sponsors

PWI Laser Systems and Technology Center

Ministry of Education and Science of Ukraine

Information Support

«The Paton Welding Journal»

www.nas.gov.ua/pwj

OPTIMAL CONDITIONS FOR PROCESS OF RAPID PROTOTYPING

M. ANYAKIN, P. KONDRASHOV, A. MUKHOID, A. STEPURA, V. KOVALENKO
Laser Technology Research Institute of NTUU «KPI», Kiev, Ukraine

Introduction. The possibility to manufacture the experimental models and ready articles from metal and composites, is a result of laser technology (sintering or cladding) and information technology mutual integration [1]. Naturally, at laser Rapid Prototyping* technique development the different schemes of processing (like in a basic technology) may be utilized: melting (sintering) of a preformed layer of a powdered material [2] or its immediate feeding into a zone of laser interaction with material [3]. Each of the schemes has the advantages and lacks. So the advantage of the first method is the possibility of sintering of the ultra disperse powdered material in a solid phase, and the lack appears at forming the «hollow» details, as the powder fills the whole volume and it is necessary to provide the technological windows for its removal. This disadvantage is absent at the second method of processing — the amount of the powdered material which occurred inside the hollow details is minimal. Common for all systems of Rapid Prototyping is:

- High level of mutual integration;
- Preparation of a drawings of the designed article with the help of CAD system;
- Manufacturing of an article via «layer by layer» technique;
- Dependence of outcome of processing on conditions of irradiation, properties of a powdered material etc.

This paper is devoted to a problem of technology and equipment for Rapid Prototyping development.

Experimental procedure and equipment. The main feature of the mentioned above schemes of manufacturing of a ready article with the help of Rapid Prototyping technique is that:

- to implement the process the use of only one source of laser radiation is possible;
- the accuracy of a ready article is determined by the movement accuracy of the focused beam across the product surface and by the powder material parameters;
- the productivity of the process (for the given powdered material) is determined by energy density of the focused laser beam on a component surface (beam power, spot size and speed of movement).

To implement the technique of Rapid Prototyping based on the scheme of sintering beforehand packed layer of a powdered material (1st scheme) and on the scheme of powder injection into a zone of laser interaction (2nd scheme), and taking into account the possibility of using the uniform source of laser radiation, the universal technological complex (Figure 1) was designed and manufactured which includes the YAG laser (position *1* at Figure 1) with 2x multiple telescope and universal coupling system (position *2*, Figure 1). The given system allows (without additional alignment) installing the system of scanning of laser radiation (position *3*, Figure 1) or the system of radiation input into a light-guide, thus changing the working scheme of the process. The designed setup is equipped with the common technological controller and controlling PC. Except for the listed units, for implementation of technique on the 1st version, the equipment consists of:

- system of scanning of the focused radiation on a machined surface (position *3*, Figure 1)
- the batch system for powder dozing (position *4*, Figure 1);
- system to compress the powdered material (position *5*, Figure 1);
- work table (position *6*, Figure 1);

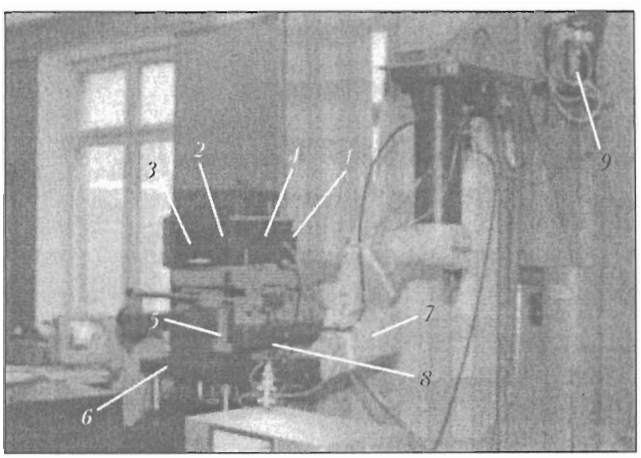


Figure 1. Universal laser technological complex for implementation the Rapid Prototyping technique: *1* — laser; *2* — coupling system; *3* — scanning system; *4* — batch system of powder dozing; *5* — system of sealing; *6* — work table; *7* — technological robot; *8* — input/output system with a flexible light-guide; *9* — system of a batching (the laser radiation safety system is not shown)

*Here and further under technique of Rapid Prototyping the laser forming of an article from the powdered materials is understood

© M. ANYAKIN, P. KONDRASHOV, A. MUKHOID, A. STEPURA, V. KOVALENKO, 2005

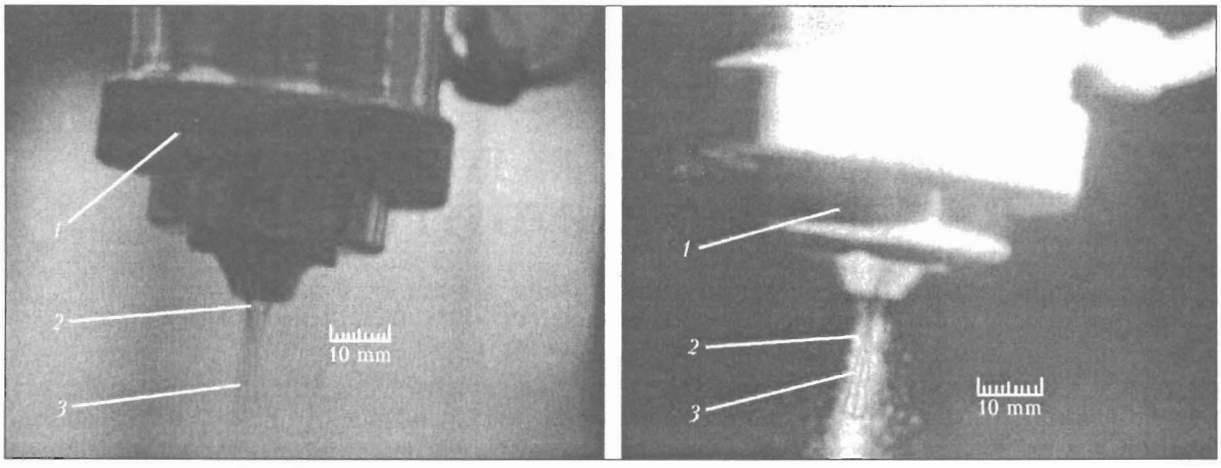


Figure 2. Different shapes of powder material flow, which are used at technology realization

• working bath playing a role of a laser radiation preventing screen;

For implementation of technique on the 2nd version the system consists of:

• the technological robot PM-01 (position 7, Figure 1);

• system of radiation input/output with a flexible light-guide and the system of monitoring of the process (position 8, Figure 1)

• the precision system of a batching of a powdered material (position 9, Figure 1);

• working bath playing a role of a laser radiation preventing screen.

The excess of a powdered material from a working bath is deleted by the express injector system. Besides in the common technological system the installation of guide rolls for drive of a polymeric film is stipulated.

The selected schemes of implementation of technique of Rapid Prototyping the most widely used and optimal [1, 2, 3]. So, as contrasted to scheme of processing, based on use «of flying optics», the system of scanning of the focused beam on a surface of a compacted powdered material is less bulky. Besides the radiation transfer into a working area with the help of an optical fiber and fixing the focusing unit in a hand of the anthropomorphic robot allow treating the large fixed details. Thus, naturally, the necessity for movement of large masses of work pieces on vertical coordinate is eliminated.

Some features of equipment. The technological YAG laser operates in a CW and pulse mode (pulse repetition rate up to 500 Hz) and equipped with closed-loop system of cooling «AFFINITY». It generates radiation with a wavelength $\lambda = 1.06$ μm and mean power up to 400 W and divergence 3–10 mrad.

The system of scanning with the beam aperture 15 mm TURBOSCAN-280 and objective (focal length 420 mm) scans the focused laser radiation on a maximum field size 280×280 mm with maximum resolution equal 0.009 mm.

The batch system for powder dozing ensures feeding of a given quantity of a powdered material in intermediate bin – feeder, which is installed between two rollers of the powder compacting system.

The system for powdered material compacting represents two rollers with intermediate bin – feeder, cylindrical guides and drive. The capacity of the intermediate bin is enough to deposit the powder layer of given width after some round-trips of the system, without replenishment from the intermediate bin.

The worktable with a closed loop allows displacing of a mass up to 400 kg on vertical coordinate with accuracy 0.01 mm. The size of a gap between the rollers of the packing system and worktable determines the thickness of a compacted (compressed) layer.

The anthropomorphic technological robot allows displacing the laser radiation focusing system with speed up to 0.5 m/s within the limits of an orb of radius 0.84 m;

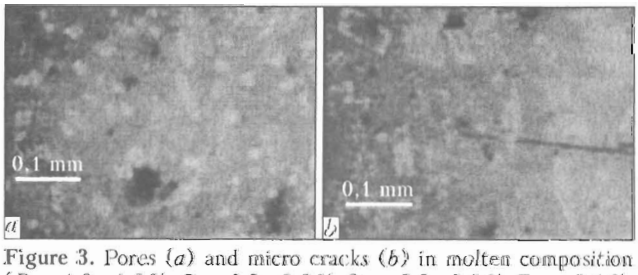


Figure 3. Pores (*a*) and micro cracks (*b*) in molten composition (*B* – 1.2...1.8 %, *C* – 0.2...0.6 %, Si – 2.3...2.8 %, Fe – 0.1 %, Ni – 94.9 %)

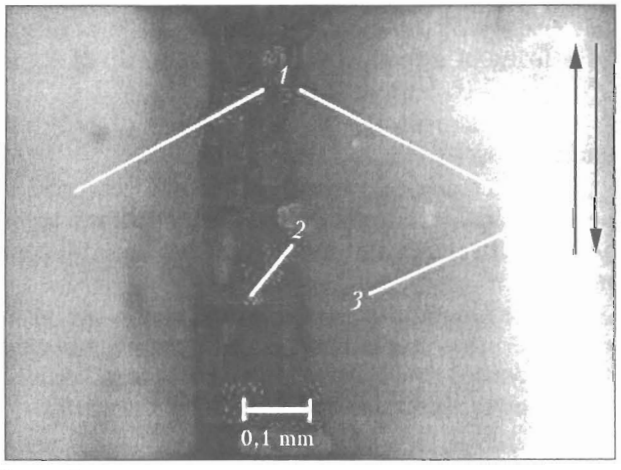


Figure 4. «Waves» which appear in laser processing of a powder from titanium oxide (Pm = 180 W, rp = 0.21 mm, V_x = 10 mm/s with step between pathes Step$X$ = 40 μm): *1* – top of «wave»; *2* – hollow (depth 0.2 mm); *3* – direction and step of scanning

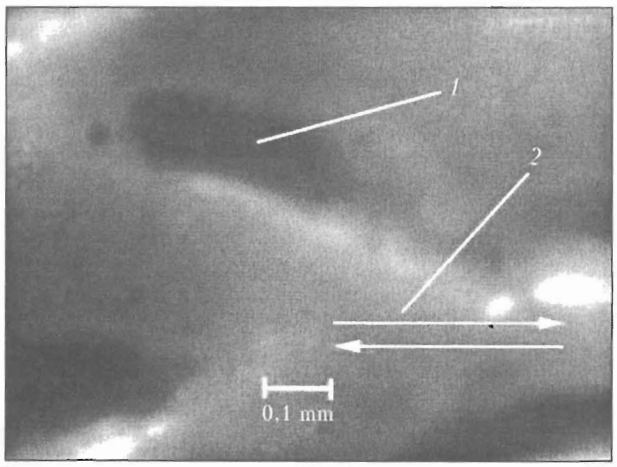


Figure 5. «Pores» which appear in laser processing of a powder from titanium oxide (Pm = 180 W, rp = 0.21 mm, V_X = 30 mm/s with step between pathes Step$X$ = 40 μm): *1* — pores; *2* — direction and step of scanning

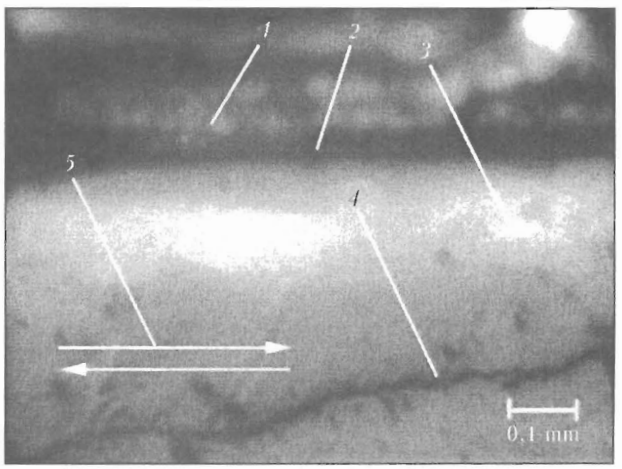


Figure 7. Cracks which arise on border of surfaces, obtained by laser processing of oxide titanium powder at different conditions (Pm = 180 W, rp = 0.21 mm, with step between pathes Step$X$ = 40 μm): *1* — speed of scanning, V_X = 20 mm/s; *2* — limit between zones with V_X = 20 mm/s and V_X = 80 mm/s; *3* — zone with V_X = 80 mm/s, *4* — crack; *5* — direction and step of scanning

The precise system of dozing allows supplying a powdered material to a working area with feed rate 0.1–5 g/s.

For quality control of the process (2nd scheme) the express device similar to that described in [4] is used. It permits to evaluate a luminous flux, reflected from a zone of laser interaction and by that to calculate the temperature in a focusing spot on a surface of a processed article [4].

Due to coaxial feeding of a powdered material into a working zone (Figure 2) the dependences of parameters of a layer under processing on all optional versions of a nozzle positions for feeding a powder are eliminated [5] as well as of focusing spot of laser radiation.

Software. Like in all systems implementing Rapid Prototyping technique, the software converts *.STL, *.DXF files of drawings interchanging into internal commands of controlling PC. As against all known systems, we designed the additional software, which allows, in some cases to recover the image of the object using their plane maps (color, black-and-white photos, engravings and paintings), and to transform them into the file, which is treated by controlling PC. For this the following methods had been used:

- shearing the image (map) on equal-luminosity planes (the image is transformed into the lined picture similar to physical map);
- the planes of equal luminosity are subjected to additional image contouring (image filtration is done with help of coefficients analysis of convolution matrixes 3×3 and more pixels);
- rays tracing (the use of Witter's model of luminance) [6, 7].

Besides the process of the additional scanning is realized with the help of software. So, using system of scanning RAZORSCAN with control panel SPC-1 together with *.DLL — libraries with ready procedures (which enter into the software of a control system) process of additional scanning along a line of movement of the focused beam is possible for carrying out with the help of formation of lists (which contain coordinates points of movement of the focused laser beam). In the second case, when laser radiation moves in a zone of processing with the help of a flexible optical fiber which is fixed in «hand» of antropomorphic robot (robot PUMA-01) with control system ARPS (Advanced Robot Programming System) scanning of radiation is possible due to built-in function GOS*WEAVE or combinations of functions of delays and movements of working units.

Factors influencing the productivity and quality. On productivity and quality of Rapid Prototyping technique (like in any other laser technology) for the given wavelength of radiation, the defining influence is rendered by integral parameter of the focused beam of laser radiation — energy density in a focused spot and thermal parameters of a workpiece. For given schemes of process implementation, effect on some technology factors (the focal length of an objective) is ambiguous and is labor consuming. However, common for both processing schemes are the following technology factors:

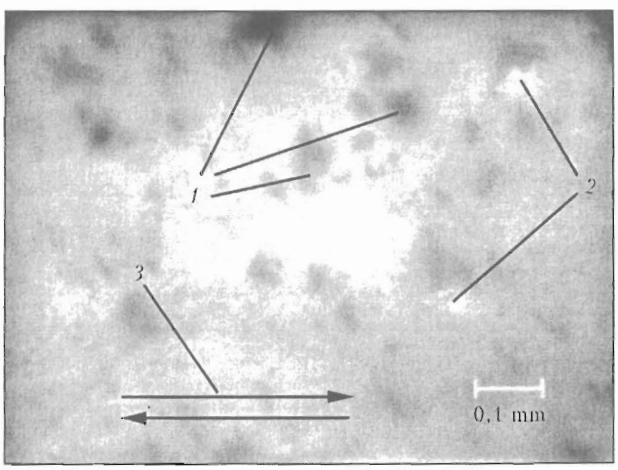


Figure 8. «Pores» which appear at laser processing with additional scaning of a powder from titanium oxide (Pm = 180 W, rp = = 0.21 mm, V_X = 80 mm/s with step between pathes Step$X$ = = 40 μm): *1* — pores; *3* — particles of melt; *2* — direction and step of scanning

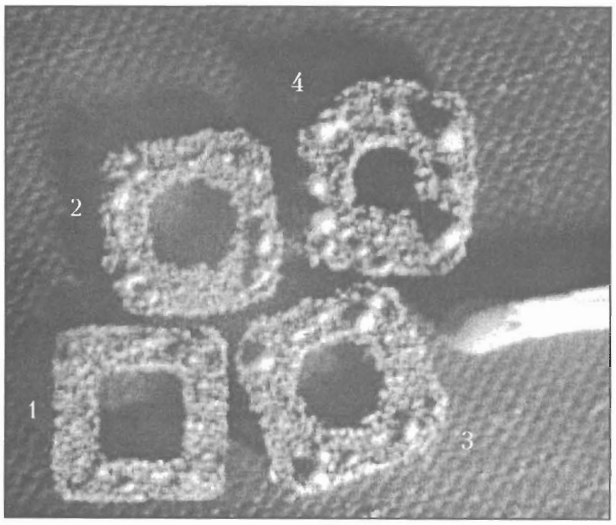


Figure 9. Appearances of samples from a powder PGSR-3 (diameter of particles 20–60 μm), obtained with the help of Rapid Prototyping technology with Pm = 180 W, rp = 0.21 mm (scheme of sintering beforehand packed layer of a powdered material): *1* — scaning speed V_X = 30 mm/s («switching-off» of laser radiation at «tops» of a trajectory of movement of a beam); *2* — V_X = 25 mm/s; *3* — V_X = 20 mm/s; *4* — V_X = 15 mm/s

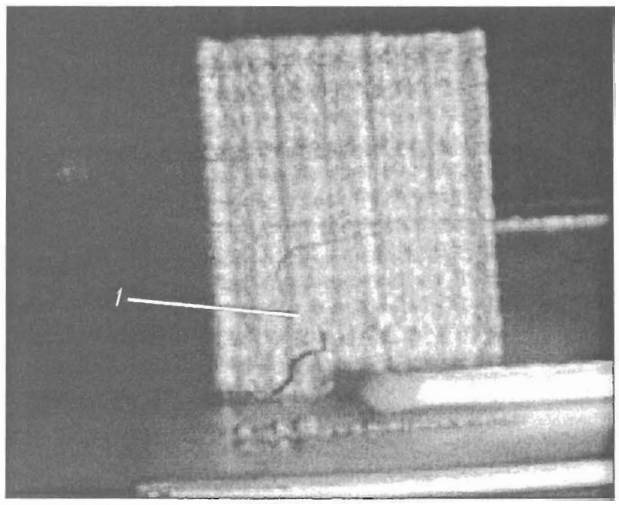


Figure 10. Sample made of an alloy on the basis of a powder PGSR-3 with a standard technology: *1* — crack

- energy, pulse duration and frequency;
- speed of the focused beam movement on a surface;
- number of passes (laser irradiation of a treated layer);
- law of movement (to decrease the stresses);
- working medium (active, inert);
- powder composition, size of particles.

The change of a focal length of focusing optics influences the size of a focusing spot and steepness of a caustic surface. At sintering of beforehand compressed layer of powdered material with a scanning laser radiation the field of processing varies as well as the accuracy of the focused beam movement on a surface of the component that causes changes of both size and manufacturing accuracy of a detail.

The packing density of a powdered material (1st scheme) is defined by a gap between a treated surface and the packing rollers, rolling speed and number of passes. At processing under the 2nd scheme, except for feed rate of a powdered material into the irradiation zone, renders influence the shape of «powder jet». The latter depends on a relation of pressures in nozzles (Figure 2) for feeding gas and powder, their relative position and size.

Powder materials for technique implementation. Apparently, the main advantage of the given schemes of implementation of Rapid Prototyping technique is the immediate manufacture of ready articles. For this reason, the properties of powdered materials are determined by the requirements to the future article, conditions of its maintenance and minimum cost. The gained experience in laser cladding testifies that the minimum porosity of coatings is reached at processing the self-fluxing powder materials on a Ni base [1], or materials with low-melting bonding. It is worth to note that unlike at sintering of packed powder composition (1st scheme), the powder injection into irradiated zone doesn't guarantee the pore absence. Thus

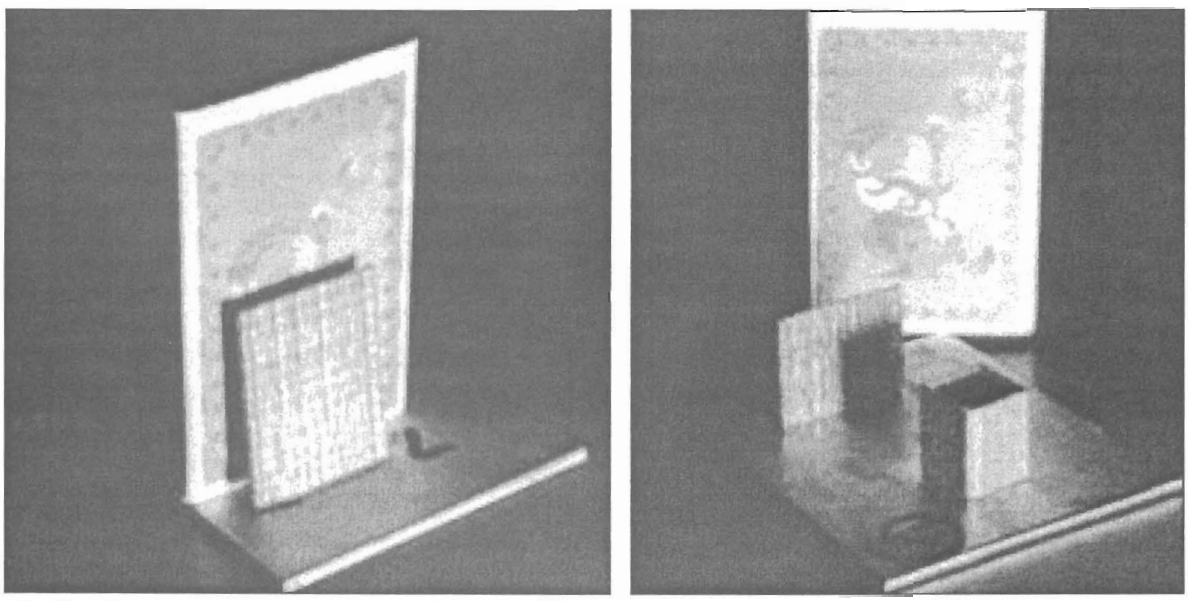


Figure 11. Sample made of an alloy on the basis of a powder PGSR-3 with additional scaning of the focused laser beam

maximum probability of their appearance is possible between the cladded layers and the paths. Figure 4 represents the cross section view of molten composition on Ni base with specific pores (laser beam power 280 W, pulses frequency 150 Hz, pulse length 4.5 μs, laser beam movement speed 30 mm/s, focused beam diameter 0.5 mm, 2nd scheme of processing).

At processing on 1st scheme [5] the surface roughness of sintered material is irregular and depends on the particles size but isn't influenced by the focused beam movement direction. So, on Figure 5, 6 the appearance of fragments of sample surfaces from various materials, which were received with the help of Rapid Prototyping technology under the scheme of rolling of powder at different processing conditions is represented. The specific effect is explained with the fact, that in this case, the processing is conducted at conditions, at which only «slight» melting of a powder is provided. At energy density of the focused laser beam, which exceeds 1500 J/cm^2, warping of melt leads to a «wavy» surface of a product (Figure 4, Figure 5), or forming «bubles», which accumulate in themselves the surrounding particles of powder (Figure 5), directly changing the product shape. Thus at Figure 5–7 the fragments of a sample from titanium oxide (fraction by diameter 5–15 μm) received at different conditions of laser processing are represented. At high density of focused laser beam energy, due to pressures, which arise at cooling of melt, waves are appearing (Figure 5), and the period between their tops does not coincide with step of scanning. At movement speed increase of the focused laser beam, the regular picture of «waves» turns to occurrence of a continuous layer of the alloyed material with pores, which change appearance of a product (Figure 6). In a case, when parts of a detail, which is being created, are processed at different conditions cracks formation is possible, direction of which coincides with the vector of speed of focused beam movement. To avoid this effect the additional scanning of laser beam in a focusing spot is desirable. At increase of speed of the focused beam movement up to 60 mm/s, it is possible to receive continuous compounds (due to partial melting of particles) without significant defects (Figure 8).

Influence of processing conditions on result is most visible at forming of details by a vector method. So, in a Figure 9 samples from a powder PGSR-3 (dispersivity 20–60 μm) are represented which are received with Rapid Prototyping technology using laser beam Pm = 180 W, focusing spot rp = 0.21 mm, which moves with different speed.

At reduction of speed of focused beam movement down to 15 mm/s, on the top of a zone (when the speed of a beam movement is equal to zero), uncontrollable accumulation of heat takes place, which conducts not only to occurrence of the alloyed particles of a powder in the form of «bubls», but also «tightening» of a core of a product. Increase of a beam speed (for the small sizes of sample) up to 30 mm/s and «switching-off» of laser radiation at «tops» of a trajectory of movement of a beam, allows to avoid the specified defects (Figure 9).

At processing on 2nd scheme the surface roughness depends both on working conditions, particles size and on the direction of focused laser beam movement. In the last case the surface roughness is more regular with some splashes (because of embedded powder particles). Such embedment may be explained by powder flow and particles size fluctuations, which has the random character [5].

During thin-walled designs manufacturing the stresses, arising in a sample, are the key factor, leading to it's destruction. A nature of these stresses, which appear in time or after laser processing, is well investigated, and the main method of it's elimination (except of bringing of «plasticizing agents») is creating favorable thermal cycles directly during processing, or volumetric tempering of a sample after it. It is known, that additional scanning of laser beam in focusing spot is a possible method of influence on «thermal history» of the zone of thermal influence. Thus, on Figure 10 the sample made of an alloy on the basis of a powder PGSR-3 with a standard technology is given. It is necessary to note, that the removal of internal stresses, that is forming of a crack, was held approximately in 60 s, after completion of treatment.

The application of special measures like:

- additional scanning of laser beam in borders of a focusing spot;
- additional heating of a sample, which occurs with help of the focused laser beam without supply of a powder material (that is at the expence of unproductive use of operating time of the equipment
- allow to avoid undesirable destruction of a thin-walled detail. Thus, on Figure 11 samples are given which are made from an alloy on the basis of a powder PGSR-3 in conbditions similar to previous one, but at additional scanning of the focused laser beam.

CONCLUSIONS

1. The equipment for 3D components forming based on two schemes of process realization had been developed;

2. The special software had been proposed to transform the flat black and white or color image into 3D virtual model;

3. Influencing the law, amplitude and frequency of additional scanning of the focused laser radiation it is possible to control the parameters of a melt bath and thus the processing quality.

Acknowlegement. *This study was done thanks to financial support of STCU (Scientific and Technological Center of Ukraine) on the project #2739.*

1. *LIA Handbook on Laser Materials Processing* (Ed. in Chief: John f. Ready), Laser Institute of America, Magnolia Publishing, Inc., 2001, 715 p.
2. J. P. Kruth, X. Wang, T. Loui, L. Froen, *Progress in selective laser sintering* / Proceeding of the 13th International Symposium for Electromachining. V. 1, p. 21–38.
3. Lijue Xue, Jianyin Chen and Andre Theriault, *Laser Consolidation of Ti–6Al–4V Alloy for the Manufacturing of Net-Shape Functional Components* / «Proceedings of International Congress» ICALEO '2002', Scottsdale, USA, Oct. 2002.
4. V. Kovalenko, M.Anyakin, J. Meijer, A. Degtyarev, A. Kozyrev, *Studying of Laser Processed Material Optical Parameters Dependencies from Temperature* / Proceedings of International Congress «ICALEO 2002», Scottsdale, USA, Oct. 2002.
5. V. Kovalenko, M. Anyakin, J. Meijer, A. W. Duley, D. Roessler, *Laser 3D prototypes forming from metal and ceramic materials* «Proceedings of International Congress «ICALEO'2003», Jacksonville, USA, Oct. 2003.
6. V. Kovalenko, M. Anyakin, V. Anyakin, *«Laser 3D objects prototyping Using Their Flat Images»* // Welding and Materials Processing «LTWMP-03», Katsiveli, Ukraine, May 2003.

STUDY OF THE PROCESS OF RAPID PROTOTYPING USING NUMERICAL EXPERIMENTS

M. ANYAKIN, K. RUDAKOV, A. LUTAY, T. KOZAKOVA, V. KOVALENKO
Laser Technology Research Institute of the NTUU «KPI», Kiev, Ukraine

Introduction. As it is known the main difference of technological process of Rapid Prototyping from related technologies (cladding, sintering) is the controlled according to the 3-dimensional drawing of a detail its layer-by-layer «growth». Modern Rapid prototyping technology allows getting the ready detail (workpiece) from metal or ceramic materials and with minimum further traditional finish machining few times faster then using the alternative technologies [1–3]. To find the possibilities to increase the productivity and the quality of processing it is necessary to study the mechanism of prototype formation.

Theoretical consideration. As well as for any kind of laser technology, the main technology factors of process of Rapid Prototyping are factors which render the direct influence on energy density $W_E(x, y)$ and power density $W_P(x, y)$ of the focused laser radiation — average power P_m, speed of movement V_x, focusing spot radius r_p and other). Among responses of the process that are possible to determine with the help of calculation experiments, are:

- Parameters of a melt bath (depth h_m, width W_m and time of existence t_m) which was formed under action of the focused laser radiation;
- The law of the focused beam movement on a surface of a detail;
- Coefficient of overlapping of paths CC_r and a step of escalating on vertical coordinate $Step_Z$ (Figure 1).

Thus at process realization the following factors had to be considered:

The minimum thickness of walls of the future detail. Thus thickness of a wall (without shrinkage) cannot be less, than width W_m of a melt bath;

A step of escalating on vertical coordinate which less or is equal to depth of a melt bath;

Time of melt existence should be sufficient for realization of diffusion processes and creation of a detail with the set of physico-mechanical properties.

At creation of a thick-walled detail, or a detail without internal emptiness when its cross-section is formed for some passes of the focused laser beam, productivity of process (for the given power of laser radiation, properties of a powder material and other) is determined by speed of movement of the focused laser beam, width and thickness of a separate path, overlapping coefficient of paths CC_r and so forth. At Figure 1 the scheme of layer-by-layer location of paths, which form a product using the technology of Rapid Prototyping, is given.

Thus, during manufacturing a detail it is necessary to define and to control the parameters of a melt bath, which was formed under action of the focused laser radiation. For this reason, for studying influence of parameters of the focused laser radiation on result of processing a series of calculation experiments has been carried out.

As model of process the nonlinear non-stationary equation of heat conductivity in view of phase transformations was used (1). At the solution of a problem the system (1) was replaced with finite-difference analogue with the implicit scheme of approximation of derivatives and non-uniform steps on spatial and time coordinates. Further the finite-difference system was solved with method of racing with the iterative scheme of the nonlianiarities account. And, dependences of thermo-physical properties of sample material from temperature were interpolated by cubic splines.

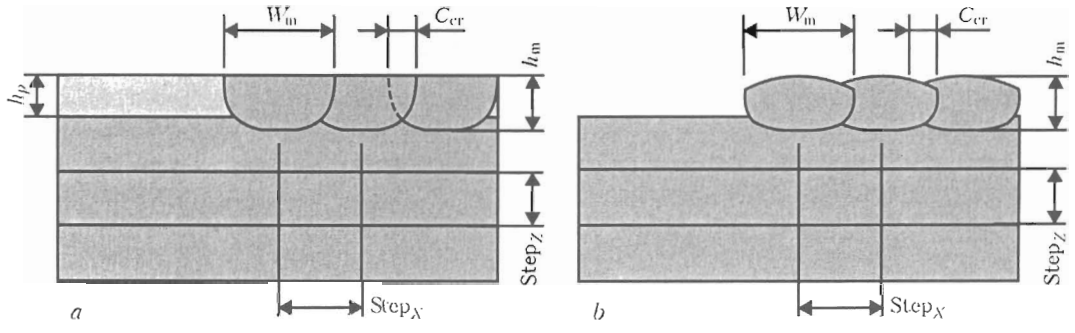


Figure 1. Scheme of layer dispositions in treated zone, which forms a detail using Rapid Prototyping technology: *a* — sintering of powder material «layer by layer» with its compaction by rollers; *b* — sintering of powder material with its injection into the focusing

© M. ANYAKIN, K. RUDAKOV, A. LUTAY, T. KOZAKOVA, V. KOVALENKO, 2005

$$c(T)\rho(T)\frac{\partial T}{\partial t} = \frac{\partial}{\partial y}\left(\lambda(T)\frac{\partial T}{\partial y}\right) + \frac{\partial}{\partial x}\left(\lambda(T)\frac{\partial T}{\partial x}\right) + \frac{\partial}{\partial z}\left(\lambda(T)\frac{\partial T}{\partial z}\right)$$

$$c_v(T) = c_v(T) + Q_f\delta(T - T_f)$$

$$T_{start} = 25\ ^\circ C$$

$$\frac{\partial T}{\partial x}\Big|_{\substack{x=0\\x=HX}} = 0;$$

$$-\lambda(T)\frac{\partial T}{\partial y}\Big|_{y=0} = A(T)W_P(x,y,t); \qquad (1)$$

$$\frac{\partial T}{\partial y}\Big|_{y=HY} = 0;$$

$$\frac{\partial T}{\partial z}\Big|_{\substack{z=0\\z=Hz}}$$

where: $c(T)$, $\rho(T)$, $\lambda(T)$ — dependencies of heat capacity, density and heat conductivity of material from temperature T; x, y, z, t — space and time coordinates; $c_v(T)$ — volumetric heat capacity, equal $c_v(T) = c(T)\rho(T)$; δ — Dirac function; Q_f — latent heat of phase transformation; T_{start} — initial temperature of the sample; HY, HX, HZ — size of sample; $A(T)$ — dependence of absorption coefficient of the laser radiation from temperature T.

At the description of dependence of power density of the focused laser radiation $W_P(x, y)$ from spatial coordinates x, y the theoretical distribution of intensity of a beam (mode TEM_{00}) was used which is described by expression:

$$W_P(x,y) = \frac{2P_m}{\pi r_P^2}\exp\left(-\frac{2((x-x_c)^2 + (y-y_c)^2)}{r_P^2}\right), \qquad (2)$$

where: P_m — average power of radiation; r_P — radius of focusing spot at a level $\frac{P_m}{e^2}$; x_c, y_c — the current coordinates of an axis of the focused laser beam.

Table 1. Percentage of alloying elements in powder compositions

Type of a powder	The elements contents (%)							
	Ni	B	C	Si	Fe	W	Cr	Co
PGSR-3 (100%)	95.9	1.2	0.4	2.4	0.1	–	–	–
PG-10K-01(100%)	28	1.2	1.3	1	0.1	2.5	21	44.9

Let's consider process of interaction of the focused laser radiation with powder materials on Ni base (a powder of type PGSR-3) and Co (a powder of type PG-10K-01) with the contents of an atmosphere of 5–15 %. Percentage of components, which alloy the specified powder materials, is resulted in Table 1.

Dependences of thermo-physical properties of powder materials from temperature (density $\rho_\Sigma(T)$, heat conductivity $\lambda_\Sigma(T)$, and thermal capacities $c_\Sigma(T)$) were determined with additivity equations (3), in view of the data resulted in Table 1 and in reference books [4, 5]. Phase transformations (solid body – melt – evaporation phase – solid body) that occur in a material of a sample during laser heating had been considered taking into account the implicit allocation of their borders (1).

Temperature dependences of absorbing ability of powder compositions have been established with the help of experiments which technique is described in report [6, 7]. These dependences (wavelength of laser radiation $\lambda = 1.06$ μm) are received up to a level of temperatures at which melting of powder components occurs. As it was marked, it is connected with effect that during carrying out the experiments with short laser pulses ($\tau = 200$ μs) simultaneously with powder melting its destruction occurs (chaotic movement and scattering), that leads to damage of a measuring path of the system. For this reason, the mentioned series of calculation experiments has been carried out without taking into account absorption of laser radiation

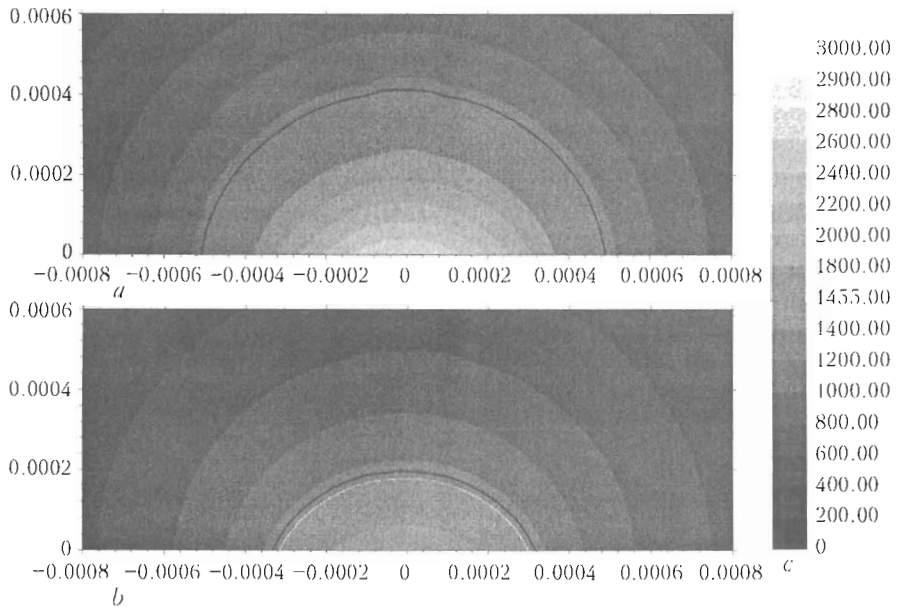


Figure 2. Distribution of temperature in samples from powders PGSR-3 and PG-10E-01 ($P_m = 150$ W, $r_p = 0.4$ mm, $V_x = 2$ mm/s, air contents of 5 %): *a* — sample from powder PGSR-3; *b* — sample from powder PG-10K-0; *c* — scale bar for temperature; dark line — molten pool for Ni; light line — molten pool for Co

in a plasma cloud that arises during phase transformations.

At realization of Rapid Prototyping technology the condensed powder material comprises surrounding atmosphere (air, argon and other) which contents depends on the particles size, thickness of a layer which is rolled, rolling load and so on. The contents of an atmosphere in a powder material also were estimated with the help of the additivity equations (3).

$$C_\Sigma = C_{\Sigma 1}(T,x,y,z)\Big|_{\substack{x=xp\\y=yp\\z=zp}} + C_{\Sigma 2}(T,x,y,z)\Big|_{\substack{x=xd\\y=yd\\z=zd}}$$

$$\rho_\Sigma = \rho_{\Sigma 1}(T,x,y,z)\Big|_{\substack{x=xp\\y=yp\\z=zp}} + \rho_{\Sigma 2}(T,x,y,z)\Big|_{\substack{x=xd\\y=yd\\z=zd}} \qquad (3)$$

$$\lambda_\Sigma = \lambda_{\Sigma 1}(T,x,y,z)\Big|_{\substack{x=xp\\y=yp\\z=zp}} + \lambda_{\Sigma 2}(T,x,y,z)\Big|_{\substack{x=xd\\y=yd\\z=zd}}$$

Where: C_i, λ_i, ρ_i — dependencies for heat capacity, heat conductivity and density for i component of composition material; k — amount of i component xp, yp, zp, xd, yd, zd — the sizes of layers of a material.

Results and discusion. Analyzing the data resulted, we shall note, that the main influencing factor on thermo-physical properties of powder is the content of the basic element:

- for powder PGSR-3 it is Ni — 95.9%;
- for powder PG-10K-01 it is Co — 44.9%.

Presence of other elements despite of their low contents is observed only on dependence of a thermal capacity of a composition at high temperatures (in the field of phase transformations of components).

The increase in percentage of atmosphere (that is the density of rolled powder) leads to reduction of its heat conductivity, density and to increase of thermal capacity. The specified changes are marked at laser heating the powder with different concentration of atmosphere [6]. It is necessary to note, that here and

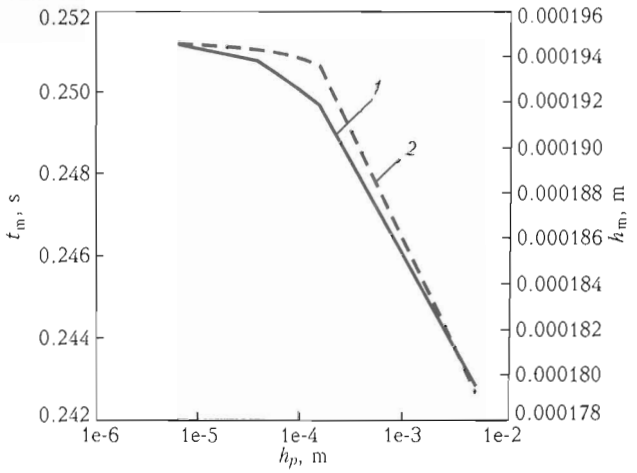


Figure 3. Dependencies of a parameters of a molten pool (depth h_m, time of existence t_m) in sample of composition powder PGSR-3 and alloy PGSR-3 on thickness of the powder layer h_p (P_m = = 150 W, d_p = 0.6 mm, 10 % air): *1* — dependence time of existence of a molten poll t_m on thickness of the powder layer h_p; *2* — dependence depth of a molten poll h_m on thickness of the powder layer

further parameters of a melt bath (depth h_m, width W_m and time of existence t_m) were defined on limiting positions of a line of temperatures of phase transformation of matrix material.

For different thermo-physical and optical properties of powder mixtures on basis PGSR-3 and PG-10K-01 under identical conditions of processing parameters of melt baths the obtained results are different. And despite the more effective laser radiation absorption by powder PG-10K-01, parameters of melt bath for powder on basis Ni is essentially higher, than that for powder PG-10K-01.

It can be explained by:

- Greater heat conductivity of basic powder metals Co (in comparison with Ni) at high temperatures;

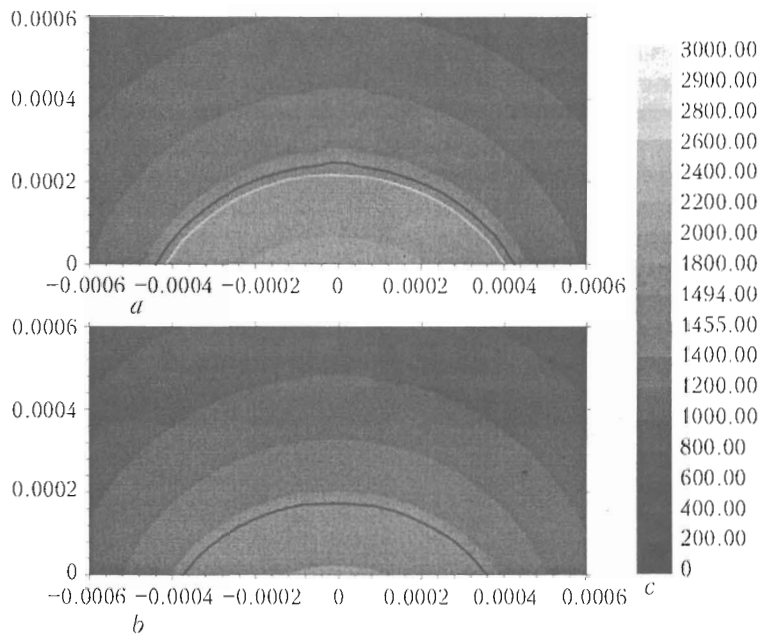


Figure 4. Distribution of temperature in sample from composition powder PGSR-3 and alloy PG-10K-01 and in sample from composition powder PG 10K-01 and alloy PGSR-3 (P_m = 150 W, r_p = 0.4 mm, V_x = 2 mm/s, thickness of the powder layer h_p = 30 μm and air contents of 10 %): *a* — sample from powders PGSR-3 — alloy PG-10k-01; *b* — sample from powders PG-10E-01 — alloy PGSR-3; *c* — scale bar for temperature; darl line — molten pool for Ni, light line — molten pool for Co

• Influence of Cr (21%) with the high specific heat of melting for which phase transformations laser energy is spent.

Thus in Figure 2 the distribution of temperature in samples from powders PGSR-3 (Figure 2, *a*) and PG-10K-01 (Figure 2, *b*) is demonstrated at their processing by the focused laser radiation at identical conditions. Taking into account the significant content of Ni in powder PG-10K-01 (Table 1), its sintering (melting) is possible due to diffusion in a liquid phase not only the basic material (Co), but also an alloying material — Ni. Therefore in Figure 2, the dependence of depth of a melt bath h_m Ni for powder PG-10K-01 is given as well. Apparently from the resulted dependences, the product forming from powder PGSR-3 is possible with the larger productivity, than for powder PG-10K-01. At increase of processing speed the probability of sintering of a product from powder PG-10K-01, due to melting of only alloying element Ni, increases.

Laser processing of multiplayer system is characterized by anisotropy of the thermo-physical properties of treated material (their dependence on spatial coordinates). The account of the given phenomenon (under condition of ideal thermal contact between layers of a material) is possible with the help of expression (3).

The work cycles of process are characterized by processing of multi-layer system: a layer of a powder thickness h_p — a layer of a monolithic material.

So, for example, at processing system which consist from layer of powder PGSR-3 with the atmosphere contents 10 % and layer of alloy on the basis of the specified powder (Figure 3) with increase of thickness of a layer of a powder h_p, parameters of a liquid bath depth h_m (dependence 2, Figure 3) and time of its existence t_m (dependence 1 Figure 3) decrease.

The phenomenon is explained by increase in volume of a material with low heat conductivity that locates heat in a superficial layer and adjoins to a monomaterial. It does not allow the front of phase transformation to move inside and leads to reduction of volume of a liquid bath and, accordingly, time of its existence.

At creation of products with the set of physical-mechanical properties, layers of the future detail may be made of various materials, for example, consecutively from layers of materials PGSR-3 and PG- 10K-01. In comparison with detail manufactured from monolithic material for the specified compositions the depth of a melt bath changes (Figure 4). So in a composition powder PGSR-3 + alloy PG-10K-01 the depth of a liquid bath increases. This phenomenon may be explained in the following way:

• Heat conductivity of the bottom layer of the molten material increases that promotes penetration of Ni fusion front deep inside;

• Ni percentage in alloy PG-10K-01 decreases, that also promotes the increase of depth of fusion front. It is necessary to note, that materials which are components of powder PG-10K-01, have significant specific heat of fusion and accumulate a significant amount of energy that is gradually spent for movement of molten Ni.

Analyzing the results given on Figure 2 — Figure 4, it is worth to note, that provision of constant thickness of a molten zone at formation of multi-layer details is possible at change of energy density of the focused laser radiation $W_E(x, y)$.

Irrespective of different schemes of realization of technology of Rapid Prototyping (the scheme with rolling, powder injection and so on), on a surface of a detail which is realized by analogy to laser marking [8], it is possible to divide conditionally the technique of getting the trajectory of movement of the focused laser radiation into two groups:

• Plane — analogue of the dots-matrix scheme of marking;

• Vector scheme.

It is obvious, that at forming thin-walled products the vector scheme provides the maximum productivity of operation (due to reduction of a total way of move-

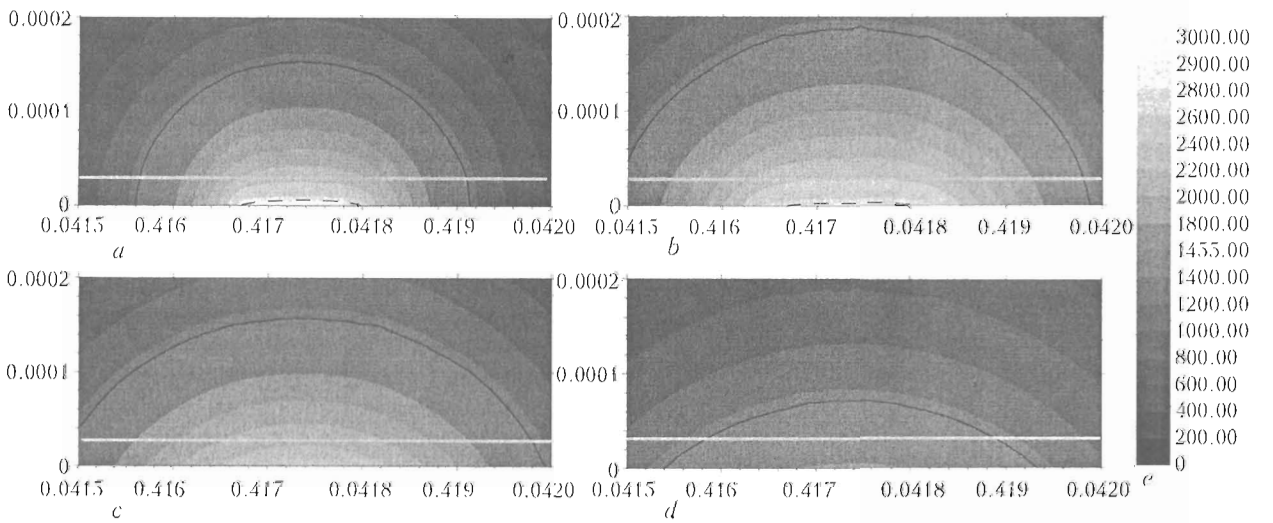


Figure 5. Distribution of temperature in sample from the composition powder PGSR-3 and alloy PGSR-3 (P_m = 150 W, V_x = 20 mm/s, thickness of the powder layer h_p = 30 mm and air contents of 10 %): *a* — the size of focusing spot r_p = 0.1 mm; *b* — r_p = 0.2 mm; *c* — r_p = 0.3 mm; *d* — r_p = 0.4 mm; *e* — scale bar for temperature; dark line — molten pool for Ni, dotted line — vapor pool for Ni

ment of the focused beam). And for both schemes of processing the common is the following:

- Parameters of a powder (the powder particles size, its thermo-physical properties) and parameters of the focused laser radiation determine the size of deviation from borders of a contour of the drawing of the detail and a step on vertical coordinate;
- The increase in thickness of walls of a product is achieved due to the certain overlapping of generated elementary «paths».

Thus, the valid increase of productivity of technology of Rapid Prototyping (for the given laser oscillator, powder mix, depth of a melt bath etc.) can be achieved for the account of:

- increases in speed of movement of the focused laser beam;
- reduction of a total way of its movement.

For the given oscillator (power, mode of generation and other), the increase in speed of movement of the focused laser beam can be achieved due to reduction of focusing spot (increase in power density of the focused laser radiation). However, change of the size of focusing spot will cause not unequivocal influence on the sizes and time of existence of a melt bath.

So, in Figure 5 the distribution of temperature (time 0.023 s) in samples from composition of powder PGSR-3 of thickness 30 μm (the atmosphere contents 10 %) and an alloy on basis PGSR-3 are given which were observed at processing by laser radiation by power P_m = 150 W, moving on a surface with speed V_x = 20 mm/s for different focusing spots. Apparently from the resulted dependences, at focusing laser radiation to a spot by radius 0.1–0.2 mm, the surface temperature of a sample exceeds temperature of evaporation of basis material of the powder mix. It is obvious, that at processing by the laser radiation focused in a spot r_p = 0.1 mm (P_m = 150 W, V_x = = 20 mm/s), the destruction of coating material occurs that does not allow getting high quality product. Focusing laser radiation to a spot r_p = 0.2 mm leads to the beginning of evaporation of material surface, thus the sizes (width and depth) of melt baths increase in comparison with the previous case. The gradual increase in size of focusing spot leads to reduction of the sizes of a melt bath, and reduction of depth h_m and time of existence t_m occurs more intensively.

Changes of speed of movement of the focused laser beam (at constant power density of the focused laser radiation) also will cause changes of parameters of a melt bath. It is obvious, that for given values W_P, increases in speed of movement of the focused laser radiation will cause reduction of the sizes of a melt bath. Thus, for example, on Figure 6 the dependences of parameters of a melt bath are presented, which take place at processing the composition of a layer of powder PGSR-3 with thickness 30 μm (atmosphere contents 10 %) and an alloy on basis PGSR-3 with the focused laser radiation (P_m = 150 W, r_p = 0.3 mm) from speed of processing.

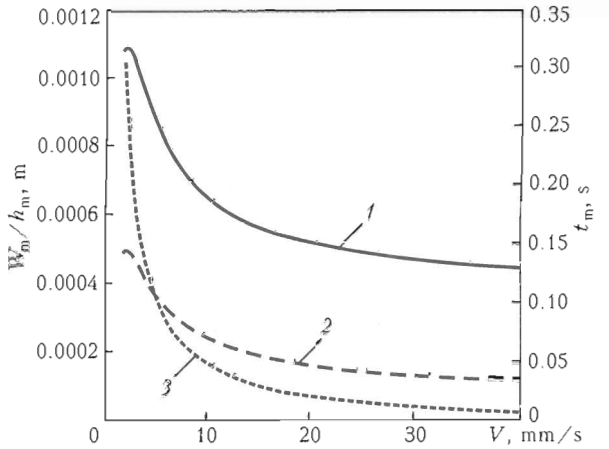


Figure 6. Dependencies of a parameters of a molten pool (depth h_m, width W_m, time of existence t_m) of sample of the composition powder PGSR-3 and alloy PGSR-3 on speed of processing V_x (P_m = 150 W, r_p = 0.3 mm, thickness of the powder layer h_p = = 30 mm, 10 % air): *1* — dependencies of a width W_m of a molten pool on speed V_x; *2* — dependencies of a depth h_m of a molten pool on speed V_x; *3* — dependencies of a time of existence t_m of a molten pool on speed V_x

At preservation of the certain speed of movement of the focused laser radiation, the set mode of generation of the laser the change of parameters of a melt bath is achieved due to change of distribution of power density $W_P(x, y)$ or distribution of energy density of $W_E(x, y)$ of the focused laser radiation [6–14].

Change of distribution of power density $W_P(x, y)$ of the focused laser radiation is possible due to use of special devices (mirrors, diffraction optics and others) that change distribution of intensity of light flow left from the resonator [9, 10]. For the given schemes of processing, use of the specified devices leads to increase in the price of process because of significant cost of equipment. For this reason, change of energy density $W_E(x, y)$ of the laser radiation focused on a surface of a detail (due to its additional scanning), in this case is ithe most simple way to control the size and time existence of a melt bath. Besides as it is marked in [11–14], increase of productivity of operation is achieved for the account of:

- Increase in efficiency of absorption of the focused laser radiation. Thus it is known, that during laser heating of a sample, with increase of temperature the absorption abilities of its surface increases. But at phase transformations, which proceed during heating (solid body — liquid — vapor), there is a «jump-like» reduction of laser energy, which has reached the surface of a detail. The given phenomenon is explained by a number of reasons:
  - plasma shielding;
  - laser radiation refocusing in plasma;
  - change of focusing spot (plasma, heated up air near a surface are the medias with square-law factor of refraction of light which depends on medium temperature of environment).

Thus to increase the productivity and quality of laser processing the use of additional scanning of the focused laser radiation in the spot of its action is recommended, and the easiest for realization is focused

laser radiation scanning under the elliptic law or the harmonious law [12–14].

At additional scanning the focused laser radiation, which moves parallel to axes OX (for example, under the elliptic law), coordinates of the center of focusing spot are described by dependence (4):

$$x_c(t) = x_0 + V_x t + A\cos(2\omega t);\ y_c(t) = y_0 + B\sin(2\omega t), \quad (4)$$

where x_0, y_0 – initial position of an axis of a beam; A, B, ω – amplitude and frequency of scanning.

Analyzing dependences (1) and (4) we shall note, that at additional focused laser radiation scanning the influence on parameters of a liquid bath is possible not only due to change of P_m, V_x, r_p, but also because of change of amplitude A, B, and frequencies of scanning ω as well.

At processing by the continuous scanning focused laser beam the temperature in considered section repeats the periodicity of heating (the moments occurrence of peak of a beam). And, as well as at laser welding and cladding, the periodicity of heating is less with depth. Besides some decrease of surface temperature is observed which is connected to high-speed movement of focusing spot on a surface of a sample. Nevertheless, at the moment of meeting of a detail and the focused beam when their resulting speed is equal to a difference of vectors of speeds of detail and beam scanning and, in some cases, is close or equal to zero, the short-term splashes in temperature on a surface of a detail are observed. This, accordingly, leads (together with laser beam multi passes treatment of zone of processing) to growth of the size of a melt bath. With the increase in frequency of scanning (in an analyzed range of change ω) the efficiency of formation of bonding of the melted powder mix and a material of a substrate grows.

Productivity and quality of formation of separate melted «paths» and their groups raises due to:

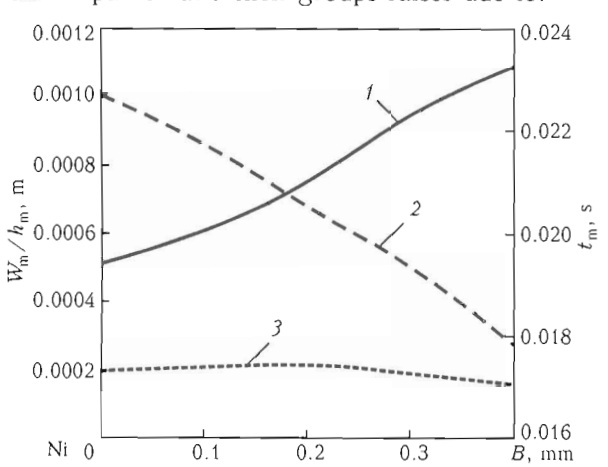


Figure 7. Dependencies of parameters of a molten pool (depth h_m, width W_m, time of existence t_m) of the sample of the composition powder PGSR-3 and alloy PGSR-3 on amplitude B of additional scanning of the focused laser radiation (P_m = 150 W, r_p = 0.2 mm, V_x = 20 mm/s, A = 0 mm, ω = 100 Hz, thickness powder layer h_p = 30 μm, 10 % air): *1* – dependencies of a width W_m of a molten pool on amplitude B of additional scanning; *2* – dependencies of a depth h_m of a molten pool on amplitude B; *3* – dependencies of a time of existence t_m of a molten pool on amplitude B

- sluggishness of systems of heating;
- high speed movement of the scanning focused laser radiation (affects reduction of energy density of the focused laser radiation) and to melt existence during 0.01–0.3 s;
- many passes of the focused laser radiation on a zone of laser influence (depends on speed V_x of beam movement, amplitude and frequency of its scanning, that allow «to warm up» a liquid phase longer, than at usual laser processing.

Apparently from the resulted dependences, at focusing laser radiation by power 150 W in a focusing spot with radius 0.1 and 0.2 mm, the power density reaches $9.5{\cdot}10^5$ W/cm^2 and $2.4{\cdot}10^5$ W/cm^2, accordingly. At focused laser radiation movement on a surface of a sample with a speed 20 mm/s, the maximum laser energy density in a zone of processing reaches $5.98{\cdot}10^4$ W/cm^2 and $2.99{\cdot}10^4$ W/cm^2, accordingly. As it was marked earlier, at laser processing the composition powder PGSR-3 – an alloy on basis PGSR-3 in the discussed conditions, there is an evaporation of surface layer that leads to destruction of coating material.

At additional focused laser radiation scanning, due to change of speed of movement of an axis of the focused beam and the area of processing, there is a change of the maximum energy density $W_E(x, y)$ of the focused laser radiation in a zone of processing and, accordingly, of a surface temperature.

In the considered range of change of focusing spot and parameters of scanning of the focused radiation, in comparison with usual laser processing that is when $\omega = 0$, there are significant changes of energy density of the focused laser radiation in zone of processing. So, at preservation of power density of the focused laser radiation and speed V_x of sample movement it is possible both increase, and reduction of the maximum energy density of the focused radiation. Obviously, the increase in energy density occurs at the moment of time, when resulting speed of movement of the focused beam is close (or is equal) to zero. Change of energy density of the focused laser radiation (due to its additional scanning) affects parameters of a melt bath. It is necessary to note, that in case of scanning laser radiation under the circular or elliptic law when the amplitude of fluctuations exceeds the size of focusing spot, the distribution of density of energy along a line of processing has significant nonuniformity, which affects change in time of parameters of a melt bath.

As it was marked earlier, at processing by the focused laser radiation with P_m = 150 W, focused in a spot r_p = 0.2 mm ($W_P = 2.4{\cdot}10^5$ W/cm^2), moving with a speed 20 mm/s ($W_E = 2.99{\cdot}10^4$ J/cm^2), the surface layer of a composition powder PGSR-3 with 10 % of air (thickness 30 mm) – alloy PGSR-3 evaporates on insignificant depth. Due to change of size and distribution of density of energy of the focused laser radiation, it is possible to avoid destruction of the top

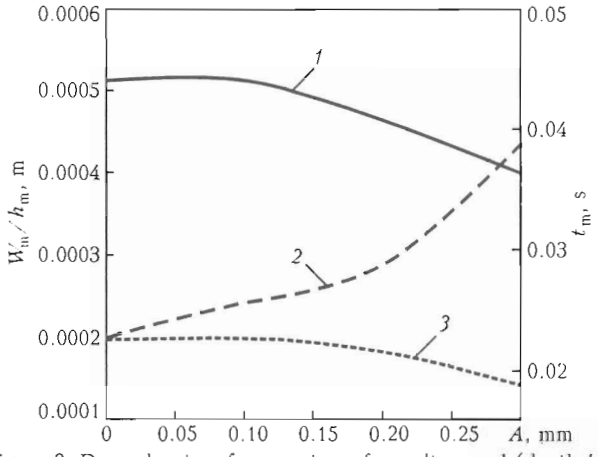


Figure 8. Dependencies of parameters of a molten pool (depth h_m, width W_m, time of existence t_m) of the sample of the composition powder PGSR-3 and alloy PGSR-3 on amplitude B of additional scanning of the focused laser radiation (P_m = 150 W, r_p = 0.2 mm, V_x = 20 mm/s, A = 0 mm, ω = 100 Hz, thickness powder layer h_p = 30 μm, 10 % air): *1* — dependencies of a width W_m of a molten pool on amplitude A of additional scanning; *2* — dependencies of a depth h_m of a molten pool on amplitude A; *3* — dependencies of a time of existence t_m of a molten pool on amplitude A

layer of a coating. At scanning the focused laser radiation on considered conditions of processing, the distribution of energy density (in comparison with processing by a beam focused in a spot r_p = 0.1 mm) has more uniform character, and, in cases when scanning of laser radiation occurs in a plane of a vector of movement of detail V_x, the excess of base value $W_E = 2.99 \cdot 10^4$ J/cm^2 is observed. Thus, for example, in case of scanning radiation (P_m = 150 W, r_p = 0.2 mm, V_x = 20 mm/s with parameters B = 0, A = 0.1 ω = 50 Hz and ω = 100 Hz) the maximum value W_E reaches $3.99 \cdot 10^4$ J/cm^2 and $3.0 \cdot 10^4$ J/cm^2, accordingly. But, due to that the increase of W_E occurs during certain time, keeping balance of energy which joins the detail and is removed from its body (due to heat conductivity), temperature of a surface does not exceed temperatures of evaporation of a material of a basis of a powder (in comparison with usual processing), and parameters of a melt bath increase.

In a Figure 7, Figure 8 dependences of parameters of a melt bath are resulted, which are observed at laser processing at different working conditions of a composition powder PGSR-3 with 10 % of air (thickness 30 mm) — alloy PGSR-3. Apparently from the resulted dependences, maximum time of existence of a melt bath is possible under conditions when the plane of scanning (B = 0) coincides with a vector of speed of laser beam movement (dependence 3, Figure 8) and grows with increase of amplitude of scanning. On the contrary, under conditions when the plane of scanning is perpendicular to a vector of speed of laser beam movement, the time of melt existence decreases (dependences 3, Figure 9). In both cases depth of a melt bath gradually decreases with increase of amplitude of scanning of the focused laser beam.

CONCLUSIONS

Thus, analyzing calculations, we can draw the following conclusions:

Influencing on the law, amplitude and frequency of additional scanning of the focused laser radiation we have an opportunity to control the parameters of a melt bath.

The increase in the size of a melt bath with the help of additional scanning is the most expedient for carrying out for usual processing at conditions, when the evaporation starts on the surface of composition;

Prevention of destruction (due to evaporation) of compositions in «dead» points of amplitude is possible probably by synchronous blocking the access of laser radiation to zone of processing.

Acknowlegement. *This study was done thanks to financial support of STCU (Scientific and Technological Center of Ukraine) on the project #2739.*

1. F. Arcella, *Titanium Alloy Structures for Aircraft Applications by the AeroMet Laser Additive Manufacturing (LAMSM) Process* // «Proceedings of International Congress «ICALEO'2003», Jacksonville, USA, Oct. 2003
2. L. Xue, J. Chen and A. Theriault, *Laser Consolidation of Ti-6Al-4V Alloy for the Manufacturing of Net-Shape Functional Components* // «Proceedings of International Congress «ICALEO'2002», Scottsdale, USA, Oct. 2002
3. L. Xue, A. Theriault, B. Rubinger, D. Parry, F. Ranjbaran and M. Doyon, *Investigation of Laser Consolidation Process for Manufacturing Structural Components for Advanced Robotic Mechatronics System (ARMS)* // «Proceedings of International Congress «ICALEO'2003», Jacksonville, USA, Oct. 2003.
4. *Thermal properties of substances.* Handbook / Ed. in Chief N. V. Vargaftik. — M.: Gosenergoizdat, 1956, 367 p.
5. *Technology Laser Handbook* / Ed. in Chief G. A. Abilsiitov. — M.: Mashinostroenie, 1991, v.1.
6. V. Kovalenko, M. Anyakin, J. Meijer, A. Degtyarev, A. Kozyrev, *Studying of Laser Processed Material Optical Parameter Dependencies from Temperature* // «Proceedings of International Congress «ICALEO'2002», Scottsdale, USA, Oct. 2002.
7. V. Kovalenko, M. Anyakin, J. Meijer, A. W. Duley, D. Roessler, *Laser 3D prototypes forming from metal and ceramic materials* // «Proceedings of International Congress «ICALEO'2003», Jacksonville, USA, Oct. 2003.
8. Peter M. Beker, *Laser marking and serialising* //SAE Techn. Pap. Ser., 1982, v. 82, 1108, 8 p.
9. Jimbou R., Inagaki M., Tamamura T., *A method for laser alloing and transformation hardening using a uniform intensity rectangular beam* // Proceeding of the first International Laser Processing Conference. November 16–17, 1981, Anaheim, CA, USA. P. 97–117.
10. Iwase, T., Shibata, K, Sakamoto, H., Dausinger, F, Hohenberger, B., Muller, M., Matsunawa, A., Seta, N., *Realtime X-Ray Observation of Dual Focus Welding of Aluminum Alloys* // «Proceedings of International Congress «ICALEO'2000», Dearborn, USA, Oct. 2000.
11. T. Arai, S. Riches, *Thick Plate Cutting with Spinnng Laser Beam* // «Proceedings of International Congress «ICALEO'97», San Diego, USA, Nov. 1997, vol B19-B-26.
12. V. Kovalenko, M. Anyakin, Y. Uno, *Modeling and Optimization of Laser Semiconductors Cutting* // «Proceedings of International Congress «ICALEO'2000», Dearborn, USA, Oct. 2000, Vol. 90, p. D82–D92.
13. V. Kovalenko, M. Anyakin,Yoshiyki Uno, Khaled Al Shaboul, *Laser technology application in transformers and electro motors manufacturing* // «Proceedings of 13th International Symposium for Electromachining (ISEM-XIII)», May 9–11th, 2001, Bilbao, Spain, Vol. II., p. 839–850.
14. V. Kovalenko, M. Anyakin, Yoshiyki Uno, Yasuhiro Okamoto, *Laser Cutting of Semiconductor Elements* //International Journal of Electrical Machining, #7, January 2002, p. 9–14.

Conference Sponsors

PWI Laser Systems and Technology Center

Ministry of Education and Science of Ukraine

Information Support

«The Paton Welding Journal»

www.nas.gov.ua/pwj

Conference Sponsors

PWI Laser Systems and Technology Center

Ministry of Education and Science of Ukraine

Information Support

«The Paton Welding Journal»

www.nas.gov.ua/pwj

Conference Sponsors

PWI Laser Systems and Technology Center

Ministry of Education and Science of Ukraine

Information Support

«The Paton Welding Journal»

www.nas.gov.ua/pwj

NEW METHOD OF LASER POWER DELIVERY TO POWDER STREAM IN LASER CLADDING AND NANOPOWDERS PRODUCTION

Yu. CHIVEL
Institute of Molecular & Atomic Physics NASB, Minsk, Belarus

The new method of laser radiation delivery to powder stream in process of selective laser cladding and nanopowders production based on conical laser beams is presented. The results of calculations of powder stream impact on beam parameters and powder particles and base heating is displayed. High efficiency of the new method in combination with precision has been demonstrated.

Introduction. Under selective laser cladding (SLC-process) [1] the powder particles are injected from one side into the focal region where the molten puddle on a substrate surface exist. The duration of particles stay in the region of laser heating is very small and particles are melted only in molten puddle. At high concentration of particles in powder stream its screen each other and surface. The maintenance of molten puddle in the case of metal object is an energy-expensive. All add up to a drop in process efficiency and accuracy which are not more then ~100 μm [1]. In article a new method of laser radiation delivery to powder stream is presented.

Principles of method. The main idea consists in provision of laser power delivery to powder stream uniformly across the surface of stream (Figure 1) and based on unique properties of conical laser beams [2]. Conical beams are formed on focus the laser beam by axicon – conical lens (Figure 2) or conical mirror.

In the case under consideration [3] the laser energy introduction to powder stream is more efficient because heating of small particles at stationary mode of operation and a total uniform absorption of laser beam energy is possible in the dense powder stream. The heat build-up of surface is easy to set up through the corresponding location of surface relative focal region of conical beam (Figure 3). Also the particles heat the surface of object at collision.

One device of doing this is shown in the Figure 3. Laser radiation in the form of ring is directed onto the axicon 6 through the use of mirror 5. In the convergence area of conical beam the focal line 3 is formed. To this region which support on surface of object 4, the dense powder stream is injected by the use of a feed device 1, 2. The other device with multipass optical scheme and conical mirror is shown in Figure 4.

The cross distribution of intensity in focus region of conical beam in transparent media is determined by the zero order Bessel function squared why this beams named as Bessel beams and is displayed in the Figure 4. For axicon with the refrective angle a the field of maximum energy concentration takes the form of cylinder with diameter $d = 2.4\ \lambda/\pi\sin\gamma$ and $\Delta Z = \Delta R/\mathrm{tg}\gamma$ for ring laser beam (Figure 1), where $\gamma = [\arcsin(n\sin\alpha)]$ – cone angle of beam. The intensity maximum grows in amplitude as the angle γ grows, but the width of central maximum is made narrow up to ~λ. Under the dense powder stream the sufficiently large cone angle must be used as a precautionary measure against the strong laser radiation reflection on the stream interface.

Calculations of process. On powder injecting the structure of beam will be modified through laser light

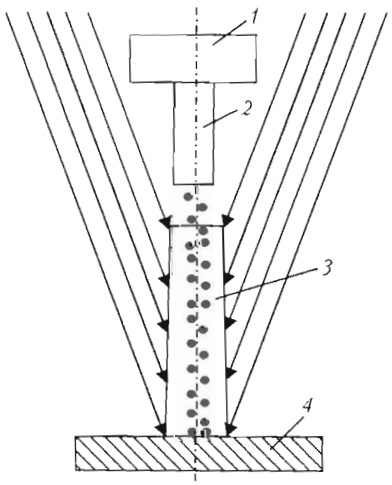


Figure 1. Scheme for delivery of laser

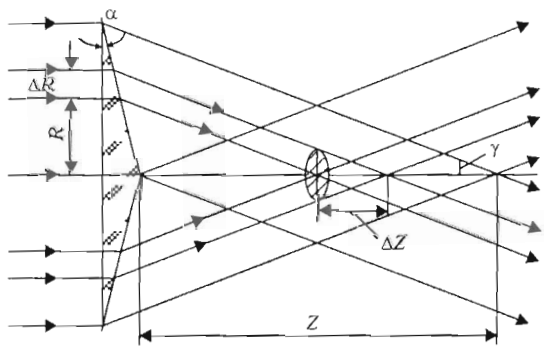


Figure 2. Chart of production of conical beam energy to powder stream

© Yu. CHIVEL, 2005

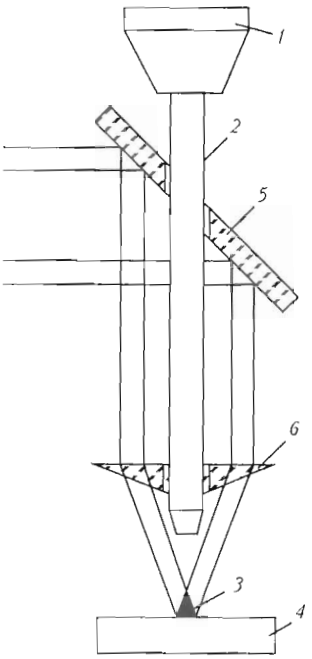


Figure 3. Optical scheme of device

absorption and scattering. We consider the amplitude variations of the beam taking into account attenuation of laser light in snugpacking dispersed layer. The calculations is carried out for metal spherical particles (material – Ti) with diameter d = 10 μm under volume density $N = 10^8$ cm^{-3}. The radius of powder beam is taking to be R = 50 μm.

For coherent light passing the exponential connection between coefficient of attenuation and layer's thickness can be used [4]:

$$T = \exp(-Q\eta) \qquad (1)$$

where $\eta = 3Rn1/2d$ – coefficient of layer's overlap, Q – effective factor of attenuation, $n_1 = 0.74(d/\delta)^3$ – dimensionless volume density of particles ($\delta = 2d$ – average distance between particles). For layer from optically hard large particles ($\pi d/\lambda > 1$, $\pi d/\lambda(n - 1) >> 1$) the effective factor of attenuation may be written:

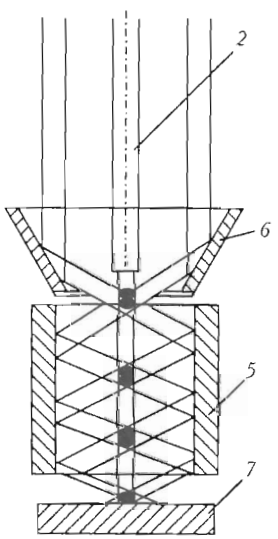


Figure 4. Modified optical scheme

$$Q = 1/1.5n_1 \ln[1 + 1.5n_1 Qi \exp(1.5n_1 Qi)] \qquad (2)$$

The transmission of powder stream has described by the relationship:

$$T = \exp[-\sigma(R - r)] \qquad (3)$$

where $(R - r)$ – depth of laser light penetration into the powder stream in μm, σ = 0,03 μm^{-1} – attenuationcoefficient, Qi – factor of attenuation of insulated particle.

Laser intensity attenuation causes the Bessel beam peak intensity to fall and the distribution of laser intensity within powder stream levels off (Figure 5). Intensity distribution of laser radiation within the powder stream in the absence of a interference has described by the following expression [5]:

$$q = q_0(R/r)[e^{-\sigma(R-r)} + e^{-\sigma(R+r)}] \qquad (4)$$

The scattered laser radiation is effectively absorbed by particles under repeated scattering. The calculations of scattered radiation attenuation in the frame of transport theory enable to determine diffuse transmission and reflection of powder stream. In the case under consideration Td = 0.16 – 0.30, a Rd = 0.02 – 0.17, depending on boundary data. Coherent laser radiation transmission per powder beam radius 50 μm is equal T = 0.3.

The calculations of laser heating of powder streams with diameters 10 μm and 100 μm from particles 1 μm and 10 μm with a high density (10^{12} cm^{-3} and 10^8 cm^{-3} respectively) are carried out. The powder streams velocity is taken as 10 m/s and length of focal line is 2 mm. The powers of laser radiation that are necessary for powder heating to a point of melting in such streams not more than 3 W and 30 W for 1 μm and 10 μm particles streams respectively. Variations in powder stream density and laser intensity distribution on the axicon are operable to optimization of sintering process.

The heating of surface of object in the region of powder delivery is the main factor in the technology of cladding. The average surface temperature on the delivery spot through particles supply is described by expression [6]:

$$Tav = 0.115Q\alpha^{1/2}G/\lambda v^{1/2}\theta^{3/2} \qquad (5)$$

where Q – particles enthalpy, G – rate of powder stream, v – velocity of spot movement, α – temperature conductivity coefficient of object, λ – thermal conductivity coefficient, θ – dispersion of particles distribution in spot. In our case under the diameter of stream 100 μm and flow rate $5{\cdot}10^{-3}$ g/s, $Tav = 0.035{\cdot}10^4/v^{1/2}$, where v – cm/s. At a velocity 0.40 cm/s the average r temperature on the surface within the the delivery spot is equal 1800 °K.

By this means the moderate heating up of the surface of object to melt temperature is readily provided by laser beam under corresponding location of surface relative focal line.

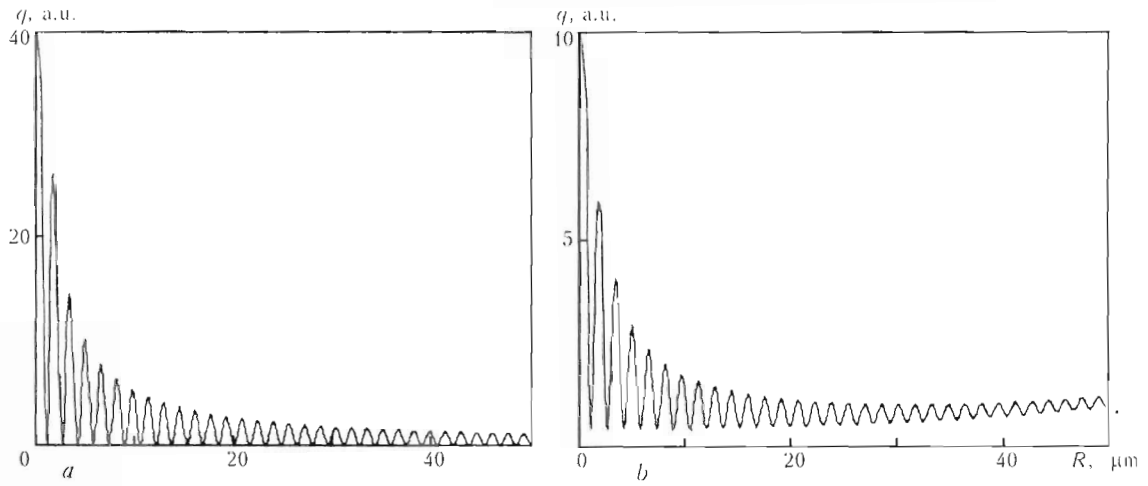


Figure 5. Intensity distribution in the conical Bessel beam: *a* — in transparent media; *b* — in powder stream

Conical beams in nanopowders production. Laser evaporation of solids followed by vapour condensation is perspective method of nanopowder production. The potentials of the new method of laser radiation energy delivery to powder stream for nanopowder production were investigated. In the model under study the dense stream ($5 \cdot 10^6$ cm^{-3}) diameter 0.5 mm from Ti-micropowders with particles 30 mm in size is injected into the focal region of conical beam 3 μm long at the rate of several m/s.

Dynamics of heating and evaporation of spherical particles describe by equations:

$$4/3\pi r^3 \rho C(dT/dt) = \pi r^2 q Q_a - E - LG; \quad (6)$$

$$dr/dt = -G/4\pi r^2 \rho; \quad (7)$$

where r — particle radius, ρ — density of particle material, C — specific heat, q — laser radiation intensity, Q_a — factor of absorption of particle, E — energy flow from particl surface, L — specific heat of evaporation, G — mass flow from surface.

Under initial step of particle heating the losses on vaporation and thermal conductivity are small and temperature dynamic may be wrute in view:

$$T = 3qtQ_a/4\rho Cr \quad (8)$$

And temperature of quasistationary evaporation are determined from next condition — $dT/dt = 0$.

Under number of reductions [7] the simple form of evaporation rate may be received:

$$dr/dt = -qQ_a/4\rho(C_1T^* + L) \quad (9)$$

According the calculations particles duration of stay in the heating region ~10^{-2} s, the required laser power for developed evaporation not exceed ~250 W and total speed of evaporation equal 36 g/hour under power imputs ~12 W hour/g.

Discussion. The calculations of efficiency of the process of 3D-object production using new method made it apparent that the consumption of energy is equal $2 \cdot 10^3$ J/g. That is one order of magnitude less than in well known LENS-process, DLF-process. The accuracy of the process can be estimate as diameter of Bessel function maximum ~1–10 μm.

A tenfold higher efficiency (2–3 times more) of the process of nanopowder production as compared to that of the process of vaporization of the pellet from compacted powder [8] has been established.

CONCLUSIONS

By this means the harnessing of the conical beams allows to carry out a laser power delivery to powder stream uniformly across the surface of stream, resulting in gain in productivity and accuracy. The laser radiation distribution within the dense streams is sufficiently uniform, excluding a small region near the axis of stream, with resulting uniform particles heating across the whole width of stream. The new method makes it possible to hold down consumption of energy and powder in SLC and nanopowder production, yet to raise the accuracy. The optimum heating of powder particles and the object surface may be achived with high efficiency.

One of the main advantage of the new method of laser radiation delivery lies in the fact that the cladding process is computatiable with high accuracy. The calculation methods of laser radiation transmission in dispersed medium are developed well and the possibilities to optimized the technological process have opened up.

The calculations of efficiency of the process of nanopowders production using new method made it apparent that the efficiency is higher that one of the process of vaporization of the pellet from compacted powder.

1. D. Thoma, G. Lewis, et al // Proc. XV ITSC. — P. 1205–1210, 1998.
2. J. McLeod // J. Opt. Soc. Am. v. 44. — P. 592. — 1954.
3. Yu. Chivel // Proceedings SPIE, V. 5399. — P. 228–233. — 2004.
4. A. P. Ivanov, V. A. Loiko, V. P. Dik, *The Propagation of Light in Snugpacking Dispersed Medium.* — Minsk. — 1988.
5. E. P. Shafer // Appl. Phys. B. V. 39. — P. 1–8. — 1986.
6. V. V. Kudinov, P. Yu. Pekshev, V. E. Belashenko et. al. *Plasma spraying coatings,* Nauka, Moscow, 1990.
7. V. Igoshin, V. Kurotchin et al // PhIAN Transactions, V. 198. — P. 33. — 1989.
8. Muller E., Oestreich Ch., Popp U. et al //Journ. KONA. Powder & Particle. — № 13. — P. 79. — 1998.

INFLUENCE OF LASER TREATMENT ON STRUCTURE AND PROPERTIES OF PLASMA CERAMIC COATINGS

O. G. DEVOJNO, M. A. KARDAPOLOVA
Belarussian State Polytechnic Academy, Minsk, Belarus

Theoretical estimations are executed and experimental data about the influence of Al_2O_3 crystal structure on tribotechnical characteristics are obtained. The dependence of physical and mechanical properties of covering Al_2O_3+TiO_2 on the contents of titanium dioxide, and the type of an underlayer and laser processing is investigated.

Introduction. Today ceramic materials (*CM*) with high wear- and corrosion-resistant characteristics represent high interest for the creation of protective covering.

In this respect special interest present the oxides, which, when introduced in a friction couple, completely change the mechanism of friction, thus preventing formation of zure bridges, which are one of the main reasons of destruction of contacting surfaces during friction [1].

In the ceramic materials which form high operational properties of superficial layers, aluminium oxide Al_2O_3 and titanium dioxide TIO_2 are of a special interest. Aluminium oxide possesses the characteristics of hardness, wear- and corrosion-resistance, it does not interact with metals at high temperature heating. Titanium dioxide, possessing good plasticity, can play the role of an adhesive. When fused in plasma spray, the particles of aluminium and titanium oxides form the solid solution of TiO_2 in Al_2O_3, the layer of eutectic pattern created. Temperature decrease of a composite fusion promotes creation of a denser covering consisting of Al_2O_3 particles, intervals between which are filled with frozen buttons on TiO_2 base.

One of the ways to improve the physical and mechanical, and operational characteristics of ceramic coverings is processing of their surfaces with laser radiation (LR) [2]. Ceramics, including oxides, absorb LR very well, especially radiation of CO_2 lasers with wavelength of $10.6 \cdot 10^{-6}$ m.

Thus, the analysis of scientific backgrounds and researches has shown that the problem of high wear-resistance can be successfully solved by application of ceramic materials as coverings and their postprocessing with LR. The possibility to change crystal structure of ceramic coverings (CCs) is especially important at the stage of laser treatment (LT), thus, providing the dominance of crystal modifications in a covering which raise operational characteristics of the latter. Taking into account chemical inertness of ceramics towards the basic constructional materials, it is important to provide possibility of carrying out LT in a sintering regime, achieving significant decrease of porosity and good adhesion of covering particles.

In the given research the following problems were solved:

1. Theoretical estimation of the influence of a crystal structure of a covering material on its friction characteristics.

2. Determination of the criteria in choosing methods of coating underlayers and coverings on a parent metal.

3. Investigation of the conditions of CCs formation, their physical and mechanical, and wear-resistant properties at laser treatment.

Technique of research. The mechanical mixes of aluminium oxide and titanium dioxide (rutile concentrate) were chosen for research with the ratio 97:3, 87:13, 60:40, 40:60, and 20:80 respectively. The materials had granulation of 0.02–0.04 mm.

The technology of coating of a steel-45 surface had the following stages: the preparation of a surface for spraying, underlayer coating, ceramic spraying, laser treatment. The preparation of a surface included degreasing with organic dissolvents and shot processing. To coat the base layer and underlayers of the thermoresponding powder PT-NA-01 (ПТ-НА-01) or alloy PH20N80 (ПХ20Н80) there was used the plasma spraying unit UPU-3D (УПУ-3Д) with the plasma generator PP-25 (ПП-25). The thickness of underlayers was 0.05–0.06 mm, that of the base layer 0.45–0.55 mm.

Before coating of a fusible tin underlayer, chemical processing was done in a flux. The following modes of tin underlayer coating were used: flux temperature, K-550, time of soaking in Sn flux, 1.5–2.0 min. The thickness of a coated tin underlayer was 0.02–0.03 mm.

For LT of ceramic coverings there was used the CO_2-laser of continuous action LGN-702 (ЛГН-702) with wavelength of $10.6 \cdot 10^{-6}$ m. LT was done on the whole surfaces of coverings without mutual overlap of processing zones. LT modes were chosen on the criterion of maximum wear-resistance (determined experimentally), and on the criterion of getting optimum density to a covering (determined by thermal calculation).

The wear resistance test was carried out on the machine for express-tests according to the following scheme: a flat surface – a counterface (alloy VK-8 (ВК-8)). The wear-out value was defined by the depth of a worn flute with the help of a surface analyser-profilometer. The tests of durability of the adhesion of covering with a base material were carried out by a pinning technique on an Instron-1195.

© O. G. DEVOJNO, M. A. KARDAPOLOVA, 2005

Calculation of adhesive force of friction. The crystal structure of a covering material can greatly influence the characteristics of friction and its wear-resistance. It is proved, that the crystal structure influences the pattern of destruction of adhesive connections at friction. The cubic structure of a crystal lattice provides a deeper tear, than a hexagonal lattice, and, hence, metals with a hexagonal lattice show a higher wear-resistance than metals with a cubic one. It is caused by various number of easy sliding systems in crystal lattices of metals with cubic and hexagonal lattices, i.e. with various mechanisms of deformation.

Thus, the crystal structure of metal influences the value of friction force. The latter is the sum of molecular (adhesive) and mechanical components. The mechanical component of friction force cannot depend on a crystal structure of rubbing materials (in its physical meaning), therefore influence of a crystal structure should be considered with reference to the adhesive component of friction force, which also confirms its physical meaning.

The calculations proved that there is less of the friction force adhesive component (FFAC) for metals with a hexagonal lattice, than for metals with a cubic one. For ceramic materials, including aluminum oxide, such data were not obtained.

According to the calculations of the temperature field, there should occur a change of the crystal structure in aluminium oxide in the aluminium oxide covering processed with the laser (transition of the cubic – modification Al_2O_3 into the hexagonal modification – Al_2O_3), so FFAC calculation for aluminium oxide with hexagonal and cubic lattices was made [3]:

As a basis of calculations was accepted the Madelung and Born classical theory of ionic crystals.

Full energy of an ionic crystal lattice develops of energy of electrostatic interaction and energy of repulsive forces at approach of ions [3]:

$$W = -\frac{N\alpha Z_1 Z_2 e^2}{L}\left(\frac{n-1}{1}\right), \qquad 1.1$$

where W – full energy of an ionic crystal lattice: N – number of opposite ions couples: α – Madelung constant: Z_1 and Z_2 – valencies of positive and negative ions: e – electron charge: L – distance between opposite ions: n – a constant for the majority of substances, including aluminium oxide = 9 [3].

Having differentiated the equation 1.1 on L, we shall receive force of interaction in a general view.

$$F = -\frac{N\alpha Z_1 Z_2 e^2}{L^2}\left(\frac{n-1}{1}\right), \qquad 1.2$$

where F – force of interaction between ions in a lattice.

Having accepted as it mentioned above, $n = 9$, we shall receive:

$$F = -\frac{0.889 \cdot N Z_1 Z_2 e^2}{L^2}, \qquad 1.3$$

The adhesive component of elementary force X to a direction of an axis is equal to a projection of force of interaction between ions on this axis:

As far as $\cos(F, x) = \frac{Xi}{\sqrt{Xi^2 + Yi^2 + Zi^2}}$ and $L2$ in the equation (1.3) is equal to $L2 = Xi^2 + Yi^2 + Zi^2$, we shall receive:

$$Fi = 0.889 \cdot N\alpha Z_1 Z_2 e^2 \frac{Xi}{(Xi^2 + Yi^2 + Zi^2)^{3/2}}, \qquad 1.4$$

where Fi – an adhesive component of elementary force of friction: Xi, Yi, Zi – projections of distance between opposite ions on the corresponding reference axes.

Having replaced in the equation (1.4) expression $\frac{NXi}{(Xi^2 + Yi^2 + Zi^2)^{3/2}}$ on B_{resh}, we shall receive:

$$Fi = 0.889 \alpha Z_1 Z_2 e^2 B_{resh}, \qquad 1.5$$

where B_{resh} is the coefficient depended on a type of a crystal lattice of an ionic crystal (lattice coefficient).

The calculation of Madelung constant was made according to the technique stated in the literature [4]. For $B_{resh} = 583360.91 \cdot 10^{20}$, $1/m^2$.

Similarly, while using corresponding model and the level-to-level scheme of an arrangement of ions in cubic aluminium oxide lattice (γ–Al_2O_3) [5], for this structural updating Al_2O_3 there was received the equation and the calculation of B_{resh} coefficient was made.

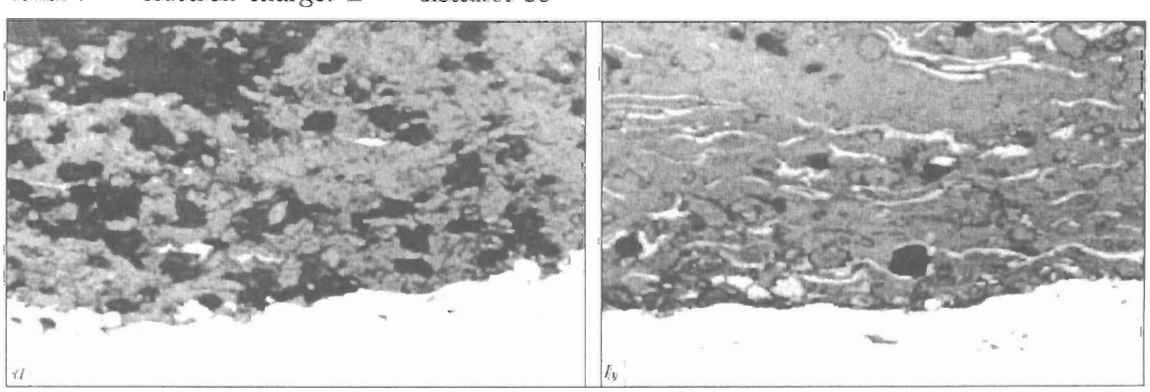


Figure 1. Microstructure of plasma spraying coatings (×200): *a* – mixture 97% Al_2O_3 + 3% TiO_2; *b* – mixture 40% Al_2O_3 + 60% TiO_2

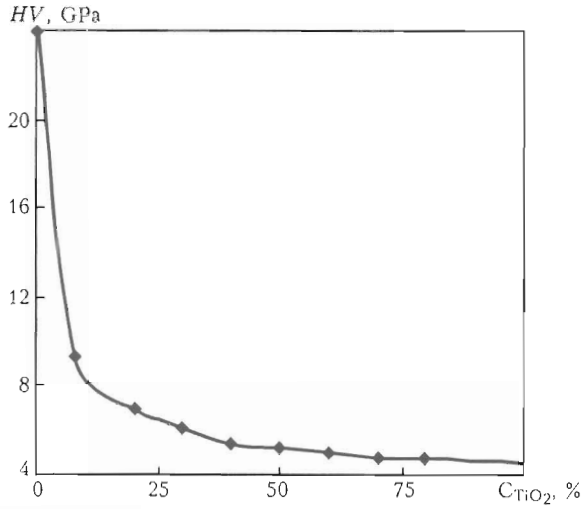


Figure 2. Dependence of coating microhardness Al_2O_3–TiO_2 on concentration TiO_2

At $t = a_0/2 = 3.95 \cdot 10^{-10}$, m [5], $B_{resh} = 1992177.5 \times \times 10^{20}$, $1/m^2$ (a_0 parameter of lattice γ–Al_2O_3).

To receive the results of FFAC calculation in terms of SI system we shall write down the formula 1.5 in the following way:

$$F_{adh} = \frac{1}{4\pi\varepsilon_0} 0.889 \cdot \alpha Z_1 Z_2 e_2 B_{resh}, \qquad 1.7$$

where F_{adh} — an adhesive component of friction force, H; ε_0 — an electric constant, $K^2/H \cdot m^2$.

Having made calculations under the formula 1.7, we receive the following FFAC values: For aluminium oxide with close-packed hexagonal lattice α-Al_2O_3-F_{adh} = 0.298957 H; for aluminium oxide with close-packed cubic lattice γ-Al_2O_3-F_{adh} = 1.253526 H.

Thus, FFAC for aluminium oxide with hexagonal lattice is more than 4 times lower than FFAC for aluminium oxide with cubic lattice. Hence, it is possible to assume, that force of friction for α-Al_2O_3 will be lower, than for γ-Al_2O_3. Despite the difference in type of connection between particles in a lattice of metals and ceramics, the dependence of FFAC and, of friction forces correspondingly, on the type of crystal structure is expressed approximately equally for them.

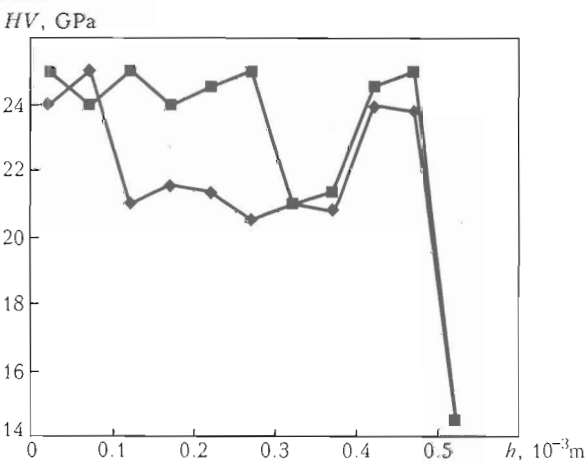


Figure 3. Distribution of microhardness on Al_2O_3 coating depth: *1* — after plasma spraying; *2* — after laser treatment

Taking into account the received results, it is necessary to assume, that wear-resistance of a covering with a hexagonal lattice, i.e. after being laser-treated (according to the above results of calculations), will be higher than wear-resistance of a covering with the cubic lattice, not exposed to the laser treatment.

Results of researches and their discussion, it was established during the researches, that the porosity and durability of adhesion of compositions Al_2O_3–TiO_2 substantially depend on the content of titanium dioxide in this mix, since the limiting wetting angle of metals for these mixes quickly increases when the content of TiO_2 changes from 0 up to 10%, and then decreases at TiO_2 content up to 50%. General dependence of durability of adhesion on the content of TiO_2 in mechanical mixes is caused by the ability of titanium dioxide to form solid solutions in aluminium oxide. The significant amount and size of pores can be observed in the covering 97%Al_2O_3 + 3%TiO_2 (Figure 1, *a*). The covering is loose, with low cohesive connection among particles. Alongside with aluminium oxide titanium dioxide is present in insignificant amount. The highest durability of adhesion and the least porosity is found in the composition of 60% Al_2O_3 + 40% TiO_2. (Figure 1, *b*) σ = 23–25 МПа. A plenty of pores is filled with titanium dioxide and solid solution of TiO_2 in Al_2O_3.

Application of a fusible tin underlayer results in growth of durability of adhesion in 1.5–1.7 times in comparison with the durability of adhesion achieved in the usage of the underlayers PKh20N80 (ПХ20Н80) and PT-HA-01 (ПТ-НА-01). It is caused by the increase of the contact area between the covering and the underlayer and by the relaxation of residual voltage on their border due to high plasticity of a fusible layer. Laser treatment of CM did not resulted in change of durability of adhesion of the covering with the base material as it had the purpose of processing the surface of a layer.

It is typical for laser-treated aluminium oxide covering, as well as for sprayed one, to have three zones with various microhardness in depth of a layer covering (Figure 2). Average microhardness of these zones coincides. However, in case of sprayed covering the top zone with high microhardness is located up to the depth of 0.1 mm, but after LT its depth is 3 times larger and reaches 0.3 mm. The zone of low microhardness at LT decreases and is located within the depth of 0.3–0.4 mm. In this case the bottom zone with high microhardness does not change and fully corresponds to the same zone for a covering after spraying. Thus, the conclusion proves to be true that LT influences only the top zone of covering with the depth up to 0.3 mm, while the bottom layers and the base material do not suffer the LT influence.

As the X-ray crystal analysis confirms, zone 1 and 3 of the sprayed covering and the laser-treated covering should be connected with a hexagonal (high-temperature, formed of γ-Al_2O_3 at heating to temperature

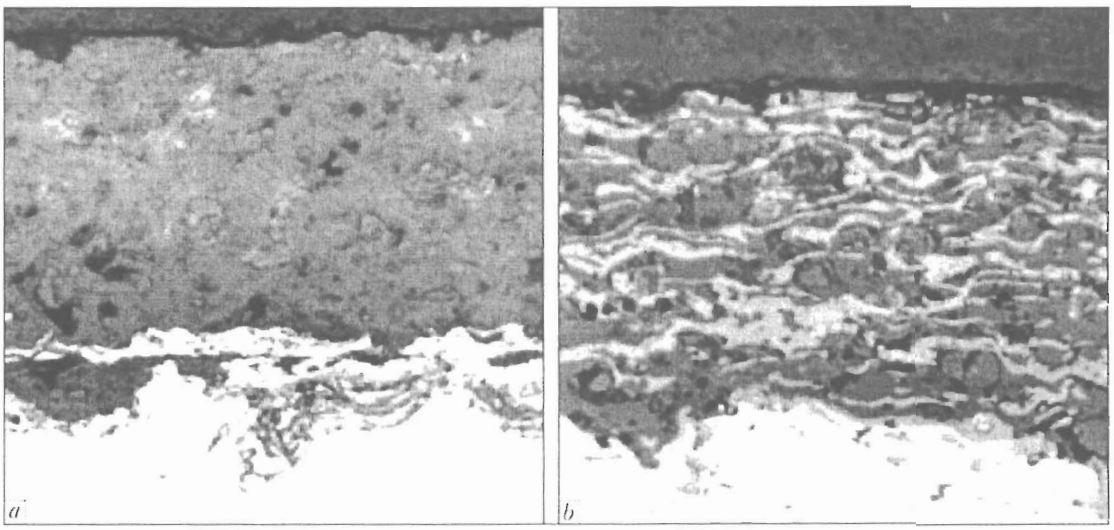


Figure 4. Microstructure of coatings after laser treatment (×200): *a* — mixture 97% Al_2O_3 + 3% TiO_2; *b* — mixture 40% Al_2O_3 + 60% TiO_2

1223–1573 K) modification of aluminium oxide, zone 2 — with a cubic (low-temperature) modification. In process of spraying the heating of a powder particles to the temperature of fusion (2323 K or close to it) takes place, and then relatively slow cooling of particles in the covering occurs. Here, in the main, the transition of aluminium oxide a-modification into y-modification has time to come to the end. However, in the top layer of the covering contacting with atmosphere, and in its bottom layer, adjoining with the base material, the cooling of particles proceeds more intensively, than in the middle layers. The formation of zone 1 occurs due to high speeds of heating and cooling of the covering up to the depth of 0.35 mm, provided by LT.

Titanium dioxide reduces the microhardness of a composition, determining a wide range of operational properties (Figure 3). The microhardness of the composition decreases intensively within 0 up to 40% of TiO_2 content, hereinafter the decrease of microhardness occurs more slowly. It is caused by significant content of Al_2O_3 when softer and softer eutectic layers are formed; at the content of titanium dioxide from 40 up to 100% aluminium oxide is not sufficient any more to form eutectic layers solid enough. In formed eutectics it is titanium dioxide that makes a base. LT results in 1.6–2.1 times reduction of porosity of compositions in comparison with sprayed coverings (Figure 4). It confirms the assumption of creation in the covering the conditions for sintering. Compared together a microstructure before and after LT (Figure 1 and 4), it is necessary to note, that the ratio of phases remains constant, but a significant seal is marked. Big pores are closed, the amount of fine pores grows with the increase in depth of a covering. To experimentally check theoretical results concerning antifrictional characteristics of a Al_2O_3 covering, the researches of friction coefficient of treated and untreated coverings were carried out. The data was obtained, that the friction coefficient of the processed coverings at friction on a similar covering and alloy BK8 is 1.1–1.35 times lower, than of the sprayed ones. Therewith, the difference grows with increase in contact pressure. At friction in the environment of «industrial oil 20» and at dry friction the laser-treated coverings wore out much more slowly (in 2–3 times), than the sprayed ones, and the effect at dry friction was even higher. It is explained by the fact that wear-out process in this case is determined by the spalling of particles, and LT seals coverings.

CONCLUSION

The calculation of friction force adhesive component FFAC is made for aluminium oxide with cubic and modifications of crystal lattice. It is shown, that FFAC for γ-Al_2O_3 with a cubic lattice (sprayed covering) is 4 times higher than FFAC for α-Al_2O_3 with hexagonal lattice (laser-treated covering). The obtained theoretical data are confirmed with the researches of friction coefficient and wear-resistance of coverings. The wear resistance of compositions raises up to 2–3 times after LT in comparison with the similar sprayed compositions.

The influence of titanium dioxide in compositions Al_2O_3 + TiO_2 on the durability of adhesion, microhardness, porosity of coverings is revealed. This influence is connected to the ability of titanium dioxide to form solid solutions in aluminium oxide and the dependence the limiting wetting angle of metals on the content of TiO_2 in composition.

1. Fedko J. P., Kalitin A. T., Bartenev S. S., *Studying of wear-resistant detonation coverings. The theory and practice of gasothermal coating of coverings.* Theses of reports V111 of All-Union meeting, V. 1, «Zinantne», Riga, 1980, p. 167–170.
2. Zaplatinsky I. *Thin Solid Films*, 1982, v. 95. — № 3. — P. 275–284
3. Nazarenko P. V., Anistratenko L. A., *Certain types of external friction on the basis of dislocation representations in the view of connection type and type of lattice of metals* // Friction and deterioration. — 1991. — V.2, № 6. — P. 987–995.
4. Kittel Ch. *Introduction in physics of solid bodies.* — M. Nauka, 1978, p. 782.
5. Kostov I. *Mineralogy.* — Mir, 1981, p. 584.

THERMAL STRESS ANALYSIS OF NOZZLE FOR POWDER FEEDING IN HIGH POWER DIODE LASER (HPDL) POWDER SURFACING

A. KLIMPEL, D. JANICKI, A. LISIECKI
Welding Department, Silesian University of Technology, Gliwice, Poland

This paper describes the influence of High Power Diode Laser (HPDL) powder surfacing parameters on the temperature of nozzle for powder feeding. Influence of material and construction of the nozzle on reflection coefficient of laser beam was determined. It was shown that the nozzle made of copper body and thin-walled tube made of austenitic stainless steel ensures much higher life time of the nozzle and also higher process efficiency compared with nozzle made of copper.

Introduction. Laser powder surfacing, as one of areas of laser application, is currently being developed in many branches of industry. Possibility of precise control of fusion depth makes that the dilution of the surfacing material by substrate material is insignificant (from 3 to 10%), especially in the laser surfacing with powder addition. The chemical composition of laser deposits is not significant different from chemical composition of the additional material even in the first layer. Therefore it is possible to obtain required utility properties in the first layer of deposit, and the material excess for finishing does not exceed 0.2–0.3 mm. The high power density of laser beam (reaches even 10^7 W/cm^2 at atmospherical conditions) ensures minimum heat effect on the workpiece. Thus, thermal stresses and deformations of the workpiece are very low or even neglectable [1–15].

The development of direct-diode laser systems has enabled recently the arrival of the new generation of high power diode lasers which are of interest for material processing because of their beneficial features, compared with molecular CO_2 and solid state Nd:YAG lasers. Thanks to rectangular shape of HPDLs laser beam, with a top hat profile in one direction and Gaussian like in the other, the HPDL beam is ideal for surface treatment applications. Additionally, in comparison to CO_2 lasers, HPDLs emit at short wavelengths in a range 808–960 nm thus the absorption of HPDL beam is significantly higher. Some authors indicate that the absorption of HPDL beam for metallic materials is even several times higher than absorption of CO_2 laser beam [1–5].

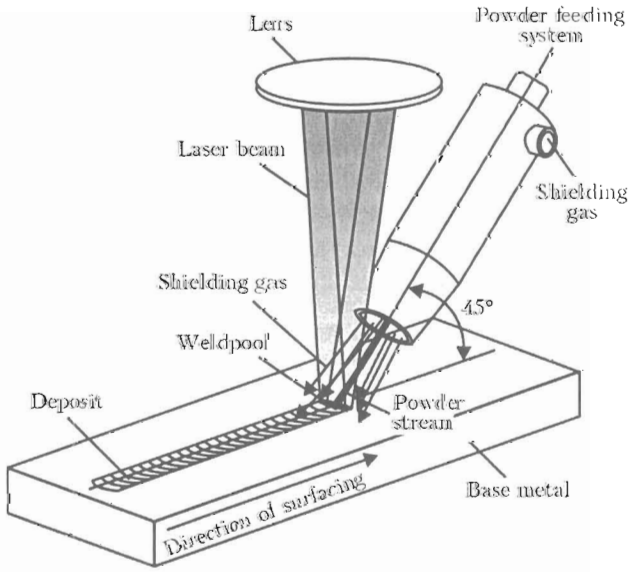


Figure 1. Scheme of laser powder surfacing process carried out along the short side of the rectangular diode laser beam spot with powder injection in front of the weld pool

© A. KLIMPEL, D. JANICKI, A. LISIECKI, 2005

There are two main techniques of laser powder surfacing, depending on the method of powder applying. The powder can be injected directly into the weld pool and melted inside the weld pool and then the deposit layer is formed. The powder can be also preplaced on the substrate surface and then remelted by the laser beam. The powder injection technique provides significantly more accurate control of fusion depth and higher efficiency compared to the powder preplacing technique. Usually the powder is injected into the weld pool via nozzle set at an angle to the substrate material [1–15]. The distance from the weld pool surface to the outlet of nozzle for powder feeding must be short to ensure high efficiency of laser cladding with powder injection technique. Thus the nozzle for powder feeding is intensive heated and the tip of the nozzle can be easily overheated and melted. That is why the construction of the nozzle for powder feeding must be designed for extreme working conditions.

The aim of this work was elaborating and designing a construction of nozzle for powder feeding which is resistant to heating during laser cladding, when short distance from weld pool surface to the nozzle outlet is applied, which is indispensable to achieve high efficiency of laser cladding process with powder injection technique.

Experimental. The laser used in the cladding process was high power diode laser with maximum output power 2.3 kW, (Figure 1, table 1). The rectangular HPDL beam spot of size 1.8×6.8 mm, at focal length

Table 1. Technical data of the HPDL ROFIN DL 020

Wavelength of the laser radiation	808 nm ± 5 nm
Maximum output power of the laser beam (continuous-wave)	2300 W
Laser power range	100–2300 W
Focal length	82 mm/32 mm
Laser spot size	1.8×6.8 mm/1.8×3.8 mm
Range of the laser intensity	0.8–36.5 kW/cm^2

82 mm, was focused on the metallic clean surface of carbon steel plates S355NL-EN 10 113, 8 mm thick (table 2). The substrate was moved under the statio-

Table 2. Chemical composition, wt.%, of S355NL steel used as the substrate for laser powder surfacing process

C	Mn	Si	P	S	Cr	Ni
0.18	1.36	0.45	0.02	0.02	0.09	0.10

nary beam by a numeric XY-table. The cladding process was carried out along both short and long side of the rectangular HPDL beam spot. The nickel base powder was supplied, by a rotary powder feeder and Ar carrier gas, via a cylindrical nozzle and also a nozzle with flat outlet, (table 3, Figure 4). The powder fe-

Table 3. Chemical composition, wt.%, of the powder used for laser powder surfacing process; particle size of powder 32–125 μm

C	Si	Cr	Ni	Co	Fe	B
0.14	3.38	0.03	base	0.01	0.75	3.16

eding system enables precise control of powder feeding rate in a rage from 0.8–25 g/min. Laser cladding experiments were carried out using two type of nozzles for powder feeding. One nozzle for powder feeding was made of copper and the second one was made of two type of materials. The nozzle body was made of copper and connected with a thin-walled tube (nozzle tip) made of austenitic stainless steel, (Figure 3 and 4). Nozzles for powder feeding made of copper are commonly used in industrial systems for laser powder cladding with CO_2 and Nd:YAG lasers. The construction of the nozzle for powder feeding with a thin-walled tube made of austenitic stainless steel was designed, manufactured and patented in Welding Department of Silesian University of Technology. To determine the temperature of the nozzle tip during laser surfacing, stringer beads of deposit were produced at different laser output power, surfacing speed, powder feeding rate, different distance of nozzle tip from weld pool surface and nozzle inclination angle. The commercial grade argon was used as a shielding gas supplied generally at 6 l/min via cylindrical nozzle. The temperature of the nozzle tip for powder feeding was measured using a temperature recorder with Ni–NiCr thermocouple. The temperature of the nozzle tip was measured for 60 seconds from start of the laser cladding process to ensure stable thermal conditions of the nozzle tip. The absorptions of High Power Diode

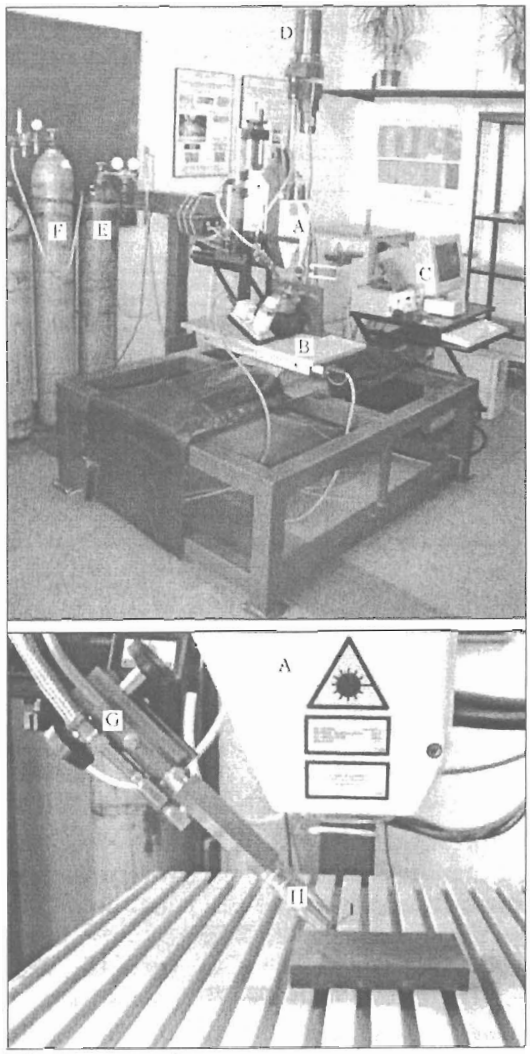


Figure 2. Experimental set-up with 2.3 kW HPDL in Welding Department of Silesian University of Technology in Gliwice, Poland; *A* – laser head, *B* – positioning system, *C* – PC controller, *D* – powder feeder, *E*, *F* – gas bottles, *G* – positioning system of nozzle for powder feeding, *H* – shielding gas nozzle, *I* – nozzle for powder feeding

Laser beam for materials used for manufacturing the nozzles (copper and stainless steel) were measured by a spherical method.

Results and discussion. It was found that, the temperature of the tip of the nozzle for powder feeding was stabilized after 6 seconds from the start of laser cladding process. The temperature of the tip of the

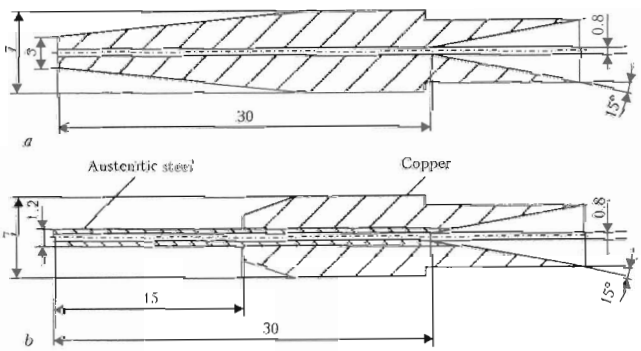


Figure 3. Construction of the nozzle for powder feeding: *a* – nozzle for powder feeding made of copper, *b* – nozzle for powder feeding made of copper body and thin-walled tube made of austenitic stainless steel

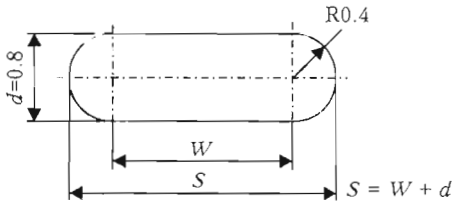


Figure 4. Cross-section of the nozzle for powder feeding with flat outlet

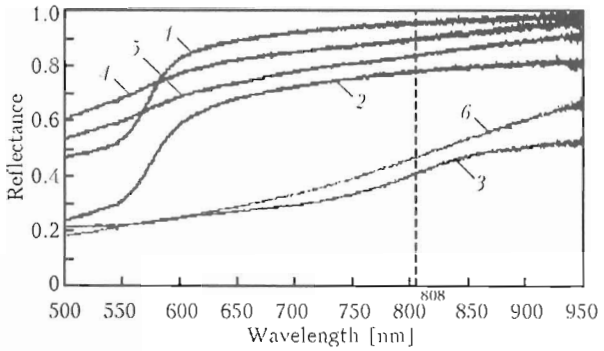


Figure 5. Influence of the material type and surface condition of the nozzle for powder feeding, on the reflection of laser radiation: *1* — polished surface of copper; *2* — surface of copper oxidized at temperature 250 °C; *3* — surface of copper oxidized at temperature 350 °C; *4* — polished surface of austenitic stainless steel; *5* — surface of austenitic stainless steel oxidized at temperature 700 °C; *6* — surface of austenitic stainless steel oxidized at temperature 1100 °C

nozzle for powder feeding does not depend directly on heat input of laser surfacing, but separately on the laser out put power and the surfacing speed. The decrease of the surfacing speed does not cause significant increase of the temperature of the tip of the nozzle for powder feeding, (Figure 7). Significant increase of the temperature of the tip of the nozzle for powder feeding was observed when the laser output power was increased, especially during laser surfacing process along the short side of the rectangular diode laser spot, (Figure 8). It was found that heating of the nozzle for powder feeding is caused mainly by the laser radiation reflected from the surface of the weld pool. A numerical analysis of laser powder surfacing process, [16], showed that the absorption coefficient of HPD laser beam at the weld pool surface is approximately 0.65. Thus, 35% of the output power of the HPD laser beam is reflected from the weld pool surface. Direction of reflected laser beam radiation

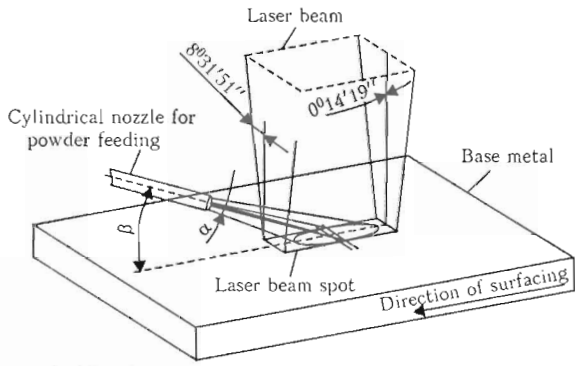


Figure 6. 3D scheme of laser powder surfacing carried out along the long side of the rectangular diode laser spot with powder feeding in front of the weld pool

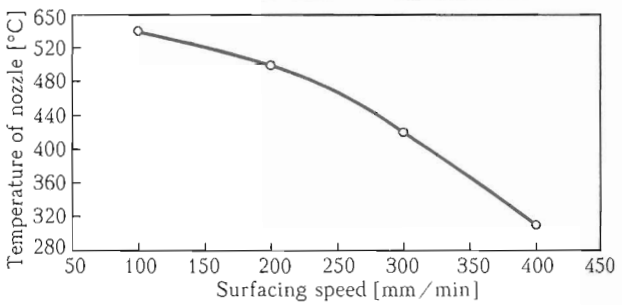


Figure 7. Influence of the surfacing speed of laser powder surfacing process on the temperature of nozzle for powder feeding. Surfacing parameters: laser output power 1000 W, powder feeding rate 8 g/min, distance from weld pool surface to the outlet of nozzle for powder feeding L = 15.0 mm, nozzle inclination angle $\beta = 45^\circ$; surfacing process carried out along the short side of the rectangular diode laser beam with powder feeding in front of the weld pool

depends strongly on the shape of HPD laser beam and shape of the weld pool, (Figure 6).

The study of the construction of the nozzle for powder feeding has shown that the nozzle made of copper was heated more intensive, in spite of very high thermal conductivity, than the nozzle made of copper body and thin-walled tube made of austenitic stainless steel. This phenomenon is a result of reflectivity of the laser energy from the surface of copper. The polished surface of copper reflects 95% of the output power of the HPD laser beam, at ambient temperature. However increase of temperature of the copper surface causes intensive oxidation of the surface and the absorption coefficient of HPD laser radiation is increased, (Figure 5). Heating of the copper nozzle for powder feeding at temperature of 350 °C, in the air atmosphere, causes formation of CuO on the surface of the nozzle tip. Layer of Cu oxides on the copper nozzle decreases the reflection of the HPD laser radiation by approximately 50%. The nozzle for powder feeding made of polished austenitic stainless steel is high oxidation resistant so the absorption of laser radiation is significantly lower, approximately 15%, in wide range of temperature, (Figure 5). Moreover, the area of absorption of the laser radiation is significantly limited when the thin-walled tube of 0.2 mm thick wall is applied. The copper body of the nozzle is not

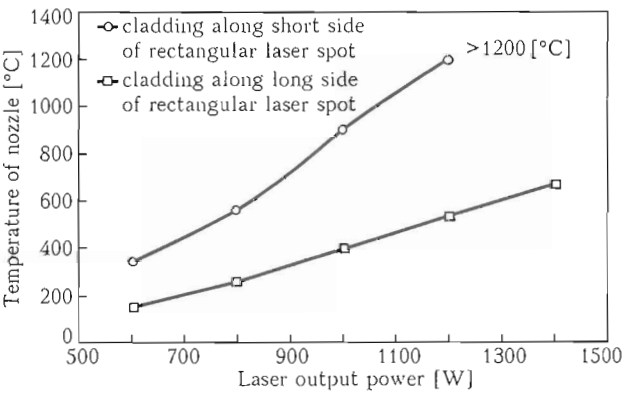


Figure 8. Influence of laser output power and the direction of laser powder surfacing on the temperature of nozzle for powder feeding. Surfacing parameters: surfacing speed 200 mm/min, powder feeding rate 8 g/min, distance from weld pool surface to the outlet of nozzle for powder feeding L = 10.0 mm, nozzle inclination angle $\beta = 45^\circ$

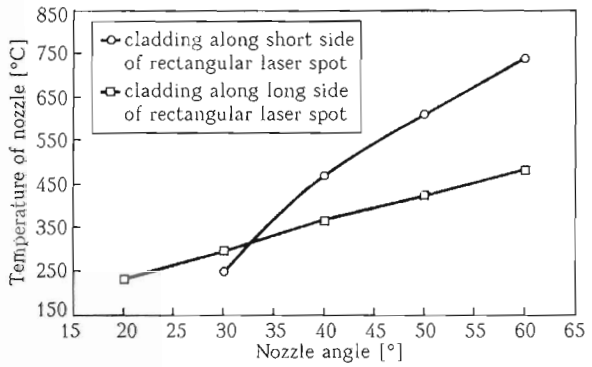


Figure 9. Influence of the nozzle inclination angle and the direction of laser powder surfacing on the temperature of the nozzle for powder feeding. Surfacing parameters: laser output power 1000 W, surfacing speed 200 mm/min, powder feeding rate 6 g/min, distance from the weld pool surface to the outlet of the nozzle for powder feeding: L = 10.0 mm in surfacing along the long side of the rectangular diode laser beam, L = 15.0 mm in cladding along the short side of the rectangular diode laser beam

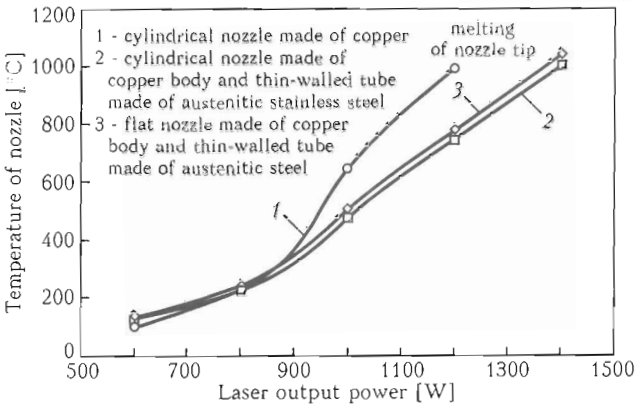


Figure 10. Influence of the construction of the nozzle for powder feeding and laser out put power of laser powder surfacing on the temperature of nozzle for powder feeding. Surfacing parameters: surfacing speed 200 mm/min, powder feeding rate 8 g/min, distance from the weld pool surface to the outlet of nozzle for powder feeding L = 14.0 mm, nozzle inclination angle β = 45°

subjected to laser radiation reflected from the weld pool and also the copper body ensures intensive heat abstraction from the austenitic stainless steel thin-walled tube. The polished surface of austenitic stainless tube ensures high oxidation resistance up to the temperature of 1100 °C. Over the critical temperature the tube surface is oxidized and the absorption of laser radiation is also radically increased. The increase of width (S) of the austenitic stainless steel thin-walled nozzle does not cause significant increase of its temperature. The reason of this phenomenon is that the increase of the external area of nozzle, when the laser radiation is absorbed, causes increase of teh internal area of the nozzle, that is cooled intensively by powder particles and the carrier gas, (Figure 10). The minimum distance from the weld pool surface to the outlet of nozzle for powder feeding, during laser surfacing process carried out along the short side of the rectangular diode laser beam spot with powder feeding in front of the weld pool, ensuring high life time of the nozzle and also high process efficiency is limited to 14.0 mm. Moreover the reflection of the HPD laser radiation from the weld pool surface limits the nozzle inclination angle β to 45°, (Figure 9).

Relative low divergence of the HPD laser beam in the plane parallel to the long side of the rectangular diode laser spot ensures a minimum heating of nozzle for powder feeding during the laser surfacing process carried out along the long side of the rectangular diode laser beam spot with powder feeding in front of the weld pool, (Figure 8). Thus in this case the minimum distance from the weld pool surface to the outlet of the nozzle for powder feeding, ensuring high life time of the nozzle and also high process efficiency, is limited to just 5.0 mm.

Summary. Intensive heating of the outlet of the nozzle tip for powder feeding during the laser powder cladding is mainly caused by the laser radiation reflected from the surface of the weld pool. Long life time of the nozzle for powder feeding and stability of the powder stream during the HPD laser powder surfacing are ensured by nozzle made of materials that are characterized by low absorption of laser radiation in wide range of temperature, e.g. austenitic steel.

Acknowledgment. *The work was supported by the Polish Committee for Science Research (KBN) under contract 4T08C 05125.*

1. Klimpel A.: *Surfacing and thermal spraying.* Technologies. WNT, W-wa. 2000,
2. L. A Dobrzacski, *Metal and material science,* WNT, Warszawa, 2002.
3. Zediker M. S.: *Direct-diode laser competes with Nd:YAG and carbon dioxide.* Industrial Laser Review. 1993, no. 8, s.17.
4. Sepold G., Iinni: *Processing with a 1.4 kW diode laser.* Industrial Laser Review. 1997, no. 12, s. 19–20.
5. Nicey T.: *Diode lasers offer welding advantages.* Welding Journal, vol. 80, 2001, no 6, s. 29–30.
6. Yellup J. M.: *Laser cladding using the powder blowing technique.* Surface and Coatings Technology, 1995, nr 71.
7. Lin J.: *A simple model of powder catchment in coaxial laser cladding.* Optics and Lasers Technology, 1999, nr 31.
8. Lin J., Hwang B. C.: *Coaxial laser cladding on an inclined substrate.* Optics and Lasers Technology, 1999, nr 31.
9. Lin J., Hwang B. C.: *Clad profiles in edge welding using a coaxial power filler nozzle.* Optics and Lasers Technology, 2001, nr 33.
10. Kathuria Y. P.: *Some aspects of laser surface cladding in the turbine industry.* Surface and Coatings Technology 132 (2000).
11. Shepeleva L., Medres B., Kaplan W. D., Bamberger M., Weisheit A.: *Laser cladding of turbine blades.* Surface and Coatings Technology 125 (2000).
12. Lin J.: *A simple model of catchment in coaxial laser cladding.* Surface and Coatings Technology 31 (1999).
13. Powell J., Henry P. S., Steen W. M.: *Laser cladding with preplaced powder: analysis of thermal cycling and dilution effects.* Surface Engineering, 1988, nr 2.
14. Picasso M., Iinni: *A simple but realistic model of laser cladding.* Metallurgical and Materials Transactions B, 1994, nr 25B.
15. Wu. X., Iinni: *Critical state of laser cladding with powder auto-feeding.* Surface and Coatings Technology, 1996, nr 79.
16. Janicki D.: *High power diode laser powder cladding of tool steel.* PhD dissertation, Silesian University of Technology, Gliwice 2003.

MODIFICATION OF SURFACE LAYER PROPERTIES BY LASER ALLOYING COMBINED WITH BURNISHING

J. RADZIEJEWSKA, W. KALITA, A. BARTOSZEWICZ
Institute of Fundamental Technological Research of PAS, Warsaw, Poland

Introduction. One kind of Laser Beam Machining [LBM] is the formation of alloying layers of improved properties. The advantages of laser alloying in comparison with other methods of surface layer modification are: high speed machining, a possibility of performing the process in atmosphere, the modification of smaller fragments of the surface freely selected (responsible for the durability of the tools and parts of mechanisms) as well as saving on the costs of material. Chemical composition, thickness and other features of the layers can be then regulated by a specific choice of the introduced elements, their amount and also by a selected set of the machining process parameters [1, 2].

The disadvantages of the LBM are the large costs of the high power lasers and the relatively high roughness of the surface after the process [2, 3, 4]. In most published works concerning laser machining related to the melting process, the problem of geometrical structure of the surface is usually omitted, despite the fact that the microgeometry of surface is an essential element describing many functional features of the machine parts. In practice an abrasive treatment of the surface is performed after LBM. However, it results in the removal of some of the formed alloying layers, which reduces a part of the positive effects of the LBM.

The results of works [5, 6] have shown that surface roughness values obtained in the alloying process are too high to apply elements without an additional abrasive machining, even at the optimal parameters of the laser treatment. Therefore, a combining of the alloying process with the burnishing process both performed at the laser stage was proposed in the work.

The aim of the work was to reduce surface roughness formed in the laser alloying process and inducement of compressive stresses.

The experiment description. The alloying process was performed on samples made of carbon steel, which had a cobalt satellite layer, 0.03 mm thick, deposited prior to treatment. The surface of samples was melted with a beam of a continuous laser CO_2, the power of which was 2 kW and two different velocities of sample motion in reference to the beam were applied: 100 mm/min and 200 mm/min. It varied time of beam interaction with material as well as temperature distribution on alloyed surface. A micro burnishing device was attached to the stage behind the laser beam.

Figure 1 presents a diagram of the machining. The device for burnishing is attached behind the laser beam. The burnishing elements made of sintered carbides are rounded with 1.5 mm radius and they are pressed against the surface using springs. Spring force on the burnishing element is controlled within the range of 50–300 N. The machining can be performed at two speeds of rotation 200, 550 rot/min. It is possible to control the position of the burnishing tool in relation to the laser beam axis, which enables us to perform the mechanical processing of the alloyed area in various temperatures. The burnishing element

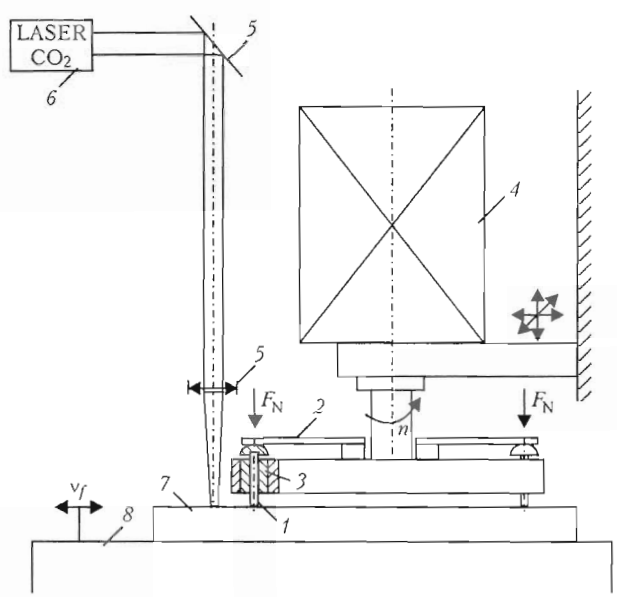


Figure 1. Diagram of the stage for laser-mechanical machining: *1* – burnishing element; *2* – springs; *3* – slide bearing; *4* – motor; *5* – mirror; *6* – CO_2-laser; *7* – specimen; *8* – laser machine table; F_N – spring force on burnishing element

Table 1. Values of 3-D roughness parameters for the whole alloyed area

V_f, mm/min	x, mm	S_a, μm	S_p, μm	S_y, μm
100		43	176	398
	4	19	78	193
	6	17	75	215
	8	21	80	252
200		30	130	252
	4	27	63	178
	6	40	71	236
	8	38	64	228

© J. RADZIEJEWSKA, W. KALITA, A. BARTOSZEWICZ, 2005

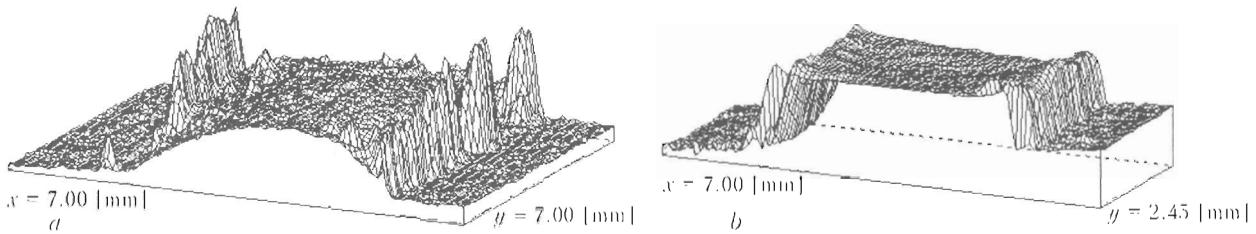


Figure 2. View of the surface obtained from scanning the profilometer: *a* — after laser alloying with speed 100 mm/min of laser beam, *b* — after alloying and burnishing

was placed at a distance of 4, 6, 8 mm from the laser beam axis.

The laser-mechanical machining was performed for the case of steel alloying with stellite cobalt at two different velocities of the alloying process: 100 and 200 mm/min at power density of laser radiation equal to $5 \cdot 10^4$ W/cm^2.

The experimental results. Measurement of surface geometrical structure was performed on a scanning profilometer after the alloying process. The thickness and microstructure of formed surface layer was determined on the basis of a cross-section made perpendicularly to the sample motion direction.

With regard to the specific geometrical structure of the surface, which forms after laser alloying roughness, parameters were determined for two regions:

- region includes the whole path; for this region the 3-D height roughness parameters were determined: S_a, S_p, S_y;
- central region in this region the 2-D profile measurements along the «axis» of path were performed, e.g. parallel to the sample motion direction, the measuring length was 12 mm depending on the roughness height; 5 profiles were recorded and then the following 2-D roughness parameters were determined and analyzed: for the unfiltered profile: P_a, P_z and for the filtered profile: roughness parameters R_a, R_z, and waviness parameters W_a, W_t. Table 1 presents the 3-D parameters determined for the hole zones, whereas Table 2 contains the 2-D parameters of roughness and waviness in central zone.

Following the process measurements of surface geometrical structure were performed on scanning profilometer. The values of 3D roughness parameters S_a, S_p, S_y, are presented in Table 1. Figures 2, *a* and *b* show the views of surface after laser alloying and after laser-mechanical treatment.

A change in shape of melted zone due to burnishing is noticeable. The heights of asperities at the boundary of the alloying zone decreased significantly while the shape of asperities in the central area of the melting underwent «flattening». The most noticeable changes

Table 2. Values of profile parameters of roughness and waviness along the laser path. Cut-off 2.5.

V_l, mm/min	x, mm	P_a	P_z	R_a	R_z	W_a	W_t
100		26	113	7	60	23	94
	4	12.3	65	4.9	34	10.3	41
	6	9.6	46	3.5	23	8.4	30
	8	11.3	56	4.1	30	10	32
200		14	63	4	34	13	45
	4	10.3	50	4.9	26	8	32
	6	15.6	68	5.1	36	13	45
	8	11	54	1.5	26	12	46

in surface geometry were observed when the process was performed at a distance of 4 and 6 mm from the beam axis. For larger distances the geometry change occurred mainly in the central zone of the melting where the temperature was the highest, while the maximal asperity heights, S_y, recognized at the boundary with unmelted material had the lowest temperature while mechanical treatment and therefore underwent lower cold work. The effect is well represented by a change of roughness parameters S_a and S_y, which is depicted in Figure 3.

In case of the laser-mechanical machining with two times larger alloying velocity — 200 mm/min a substantial reduction in asperity heights was noticed at the lowest distance between the tool and the laser beam, 4 mm, which is shown in Figure 4. The para-

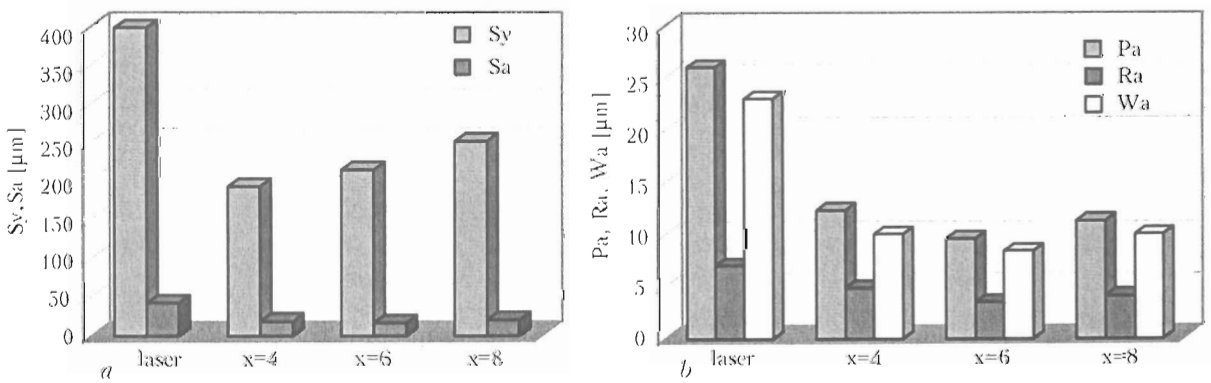


Figure 3. Change in 3D (*a*) and profile roughness parameters (*b*) as function of the distance between the burnishing tool and the beam axis; Stellite alloying at 100 mm/min velosity

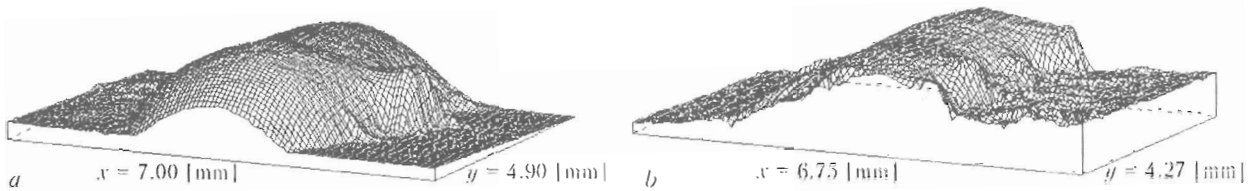


Figure 4. View of surface obtained from scanning profilometer: *a* — after laser alloying with speed 200 mm/min of laser beam, *b* — after alloying and micro burnishing

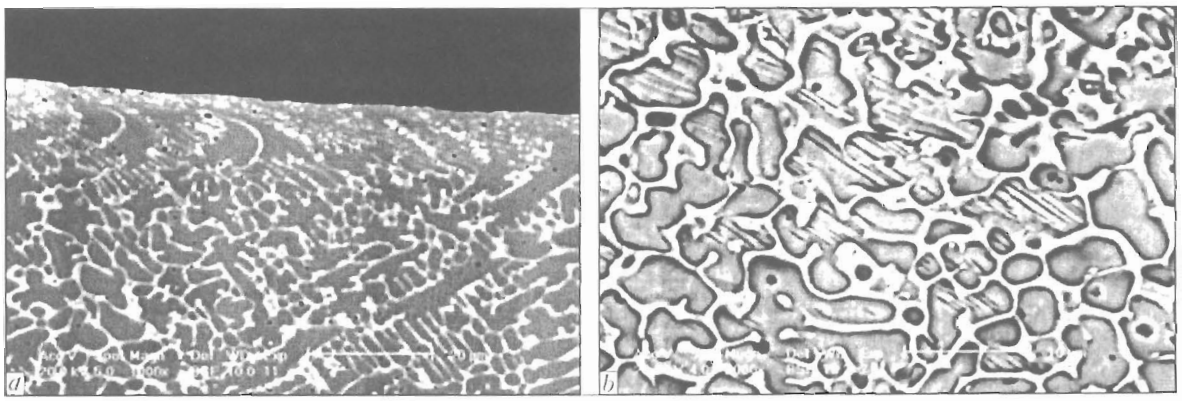


Figure 5. Microstructure of alloyed layer: *a* — structure of deformed grains, *b* — slip bands 50 μm below the surface

meter analysis of 3D roughness as a function of the distance between the tool and the laser beam indicates that the highest single asperities of the melted zone have the most their size. Roughness and waviness of surface in the central zone of the melting is also lower only for the closest position of the tool and the laser beam. In this case we could observe asymmetric shape of the melting, which was due to a larger difference in temperature on the surface between the output and input of the burnishing tool in the alloying zone compared with the machining at lower velocity.

The microstructure tests of material were made on the scanning microscope. The structure analysis performed on microsections perpendicular to the motion of specimen has shown intensely deformed grains 20 μm thick beneath the surface — Figure 5, *a*.The direction of deformation is the same as the direction of the burnishing tool machining. In the layer of 50–80 μm thick many slip bands were observe and hardness of the layer material has increased. This is shown in Figure 5, *b*.

The results of microhardness measurements (perpendicular to the surface) have revealed that in the zone around 100 μm thick below the surface the microhardness of material is 620 $HV_{0.02}$ and it is higher than of the rest the melted zone (550 $HV_{0.02}$). The noticed slip bands and the increase in hardness can indicate occurrence of stresses in the layer 100 μm thick, however there is a necessity to verify the observation.

CONCLUSIONS

The presented results of the laser alloying process combined with the micro burnishing can provide two times reduction of surface roughness heights in reference to the values of asperity heights obtained in the alloying process. The shape of the melted zone has improved as well. The layers obtained in the alloying process combined with burnishing have improved the structure, its hardness has increased and the cracks in surface layer were not detected.

1. Grigorijanc A. G., Safonow A. H.: *Metody Powerhnostnoj Lazernoj Obrabotki*, (1989), Lazernaja Technika i Technologia.
2. Viedenov A. A., Gladusz G. G.: *Fizyczeskije Processy pri Lazernoj Obrabotke Materialow*, Energoatomizdat, (1985), Moskwa.
3. Anthony T. R., Cline H. E.: *Surface Rippling Induced by Surface-Tension Gradients During Laser Surface Melting and Alloying*, J. Appl. Phys., 48, (1977), 9.
4. Arutiunian R. W., et. al.: *Wozdejstwie Lazernogo Izluczenia na Materialy*, «Nauka», (1989),Moskwa.
5. Gladusz G. G., et. al.: *Termokapilliarnaja Konwekcija w Zidkosti pod Dejstwiem Moszcznogo Lazernogo Izluczenija*, 9, (1982) Kwantowaja Elektronika, 4.
6. Radziejewska J.: *«The application of the surface topography measurement for the laser alloying process description»*, X International Colloquium on Surfaces, January 2000. Chemnitz.

Conference Sponsors

PWI Laser Systems and Technology Center

Ministry of Education and Science of Ukraine

Information Support

«The Paton Welding Journal»

www.nas.gov.ua/pwj

Conference Sponsors

PWI Laser Systems and Technology Center

Ministry of Education and Science of Ukraine

Information Support

«The Paton Welding Journal»

www.nas.gov.ua/pwj

LASER WELDING AND FORMABILITY STUDY OF TAILOR-WELDED BLANKS OF DIFFERENT THICKNESS COMBINATIONS AND WELDING ORIENTATIONS

C. H. CHENG[1], L. C. CHAN[1], C. L. CHOW[2], T. C. LEE[1]
[1]Department of Industrial and Systems Engineering, Hong Kong Polytechnic University, China
[2]Department of Mechanical Engineering, University of Michigan-Dearborn, USA

Tailor-welded Blanks (TWBs) are tailor-made for different complex component designs by welding multiple metal sheets with different thicknesses, shapes or strengths prior forming. However, the forming performance of an intrinsic TWB is critically related to its own structures and designs, such as the thickness combination, as well as the location and orientation of weldment. In this study, a 2kW Nd:YAG laser were used to butt-weld approximately 180 samples of stainless steel (AISI 304) TWBs with different dimensions (i.e., from 12.7 mm to 165.1 mm in width), thickness combinations (i.e., 1/1 mm, 1/1.2 mm, 1/1.5 mm, 1.2/1.2 mm, 1.2/1.5 mm and 1.5/1.5 mm) and welding orientations (i.e., 0°, 45° and 90°). Subsequently, Swift forming tests were carried out to study the forming performance of those TWBs. It was found that the formability of TWBs critically related to the quality of weld was very much affected by the welding parameters of the Nd:YAG laser. Also, the effects of different thickness combinations on the formability of TWBs were investigated through the constructed forming limit diagrams (FLDs). The results showed that the thinner part of TWBs dominated the majority of deformation similar to the FLD of the parent metal. The effects of different welding orientations on the forming performance of TWBs were examined from the failure analysis.

Introduction. The use of tailor-welded blanks (TWBs) has increased in practice in the automotive industry and it is being introduced to other potential industrial applications, such as electrical goods, package and construction markets [1]. As TWBs are usually tailor-made for different components, the forming performance of the TWBs is a major concern for the industry who implements TWBs in their production. In recent years, researchers have analyzed the forming performance of steel TWBs using different tests. Saunders and Wagoner [2] have identified two failure modes of TWBs and indicated that the press formability of TWBs related to the changing deformation patterns depended on the differential strength of TWBs. Heo et al. [3] indicated that a higher thickness strain distribution led to a larger movement of weld line during deep drawing. Also, Chan et al. [4] claimed that the formability of TWB decreased against the increase of the thickness ratio of a TWB. Thus, in this paper, an effective laser-welding process of stainless steel (AISI 304) TWBs with different welding orientations and thickness combinations is presented, while the effects of welding orientation and thickness combination on the formability of TWBs are investigated.

Laser wedling of twbs. In this study, AISI 304 stainless steel TWBs were butt-welded using a 2kW Nd:YAG laser. Three stainless steel sheets with thicknesses of 1.0mm, 1.2mm and 1.5mm were used to produce approximately 180 samples of TWBs having different welding orientations (i.e., 0°, 45° and 90°) and thickness combinations (i.e., 1/1 mm, 1/1.2 mm, 1/1.5 mm, 1.2/1.2 mm, 1.2/1.5 mm and 1.5/1.5 mm). Before the laser welding, the edges of the specimens to be welded were milled and degreased to attain the clean edges without any burrs, contaminates, or oils. Each pair of specimens was assembled on a welding fixture for laser-beam alignment and specimen fit-up, as shown in Figure 1. After exhaustive welding trials, the optimal welding parameters of TWBs for each thickness combinations were identified. In accordance with the British Standards EN ISO 13919-1 and 15614-11, the weld integrity was examined with respect to the conditions of weld surface and cross-sectional weld profile, while the general mechanical properties of the TWBs were measured using the tensile test.

Formability test of twbs. The formability of those produced TWBs was studied using the Swift forming test. FLDs were constructed by the major and minor strains measured from the TWB specimens with different widths, whilst the forming behavior and the failure modes of the TWBs were also investigated. The effects of every welding orientation and the thickness ratio were analyzed accordingly. Despite different orientations, almost all the welds were located in the center of TWBs, as shown in Figure 2. A forming tester with a hemispheric punch (50 mm in diameter)

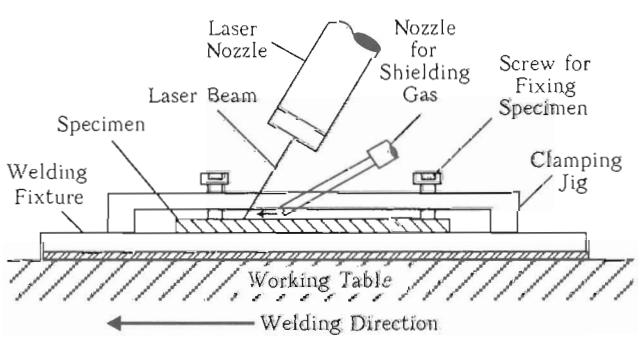


Figure 1. Schematic diagram of the welding

© C.H. CHENG, L T CHAN, C.L. CHOW, T.C. LEE, 2005

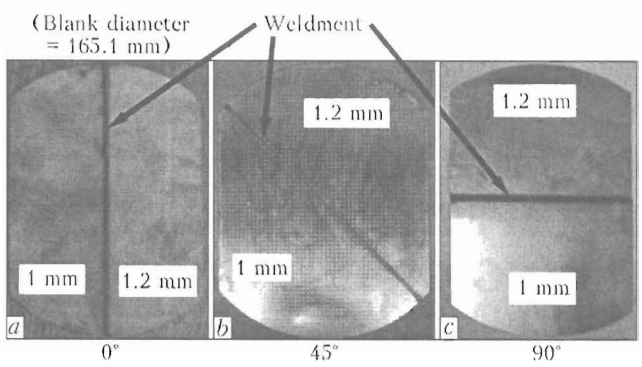


Figure 2. TWBs with different welding orientations

was used while a large blank-holding force of 100 kN was applied to control the material flow. In order to balance the thickness difference within a TWB, tailor-made spacers were designed and applied during the test.

Results and discussion. *Results of laser welding.* After exhaustive trials, AISI 304 stainless steel TWBs with different welding orientations (i.e., 0°, 45° and 90°), thickness combinations (i.e., 1/1 mm, 1/1.2 mm, 1/1.5 mm, 1.2/1.2 mm, 1.2/1.5 mm and 1.5/1.5 mm) and specimen widths (i.e., from 12.7 mm to 165.1 mm) were produced using the 2kW Nd:YAG laser, as some samples were shown in Figure 2. The optimal sets of welding parameters for welding TWBs with different thickness combinations are listed in Table 1. It is apparent that the optimal welding parameters can be obtained by only varying the welding speed according to the total thickness of base metals on both sides of TWB, whereas a lower welding speed is employed for a thicker material. Meanwhile, the laser power could be fixed within a narrow range from 1000 W to 1100 W. For all thickness combinations, the laser beam was focused on the joint of the top surface of the specimen or the thicker base metal while Argon gas with a flow rate of 20 L/min was used for shielding.

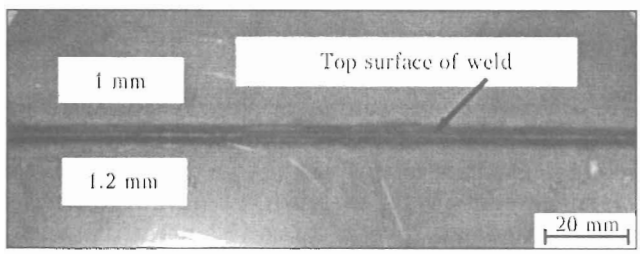


Figure 3. Weld surface of TWB produced under optimal parameters

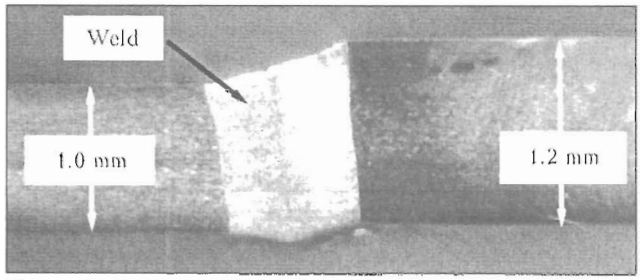


Figure 4. Cross-sectional weld profile of TWB produced under optimal parameters

Table 1. Optimal welding parameters

Thickness combination	Laser power	Welding speed	Focus	Shielding gas
1/1 mm	1100W	27 mm/s	Surface	Argon (20 L/min)
1.2/1.2 mm	1000W	23 mm/s		
1.5/1.5 mm	1100W	15 mm/s		
1/1.2 mm	1000W	25 mm/s	Surface of thicker base metal	
1/1.5 mm	1100W	20 mm/s		
1.2/1.5 mm	1100W	15 mm/s		

Figures 3 and 4 show, respectively, the weld surface and the cross-sectional weld profile obtained from a TWB (i.e., 1.2/1.5 mm) welded using a set of the optimal parameters. The weld surface was found clean and continuous throughout the entire length of the TWB without any observed cracks or porosity, while an acceptable weld profile was attained without any defect such as underfill, undercut or weld-sagging. The tensile properties of the TWBs with different thickness combinations of transversal welds were evaluated using subsize specimens of TWBs. The tensile test was carried out under a constant cross-head speed of 1mm/min until the initiation of localized necking. As shown Figure 5, most failures were typically found in the base metal rather than the weld or the heat-affected zone (HAZs), indicating that the acceptable welds, as well as the quality TWB, can be obtained using such welding parameters. The stress-strain curves of the TWBs were measured as shown in Figure 6. The curves (1), (2) and (3) showed that the TWBs with similar thickness combinations (i.e., 1.0/1.0 mm, 1.2/1.2 mm and 1.5/1.5 mm) possessed similar stress and strain values as those of their base metals. However, for the TWBs with dissimilar thickness combinations (i.e., 1.0/1.2 mm, 1.0/1.5 mm and 1.2/1.5 mm), a larger difference in thickness with the TWB resulted in lower strain values, as shown in curves (3), (4) and (5) in Figure 6. This was because the deformations of TWBs were predominated by the thinner base metals, as shown in Figure 5.

Results of formability test. Swift forming tests were carried out to study the forming behavior of the TWBs, as well as their formability. Figure 7 shows the formed TWBs (thickness combination of 1/1.2 mm) with different welding orientations. It was found that the locations of failures for all the TWBs with different welding orientations were similar and all the

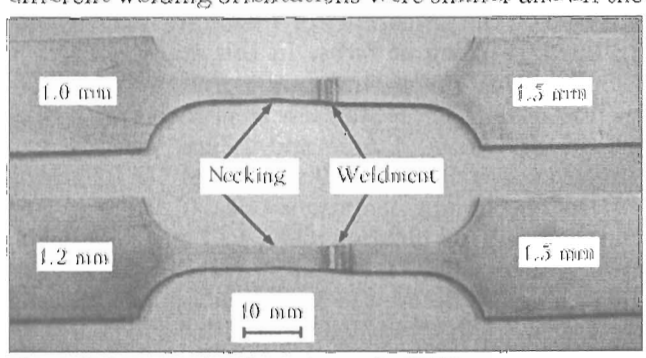


Figure 5. Some results of tensile test for TWBs

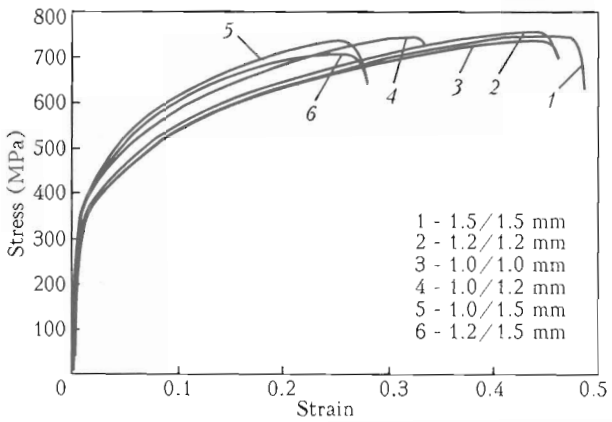


Figure 6. Tensile curves for TWBs with different thickness combinations

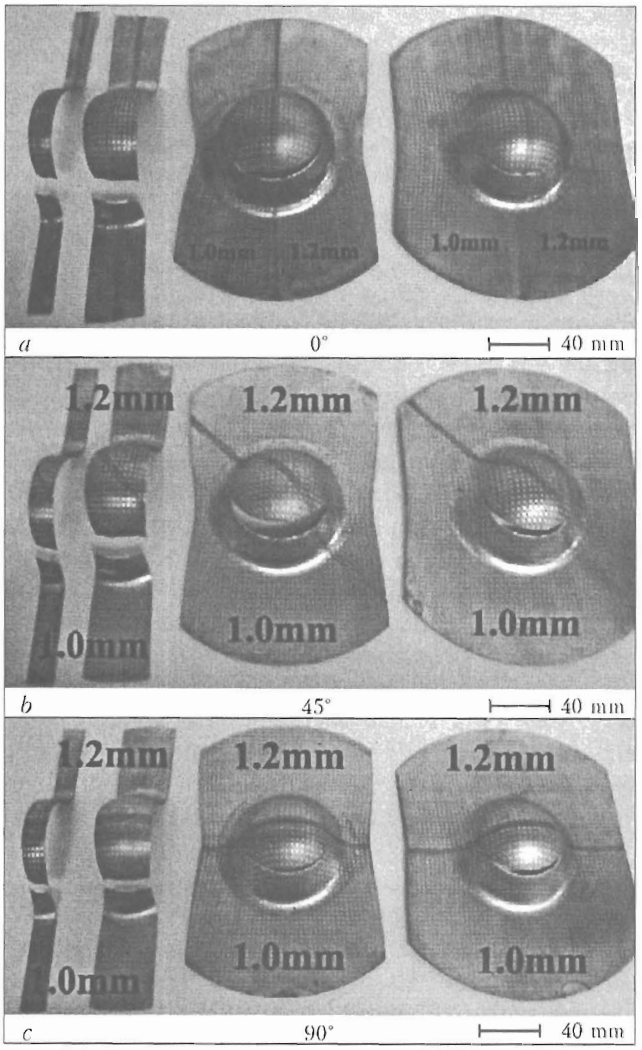


Figure 7. Formed TWBs with different welding orientations

failures propagated perpendicular to the major loading direction. Failures of TWBs with 45° and 90° welding orientations (Figs. 7, *b* and 7, *c*) were found to occur in their thinner base metal away from the weld, while failures initiated at the weld of the TWBs with 0° welds (Figure 7, *a*). Thus, the quality welds with different orientations may be concluded to have insignificant effect on the forming behavior and the failure mode of TWBs as the failures mainly occur in

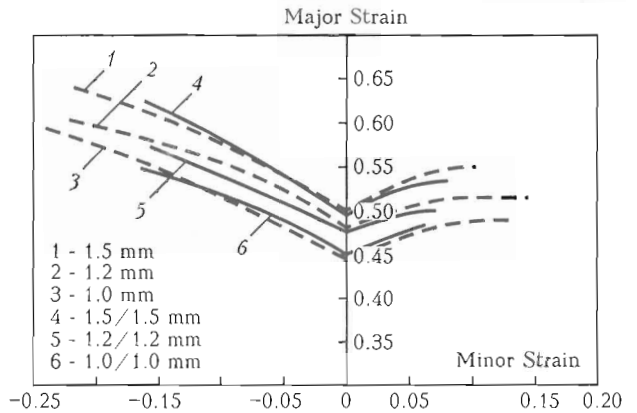


Figure 8. FLDs of stainless steel TWBs (welding orientation of 90°) with similar thickness combinations

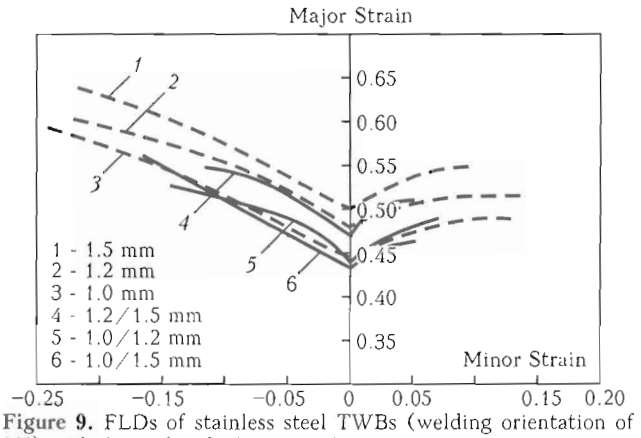


Figure 9. FLDs of stainless steel TWBs (welding orientation of 90°) with dissimilar thickness combinations

the thinner base metals perpendicular to the major loading direction.

In order to study the formability of the TWBs, their FLDs were constructed by measuring the major and minor strains of circular pre-printed grids on the surface of TWBs. Figures 8 and 9 show, respectively, the FLDs of TWBs (welding orientation of 90°) with both similar and dissimilar thickness combinations. Comparing to the FLDs of base metals (i.e., curves in dotted line), the TWBs with similar thickness combinations possessed the similar formability as their corresponding base metals. This revealed that the weldments with 90° orientation to the major loading direction had slight effect to the TWBs with similar thickness combinations. As shown in Figure 7, *c*, most of the failures in TWBs with dissimilar thickness combinations located in the thinner base metal so that similar FLDs were obtained as those of their thinner base metals.

CONCLUSIONS

In this study, AISI 304 stainless steel TWBs with different welding orientations and thickness combinations were produced using a 2kW Nd:YAG. Optimal set of welding parameters for different thickness combinations were identified based on the weld integrity and the tensile properties of the TWBs. On the other hand, similar failure modes were observed

on the TWBs with different welding orientations. Once the quality weld is attained, failure generally occurs in the thinner base metal of TWB similar to the FLDs of their corresponding thinner base metal. One may also conclude that the FLD alone was not able to reveal any meaningful limit strain data of TWB made of dissimilar thickness combination.

Acknowledgment. *The work described in this paper was partially supported by grants from the Research Grants Council of the Hong Kong Special Administrative Region, China (Project No. PolyU 5178 / 01E) and the Research Committee of the Hong Kong Polytechnic University (Project No. G-T906).*

1. R. J. Pallett and R. J. Lark, «*The use of tailored blanks in the manufacture of construction components*», Journal of Materials Processing Technology, 117, p. 249–254 (2001).
2. Saunders, F. I., and Wagoner, R. H., 1996, «*Forming of Tailor-Welded Blanks*» Metallurgical and Materials Transactions A, 27A, pp. 2605–2615.
3. Y. Heo, Y. Choi, H. Y. Kim and D. Seo, «*Characteristics of weld line movements for the deep drawing with drawbeads of tailor-welded blanks*», Journal of Materials Processing Technology, 111, p. 164–169 (2001).
4. S. M. Chan, L. C Chan and T.C. Lee, «*Tailor-welded blanks of different thickness ratios effects on forming limit diagrams*», Journal of Materials Processing Technology, 132, p. 95–101 (2003).

TRUE STRESS-STRAIN ANALYSIS ON WELDMENT OF HETEROGENEOUS TAILOR-WELDED BLANKS — AN EXPERIMENTAL APPROACH

C. H. CHENG[1], L. C. CHAN[1], C. L. CHOW[2], T. C. LEE[1]
[1]Department of Industrial and Systems Engineering, Hong Kong Polytechnic University, China
[2]Department of Mechanical Engineering, University of Michigan-Dearborn, USA

Laser welding technique is widely adopted to produce tailor-welded blank (TWB). However, due to the thickness difference of welded blanks and the existence of their weldment, TWBs should be considered as heterogeneous structures. Therefore, for more accurate assessment of TWBs, the properties of the parent metals and their weldment should be considered independently rather than that of an entire TWB. This paper presents a novel experimental approach to acquire the independent tensile properties of the weldment. Specially specimens were designed and cut from the AISI 304 stainless steel TWBs with a thickness combination of 1 mm/1.2 mm for the tensile test. A real-time microscopic recording system is used to analyze the relationship between the deformation of the laser-marked circular grids premade on the weldment and the applied load. Eventually, the true stress-strain curve of the weldment of the TWB can be successfully measured.

Introduction. In order to achieve the maximum forming performance of TWBs, a variety of experimental studies and finite element analyses (FEA) were carried out to determine mechanical properties of the TWBs, as well as their formability and forming behavior. However, due to the difficulty of assessing the weld of an indiscernible size, the independent properties of the weldment have sometimes been neglected while their distinctive effects have also not been taken fully into account in the formability analysis. In particular, the weldment in steel TWBs is typically stronger than the base metals [1]. Abdullah et al. [2] and Zhang et al. [3] have evaluated the mechanical properties of weldment in the steel TWBs, respectively, using the rule of mixtures and the load separation principle on a notched specimen. However, all these studies have evaluated the weldment properties based on the concurrent mathematical models of the homogeneous material.

In view of the above shortcomings, this paper is intended to present an experimental method of analysis to accurately determine the true stress-strain data of the weldment in a heterogeneous TWB. The method employs a real-time microscopic recording system. From the localized deformation of laser-marked circular grids, the true stress-strain relationship of the weldment was analyzed after the measurement of the localized deformation and the computation of the applied load.

Experimental procedures. *TWB and Weldment.* AISI 304 stainless steel blanks with thicknesses of 1.0 mm and 1.2 mm were used to produce the TWBs (Figure 1). A 2 kW Nd:YAG laser was selected to butt-weld the TWBs with a thickness combination of 1.0 mm/1.2 mm. Applying continuous-wave (CW) laser with power of 1000 W and traveling speed of 25 mm/s, the optimal welding parameters were identified. Argon gas with a flow rate of 20 L/min was used for shielding the weld pool during welding. The weld quality of TWBs was examined by a conventional tensile test of the specimen with a transversal weldment. As shown in Figure 2, failure was found on the thinner base metal away from the weldment, indica-

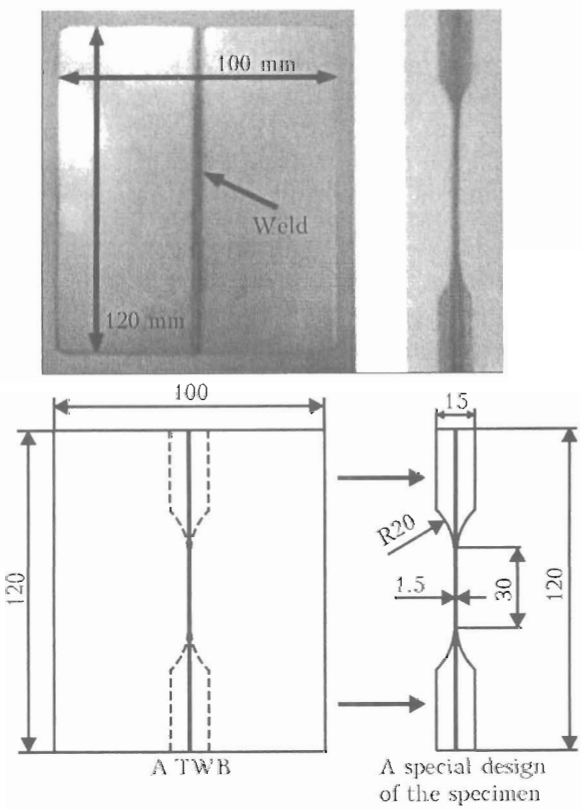


Figure 1. Stainless steel TWB and design of specimen for tensile test

© T. H. CHENG, L. T. CHAN, T. L. CHOW, T. C. LEE, 2005

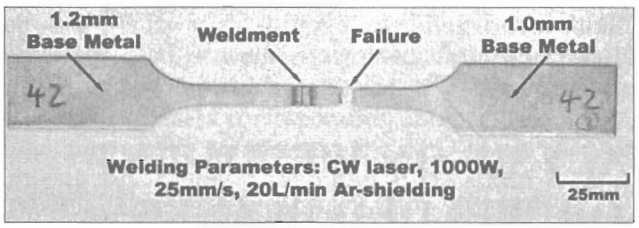


Figure 2. Result of tensile test on TWB with transversal weldment

ting that the weldment is typically stronger than the base metals.

Design of specimen and tensile test. In order to acquire the independent stress-strain data of weldment, a special tensile specimen of TWB (Figure 1) was designed and cut precisely from the TWB produced using the wire-EDM. The gage width of the designed specimen is approximately equal to the width of weldment (i.e., 1.50 ± 0.05 mm) to ensure that the entire gage length of specimen was made of welded material. This was done to ensure that the effects of

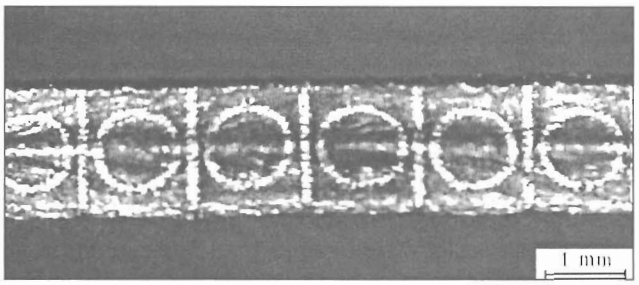


Figure 3. Row of circular laser-marked grids on the surface of weldment

base metals and HAZs could be eliminated. A tensile test was carried out under a constant cross-head speed of 1 mm/min until the threshold of localized necking.

In order to observe the deformation of weldment during the test, a row of circular grids (Figure 3) with a diameter of 1.0 mm and a depth of 10 μm were laser-marked on the bottom surface along the weldment. The circular laser-marked grids were produced by a 90 W Nd:YAG laser marker using a parameter setting of (i) a current of 12 A, (ii) a traveling speed of 10 mm/s, (iii) a pulse frequency of 1000 Hz, and (iv) three repetitions of marking cycle.

Determination of true stress-strain data for weldment. *Real-time microscopic recording system.* During the tensile testing, the circular laser-marked grids on the surface of the weldment were found to distort and deform during the stretching of the specimen. A real-time microscopic recording system was developed and employed to record the information required for determining the true stress-strain data of the weldment (Figure 4). The recording was consisted of two systems.

For division I (D-I) system, a Mitutoyo microscope equipped with a 2X magnification lens was mounted on a tailor-made adjustable stand in front of the specimen for capturing the deformation of circular grids. During the tensile test, the progressive deformation

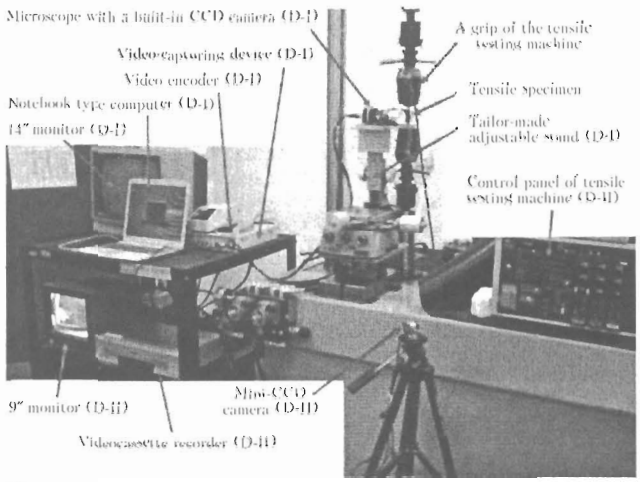


Figure 4. Real-time microscopic recording system

of the circular grids laser-marked on weldment was clearly observed and captured by a built-in CCD camera in the microscope. The major strains of the deformed circular grids were measured from the captured images (Figure 5, *a*) using an image processing software which could digitize data from an image to numerical values. Actually, only the circular grid (Figure 6) where localized necking occurred was considered because only the data obtained from this grid could reveal the entire localized deformation of weldment.

For division II (D-II) system, a mini-CCD camera and a videocassette recorder were used to record the variation of the applied tensile load on specimen, which was instantaneously displayed on the control panel of the MTS machine (Figure 5, *b*). In order to synchronize both the captured images from two system divisions, their recording procedures were activated simultaneously at the start of the tensile test such that

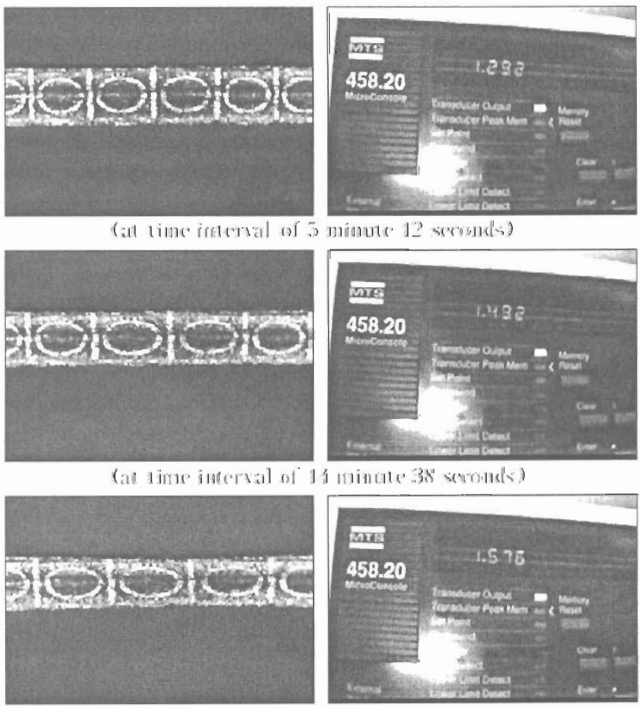


Figure 5. Some captured images from the recording system

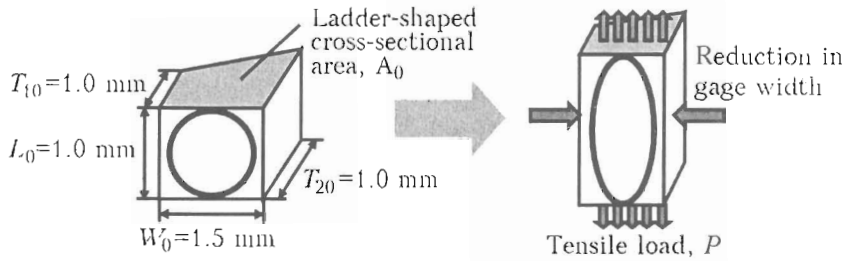


Figure 6. Deformation of circular grid under constant volume assumption

the images would be correlated at the same time intervals, as shown in Figure 5.

Computation of true stress-strain data. Based on the measured major strain values of circular grid and their corresponding tensile loads, the true stress-strain data of the weldment were computed accordingly. As shown in Figure 6, only the materials beyond the circular grid where localized necking occurred were chosen for the computation. It is assumed that the applied tensile load was evenly distributed at the ladder-shaped cross-sectional area, A_0, of the gage, as shown in Figure 6, with an upper edge of 1.0 mm (i.e. thickness of thinner base metal in the TWB, T_{10}), a lower edge of 1.2 mm (i.e. thickness of thicker base metal in the TWB, T_{20}) and a width of 1.5 mm (i.e., the width of gage, W_0).

$$A_0 = \frac{W_0(T_{10} + T_{20})}{2} \qquad (1)$$

In the elastic deformation, $\tilde{\varepsilon}$ and $\tilde{\sigma}$ data of the weldment are the same as their engineering values. However, in the plastic region, $\tilde{\varepsilon}$ and $\tilde{\sigma}$ data are of significantly importance, while they can be calculated using the constant volume assumption.

$$AL = A_0L_0 \qquad (2)$$

where A, L and L_0 are the instantaneous cross-sectional area of the gage, the instantaneous major strain and the original diameter of circular grid, respectively.

$$A = \frac{A_0L_0}{L} = \frac{W_0L_0(T_{10} + T_{20})}{2L} \qquad (3)$$

Then,

$$\tilde{\sigma} = \frac{P}{A} = \frac{2PL}{W_0L_0(T_{10} + T_{20})} \text{ and } \tilde{\varepsilon} = \int_{L_0}^{L} \frac{dL}{L} = \ln\frac{L}{L_0} \qquad (4) \text{ and } (5)$$

where P is the applied tensile load changing with the time.

It should be noted that computation of $\tilde{\varepsilon}$ and $\tilde{\sigma}$ data in plastic deformation is based on the constant volume assumption prior to localized necking.

Results and discussion. *Validation of Methodology.* In order to evaluate the validity of the experimental method developed in this study, the standard tensile testing of the AISI 304 stainless steel blanks without welding was carried out. The $\tilde{\varepsilon} - \tilde{\sigma}$ curves were measured directly from the MTS machine. Both the laser grid and standard tensile measured curves were compared in Figure 7. It can be observed from the figure that the curve profile of the experimental $\tilde{\varepsilon} - \tilde{\sigma}$ curves from both methods shows excellent agreement, including yield stress, ultimate tensile stress and necking strain.

True stress-strain curve of weldment. By using the proposed approach in this study, the experimental $\tilde{\varepsilon} - \tilde{\sigma}$ curve (i.e. curve (1) in Figure 8) of the weldment in our TWBs with a thickness combination of 1.0 mm/1.2 mm was successfully determined. It is found that the weldment has a significantly higher necking $\tilde{\varepsilon}$ (~1281 MPa) than that of the 1.0 mm base metal (~1103 MPa) and 1.2 mm base metal (~1180 MPa), while its necking a (~0.35) is slightly lower (~0.37 and ~0.39). The data revealed that, after laser welding, the weldment metal has been hardened and become the strongest region in the TWBs to sustain the highest loading during the tensile test. This

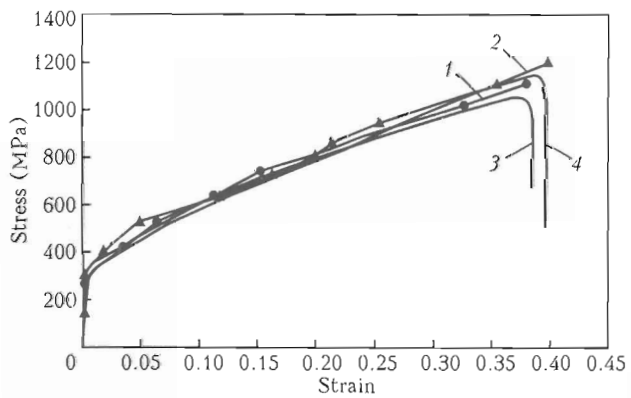


Figure 7. Experimental and measured $\tilde{\varepsilon} - \tilde{\sigma}$ curves of base metals: *1* — 1.0 mm, *2* — 1.2 mm; *3* — 1.0 mm, *4* — 1.2 mm

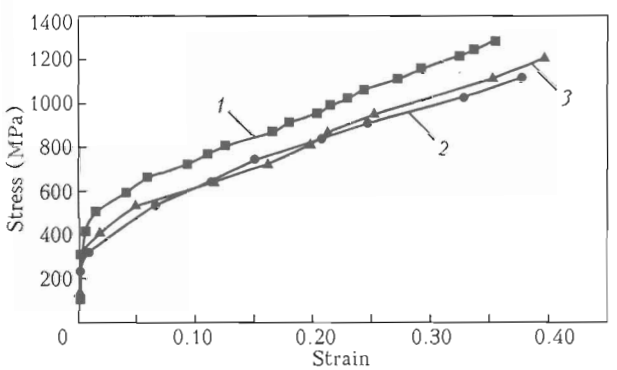


Figure 8. Experimental $\tilde{\varepsilon} - \tilde{\sigma}$ curves of weldment and base metals: *1* — weldment in a TWB (1.0 mm/1.2 mm), *2* — base metal (1.0 mm), *3* — base metal (1.2 mm)

can be confirmed by the results of the tensile test, as shown in Figure 2, where failure is found in the thinner base metal rather than the weldment. In other words, for stainless steel TWBs, the tensile properties, as well as its formability, are somehow dependent on the properties of the thinner base metal rather than the weldment.

CONCLUSIONS

This study successfully presents an experimental method of analysis to acquire the true stress-strain data of the weldment for our AISI 304 stainless steel TWBs with a thickness combination of 1.0 mm/ 1.2 mm. The weldment is found to be the strongest region/material with the highest necking strength within a TWB. In order to accurately predict formability of TWBs, the mechanical properties of the weldment should therefore be fully taken into account.

Acknowledgments. *The work described in this paper was partially supported by grants from the Research Grants Council of the Hong Kong Special Administrative Region, China (Project No. PolyU 5178/01E) and the Research Committee of the Hong Kong Polytechnic University (Project No. G-T906).*

1. B. Y. Ghoo, Y. T. Keum, and Y. S. Kim, *«Evaluation of the mechanical properties of welded metal in tailored steel sheet welded by CO_2 laser»*, Journal of Materials Processing Technology, 113, p. 692–698 (2001).
2. K. Abdullah, P. M. Wild, J. J. Jeswiet, and A. Ghasempoor, *«Tensile testing for welding deformation properties in similar gage tailor welded blanks using the rule of mixtures»*, Journal of Materials Processing Technology, 112, p. 91–97 (2001).
3. Z. L. Zhang, M. Hauge, C Thaulow, and J. Odegard, *«A notched cross weld tensile testing method for determining true stress-strain curves for weldments»*, Engineering Fracture Mechanics 69, p. 353–366 (2002).

LASER-MIG HYBRID WELDING OF ALUMINIUM ALLOYS

J. GEDOPT, J. VERWIMP, E. GEERINCKX
VITO Materials Technology, Mol, Belgium

In the field of welding of aluminium characteristics required for the welding are: a good weld quality (defect free), high productivity and low costs (high welding speed), freedom in term of design (complex shapes) and freedom in the execution of the welding (bridging root gap). The ability of the laser to bridge root gap is low due to its very small focal diameter, but this small focal diameter allows high welding speeds. The MIG (GMAW) arc welding process has a much lower energy density due to its larger focal spot, but the wire fed electrode allows bigger root opening. By combining both welding processes several synergies can be obtained, thus creating a welding technique that offers interesting advantages for applications in automotive industry. However, laser welding of aluminum alloys is susceptible to porosity formation. Hybrid laser-MIG welding offers a number of advantages over laser welding, especially in preventing pore formation and gap bridging ability. This requires the control of all the complexly related process parameters. The complete set of process parameters is a combination of the MIG, laser and interaction parameters. In order to obtain a stable hybrid welding process, free of defects, several process parameters are altered. Among these are shielding gas, welding speed and the distance between laser focal point and impingement of the arc. All welding tests are performed on aluminum sheet of the 5xxx and 6xxx series, alloys applicable in industry. In this paper results of welding experiments are reported as well as mechanical properties obtained.

Introduction. The light metal aluminum has become more and more important for the automotive industry. The use of aluminum parts in the construction of a car will result in a lower weight due to the low density of aluminum alloys. Conventional welding of aluminum alloys with high mechanical properties, due to a thermal treatment, will result in fairly low mechanical properties. To obtain high strength levels the heat input of the welding process has to be limited. Although hybrid laser welding [1] has a higher heat input compared with laser welding, still the heat input is acceptable. Especially in automotive applications, where the low tolerances of the work pieces can cause problems for plain laser welding, the high gap bridging ability of the hybrid laser welding process can be the solution of this problem. Another advantage of hybrid laser welding for the use in automotive applications is the flexible use of different kind of filler wires. This can prevent hot cracks in the case of plain laser welding of certain 6xxx alloys, which are of special interest for the automotive industry. The hybrid laser welding process has already several applications in the automotive industry: Audi uses the welding process to weld parts of the A8 version and VW uses the process to weld the doors of the VW Phaeton.

Laser-MIG process. Unlike a sequential configuration where two separate weld processes act in succession, hybrid welding may be viewed as a combination of both weld processes acting simultaneously in one and the same process zone [2]. Depending on which arc or laser process is used, and on the process parameters, the processes will influence one another to a different extent and in different ways. Thanks to the combination of the laser process and the arc process, there is also an increase in both the welding penetration and the welding speed. The metal vapor escaping from the vapor cavity retroacts upon the arc plasma. Absorption of the Nd:YAG laser radiation in the processing plasma remains negligible. Depending on what ratio of the two inputs is chosen, the character of the overall process may be determined to a greater or smaller degree either by the laser or by the arc. Before the laser welding can get underway, the initial reflectance must first be overcome, especially on aluminum surfaces. This can be achieved by starting welding with a special start program. After the vaporization temperature has been reached, the vapor cavity is formed, with the result that nearly all the radiation energy can be absorbed in the work piece. In laser-MIG welding, vaporization takes place not only from the work piece but also from the filler wire, meaning that there is more metal vapor available, which in turn facilitates the laser radiation. Figure 1 shows the principle setup of the hybrid laser-MIG welding process.

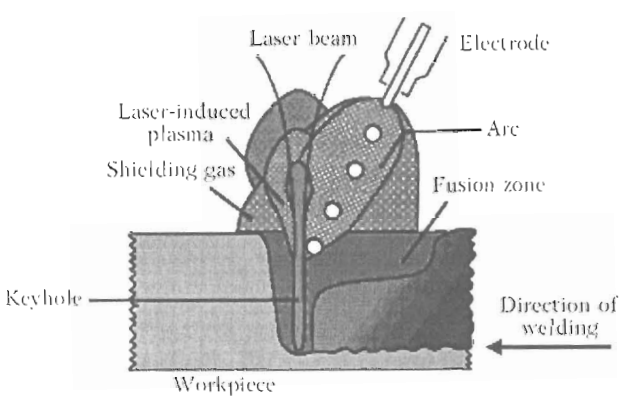


Figure 1. Setup of the hybrid laser-MIG welding process

© J. GEDOPT, J. VERWIMP, E. GEERINCKX, 2005

Benefits of the HLW process. The merging of the arc and laser beam results in the following advantages of laser hybrid welding over laser welding [3, 4]:

1. Higher process stability
2. Higher bridging ability
3. Deeper penetration
4. Lower capital investment costs because of savings in laser energy
5. Greater ductility

The advantages of laser hybrid welding over MIG welding are the following:

1. Higher welding speeds
2. Deeper penetration at higher welding speeds
3. Lower thermal input
4. Higher tensile strength
5. Narrower weld joints

The arc welding process is characterized as a low cost energy source, good root opening bridge ability, and the facility for influencing the structure by adding filler metals. The laser beam process, on the other hand, allows large welding depth, high welding speed, low thermal load and narrow joints. Laser hybrid welding thus allows higher welding speeds, process stabilization due to the interaction between the arc and the laser beam, increased thermal efficiency and greater work piece tolerances. As the weld pool is smaller than with the MIG process, there is less thermal input and a smaller heat-affected zone. This results in less weld distortion, which reduces the amount of subsequent post weld straightening work. Turning now to the economic advantages of hybrid welding over laser welding, the following statements can be made: the weld joint consists partly of a MIG weld and partly of a laser weld. The hybrid process makes it possible to reduce the power of the laser beam, thereby greatly reducing the energy consumption of the laser source. In Figure 2 the synergies of the hybrid laser-MIG welding process is shown.

Aluminum weld ability Although some problems may be encountered in hybrid laser welding of aluminum alloys, sound joints can be produced with proper precautions. However, there are also some inherent difficulties in fusion welding of aluminum alloys. These alloys are prone to a high level of porosity and some alloys to cracking. Factors that may influence

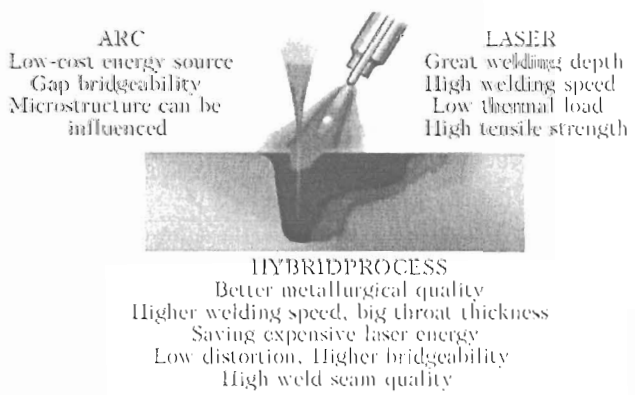


Figure 2. Synergies of the hybrid laser-MIG welding process

the hybrid laser welding of aluminum alloys include [5]:

1. Aluminum oxide layer: this layer forms immediately on aluminum surfaces upon exposure to air, must be removed prior to welding in order to obtain sound welds. If the oxides are not removed, oxygen and humidity may be entrapped in the weld, with detrimental effect on the weld properties

2. Thermal Conductivity: the thermal conductivity of aluminum is four times that of low carbon steel. This means that heat must be supplied four times as fast to aluminum alloys as to steel to raise the temperature locally by the same amount. Energy density of the laser beam is sufficient to overcome this difficulty

3. Wide Solidification-Temperature Range: aluminum alloys exhibit relative wide solidification-temperature ranges. This relatively wide range combined with a high coefficient of thermal expansion and solidification shrinkage makes these alloys, particularly heat-treatable alloys, susceptible to cracking

4. Hydrogen Contamination: porosity may be formed in aluminum alloys when hydrogen gas is entrapped during solidification because aluminum displays an abrupt drop in its hydrogen solubility when going from liquid to solid. Hydrogen is entrapped into the molten pool during welding due to its high solubility in the liquid phase and forms gas pores upon solidification as a result of the decrease in solubility

5. High Reflectivity: difficulties are encountered due to the high reflectivity of the laser beam on the aluminum surface. Proper welding procedures should be utilized in order to achieve adequate penetration

During laser welding of aluminum alloys the keyhole is very instable due to the low viscosity of the aluminum melt [6]. This leads to numerous collapses of the keyhole and a lot of big pores, so called process pores. The out gassing of these pores is very difficult due to the very small weld pool and short solidification times in case of laser welding of aluminum alloys. The phenomenon of process pores is limiting the welding depths in case of laser welding aluminum. To solve this problem some strategies were developed, e.g. the welding with two laser spots for the enlargement of the weld pool. In principle all these strategies lead to a higher necessary laser power at constant welding depths. The laser-MIG hybrid welding is a good possibility to realize the higher power at the working piece. With the coupling of the laser beam and the arc high welding depths and high welding speeds are also possible on aluminum alloys with less danger of process pores. The bigger weld pool and the modified flow conditions in the melt allows the out gassing of pores. Furthermore, the override of the metallurgy of the weld with the melting of filler wire is much better compared with pure laser welding.

HLW process parameters. Since Hybrid Laser Welding is the combination of a conventional arc welding process and laser welding, the parameter sets of both welding techniques have to be considered. Due

to the combination of both techniques several other process parameters become important. A list of the most important parameters is presented:

MIG:

1. Arc voltage, arc current, pulse frequency
2. Wire speed, wire diameter, welding speed, wire type
3. Torch orientation, stick out
4. Gas shielding, edge preparation, ...

Laser:

1. Laser power, laser type
2. Welding speed, focal position, spot size
3. Gas shielding, edge preparation, ...

The effect of these parameters on both separate processes is sufficiently known and not discussed in this paper.

Besides the MIG and laser parameters, the interaction parameters of both processes are very important [7, 8, 9]:

1. Distance between laser focal point and impingement point of the arc
2. Geometrical formation of the laser beam and the arc torch
3. Shielding gas of the combined process

The distance between laser focal point and impingement point of the arc is an important parameter since it will determine the weld pool geometry. The bigger the weld pool geometry, the easier the out gassing of pores will happen. A small difference between the impingement points will assure the interaction of the processes, but when the distance is growing too much the processes will become more separate and the interaction will perish. The arbitrary geometrical formation of the laser beam and the torch (torch before or behind the laser) and the angle between laser and MIG are both important parameters to insure a proper interaction between laser and MIG. To weld aluminum the laser beam is always leading the arc, the angle between laser and MIG is in most cases fixed at 30°.

The usable shielding gas is one of the biggest difference between the hybrid welding with a CO_2 laser and Nd:YAG or fiber laser. For the work with the CO_2 laser gas mixtures with high helium content are necessary to suppress plasma formation. The amount of laser power absorbed in a plasma is proportional with λ^2 of the laser beam. For a CO_2 laser ($\lambda = 10.6$ μm), this means that plasma formation should be suppressed using helium as the shielding gas, since helium is less sensitive for plasma formation. In case of the Nd:YAG (or fiber) laser pure argon can be used as a shielding gas since the risk on laser power absorption in the plasma is not present ($\lambda \pm 1.06$ μm). The type of shielding gas chosen to perform the HLW process will influence the stability of both processes and will also influence the weld pool formation.

The gap bridging ability is very limited in case of laser welding. Combining laser and MIG in one hybrid process will significantly increase the gap bridging ability. This means that work piece preparation costs can be reduced. The edge preparation of the parts is an important issue since it will determine the amount of filler wire (MIG wire) needed to reach an acceptable welding result.

Experimental equipment and materials. *Nd:YAG laser:* The laser used in the experimental runs is a 4.4 KW diode pumped Nd:YAG laser of Rofin Sinar (DY044). The laser beam is delivered by a fibre of 400 μm core diameter and collimated with a focal length of 200 mm. The hybrid laser welding head contains a focal lens of 250 mm, resulting in a laser spot size of 500 mm. The resulting maximum energy density of the laser is 2.2×10^6 W/cm^2.

MIG welding: The MIG welding source used in all experimental runs is a Fronius Transpuls Synergic 5000. It has a synergy action according to the filler wire speed and also standard parameters for different materials and filler wires. Direct current is used in all the experimental runs, all test pieces were grounded.

Hybrid laser welding head: The hybrid laser welding head used in all the experimental runs is a Fronius HLW head, shown in Figure 3. An important part of the head is the spatter-guard. This part will prevent spatters from the welding process to move towards the laser optics. This will increase the length of life of the protective glass in the laser optic. The functioning of the spatter-guard is guaranteed by blowing high pressure (minimum 2.8 bar) compressed air into the part. As mentioned before, the length of the focal lens is 250 mm.

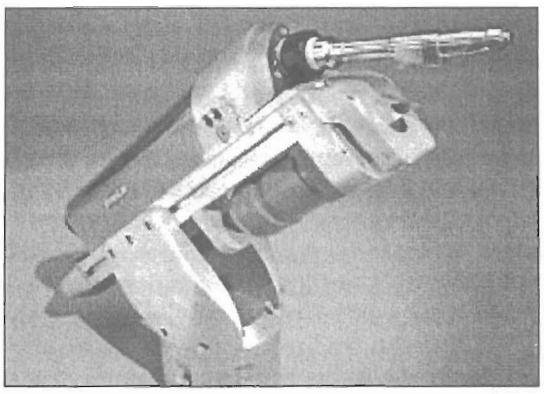


Figure 3. The Fronius hybrid laser welding head

Materials: The aluminum alloys welded during this work are:

1. The EN AW 5083 alloy is a non-heat-treatable wrought alloy, which can only be strengthened by cold deformation. The temper condition of the plates is a H111-temper, which means strain-hardened less then the amount required for a controlled H11 temper (this condition is a temper between O («dead soft» or fully annealed) and H12 (strain hardened only to a quarter hard condition). The main alloying elements for the 5083 are: Mg (4.0–4.9%) and Mn (0.4–1.0%). The yield strength (0.2%) is minimal 125 MPa, the tensile strength is between 275 and 350 MPa. Typical application fields of this alloy are: automotive (welded

tank trailers, welded dump bodies), vessels, tubing, piping, ...

2. The EN AW 5182 alloy is a non-heat-treatable wrought alloy, which can only be strengthened by cold deformation. The temper condition of the plates is a H111-temper, which means strain-hardened less then the amount required for a controlled H11 temper (this condition is a temper between O («dead soft» or fully annealed) and H12 (strain hardened only to a quarter hard condition). The main alloying elements for the 5182 are: Mg (4–5%) and Mn (0.2–0.5%). The yield strength (0.2%) is minimal 110 MPa, the tensile strength is between 255 and 315 MPa. Typical application fields of this alloy are: automotive (body panels, transportation), can stock, containers, ...

3. The EN AW 6061 alloy is a heat-treatable wrought alloy. The main precipitation hardening component is Mg_2Si. The temper condition of the extruded profiles is a T6 condition. This temper corresponds with solution heat-treated and then artificially aged. The main alloying elements for the 6061 are: Mg (0.8–1.2%), Si (0.4–0.8%) and Fe (max. 0.7). The yield strength (0.2%) is minimal 240 MPa, the tensile strength is minimal 260 MPa. Typical application fields of this alloy are: automotive (truck frames, transportation), heavy duty structures, aerospace applications, piping, ...

4. The EN AW 6082 alloy is a heat-treatable wrought alloy. The main precipitation hardening component is Mg_2Si. The temper condition of the extruded profiles is a T6 condition. This temper corresponds with solution heat-treated and then artificially aged. The main alloying elements for the 6082 are: Mg (0.6–1.2%), Si (0.7–1.3%) and Mn (0.4–1.0 %). The yield strength (0.2%) is minimal 250 MPa, the tensile strength is minimal 290 MPa. Typical application fields of this alloy are: automotive (truck frames, transportation), heavy duty structures, nuclear applications, piping, tubing...

Experimental results: parameter optimization. Hybrid laser-MIG welding offers a number of advantages over laser welding, especially in preventing pore formation and gap bridging ability. This requires the control of all the complexly related process parameters. The complete set of process parameters is a combination of the MIG, laser and interaction parameters. In order to obtain a stable hybrid welding process, free of defects, several process parameters are altered. Among these are shielding gas, welding speed and the distance between laser focal point and impingement of the arc. The parameter optimization of hybrid laser welding is a topic of which not much information is available in literature. Based on results of preliminary tests, experimental programs to optimize the hybrid laser welding process are often limited to the variation of one or two process parameters, of which the influence on the welding result is examined. This experimental program will identify the most important process parameters and the influence on the resulting weld. The effect of gap tolerances on the resulting weld quality is also examined. All welding tests are performed on aluminum sheet of the 5xxx and 6xxx series, alloys applicable in automotive industry.

In a first experimental run the synergy between laser and MIG is demonstrated. To prove this synergy 3 separate welding tests were performed. In a first test laser welding parameters are determined for a butt weld in a 4 mm thick 6082 alloy. A micrograph of the weld is shown in the left part of Figure 4. In a second test the parameters for the hybrid laser welding process of the same configuration are determined. The macrograph of this weld is shown in the right part of Figure 4. Finally a weld test is performed using only the MIG parameters of the hybrid process for the same configuration. This micrograph is shown in the middle part of Figure 4. Comparing these 3 micrographs it is immediately clear that the hybrid process is not just the addition of the laser and the MIG process. The weld pool in case of the hybrid laser welding process is considerably larger then the addition of the separate weld processes. This leads to conclude that both processes interact in the hybrid process. These interactions are investigated in the next experimental runs.

Effect of welding speed, distance between laser and MIG and shielding gas on alloy 5083: The alloy 5083 (thickness 5 mm) is butt welded using a filler wire type AA 5183 (AlMg4.5Mn). In a first experimental run the welding speed is varied between 0.5 and 2.5 m/min. A welding speed of 2.5 m/min requires full laser power to ensure full penetration welding. This means that for this thickness the maximum welding speed is limited to 2.5 m/min. The distance between laser and MIG is set at 4 mm, the shielding gas used is pure argon. The influence of the welding speed on the mechanical properties and porosity formation is studied. The amount of porosity in the weld is determined using X-ray (radiographic) inspection,

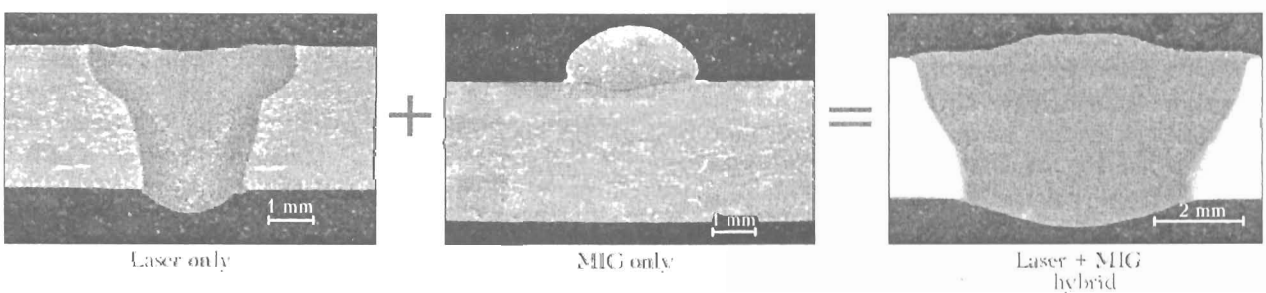


Figure 4. Macrographs of 3 welding processes: laser, MIG and laser-MIG hybrid

the tensile strength is the result of a transverse tensile test. The results are shown in Table 1. The radiographic analyses revealed that in case of welding speeds higher than 1 m/min the welds contained too much porosity. The high amount of porosity results in relatively low tensile strength of the welded plates (Average tensile strength 70 MPa lower in case of high amount of porosity).

In a second experimental run the distance between laser and MIG is varied between 0 and 4mm. The influence of the distance between laser and MIG on the mechanical properties and porosity formation is studied. The radiographic analyses revealed that in case of laser – MIG distance = 0 mm, both welding processes are disturbed by each other, and no stable welding process could be obtained. The best results are obtained using a relatively small distance between laser and MIG. A distance of 2 mm resulted in pore free welds, even with a welding speed of 1.5 m/min. The radiographic inspection revealed that welding speeds of 2 m/min and more result in excessive pore formation. The results obtained using a laser – MIG distance of 1 mm are slightly worse than the 2 mm results. When the distance is growing too much, the processes will become more separate and the interaction will perish. The radiographic analyses of a 2 mm laser – MIG distance combined with welding speeds of 1.5 and 2 m/min are shown in Figure 5.

The tensile strength obtained with the optimal welding parameters (distance laser – MIG = 2 mm and welding speed = 1.5 m/min) equals 280 MPa, slightly higher than the specified minimum tensile strength (275 MPa) in the standard EN 485-2. Both root and face bend test showed good results according to EN 910 (bending angle of 180° and former diameter of 6*thickness). Micro hardness was tested (HV0.5; 30s) and no softening in the HAZ or weld metal was found.

In a third experimental run the shielding gas is altered between pure argon and a mixture of 30% helium in argon. The results obtained with this gas mixture did not significantly differ from the results previously obtained.

As a preliminary conclusion can be pointed out that:

1. Welding speed has a large influence on weld quality. Optimal results could be obtained with a welding speed of 1.5 m/min.

2. Distance between laser and MIG has a large influence on the welding process. A too small distance results in a disturbed process stability, a too large distance results in two separate processes. An optimum of 2 mm is found in case of welding aluminum alloy 5083 in 5 mm thickness.

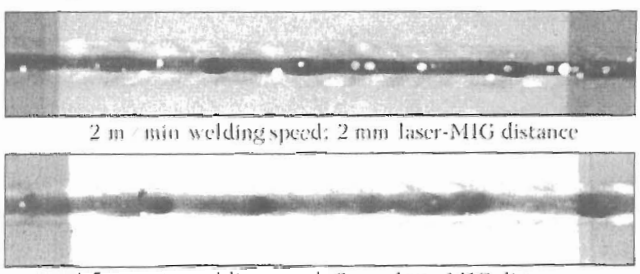
Table 1. Influence of a variation in welding speed on the weld quality for alloy 5083

Welding speed [m/min]	0.5	1	1.5	2	2.5
Av. tensile strength [MPa]	274	271	210	200	200
Radiographic inspection	Free of pores	Free of pores	Pores	Pores	Pores

3. Shifting from pure argon to argon/helium mixtures has no significant influence on the weld quality.

Effect of the welding speed on aluminum alloy 5182: The alloy 5182 (thickness 1.5 mm) is butt welded using a filler wire type AA 5183 (AlMg4.5Mn). A comparison is made between laser and hybrid laser welding. For both welding processes the welding speed is altered between 3.6 and 8.4 m/min. Table 2 shows the resulting average tensile strengths for both welding processes. In this table HLW stands for hybrid laser welding, LW for laser welding.

For the laser welding process the average tensile strength increases as the weld speed increases. For the hybrid laser welding process the average tensile strength is constant except for the highest welding speed. A welding speed of 8.4 m/min results in an unstable weld process with considerable lower mechanical properties. A possible explanation is that the MIG process is unstable for these very high welding speeds and even the stabilizing effect of the laser cannot compensate this inconvenience. Since the weld metal is too small when welding 1.5 mm thick plates, no radiographic inspection could be performed. All the test specimen of the tensile test broke in the weld metal. Inspection of the fracture surface showed that no pores were present. The specified minimum tensile strength (255 MPa) in the standard EN 485-2 is reached in 6 out of 9 test runs. Both root and face bend test showed good results according to EN 910 (bending angle of 180° and former diameter of 6*thickness). Micro hardness was tested (HV0.5; 30s) and no softening in the HAZ or weld metal was found.



2 m/min welding speed; 2 mm laser-MIG distance

1.5 m/min welding speed; 2 mm laser-MIG distance

Figure 5. X-ray analyses with varied welding speed

Table 2. Average tensile strength obtained for both welding processes using different weld speeds

Welding process	HLW	HLW	HLW	HLW	HLW	HLW	LW	LW	LW
Welding speed [m/min]	3.6	4.2	4.8	6	7.2	8.4	3.6	6	8.4
Average tensile strength [MPa]	260	270	262	250	255	200	252	256	270

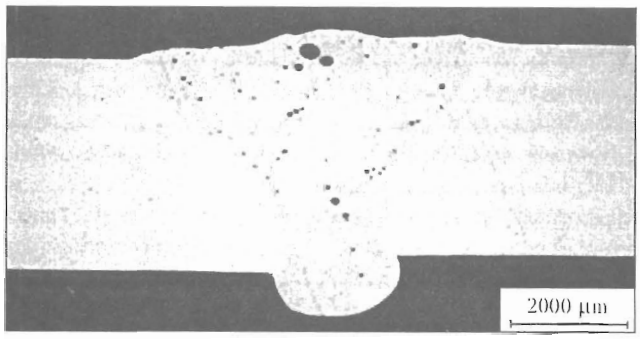


Figure 6. Macrograph of a 6061 T6 alloy, hybrid laser welding speed = 1.8 m/min

As a preliminary conclusion can be pointed out that welding speeds of 8.4 m/min and higher result in an unstable weld process. Under stable conditions both hybrid and laser welding resulted in comparable mechanical properties. To be able to obtain these results in laser welding edge preparation (milling) of the parts is important. In automotive applications precise edge preparation will often limit the suitability of the laser welding process.

Effect of welding speed and shielding gas on alloy 6061: The alloy 6061 (thickness 4 mm) is butt welded using a filler wire type AA 4043 (AlSi5). In a first experimental run the welding speed is varied between 1.2 and 1.8 m/min. For 3 welding speeds (1.2; 1.5 and 1.8 m/min) the influence of the speed on the mechanical properties and porosity formation is studied. The amount of porosity in the weld is determined using X-ray (radiographic) inspection, the tensile strength is the result of a transverse tensile test. The X-ray analyses clarified that even with the highest welding speed no or very low amount of porosity was found in the welds. A macrograph of the weld with the highest welding speed is shown in Figure 6.

The results of the X-ray analyses and the transverse tensile test are shown in Table 3.

Table 3. Influence of a variation in welding speed on the weld quality for alloy 6061

Welding speed [m/min]	1.2	1.5	1.8
Av. tensile strength [MPa]	240	249	245
Radiographic inspection	Free of pores	Free of pores	Free of pores

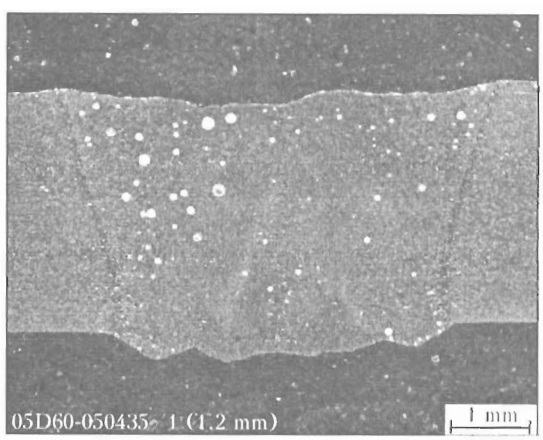


Figure 7. Macrograph of a weld in AA 6082 (3 mm) with a gap size set at 1.2 mm

The influence of the welding speed on porosity and mechanical properties seems limited. In the second experimental run the shielding gas is altered between pure argon and a mixture of 30% helium in argon. The results obtained with this gas mixture did not significantly differ from the results previously obtained. The effect of the shielding gas seems limited and this seems independent of the alloy type welded.

As a preliminary conclusion can be pointed out that, for the 6061 alloy:

1. Welding speed has a limited effect on the resulting weld quality.
2. Shifting from pure argon to argon/helium mixtures has no significant influence on the weld quality.

Effect of gap tolerances on alloy 6082: The gap bridging ability of a welding process is a very important topic for the automotive industry. Since the tolerances on the parts to be welded for automotive applications are oftentimes relatively low due to the size of the parts, the gaps that need to be bridged are large. In pure laser welding the gap bridging ability is very low because no filler metal is added during the welding process. For this reason the use of laser welding in some automotive applications is limited. Hybrid laser welding has a relatively large gap bridging ability compared with this process. The size of gaps that can be bridged with the hybrid process are examined during the final experimental run.

The alloy 6082 (thickness 3 mm) is butt welded using a filler wire type AA 4043 (AlSi5) with a gap size altered between 0 and 1.2 mm. The size of the gap is guaranteed using spacers to keep the plates in position. The results obtained in the experimental program are promising. Since the size of the Nd:YAG laser spot in the focal position is only 0.5 mm, it is expected that the gap size that can be bridged is limited to more or less this value. Nevertheless, gaps up to 1.2 mm can be bridged in the given configuration. The weld quality obtained for this gap is still acceptable. As an example, a macrograph of a weld with a gap size of 1.2 mm is shown in Figure 7.

It should be clear that the upper limit of the gap size depends on several process parameters. The most important are: plate thickness, laser spot size, alloy type, weld speed and filler wire type.

As a preliminary conclusion can be pointed out that in case of welding 3 mm thick plates in aluminum 6082 a maximum gap size that still can be bridged by the process is 1.2 mm. The weld quality obtained for this gap is still acceptable.

It is important to know that the influence of a parameter depends on the alloy type as well as the material thickness. The absolute values obtained in this work depend strongly on the laser source and optics used, as well as the arc source used. Nevertheless the relative values obtained should be transferable to other experimental setups using other laser and arc sources. It seems that alloys of the 5xxx series are more susceptible to pore formation and unstable weld processes than alloys of the 6xxx series. An explana-

tion for this inconvenience is the high content of magnesium in the 5xxx series. Magnesium will disturb the welding process because the element is volatile at welding temperatures. The magnesium fumes will disturb the stability of the keyhole of the laser welding process and they will result in weld porosity if the fumes cannot escape from the weld pool. Increasing the welding speed will significantly increase the risk of weld porosity.

In the near future new welding tests will be performed to determine the influence of all weld parameters and gap size on the resulting weld quality.

CONCLUSIONS

Hybrid laser welding of aluminum, combining laser and MIG in one process, is an excellent welding process for applications in the automotive industry. The influences of several parameters on the hybrid laser welding process are studied in this work. Some important influences are found:

1. Welding speed: depending on alloy type and thickness, welding speed can have a large impact on porosity formation. Too high welding speeds result in an unstable process and a poor weld quality.

2. Distance laser – MIG: depending on alloy type and thickness, distance laser – MIG has a large impact on weld quality. For each alloy type, plate thickness and welding speed the optimal value should be determined. If the distance is too small both welding processes are disturbed by each other, and no stable welding process could be obtained. If the distance is growing too much, the processes will become more separate and the interaction will perish.

3. Shielding gas: shifting from pure argon to argon/helium mixtures has no significant influence on the weld quality.

4. Gap size between plates: for alloy 6082 (3 mm thick) a maximum gap size of 1.2 mm is found. The weld quality obtained for this gap is still acceptable.

5. Aluminum alloy type: alloys of the 5xxx series are more susceptible to pore formation and unstable weld processes than alloys of the 6xxx series. An explanation for this inconvenience is the high content of magnesium in the 5xxx series, which will disturb the welding process.

1. Steen et al.: *Arc-Augmented Laser Welding*, 4th Int. Conf. on Advances in Welding Processes, Paper No. 17, 1978, pp. 257–265.
2. H. Stauffer, M. Ruhrnobl, G. Miessbacher, *Laser-MIG for the Automotive*, Welding & Assembly, October 2003, pp. 103–105.
3. H. Staufer, *Hybrid laser welding*, Welding journal, January 2003, pp. 43–48.
4. H. Staufer, *Laser-hybrid welding of ships*, Welding Journal, June 2004, pp. 39–43.
5. G. Cam, J. F. dos Santos, M. Kocak, *Laser and Electron Beam Welding of Aluminium Alloys: Literature Review*, GKSS-Forschungszentrum Geesthacht GmbH, 1997, GKSS 97/E/25.
6. G. Aichele, *The joining of aluminium remains a lively topic, part I*, Aluminium. 79, January, 2003, pp. 1059–1068.
7. T. Jokinen, P. Jernstrom, M. Vanttaja, V. Kujanpaa, *Optimisation of parameters in hybrid welding of aluminium alloy*, Proceedings of the society of photo-optical instrumentation Vol. 4831, 2003, pp. 307–312.
8. E. Schubert, B. Wedel, G. Kohler, *Influence of the process parameters on the welding results of laser-GMA welding*, ICALEO 2002
9. M. Ema & S. Sasabe, *Joint strength of Al–Mg–Si alloys for automobiles by advanced welding techniques*, Welding International 2004, 18, pp. 11–15.

PROPERTIES OF CO_2-LASER WELDED JOINTS OF DISSIMILAR MAGNESIUM ALLOYS

W. KALITA[1], P. KOLODZIEJCZAK[2], L. KWIATKOWSKI[3], M. GROBELNY[3], J. HOFFMAN[1]
[1]Institute of Fundamental Technological Research of PAS, Warsaw, Poland
[2]Warsaw Technical University, Poland
[3]Institute of Precision Mechanics, Warsaw, Poland

This paper provides the results of investigation that has been carried out on the keyhole laser beam welding of dissimilar magnesium alloys. Welding of workpieces of alloys of MgAlZn (brittle) and MgAlMn (ductile) groups has been performed with the CO_2-laser of maximum power of 2.5 kW. With the chosen flow rate of helium shielding and the beam focal position set on the metal surface the welds with no defects and with nearly parallel boundaries were obtained. The analysis of microstructures of the joints, measurements of hardness distributions and the elemental distributions in the weld cross-sections allowed to find the changes due to beam action and recrystallization. The static tensile strength tests have permitted to determine the conditions when the joints of satisfactory mechanical properties could be acquired. The corrosion immersion tests are also reported.

Increasing interest of automotive and aeronautic industries in magnesium alloys is mainly due to their much lower density with respect to traditional materials like steel and aluminum alloys. Development of new magnesium alloys with mechanical properties comparable with traditional materials [1] gave the way to their applications as die-casting parts [2]. That resulted in appropriate fulfilling the sharpening requirements for enviromental protection [3] and transportation safety [4] through the mass reduction and fuel savings. However, the production and processing of sheet elements and modular lightweight structures are still in progress. In this matter the special concern is given to welding, particularly to laser beam welding of magnesium alloys [5–18]. Most of the studies done so far is related to welding of similar alloys. But, the extending application of tailored blanks gave attention to laser welding of dissimilar alloys [5].

Experimental. Two cast magnesium alloys AM50 and AZ91, with the chemical composition given in the Table, were machined from the bars to the plates with thicknesses of 4.5 mm, widths of 50 mm and the lengths of welding edges of 100 mm.

The butt welding of plates of similar and dissimilar alloys has been performed with CO_2 FAF (fast axial flow) laser with the beam of the mode close to TEM_{10} focused to the diameter of 0.25 mm by the ZnSe lens of 5". No filler metal has been used. After some attempts to find the optimal conditions of welding, the laser power has been set at 2.0 kW, the velocity of welding at 4 m/min and, after evaluation of the influence of the **focal point** position (with respect to material surface) **on the** shape of the seam, the focal position of the **beam has** been chosen on facing surface of plates. The helium shielding of the facing surfaces was provided from the nozzle of 4 mm in diameter with the flow rate of 15 l/min and the bottom surfaces were shielded by the blow of argon.

Table. Chemical composition of welded alloys

Alloy	Alloying elements (wt.%)		
–	Al	Mn	Zn
AM50	5	0.3	0.2
AZ91	9	0.17	0.7

The microstructures and the hardness profiles have been evaluated on the cross-sections perpendicular to the direction of beam scanning as well as on the cross-sections done parallelly to the facing surface along the seam. In order to find any changes due to the action of laser beam (e.g. evaporation of material and convection) the analysis of elemental distribution of basic elements has been performed with X-ray microprobe. The mechanical properties of the joints have been revealed by the tests on the Instron stand for static tensile strength. After the fracture of workpieces the SEM images of fractures were obtained to compare with fractures of the parental material. Welded samples were also exposed to neutral 0.15 M NaCl for a 22 days and periodically inspected by a naked eye. After 3 days of exposure pH of solutions has changed to approximately 11 and was stable to the end of experiment.

Results. The macrostructures of the butt-welded joints for similar and dissimilar alloys are presented in Figure 1. The boundaries of the fusion zones are nearly parallel and the aspect ratios of welds (thickness of a plate to mean width of the fusion zone) are of high value indicating that the keyhole effect of beam penetration was responsible for the joining. The parental materials contained no pores and after welding the fusion zones are practically free of them. Also, no cracks are observed.

© W. KALITA, P. KOLODZIEJCZAK, L. KWIATKOWSKI, M. GROBELNY, J. HOFFMAN, 2005

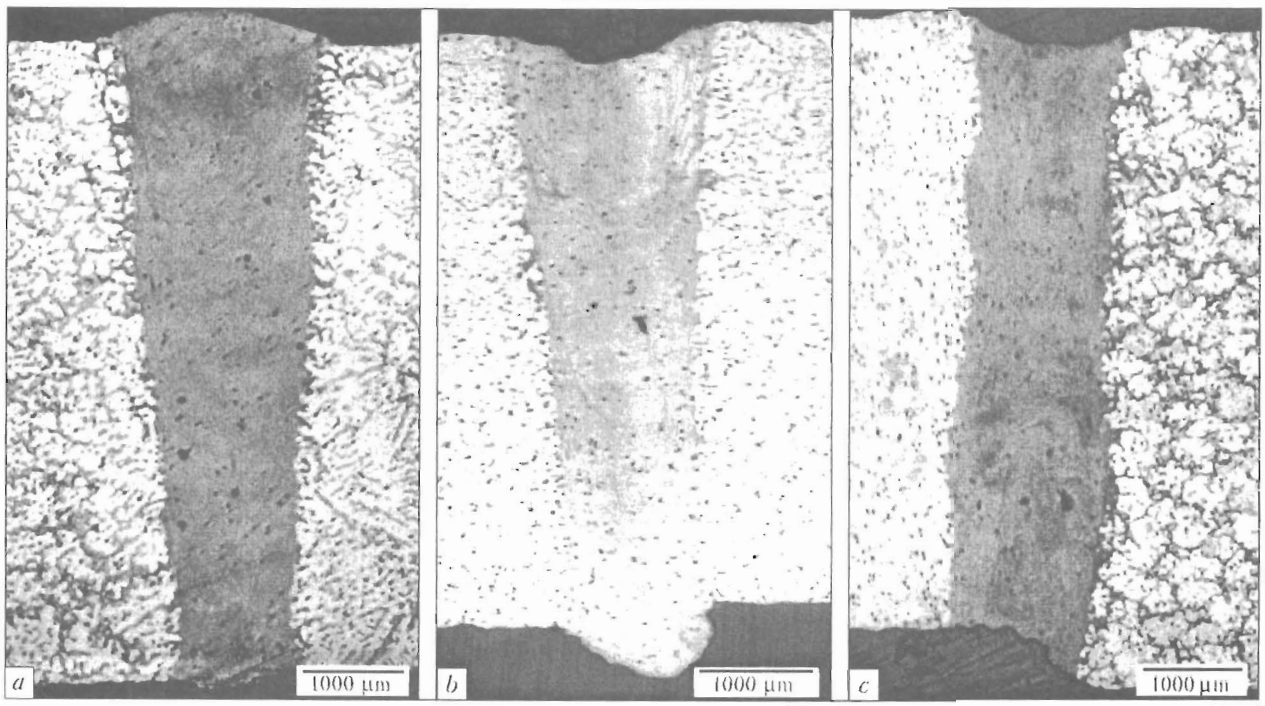


Figure 1. Macrostructures of the butt-welded joints: *a* — AZ91-AZ91, *b* — AM50-AM50, *c* — AM50-AZ91

Due to the short time of irradiation (determined approximately as the ratio of beam diameter and velocity of welding: less than 4 ms) and fast solidification the fusion zones are characterized by significant grain refinement, Figure 2. The sharp transitions from the base metal to the fusion zone with no distingusihed direction of solidification at boundaries of these zones may indicate that there is no heat affected zone that, on contrary, may easily be found e.g. for joints of steel or titanium alloys.

The measurements of hardness distributions in the cross sections of welds (perpendicular to the direction of welding) have shown significant increase of hardness in the fusion zones in comparison to the base material. These results, presented in Figure 3, may be associated not only with the high grain refinement in the weld but also with the increase of precipitations at the grain boundaries and appearance of intermetallic compounds. A share of these factors need further investigations.

For the determination of the changes in the chemical composition of materials caused by the influence of beam action the measurements of elemental distributions have been performed by means of X-ray microprobe. It was found that due to the very low boiling point of magnesium in comparison with that of aluminum, the percentage share of magnesium in the joints of similar alloys has been slightly decrased by evaporation of this element.

The static tensile tests of samples of parental alloys and the welds have been performed on the Instron stand. The stress vs. strain curves for joints of similar alloys and the base metals are presented in Figure 4. It has been observed that the fracture of welded samples for all alloys appeared far from the fusion zone boundaries — in the region of base metal. As it could be expected the joints of similar alloys have smaller elongation at fracture than the parental materials however there are differences for tensile stress: for AM50-AM50 joint the stress at fracture is lower and for AZ91-AZ91 higher than those for base metal samples.

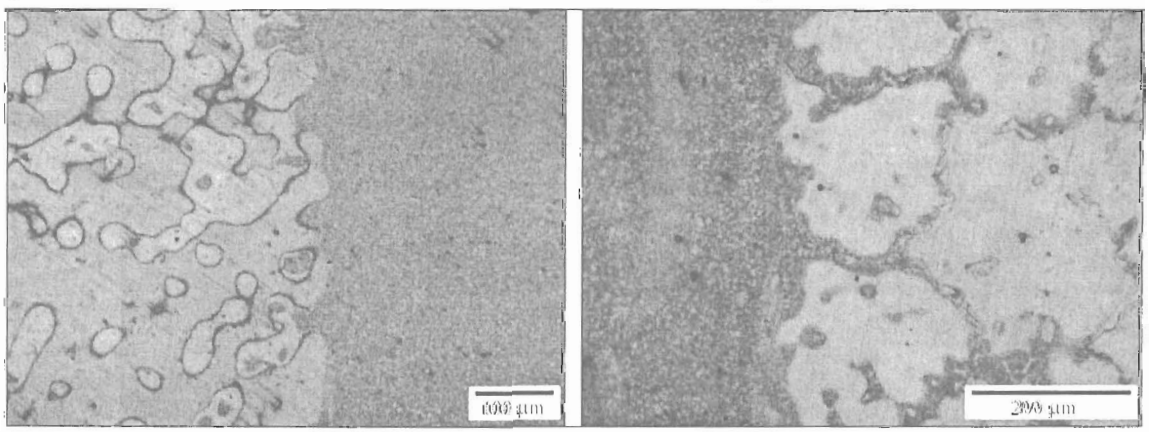


Figure 2. Microstructures of the transition from the fusion zones (FZ) to base material in the joint of disssimilar alloys AM50-AZ91: *a* — AM50 on the left to FZ, *b* — FZ to AZ91 on the right

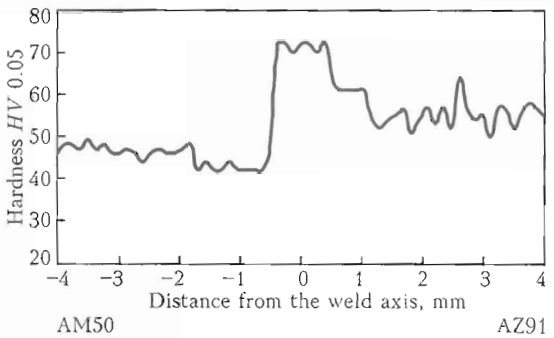


Figure 3. Hardness profile across the weld on dissimilar alloys measured 1.5 mm from the facing surface

For the joints of dissimilar alloys the workpieces broke at the AZ91 side, also far from the fusion zone.

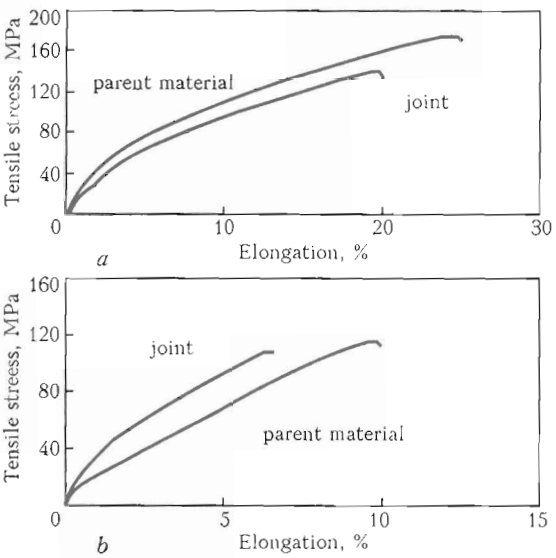


Figure 4. Stress-strain diagrams for the joints of similar alloys: *a* — AM50, *b* — AZ91

The comparison of stress-strain curves for all welded joints is given in Figure 5. According to anticipations the elongation at fracture for dissimilar joints has the value between those of the joints of brittle alloy AZ91 and the ductile alloy AM50.

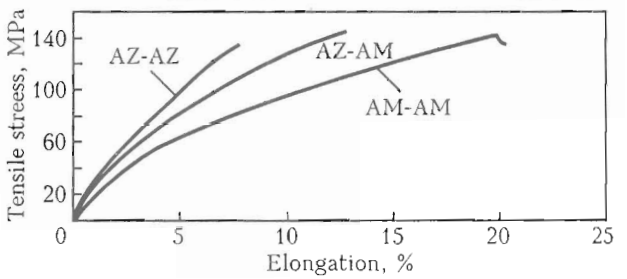


Figure 5. Stress-strain diagram for the joints of similar and dissimilar alloys

Since the fracture of the welded samples occurred far from the fusion zones the SEM images of fracture surfaces of the workpieces made of parental materials and samples with the joints displayed no differences.

For the corrosion behaviour of welded samples the corrosion immersion tests have been performed. The results of 22 days of samples immersion in 0.15 M NaCl is shown in Figure 6. The changes on surfaces for both sides of the samples (front, rear) are very similar therefore only the front view is given. It is seen that galvanic couple is being formed between dissimilar alloys. It is worthy to note that AZ91 in this galvanic couple is protected and exhibits much better properties than AZ91-AZ91 couple while AM50 work as sacrificial electrode. It is also important to underline that a welded joint in AZ91-AM50 couple plays insignificant role in corrosion process. More corrosion effects is seen on a joint for AZ91-AZ91 couple. This very interesting example is being studied in order to clarify observed behavior since differences in electrode potentials are not very large. From our previous studies [18] the following results were obtained:

- for AZ91 $E_{COR} = -1.5473$ *V* versus *SCE*;
- for AM50 $E_{COR} = -1.5826$ *V* versus *SCE*.

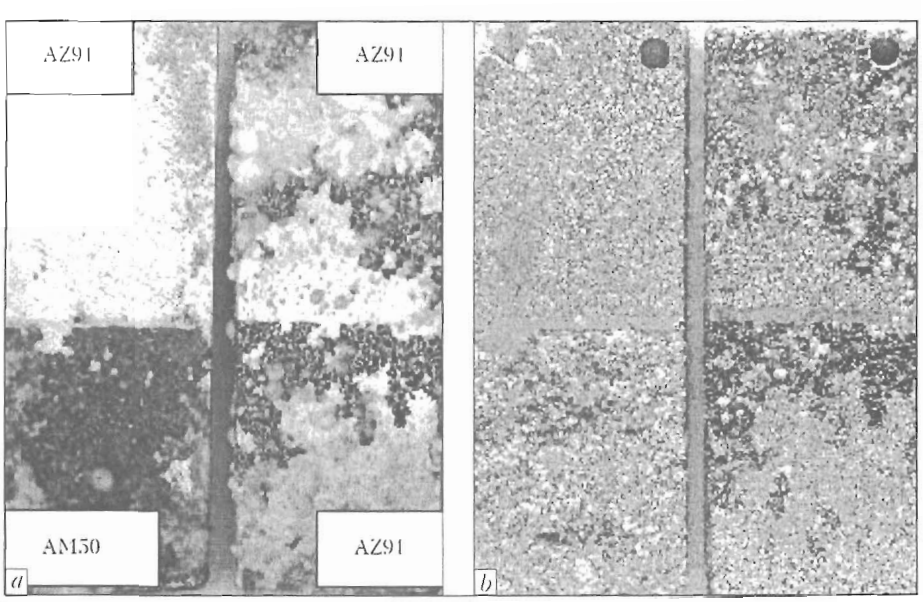


Figure 6. Images of corroded surfaces after 22 days of immersion in 0.15 M NaCl: *a* — just after withdrawing from the solution; *b* — after removal of precipitates during pickling in H_2SO_4

Therefore a difference is approximately 35 mV which is not extremely high for the occurrence of galvanic corrosion. Usually 50 mV is considered as a limit. Detailed explanation will be given after collection of additional results.

CONCLUSIONS

The following remarks can be made regarding the CO_2-laser beam welding of similar and dissimilar magnesium alloys:

1. Welding of similar and dissimilar alloys in the same conditions (for plate thicknesses equal to 4.5 mm: 2 kW laser power, velocity — 4 m/min, helium shielding, focal position at facing surface) resulted in nearly the same high aspect ratios of the fusion zone, with practically no porosity and without cracks. No heat affected zone may be observed and no distinguished direction of solidification can be noticed at fusion zones boundaries.

2. In all cases the high grain refinement and increased precipitations in the fusion zones may be observed that heightened the hardness in these regions.

3. In the static tensile tests the fractures occurred far from the weld (in the base material): in dissimilar weld on the side of brittle alloy AZ91. The plastic properties of samples with welds are lower than for the parental materials.

4. The results of corrosion immersion tests performed in 0.15 M NaCl showed that welding of dissimilar Mg alloys, in this case AZ91-AM50, increases a susceptibility to galvanic corrosion even if the difference between electrode potential values are not apart each other. However an influence of a weld is rather negligible. An exact interpretation requires further studies.

Acknowledgements. *This work was done within the framework of research project No. 4 T08C 009 25 supported by the National Committee for Scientific Research in 2003–2005.*

1. Friedrich H., Schumann S.: *Research for a «new age of magnesium» in the automotive industry.* Journal of Materials Processing Technology, vol. 117, 2001, pp. 276–281
2. Longworth S.J.P.: *The Bolting of Magnesium Components in Car Engines.* Dissertation for the degree of Master of Philosophy to the University of Cambridge, August 2001.
3. Aghion E., Bronfin B., Eliezer D.: *The role of the magnesium industry in protecting the environment.* Journal of Materials Processing Technology, vol. 117, 2001, pp. 381–385.
4. Mordike B. L., Ebert T.: *Magnesium. Properties – applications – potential.* Material Science and Engineering. A302, 2001, pp. 37–45.
5. Weishait A.; Galun R.; Mordike L.: *CO_2-Laser Beam Welding of Magnesium-Based Alloys.* Welding Journal, Vol. 77, No. 4, 1998, pp. 149–154.
6. Draugelates U.; Schram A.; Kettler C.: *Joining of magnesium alloys.* Materialwissenschaft und Werkstofftechnik, Vol. 30, no. 10, 1999, pp. 623–627.
7. Dhahri M.; Masse J. E.; Mathieu J. F.; Barreau G.; Autric, M.: *CO_2-Laser Welding of Magnesium alloys.* In: SPIE (High-Power Lasers in Manufacturing), Vol. 3888, 2000, pp. 725–732.
8. Dhahri M.; Masse J. E.; Mathieu J. F.; Barreau G.; Autric, M.: *Laser Weldability of WE43 Magnesium Alloy for Aeronautic Industry.* In: Geiger M., Otto A. (Edtrs.): Proc. of the LANE 2001, August 28–31, 2001, Erlangen, Germany, pp. 297–310.
9. Zhao H.; DebRoy T.: *Pore Formation during Laser Beam Welding of Die-Cast Magnesium Alloy AM60B – Mechanism and Remedy.* Welding Research Suppl., 2001, pp. 204–210.
10. Sun Z.; Wei J.; Pan D.; Tan Y. K.: *A Comparative Evaluation on Microstructures in TIG and Laser Welded AZ31 Magnesium Alloy.* SIMTech Technical Report, PT/01/008/JT, 2001, pp. 1–8.
11. Haferkamp H.; Goede M.; Bormann A.; Cordini P.: *Laser Beam Welding of Magnesium Alloys – New Possibilities using Filler Wire and Arc Welding.* In: Geiger M., Otto A. (Edtrs.): Proc. of the LANE 2001, August 28–31, 2001, Erlangen, Germany, pp. 333–338.
12. Lathabai S.; Barton K. J.; Harris D.; Lloyd P. G.; Viano D. M.; McLean A.: *Welding and Weldability of AZ31B by Gas Tungsten Arc and Laser Beam.* In: Kaplan H.I. (Edtr.): Proc. Magnesium Technology 2003, March 2–6, 2003, San Diego, CA, USA, pp. 157–162.
13. Watkins K. G.; *Laser Welding of Magnesium Alloys.* In: Kaplan H. I. (Edtr.): Proc. Magnesium Technology 2003, March 2–6, 2003, San Diego, CA, USA, pp. 153–156.
14. Stern A.; Munitz A.; Koln G.: *Application of Welding Technologies for Joining of Mg Alloys. Microstructure and Mechanical Properties.* In: Kaplan H. I. (Edtr.): Proc. Magnesium Technology 2003, March 2–6, 2003, San Diego, CA, USA, pp. 163–170.
15. Kalita W.; Kolodziejczak P.; Pokhmurska, H.: *Welding of Mg-Based Alloy AM20 by CO_2-Laser Beam.* In: Paton B. E., Kovalenko V. S. (Edtrs.): Proc. International Conference on «Laser Technologies in Welding and Materials Processing», May 19–23, 2003, Katsiveli, Ukraine, pp. 214–216.
16. Dasgupta A. K., Mazumder J.: *Laser Welding of AM60 Magnesium Alloy.* In: Luo A. A. (Edtr.): Proc. Magnesium Technology 2004, March 14–18, 2004, Charlotte, NC, USA, pp. 43–48.
17. Kolodziejczak P., Kalita W., Hoffman J., Kolasa **A.: *Laser welding of magnesium-based alloys of MgAlZn group.*** Advances in Manufacturing Science and Technology, vol. 28, no. 4, 2004, pp. 45–53.
18. Kalita W., Kolodziejczak P., Kwiatkowski L., Hoffman J.: *Properties of the butt-welded joints of CO_2-laser welded Mg alloys.* In: Geiger M., Otto A. (Edtrs.): Proc. of the LANE 2004, Sept. 21–24, 2004, Erlangen, Germany, vol. 1, pp. 317–328.

THE EFFECT OF THE PRESENCE OF THE ACTIVE METAL IN ODS LASER WELD METAL

M. K. KARFOUL
Al-Baath University, Homs, Syria

Introduction. The increasing of using of mechanically alloyed materials in the last decay put the question of their welding in the view of their wide exploitation in industry. The powder metallurgy allows now to produce mechanical alloys containing dispersed oxide particles of reactive metals* (REM) as Y_2O_3 or ZrO_2. The question of high temperature instability of aluminum oxide layer on the surface of oxide dispersion strengthened stainless steel (ODS) weld metal prevented their wide using in welded form. Some investigations proved that if the welding process keeps the dispersed reactive metal in the weld metal, then the Al oxide (Al_2O_3) layer on the surface of ODS weld metal will be in tight contact with the steel surface without defects [1, 2]. This layer will protect the ODS weld metal from high temperature corrosion. It was proved that the Al will diffuse from inside the ODS to its surface to react with oxygen for producing the Al oxide type Al_2O_3 [4, 5]. A lot of propositions were done for explanation of the effect of dispersed REM oxide particles in the mechanical alloy [3–7]. These propositions put the effect of the dispersed REM oxide particles in the structure of the ODS as the main reason for the decreasing of the high temperature diffusion of Al from inside of the ODS structure to the surface for producing of Al-oxide layer. The role of the REM oxide particles is to inhibit the forming of a thick Al_2O_3 layer on the metal surface. and to avoid the spallation and cracks forming of this layer [6, 7]. On the other hand, the smoothening of the weld surface should allow the Al oxide layer to have a good adherence to the metal surface [7–11]. It is very difficult to keep the presence of the REM particles inside the fusion weld metal during the fusion welding. There were some attempts to use the pulse laser welding that the oxide particles could remain inside the weld metal [1, 2]. But in practice by using the pulse laser welding of ODS it was noticed that the Al oxide layer has defects as cracks or spallation, etc:and as a result the weld metal failed in the high temperature corrosion test [8]. It was not proved whether the cracks on those Al oxide layer appeared as result of the weld metal roughness or the weld metal compositions. Therefore, it is important to study the behavior of the REM in the base metal in addition to the presence of strengthening REM oxide particles. Excess of REM in the base metal should play a part of REM sours for their transferring to the weld metal during the welding process. In this paper the role of REM presence in the laser welding joint metal on the forming of REM oxide particles was studied.

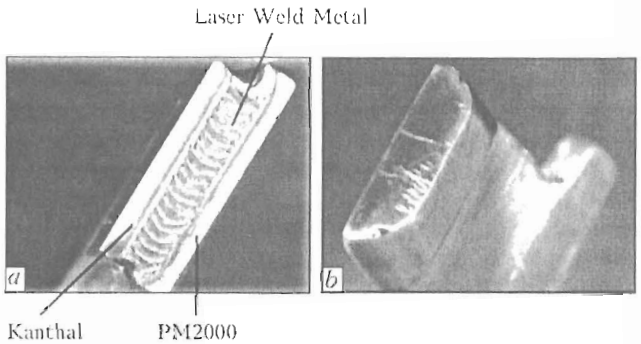


Figure 1. Pulse laser welded joint: *a* — welded pieces; *b* — smoothed laser weld metal.

Experimental procedures. The welded samples were prepared from PM 2000 ODS Steel plate 1.5 mm thickness which was laser welded to 1.5 mm thickness Kanthal AF ODS Steel plate. The Kanthal plate has 7mm width and 20 mm length. The PM 2000 has 20 mm width and 30 mm length. The two steel plates were jointed by pulse laser welding as it is illustrated on Figure 1. The data of the pulse laser welding was the following: The pulse length = 20 msec. the input energy = 51 J, the pulse frequency = 2 Hz, the welding velocity = 60 mm/min, the shielding gas was the Argon with flow rate = 20 liters/minute.

The welding process was done by using R56000 CO_2 apparatus. The welded surfaces of the laser welded samples were ground by silicon carbide papers up to No 600. The smoothed surfaces sample was tested

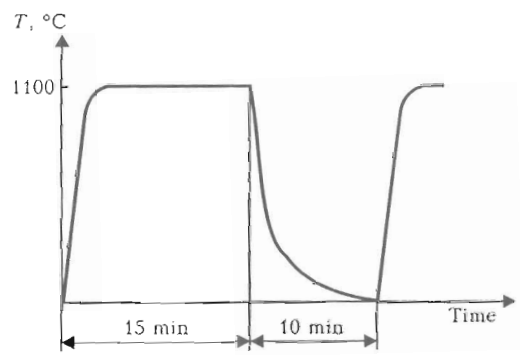


Figure 2. Cyclic high-temperature corrosion process

* The reactive metal is chemically active metal that was mentioned in the paper title.

© M. K. KARFOUL, 2005

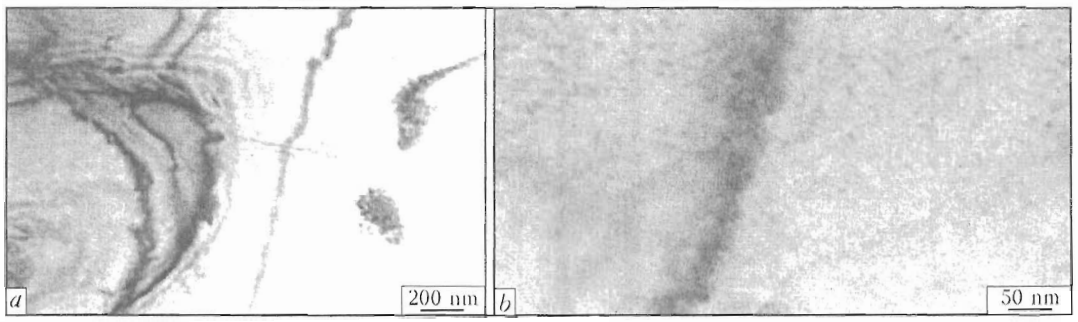


Figure 3. TEM-image of the PM 2000 HAZ closed to the weld metal (*a*), and the low middle zone (*b*) of figure (*a*), where the dispersed oxide particles are shown

for high temperature corrosion process. The corrosion test was done for the PM 2000 Kanthal AF welded couple on a special apparatus [8], which made a cyclic high temperature (1100 °C) corrosion process in air atmosphere as it is shown on Figure 2 (the heating time was 2–3 minutes and the average cooling rate was 100 °C/min). Such hard air corrosion process can illustrate a real corrosion behavior of the welded sample. The frequency of the high-temperature corrosion process was 1200 times which equals to 300 hours of corrosion process. From the welded and corroded samples a specimens were prepared for scanning and transmission electron microscopy study on Hitachi 2600 N scanning electron (SEM) and Joel JEM Fx II transmission electron (TEM) microscopes.

The experimental results and discussion: From the results of works [1, 2] it was not possible to propose a specific conclusion as well from the results of the work [8] about the rightness of these laser welding processes. To be sure that the welding process has right metallurgical data, the active metal oxide particles should be kept in the laser weld metal. In this view two different ODS-PM 2000 and Kanthal AF were chosen for laser welding. Both chosen ODS plates were laser welded together as it is illustrated on Figure 1. The used steel alloys have a chemical compositions as it is shown in Table 1. The Kanthal AF has in its structure a small quantity of soluble Zr and lesser Y. This Zr and Y-quantities are chemically free REM quantities, they can react with free soluble oxygen, which can appear in the weld metal during the short melting period of laser welding regime, or with less stable thermodynamically metal oxides.

The TEM image of the PM 2000 base metal at the HAZ closed to the weld metal (Figure 3) shows some structure deviation from the normal PM 2000 metal structure, but this zone still has a small dispersed oxide particles. On Figure 3 there are shown grain boundary lines on the weld metal side of the HAZ of the PM 2000. These lines indicate the removal of crystallization lines in relation to the heat transfer mechanism in the crystallized weld metal boundaries. At these intermediate boundaries the fine oxide particles are accumulated, but they still disperse in the melted HAZ structure. The strengthening oxide particles in the weld metal boundary HAZ structure are aspiring to agglomerate together in bigger size particles as it is shown on Figure 3, *a*, but the fine ones are still in the metal structure Figure 3, *b*. This HAZ metal structure is sufficient to give adhesion constancy, integrity and stability to the formed Al oxide layer by the high temperature corrosion process. The TEM image of the spot inside the weld metal (Figure 4, *b*) shows that

Table 1. Chemical compositions (wt.%) of the ODS used

Material	Fe	Cr	Al	Ti	Y	Zr	Y_2O_3	Mn	Si
Kanthal AF	Bal.	21.74	5.2	0.09	0.03	0.06	–	0.06	0.19
PM2000	Bal.	20	5.5	0.5	–	–	0.5	0.12	0.03

there are another formed oxide particles. It was proved by the EDX analysis (the spectrum on Figure 5, *b*) that these particles are mostly formed from Zr oxide. The Zr oxide particles appeared in the laser weld metal as result of the Zr reaction with the oxygen, which

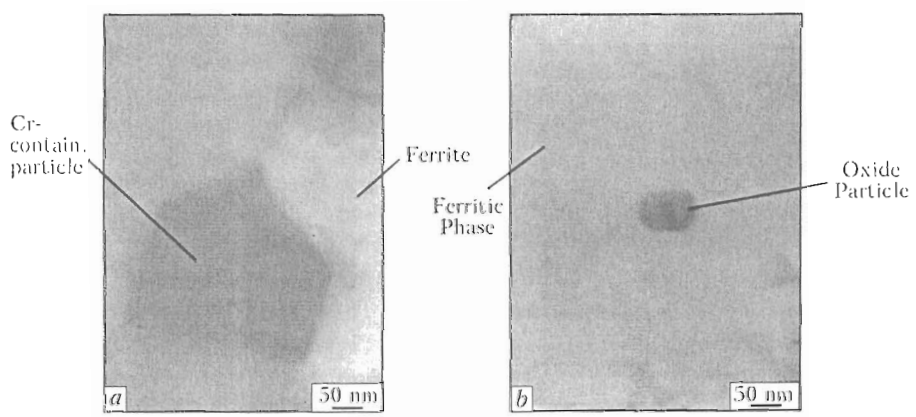


Figure 4. High magnification TEM-image of the Kanthal base metal structure in the HAZ (*a*) and the laser welded couple PM2000-Kanthal AF weld metal (*b*)

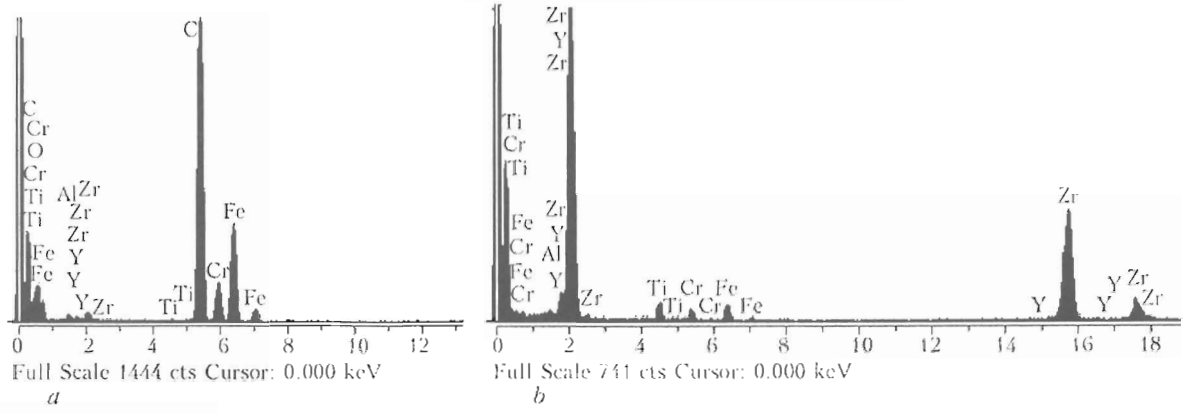


Figure 5. EDX spectrums of the particles: *a* — in HAZ Kanthal AF; *b* — in laser weld metal

was transformed to a reacting form as result of the heating to a high temperature during welding process. Zr was transferred from the Kanthal AF side of welded couple. The TEM study of the Kanthal AF base metal at the HAZ closed to the weld metal (Figure 4, *a*) shows agglomerated particles in base metal structure. The particles agglomeration took place as result of the welding temperature effect. It can be speculated that the combination of welding residual plastic deformation, possibly in conjunction with locally melted regions at grain boundaries (see Figure 4, *a*), promotes agglomeration of small particles (possibly these particles may contain chromium carbide, Ti, and Zr compounds) with larger Cr (C, N). Such process can go on easily at the positions of triple grain boundary junction as it is shown in Figure 4, *a*. It was proved by EDX analysis for these particles (Figure 5, *a*). Figure 5, *a* shows that these particles are mostly chromium containing particles as carbides with small quantities of Ti and Zr compounds (a similar proposal was promoted for explanation of agglomeration of small oxide particles during the friction welding of MA956 super alloy [12]). As result of re-crystallization process during the laser welding the Kanthal HAZ closed to the weld metal boundary should have high temperature corrosion resistance less than the base metal corrosion resistance. The high temperature (1100 °C) cyclic corrosion test (Figure 2) of the welded couple PM 2000-Kanthal AF (Figure 6) shows that on the surface of weld metal and the PM 2000 a good oxide layer has been formed. The results that were illustrated in Figure 6 prove the existence of good high temperature corrosion resistance of the laser weld metal and the PM 2000 base metal (including the HAZ). The oxide layer on their surfaces is without cracks and spallation. This result was mentioned earlier in this paper when the TEM image of the HAZ — weld metal zone microstructure was discussed (Figure 3). The EDX analysis of the formed oxide layer on the welding joint surface is shown on spectrum in Figure 7. This spectrum proves that the formed oxide layer is Al oxide.

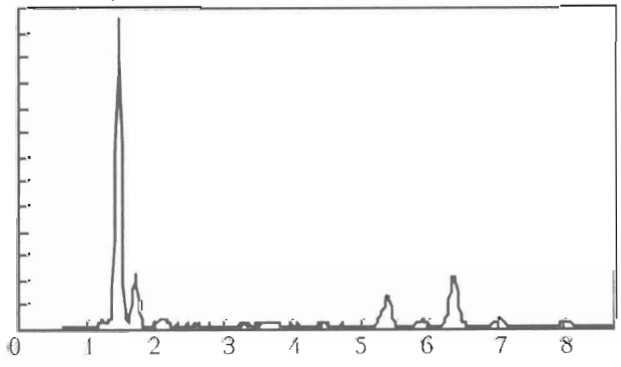


Figure 7. EDX analysis of the Al oxide layer

On the Kanthal AF side of the laser welding joint a roughness shape was noticed on the Al oxide surface (Figure 8). This roughness appears as result of the REM oxide particles absence in the Kanthal structure. The morphology of those Al oxide layer contains

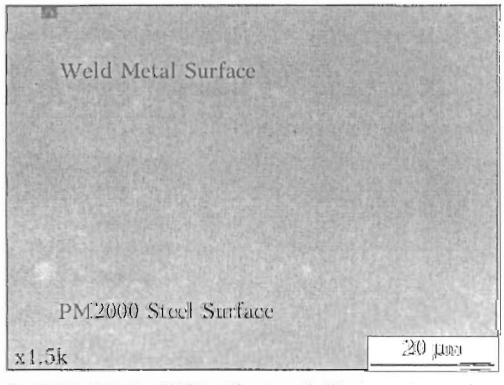


Figure 6. SEM-image of Al oxide morphology surface of laser welded joint

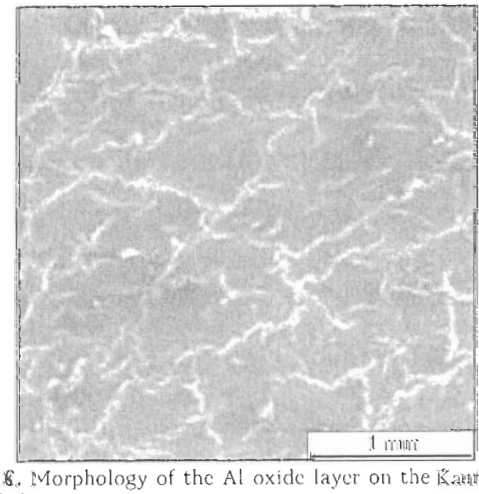


Figure 8. Morphology of the Al oxide layer on the Kanthal zone of welded joint

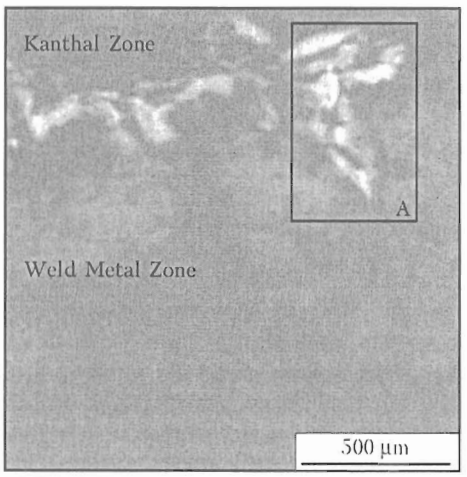


Figure 9. SEM-image of Al oxide layer on the welded joint surface

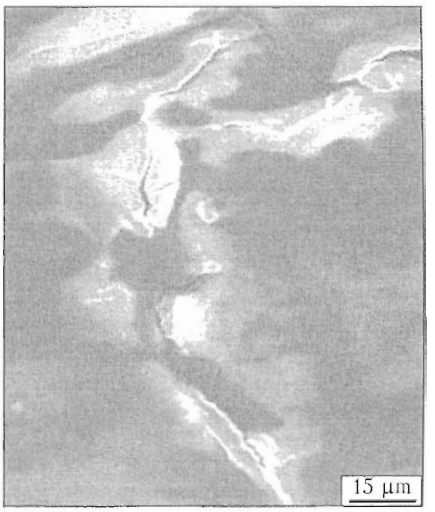


Figure 10. Morphology of α-alumina layer on the on the Kanthal–weld metal boundary zones (zone *A* in Figure 8)

cracks and other defects on the boundary zone between the Kanthal and the weld metal (Figure 9 and 10).

These defects on the oxide morphology of HAZ prove the proposition about the metallurgical aspects of the HAZ metal re-crystallization which was commented before. This means that the Y_2O_3 particles in the HAZ of PM 2000 did not loose the small sized strengthening yttrium oxide particles, and the ZrO_2 particles appeared in the weld metal structure, therefore the HAZ of PM 2000 base metal kept its high temperature corrosion resistance and the weld metal acquired such resistance after welding. The Al oxide layer morphology shows a constancy of non defected shape on these metal surfaces. These results coincides with the microstructure study of the welding joint metal (Figure 3 and 4).

CONCLUSIONS

1. It is possible to carry out successfully pulse laser welding of two different ODS steels.

2. The ODS laser weld metal will have high temperature corrosion resistance when the REM oxide particles exist in the weld metal structure.

3. The ODS welding joint will obtain a high corrosion resistance when the welded ODS couple has strengthening dispersed REM oxide particles in addition to a small concentration of REM in both ODS structures.

Acknowledgment. *The author wish to thank Prof. Dr. G.J. Tatlock and his staff in the department of Materials Science, The University of Liverpool UK for the help during the experimentation in 2003. The author would like to acknowledge his debt to Professor G.J. Tatlock for his guidance and fellowship during this work effort.*

1. T. J. Kelly, *Welding of Mechanically Alloyed ODS Materials*, American Society for Metals, Metals Park, Ohio 44073, 1982 p. 471.
2. P. A. Molian, Y. M. Yang, P. C. Patnaik, *Laser Welding of Oxide Dispersion-Strengthened Alloy MA 754*, Journal of Materials Science, 27, 1992, 2687–2094.
3. G. Merceron, R. Molins and J-L Strudel. *Oxidation behavior and microstructural evolution of FeCrAl ODS alloys at high temperature*, In Book «Microscopy Of Oxidation», Proceeding of the Fourth International Conference, Cambridge, September 1999, p. 87.
4. H. Al-Badairy and G. J. Tatlock. *The Application of a Wedge-Shaped Sample Technique for the Study of Breakaway Oxidation in Fe–20Cr–5Al Base Alloys*, Oxidation of Metals, Vol. 53, Nos. 1/2, 2000, p. 157.
5. G. Strhl, D. Naumenko, H. Al-Badairy, L. M. Rodriguez Lobo, G. Borchardt, G. J. Tatlock and W. J. Quadakkers. *«The effect of aluminium depletion on the oxidation behaviour of FeCrAl foils»*, In Book: Microscopy of Oxidation, Proceeding of fourth International conference, Cambridge, September 1999, p. 87.
6. A. Rahmel and M. Schtze, *Mechanical Aspects of the Rare-Earth Effect*, Oxidation of Metals, Vol. 38, 3/4, 1992, p. 255.
7. Vladimir K. Talpygo, The Morphology of Thermally Grown α-Al_2O_3 Scales on Fe–Cr–Al Alloys, Oxidation of Metals, Vol. 51, Nos. 5/6, 1999, p. 449.
8. P.Muangjunburee and G.J. Tatlock. *The study of α-alumina scale failure at welded joint in high temperature ODS alloys*. International Symposium Corrosion Science in the 21 century, The University of Manchester, UK, 6–11 July 2003, p-r H028.
9. A. G. Evans, G. B. Crumleym, and R. E. Demaray, On the *Mechanical Behavior of Brittle Coating and Layers*, Oxidation of Metals, Vol. 20, Nos. 5/6, 1983, p. 193.
10. Michael Schutze, *Mechanical Properties of Oxide Scales*, Oxidation of Metals, Vol. 44, Nos. 1/2, 1995, p. 29.
11. S. Uran, B. Veal, M. Grimsditch, J. Pearson, and A. Berger, *Effect of Surface Roughness on Oxidation: Changes in Scale Thickness, Compositio, and Residual Stress*, Oxidation of Metals, Vol. 54, Nos. 1/2, 2000, p. 73.
12. K.Shinozaki, C.Y. Kang, Y.C. Kim, M. Aristoshi, T.H. North and Y. Nako, *The Metallurgical and Mechanical Properties of ODS Alloy MA 956 Friction Welds*. Welding Journal, August 1997, 290 s.

SOME RESULTS OF RESEARCH IN HYBRID LASER-ARC TECHNOLOGIES AT THE E.O. PATON ELECTRIC WELDING INSTITUTE OF NASU

V. D. SHELYAGIN, I. V. KRIVTSUN, V. Y. KHASKIN, T. N. NABOK
E.O. Paton Electric Welding Institute, NASU, Kiev, Ukraine

Techniques based merely on the use of laser radiation, in determinate cases do not let obtain positive effect without supplementary process. It is so, for example, in butt welding of aluminium alloys essential to form the root and top rolls of amplifying which demands the infusion of filler substance. Such technological receipt demands the significant upswing of the power of laser radiation, and consequently boosts the cost of linear metre of joint.

In the deposition of coatings sometimes is needed so to localize thermal stress, in order it was close to stress in microplasma sputtering, but in this case the durability of linking of layers with basis must correspond durability welding deposition.

Generally speaking, it is desirable to raise peak the productivity of laser processes in combination with minimizing of cost of laser radiation power. To manage with such goals hybrid laser-arc processes allow.

Therefore the purpose of the research was to investigate of interaction between two heat sources (the laser beam combined with MIG/MAG, plasma transferred arc or plasma jet) to find out the peculiarities of the hybrid process, of their influence on formation of welds or on surface modification, as well as to combine the advantages of these sources and overcome their limitations.

For the achievement of this target by us were solved the following tasks:

1. On the basis of the analysis of existing variants were fetched the schematics of the processes of welding and the deposition of coatings.

2. On the ground of the family of experiments were cleared up the technological features of the processes of welding of steels up to 20 mm thick and aluminium alloys up to 6 mm thick.

3. Experimentally were determined the technological features of the process of hybrid laser-microplasma deposition of coatings.

4. According to obtained effects were developed the basic technological receipts of hybrid bonding butt joints and sawn joints, of the combined deposition of coats.

When carrying out the researches as a substance of patterns were utilized steels 20, St3kp, 18G,17G1S, 13G1S, 09G2S, 09M2SF, 10KhSND, 10G2FBYu, 38KhN3MFA, Kh18N10T, 08Kh17T up to 20 mm thick, as well as aluminium alloys AMg-5, AMg-6, 1915 and technical aluminum up to 6 mm thick.

In welding were utilized filler (electrode) wires Sv-08G2S (0.8... 1.6 mm), Sv-12Kh18N9T (0.9 mm and 1.0 mm). In the analysis of the combined processes laser-micro plasma doping and the application of fine coats were applied dusts by granularity of 0... 40, 60... 100, 50... 160 and 100... 300 μm of the alloys of system Ni–Cr–B–Si (PG-AN6, PG-AN9, PG-12N-01, PG-12N-02, PG-10N-04), of system Ni–Fe–B–Si (PG-N1, PG-N3), on the basis of iron (PG-S27), as well as the dusts of chrome, of nickel, Relite (of the carbide of tungsten), of the nitride of titanium.

In the process of experiments were utilized technological lasers LT-104 with maximum power 10 kW [3] and DF-020 HQ (Rofin-Sinar, Germany) with maximum power 2 kW. Apart from that, for hybrid welding with the arc of consumable electrode were utilized power supplies WDU-601 and PSG-500; for hybrid welding with plasma utilized the origin of proprietary design allowing to adjust welding current to 110 A, for the combined application of coats utilized upgraded power supply MPU-4, allowing to adjust current up to 60 A.

Experiments were realized on the workbench performed on the base of two-coordinate manipulator with operable margin X:Y = 2000:1200 mm, positional resolution up to 0.1 mm and the rates of operable transpositions up to 600 m/h, as well as on workbenches performed on basis of turning-screw-cutting tools. In this case we utilized the production accessories of native design.

Experiments on hybrid welding low-carbon low-alloyed steels by laser radiation with the arc of consumable electrode in guard by carbon dioxide were carried out as to schema, mentioned in [4]. They showed that cast metal of welded joints had preemptively ferrite-pearlite construction (relatively plastic with low hardness HV1-200... 250), and in HAZ are present tempering bainite constructions HV1-250... 300. In case of laser welding of patterns from the same substance with the same rate, as in cast metal of joint, so in HAZ predominate tempering bainite and martensitic constructions.

However despite the presence of tempering constructions and high hardness joints performed by laser

© V.D. SHELYAGIN, I.V. KRIVTSUN, V.Y. KHASKIN, T.N. NABOK, 2005

radiation, also have high enough meanings of durability and plasticity. This is concatenated with presence fine-grained equiaxial martensite [5].

Nevertheless, it is traditionally adopted to believe inadmissible the heightened hardness of joints and presence in them of tempering structures. Thus, for welding of tube steels requirement to joints and HAZ restrict their hardness at the level HV1-260... 280. In such cases laser-arc welding turns out to be preferable.

Another positive moment of laser-arc welding is the removal of root defects of laser welds, peculiar for welding by any high-concentrated energetic source and revealed in the peril of appearance scores and pores [6]. This is concatenated with the alteration of the hydrodynamics of weld pool.

With hydrodynamic processes going in weld pole during hybrid welding, are concatenated also periodic increases of and the reduction of depth of penetration as compared with laser welding in equal rates and capacity laser radiation [4]. The analysis of these processes allows to introduce correctives in process for amplifying of demonstration hybrid effect.

We had installed that in hybrid welding of steels by thickness up to 4... 5 mm 1 kW the arc of melted electrode is able to replace 1 kW the capacity of laser radiation, and in bonding of steels greater thicknesses — 1 kW arc replaces 0.5 kW the capacities of laser radiation.

By us was installed, what in hybrid welding depending on the rate of process occur the periodic deviations of the shareable height of weld and depth of weld penetration from monotonic dependence, peculiar for laser welding. Mathematical processing of experimental data showed [4], that such deviations were not occasional and exceeded the value of inaccuracy of the experiment. Such phenomenon can be explained in such a way. The wet metal of weld pool, formed by laser radiation, has native waves (their frequency can lie in the range 80... 200 Hz). On the back wall of steam-to-gas channel will form a stagnant wave. When the drop of the drops of the metal of melted electrode coincides with the frequency of autooscillations of weld pool, the resonant effect is observed.

Wet metal totally is eliminated from the bottom of steam-to-gas channel, deallocating the access to laser radiation to have not yet melted metal. The depth of weld penetration swells. In case of the mismatch of specified frequencies the wet metal of tail-end of weld pole saturates steam-to-gas channel, and the penetration depth descends.

Was established, that in laser-arc welding at power of sources up to 3... 4 kW is advisably for one pass to weld steel by thickness up to 10 mm. Greater thicknesses demand whether en-hancements of capacity (primarily laser forming) whether usages of multipass welding. By us was carried out technological aprobation of multipass laser and hybrid laser-arc welding steels by thickness 10... 20 mm. For welding by laser radiation with filler wire Sv-08G2S (∅ 1.2 mm) of low-carbon 20 mm thick steel had required 6... 8 passes

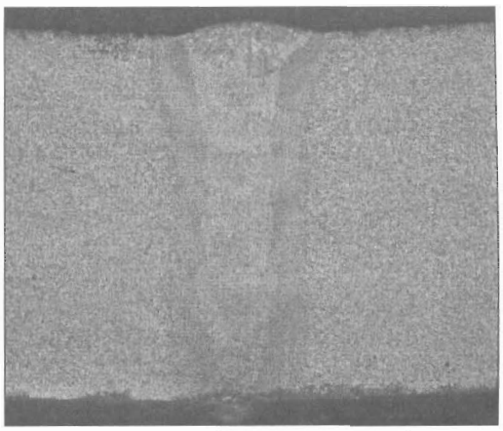


Figure 1. Macrostructure of butt from steel 20 (δ = 20 mm), obtained by laser welding with filler wire Sv-08G2S 1.2 mm for eight passes (P = 2. 8 kW, V_w = 12 m/h, V_{pr} = 250 m/h)

(Figure 1). The usage of hybrid welding allowed to flatten the Figure of passes up to four.

In the event of hybrid welding laser radiation will stabilize electrical arc and force her to go down in the narrow gap of V-similar grooving (of sequence 10°) on depth up to 20 mm. This effect is put in the basis of the developed technological receipts of hybrid welding of thick steels (Figure 2). Weld pool has relatively not large dimensions (length up to 30 mm).

The rigid thermal cycle, typical for single-pass laser welding, is softened at the expense of an arc component, and at the expense of repeated passes the propensity to formation of hardening structures is reduced. In case of laser welding with filler the heat input had made 0.84 MJ/m at speed of welding 12 m/h.

In case of hybrid welding the linear energy has made 1.125 MJ/m at speed of welding 24 m/h. Thus, the increase of linear energy approximately on third has allowed to increase general productivity of process of multipass welding twice under condition of transition from laser to hybrid laser-arc process.

The definition of shock viscosity of seams and HAZ on standard samples with a U-shaped cut was carried out at temperature +20 °C and V-shaped cut at temperature −20 °C. Samples were cut out from a medium part of connections welded by laser and hybrid ways

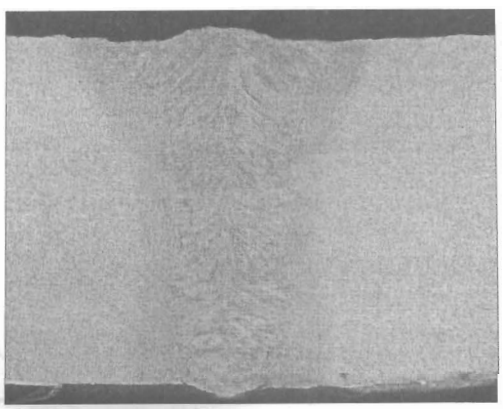


Figure 2. Macrostructure of butt from steel 10G2FBYu (δ = = 18.7 mm), welded by a laser MAG for 4 passes (P = 2.5 kW, V_w = 24 m/h, V_{pr} = 400 m/h, I = 200 A, U = 26 V, wire Sv-08G2S 1.2 mm)

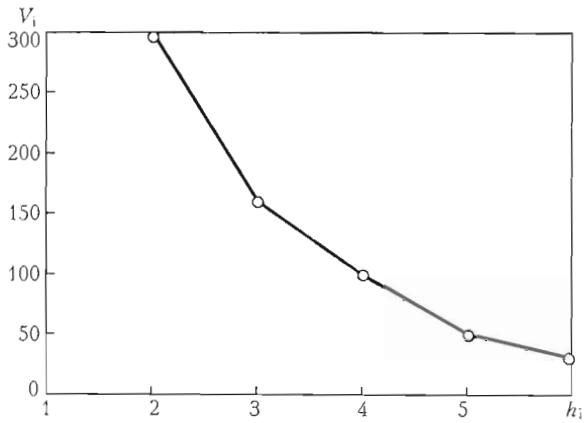


Figure 3. Relation of speed V [m/h] of hybrid welding of aluminium alloys from depth of a sheet h [mm] (P = 2.8 kW, V_{pr} = = 400 m/h, I = 200 A, U = 20 V)

(three samples each). Moreover, for comparison of the obtained meanings with a level of the basic metal from this metal was made and tested two similar samples. Decrease of shock viscosity in case of samples with a U-shaped cut (temperature of tests +20 °C) did not exceed 7...8 %. In case of samples of hybrid welding with a V-shaped cut (temperature of tests −20 °C) the shock viscosity of cast metal of a seam amounted 60...70 J and zone of thermal influence — 100...150 J/cm^2.

It is possible to consider the obtained results as satisfactory parameters of plasticity (7). In case of laser welding with filler wire, as expected, shock viscosity of a seam exceeds this parameter for HAZ. It is interesting to note, that in case of hybrid welding the inverse picture irrespective of temperature of tests takes place.

For welding of volumetric designs it is important to know behaviour of a welding pool and change of quality of a seam depending on spatial positions, in which the welding is conducted. Therefore we carried out the appropriate experiments, at which laser and laser-arc welding order in lower and upper (ceiling) positions, on rise and on descent. There was established, that a unsatisfactory quality (the presence of pores) and reduction of a weld penetration depth on 40...50 % concerning welding in lower position is ob-

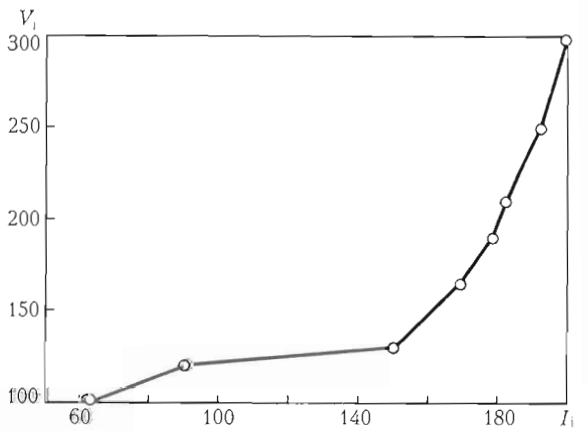


Figure 4. Relation of speed V [m/h] of hybrid welding of aluminium alloy AMg-6 (δ = 2mm) from an arc current I [A] (P = 2.8 kW)

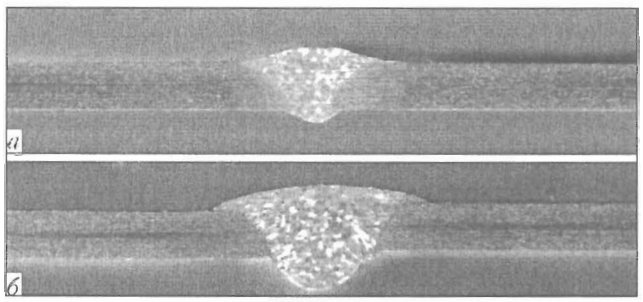


Figure 5. Macrostructures of butt joints AMg-6 (δ = 2 mm) performed by hybrid (*a*) and arc (*b*) methods

served at welding on descent. It is connected that the liquid metal from a tail part of a welding bath becomes numb in vapour-gas channel, forcing it to collapse. At welding the depth of weld penetration is increased by rise approximately on 20 % concerning welding in lower position, and the presence of filler material of metal often is not required.

It is caused by the improved conditions of outflow of liquid metal from vapour-gas channel into a tail part. The welding in ceiling position practically is identical to welding in the lower position.

The laser welding of aluminium alloys differs from welding steels not only because of high heat conductivity of aluminium. For achievement of stable process of welding of aluminium alloys by laser radiation with length of a wave λ = 10.6 microns are necessary to exceed the certain threshold of capacity — otherwise there will be a complete reflection of laser radiation from the surface of a sample, that can result in destruction of a focusing lens, to hit of radiation on the man etc. For materials by thickness up to 4 mm this threshold makes 2 kW. In a case of utilizing of smaller lengths of waves (Nd:YAG laser from 1.06 micron or diode laser with λ = 0.808/0.940 micron) such threshold is significant reduces. It is connected with dependence of absorbing ability of a surface of metal on length of a wave of laser radiation.

The comparative experiment was carried out at welding an alloy AMg-5 (δ = 3 mm) radiation CO_2-laser in protection by argon. In all cases the capacity of the laser radiation, focused on a sample, made 2 kW. At laser welding without filler the speed of process made 60 m/h.

The presence of a filler wire Sv-AMg-6 (1.2 mm) caused a reduction of speed of welding in 2 times. The hybrid process, in which besides laser radiation the arc with metal-electrode of the same wire was used at a welding current 100 A and voltage on an arc 20 V, has allowed to raise speed of welding up to 120 m/h. As a result of experiments on hybrid welding of aluminium alloys the graphic dependences, shown in Figure 3 and 4 were received. From Figure 4 it is visible, what in case of hybrid welding of aluminium alloys there is a threshold meaning of force of a current, which for AMg-6 (δ = 2 mm) corresponds 150 A. Before overcoming this threshold the increase of force of the current on 3 A raises speed of welding no more than on 1 m/hour, and after — the increase of force

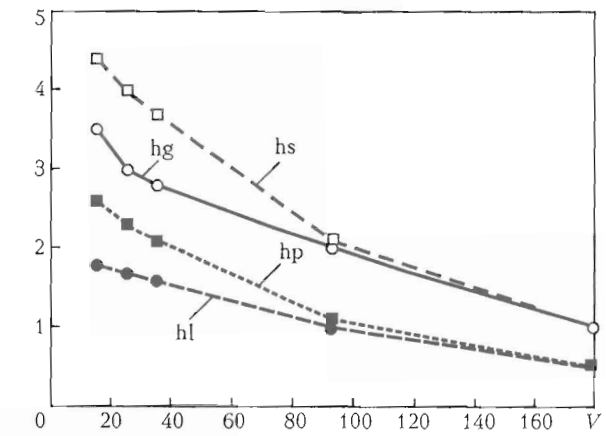


Figure 6. Dependence of laser hl, gas-plasma hp and hybrid hg [mm] weld penetration depth of stainless steel sheets on the rate of welding V [m/h] at the power of diode laser 2 kW and argon plasma 2 kW (hs — sum of depth of laser and gas-plasma weld penetration, mm)

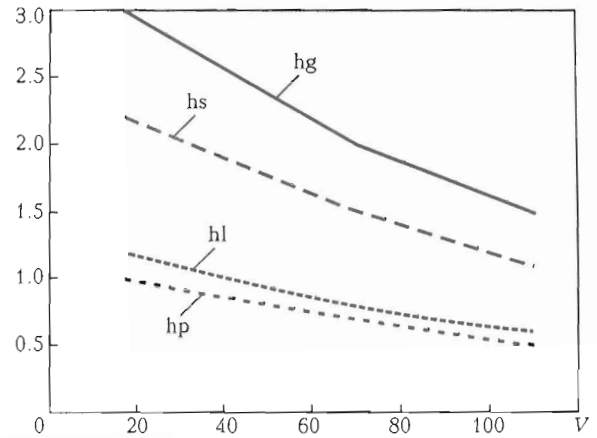


Figure 7. Dependence of depth of laser hl, gas-plasma hp and hybrid hg [mm] weld penetration of aluminium alloy AMg-6 sheets on the speed of welding V [m/h] at diode laser beam power 1.2 kW and argon plasma 0.8 kW (hs — sum of depth of laser and gas-plasma weld penetration, mm)

of a current on 1 A raises speed of welding approximately on 3 m/h. As a result of hybrid welding of an alloy AMg-6 the satisfactory formation of the upper and lower beads of strengthening of a seam was achieved at speed 300 m/h (Figure 5). Thus the residual deformations considerably have decreased in comparison with consumable electrode welding, and the structure of seams became more small-grained and equiaxial.

One of the basic lacks of welding aluminium and of titanic alloys, and also stainless steels by radiation CO_2-laser is the partial absorption of laser radiation by argon plasma and opportunity to refocus it in case of occurrence of a so-called plasma lens [8]. For elimination of this lack as a laser component of hybrid process was used radiation of the diode laser, for which the argon plasma is transparent because of shorter length of a wave (λ = 0.808/0.940 microns). However, in connection with unsufficient density of power (the focus spot made up ~1.2 mm) on stainless steel hybrid effect was not showed, as against welding aluminium alloys (Figures 6, 7). It is explained to the following. The hybrid effect is shown the more strongly, than more intensively welded materials under influence of laser radiation evaporate, i.e. than the laser plasma is more intensively formed, by which occurs an arc-over. In aluminium alloys easily evaporated magnesium was comprised.

Besides researches in the field of hybrid welding, we carried out researches of hybrid laser-microplasma deposition of coats and alloying. The firms LERMPS-IPSe and IREPA-Laser have developed and have patented technology «Protal», which at the expense of incomplete overlapping by zone of laser heating of plasma deposition zone provided effect of preparation of a surface, excluded necessity of jet-abrasion processing [9]. As distinct from such technology the processes of deposition of coverings and alloying, offered by us, come nearer to laser surfacing and laser alloying. Thus the presence of laser radiation allows to eliminate the necessity of pre-liminary preparation of a surface of a sample, and the microplasma component allows to remove characteristic for laser weld deposition formation of microcracks in deposited layers. The laser-microplasma processes were carried out according to the scheme shown in Figure 8. On it the basic parameters of processes of drawing of coverings and alloying are shown. In conditions of accomplished experiments are determined most significant from these parameters (Figure 9). Carried out metallography researches have shown a presence of a narrow transitive zone (3... 5 microns) and an absence of HAZ in case of deposition of coverings, and also presence of HAZ (up to 0.2... 0.3 mm) in a case of alloying. In both cases in the top layers of coverings (pathes of alloying) the fall of hardness on 20... 30 % from hardness of a filler material takes place. It is not critical, as the size of these layers is comparable to size of allowance under finishing machining. On height deposited for one pass of coverings the greatest influence renders the mass consumption of a powder and factor of overlapping of pathes. Speed of moving of a sample and density of capacity of laser radiation to a lesser degree influences. Influence of change of a corner between axes

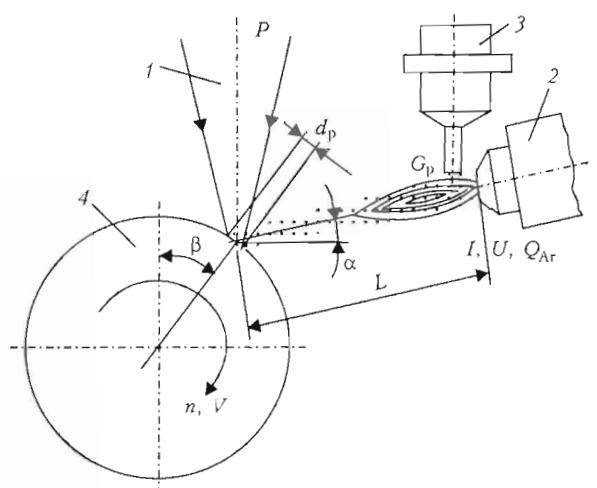


Figure 8. Scheme of laser-microplasma of deposition of coating and doping: *1* — laser radiation; *2* — microplasmotron; *3* — metering device; *4* — sample

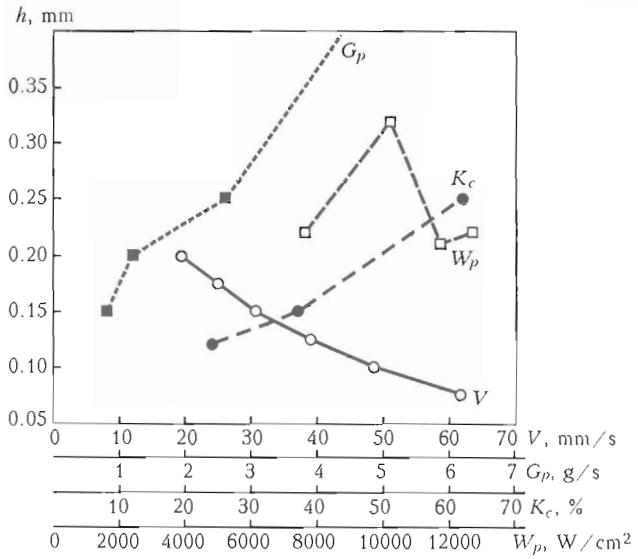


Figure 9. Relations of the altitude (mm) of layer from the parameters of combined deposition of coatings from dusts PG-AN9 and PG-N1 obtained in following conditions: $h = f(V)$ in $W_p = 10.19$ kW/cm², $G_p = 0.26$ g/s, $K_c = 37\%$; $h = f(G_p)$ in $W_p = 10.19$ kW/cm², $V = 30.6$ mm/s, $K_c = 24\%$; $h = f(K_c)$ in $W_p = 10.19$ kW/cm², $V = 30.6$ mm/s, $G_p = 0.26$ g/s; $h = f(W_p)$ in $V = 30.6$ mm/s, $G_p = 0.26$ g/s; $K_c = 62\%$

of laser radiation and microplasma jet on height of a covering during the carried out experiments is not established.

On the ground of suggested review of works can be made the following conclusion:

1. An influence of the drops of electrode metal on the surface of welding pool in hybrid welding results in resonant phenomena, for account of which can be increased penetrative ability of laser component.

2. The demonstration of hybrid effect is in direct proportion to development of the density of power of laser component. Laser beam creates intensive narrow-directed stream of the vapors of metal expiring from the heating spot. This stream promotes the compaction and the stabilization of electrical arc and forces her to go down into vapour-gas channel or narrow gap in welding of thisk-sheeted steels.

3. The supplementary thermal stress of electrical arc lets goal-seeking to manage the thermal cycle of process for obtaining of the demanded constructions of weld metal and HAZ. In this case at welding thermal cycle of hybrid process the steepness of anterior front is approached to laser, and slope of back front is adjusted so, in order to eliminate the formation of tempering constructions in weld metal and HAZ.

4. In the laser beam power up to 3...4 kW the usage of the hybrid process of welding of steels advisably up to the thickness of sheet 10 mm, over which penetration depth does not grow, regardless of abatement of the rate of welding. Welding of greater thicknesses is possible for account of usage multipass laser or hybrid welding without upswing of the capacity of laser radiation.

5. The analysis of hybrid welding in differential spatial positions showed the universality of this method. Is installed, what penetration depth in bottom and top positions is identical, in welding «on raising« depth swells on ~20, and in welding «on lowering» descends on ~40% with the formation of pores. This is caused by hydrodynamic processes in welding pool.

6. Combined laser-microplasma doping of steels and deposition on them fine coatings (50–300 μm) allow to eliminate the formation of microcracks, the requisite of the abrasive-jet preparation of deposited surfaces and decrement allowance on finish machining up to 30–150 μm.

1. *The technology of electric welding of metals and alloys by melting.* Edited by B.Paton. — Moscow, «Mashinostroeniye», 1974–768.
2. Shelyagin V. D, Khaskin V. Yu. (2002) *Tendencies in development of laser-arc welding (Review)*, Avtomatich. Svarka, 6, 28–33.
3. Garashchuk V. P., ShelyaginV. D, Nazarenko O. K. et al (1997) *Technological CO_2-laser LT-104 of 10kW power*, Avtomatich. Svarka, 1, 36–39.
4. Shelyagin V. D, Khaskin V. Yu., Garashchuk V. P., Siora A. V., Bernatsky A. V., Sakharnov A. V. (2002) *Hybrid CO_2-laser and CO_2 consumable-arc welding*, Avtomatich. Svarka, 10, 35–37.
5. Gulyaev A. P. *Metal science.* — Moscow, Oborongyz, 1963. — 464.
6. *The electron-beam welding*, Nazarenko O. K. Kaydalov A. A., Kovbasenko S. N. et al.; Edited by B. Paton. — Kyiv, Naukova dumka, 1987. — 256.
7. Semyonov S. E., Mandelberg S. L., Goncharenko L. V. (1989) *Concerning optimal level of shock viscosity of seams of metal gas-pipes*, Avtomatich. Svarka, 11, 55–57.
8. *The laser engineering and technology*. In 7 vol. VI. 5. The laser welding of metals: The manual for higher education establishments // Grigoryants A. G., Shiganov I. N., Edited by Grigoryants A. G. — Moscow, Visshaya Shkola, 1988. — 207.
9. Coddet C., Montaron G., Marchione T., Freneaux O. *Surface preparation and thermal spray in a single step: the PROTAL process*, Proc. of 15 th ITSC, Nice, France, 1998, vol. 2, p. 1321–1325.

STUDY OF CHEMICAL ELEMENT DISTRIBUTION IN A LASER WELD JOINT

T. N. SOKOLOVA, E. L. SURMENKO
Saratov State Technical University, Russia

Laser is one of the most frequently used welding instrument when a high locality, a short duration of influence and an aesthetic view of the weld joint are important. Numerous researches revealed significant changes of structure, element composition and physical properties of substances in laser processing zones. These data show, that despite of short duration of action of high-energy laser beams on materials, in zones of defeat the processes of carry of substance take place. Thus, the distribution of alloying elements after the termination of influence of a laser pulses differ from initial [1–2]. Redistribution of impurities, in turn, influences physical, mechanical and operational properties of materials.

After the beginning of laser-matter interaction a thin layer of liquid metal is formed near to the border of destruction. Its thickness is the less, than the higher the power density of radiation. The higher the power density of a laser radiation, the less the thickness of a melt zone in the material being processed for every definite energy or power level. This narrow layer of the melted material during the process of laser-matter interaction can be enriched or impoverished by alloying elements and impurities because of the different elasticity of vapours of alloying elements and base metal. Thus, when the border of destruction is moving the process of evaporation occupies atoms from a surface of the border layer and some part of impurity atoms from the transitive layer δ_D adjoining to a border.

There is one more reason of redistribution of chemical elements in the layer adjoining to a zone of a laser influence. The border «liquid phase – solid material» moving during the laser pulse action onto a zone being processed takes from a solid phase the impurities whose solubility in a liquid phase is more than in solid. Velocity of dissolution is defined by temperature in a liquid phase, by time of a contact between liquid and solid phases, by physical nature of impurity atoms and by concentration of the element. For the most of materials their solubility in a liquid phase is higher than in a solid phase. That is why before a border of a liquid phase from the side of a base material the layer impoverished by impurities have to be formed.

Thus, the initial distribution of impurities in the zone adjoining to the place of laser influence should differ from the final distribution.

Object. As the investigated objects, as an example, ten weld joints of aluminum-magnesium alloy (AMg3) were taken. This alloy contains 3.2–3.8% of Mg depending on mark and the set of standard impurities, such as Fe, Cu, Ti, Mn etc. The welding of aluminum and its alloys represent a special interest and specificity because of singularities of interaction with an atmosphere [3]. That is why the multifold study of aluminum weld joints is important.

We studied redistribution of impurities in weld joints in depth of fusion and in horizontal zones of joints (Figure 1).

Laser jam welding was produced by CW Nd:YAG-laser, $\lambda = 1.06$ μm, $P = 1$ kW. The thickness of welded ridges was about 3 mm. The width of weld joints was about 2–5 mm on the side of a laser action and about 0.5–3 mm on the reverse side of joints.

The wide laser weld joints (4–5 mm) were studied on 3 horizontal zones (Figure 1): a boundary zone on the edge of the joints, a center zone of the joints and an intermediate zone – between two previously mentioned. When the width of joints was less than 4 mm the intermediate zone was eliminated from reviewing and only the border and the center of such weld joints was studied.

Eight vertical zones were taken for investigation: three on the side of a laser action with consequent deepening, each to depth about 250 μm; three on the

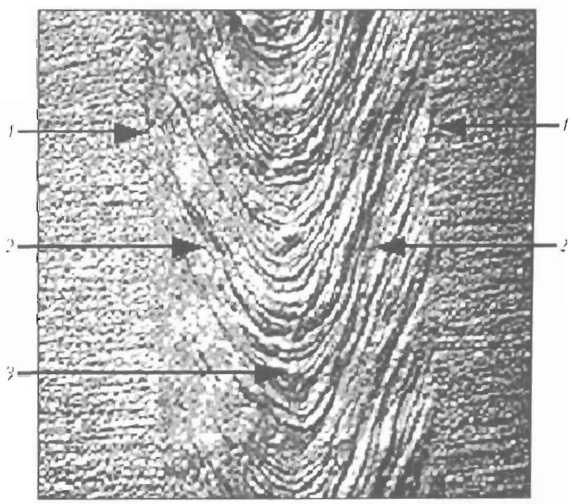


Figure 1. Horizontal zones of aluminum laser weld joint (5 mm width): *1* – border of a joint and a base material; *2* – intermediate zone; *3* – center zone

© T. N. SOKOLOVA, E. L. SURMENKO, 2005

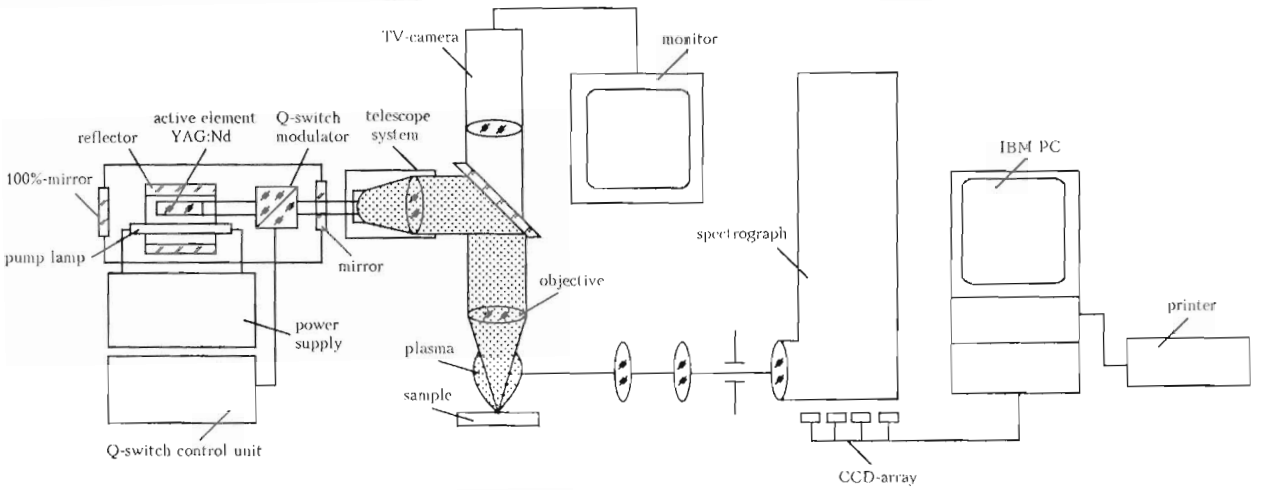


Figure 2. Schematic of the laser analytical setup LDMA

reverse side of joints the same way; two on the cross-section of joints apart about 1 mm from the laser action side and from the reverse side of the weld joint.

Method. The chemical elements distribution in a laser weld joint was studied by laser emission microspectral analysis or, in other words, LIBS – laser induced breakdown spectroscopy. The study was carried out on device of LIBS-analysis LDMA [4] (Figure 2). In this device the radiation of laser plasma without additional excitation by electric discharges is used.

The source of spectra excitation is Nd:YAG-laser (λ = 1.06 μm), Q-switched. A pulse repetition rate is 25 Hz. The power density in a monopulse mode is 10^{10}–10^{12} W/cm^2. The focus spot size is from 10.8 μm.

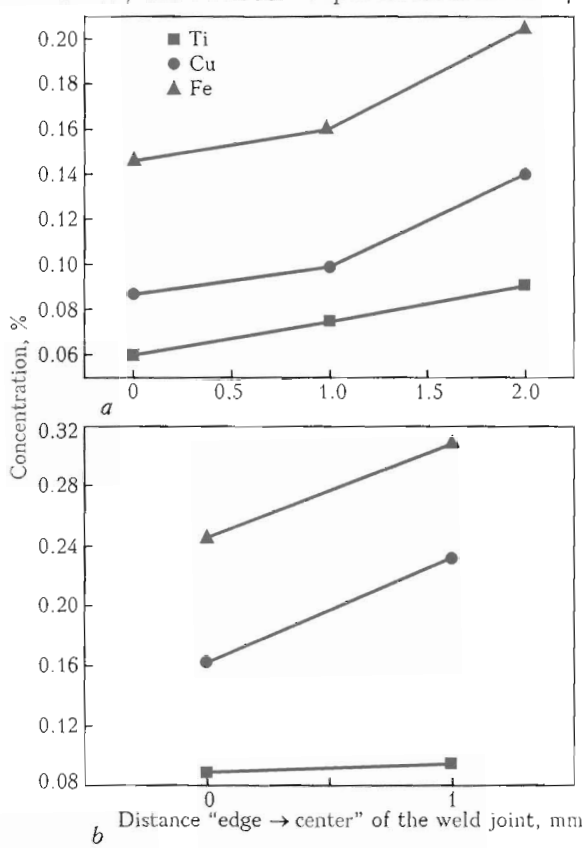


Figure 3. Behavior of Fe, Ti, Cu in horizontal zones: *a* – side of a laser action during welding; *b* – reverse side of the samples

The diameter of a laser crater on the surface of the material is up to 300 μm for different substances. The limit of element detection is 10^{-10} g; the relative limit of detection is about 0.001 %.

The spectrograph with gratings 900, 1200, or 1800 mm^{-1} and CCD camera ensuring the analysis in the spectral range 200–800 nm, as well as the special software for processing of spectra were used.

The aluminum samples were clamped and positioned beneath the laser beam. The sampling from joints was implemented by three consequent deepening into one point. Exposition time of each analytical act was 1 s. For each zone four sets of laser sampling were made. The calibration graph for quantitative analysis was constructed using the special set of etalons for quantitative spectral analysis of aluminum.

Results. The first part of the experiment was devoted to the investigation of a chemical elements behavior on the distance from the edge of laser weld joints to the center zone.

Two graphs for such impurities as Fe, Cu and Ti are shown on Figure 3, *a*, *b*. These are the pictures for one weld joint, they are typical for the enough wide «upper» side of a weld joint (from the side of a laser action) and the narrow reverse side.

Evidently, the border «liquid phase – solid material», which is represented by the edge of laser weld joints in a horizontal plane, is really impoverished by impurities. This is an important enough conclusion, because it proves that impoverishment takes place not only in direction of the laser beam but also on the lateral surface of laser weld joints.

The results for the investigation of a chemical elements behavior on the deepening in the direction of the welding laser beam action are not the same for different elements (see Figure 4, *a*, *b*, *c*). On the Figure 4 the abscissa axis represents the set of vertical zones, each of which conditionally defines the degree of deepening into a laser weld joint. Digits 1, 2, 3 for laser action and reverse sides mention the number of a sampling; «1, cr.-s.» is the laser sampling from cross-section of a joint near the action side, «2, cr.-s.» is the same near the reverse side.

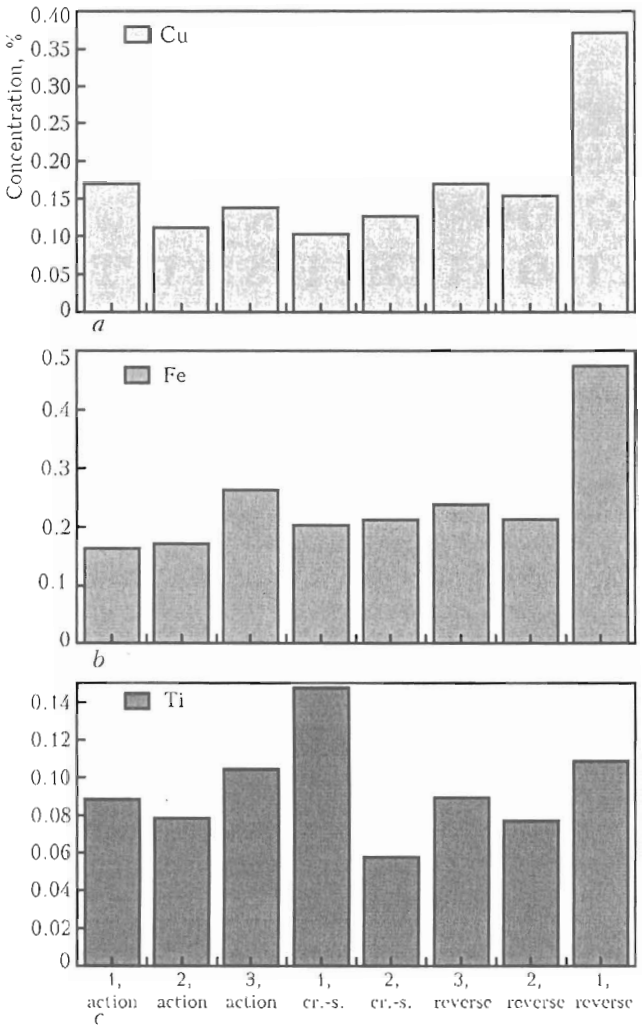


Figure 4. Behavior of Cu, Fe, Ti in vertical zones on the depth into the central horizontal zone of the laser weld joint (for details see the text)

The concentration of iron shows the quite stable tendency to an increase. The border of a liquid phase moving in the direction of the laser beam carries away the atoms of Fe. It apparently is linked with the process of crystallization after cancellation of action of welding laser light and with the consequent cooling of a laser weld joint.

Another tendency show copper and titanium. Besides an apparent maxima on the border of the stiffened liquid phase these elements have intermediate extremums of concentration, and, that is typical, in the same zone — approximately on the third of the joint width. This difference can be linked with the different densities of these substances (they are practically opposite on this item) and the polymorphic transmutation of heated titanium. Apparently on T = 882 [5] the high-temperature modification of Ti is concentrated on the layer on which it initially reached this temperature.

CONCLUSIONS

The distribution of chemical elements in a laser weld joint really varies at removal from the border of the liquid phase and depending on depth of a fusion. Impoverishment by impurities takes place on the edges of weld joints. The curves of concentration of elements on the different depth of a laser weld joint have individual natures for each element depending of physical and chemical properties of the materials.

1. A.A. Uglov, A.N. Kokora, M.A. Krishtal, *«About distribution of some elements in zones of action of a laser beam in alloys processing»*, Physics and Chemistry of Materials Procesing, N4, pp. 3–7, 1973.
2. J.O. Milewski, M.B. Barbe, *«Modeling and analysis of laser melting within a narrow groove weld joint»*, Supplement to the Welding Journal, pp. 109–115, April. 1999.
3. C.A. Huntington, T.W. Eager, *«Laser welding of aluminum and aluminum alloys»*, Welding Journal, 62 (4), pp. 105–107, 1983.
4. A.E. Kriger, E.L. Surmenko, L.A. Surmenko, V.V. Tuchin, *«Applications of direct atomic laser spectral analysis of laser plasma for determination of inorganic components presence in biological objects»*, Proc. SPIE. Bellingham, SPIE, v. 4001, pp. 299–303, 1999.
5. *Materials technology*. B.N. Arzamasov, I.I. Sidorin, G.F. Kosolapov et al; ed. by B.N. Arzamasov, Moscow, Machine Engineering Publishing, 1986, 384 pp.

LASER WELDING OF STEEL SHEETS DIFFERENTIATED IN THICKNESS FOR TAILORED BLANKS. INVESTIGATIONS CONDUCTED AT THE INSTYTUT SPAWALNICTWA

S. STANO, M. BANASIK, J. DWORAK, J. PILARCZYK
Institute of Welding, Gliwice, Poland

The investigations conducted at the Instytut Spawalnictwa in Gliwice into technology of laser welding of galvanized car body sheets, dissimilar in thickness, designed for tailored blanks, have been presented. It has been described the essential requirements imposed on the joints of this type. Different techniques of laser welding, such as dual beam laser welding and hybrid welding have been discussed. Keywords: laser welding, laser CO_2, tailored blanks, hybrid welding, dual beam, twin spot

Implementation of laser welding technology to industry is generally considered to be one of the most important directions of modernization of technological processes. World competition in this field forces for ever the application of new conceptions, both in laser equipment design and laser welding technique. Fundamentally, to-day in manufacturing processes, there are used most often welding lasers of two types, which provide the proper power level, high reliability and operational stability. These are CO_2 lasers (laser beam wavelength being 10.6 μm) and solid state lasers of the YAG type (laser beam wavelength being 1.06 μm). After the time of intensive development, especially in the last decade or so, nowadays dozens of companies offer a variety of laser radiation generators and specialistic or general purpose welding equipment based on them.

Laser welding enables to perform welded joints of various kinds, at any welding position, within the wide range of material thickness, both with addition and without filler metal. Specific properties of laser radiation enable to concentrate the beam very strongly and to obtain huge temperature gradients in the place of its impact, resulting thereby in very quick melting or evaporation of the material. It allows to achieve very high welding speed while only a small amount of the parent material is molten and the area of thermal influence is not large. In comparison to arc welding methods, in laser welding processes, the heat affected zone, where structural changes and thermal distortions appear, is more constrained, whereas the productivity is much higher.

Laser welding is bound together with overcoming a number of difficulties arising from very high power density possible to obtain in the zone of the laser beam influence. For instance, very high speed of metal heating or cooling (the cooling time from 800 °C to 500 °C in welding of constructional steel with typical CO_2 or YAG industrial lasers is most often within the range of $0.5\,s \leq t_{8/5} \leq 10\,s$) can bring about the local increase in the hardness, even in easy-to-weld by arc methods unalloyed and low-alloy constructional steels. Moreover, different conditions of weld formation, such as high welding speed, low heat input and low values of weld-shape factor (weld face width to penetration depth ratio) within the range of 1:5 to 1:7 are conducive for weld hot cracking and pore formation [1, 2]. This gives rise to necessity of development of welding technology very precisely, for individual devices and applications. Thanks to the advance in equipment design and intensive technological investigations on new techniques, laser welding becomes to-day an industrial method, competitive to arc welding and resistance welding.

Laser welding is applied in different industrial branches, but automotive industry is at present and will be in the nearest future the pioneer in implementation of this technology. In automotive industry, the widest range of laser methods is used nowadays. In car manufacture, lasers are applied to welding, cutting, marking, building up and surface treatment. Laser technology is employed for processing of materials of various kinds used in car manufacture, for instance constructional steels of different grades, aluminium and magnesium alloys, plastics, woven fabrics and so on. There are applied technological lasers of all types: CO_2 lasers, YAG lasers and also high power diode lasers. One of examples of effective use of laser welding technology in automotive industry, in technical and economical aspect, is welding of semi-finished components of car bodies, so called «tailored blanks».

In structures consisted of press formed elements, such as car bodies, operational aspects show that in case of large-size body panelling drawpieces it would be advantageous to use, inside the same drawpiece, a sheet locally thickened or that of higher-strength steel in the places determining passive safety of users and the strength of the structure, and a sheet locally thinned in these places in which the sheet is only a fragment of body panelling (Figure 1). These constructional and operational needs are satisfied by charges for press forming of a new type, so called

© S. STANO, M. BANASIK, J. DWORAK, J. PILARCZYK, 2005

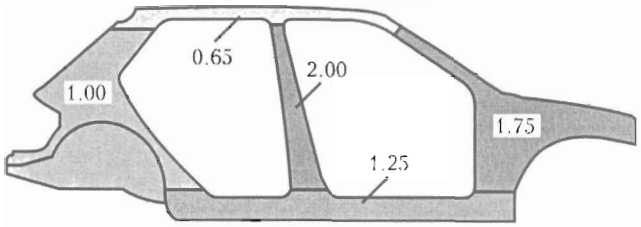


Figure 1. Example of making use of tailored blanks in construction of car bodies

tailored blanks. The conception of manufacture of such a charge consists in joining (mainly by laser welding method) of component parts cut out of flat steel sheets dissimilar in thickness, chemical composition, mechanical and plastic properties and covered with different protective coatings. Flat components are laser welded and next, the whole is pressed to form suitable shape and dimensions [3–6].

Conventional methods of joining of car body elements, such as resistance welding or arc welding, do not yield satisfactory results in case of joining of advanced steel plates covered with protective coatings. High heat input brought into the joint in arc welding of car body sheets, besides substantial distortions difficult to control and low mechanical properties of welded joints, results also in damage of protective coatings on a large area along the joint line.

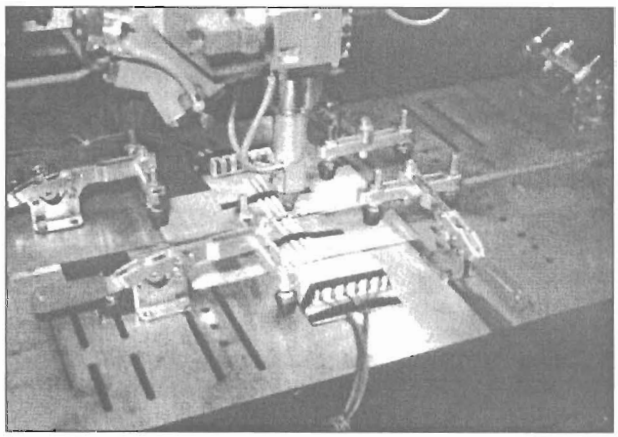
Application of laser welded blanks for press forming of car body elements yields a number of advantages among which the following should be accentuated:

- reduction in the vehicle weight resulting from possibility of optimum selection of the material for individual fragments of body panelling (sheet thickness, yield point and strength of the material),
- decrease in the number of drawpieces and technological-assembling operations, considering the possibility of resignation of internal drawpieces strengthening the structure,
- reduction in the amount of charge material in consequence of better utilization of the sheet metal and pressing the product practically without technological waste,
- improvement in operational features of the vehicle. The use of tailored blanks for press forming depends on resolving a number of technological problems connected with the manufacture of the blanks (cutting and welding) and with the design of charge blanks and press forming processes.

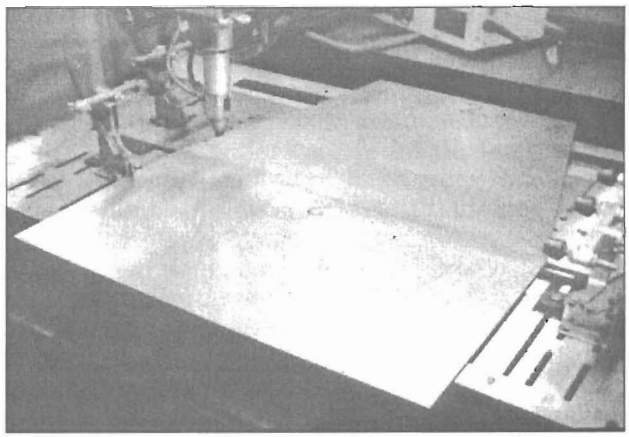
The problems relevant to the manufacture of a blank are, in the main, those related to cutting and welding of galvanized deep-drawing sheets differentiated in thickness, and determination of technological conditions for these processes providing optimum quality of welded joints.

The joints of laser welded blanks should meet the following requirements:

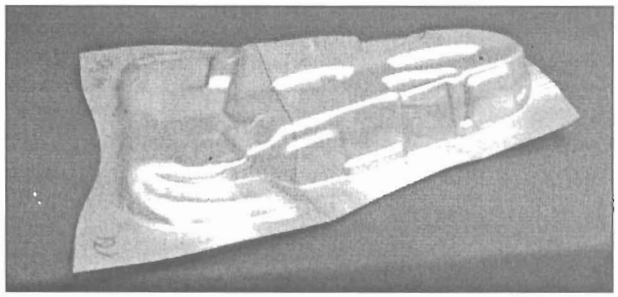
- they should be homogeneous to the last degree, without welding imperfections such as porosity, cracks, undercutting and incomplete penetration, while the weld face and root should be shaped in the best possible manner,



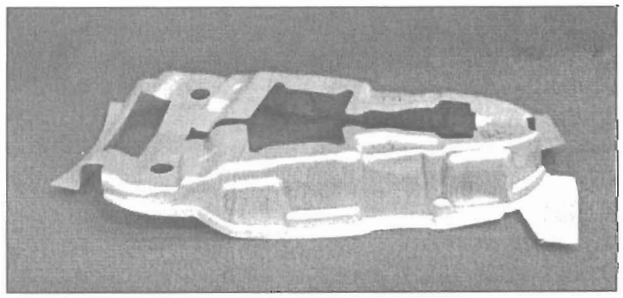
Experimental station with the set of thermocouples for testing of thermal cycles in laser welding of sheets designed for tailored blanks



A tailored blank after laser welding appropriated for press forming



An element of the tailored blank type welded at the Instytut Spawalnictwa, after pressing operation



Ready element of car body after three-dimensional laser cutting out

Figure 2. Test welding station at the Instytut Spawalnictwa for manufacture of tailored blanks, equipped with Trumpf Lasercell 1005 system with 3.8 kW CO_2 laser and ready tailored blanks for car bodies

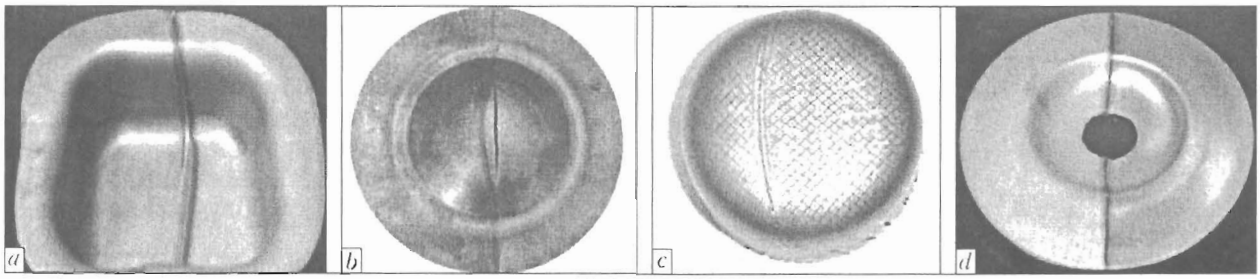


Figure 3. Photographs of drawpieces obtained from laser welded blanks made of sheets dissimilar in thickness and of different steel grades; *a* – cup drawing test with the use of the punch, square in cross-section, with flat bottom; *b* – bulging test with the use of ball-shaped punch; *c* – cup drawing test acc. to Swift; *d* – KWI test

• they should be characterized by the narrow and very plastic heat affected zone (the width of HAZ should approximate the thickness of joined sheets),

• properties of all joint areas should be similar as much as possible to those of component sheets.

Investigations into the development of welding procedures for the blanks refer, first of all, to determination of the optimum manner of aiming of the beam at the contact place, determination of suitable gas shielding for the molten metal pool and the manner of influencing on vapor plume as well as to the selection of such technological parameters which would ensure the process stability and the required joint properties. Different thickness of the sheets in the contact line of their edges imposes requirements as for the selection of the point and angle of aiming the beam at the contact line and such a positioning of the focus in relation to the situated at different height sheet edges that the smooth weld-to-parent metal interface without appreciable structural notches may be obtained. The manner of the blow in and the flow velocity of the shielding gas (helium or argon) shall be selected so that the influence of vapor plume arising from the welding process is optimized and the proper shielding of the molten pool is provided.

The construction of the tooling system for positioning and fastening of components to be welded is no less important than the choice of suitable process conditions. Such a system should secure the proper repeatability and precision of matching the sheets to be joined and to make allowances for stresses and strains generated in the joint in the course of welding.

At the Instytut Spawalnictwa it was made complex investigations into CO_2 laser butt welding of sheets designed for tailored blanks with the use of three different welding techniques:

• single spot laser welding,

• twin spot laser welding,

• laser – TIG hybrid welding.

In Figure 2 it is shown the experimental station for welding of tailored blanks and an example of welded, ready, tailored blank – an element of car body. At the Instytut Spawalnictwa, in collaboration with the Silesian Technical University in Katowice it was developed procedures of welding and press forming tailored blanks of particular type.

The general principle of the choice of sheets for joining them into one press forming charge blank is the selection of sheets differentiated in strength and in thickness to as low degree as indispensable. The minimization of the difference in sheets thickness is aimed at the elimination of the geometrical notch which is formed in consequence of joining two sheets dissimilar in thickness. Such a procedure is justified especially in case of press forming of sub-assemblies of car bodies which are strongly loaded in the course of the car operational use or determine the passive safety of its passengers. The basis of design of the press forming process, however, is the quantitative analysis of the mechanical state of the distortion zone and the analysis of the process of plastic flow of the charge blank. The assessment of press-formability of laser welded blanks, and more precisely, the recognition of the problem of the influence of weld metal on the process of plastic flow of welded blank sheet, is conducted on the grounds of laboratory testing and industrial press forming tests (Figure 3). The weld metal and the heat affect zone are a geometrical notch and their metallographic structure influences substantially the usability of the elements for deep drawing. It imposes the necessity of precise selection and control of welding process parameters in order to ensure repeatability of the joints quality.

In order to limit the influence of structural and geometrical notches in welded joints of tailored

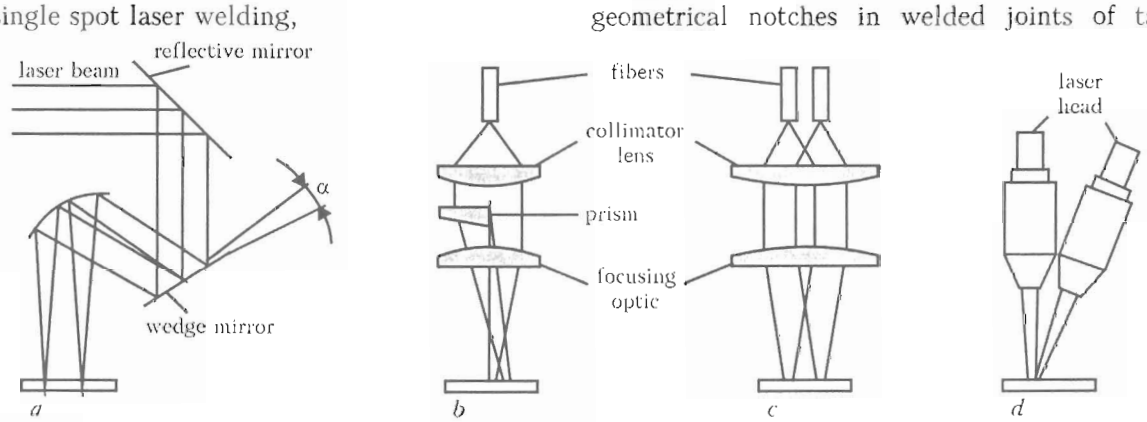


Figure 4. Different means of obtainment of two laser beams in twin spot laser welding

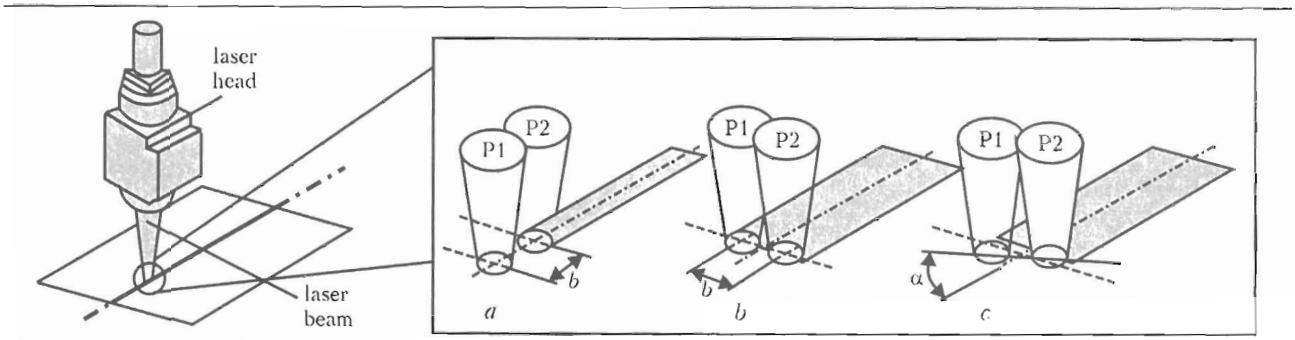


Figure 5. One to the other orientation of two laser beams in twin spot laser welding

blanks, the investigations on the application of various laser welding techniques for performing such joints are conducted at the Instytut Spawalnictwa.

Twin spot laser welding consists in the obtainment on the welding area two laser beams focused in two different points. It can be carried on through splitting the laser beam in two separate ones by means of special wedge mirrors or prisms (Figure 4, *a* and *b*) or delivery of two laser beams to the optical system (Figure 4, *c*) or application of two separate welding heads (Figure 4, *d*). Laser beam focuses can be positioned in tandem (in single file) in accordance with welding direction or one next to the other, perpendicular or at an angle to welding direction (Figure 5).

Positioning of two laser beams in tandem enables to influence the quality of the joint, for instance through the decrease in weld cooling rate. In consequence, the fraction of hardening structures in HAZ is reduced and the hardness grows less. Additional debunching of the drag beam allows to diminish the cooling rate more effectively. In welding of aluminium alloys it was observed the decrease in porosity and in tendency to formation of weld cracks when the focus of the drag beam was situated above the material under welding (the pilot beam was focused on the surface of the material) [7]. On account of necessity to keep up the power density above the threshold limit value and to create the forced gas draft, the welding speed must be decreased to the degree depending on the proportion of the power distributed among two component beams.

Application of this welding technique for performing tailored blanks brought about the change of weld shape and lessened geometrical and structural notches. The change in the means of heat input to the material to be welded affects the shape of the weld (Figure 6) and the welding thermal cycle, influencing thereby the structural transformations in the weld and heat affected zone. The use of dual beam laser technique for welding sheets designed for tailored blanks made it possible to decrease the hardness of the weld and HAZ by about 30%.

In welding of sheets for tailored blanks, the preparation and positioning of sheets is of essential importance to guarantee high quality joints. The weld gap should not exceed 0.1 mm. Enlarging of it can bring about defects such as excessive penetration bead or incompletely filled groove and, in extreme cases, lack of joining.

Dual beam laser welding technique with placing laser beams in position one next to the other, perpendicular to welding direction, besides changes in the thermal cycle run in the weld and HAZ, enables to increase remarkably the tolerance on fit-up of sheet edges. The tests of butt welding of car body sheets dissimilar in thickness (1.5 mm thick sheet welded to that of 0.7 mm thick) with variable weld gap have shown, that it is possible to obtain a correct joint, if the gap does not exceed about 0.2 mm.

Hybrid welding — the process in which it is used the heat source in the coupled form, namely the laser beam and electric arc operating together in the same place and time. The process shows a number of advantages in relation to laser welding and electric arc welding applied separately. Simultaneous operation of laser beam and electric arc stabilizes the welding process and improves the thermal efficiency and elasticity of the method, making it possible, for instance, to weld elements, the edges of which are less precisely prepared than it would be necessary for laser welding while the smaller distortions of heavy-gauge elements are obtained than in arc welding.

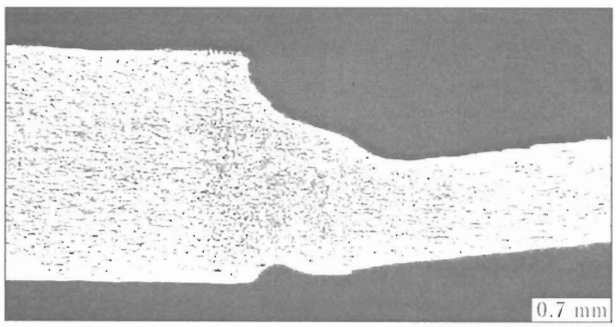
Electric arc brought into the laser affected zone delivers heat to metal in the upper part of the joint being formed, resulting in the change of «I» weld shape, typical for laser welding. Usually, the weld assumes the «U» shape.

Nowadays, research and development works on specialistic equipment are focused on three fundamental methods of the hybrid welding process:

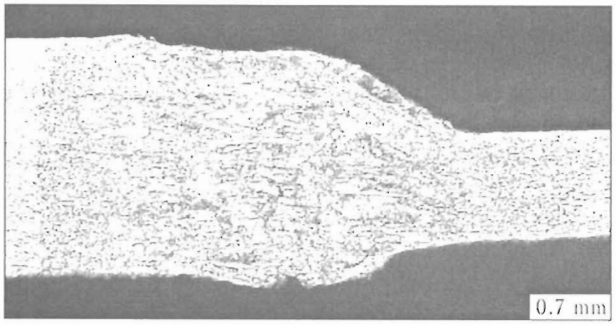
1. Laser-plasma arc hybrid welding,
2. Laser-MIG hybrid welding and «HyDRA» welding,
3. Laser-TIG hybrid welding.

At the Instytut Spawalnictwa there are conducted investigations into laser-TIG hybrid welding, including the application of this process to welding of car body sheets to produce tailored blanks. In investigations it is used Trumph Lasercell 1005 system together with the special instrumentation developed at the Institute, which affords possibilities for regular and safe co-operation of laser with the power source (Figure 7).

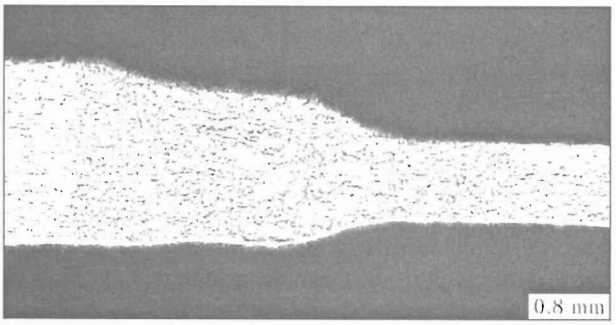
The process of hybrid laser welding, in which the heat source is the CO_2 laser beam and electric arc burning in gas shield between nonconsumable electrode and the material under welding, is suitable, first of all, for joining of rather thin elements. The laser beam stabilizes the anode spot owing to the vapor plume induced by laser and forced gas draft, characteristic for this process. The most visible advantage of the hybrid laser welding process is the remarkable increase in the rate of production yield in comparison to each of the component processes considered sepa-



Single spot laser welding technique



Twin spot laser welding technique with equipartition of power; the beam focused in two points 0.7 mm apart, positioned in tandem, parallel to welding direction



Twin spot laser welding technique with equipartition of power; the beam focused in two points 0.7 mm apart, positioned perpendicular to welding direction

Figure 6. Macrostructures of butt joints in car body sheets, differentiated in thickness (1.5 mm and 0.7 mm thick), made of electrogalvanized steel, welded with 3.8 kW CO_2 lasers by different techniques

rately. The essence of this process is the fact that during simultaneous use of low power laser beam and electric or plasma arc it is possible to achieve such a penetration depth as in each of these processes separately but with the use of remarkably higher power. The characteristic feature is also the possibility of substantial increase in welding speed in comparison to that of component processes. The difficulties in conducting of hybrid processes resolve themselves into three questions: selection and co-ordination of the work of laser and arc welding unit, precise spatial positioning of welding torch in relation to the laser beam axis and determination of proper power level for each heat source used in the process.

The tests of welding of butt joints in galvanized sheets designed for tailored blanks for car bodies confirmed the usability of this method to manufacture high quality joints of this type. The use of two coupled

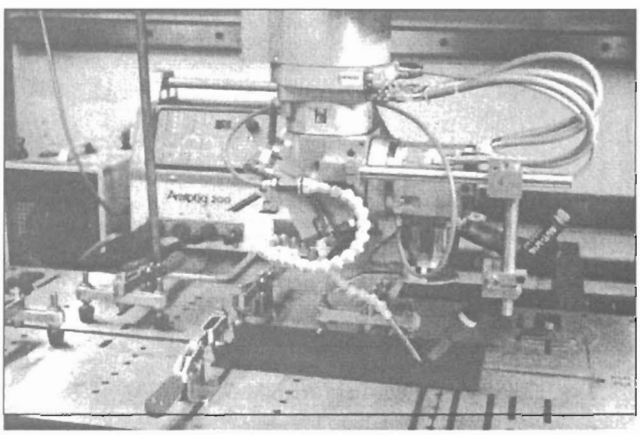


Figure 7. Test station for laser-TIG hybrid welding at the Instytut Spawalnictwa

heat sources, and thereby the change in the manner of heat delivery and in the amount of the heating input into the joint region, changes the shape of the joint zone, providing smooth interface on the area of elements, differentiated in thickness (Figure 8). At the same time it was achieved the hardness drop in the weld and heat affected zone by about 30% (just as in dual beam laser welding) and more than 40% increase in welding speed in comparison to conventional laser welding.

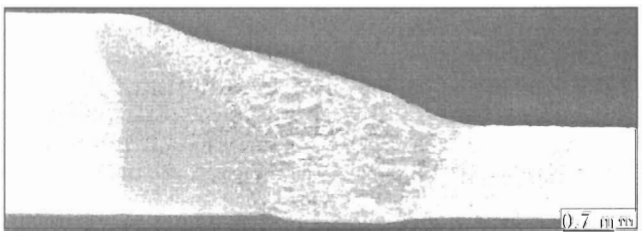


Figure 8. Macrostructure of butt joint in car body sheets differentiated in thickness (1.5 mm and 0.7 mm) made of electrogalvanized sheet, welded by hybrid laser-TIG technique

Despite of evident advantages of this method, demonstrated in laboratory tests, the process of hybrid laser welding did not find up to now any wide industrial application, on account of, among other reasons, large number of variable parameters and the risk of lack of repeatability of the results under industrial conditions connected with this fact.

1. G. Cam, S. Erim, C. Yeni: *Determination of mechanical and fracture properties of laser beam welded steel joints.* Welding Journal, 1999, no. 6.
2. G. Cam, M. Kocak, J. K. Dos Santos: *Developments in laser welding of metallic materials and characterization of the joints*, Welding in the World, 1999, no. 3, 4.
3. S. M. Chan, L. C. Chan, T. C. Lee: *Tailor welded blanks of different thickness ration effects on forming limit diagrams*, Journal of Material Processing Technology 132/2003.
4. J. Baysore, M. Williamson, Y. Adonyi, J. Milian: *Laser Beam Welding and Formability of Tailored Blanks.* Welding Journal, 1995, no. 10.
5. K. Ayres, P. Hilton: *CO_2 laser butt welding of coated steels for the automotive industry.* Welding and Metal Fabrication, 1994, no. 1.
6. W. Waddell, G. Davies: *Laser welded tailored blanks in the automotive industry.* Welding and Metal Fabrication, 1995, no. 3.
7. J. Xie: *Dual beam laser welding.* Welding Journal, 2002, no. 10.

BASICS AND APPLICATIONS OF LASER GMA HYBRID WELDING

C. THOMY, T. SEEFELD
BIAS-Bremen Institute of Applied Beam Technology GmbH, Germany

A basic requirement for exploiting the specific advantages of laser GMA hybrid welding is a comprehensive, fundamental understanding of the interactions of the two sub-processes laser welding and GMA welding, as their synergetic interactions significantly contribute to the advantages of hybrid welding. However, for an effective as well as efficient industrial application, a thorough analysis of the requirements of the specific applications and the industrial environment is a prerequisite. Thus, within this paper, after an overview on hybrid welding, some interaction phenomena between the sub-processes are given a closer look. Based on these considerations, two applications (Laser GMA hybrid welding in pipe production and in welding of extruded aluminium profiles in the railway industries) are discussed.

Introduction. Among others, the hopes for a reduction of investment and operating costs, of decreasing cycle time and of improving product quality are often the driving forces for developing and applying innovative welding processes such as laser GMA Hybrid Welding. This welding process is generally characterised by the combination of laser beam welding and GMA welding in one common process zone (melt pool and plasma) and was first investigated in the 1970s [1]. Among the advantages commonly associated with hybrid welding is a significant process stabilisation, higher achievable welding speeds especially compared to arc welding, lower tolerance requirements compared to laser welding and, in some cases, improved weld properties.

Exploiting these advantages, a variety of application potentials arises, in special in welding of thicker steel materials [2, 3, 4, 5]. Due to the laser powers required for these sheet thicknesses, up to now mainly CO_2-Lasers (typically with beam powers exceeding 8 kW) have been applied for these tasks.

In contrast, for welding of aluminium alloys in sheet thicknesses normally used in the automotive industries, the beam powers delivered by today's Nd:YAG-Lasers (accepting some restrictions considering welding speed) suffices. Consequently, due to the easy beam delivery (fibres instead of mirror systems as for CO_2-Lasers) and certain process properties, Nd:YAG-Laser GMA hybrid welding is often applied [6]. Moreover, the development of commercially available hybrid welding systems is currently focussing on Nd:YAG-Laser GMA hybrid welding.

However, Nd:YAG-Laser GMA hybrid welding is (due to the comparably low laser powers) normally restricted in view of sheet thickness and consequently not capable of covering the complete range of thicknesses encountered e.g. in welding of extruded aluminium profiles for railway structures. Thus, there is a demand for higher and easily deliverable beam powers which may be answered by the high-power fibre laser.

Interaction Phenomena in Laser GMA Hybrid Welding. To be able to fully exploit the benefits arising from the combination of a gas metal arc and a laser beam to a hybrid welding process, a wide variety

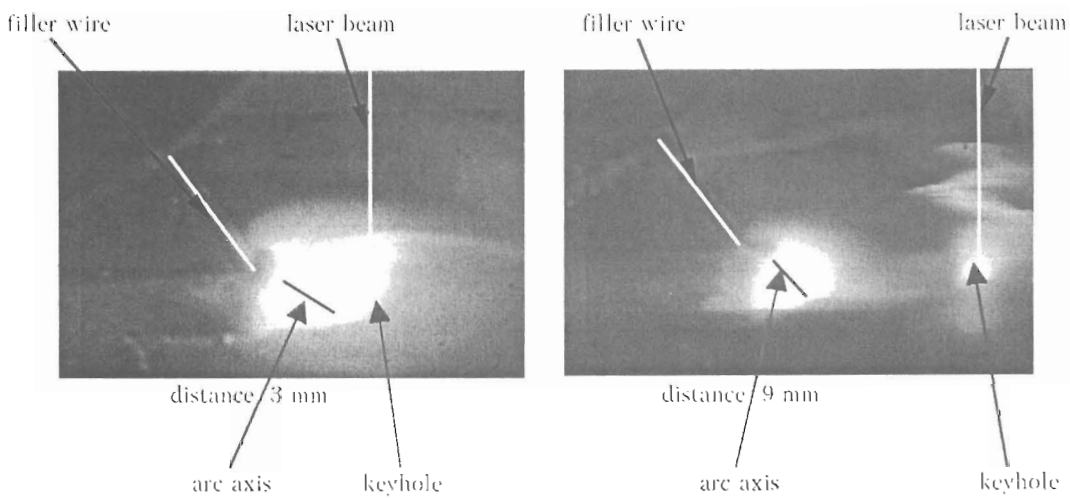


Figure 1. Influence of the laser beam on the arc

© C. THOMY, T. SEEFELD, 2005

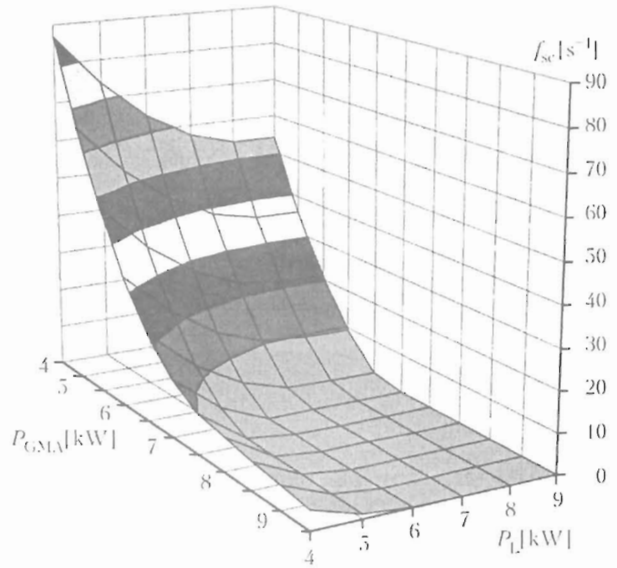


Figure 2. Influence of laser power P_L and arc power P_{GMA} on short-circuiting frequency f_{SC}

of parameters have to be optimized in view of the specific demands of the task. However, as these parameters (e.g. laser power or welding voltage) often significantly interact, a fundamental understanding of these interactions is required.

The mutual interaction between laser beam and GMA becomes obvious if high-speed videos of the process are analysed. Taking the position of the arc axis, on the one hand, for a laser-arc distance of 9 mm, no arc deviation is observed (Figure 1).

Consequently, it does not seem to be justified to talk of hybrid welding for such a process distance. Rather, it has to be expected that for this spatial arrangement, the advantages of hybrid welding resulting from process interactions are reduced to the effects of temperature field modifications. On the other hand, for a laser-arc distance of 3 mm, i.e. for a «real» hybrid welding process, the arc axis is significantly deviated towards the keyhole, and a common process plasma is formed. Comparable observations can be made for the influence of the beam power applied, so the optimisation of the relation of laser power to arc power may be of significance, too.

Taking the example of CO_2-Laser GMA hybrid welding of steel, the interactions of laser beam and GMA were given a closer look. Within these experiments (P_L = 4...9 kW, welding speed v = 1.8 m/min, U = 19...30 V, wire feed rate = 9 m/min, Ar/He shielding gas) it was established that both increasing arc power P_{GMA} and increasing laser power P_L contribute to a significant reduction of short-circuiting frequency and thus greatly influence the mode of metal transfer (Figu-re 2).

CO_2-Laser GMA Hybrid Welding in Pipe Production. In order to implement CO_2-Laser GMA hybrid welding on an existing production unit for longitudinally and continuously welding stainless steel linepipes by the help of an 8 kW CO_2-laser, a welding head (Figure 3) integrating both sub-processes was developed, built and tested by BIAS, paying special attention to the thermal loads resulting from continuous welding times of several hours. These loads are not only due to the arc, but also due to the laser plasma and back-reflections of the laser beam.

During the production tests, a welding speed of 1.2 m/min was achieved for pipelines up to Ø 273×8 mm (steel 12Cr 4.5Ni 1.5Mo) using laser powers up to 7 kW and arc powers up to 8 kW. This welding speed means an increase in processing speed of more than 300 % compared to conventional arc welding processes. It was not limited by the welding process itself but rather by the restrictions of the forming unit. Considering quality, 100% X-ray testing (DIN EN 25817 C) demonstrated that the produced welds were 100% defect-free according to the company's requirements in view of cracks, pores and other imperfections. Figure 4 shows a cross-section of a pipe Ø 273×5 mm.

From this application, it became obvious that, if hybrid welding is integrated in production systems mainly designed for arc welding processes, the welding speed is often not the critical factor for reducing cycle time. Rather, new bottlenecks in operations before or after welding (such as handling processes) arise, making additional efforts necessary to be able to fully exploit the benefits of hybrid welding.

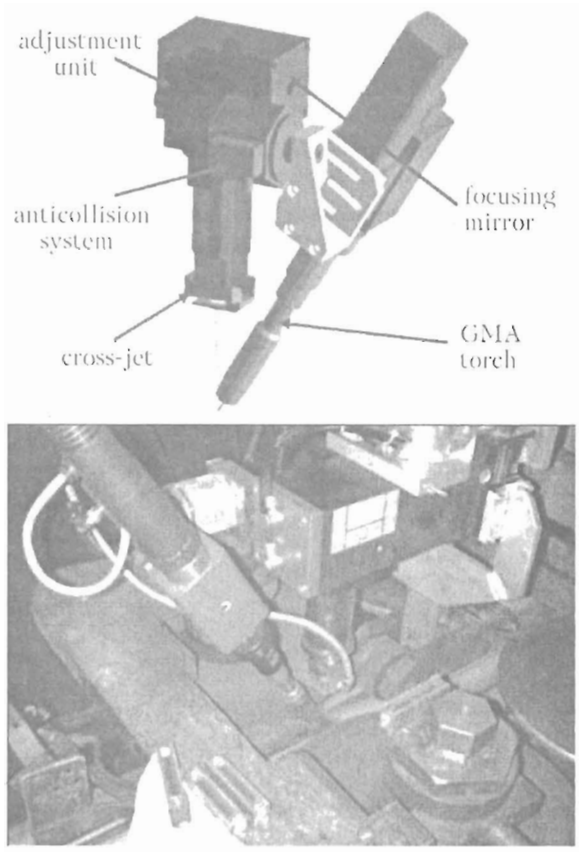


Figure 3. CO_2-Laser GMA hybrid welding head – design and industrial application

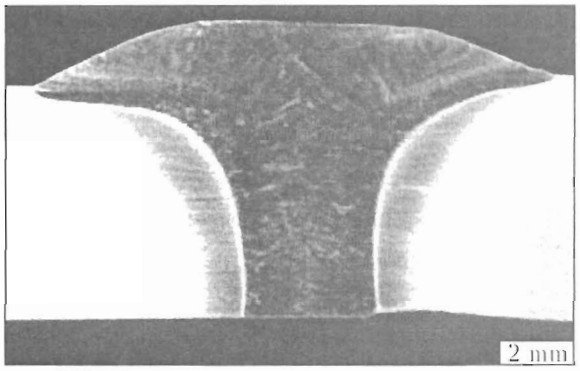


Figure 4. Cross-section of pipe (Ø 273×5 mm, 12Cr4.5Ni1.5Mo)

Solid-State Laser GMA Hybrid Welding of Railway Structures. One of the central targets of the study on Nd:YAG-Laser GMA hybrid welding of extruded aluminium profiles was the production of test panels. The roof segment displayed in Figure 5 is a prototype section of the roof of the ICN train produced from six extruded aluminium profiles (AlMgSi0.7, t = 3 mm, filler wire AlSi12) with a length of 2 m. No special clamping devices were used. With a laser power of 4 kW at workpiece and an arc power of the pulsed GMA of 3.65 kW, a welding speed of 4 m/min was achieved.

It was demonstrated that Nd:YAG-Laser GMA welding is a feasible process especially in view of the requirements considering gap bridging. Consequently, special efforts considering seam preparation, clamping technology or gantry precision are not required. Moreover, compared to pure GMA welding, Nd:YAG-Laser GMA welding allows a significant increase in welding speed, which is associated with a reduction of seam volume and total heat input (up to 85%), thus resulting in a considerably lower distortion [7].

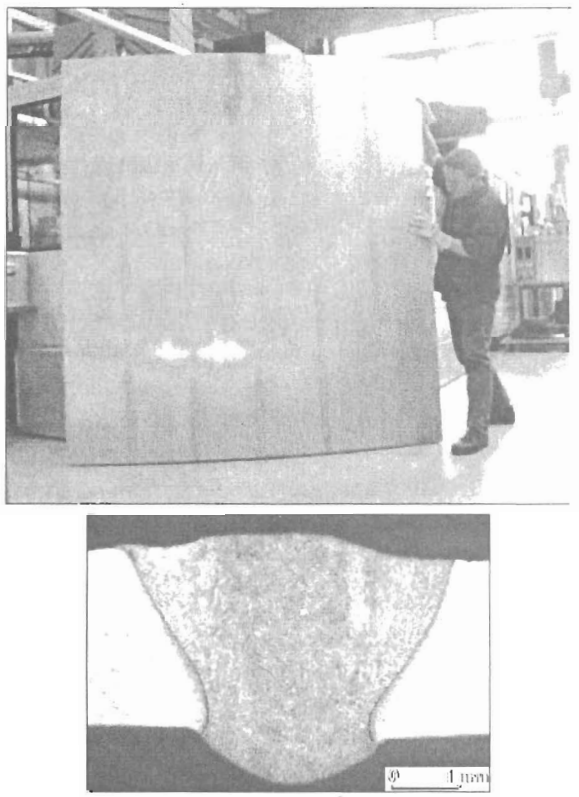


Figure 5. Roof segment of the ICN train, and weld cross-section

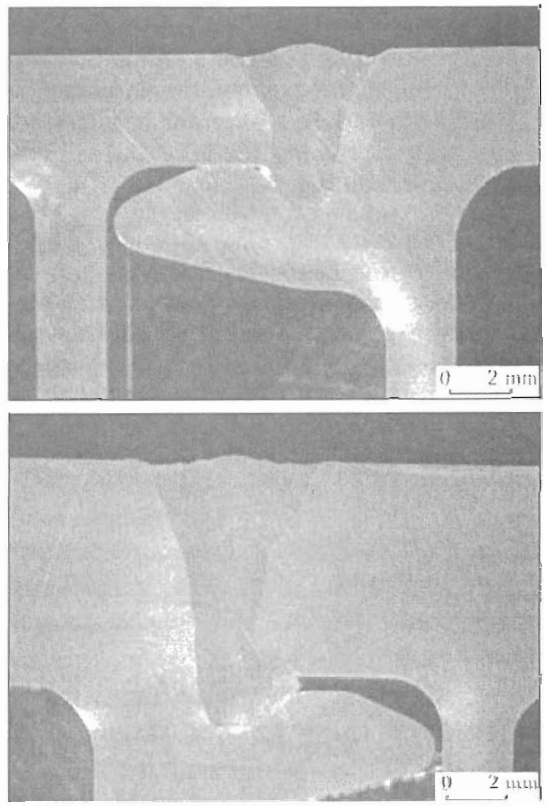


Figure 6. First fibre laser GMA hybrid welds (EN-AW 6008, 4 mm and 8 mm)

To surpass the limitations imposed by a laser power restricted to 4 kW, an IPG fibre laser of the 10 kW class was applied to hybrid welding, too. Figure 5 shows two first results obtained on EN AW 6008 (wall thickness 4 and 8 mm, respectively) with filler wire AlSi 5. Welding speed was 6 m/min in all cases with laser powers up to 10.5 kW for the 8 mm material.

The process was very stable and weld quality was acceptable. Further optimisation might result in even higher welding speeds especially for a wall thickness around 4 mm. These results have been rated so promising that further tests to pre-qualify fibre laser GMA hybrid welding for this application are scheduled.

CONCLUSIONS

As a conclusion, it is safe to say that Laser GMA hybrid welding in its various forms especially considering the type of laser has found and will find numerous interesting industrial applications. However, for a successful industrial implementation of laser GMA hybrid welding a deepened understanding of the process as well as an exact analysis of both the welding process and the production system is required. In special, the significant increase in welding speed has to be considered.

Recently, the high-power fibre laser enhances the application potentials of hybrid welding, as it combines the easy beam handling of the Nd:YAG-Laser with

the power of the CO_2-Laser and possesses numerous other specific advantages such as a high efficiency and a small footprint. Consequently, this laser can be applied to tasks where lasers have not been considered previously, thus increasing the potential application fields for hybrid welding, too.

Acknowledgements. *The authors are particularly grateful to the European Commission («Development of Advanced Joining Technologies for Supermartensitic Stainless Steel Line Pipes – JOTSUP» (GRD1-1999-10278)) as well as to the Bremer Innovationsagentur GmbH (funding on behalf of the Senator fur Wirtschaft und Hafen der freien Hansestadt Bremen (AMST P2)) and the BMBF (project Leichter: 13N7460-5) and the Deutsche Forschungsgemeinschaft DFG (Gottfried-Wilhelm-Leibniz-Programm, VO530/7) for funding considerable parts of the work presented.*

1. Steen, W.M. and Eboo, M.: *Arc Augmented Laser Welding*. Met. Constr. 11 (1979), H. 7, 332–333, 335.
2. Wieschemann, A.: *Entwicklung des Hybrid-und Hydrasch weißverfahrens am Beispiel des Schiffbaus*. Aachen: Shaker 2001.
3. Thomy, C., Sepold, G., Seefeld, T., Walz, C., Hoffmann, R., Stiebe-Springer, I., Kocak, M. and Segar, R.: *Industrial implementation of Laser/GMA welding and mechanical properties of the welds*. Supermartensitic Stainless Steels Conference, Brussels 2002, 147–155.
4. Kaierle, S., Dahmen, M., Bongard, K. et al.: *Hybridschweißen von Öltanks – Ein innovativer Fügeprozeß*. Große Schweißtechnische Tagung 2002, Nurnberg 2002, 207–209.
5. Miebach, R.; Lembeck, H.: *Die neue Fertigung der Meyer-Werft-Laserhybridschweißen als Kerntechnologie*. Große Schweißtechnische Tagung 2003, Berlin 2003, 187–192.
6. Stäufer, H.; Helten, S.: *Laser-Hybridschweißen fur neuartige Leichtbaukonzepte im Automobilbau*. Große Schweißtechnische Tagung 2003, Berlin 2003, 175–180.
7. Harlfinger, N.: *Laserstrahlgeschweißte Leichtbaustrukturen im Schienenfahrzeugbau. Verbundprojekt Innovativer Leichtbau durch energiereduziertes Fugen mit Lasersystemen neuester Generation (LEICHTER)*, VDI-Technologiezentrum, 2003, 61–68.

Name Index

Ajayi O. 116
Albert F. 19
Anyakin M. I. 67, 135, 141

Bachmann F. 24
Banasik M. 198
Bartoszewicz A. 162
Beliavin K. E. 113
Borisov Yu. 57
Borisova G. V. 73
Bushma A. 57

Chan L.C. 167, 171
Cheng C. H. 167, 171
Chivel Yu. A. 113, 151
Chow C. L. 167, 171

Daszherdi A. 80
Devojno O. G. 154
Dilthey U. 29, 49
Dworak J. 198

Etsion I. 116
Exsan O. 121

Fomakin A. 57

Garashchuk V. P. 60
Gavrilov S. P. 130
Gedopt J. 175
Geerinckx E. 175
Golovko L. F. 76, 80, 121
Golubev V. S. 34
Goncharuk A. A. 121
Grigoriev A. 49
Grobelny M. 182
Gumenyuk A. 29, 49, 96
Guo X. 43

Hoffman J. 182

Jahrsdoerfer B. 19

Janicki D. 39, 158

Kaglyak A. D. 76
Kalita W. 162, 182
Kardapolova M. A. 154
Karfoul M. K. 186
Khaskin V. Y. 57, 190
Kislitsa A. 57
Klimpel A. 39, 158
Klyuchnikov Y. V. 80
Kohn H. 46
Kolodziejczak P. 182
Kolpakov V. 64
Kondrashov P. 135
Korovina N. A. 73, 85
Kovalchenko A. 116
Kovalenko V. S. 9, 64, 67, 91, 121, 135, 141
Kozakova T. 141
Krasavin A. P. 76
Kravets O. L. 73
Krivtsun I. V. 57, 190
Kwiatkowski L. 182

Lee T. C. 167, 171
Lisiecki A. 39, 158
Lopota V. 49, 96
Lutay A. 141
Lysenko A. A. 73
Lysenko A. B. 73, 85

Makhnenko O. 103
Malkin P. E. 96
Mamalis A. 64
Man HC 43
Mukhoid A. 135
Mys I. 19

Nabok T. 190
Novikov N. V. 121

Oleschuk L. M. 67

Pavlenko V. K. 113
Pavluchenkov I. A. 85
Petrushina M. V. 113
Pilarczyk J. 198
Pozdeeva E. 49
Pretorius T. 100

Radziejewska J. 162
Rudakov K. 141

Schmidt M. 19
Seefeld T. 203
Serditov A. T. 80
Seyffarth P. 103
Shelyagin V. D. 57, 190
Shepelev A. A. 121
Sidorets V. N. 60
Sokolova T. N. 195
Soroshenko V. G. 76, 121
Stano S. 39, 198
Stepura A. 135
Surmenko E. L. 195

Teplova L. A. 126
Thomy C. 46, 203
Turichin G. 29, 49, 96

Valdaitseva E. 96
Vertiy A. A. 130
Verwimp J. 175
Vollertsen F. 46, 100
Voynarovich S. 57

Woitschig J. 100

Zemliakov E. 49
Zhang S. 43
Zhuk R. O. 67, 91